

Molecular and Integrative Toxicology

Andrea B. Weir
Margaret Collins *Editors*

Assessing Ocular Toxicology in Laboratory Animals

 Humana Press

Molecular and Integrative Toxicology

Series Editor

Rodney R. Dietert

For further volumes:

<http://www.springer.com/series/8792>

Andrea B. Weir • Margaret Collins
Editors

Assessing Ocular Toxicology in Laboratory Animals

 Humana Press

Editors

Andrea B. Weir
Charles River Laboratories
Preclinical Services
Reno, NV, USA

Margaret Collins
Charles River Laboratories
Preclinical Services
Reno, NV, USA

Series Editor:

Rodney R. Dietert
Department of Microbiology
and Immunology
College of Veterinary Medicine
Cornell University
Ithaca, New York, USA

ISBN 978-1-62703-163-9 ISBN 978-1-62703-164-6 (eBook)
DOI 10.1007/978-1-62703-164-6
Springer New York Heidelberg Dordrecht London

Library of Congress Control Number: 2012951925

© Springer Science+Business Media, LLC 2013

This work is subject to copyright. All rights are reserved by the Publisher, whether the whole or part of the material is concerned, specifically the rights of translation, reprinting, reuse of illustrations, recitation, broadcasting, reproduction on microfilms or in any other physical way, and transmission or information storage and retrieval, electronic adaptation, computer software, or by similar or dissimilar methodology now known or hereafter developed. Exempted from this legal reservation are brief excerpts in connection with reviews or scholarly analysis or material supplied specifically for the purpose of being entered and executed on a computer system, for exclusive use by the purchaser of the work. Duplication of this publication or parts thereof is permitted only under the provisions of the Copyright Law of the Publisher's location, in its current version, and permission for use must always be obtained from Springer. Permissions for use may be obtained through RightsLink at the Copyright Clearance Center. Violations are liable to prosecution under the respective Copyright Law.

The use of general descriptive names, registered names, trademarks, service marks, etc. in this publication does not imply, even in the absence of a specific statement, that such names are exempt from the relevant protective laws and regulations and therefore free for general use.

While the advice and information in this book are believed to be true and accurate at the date of publication, neither the authors nor the editors nor the publisher can accept any legal responsibility for any errors or omissions that may be made. The publisher makes no warranty, express or implied, with respect to the material contained herein.

Printed on acid-free paper

Humana Press is a brand of Springer
Springer is part of Springer Science+Business Media (www.springer.com)

*This book is dedicated to all toxicologists,
ophthalmologists and other scientists who
have furthered knowledge in the field of
ocular toxicology.*

Preface

The goal of this text is to provide a concise reference addressing ocular anatomy and physiology across species, approaches for assessing ocular toxicity and regulatory expectations regarding ocular toxicology. The text is intended for toxicologists and other scientists involved in conducting toxicology studies for regulatory purposes and/or reviewing data from such studies.

Ocular toxicity is known to occur following intended or unintended exposure of ocular tissues to xenobiotics. It can occur following local exposure of the eye to an agent or after exposure via oral or other routes of administration. In order to define the risks that pharmaceuticals, pesticides and other toxic substances pose to the eye, an assessment of ocular toxicity is routinely included in general toxicology studies conducted for regulatory purposes. Because anatomical and physiological differences between species can impact the nature of the ocular effects observed, understanding species differences is important. Although it is possible to detect some ocular effects, such as conjunctivitis, with the naked eye, more sensitive techniques are routinely used to assess ocular toxicity. Slit lamp biomicroscopy and indirect ophthalmoscopy are routinely utilized to more closely evaluate the anterior and posterior segments of the eye, respectively, during the course of toxicology studies. In some cases, more advanced diagnostic procedures that are not routinely performed in standard studies are needed. At the time of necropsy, ocular tissues are collected and processed for histopathological evaluation. More specialized endpoints, such as electroretinography, can be incorporated, as needed. The United States Food and Drug Administration (FDA) ensures the safety of medicinal products for human and animal use, food additives, cosmetics and other products. Similarly, the Environmental Protection Agency (EPA) ensures the safety of pesticides and other products. Toxicology studies are conducted to support the safety of FDA- and EPA-regulated products. The design of those studies includes an assessment of ocular toxicity, with the nature of the assessment dependent upon the regulatory authority, nature of the product and other factors.

We began this text with a discussion of ocular anatomy across various species of laboratory animals used in toxicology studies being conducted for regulatory purposes, which lays the groundwork for subsequent chapters. The next three chapters

address ocular diagnostic techniques, with Chap. 2 focusing on techniques that are routinely included in toxicology studies and Chaps. 3 and 4 on advanced diagnostics, including electrophysiology and imaging, which are used as scientifically warranted. Chapters 5 and 6 address ocular pathology and include a detailed description of appropriate techniques used to process ocular tissues as well as lesions that can be encountered in laboratory animals. Finally, Chaps. 7 and 8 focus on the regulatory expectations from FDA, EPA and other agencies for assessing ocular toxicity.

Acknowledgements

We would like to acknowledge the contributors for their efforts in creating this text. Each of the contributors has a full time career, and projects such as this one place even more demands on their limited time.

Contents

1 Comparative Ocular Anatomy in Commonly Used Laboratory Animals	1
Mark Vézina	
2 Assessment of Ocular Toxicity Potential: Basic Theory and Techniques	23
Robert J. Munger and Margaret Collins	
3 Emerging Imaging Technologies for Assessing Ocular Toxicity in Laboratory Animals	53
T. Michael Nork, Carol A. Rasmussen, Brian J. Christian, Mary Ann Croft, and Christopher J. Murphy	
4 Emerging Electrophysiological Technologies for Assessing Ocular Toxicity in Laboratory Animals	123
James N. Ver Hoeve, Robert J. Munger, Christopher J. Murphy, and T. Michael Nork	
5 Toxicologic Pathology of the Eye: Histologic Preparation and Alterations of the Anterior Segment	159
Kenneth A. Schafer and James A. Render	
6 Toxicologic Pathology of the Eye: Alterations of the Lens and Posterior Segment	219
Kenneth A. Schafer and James A. Render	
7 Nonclinical Regulatory Aspects for Ophthalmic Drugs	259
Andrea B. Weir and Susan D. Wilson	

**8 Ocular Toxicity Regulatory Considerations for Nondrug
Food and Drug Administration (FDA) Products
and the Environmental Protection Agency (EPA) 295**
Christopher Bartlett

About the Editors..... 307

Index..... 309

Contributors

Christopher Bartlett, Ph.D. SciMetrika LLC, Durham, NC, USA

Brian J. Christian, Ph.D., DABT Covance Laboratories, Madison, WI, USA

Margaret Collins, M.S. Charles River Laboratories, Preclinical Services, Reno, NV, USA

Mary Ann Croft, M.S. Department of Ophthalmology and Visual Sciences, University of Wisconsin-Madison, Madison, WI, USA

Robert J. Munger, D.V.M., DACVO Animal Ophthalmology Clinic Inc., Dallas, TX, USA

Christopher J. Murphy, D.V.M., Ph.D, DACVO Ocular Services On Demand, LLC (OSOD) and Department of Ophthalmology & Vision Science, School of Medicine and Department of Surgical and Radiological Sciences, School of Veterinary Medicine, University of California, Davis

T. Michael Nork, M.D., M.S., DABO, FARVO Ocular Services On Demand, LLC (OSOD) and Department of Ophthalmology and Visual Sciences, University of Wisconsin School of Medicine and Public Health, Madison, WI, USA

Carol A. Rasmussen, M.S. Ocular Services On Demand, LLC (OSOD) and Department of Ophthalmology and Visual Sciences, University of Wisconsin School of Medicine and Public Health, Madison, WI, USA

James A. Render, D.V.M., Ph.D., DACVP NAMSA, Northwood, OH, USA

Kenneth A. Schafer, D.V.M., DACVP, FIATP Vet Path Services Inc., Mason, OH, USA

James N. Ver Hoeve, M.S., Ph.D. Ocular Services On Demand, LLC (OSOD) and Department of Ophthalmology and Visual Sciences, University of Wisconsin School of Medicine and Public Health, Madison, WI, USA

Mark Vézina, B.Sc Charles River Laboratories, Preclinical Services, Department of Ocular and Neuroscience, Senneville, QC, Canada

Andrea B. Weir, Ph.D., DABT Charles River Laboratories, Preclinical Services, Reno, NV, USA

Susan D. Wilson, D.V.M., Ph.D Aclairo Pharmaceutical Development Group, Inc., Vienna, VA, USA

Chapter 1

Comparative Ocular Anatomy in Commonly Used Laboratory Animals

Mark Vézina

Abstract Interspecies differences in ocular anatomy can alter the way a drug interacts locally within the eye, whether administered directly to the eye or systemically. It is therefore important to understand these differences and how they can influence the outcome and interpretation of safety or efficacy data for ocular therapeutics. The eye is a complex system of tissues integrated into a functional sense organ. Oriented toward the toxicologist or ocular researcher, this chapter will discuss the individual ocular tissues in commonly used laboratory animals in comparison with humans and will provide a basic understanding of ocular anatomy including quantitative comparisons when possible in these species. It will also act as a reference to the terminology that will be encountered in subsequent chapters.

1.1 Introduction

The eye is a complex organ system consisting of many specialized tissues that work in conjunction to make vision as we know it possible. Indeed, the malfunction of just one of these tissues can impair vision. In the clinical field, the eye's complexity has resulted in the development of specialists for individual tissues such as the cornea and retina. Since vision is arguably the most important of our senses, conducting ocular toxicology and tissue distribution studies in laboratory animals is essential to ensure the safety of therapeutics applied directly to or injected into the eye to treat ocular disease before they are administered to humans. Ocular toxicology is also assessed for drugs administered via non-ocular routes, such as oral and intravenous, to treat ocular

M. Vézina, B.Sc (✉)
Charles River Laboratories, Preclinical Services, Department of Ocular and Neuroscience,
Senneville, QC, Canada
e-mail: mark.vezina@crl.com

and other diseases. As well, an understanding of the pharmacodynamics or efficacy of an ocular therapeutic can be determined with the use of laboratory animals. Therefore, knowing the ocular anatomy of the species of laboratory animals commonly used for nonclinical studies (i.e., pharmacology, pharmacokinetics, and toxicology studies conducted in laboratory animals), such as those conducted to support drug development, is important because the anatomy can influence how the eye will react to a drug or foreign substance, whether administered systemically or directly onto or into the eye. Though many of the basic elements of the eye are conserved among species, significant anatomical diversity exists and has the potential to influence study results. However, there has been a lack of comprehensive information readily available to toxicologists or researchers to aid in the decision-making process when choosing a suitable species for ocular toxicology testing, or when evaluating the relevance of animal data to the human clinical situation. Therefore, this chapter is oriented toward the toxicologist, and the goal is to assemble the diverse anatomical characteristics of the eyes of mice, rats, rabbits, dogs, cats, minipigs, and nonhuman primates (NHP) in relation to humans to aid in study design and interpretation of results. In this chapter, references to mice, rats, cats, and rabbits pertain to normal, non-transgenic stock, dogs typically beagles or similar sized dogs, minipigs, Göttingen or Yucatan (occasionally a domestic strain or other minipig of similar size) and nonhuman primates (NHP), cynomolgus or rhesus. Anatomic terminology used in subsequent chapters of this book will also be covered. When relevant, quantitative anatomical comparisons have been included for certain tissues. However, when anatomical comparisons take on a quantitative nature, a range of measurements for the same tissue can often be found in the literature for the same species, primarily due to inter-laboratory differences in methodology. As technologies for making quantitative assessments advance, methods become more precise (although not always more accurate!) and these ranges may change, altering the “conventional wisdom.”

As an introduction, a gross view of the eye is presented in Fig. 1.1, illustrating the common structures possessed by all of the species that will be covered.

1.2 Eyelids

The eyelids are often ignored in ocular studies being considered “in the way” of the true region of interest, the eye itself. However, the eyelids do play a key role in ocular maintenance in the form of the blink. The true mechanism of blink control is not fully understood. It is likely a combination of a central nervous system mediated “blink center” that receives sensory input from the ocular surface as well as reflex from visual and mental sources. In humans, blinking can occur automatically (but not at truly fixed intervals), as a reflex to a visual or sound stimulus and at will. Most mammals can do the same. Blinking cleans the surface of the eye, results in the application of the lubricating tear film to the ocular surface, and prevents complete photobleaching of the photoreceptors by providing brief instances of darkness. In humans, the duration

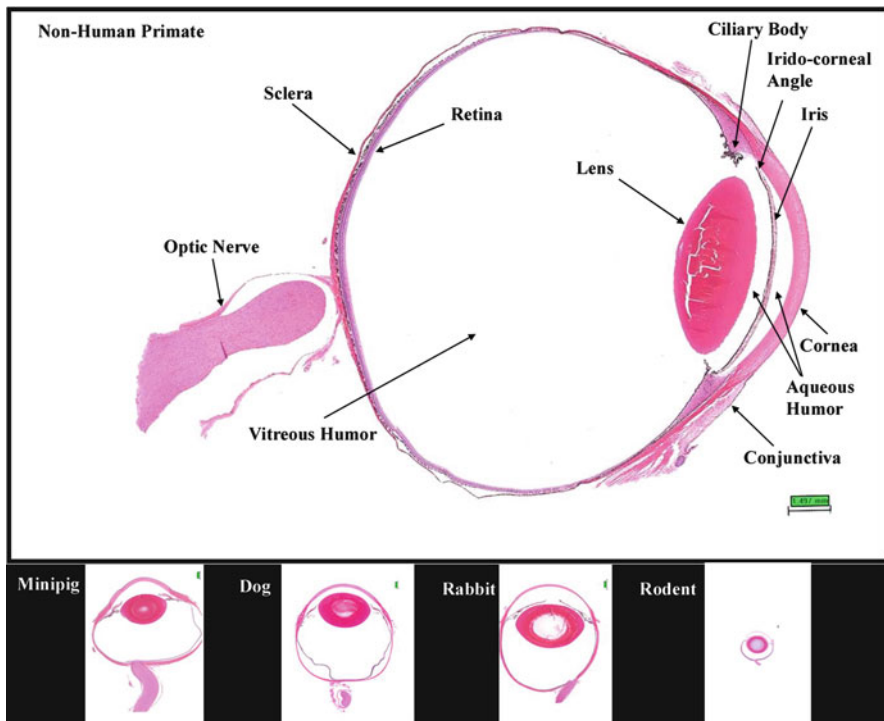


Fig. 1.1 Gross ocular anatomy. Human and nonhuman primate eyes are similar, with the NHP eye at approximately half the scale of the human eye. Other species presented for comparison demonstrate the more obvious differences such as lens size, vitreous and aqueous chamber size, and corneal thickness

of a blink is approximately 250–400 ms [43], which translates into an additional 5–7 min of “darkness” each day during normal waking hours for humans. Although blinking speed has not been well studied in laboratory animals, it has been observed in dogs and nonhuman primates to be in the range of approximately 100–300 ms [11], which is not dissimilar to humans. In addition to applying the tear film, the eyelids are also involved in draining excess tear film, or topical drops for that matter, from the ocular surface. All mammals have two functional eyelids; however, they are not all created equally. Of interest to the toxicologist is the drainage system since it will impact on the duration of the presence of a liquid eye drop on the surface of the eye and by inference the amount of systemic exposure that might occur. Normal tear film is drained from the eye by small openings in the eyelids called puncta. The puncta are connected to nasolacrimal ducts which drain into the sinus onto the nasal mucosa. Their location on the eyelid can vary somewhat, but in general they are located in the medial canthal area, near the edge of the eyelid where the conjunctiva and skin meet. Most laboratory species as well as humans have one punctum on

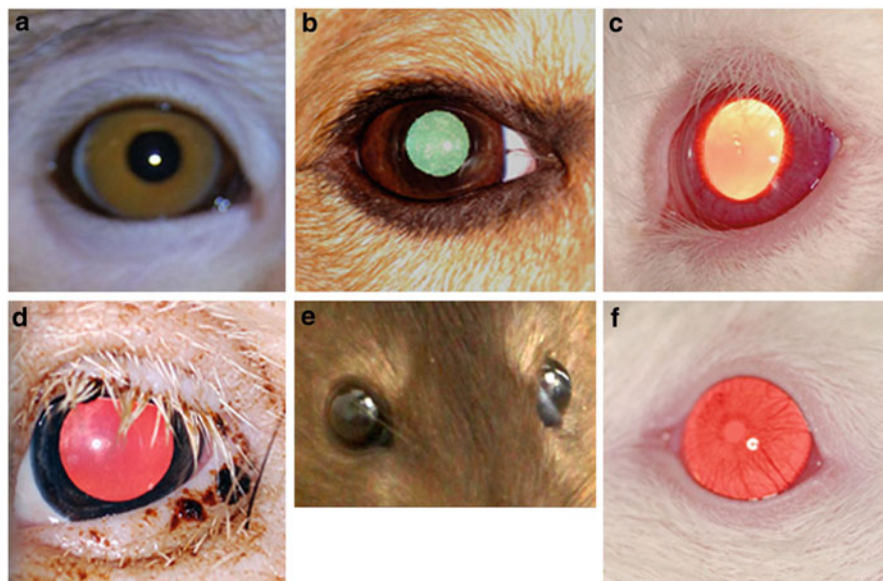


Fig. 1.2 Relative eyelid configuration and eyeball exposure. (a) *Cynomolgus* monkey, (b) dog, (c) New Zealand White rabbit, (d) Göttingen minipig, (e) Brown Norway rat, (f) albino mouse

each upper and lower eyelid. Minipigs (pigs in general) only have puncta on the upper eyelid and rabbits only on the lower eyelid. In humans, approximately 75–80% of tear volume is drained with each blink. It has been estimated that up to 80% of a topical drop can be absorbed systemically [32, 51], with some absorption through the conjunctival vasculature and most of the fluid arriving directly on the highly absorbent nasal mucosa via the nasolacrimal duct system. Mechanically, the drainage occurs by the suction force created when the upper and lower eyelids part, when fluid is drawn into the nasolacrimal drainage system. The size and shape of the eyelids also plays a role in systemic absorption. A species with looser eyelids and larger conjunctival sac such as a rabbit may have more “drop” available for absorption on a subsequent blink than a nonhuman primate which has eyelids more tightly pressed to the eye, where runoff onto the surrounding skin and/or fur from the initial blink is likely to be higher (refer to Fig. 1.2). Similar systemic absorption after topical ocular instillation has been observed in dogs and rabbits [11]. The concern with the systemic absorption is the potential for unwanted systemic side effects. In adult humans, the unintended systemic dosage is usually relatively low on a body weight basis, and consequently, the risk of side effects in the general population is also low, with exceptions for certain susceptible populations. However, when the dose/body weight ratio becomes higher such as in children, the side effects can be more serious [23]. Scale that effect to a 2-kg rabbit or nonhuman primate and the potential for systemic toxicity increases further.

Because blinking can influence the residence time of a topically applied test substance in the eye as well as the tear film, the blink rate may provide some insight

Table 1.1 Average blink rates by species

Human	Every 5 s (task dependent) [60]
Nonhuman primate	Every 6 s [31]
Pig	Every 20–30 s [11]
Dog	Partial blink: Every 4 s [10] Complete blink: Every 10–20 s [10]
Cat	Every 18 s [9]
Rabbit	Every 6 min [59]
Rat	Every 5 min [58]
Mouse	Similar to rats

Table 1.2 Species with nictitating membranes

Human	Nonhuman primate	Minipig	Dog	Cat	Rabbit	Rat	Mouse
No	No	Yes	Yes	Yes	Yes	Yes ^a	Yes ^a

^aThe nictitating membrane in rodents is effectively nonfunctional

into interspecies local or systemic reaction to treatment. A faster blink rate can result in decreased residence time on the eye as well as alter the systemic absorption characteristics of a topically applied product compared to a slower blink rate. Blink rates for the various species are presented in Table 1.1.

The nictitating membrane, or 3rd eyelid, is a translucent to opaque structure that supplies additional lubrication and cleaning of the corneal surface. It is not easily visible in most laboratory species, and though it has some sympathetic innervation with minor musculature in some species (like cats), its motion is mostly passive occurring with slight retraction of the eyeball and/or the action of blinking. It is also thought to be a protective structure in the animals’ natural environment. The presence of this structure in laboratory species needs to be considered when conducting certain ocular evaluations such as scoring of local irritation or when comparing tear film or corneal changes between species. For example, a protruding or inflamed nictitating membrane may be confused for severe conjunctival hyperemia or may physically mask other ocular changes, and the absence or presence of the third eyelid could be the difference in why one species exhibits symptoms of ocular dryness or erosion and another does not after receiving the same topical drug (Table 1.2).

1.3 Conjunctiva

The conjunctivae are the transparent membranes that line the underside of the eyelids and cover the sclera. There are three primary classifications: (1) the *palpebral*, covering the underside of the eyelids, is thick and can be reddish in appearance; (2) the *bulbar*, covering the sclera, is thinner, vascularized, and transparent but may contain

some pigment in more heavily pigmented animals, such as nonhuman primates; and (3) the *fornix*, forming the junction where the palpebral turns to meet the bulbar. The conjunctival sac or cul-de-sac is the space formed by this arrangement.

The conjunctivae serve several purposes. They provide lubrication, help to hold the eye in place, and allow it to move smoothly within the eye socket.

The amount of conjunctiva visible when observing an eye varies by species (as seen in Fig. 1.2), with a larger amount visible in rabbits compared to nonhuman primates. The differences in the amount of visible conjunctiva can make it more or less difficult to evaluate surface irritation (conjunctivitis) after administration of a test substance.

1.4 Pre-corneal Tear Film and Ocular Glands

The pre-corneal tear film is composed of aqueous and lipid layers and is secreted by several glands mostly located around the eye. The tear film is spread over the cornea during blinking, and its composition is related to the blink rate of the various species. A more aqueous tear film is subject to more evaporation and requires more frequent reapplication than a more lipid-based tear film. The glands involved in the secretion of the tear film include the lacrimal gland (located in the orbit), the Harderian gland (located on or near the nictitating membrane and therefore not found in the primates), accessory lacrimal glands, Meibomian glands (located on the eyelid margin), and goblet cells (located in the conjunctiva (palpebral and fornix). In general, the tear film has three layers. A mucin layer secreted by the goblet cells is the innermost layer. The middle layer is more aqueous and is secreted by the lacrimal glands with contributions from the Harderian gland in some species such as dogs and cats (where the Harderian gland is more similar to a lacrimal gland). The outermost layer is a lipid layer secreted by Meibomian glands and Harderian glands. In rodents, the Harderian glands also secrete porphyrins, which when over-secreted can cause a reddish deposit around the eye [16]. The reason for the presence of porphyrins in the Harderian gland of rodents is unknown, but it suggests a sensitivity to light and a possible relationship to the pineal gland [8].

1.5 Cornea

The cornea is a transparent multilayered structure at the front of the eye that is responsible for allowing light to enter the eye as well as for approximately 2/3 of light refraction (focusing). It joins the sclera in a zone called the limbus. The cornea is avascular, but it has the highest concentration of nerve endings in the body.

The layers of the cornea from outer to inner generally consist of:

Epithelium: The corneal epithelium is several cell layers thick and is continuous with the bulbar conjunctiva. It desquamates at the surface and rapidly regenerates. The epithelium is the primary barrier within the cornea to drugs and bacteria. It is

Table 1.3 Average central corneal thickness (mm)

Mouse	Rat	Rabbit	Dog	Cat	Pig	NHP	Human
0.089–0.123 [36, 52]	0.16–2 [11, 52]	0.36 [52]	0.5–0.66 [24, 37]	0.57 [55]	0.8 [54]	0.42 [39]	0.54 [17]

damaged easily and, therefore, alterations to the corneal epithelium may alter drug penetration into the anterior section of the eye. It does not present a uniform surface, and the mucin layer of the pre-corneal tear film fills in the gaps to provide the required optical quality.

Bowman's membrane: This layer underlies the epithelial layer and acts as a barrier protecting the stroma. Not all species have this structure, including rabbits, dogs, cats, and rodents [30, 56].

Stroma: This is the thickest layer. It is composed of parallel collagen fibrils and is responsible for the refractive power of the cornea.

Descemet's membrane: This layer underlies and supports the stroma. It is collagenous and elastic and acts as the basement membrane of the corneal endothelium.

Endothelium: The corneal endothelium is a single layer of cells that maintains the proper relative water content of the stroma. Additionally, it transports nutrients to the stromal cells from the aqueous humor and removes waste. It is effectively non-regenerative. In the event of damage to this layer, some cells will enlarge to fill in gaps left by dead cells. A healthy endothelial layer is critical for corneal function. An unhealthy endothelial layer will eventually result in corneal edema (thickening due to increased water content) which will interfere with vision.

The cornea, being avascular, obtains its nourishment from sources such as the tear film, aqueous humor, and a ring of perilimbal vessels located approximately 1–3 mm from the edge of the corneoscleral junction (limbus).

Corneal thickness varies by regions within the cornea, with the time of day, with age, with external influences (e.g., contact lenses), damage, disease, and species. Because of this variability, average central corneal thickness is usually the parameter that is measured and quoted for comparison purposes. Some measurements for laboratory species are presented in Table 1.3.

1.6 Sclera

The sclera is the protective white fibrous sheath around the eye. It is continuous with the cornea and is composed of the same type of collagen fibrils as the stroma. However, as opposed to being aligned in a parallel fashion, the fibrils are in a cross-matrix pattern, which results in the white reflective appearance. Other scleral components include proteoglycans and mucopolysaccharides.

Scleral thickness varies over the ocular surface as well as among species. However, direct comparison of quantitative data is difficult due to the inconsistent

methods used to determine thickness. Methods used include measuring thickness on excised fresh tissue with calipers, measuring fixed tissue with calipers or microscopically, as well as *in vivo* with various imaging techniques. In many species, including NHPs, dogs, and cats, the sclera is thickest at the limbus and thinnest at the equator and somewhere in between near the optic nerve. In humans, it is thickest near the optic nerve, thinnest at the equator, and thicker again near the limbus. In pigs, however, the thickest region is approximately 5–6 mm from the limbus [45], being otherwise comparable to human. In rabbits, measurements are about half as thick as human over most of the sclera surface, thickening only at the limbus [44, 48]. Rodents tend to have thinner scleras than the larger-eyed species.

Much has been said about the relative sclera thickness of various species compared to human and its relationship to penetration of externally applied drugs into the eye. However, though the sclera does play a role in this respect, hydrophilic molecules pass through the sclera fairly easily. An additional significant barrier to ocular penetration appears to be Bruch's membrane and the vascular choroidal layer which can easily carry away a drug in the circulation.

1.7 Aqueous Humor (Part I)

The aqueous humor is a clear, watery fluid that contains ions, proteins, and other nutrients. It provides nutrients to avascular structures such as the cornea, lens, and trabecular meshwork and removes waste products. It plays a significant role in ocular pressure and maintaining the shape of the globe and therefore the optical quality of the eye.

Aqueous humor is in a constant state of relatively rapid flow and is subject to diurnal fluctuations. The flow rate is an important consideration when evaluating the relative kinetics of a drug in the anterior portion of the eye. A higher flow rate may contribute to increased clearance. Complete turnover can take as little as an hour. Average aqueous humor flow rates are presented in Table 1.4 and estimated aqueous volumes are presented in Table 1.5.

1.8 Iris, Ciliary Body, Trabecular Meshwork, and Aqueous Humor (Part II)

The iris is the muscular diaphragm that controls the amount of light entering the eye by enlarging or narrowing the pupil. It is circular in shape except for cats where it is in the form of a vertical slit-shaped oval. The iris separates two chambers in the anterior segment of the eye. The *anterior chamber* represents the space between the cornea and the iris and the *posterior chamber* the space between the lens and the iris. The iris joins the cornea at the irido-corneal angle.

The ciliary body lies in the posterior chamber and is responsible for production of aqueous humor, lens accommodation, and uveoscleral outflow. It consists primarily of ciliary muscle but has extended villus-like components called ciliary processes that are responsible for the production of the aqueous humor. The ciliary processes

Table 1.4 Average aqueous humor flow ($\mu\text{L}/\text{min}$)

Mouse	Rat	Rabbit	Dog	Cat	Pig	NHP	Human
0.18 [1]	0.35 [41]	2.7 [19]	4.5 [62]	5.5–8.5 [13, 33]	^a	1.95 [47]	2.8 [46]

^aUndetermined *in vivo***Table 1.5** Average aqueous humor volume (μL)^b

Mouse	Rat	Rabbit	Dog	Cat	Pig	NHP	Human
5.9 [1]	13.6 [27]	287 [12]	770 [22]	853 [38]	^a	123 [7]	310 [57]

^aUndetermined *in vivo*^bVolumes derived from direct aspiration or anterior/posterior chamber measurements

are also connected to the lens via proteinaceous filaments called zonules. The zonules hold the lens in place and allow the ciliary muscle to exert force on the lens for accommodation.

The plasma-derived aqueous humor is secreted from the epithelial cells of the ciliary processes into the posterior chamber. It flows through the pupil into the anterior chamber where most of it flows out of the eye at the irido-corneal angle via the trabecular meshwork.

The trabecular meshwork, located in the irido-corneal angle in the anterior chamber, consists of a net of cross-linked collagen fibers with some endothelial-like cells. It filters the aqueous humor into Schlemm's canal (not specifically present in all species), scleral collector channels, the episcleral veins, and finally into the general venous circulation. This constitutes the conventional outflow pathway and accounts for most of the aqueous humor drainage. Damage to the trabecular meshwork or narrowing of the irido-corneal angle can result in reduced outflow and subsequent increased intraocular pressure.

The unconventional pathway, also known as uveoscleral drainage, consists of drainage of aqueous humor through the supraciliary spaces in the ciliary body through to the sclera and choroid. It is difficult to measure, and therefore, there are a wide range of values associated with the amount of aqueous it actually drains. Some estimates place it as a major contributor. For example, in humans, estimated uveoscleral drainage can account for as little as 4% and as much as 60% of total outflow [64]. In rabbits, 3–8% has been reported [6] and in nonhuman primates, up to 60% has been reported [5]. Currently, it is considered to be a secondary outflow pathway in laboratory species.

1.9 Lens

The lens provides the final fine tuning for focus of incoming light and is comprised of three major components:

The capsule: The lens capsule is a collagenous membrane that surrounds the lens and provides support by elastic tension.

The lens epithelium: This structure is located in a layer beneath the anterior capsule. The cells of this structure provide homeostatic support and are regenerative.

As they age, they migrate to the lens equator, compress into an elongated form, lose their nucleus, and become new lens fibers.

The lens fibers: The lens fibers are elongated transparent cells that contain the crystallins, which are essential for the refractive properties of the lens. The lens fibers have no light-scattering internal organelles such as a nucleus, endoplasmic reticulum, and mitochondria. They rely on the aqueous humor for nutrients and waste removal. The lens fibers are divided into cortex and nucleus. Crystallins are a complex group of structural water-soluble proteins that are organized within the lens fibers in such a way as to increase the refractive index of the lens while maintaining transparency. The lens fibers are classified as cortical and nuclear based on their age and location. The cortical fibers are the newer, softer lens fibers in the outer regions of the lens. As they age and become more compressed by the development of new cortical fibers, they locate more centrally and become part of the lens nucleus which itself becomes larger and harder with age as more cells are incorporated in this region.

The size and shape of the lens varies with species, as demonstrated in Table 1.6 (to scale). In rodents, the lens occupies approximately 70% of the entire volume of the eye.









When discussing general regions of the lens, terminology is similar to that used to describe the Earth. The *anterior pole* refers to the center of the anterior surface and the *posterior pole* the center of the posterior surface. The lens is divided into two hemispheres at the *equator* which is the circumference between the two poles.

1.10 Vitreous Humor

With the exception of mice and rats, the vitreous humor occupies the majority of the volume of the eye. Its clear, gel-like consistency is composed primarily of water with some hyaluronic acid, a small amount of salts, and a few cells. It also has an ultrastructure composed of collagen and some proteins that give it the gel-like consistency. As the vitreous ages, it becomes less gel-like and more aqueous. It is generally non-regenerative. Vitreous that has been removed will be replaced eventually with aqueous humor. Vitreous flow has been reported, but there is controversy over whether a front-to-back convection-related flow exists or whether the flow is the result of the shear-related forces associated with saccadic eye movements [15, 20]. In any case, the vitreous humor is not completely stagnant.

Average vitreous volumes are presented in Table 1.7. For humans, the reported range is approximately 3.5–5.4 mL [3]; however, the currently accepted average is 4 mL as presented in the table. Knowledge of the vitreous volume (and hence general shape of the vitreous chamber) is important for determining scaling comparisons of animals to humans, as well as in the consideration of the diffusion of a material within the vitreous and its inevitable contact with the sensory retina in pharmacology and toxicology studies using intravitreal injection.

Table 1.6 Comparative lens shape and dimensions

Species	Mouse	Rat	Rabbit	Dog	Cat ^b	Minipig	NHP	Human
Shape								
Axial length (mm) ^a	2.15 [49]	3.87 [40]	7.9 [26]	6.7 [65]	8.5 [61]	9 [11]	2.98 [34]	4 [25]

^a Axial length measured anterior to posterior. The anterior face of the lens is the upper surface in this diagram

^b Cat lens image courtesy of Julia Baker

Table 1.7 Average vitreous volumes by species (mL)

Mouse	Rat	Rabbit	Dog	Cat	Minipig	NHP	Human
0.0053 [50]	0.013–0.054 [18, 27]	1.5–1.8 [2, 11]	3 [2, 11]	2.4–2.7 [11, 63]	3–3.2 [2, 11] 2–2.7 [53]	1.8–2.0 [29]	4

1.11 Fundus, Retina, and Choroid

The term “fundus” represents all of the structures that can be seen at the back of the eye when looking directly through the pupil with an adequate light source. This includes the optic nerve head (ONH), retinal vessels, sensory retina, underlying pigmented layer, reflective tapetal layer (for those species that have one), and choroidal vessels (when not obscured by overlying pigment). Examples of the diversity of the view of the fundus are demonstrated in Fig. 1.3.

Clearly, there are some major differences between species that could be important for both species selection and interpretation of drug-related ocular changes. The human fundus most closely resembles that of the nonhuman primate species commonly used in the laboratory, including specialized structures not present in the other laboratory species such as the macula and fovea.

The optic nerve head, also known as optic disc or the blind spot (as there is no sensory retina in the region), is the point of entry into the eye for the optic nerve as well as the major retinal veins and arteries. Its myelination (in most cases) gives it a white appearance, and its location in the eye can vary somewhat, usually out of the way of central vision (see Fig. 1.3). In rabbits, the myelination extends into the nerve fibers in a horizontal plane on either side of the optic nerve head. The optic nerve head is also cup shaped, with rabbits having one of the deeper cups of all the species used in the laboratory. Alterations in the shape and orientation of the ONH can be affected by chronic elevations in intraocular pressure, a hallmark of glaucoma.

The retinal vessels provide nourishment to the inner retinal components such as the interstitial and ganglion cells. As well, the retinal vascular system provides structural support to the retina and helps dissipate the heat associated with the light energy entering the eye. Most of the laboratory species as well as humans have a well-developed retinal vasculature throughout the inner retina termed holangiotic. Rabbits are the exception with a limited retinal vasculature known as merangiotic, where the retinal vasculature is limited to axial vessels in a horizontal plane radiating from the optic nerve over top of the myelinated nerve fibers (Fig. 1.4).

The sensory retina itself consists of several layers (Fig. 1.5). In the outermost layer are the photoreceptors, the rods and cones that contain the pigment rhodopsin, which reacts with light and makes vision possible. In very general terms, cones are responsible for daytime color vision (the wavelengths determined by the subtype of rhodopsin within the cone outer segment) and higher visual acuity. They require substantial light to function. The rods are designed for low-light function, have less visual acuity, and are not sensitive to color. Rods outnumber cones in most vertebrate species. Subsequent layers include the outer nuclear layer, comprised of the nuclei

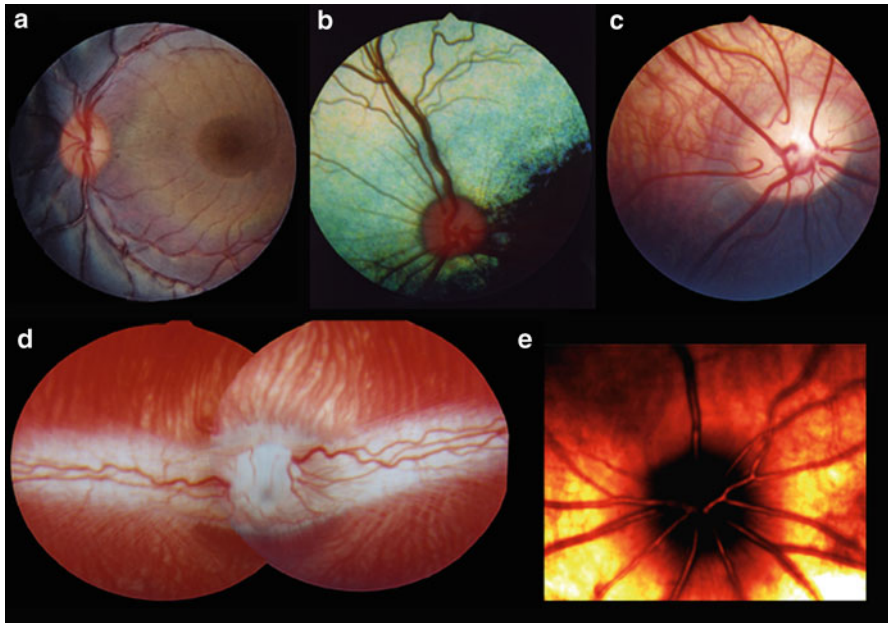


Fig. 1.3 (a) Nonhuman primate showing macula and fovea. The vascular pattern cradles this region and is similar to human fundus. (b) Dog fundus showing reflective tapetal layer. Cat is similar. (c) Minipig fundus with pigment variation and choroidal vessels visible in a nonpigmented region superior to the optic nerve head (ONH). (d) Albino rabbit with myelinated nerve fibers and merangiotic vasculature with clearly visible choroidal vessels inferior and superior to the ONH. (e) Albino rat with radial vasculature extending from optic nerve head. Mouse is similar

of the photoreceptors, followed by the outer plexiform layer, the synapses between the photoreceptors and the bipolar cells. The bipolar, amacrine, horizontal, and Müller cells are located in the inner nuclear layer. These cells are involved in chaperoning and secondary signal processing. The synapses between these cells and the ganglion cell layer are the inner plexiform layer. The ganglion cell layer contains the bodies of the ganglion cells that further process the signal before it is transmitted to the visual cortex in the brain. The innermost layer, the nerve fiber layer, is comprised of the axons of the ganglion cells which run toward and become the optic nerve. Covering the nerve fiber layer is a protective membrane called the inner limiting membrane. This membrane can be a barrier to intravitreally injected therapeutics, such as certain adeno-associated viral (AAV) vectors [14], preventing exposure to the underlying cellular structures. The thickness or number of cells within these retinal layers varies by location, from central (generally a higher concentration of cells for more acute vision) to peripheral (generally fewer signal processing cells/photoreceptor). The constituency of these layers can also vary significantly by species. Figure 1.5 compares a microscopic view of a cynomolgus monkey retina and a Sprague Dawley rat retina. The monkey is primarily a visually oriented animal and

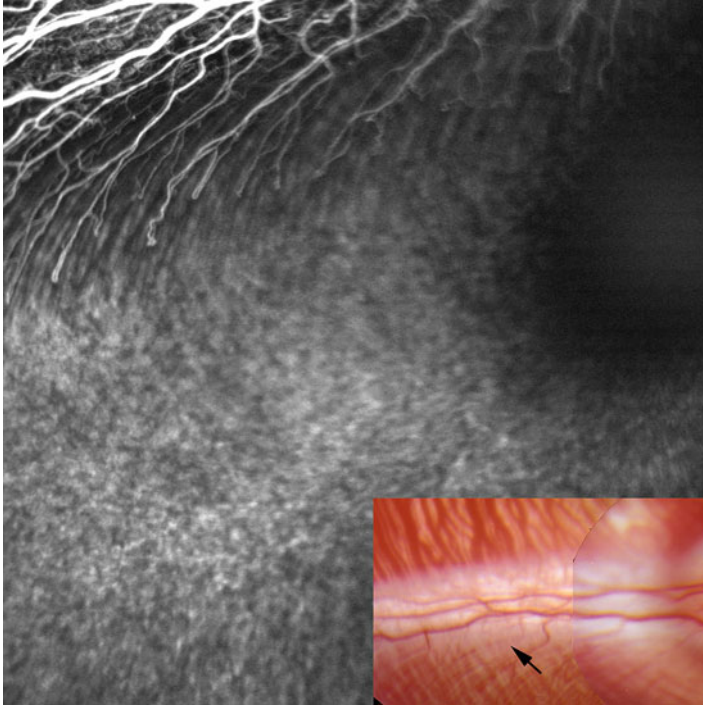


Fig. 1.4 Fluorescein angiogram of rabbit fundus demonstrating the merangiotic vascular arrangement. Retinal vessels are limited to a small region of the sensory retina (*upper left corner*). *Color inset* and *arrow* indicate general region of vessels in the angiogram

the nocturnal rat has rather poor vision (it does not need good vision in a dark environment), which is evident in the relative difference in complexity of the two eyes.

Most animals have a region in the retina with a higher concentration of cones for increased visual acuity. It is most often, but not always, in the central region of the retina, central vision usually being the most important for survival (rabbits being an exception). In humans and nonhuman primates, this region is called the macula and within the macula is a smaller (1–2 mm) region called the fovea, exclusively containing cones, that is responsible for the majority of our high-resolution daytime vision. The macula is easy to detect due to its yellowish pigmentation. The pigment is protective, acting as a UV filter. The area overlying the fovea is devoid of the usual retinal cells and retinal vessels in order to allow light to reach the photoreceptors with as little interruption as possible (Fig. 1.6). This results in a depression in the retina known as the foveal pit (Fig. 1.7).

In the other species, the region of concentrated cones is most often referred to as the area centralis or visual streak depending on its shape. Figure 1.8 shows some examples of its shape and general location. It is difficult to detect visually because it lacks the yellow pigment that is present in the macula.

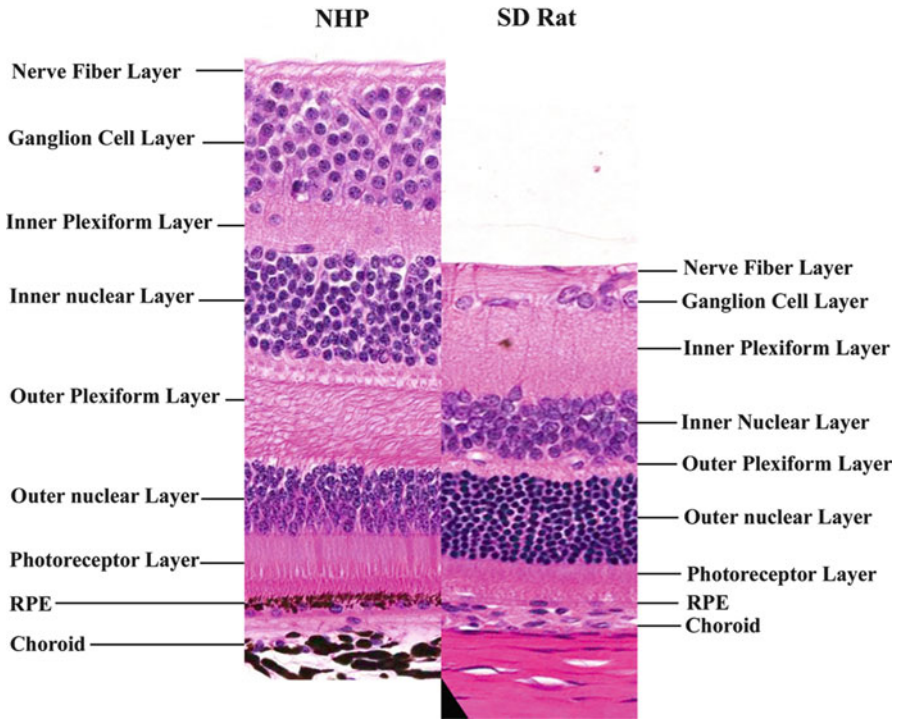


Fig. 1.5 Comparison of the cellular anatomy of the retina of a nonhuman primate (*NHP*) and Sprague Dawley albino rat, aligned at the retinal pigment epithelium (*RPE*). Note the significantly higher number of signal processing cells in the inner nuclear and ganglion cell layers of the NHP



Fig. 1.6 Fluorescein angiogram of the macular region of a cynomolgus monkey showing the avascular foveal region in the center (approximately 1-mm diameter)

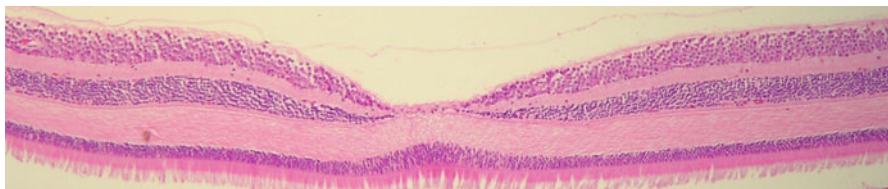


Fig. 1.7 H&E histology section of the foveal pit of a cynomolgus monkey

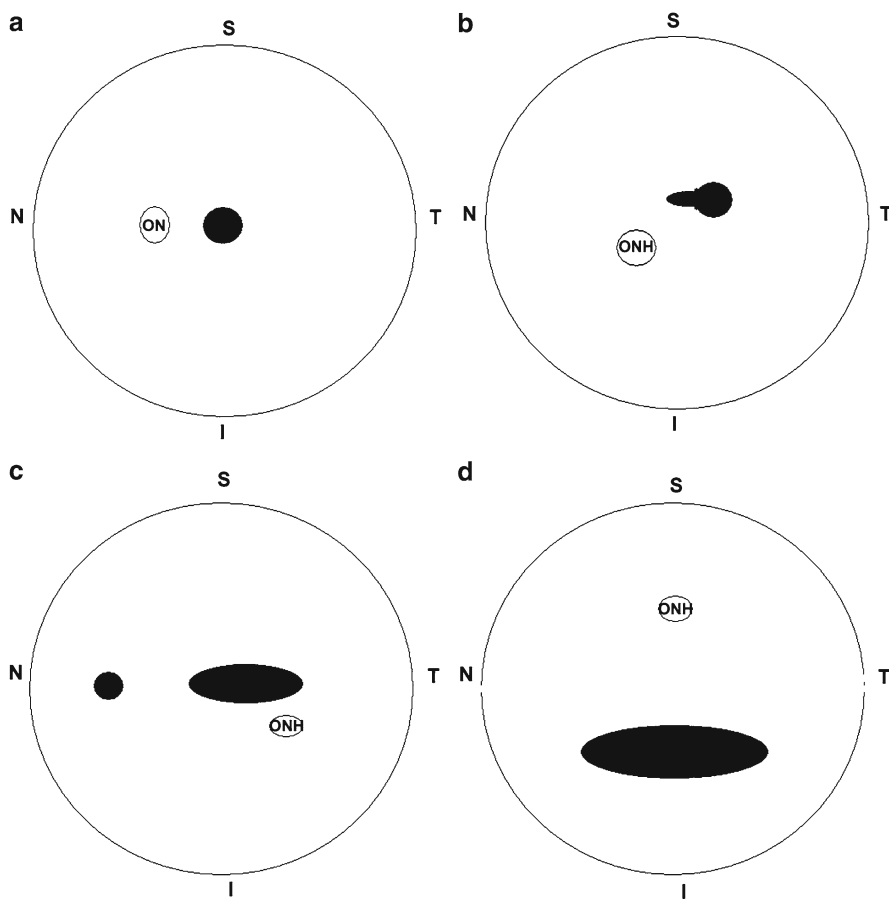


Fig. 1.8 Examples of the relative positions of the optic nerve head (*ONH*) and area centralis/visual streak (*dark regions*). (a) Human and nonhuman primate, (b) dog [42], (c) minipig [11, 21], and (d) rabbit [28]; Of note, the foraging/hunting species have a more centrally located concentration of cones while the low to the ground rabbit, a prey animal, is primarily concerned with predators approaching from above and has the region of higher visual acuity arranged as such. *S* superior, *I* inferior, *N* nasal, *T* temporal

Underlying the photoreceptors is a single layer of epithelial cells known as the retinal pigment epithelium (RPE), even if the animal is albino. These cells are responsible for photoreceptor maintenance and nourishment. They are only loosely attached to the photoreceptors, and therefore, this junction is the primary location of retinal detachments, both *in vivo* and artifactually during histology processing. In non-albino animals, these cells contain varying degrees of melanin.

The tapetum lucidum is a reflective blue/green/yellow layer that among nonclinical laboratory species is exclusive to dogs and cats. Its size is variable from animal to animal, and it is located in the superior hemisphere of the fundus. It is thought that the reflective properties of this structure amplify light in dim light situations, thus enhancing low-light vision. However, as the light is now diffused, it does not increase visual acuity. There are various structural differences among the species that possess a tapetum lucidum. Dogs and cats both have a layer of lamellated cells in the choroidal region underlying the RPE, and thus, it could be considered part of the choroidal layer. The cells are elongated and polygonal in shape. They contain rod-like structures within that are generally arranged parallel to the retina. The cell depth, number of rod-like structures with them, and their precise orientation influence the wavelengths (colors) that are reflected. In eyes with a reflective tapetal layer, the overlying RPE has less pigment or no pigment at all (which would otherwise defeat the purpose of the light amplification), allowing the color of the tapetum to show through. In dogs, the range of thickness has been reported to be 18–20 layers of cells [35] at the center of the eye, while in cats, it is slightly thicker with approximately a 35-cell thickness at the center [4]. The potential contribution of this layer to the pharmacokinetics/tissue distribution of a drug within the eye is unknown. Bruch's membrane has been shown to be thinner (or nonexistent) over the tapetal area [4, 35].

The last outer layer related to the retina is the choroid. The choroid is a multiplex pigmented vascular layer that provides the nourishment and removes waste from the RPE and photoreceptors. At the innermost region of the choroid, underlying the RPE is a structure called Bruch's membrane. This structure consists of five layers and is 2–4 μm thick. It is an important part of the blood-retinal barrier and tends to thicken with age. The RPE must transport nutrients and waste products across Bruch's membrane, and it is thought the age-related thickening may contribute to waste buildup and the formation of drusen (precursors to macular degeneration) in humans. The outermost region of the choroid borders on the sclera. The region between sclera and choroid, the suprachoroidal space, can accept the administration of small amounts of fluid or suspension and has been reported as an alternative intraocular dose route for depot drug delivery.

1.12 Additional Terminology

During the course of designing and/or conducting ocular research or toxicology studies, the researcher may encounter anatomic terminology that may not specifically describe a single ocular tissue or geographic region. Some of the more common terms are presented.

1.12.1 The Uvea

The uvea is a frequently used term that describes the vascular layer or tunic of the eye. It is comprised of the choroid, ciliary body, and iris. Uveitis is the inflammation of this layer, often posterior (choroidal origin) or anterior (iris/ciliary body origin).

1.12.2 Subretinal Space

The subretinal space is a theoretical space located between the retinal pigment epithelium (RPE) and the photoreceptors. In a normal healthy eye, this space does not exist. In a diseased eye that is undergoing some kind of exudative process, fluid may accumulate within the subretinal space and result in a retinal detachment (a separation of photoreceptors from RPE). It is a common space for the local delivery of viral vector or cell-based ocular therapeutics.

1.12.3 Suprachoroidal Space

The suprachoroidal space is another theoretical volume that is located between the choroid and sclera. As with the subretinal space, it does not exist in a healthy eye. Fluids can be administered into the suprachoroidal space, and therefore, it can serve as another delivery route for ocular therapeutics.

1.12.4 Tenon's Capsule/Sub-Tenon's Space

Tenon's capsule, also known as the fascia bulbi, is a thin membrane that encompasses the outside of the eyeball from optic nerve to limbus. Beneath it lies the periscleral lymph space, which in turn overlies the sclera. This region may also be known as the sub-Tenon's space, and it can accept the administration of ocular therapeutics or anesthetics. The periscleral lymph space is continuous with the subdural and subarachnoid spaces.

1.13 Summary

The eye is composed of many individual tissues that work together to focus reflected light, capture an image, and process and transmit that image to the brain via the optic nerve. The anatomical descriptions and quantitative information presented in this chapter represent a small amount of the information available for each of these substructures,

and the reader engaged in ocular research or toxicology is encouraged to explore the references as well as the subsequent chapters in this book to gain further insight into the nature of the individual substructures as well as how they interact as a whole.

References

1. Aihara M, Lindsey JD, Weinreb RN. Aqueous humor dynamics in mice. *IOVS*. 2003;44:5168–73.
2. Altman PL. In: Dittmer DS, editor. Blood and other body fluids. Washington, DC: Federation of American Societies for Experimental Biology; 1961.
3. Balazs EA, Denlinger JL. Aging changes in the vitreous. In: Sekulker R, Kline D, Dismukes K, editors. Aging and human visual function, Modern aging research, vol. 2. New York: Alan R Liss; 1982.
4. Bernstein MH, Pease DC. Electron microscopy of the tapetum lucidum of the cat. *J Biophys Biochem Cytol*. 1959;5:35–40.
5. Bill A. Conventional and uveo-scleral drainage of aqueous humour in the cynomolgus monkey (*Macaca irus*) at normal and high intraocular pressures. *Exp Eye Res*. 1966;5:45–51.
6. Bill A. Uveoscleral drainage of aqueous humor: physiology and pharmacology. In: The ocular effects of prostaglandins and other eicosanoids. New York: Alan R Liss; 1989.
7. Bill A, Hellsing K. Production and drainage of aqueous humor in the cynomolgus monkey (*Macaca irus*). *IOVS*. 1965;4:920–6.
8. Blackshaw S, Snyder SH. Developmental expression pattern of phototransduction components in mammalian pineal implies a light-sensing function. *J Neurosci*. 1997;17(21):8074–82.
9. Blount WP. Studies of the movements of the eyelids of animals: blinking. *Exp Physiol*. 1927;18:111–25.
10. Carrington S, Bedford P, Guillon J-P, Woodward E. Polarized light biomicroscopic observations on the pre-corneal tear film. 1. The normal tear film of the dog. *JSAP*. 2008;7:605–22.
11. Charles River unpublished in-house data.
12. Conrad JM, Robinson JR. Aqueous chamber drug distribution volume measurement in rabbits. *J Pharm Sci*. 1977;66:219–24.
13. Crumley WR. Aqueous humor flow rate in normal cats and the effect of topical 2% dorzolamide on aqueous humor flow and intraocular pressure. Dissertation, University of Kentucky; 2011.
14. Dalkara D, Kolstad KD, Caporale N, Visel M, Klimczak RR, Schaffer D, Flannery JG. Inner limiting membrane barriers to AAV-mediated retinal transduction from the vitreous. *Mol Ther*. 2009;17(12):2096–102.
15. David T, Smye S, Dabbs T, James T. A model for the fluid motion of vitreous humor of the human eye during saccadic movement. *Phys Med Biol*. 1998;43:1385.
16. dos Reis ER, Nicola EMD, Nicola JH. Harderian gland of wistar rats revised as a protoporphyrin IX producer. *Braz J Morphol Sci*. 2005;22:43–51.
17. Doughty MJ, Zaman ML. Human corneal thickness and its impact on intraocular pressure measures: a review and meta-analysis approach. *Surv Ophthalmol*. 2000;5:367–408.
18. Dureau P, Bonnel S, Menasche M, Dufier J-L, Abitbol M. Quantitative analysis of intravitreal injections in the rat. *Curr Eye Res*. 2001;22(1):74–7.
19. Elman J, Caprioli J, Sears M, Mead A, Rubion P. Chorionic gonadotropin decreases intraocular pressure and aqueous humor flow in rabbit eyes. *IOVS*. 1987;28:197–200.
20. Fatt I. Flow and diffusion in the vitreous body of the eye. *Bull Math Biol*. 1975;37:85.
21. Gerke Jr CG, Hao F, Wong F. Topography of rods and cones in the retina of the domestic pig. *HKMJ*. 1995;1(4):302–8.
22. Gilger BC, Reeves KA, Salmon JH. Ocular parameters related to drug delivery in the canine and equine eye: aqueous and vitreous humor volumes and scleral surface area and thickness. *Vet Ophthalmol*. 2005;8(4):265–9.

23. Gray C. Systemic toxicity with topical ophthalmic medications in children. *Paed Perin Drug Ther.* 2006;7:23–9.
24. Gwin R, Lerner I, Warren JK, Gum G. Decrease in canine corneal endothelial cell density and increase in corneal thickness as functions of age. *IOVS.* 1982;22:267–71.
25. Hemenger RP, Garner LF, Ooi CS. Change with age of the refractive index gradient of the human ocular lens. *IOVS.* 1995;6:703–7.
26. Hughes A. A schematic eye for the rabbit. *Vision Res.* 1972;12:123–38.
27. Hughes A. A schematic eye for the rat. *Vision Res.* 1979;19:569–88.
28. Juliusson B, Bergström A, Röhlich P, Ehringer B. Complementary cone fields of the rabbit retina. *IOVS.* 1994;35(3):811–18.
29. Kaufman P, Calkins B, Erickson K. Ocular biometry of the cynomolgus monkey. *Curr Eye Res.* 1981;1(5):307–9.
30. Kaye GI, Pappas GD. Studies on the cornea I: The fine structure of the rabbit cornea and the uptake and transport of colloidal particles by the cornea in-vivo. *J Cell Biol.* 1962;12:457–79.
31. Kleven MS, Koek W. Differential effects of direct and indirect dopamine agonists on eye blink rate in cynomolgus monkeys. *J Pharmacol Exp Ther.* 1996;297(3):1211–19.
32. Korte JM, Kaila T, Saari KM. Systemic bioavailability and cardiopulmonary effects of 0.5% timolol eyedrops. *Graefes Arch Clin Exp Ophthalmol.* 2002;240(6):430–5.
33. Langham M. Secretion and rate of flow of aqueous humor in the cat. *Br J Ophthalmol.* 1951;35:409.
34. Lapuerta P, Schein SJ. A four-surface schematic eye of macaque monkey obtained by an optical method. *Vision Res.* 1995;35:2245–54.
35. Lesiuk TP, Braekevelt CR. Fine structure of the canine tapetum lucidum. *J Anat.* 1983;136:157–64.
36. Lively GD, Jiang B, Hedberg-Buenz A, Chang B, Petersen GE, Wang K, Kuehn MH, Anderson MG. Genetic dependence of central corneal thickness among inbred strains of mice. *IOVS.* 2010;51:160–71.
37. Lynch G, Brinkis J. The effect of elective phacofragmentation on central corneal thickness in the dog. *Vet Ophthalmol.* 2006;9(5):303–10.
38. Macri FJ, Dixon RL, Rall DP. Aqueous humor turnover rates in the cat. I: Effect of acetazolamide. *Invest Ophthalmol.* 1965;4(5):927–34.
39. Madigan M, Gillar-Crewther S, Kiely P, Crewther D, Brennan N, Efron N, Holden B. Corneal thickness changes following sleep and overnight contact lens wear in the primate (*Macaca fascicularis*). *Curr Eye Res.* 1987;6(6):809–15.
40. Massof RW, Chang FW. A revision of the rat schematic eye. *Vision Res.* 1972;12:793–6.
41. Mermoud A, Baerveldt G, Minckler D, Prata J, Rao N. Aqueous humor dynamics in rats. *Graefes Arch Clin Exp Ophth.* 1996;234:S198–203.
42. Mowat FM, Peterson-Jones SM, Williamson H, Williams DL, Luthbert PJ, Ali RR, Bainbridge JW. Topographical characterization of cone photoreceptors and the area centralis of the canine retina. *Mol Vis.* 2008;14:2518–27.
43. Nuhoglu A, Bozkurt H. Assessment of electrode-based spontaneous eye blink analysis. In: *Proceedings from: recent advances in applied biomedical informatics and computational engineering in systems applications.* 2011. Accessed on-line 05 March 2012.. ISBN 978-1-61804-028-2.
44. Olsen T, Aaberg S, Geroski D, Edelhauser H. Human sclera: thickness and surface area. *Am Jour Ophth.* 1988;125(2):237–41.
45. Olsen T, Sanderson S, Feng X, Hubbard W. Porcine sclera: thickness and surface area. *IOVS.* 2002;43:2529–32.
46. Oshika T, Araie M. Time course of changes in aqueous protein concentration and flow rate after oral acetazolamide. *IOVS.* 1990;31:527–30.
47. Podos S, Lee P, Severin C, Mittog Y. The effect of vanadate on aqueous humor dynamics in cynomolgus monkeys. *IOVS.* 1984;25:359–61.

48. Prince J, Diesem D, Eglitis I, Ruskell G. The rabbit. In: *Anatomy and histology of the eye and orbit in domestic animals*. Springfield: Charles C Thomas; 1960. p. 260–93.
49. Puk O, Dalke C, Favor J, Hrabe de Angelis M, Graw J. Variations of eye size parameters among different strains of mice. *Mamm Genome*. 2006;17:851–7.
50. Remtulla S, Hallet PE. A schematic eye for the mouse and comparison with the rat. *Vision Res*. 1985;25:21–31.
51. Salminen L. Review: systemic absorption of topically applied ocular drugs in humans. *J Ocul Pharmacol Ther*. 1990;6(3):243–9.
52. Schulz D, Iliiev M, Frueh B, Goldblum D. In vivo pachymetry in normal eyes of rats, mice and rabbits with the optical low coherence reflectometer. *Vision Res*. 2003;43(6):723–8.
53. Shafiee A, McIntire GL, Sidebotham LC, Ward KW. Experimental determination and allometric prediction of vitreous volume and retina and lens weights in Göttingen minipigs. *Vet Ophthalmol*. 2008;11:193–6.
54. Shiratani T, Shimizu K, Fujisawa K, Uga S, Nagano K, Murakami Y. Crystalline lens changes in porcine eyes with implanted phakic IOL (ICL) with a central hole. *Graefes Arch Clin Exp Opth*. 2008;246(5):719–28.
55. Slatter DH. Cornea and sclera: Chapter 91. In: *Textbook of small animal surgery*. 2nd ed. Philadelphia: WB Saunders; 1993.
56. Slatter D. *Fundamentals of veterinary ophthalmology*. 3rd ed. Philadelphia: WB Saunders; 2001.
57. Solomon IS. Aqueous humor dynamics. 2002. The New York Eye and Ear Infirmary Online. From <http://www.nyee.edu/pdf/solomonaqumor.pdf>. Accessed 1 Mar 2012.
58. Swarbrick HA et al. IOVS 35: ARVO Abstract No. 1690; 1994.
59. Toshida H, Nguyen D, Beuerman R, Murakami A. Neurologic evaluation of acute lacrimomimetic effect of cyclosporine in an experimental rabbit dry eye model. *IOVS*. 2009;50:2736–41.
60. Tutt R, Bradley A, Begley C, Thibos L. Optical and visual impact of tear break-up in human eyes. *IOVS*. 2000;41:4117–23.
61. Vakkur GJ, Bishop PO. The schematic eye in the cat. *Vision Res*. 1963;3:357–81.
62. Ward D, Cawrse M, Hendrix D. Fluorophotometric determination of aqueous humor flow rate in clinically normal dogs. *Am J Vet Res*. 2001;62(6):853–8.
63. Watanabe M, Inukai N, Fukuda Y. Survival of retinal ganglion cells after transection of the optic nerve in adult cats: a quantitative study within 2 weeks. *Vis Neurosci*. 2001;18:137–45.
64. Weinreb R, Toris CBA, Gabelt BT, Lindsey JD, Kaufman PL. Effects of prostaglandins on the aqueous humor outflow pathways. *Surv Ophthalmol*. 2002;47:S53–64.
65. Williams DL. Lens morphometry determined by B-mode ultrasonography of the normal and cataractous canine lens. *Vet Ophthalmol*. 2004;7:91–5.

Chapter 2

Assessment of Ocular Toxicity Potential: Basic Theory and Techniques

Robert J. Munger and Margaret Collins

Abstract The toxicity assessment of drugs includes an assessment of ocular toxicity, with the extent of the ocular examination depending upon a number of factors. The eyes are unique in that it is possible to conduct a detailed assessment during the in-life portion of a study. This chapter will focus on routinely used approaches for assessing ocular toxicity in toxicology studies. Systemic and ocular toxicology studies include an assessment of systemic toxicity using techniques such as clinical observations, body weight measurement, clinical pathology and histopathology, and an assessment of ocular toxicity, with the ocular toxicology study having a more detailed ocular assessment. At a minimum, ocular assessment includes examination of the eyes, and this chapter discusses various forms of ocular examination as well as grading scales for qualification of findings. Additional assessments, such as intraocular pressure measurement, fundus photography, and other specialized techniques, are discussed. When establishing a protocol for a toxicology study, careful consideration must be given to planning which examinations are required to best accomplish the study objectives and the timing of those examinations relative to other study procedures.

R.J. Munger, D.V.M., DACVO (✉)
Animal Ophthalmology Clinic Inc., Dallas, TX, USA
e-mail: eyedvm@aol.com

M. Collins, M.S.
Charles River Laboratories, Preclinical Services, Reno, NV, USA
e-mail: margaret.collins@crl.com

2.1 Introduction

The evaluation of the toxic potential of drugs and other chemicals is a complex process involving multiple disciplines, such as pharmacology, toxicology, pathology, and ophthalmology. Drugs intended for the diagnosis, prevention, and treatment of diseases in humans are administered via a variety of routes, including oral, intravenous, subcutaneous, and more specialized routes, such as dermal, inhalation, and ocular. Regardless of the route of administration and intended indication, the toxicity assessment of drugs includes an assessment of ocular toxicity, with the extent of the ocular examination depending upon a number of factors. For example, drugs that are applied directly to or injected into the eye typically undergo a more extensive ophthalmological evaluation than drugs administered via other routes. During the course of toxicology studies, effects of a drug or other chemical can be assessed during the course of a study (i.e., in-life or prior to sacrifice of the animals) or following sacrifice. The eyes are unique in that it is possible to conduct a detailed assessment during the in-life portion of a study.

Toxicology studies conducted for regulatory purposes need to be conducted in compliance with Good Laboratory Practice (GLP), which is addressed in more detail in Chap. 7 of this text. According to GLPs, a protocol defining techniques to be used for toxicity assessment, including ocular toxicity, is needed for toxicology studies conducted for regulatory purposes. This chapter will focus on routinely used approaches for assessing ocular toxicity in toxicology studies. Chapters 3 and 4 will focus on emerging technologies for the in-life assessment of ocular toxicity.

For the purpose of this chapter, it can be stated that there are two types of toxicology studies, systemic (i.e., using oral, iv, and/or subcutaneous routes of administration) and ocular (i.e., test article applied to or injected into eyes). Both types of studies include an assessment of systemic toxicity using techniques such as clinical observations, body weight measurement, clinical pathology, and histopathology. Similarly, both types of studies include an assessment of ocular toxicity, with the ocular toxicology study having a more detailed ocular assessment.

2.2 Examination Techniques

In toxicology studies, it is important to note the location of lesions noted on the various examinations so that they may be correlated with histopathological findings and other diagnostic measures. Correlation between dose groups is also important when evaluating the incidence and severity in lesions so that any association with the test article administration can be assessed.

Examination of the eye should be pursued systematically using the examination techniques defined in the study protocol. Slit-lamp biomicroscopy and indirect ophthalmoscopy comprise the mainstay of most evaluations for ophthalmic toxicity. Additional examinations, including but not limited to tonometry, pachymetry, specular

endothelial microscopy, electroretinography, fluorescein angiography, ultrasonography, and optical coherence tomography (OCT), may be included as determined by the goals of the study and the nature and known effects of the test article. With slit-lamp biomicroscopy and indirect ophthalmoscopy, dilation of the pupil with a mydriatic such as tropicamide is required to allow complete evaluation of the lens and the ocular fundus. However, with few exceptions, such dilation should be postponed until after the anterior segment of the eye has been examined and the pupillary light response evaluated. Also, any tests such as tonometry for the evaluation of intraocular pressure should generally be performed prior to dilation of the pupil. When multiple testing procedures are performed that will require contact of the instrument with the cornea (pachymetry, tonometry, etc.) and/or sedation is required that may result in decreased blinking, such procedures may disturb the pre-corneal tear film or cause corneal haze to a degree that will blur the view of intraocular structures and cause artifactual corneal haze at the sites of contact, drying, and/or exposure. Therefore, examinations must take such variables into account. Additionally, the order of evaluation must be given careful consideration. Electroretinography is an important safety assessment but should not be conducted immediately after ophthalmic examinations due to effects of the light on the retina. Tonometry may be included if the drug is expected to cause alterations in intraocular pressure (IOP) or to assess the effects of inflammation; however, measurements should be done at approximately the same time of day for each time point in order to account for diurnal fluctuations. Additionally, if the drug is being introduced directly into the eye (e.g., intravitreal injection), there will be a transient increase in IOP immediately following the injection. Pachymetry is appropriate for assessing changes in corneal thickness, but may not be needed for all topical drugs or those that are introduced into the eye. Fluorescein angiography, ultrasonography, and OCT may be used in addition to histologic assessment of the eye, but would typically not replace histology.

When establishing a study protocol, careful consideration must be given to planning which examinations are required to best accomplish the study objectives and the timing of those examinations relative to other study procedures. As mentioned above, intravitreal injections will cause a transient rise in IOP. For topically applied drugs, consideration should be given to timing relative to dose administration. Administration of topical agents required for ophthalmic examinations may interfere with drug absorption if given too soon after dose administration. In some species, sedation is required for ophthalmic examinations, but this may have an effect on other study parameters depending on timing (e.g., clinical observations, food consumption, or clinical pathology assessment following sedation procedures). A balance must be struck between scheduling multiple procedures on a single day versus repeated days of sedation for ocular and other study procedures.

The examination techniques described in this chapter can generally be applied to or performed on most species although limitations or study requirements may make some modifications of techniques or scoring necessary. For example, while biomicroscopy is easily performed on rodents, that species is not well suited for topical ocular studies and scoring of parameters for ocular irritation.



Fig. 2.1 A table-mounted slit-lamp biomicroscope offers excellent optics with multiple options for magnification and greater numbers of options for varying slit-beam width, height, and light color, and cameras may be added to the configuration to provide greater potential for stability and photographic documentation of lesions than camera options on handheld portable slit lamps

2.2.1 Slit-Lamp Biomicroscopy

As the name of this examination technique implies, biomicroscopy is the examination of the living eye by means of a microscope combined with a slit lamp that provides a bright light that may be modified in intensity, shape (diffuse or finely focused beam of varying widths and lengths), and color (white, cobalt blue, or red-free). Magnification can also be varied depending on the type of biomicroscope. The slit lamp is mounted on the binocular microscope on a pivot that allows the light to be directed toward the eye from multiple directions and orientations. Thus, slit-lamp biomicroscopy allows the direct evaluation of the eyelids, tear film, conjunctiva, cornea, anterior chamber and aqueous humor, iris, lens, and the anterior vitreous. This examination technique and ophthalmoscopic examination of the ocular fundus form the mainstay of ocular examinations for the in-life portion of toxicology studies.

Both table-mounted (Fig. 2.1) and portable (Fig. 2.2) models of slit-lamp biomicroscopes are available. Portable models are less expensive and more versatile for



Fig. 2.2 The Kowa handheld slit lamp offers good optics and portability for the examination of eye in animals that are not sedated or that cannot be easily presented for examination by a table-mounted slit-lamp biomicroscope

exams of animals in a variety of situations than the table-mounted models. For small animals that are not sedated, this portability may facilitate a more complete exam while table-mounted slit lamps offer a wider range of magnifications with superior optics, greater variability of slit-beam width and orientation, and better potential for photography. When combined with specialized lenses (e.g., gonioscopy lenses or specialized indirect ophthalmoscopy lenses), the iridocorneal angle, ciliary cleft, pars plana, and even the ocular fundus may be examined with the table-mounted slit lamp.

With a very narrow (slit) beam, a highly magnified optical section of the eye is obtained, and the direction may be varied so that the structures may be viewed either directly (with direct illumination) or by illumination from the reflection of light from more posterior segments of the eye (retroillumination). Lesions may thus be evaluated for where they are in the eye with respect to other structures, and their nature can be evaluated by shadows cast by illumination cast from different directions. With broad beams of light, pupillary responses, as well as the characteristics of the surfaces of the ocular structures, can be evaluated. Protein in the aqueous can be detected as evidence of inflammation because of the Tyndall effect by which the beam of light can be seen passing through the aqueous humor. Similarly, cells (pigmented and nonpigmented) can be detected in narrow beam as the light passes through the anterior chamber or the anterior vitreous. Nonpigmented cells typically indicate an inflammatory response, while pigmented cells arising from the uvea or



Fig. 2.3 External ocular photograph of the normal eye of a Dutch belted rabbit

retinal pigment epithelial cells may arise from an inflamed uvea (iris, ciliary body, or choroid) or from trauma to uvea or retinal pigment epithelium. It is not uncommon to see some pigmented cells in the anterior vitreous following intravitreal injections due to the passage of the needle through or near the pars plana during the injection.

It is customary for the eyes to be examined prior to dilation for best examination of the iris and pupillary light responses. Thereafter, the pupils are dilated by the application of a mydriatic such as 1% tropicamide so that the lens and anterior vitreous may be examined and that direct or indirect ophthalmoscopy can be performed.

Interpretation of the findings on slit-lamp biomicroscopy requires extensive knowledge of normal findings as well as background lesions that occur as incidental findings in the species and breed examined. These include, but are not limited to, embryonic remnants (e.g., persistent pupillary membranes, persistent or absorbing hyaloid arteries), corneal opacities (e.g., corneal scars, corneal degeneration/dystrophy in Sprague-Dawley rats, epithelial dystrophy in Dutch belted rabbits), cataracts, and lesions that may be associated with incidental trauma or inflammation (e.g., synechiae, traumatic cataracts, corneal scars).[1, 2, 10, 16–19] Examples of normal and abnormal slit-lamp findings are noted in Figs. 2.3, 2.4, 2.5, 2.6, 2.7, 2.8, and 2.9. Whenever possible, animals with such background lesions noted at pre-study examinations should not be placed on study. However, in some animals such as the Sprague-Dawley rat, the incidental lesions may be so pervasive that use of affected animals cannot be avoided and randomization will usually ensure the lesions are seen with equal representation across all groups. It is then important to ensure the test article administration does not result in worsening of the lesions. Testing in more than one species is the norm for topical ocular studies and provides additional confirmation of safety.

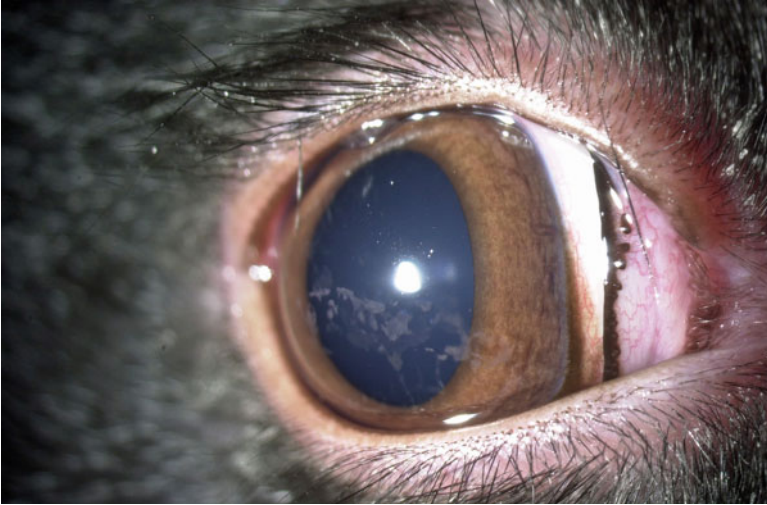


Fig. 2.4 Corneal epithelial dystrophy in a Dutch belted rabbit. Slit-lamp photo in diffuse light. Compare the multiple faint irregular corneal opacities to the clear cornea of a Dutch belted rabbit in Fig. 2.3. Such corneal opacities may develop later in a study after initial pre-screening examinations especially following anesthesia or manipulations of the eye. When that occurs, it is necessary to differentiate whether the opacities arise *de novo* or as a test article-related effect occurring in greater incidence in treated eyes versus untreated controls

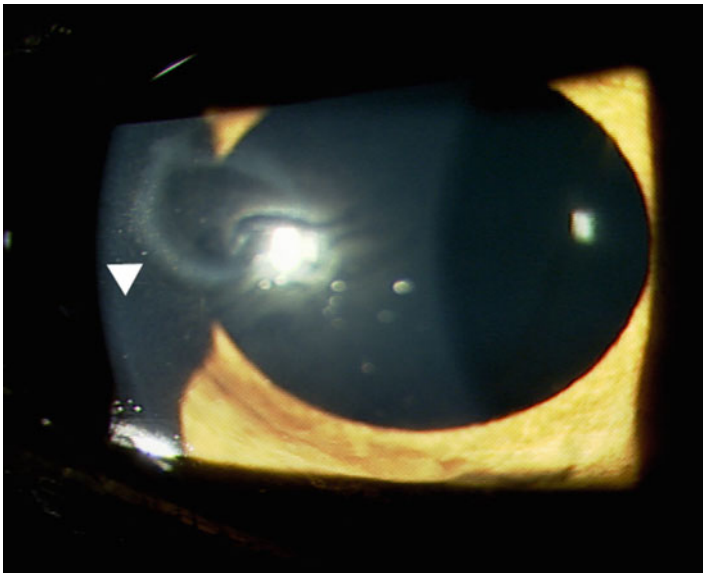


Fig. 2.5 Incidental circular superficial corneal scar (*arrowhead*) with denser outer ring in broad beam of slit lamp. Such corneal scars are seen sporadically in primates as incidental lesions. In Fig. 2.6, the narrow slit-lamp beam (optical section) reveals the superficial nature of the lesion



Fig. 2.6 An optical section of the cornea is created as the very narrow slit-lamp beam passes from *left to right* through the cornea, thus demonstrating the superficial nature of the corneal scar from Fig. 2.5. The scar is noted as a denser white curvilinear area in the superficial cornea (*small solid arrows*). The corneal endothelial layer is adjacent to the open arrow, and the anterior surface of the lens is visible and slightly out of focus further posterior in the light beam (*open arrowhead*). A small persistent pupillary membrane (*embryonic remnant*) is visible in the anterior chamber (*closed arrowhead*)

When slit-lamp examinations are used in systemic toxicology studies, it may be sufficient to simply record abnormal findings, but in topical ocular studies, it is customary to quantify findings and modifications of scoring systems such as the Hackett-McDonald scoring system (Table 2.1) [8, 11] and others such as outlined in the Standardization of Uveitis Nomenclature or SUN system [15]. Such scoring systems are designed to detect very subtle microscopic ocular changes, and they may be commonly employed in both preclinical and clinical studies. When evaluating the lens, the examination should include the notation of whether the lens is normal or abnormal and should be accompanied by a comment describing the extent and location of the lens abnormalities as determined by direct and indirect (i.e., retroillumination) illumination. Cataracts may be noted as mild (or incipient involving less than 10% of the lens), moderate (immature), or severe (involving the entire lens), and the location of the opacities may be described or defined by where they are localized in the lens (noted by the positions of the opacities in the slit beam as the light passes through the lens). Localization may thus be defined as anterior capsular, anterior subcapsular, anterior cortical, nuclear, posterior cortical, posterior subcapsular, posterior capsular, or equatorial with combinations of the preceding

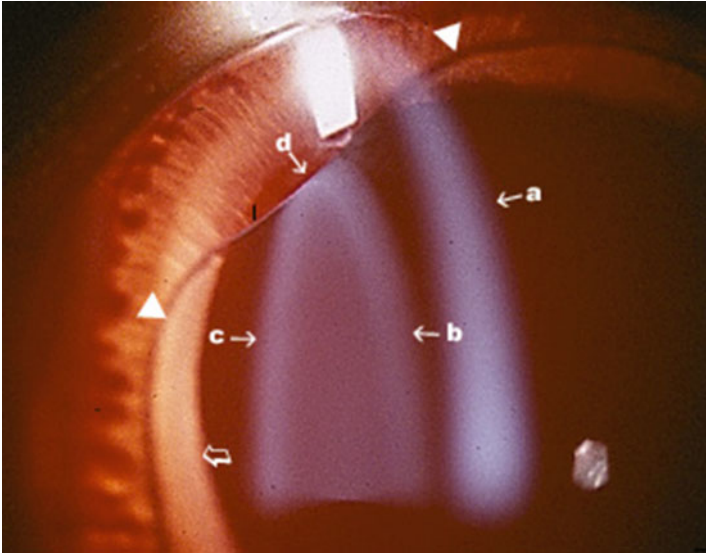


Fig. 2.7 Photograph of an optical section taken with a photo slit lamp. The beam from the slit lamp is directed from right to left with the anterior section of the beam highlighting the cornea (*a*) which is out of focus. The beam is focused on the lens which is thus in cross section with the anterior lens capsule on the *right* of the beam (*b*) and the posterior lens capsule on the *left* (*c*). The aqueous in the anterior chamber (between *a* and *b*) and the anterior vitreous immediately posterior to the lens (and to the *left* of *c*) are clear (i.e., there is no Tyndall effect and no cells are present). The pupil margin (*open arrow*) and most of the iris are illuminated indirectly from behind (retroilluminated) as are the equatorial edge of the lens and the adjacent ciliary processes visible through the nonpigmented iris in this New Zealand white rabbit. Note the congenital deformity of the lens (*d*) visible between the *solid arrowheads*

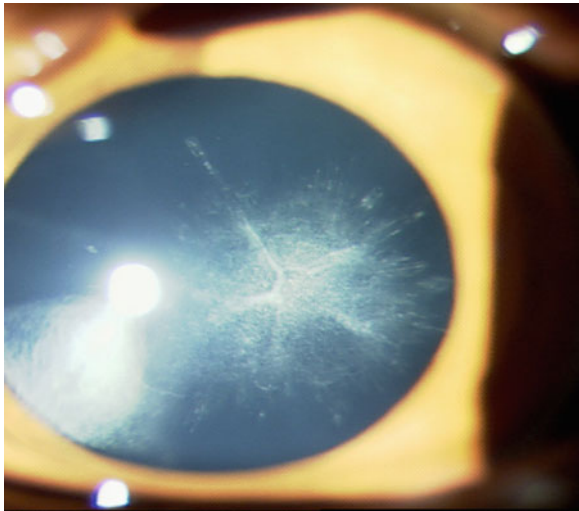


Fig. 2.8 Axial, posterior, cortical cataract in a cynomolgus macaque viewed in a diffuse beam. Such cataracts are occasionally observed as incidental lesions in otherwise normal macaques

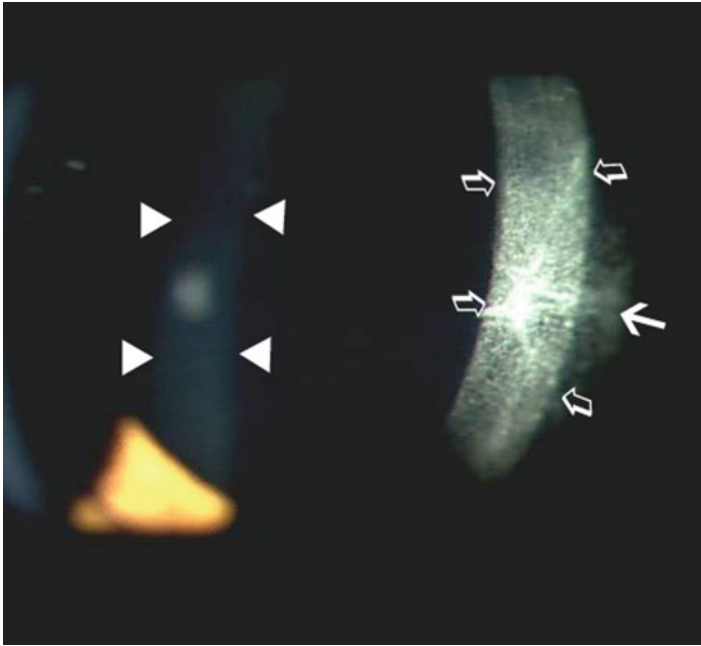


Fig. 2.9 A wide slit beam clearly reveals the posterior location of the axial cortical cataract noted in Fig. 2.8. The slit beam is evident and slightly out of focus on the anterior lens capsule (*solid arrowheads*). A flash artifact is visible in the beam between the arrowheads. The slit beam passed left to right through the clear normal portion of the lens and directly illuminates the posterior cortical (subcapsular) cataract in a curved or concave beam (*open arrows*). A portion of the cataract is retroilluminated to the right of the beam (*solid arrow*)

used if there is more than one opacity. In some instances, drawing of the lens with frontal and cross-sectional views may be used to further document the opacities. With such data recorded, it is thus possible to determine if a cataract is progressing during the study.

In addition to evaluating the solid structures of the eye, the aqueous and anterior vitreous can also be evaluated as the slit beam passes through the anterior chamber and the anterior vitreous just posterior to the lens. Uveitis can result in an increase in protein and cells in the aqueous and vitreous in association with breakdown of the blood-ocular barrier. Increase in protein in the aqueous humor results in a Tyndall effect, referred to as aqueous flare, such that the light of the slit beam can be seen as it passes through the aqueous. As noted in Table 2.1, the flare may be scored from 0 to +3 where 0 equals the normal absence of a visible light beam as it passes through the aqueous, +1 equals a visible light beam that is less intense than the beam as it passes through the normal lens (this includes a barely visible beam which may be further described as trace flare), +2 equals a visible light beam equal in intensity to the beam as it passes through the normal lens, and +3 equals a visible light beam that is greater

Table 2.1 Summary of a modified Hackett-McDonald ocular scoring system

<i>Conjunctival congestion</i>	
Normal (0) =	Normal in appearance <i>for the species</i> . May appear blanched to reddish pink without perilimbal injection (except at 12 and 6 o'clock positions) with vessels of the palpebral and bulbar conjunctiva defined and easily observed
1+ =	<i>Mild</i> . A flushed, reddish color predominantly confined to the palpebral conjunctiva with some perilimbal injection, primarily located but not confined to the upper and lower regions of the eye
2+ =	<i>Moderate</i> . The palpebral conjunctiva appears bright red with accompanying perilimbal injection covering at least 75% of the circumference of the perilimbal region
3+ =	<i>Severe</i> . Both the bulbar and palpebral conjunctiva exhibit a dark, beefy-red color with pronounced perilimbal injection. Petechiae on the conjunctiva may be present. The petechiae generally predominate along the nictitating membrane and/or the upper palpebral conjunctiva
<i>Conjunctival swelling</i>	
Normal (0) =	No swelling of the conjunctival tissue is observed
1+ =	<i>Minimal</i> . Swelling above normal but without eversion of the eyelids. Swelling generally begins in the lower cul-de-sac near the inner canthus
2+ =	<i>Mild</i> . Swelling with misalignment of the normal approximation of the lower and upper eyelids. In this stage, swelling is confined generally to the upper eyelid, with some swelling observed in the lower cul-de-sac
3+ =	<i>Moderate</i> . Swelling is definite, with partial eversion of the upper and lower eyelids essentially equivalent. Eversion of the eyelids may be determined by looking at the animal head-on and observing the positioning of the eyelids
4+ =	<i>Severe</i> . Eversion of the upper eyelid is pronounced with less pronounced eversion of the lower eyelid. At this level, it is difficult to retract the lids and observe the perilimbal region
<i>Conjunctival discharge</i>	
Normal (0) =	May include a small amount of clear, mucoid material that is normally found in the medial canthus of a substantial number of animal eyes
1+ =	<i>Mild</i> . Discharge is above normal and present on the inner portion of the eye but not on the lids or hairs of the eyelids
2+ =	<i>Moderate</i> . Discharge is abundant, easily observed, and has collected on the lids and around the hairs of the eyelids
3+ =	<i>Severe</i> . Discharge has been flowing over the eyelids so as to substantially wet the hairs on the skin around the eye

(continued)

Table 2.1 (continued)

<i>Iris congestion</i>	
<i>Normal (0) =</i>	Normal iris without any hyperemia of the iris vessels. Note: In rabbits, around the 12 to 1 o'clock position and the 6 to 7 o'clock position near the pupillary border, there may be a small area (approximately 1–3 mm in diameter) in which both the secondary and tertiary vessels may be slightly hyperemic. This is normal
<i>1+ =</i>	<i>Minimal.</i> Minimal injection of secondary and tertiary vessels observed. Generally, it is uniform, but may be of greater intensity at the 12 to 1 o'clock or 6 o'clock position. If it is confined to this area, the tertiary vessels must be substantially hyperemic
<i>2+ =</i>	<i>Mild</i> injection of tertiary vessels and minimal to moderate injection of the secondary vessels observed
<i>3+ =</i>	<i>Moderate</i> injection of the secondary and tertiary vessels with slight swelling of the iris stroma (this gives the iris surface a slightly rugose appearance, which is usually most predominant near the 3 and 9 o'clock positions)
<i>4+ =</i>	<i>Severe.</i> Marked injection of the secondary and tertiary vessels with definite swelling of the iris stroma. The iris appears rugose and may be accompanied by hemorrhage in the anterior chamber
<i>Pupillary light reflex</i>	
<i>Normal (0) =</i>	Normal pupillary light reflex
<i>1+ =</i>	Sluggish pupillary light reflex
<i>2+ =</i>	Maximally impaired pupillary reflex (pupil dilated and unresponsive)
<i>Aqueous flare</i>	
<i>Normal =</i>	Absence of visible light beam in the anterior chamber (no Tyndall effect)
<i>1+ =</i>	<i>Mild.</i> The Tyndall effect is barely discernible. The intensity of the light beam in the anterior chamber is less than the intensity of the slit beam as it passes through the lens
<i>2+ =</i>	<i>Moderate.</i> The Tyndall beam in the anterior chamber is easily discernible and is equal in intensity to the slit beam as it passes through the lens
<i>3+ =</i>	<i>Severe.</i> The Tyndall beam in the anterior chamber is easily discernible; its intensity is greater than the intensity of the slit-lamp beam as it passes through the lens

Corneal cloudiness severity

- Normal* = *Normal.* Appears with the slit lamp as having a bright gray line on the epithelial surface and a bright gray line on the endothelial surface with a uniform marble-like gray appearance of the stroma
- I+* = *Minimal.* Some loss of transparency. Only the epithelium and/or the anterior half of the stroma is involved as observed with an optical section of the slit lamp. With diffuse illumination, the underlying structures are clearly visible, although some cloudiness may be readily apparent
- 2+* = *Mild.* Some loss of transparency. The cloudiness extends past the anterior half of the stroma. The affected stroma has lost its marble-like appearance and is homogeneously white. With diffuse illumination, underlying structures are visible, although there may be some loss of detail
- 3+* = *Moderate.* Involvement of the entire thickness of the stroma. With optical section, the endothelial surface is still visible. However, with diffuse illumination, the underlying structures are just barely visible (to the extent that the observer is still able to grade flare and iritis, observe for pupillary response, and note lenticular changes)
- 4+* = *Severe.* Involvement of the entire thickness of the stroma. With optical section, the endothelium is not clearly visualized. With diffuse illumination, the underlying structures cannot be seen so that the evaluation of aqueous flare, iritis, pupillary response, and lenticular changes is not possible

Ocular surface are involvement (applied to corneal clouding and staining of the cornea with fluorescein)

- Normal (0)* = No area of cloudiness
 - I+* = Less than one fourth the corneal area
 - 2+* = One fourth to less than one half the corneal area
 - 3+* = One half to less than three fourths the corneal area
 - 4+* = Three fourths or greater of the corneal area
- Pannus (corneal vascularization)*
- Normal (0)* = No pannus
 - I+* = Vascularization is present but vessels have not invaded the entire corneal circumference. Where localized vessel invasion has occurred, the vessels have not penetrated beyond 2 mm
 - 2+* = Vessel invasion is greater than 2 mm in one or more areas or involves the entire corneal circumference

(continued)

Table 2.1 (continued)

<i>Fluorescein staining intensity (area scored as above)</i>	
Normal (0) –	No staining. This may include a small number of faint focal or hazy areas of fluorescein staining which may be present in normal eyes
1+ =	<i>Slight fluorescein staining.</i> With diffuse illumination, the underlying structures are easily visible. (The outline of the pupillary margin can be seen as if there were no fluorescein staining)
2+ =	<i>Mild fluorescein staining.</i> With diffuse illumination, the underlying structures are visible, although there is some loss of detail
3+ =	<i>Marked fluorescein staining.</i> With diffuse illumination, underlying structures are barely visible but not completely obscured
4+ =	<i>Severe fluorescein staining.</i> With diffuse illumination, underlying structures cannot be observed
<i>Lens</i>	
<i>Normal (N or 0) or abnormal (A or 1) - Describe the lenticular opacities and note position(s) in comments</i>	

Table 2.2 SUN^a grading scheme for aqueous flare

Grade	Description
0	None
1+	Faint
2+	Moderate (iris and lens details clear)
3+	Marked (iris and lens details hazy)
4+	Intense (fibrin or plasmoid aqueous)

^aSUN Standardization of Uveitis Nomenclature**Table 2.3** Alternate scoring scheme for anterior chamber fibrin

Grade	Description (based upon degree of anterior chamber filled)
0	None
1+	Faint (<25% of anterior chamber)
2+	Mild (25–50% of anterior chamber)
3+	Moderate (51–75% of anterior chamber)
4+	Marked (>75% of anterior chamber)

Table 2.4 SUN^a grading scheme for cells

Grade	Cells in field ^b
0	<1
0.5+	1–5
1+	6–15
2+	16–25
3+	26–50
4+	>50

^aSUN Standardization of Uveitis Nomenclature^bField size is a 1 mm by 1-mm slit beam

in intensity than the beam as it passes through the normal lens. As noted in the SUN system (Table 2.2), some systems adapt a slightly different mode for scoring aqueous flare to accommodate noting the presence or absence of fibrin in the aqueous. However, there can be varying amounts of fibrin formation, and some prefer to score fibrin formation in a class by itself (Table 2.3). Since the presence of fibrin in the anterior chamber generally indicates a greater degree of breakdown of the blood-aqueous barrier and hence greater inflammation, this latter practice allows better quantification if fibrin formation is encountered with any frequency in studies.

The presence of cells in the aqueous and anterior vitreous can be observed with slit-lamp biomicroscopy, and the SUN system developed a reasonable method for scoring the quantity of cells observed in the aqueous in a 1 X 1 mm beam (Table 2.4). The observer should concentrate on counting the cells at the same point (usually in the central anterior chamber) without moving the beam since cells are heavier than the surrounding aqueous and will settle inferiorly. In addi-

tion to noting the number of cells in the aqueous, it is important to note the types of cells as they may be pigmented arising from the uvea or retinal pigment epithelium (due to injury to or shedding from those structures), nonpigmented (white blood cells arising from an inflammatory response), or red blood cells (arising from damaged vasculature) as may occur with surgical or other invasive procedures (intraocular injections, aqueous or vitreous aspirations, lens extraction, placement of intraocular implants, subretinal injections, etc.). When nonpigmented cells are present in such numbers that frank hypopyon (pus in the anterior chamber) occurs, that should be noted as a comment in addition to the scoring [9, 15]. Likewise, when frank hemorrhage is noted (hyphema with or without clots), that too is worthy of separate comment and clarification.

The evaluation of cells in the vitreous is problematic in that no consensus has been reached with respect to exact scoring and significance of the degree of inflammation [15]. While it is certainly possible to see cells in the anterior vitreous and even determine if they are pigmented, nonpigmented, or red blood cells, such cells may not be uniformly distributed throughout the vitreous, and the vitreous does not circulate like the aqueous so turnover or clearing of cells does not occur as rapidly as in the aqueous. In addition, aspiration of vitreous to perform cell counts adds to the ocular trauma and has the very real potential for causing the release of more cells due to the aspiration procedure alone. Further, the number of cells in the vitreous may not be uniformly distributed so the aspirated vitreous may not provide an accurate assessment of the total cell count in the vitreous. In recognition of these limitations, it must fall to the personnel conducting the examinations to agree at the outset of the study on a method of empirically quantifying the number and types of cells. Possibilities include applying the technique for assessing aqueous cells and counting cells in the slit beam at a certain point (e.g., immediately posterior to the axial lens) or assigning general degrees of cellularity as mild, moderate, or severe. When this is done concurrently with other examinations such as indirect ophthalmoscopy, a meaningful assessment can result (see assessment of vitreal clarity under indirect ophthalmoscopy). One other complicating factor worthy of mention is that when evaluating intravitreal injection studies, it may be difficult to differentiate nonpigmented cells from individual particles of an injected suspension.

Because some references to the Draize scoring system occasionally arise in the planning stages of topical ocular toxicology studies, a brief discussion of this system is warranted. The Draize system, first described by Draize and Woodard in 1944 [5], is outmoded and has received a very negative reputation among animal welfare proponents. It is a system for grading ocular irritancy of liquids, solutions, or ointments after the one time instillation of 0.1 ml of the agent into the inferior conjunctival sac of albino rabbits. Scoring by this system is based upon the gross evaluation of damage to the cornea, conjunctiva, and iris at 1, 24, 48, and 96 h (if there are findings at 48 h) [3]. It was primarily used for evaluating cosmetics and other manufactured agents such as shampoos and not for the evaluation of ophthalmic products intended for use in the eye. The system was not designed for microscopic evaluation after repeated dosing and is not an acceptable alternative to the systems commonly employed today in ophthalmic toxicology studies.



Fig. 2.10 The indirect ophthalmoscope with lenses of varying dioptric powers allows great flexibility for examining the ocular fundus with varying magnification. It is superior to the direct ophthalmoscope for evaluation of the fundus with respect to evaluating the greatest area of the fundus and assessing the overall appearance of the retina, choroid and optic disc

2.2.2 *Direct and Indirect Ophthalmoscopy*

Ophthalmoscopy is the examination of the ocular fundus performed most commonly with either a direct or indirect ophthalmoscope after dilation of the pupil with a short-acting mydriatic (usually 0.5–1% tropicamide, a short-acting parasympatholytic agent, either alone or in combination with a sympathomimetic agent such as 2.5% phenylephrine). By this examination, changes in vitreous, retina, vessels of the retina and choroid, and the optic disc may be evaluated. The direct ophthalmoscope provides a highly magnified but monocular view of the real (neither inverted nor reversed) image of the fundus, while the indirect ophthalmoscope provides a binocular view of an inverted and reversed aerial image obtained by the positioning of a condensing or converging lens between the eye and the examiner.

Direct ophthalmoscopy provides a highly magnified image, but it has the disadvantage of a small field of view (approximately 2 optic disc diameters) so that the exam can be very time-consuming, and lesions may be missed. In addition, it requires the examiner's face be very close to the animal's face and mouth with greater risk to the examiner, it is harder to examine the peripheral fundus, and there is greater distortion of the view of the fundus when any opacities are present in the visual axis whether



Fig. 2.11 (a) The direct ophthalmoscope allows a highly magnified view of a lesion of the ocular fundus but has the disadvantage that the area examined is small (generally a few disc diameters in diameter). As a result, the time for examination of the entire fundus is greatly increased, and lesions may be inadvertently missed, especially in an animal that is awake and moving. (b) Note that direct ophthalmic examination requires very close proximity of the examiner's face to the animal, thus increasing risk of exposure of the examiner to diseases carried by primates and inadvertent injury to the examiner from bites or scratches

in the cornea, aqueous humor, lens, or vitreous. Such opacities may so degrade the visibility that the fundus may only be visible with indirect ophthalmoscopy if at all.

Binocular indirect ophthalmoscopy provides a wider, stereoscopic view of the fundus (albeit with less magnification) than with direct ophthalmoscopy, and it is easier to restrain the animal while more easily and quickly examining the entire fundus. As mentioned above, it produces an image that is both inverted and reversed that can confuse novice examiners during the examination and recording of findings. An easy method to facilitate orientation during the examination is to remember to move toward the observed image during the examination. This results in directing the light entering the eye opposite the direction the examiner moves, thus illuminating the lesion. By using different lenses, the magnification of the fundus may be increased with a consequent decrease in the field of view.

As mentioned above, the advantage of the indirect ophthalmoscope is that the fundus is more easily visible with indirect ophthalmoscopy than with direct ophthalmoscopy even when the view of the fundus is partially obscured because a wider view of the fundus can be achieved, thus allowing the examiner to better look around or through opacities in the ocular media. One scoring system of posterior uveitis devised by Nussenblatt et al. utilizes the degradation of the visualization of the fundus during indirect ophthalmoscopy using a 20-diopter condensing lens as a measure of the severity of the uveitis [13]. This scoring, summarized in Table 2.5, can be used

Table 2.5 Nussenblatt vitreous haze scoring for posterior uveitis

Grade	Description
0	Optic nerve and retinal vessels visible in detail with no impairment
Trace	Slight blurring of optic disc margins. Normal striations and reflex of the nerve fiber layer not visible
1+	Optic nerve and retinal vessel details easily discernible
2+	Optic disc margins blurred; retinal vessels well visualized
3+	Optic disc borders and retinal vessels markedly blurred
4+	Optic disc and retinal vessels obscured

to advantage in ophthalmic toxicology for evaluating the severity of vitreal haze that may occur with adverse reactions.

As with slit-lamp biomicroscopy, the examiners must have a thorough knowledge of normal findings as well as background lesions that occur as incidental findings in the species and breed examined, and whenever possible, animals with lesions noted at pre-study examinations should be excluded from the study. Documentation of lesions by photography should be performed whenever animals with findings are included in the study and whenever new lesions develop during a study (Figs. 2.12, 2.13, 2.14, 2.15, 2.16, 2.17, 2.18, 2.19, 2.20, and 2.21). Photographic documentation of vitreous haze can also be utilized [4].

Ophthalmoscopy thus has the advantages of allowing a real-time examination of the ocular tissues that is noninvasive, is documentable through photography or videography, and, to a certain extent, is to some degree a three-dimensional view. Ophthalmoscopy is time sensitive in that lesions may be followed over time, but it is thus problematic in that the histopathological characterization of a lesion is not possible at all time points since the ocular tissues cannot be harmlessly obtained. In some cases, concurrent advanced studies such as optical coherence tomography (OCT) and ultrasonography can be employed to better characterize the nature and location of a lesion (see Chap. 3). Ultimately, at specified intervals when animals are sacrificed and the eyes are submitted for histopathological evaluation, it is imperative to ensure that the type and location of lesions in the eyes are conveyed to the pathologists examining the tissues, and every effort should be made to ensure the lesions are present in sections of the ocular tissues in order to characterize the nature of the lesion at the cellular level.

2.2.3 Photography

As noted in the following images, ocular photography can be a useful method of documenting ocular findings. Photographs taken at different time points in the study can be used to document the progression or lack thereof of lesions. However, photographing a large number of animals is very time-consuming (and thus expensive), and it subjects the animals to another level of stress. Since in most large studies the incidence of adverse findings associated with the administration of the test article is low

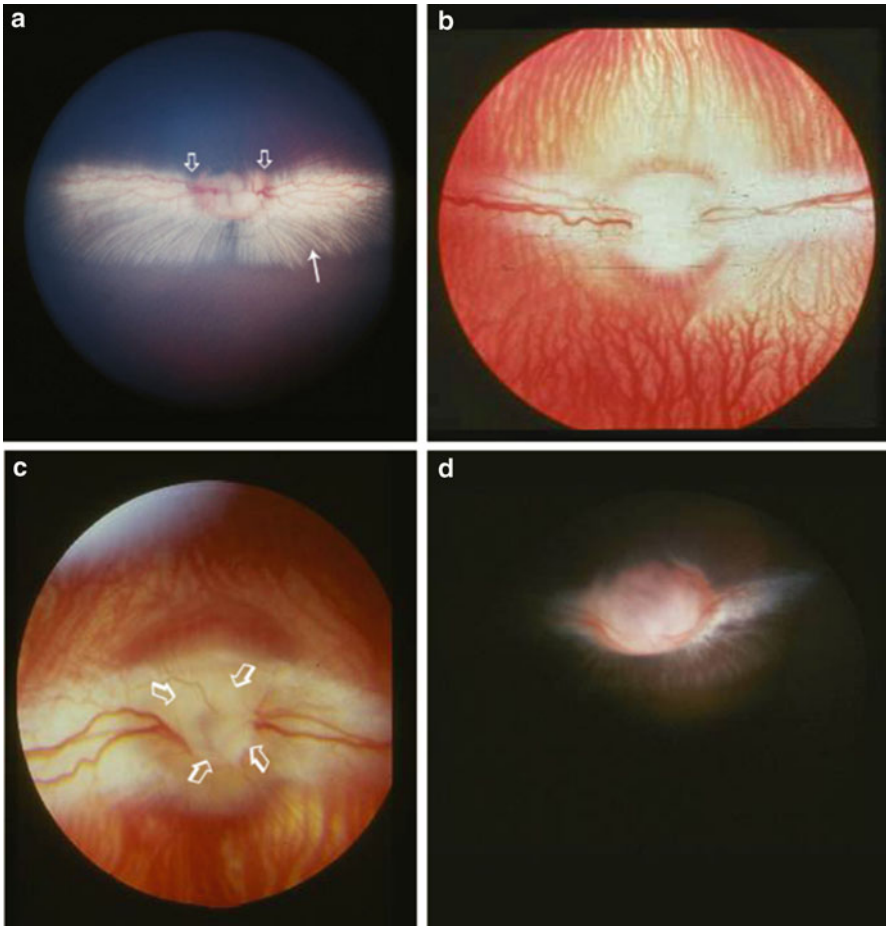


Fig. 2.12 Normal rabbit fundus (a–c), glaucomatous cupping of optic disc (d). (a) Normal New Zealand red (NZR) rabbit. The rabbit fundus is merangiotic with the retinal vessels confined to a horizontal zone on either side of the horizontally ovoid optic disc in the medullary rays. *Open arrows* show the nasal and temporal margins of the optic disc. *Long arrow* shows individual myelinated nerve fibers. The myelinated fibers are more densely packed immediately nasal and temporal to the optic disc. The choroidal vessels are not visible in pigmented fundus. (b) Normal New Zealand white (NZW) rabbit. The typical numerous choroidal vessels are visible in this nonpigmented rabbit. (c) The details of the optic disc are more visible in this photograph of a normal NZW rabbit. The *open arrows* delineate the prominent physiologic cup in the optic disc. (d) Glaucomatous cupping of the optic disc in a NZR rabbit. Note the myelinated nerve fibers are less prominent

(in many cases, pilot studies will have eliminated test articles or drugs that will cause problems or produce unacceptable findings), addition of photography in most instances will not add to the study and will be cost ineffective. Therefore, photography is most often built into a protocol as an option to be employed to document unexpected findings or as part of a smaller research study to better characterize the cause and occurrence of an effect of a test article on ocular tissues.

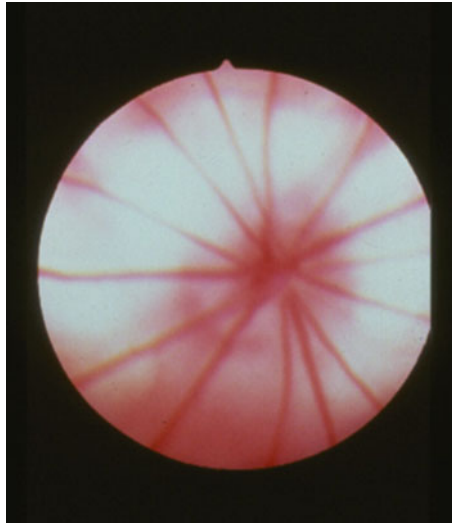


Fig. 2.13 Normal albino rat fundus. The choroidal vessels are indistinct and the reddish border of the optic disc is poorly differentiated from the surrounding field. The retinal arterioles and venules radiate from the central optic disc



Fig. 2.14 Normal canine fundus. While there are numerous breed-related variations in the appearance of the normal canine fundus, the fundus of the beagle has fewer variations. The optic disc may be pink to white, and its shape varies from round to triangular and is occasionally multilobed with varying degrees of myelination. A small physiologic cup is usually visible in the center of the disc as a small pit. The optic disc may be entirely within the tapetal zone, at the junction of the tapetal and non-tapetal fundus or entirely in the non-tapetal fundus. Three to four major venules and up to 20 smaller arterioles radiate from the optic disc. The color of the tapetum may vary and in some cases may be entirely absent

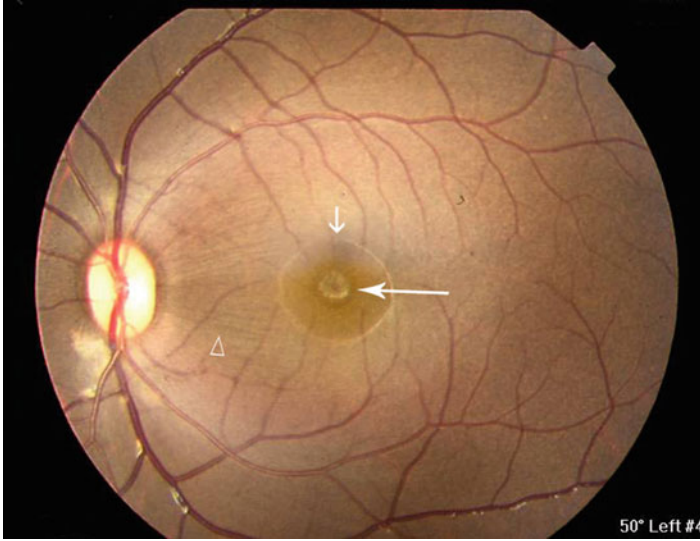


Fig. 2.15 Normal primate fundus (cynomolgus macaque) with uniform pigmentation. The vertically ovoid optic disc is present at the left with the normal macula (*short arrow*) located temporally (in the *center* of the photograph). The fovea (*long arrow*) is present in the center of the macula. Note that individual nerve fibers (*open arrowhead*) are visible between the optic disc and macula (in the papillomacular bundle)



Fig. 2.16 Normal primate fundus (cynomolgus macaque) with irregular pigmentation of the retinal pigment epithelium (RPE) and choroid. The darker retinal vessels (*open arrows*) are visible as usual, and the paler choroidal vessels (*small arrows*) are visible due to the lesser pigmentation of the RPE and choroid



Fig. 2.17 Excessive peripapillary myelination, a normal variant in a cynomolgus macaque. The excessively myelinated nerve fibers are visible involving and inferior to the optic disc

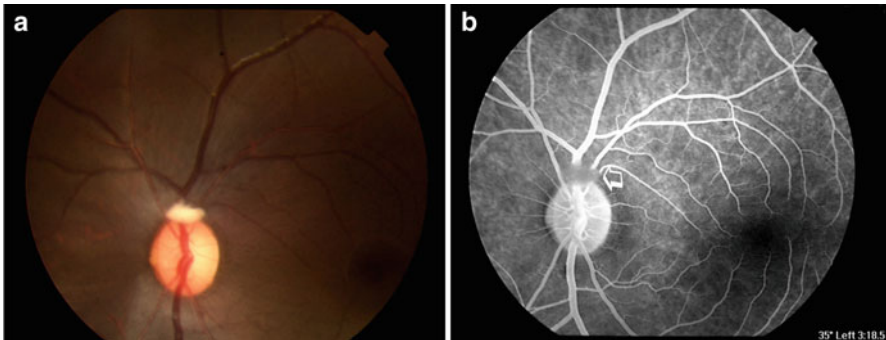


Fig. 2.18 Glial (neuroepithelial) choristoma in a cynomolgus macaque. Such glial choristomas or proliferations are occasionally seen as incidental background findings. **(a)** Color fundus of the left eye with the glial proliferation at the 12:00 margin of the optic disc. **(b)** Fluorescein angiography revealing blocked fluorescence by the glial proliferation (*open arrow*) [12]

When photography is employed, it is important as much as possible to standardize the exposure of illuminating flashes since even small variations in either the direction of gaze (angle of incident light) or the exposure can alter the appearance of a lesion. It is relatively easy to document a lesion with photography but much more difficult to demonstrate subtle progressions or regressions. Histopathology and other examination techniques such as optical coherence tomography, confocal microscopy, and ultrasonography can be utilized to characterize the lesions photographed and establish a more meaningful assessment of the nature and origin of such lesions.

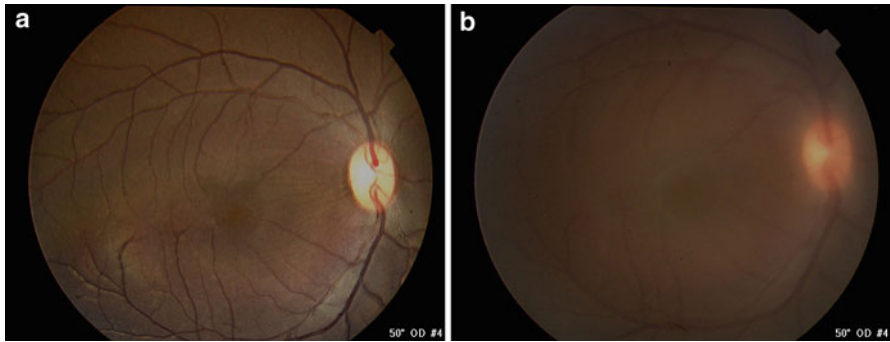


Fig. 2.19 Example of scoring of vitreous haze. (a) Normal primate (*cynomolgus macaque*) fundus. The details of the retina, its vessels, and the optic disc are visible in crisp detail. (b) Vitreous haze has significantly blurred the details of the optic disc margins, and to some degree the view of the retinal vessels, while discernible, is indistinct. This would warrant a score of 2–3+ using the Nussenblatt scoring system [13]

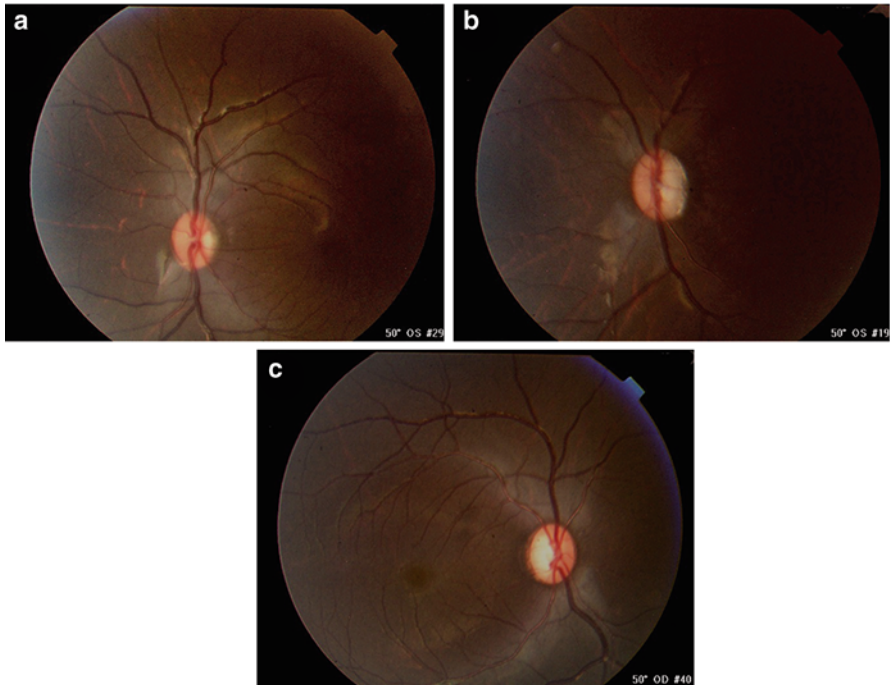


Fig. 2.20 Bilateral optic atrophy (BOA) in a Cambodian-origin *cynomolgus macaque*. Compare photos with normal *cynomolgus macaque* optic disc (Figs. 2.14, 2.15, 2.16a, and 2.22a). (a) Minimal or slight manifestation of BOA. (b) Mild/moderate manifestation of BOA. (c) Marked or severe manifestation of BOA. Grading was based upon findings on histopathological evaluations. BOA has been described as a subtle bilateral background finding in rhesus and *cynomolgus macaques* that is characterized histologically by decreased ganglion cells in the inner macula with a corresponding decrease in axons in the nerve fiber layer and temporal optic nerve (See Fig. 2.20) [6, 7]

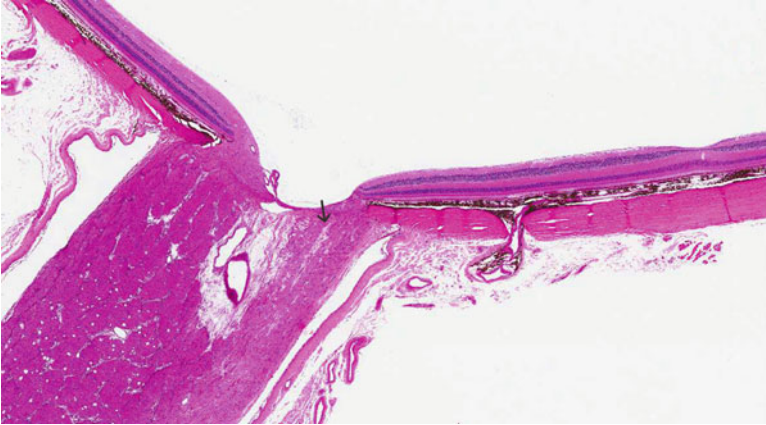


Fig. 2.21 Histologic section through the optic nerve and temporal retina. Note the decrease in axons in the temporal optic nerve (*arrow*)

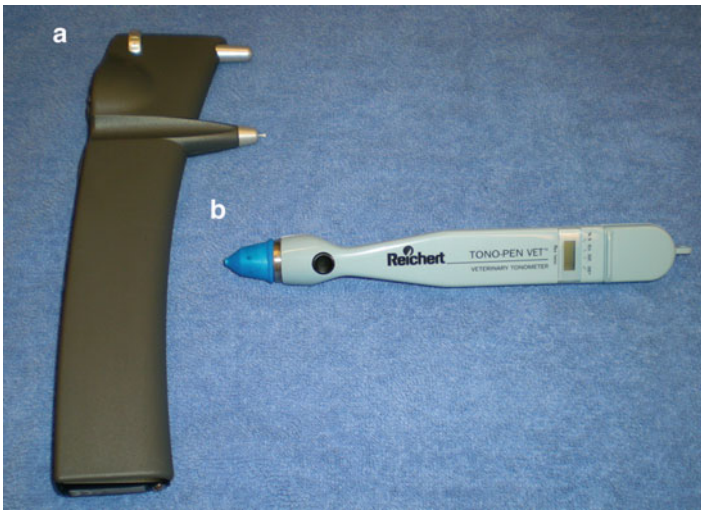


Fig. 2.22 (a) The TonoVet® is a rebound tonometer that measures intraocular pressure by induction-impaction through a technique that measures the rebound action of a magnetic probe as it contacts the cornea and bounces back. (b), The TonoPen XL® measures intraocular pressure by applanation of the cornea. Both of the above instruments are calibrated internally

2.2.4 Tonometry

Tonometry as applied to ophthalmic toxicology is an indirect measurement of the intraocular pressure (IOP) either by applanation of the cornea (TonoPen XL®, pneumotonograph – Figs. 2.22b and 2.23) or by induction-impaction through a technique that measures the rebound action of a magnetic probe as it contacts the cornea and



Fig. 2.23 The pneumotonograph is a tonometer that measures intraocular pressure by applanation of the cornea. Calibration is accomplished by placing the probe against a membrane in a manometer on the *right*, where the pressure is determined by the water level in the manometer. The intraocular pressure is recorded on the recording paper at the *left side* of the machine

bounces back (TonoVet® – Fig. 2.22a). In most animals, the accepted normal intraocular pressure is between 15 and 25 mmHg, but intraocular pressure can be highly variable and the difference between fellow eyes can range as high as 8 mmHg [14]. Variables that can affect intraocular pressure include effects of circadian rhythm, degrees of stress, location and environmental conditions, physical restraint, eye position, systemic blood pressure, water consumption, and sedation or anesthesia. Animals may even react differently to different personnel performing intraocular pressures. Such variables must be considered in construction of study protocols with proper controls established.

In general toxicology studies where baseline conditioning is not usually performed, the variables can be limited by the proper use of controls, measuring the intraocular pressures for all animals in all groups at the same time each day and using the same personnel when measuring the pressures. In such studies, evaluating mean intraocular pressure for each group and comparing it both to the initial mean intraocular pressure as well as the control group can further decrease variability between groups.

In studies that are intended to evaluate the effects of a particular test article of compound on intraocular pressure, it is imperative to acclimatize the animals over a 2–3-week period with repeated measurement of IOP under identical conditions. Whenever possible, the animals should be conditioned to allow measurement without sedation by the same personnel at the same time each day. Also the animals should be housed and their intraocular pressures checked in rooms that stringently limit “climate” variations and environmental noise from other areas of the facility.

2.2.5 *Electroretinography*

Simply put, electroretinography is the measurement of electrical potentials generated by the retina in response to light stimuli on the retina. As such, electroretinography may be used in selected studies for detection or documentation of adverse effects of a test article or procedure on retinal function. Because the procedures involved are complex and time-consuming, such testing is most commonly used in systemic toxicology studies or in studies involving test article or device delivery inside the eye. In most studies, a full-field flash electroretinography is utilized, but more specialized studies may be indicated in certain studies. Electroretinography and its various applications are discussed in detail in Chap. 4.

2.2.6 *Specialized Studies*

Pachymetry and specular endothelial microscopy are primarily used as adjunct examinations in topical ocular and intraocular drug studies as well as surgical studies (including evaluation of surgical implantations of devices such as intraocular lenses or drug delivery implants as well as intraocular injections). *Pachymetry* is simply the measurement of corneal thickness and is most often performed by contact ultrasound, high-resolution ultrasound, or optical coherence tomography (OCT). Pachymetry will allow examiners to evaluate changes in corneal thickness in advance of notable corneal edema. When such studies are conducted, the protocol should provide for standardization such that in all groups and all eyes, the same area or areas of the cornea are evaluated at each time point.

Specular endothelial microscopy is similarly standardized and usually a specified area of the central corneal is evaluated for cell area, cell density, polymegathism, and percentage of cellular pleomorphism. Both contact and noncontact instruments are available, and in recent years, automation has greatly aided in the ease of conducting both types of studies. However, the examinations can be time-consuming, and sedation is usually required for laboratory animal species. Corneal opacities, haze, and edema can make specular endothelial microscopy impossible.

Corneal wound healing studies are generally reserved for small studies designed to evaluate the effects of topical drugs and preservatives on wound healing and involve creating a standardized wound on the cornea, applying the test article and a known control, and evaluating wound area stained by fluorescein at successive time points until the corneas are healed. Because such corneal wounding involves pain, such studies should be limited and carefully evaluated by animal care and use committees to determine their necessity.

Corneal perfusion studies are performed on corneal buttons harvested from the cornea and perfused or irrigated with intraocular irrigating solutions with constituents added to evaluate the effects of such agents on the corneal endothelium by examining the corneal endothelium by microscopy.

2.2.7 Fluorescein Angiography

Fluorescein angiography (FA) is a specialized photographic technique for evaluating the vessels of the eye, usually in the retina and choroid but sometimes in the iris, for defects by means of sequential timed photographs after the intravenous injection of fluorescein. It is a demanding procedure that requires specialized equipment and handling, and sedation of animals is required. Potential reactions are rare but include tissue irritation in the event of leakage at the injection site, vomiting after administration of the intravenous bolus, and anaphylaxis. Equipment requirements for the test include a fundus camera capable of taking digital, multiple time-sequenced photographs that is equipped with an exciter filter (blue light at 490 nm) plus a barrier filter to record the yellow-green fluorescein light (520–530 nm) as the fluorescein courses through the ocular vessels. A baseline color photograph of the fundus (or the iris) is recorded before the injection, and sequential black and white images are then recorded every second for 20 seconds; then less often to record the phases of vascular filling.

The phases of FA in order are prearteriolar (choroidal flush), retinal arteriolar, capillary transition stage, early venous (also known as lamellar or arterial-venous), late venous, and late recirculation phases as shown in Fig. 2.24a–g.

Abnormalities noted in FA include hyperfluorescence and hypofluorescence. Hyperfluorescence will be noted in areas of neovascularization, aneurysm, capillary leakage, pooling defects, staining of surrounding tissues from leakage of the fluorescein from vessels, and abnormal vessels. Hypofluorescence will be noted with filling defects in the vessels themselves or with lesions that block the visualization of the vessels such as blood clots, fibrin, or other masses anterior to the retina. Fluorescein angiography is most commonly used in evaluating efficacy of test articles on reduction of experimentally induced choroidal neovascularization induced prior to conduction of ocular toxicology studies.

2.2.8 Ocular Ultrasonography

Ocular ultrasonography is a noninvasive technique by which acoustic waves are used to image (echo) ocular structures or implants, and to perform biometric measurements of ocular structures. This may involve the use of A-scan, B-scan, or ultrasound biomicroscopy. It is uncommonly used in ocular toxicity studies, and its most common use in studies with large numbers of animals may be to demonstrate the position and size of implants in the vitreous.

2.2.9 Optical Coherence Tomography

Optical coherence tomography (OCT) is a noninvasive high-resolution imaging technique that allows real-time evaluation of ocular structures, most commonly the retina and optic nerve head, and can provide cross-sectional images with an axial

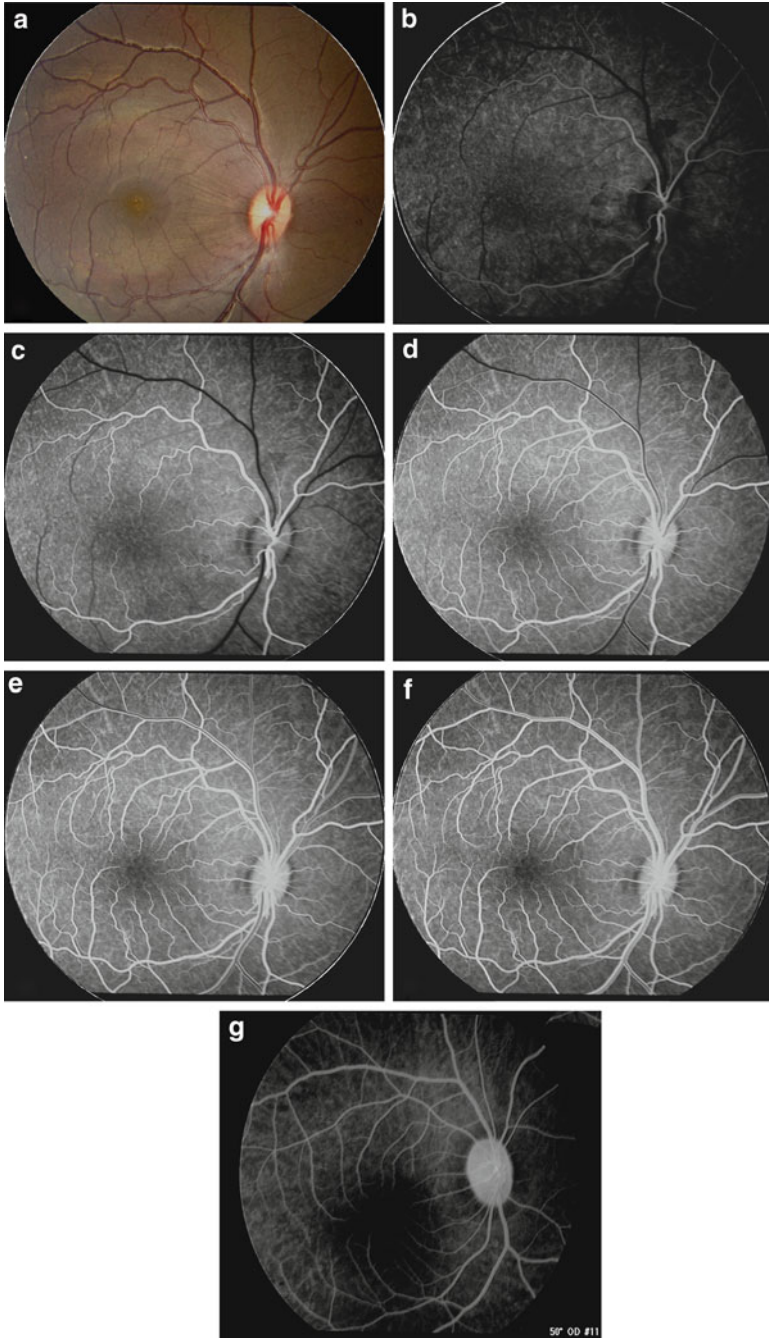


Fig. 2.24 Fluorescein angiography stages. (a) Baseline color photograph. (b) Prearteriolar (choroidal flush). (c) Arteriolar phase. (d) Capillary transition stage. (e) Early venous (arteriolar-venous) phase. (f) Late venous phase. (g) Late recirculation phase

resolution of 8–10 μm . Such images allow analysis of the ocular structures without sacrifice of the eye. OCT requires specialized equipment and precise positioning so it can be time-consuming, and there are some lesions in the peripheral fundus that cannot be imaged. It is an uncommon examination technique in routine ocular toxicity studies but may be beneficial in evaluating the eyes in smaller targeted studies as will be discussed in Chap. 3.

References

1. Bellhorn RW, Korte GE, Abrutyn D. Spontaneous corneal degeneration in the rat. *Lab Anim Sci.* 1988;38(1):46–50.
2. Bruner RH, et al. Spontaneous corneal dystrophy and generalized basement membrane changes in Fischer-344 rats. *Toxicol Pathol.* 1992;20(3):357–66.
3. Daston GP, Freeberg FE. Ocular irritancy testing. In: Hobson DW, editor. *Dermal and ocular toxicology: fundamentals and methods.* Boca Raton: CRC Press; 1991. p. 510–2.
4. Davis JL, et al. Scale for photographic grading of vitreous haze in uveitis. *AJO.* 2010;150(5):637–41.
5. Draize JH, Woodard G, Calvery HO. Methods for the study of irritation and toxicity of substances applied topically to the skin and mucous membranes. *J Pharm Exp Ther.* 1944;82:377.
6. Dubielzig RR et al. Bilateral optic atrophy: a background finding in cynomolgus macaques used in toxicologic research. In: *Proceedings, annual meeting of Association for Research in Vision and Ophthalmology;* 2009.
7. Fortune B, Wang L, Bui BV, Burgoyne CF, Cioffi GA. Idiopathic bilateral optic atrophy in the rhesus macaque. *IOVS.* 2005;46(11):3943–56.
8. Hackett RB, McDonald TO. Ophthalmic toxicology and assessing ocular irritation. In: Marzulli FN, Maibach HI, editors. *Dermatotoxicology.* 5th ed. Washington, DC: Hemisphere Publishing Corp; 1996. p. 749–815.
9. Hogan MJ, Kimura SJ, Thygeson P. Signs and symptoms of uveitis: I. Anterior uveitis. *Am J Ophthalmol.* 1964;47:155–70.
10. Losco PE, Troup CM. Corneal dystrophy in Fischer 344 rats. *Lab Anim Sci.* 1988;38(6):702–10.
11. Munger RJ. Veterinary ophthalmology in laboratory animal studies. *Vet Ophthalmol J.* 2002;5(2):167–75.
12. Munger RJ, Jensen VB, Bouldin TW, Peiffer Jr RL. Bilateral neuroepithelial choristomas of the optic disc in a cynomolgus monkey (*Macaca fascicularis*): a case report. *Vet Ophthalmol J.* 2002;5(2):221–6.
13. Nussenblatt RB, et al. Standardization of vitreal inflammatory activity in intermediate and posterior uveitis. *Ophthalmology.* 1985;92:467–71.
14. Ollivier FJ, Plummer CE, Barrie KP. Ophthalmic examination and diagnostics. In: Gelatt KN, editor. *Veterinary ophthalmology.* 4th ed. Ames: Blackwell Publishing; 2007. p. 469.
15. The Standardization of Uveitis Nomenclature (SUN) Working Group. Standardization of uveitis nomenclature for reporting clinical data. Results of the first international workshop. *Am J Ophthalmol.* 2005;140:509–16.
16. Taradach C, Graves P. Spontaneous eye lesions in laboratory animals: incidence in relation to age. *CRC Crit Rev Toxicol.* 1964;12(2):121–47.
17. Wegner A, Kaegler K, Stinn W. Frequency and nature of spontaneous age-related eye lesions observed in 2-year inhalation toxicity study in rats. *Ophthalmic Res.* 2002;34:281–7.
18. Wojcinski ZW, et al. Spontaneous corneal change in juvenile wistar rats. *J Comp Path.* 1999;120:281–94.
19. Yamaguchi K, Yamaguchi K, Turner JE. Corneal endothelial abnormalities in the Royal College of Surgeons rat. *Cornea.* 1990;9(3):217–2.

Chapter 3

Emerging Imaging Technologies for Assessing Ocular Toxicity in Laboratory Animals

T. Michael Nork, Carol A. Rasmussen, Brian J. Christian,
Mary Ann Croft, and Christopher J. Murphy

Abstract Recent decades have seen a dramatic increase in ocular imaging technologies—both for the anterior and posterior segments. This has been largely the result of increased computer processing power as applied to hardware control and data analysis. For example, the theoretical basis for ocular coherence tomography (OCT) was developed by Michelson in the nineteenth century, but only recently, thanks to computers, lasers, and electronic control circuitry, has it become a practical tool in the clinical and for toxicological studies.

In the aggregate, the use of advanced imaging may be expected to improve the drug development process by providing high-quality and clinically relevant data, which enable earlier and more informed decision making at the preclinical stage of

T.M. Nork, M.D., M.S., DABO, FARVO (✉) • C.A. Rasmussen, M.S.
Ocular Services On Demand, LLC (OSOD)

Department of Ophthalmology and Visual Sciences, University of Wisconsin
School of Medicine and Public Health, Madison, WI, USA
e-mail: tmnork@wisc.edu; tmnork@ocularservices.com;
crasmussen@wisc.edu; crasmussen@ocularservices.com

B.J. Christian, Ph.D., DABT
Covance Laboratories, Madison, WI, USA
e-mail: brian.christian@Covance.Com

M.A. Croft, M.S.
Department of Ophthalmology and Visual Sciences, University of Wisconsin-Madison,
Madison, WI, USA
e-mail: macroft@wisc.edu

C.J. Murphy, D.V.M., Ph.D., DACVO (✉)
Ocular Services On Demand, LLC (OSOD)

Department of Ophthalmology and Vision Science, School of Medicine
and Department of Surgical and Radiological Sciences, School of Veterinary Medicine,
University of California, Davis
e-mail: cjmurphy@ucdavis.edu; cjmurphy@ocularservices.com

drug development. This accompanied with gains in efficient use of resources can reduce the overall time and cost required to bring a new drug to market.

In this chapter, we review the capabilities and limitations of advanced ocular imaging and diagnostic tools that are commercially available and appropriate for inclusion in the design and execution of preclinical programs in ocular drug development.

3.1 Introduction

Advanced ocular imaging and other analytic techniques are being used more frequently in preclinical safety studies. This trend is largely driven by rapid technological advances which have enabled increased application of these techniques during starting in the experimental stages of drug discovery and continuing through the clinical management of ocular disease in patients. This provides advantages to and synergies with conventional safety endpoints:

- Imaging and other advanced analytical techniques such as electroretinography provide symmetry between efficacy data obtained from animal models of disease, pharmacodynamic endpoints in safety studies, as well as clinical program outcomes.
- Nonconsumptive endpoints provide the opportunity for serial data collection over time in a single animal. This longitudinal evaluation provides a more robust data set for statistical analysis and hence the ability to more clearly discerns effects of drug treatment. Obtaining multiple evaluations from an individual animal also mitigates the need for separate satellite groups of animals for terminal procedures, thereby reducing the overall number of research animals necessary to conduct a study.
- Imaging data including optical coherence tomography (OCT) complement those of conventional safety endpoints, such as light microscopic histomorphological evaluation by providing a more complete characterization of effects. For example, the specific location and size of a lesion may be documented in three dimensions using OCT and thus alleviate the need for expensive and time-consuming histological sectioning and microscopic evaluation procedures. These techniques may also enhance conventional methods by removing some subjectivity from the evaluation by utilizing software that provides, for example, objective measurements of lesion size.
- Novel modalities with continuing technological advances such as increasing spatial resolution for imaging techniques combined with functional endpoints such as electroretinography have the potential to identify more sensitive biomarkers of adverse drug effects. The development of biomarkers that reliably predict the human experience is recognized by the Food and Drug Administration as a critical factor in improving the drug development process.

Advanced ocular imaging and electrodiagnostic techniques (see the following chapter) are specialized fields of expertise in their own right, and implementing them in preclinical studies requires expert knowledge of the instrumentation with respect to testing strategy, data capture, and evaluation. Differences in the anatomical and physiological aspects of vision between laboratory animal species in conjunction

with the specific mode of action of the test material should be considered when designing the most applicable testing protocol. For example, the relative distribution of rod and cone photoreceptor cells between nonhuman primates and rabbits should be considered when designing specific electroretinography (ERG) testing protocols that are capable of assessing responses of different retinal cell types.

While there is ongoing development of instrumentation specifically designed to evaluate laboratory animals, much of the available technology is designed for use in humans. Similar to the intraocular anatomy, the external anatomy of the laboratory animal species commonly used for ocular research varies widely. Physical attributes such as animal size which may range from mice to mini pigs, position of the eyes within the skull such as forward vs. lateral placement, the presence of extraocular tissue such as nictitating membranes, and physiological differences including blink rate and ocular muscle movement must be understood and accounted for to obtain optimal data. Consequently, it may be necessary to modify the instrument or design specific equipment to aid in positioning the animal in front of the instrument. High-quality evaluation requires that eye movement be kept to a minimum and as a result, most procedures are performed in anesthetized animals. Since anesthesia may also affect the ability to capture data such as anesthetic-induced eye movement or to affect the quality of the data when measuring ERG response, it is critical to develop and validate reliable anesthesia protocols specific to each species tested. There are also specific requirements for optimal data capture that may be unique to specific evaluation techniques, and are discussed in the sections to follow.

3.1.1 Future Directions

In 2009, the National Eye Institute sponsored a symposium entitled “Advances in Optical Imaging and Biomedical Science” [1] during which a number of technical challenges for developing the next generation of ophthalmic imaging devices were discussed. The key points are listed below:

- Improving the speed of image acquisition. The development of spectral-domain optical coherence tomography (SD-OCT) has greatly increased image acquisition speed; however, it still limits the scientific and clinical value of new imaging technologies.
- Removing the artifacts of eye motion from retinal images. Active tracking and stabilization during image acquisition or post-processing techniques following image acquisition are needed to correct for eye movement.
- Developing better and faster software for processing ocular images. The time currently required to process large amounts of digital imaging data is hampering eye research. Automated software is needed that provides eye motion correction and visualization and improved algorithms for identifying specific retinal layers of interest. Longitudinal studies of disease progression and efficacy of therapy could be facilitated by software enabling researchers to repeatedly return to the same retinal location.

- Understanding the safety limits of light intensity. Evidence suggests current light safety standards do not adequately protect the eye under some conditions and estimates of safe light levels need to be refined.
- Integrating multiple imaging modalities. Using adaptive optics–optical coherence tomography as an example, existing technologies can be combined to form new devices with new and specialized ocular imaging capabilities.
- New noninvasive measures of functional activity are needed which can be used in conjunction with structural imaging techniques.

3.1.2 Summary

In the aggregate, the use of advance imaging and electrodiagnostic techniques may be expected to improve the drug development process by providing high-quality and clinically relevant data, which enable earlier and more informed decision making at the preclinical stage of drug development. This accompanied with gains in efficient use of resources can reduce the overall time and cost required to bring a new drug to market.

In this chapter, we review the capabilities and limitations of advanced ocular imaging and diagnostic tools that are commercially available and appropriate for inclusion in the design and execution of preclinical programs in ocular drug development.

3.2 Traditional Ophthalmic Fundus Imaging in Ocular Research

We live in an exciting era that is being transformed by computer processing power and many other technological advances. The other sections of this chapter will concentrate on some, but by no means all of the recent advances in ocular imaging as well as ocular functional analysis; however, it is important to recognize the role of traditional ophthalmic imaging in the clinic, research, and ocular toxicologic studies. This section reviews some of the advantages of standard ocular imaging and why it has not become obsolete.

A well-designed preclinical ocular drug study in which retinal toxicity is to be evaluated should include photographic ocular imaging and interpretation of those images by an individual who is both qualified and financially disinterested in the outcome of the trial. Ideally, this person should also be blinded to the treatment groups until the image interpretations are completed. As we enter a new era of fundus imaging with such modalities as spectral-domain optical coherence tomography (SD-OCT), confocal scanning laser ophthalmoscopy, scanning laser polarimetry, and in the near future, adaptive optics imaging, it is important to understand the

continued indispensable role that subjective analysis of standard fundus images including color fundus photos, fluorescein angiograms, and fundus autofluorescence plays in this era of advanced imaging. Although clinical exams are also indispensable, photography and its skilled interpretation provide important advantages.

3.2.1 Baseline Images

Biological variability is a fact of life. Unusual morphological features such as pigmentary irregularities of the retinal pigment epithelium or odd vascular patterns are important to document photographically prior to drug dosing. We have encountered instances where subtle findings were noted on the ocular clinical exam following dosing. Fortunately, baseline fundus images were available to confirm that the condition was preexisting and not due to a toxic effect of the drug.

3.2.2 High-Resolution Images

The images obtained by modern digital fundus cameras have much higher resolution than what is available to the clinician using an indirect ophthalmoscope with a 20 diopter lens. Although it is theoretically possible to obtain better resolution with a table-mounted slit lamp and a corneal contact lens such as a Goldmann lens, this would be excessively time-consuming and, even if done, would provide no permanent image record. We have documented specific examples of subtle signs of toxicity that were missed on the clinical exam.

3.2.3 Stereopsis

Fundus images including standard color photographs and fluorescein angiograms are taken and reviewed in stereo. Thickening of the retina or optic nerve are thus apparent that would not be on clinical examination with the indirect ophthalmoscope. Although optic nerve and retinal thickening can sometimes be documented with the SD-OCT, the advantage of photographic imaging is that it provides a wide-field view of the ocular fundus. Areas that might be missed by the 2-dimensional SD-OCT scan are evident on the wide-field camera images which typically include 50° of arc.

3.2.4 Second Opinions

The fundus images are stored permanently. When digital images are obtained, an exact copy can be given to the client for review. If desired, the images can be sent to another ocular specialist to obtain an independent review.

3.2.5 Retrospective Analysis

When did the suspected changes first occur and are they progressive? Or are there signs of reversal on discontinuing the test material? The use of photographic imaging enabled us to address these questions in a recent ocular toxicity study.

3.2.6 Dose-Response Changes

Although a number of endpoints are often used in ocular toxicity studies such as histopathology, color photography and fluorescein angiography can provide additional dose-response information.

3.2.7 Recovery

If lesions are observed on fundus imaging, very often the next question is, to what extent, if any, they resolve with discontinuation of drug dosing? Also, the absorption and settling of opaque test materials injected into the vitreous over time can be documented photographically – especially with the ultrawide-field Staurengi™ 150° contact lens (Heidelberg Engineering).

3.2.8 Rapid, Subjective Interpretation by a Retinal Specialist

Much emphasis is placed on quantitation, but subjective interpretation remains important for at least a couple of reasons. First, it is rapid, and therefore large number of animals and test points can be screened relatively inexpensively. Second, subjective interpretation is sometimes superior to quantitation. That is how pathologists diagnose cancer, for example. Facial recognition is another example of highly effective subjective assessment.

3.2.9 Limitation of Cross-Sectional Analysis

The SD-OCT and histopathology only look at cross sections of the ocular fundus. They can and do sometimes miss focal lesion that would be evident photographically. Fundus photography can be used to direct optical or histopathological sectioning.

3.2.10 *Fluorescein Angiography*

The small molecular size of the fluorescein molecule can provide information about the integrity of the blood–retinal barrier in the living eye which is not obtainable by other diagnostic means. The blood–retinal barrier in the eye is located in two places: the endothelial cell tight junctions in the retinal vessels and the *zonula adherens* of the retinal pigment epithelial cells. This barrier often breaks down during ocular inflammation and can be observed as fluorescein leakage. The optic nerve can also leak when inflamed and even when it is not swollen and would thus not be apparent on the color images alone.

The eye absorbs most of the light incident upon it and any white material in the vitreous reflects back the intense light used during examination such as that from a photographic flash or ophthalmoscope light in a way that may dazzle the viewer. A better way to determine possible symptoms for the subject is to look a light *emanating* from the eye. This is effectively what happens in fluorescein angiography, where the intense incident blue light is filtered out by the barrier filter in the camera and only the green fluorescent light that originates in the fundus contributes to the image. An example is shown in the accompanying figure. This human patient has asteroid hyalosis or calcium deposits in the vitreous that is so dense it is nearly impossible to make out the retinal details; however, these features are readily apparent on the fluorescein angiogram (Fig. 3.1). From the color picture alone, one might guess that the asteroid hyalosis would be symptomatically devastating. Yet, these patients are virtually symptom free! The fluorescein is therefore a better predictor of how well a similar white drug material would be tolerated by humans.

3.2.11 *Correlation with SD-OCT and Functional (Electrophysiologic) Findings*

Using a combination of testing modalities can help the investigators detect and localize potential drug-related toxic effects early on in preclinical studies. An example of this from clinical medicine is looking for convergence of various testing modalities. In other words, if physicians have a human patient with a puzzling retinal condition, they often employ a combination of anatomic and functional measures which hopefully point to a single diagnosis. Some of these are recently developed and often expensive tests, but fundus photography is nearly always included. A case in point is hydroxychloroquine (Plaquenil®) toxicity. Hydroxychloroquine is used to treat rheumatologic conditions such as rheumatoid arthritis and systemic lupus erythematosus. In patients who are on the drug for many years, retinal (macular) toxicity can develop, which is unfortunately irreversible. Therefore, it is critical to make the diagnosis of toxicity as early as possible. In addition to visual field testing, electrophysiology, and SD-OCT, we also rely on fundus photography to monitor for subtle changes in macular pigmentation.

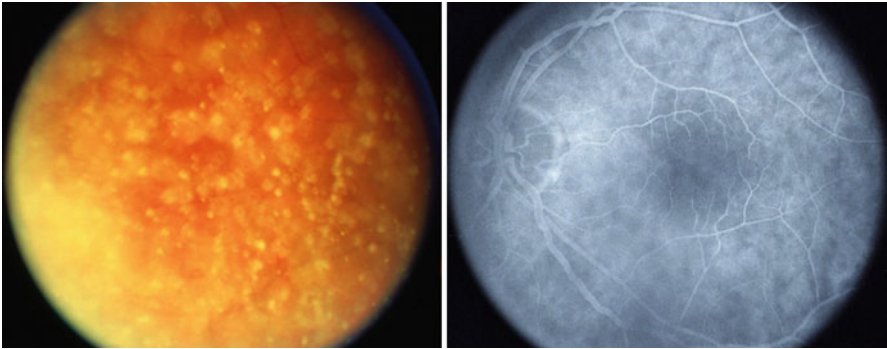


Fig. 3.1 Two images from the same eye of a patient with asteroid hyalosis. The highly reflective calcium deposits in the vitreous obscure retinal details (*left frame*). However, with fluorescein angiography (*right frame*), the light source (i.e., *fluorescing green light*) is the retina itself. So, reflections are avoided and more retinal details are apparent

3.3 Corneal Confocal Microscopy

3.3.1 Basic Principles

Unlike conventional light microscopes, the confocal microscope overcomes the problem of defocused light by using the confocal principle [2]. Light from a pinhole light source is focused by an objective lens onto a tissue specimen. The reflected light is collected by a parallel objective lens and focused onto a second pinhole aperture where it is collected by a detector. Light reflected by the specimen focal point is “co-focused” with the detection aperture and said to be confocal, meaning that the illumination and detection paths share the same focal plane. Light reflected from tissue slightly in front of or behind the specimen focal point is “defocused” and undetected (Fig. 3.2). The confocal design provides high-resolution and superior image contrast (Fig. 3.3). See Guthoff et al. [3], for a review of human clinical applications [3].

3.3.2 Performance Parameters

Corneal confocal microscopy is a useful tool for studying the anatomy of the eye and particularly the cornea [4–9] such as measuring corneal thickness *in vivo* [10, 11] and corneal edema [12].

Based on the morphologic appearance of keratic precipitates, *in vivo* corneal confocal microscopy may aid in the diagnosis of extramammary Paget’s disease [13] and uveitic syndromes including Behçet’s disease [14], and it can be used as an

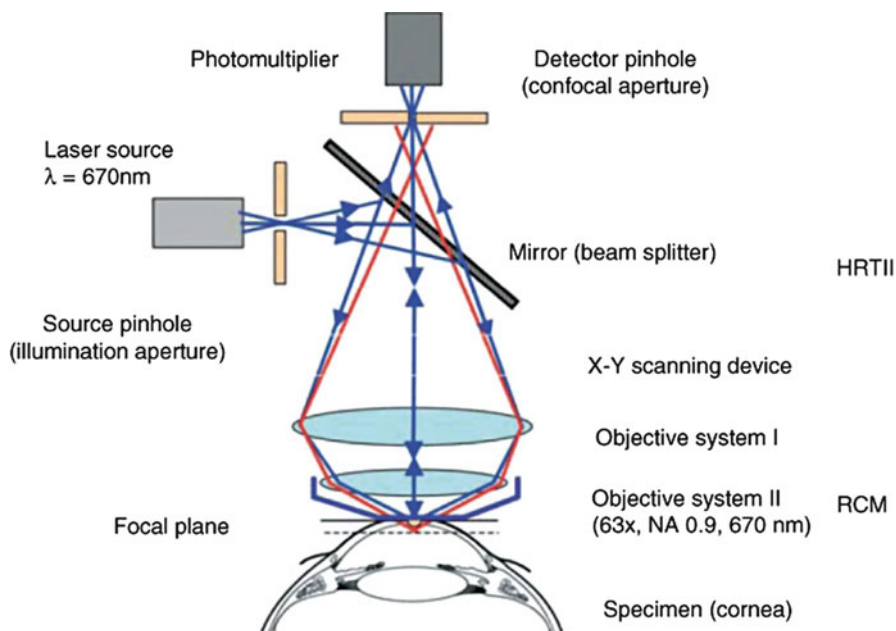


Fig. 3.2 Schematic principle of the confocal arrangement implemented in the HRT-II+RCM system for in vivo confocal microscopy of the cornea. HRT, Heidelberg Retina Tomograph; RCM, Rostock Cornea Module (Guthoff et al. [3]; used with permission)

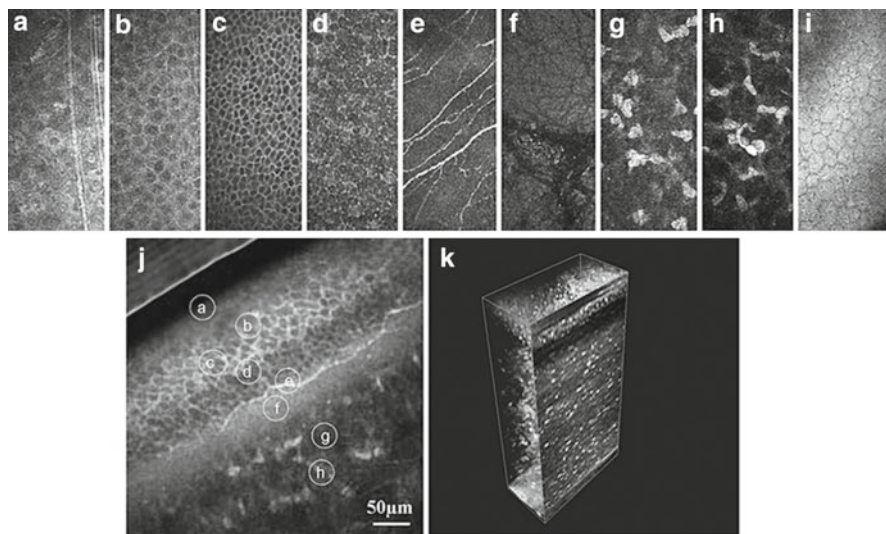


Fig. 3.3 In vivo confocal images of the normal cornea. **(a)** Superficial cells. **(b)** Upper wing cells. **(c)** Low wing cells. **(d)** Basal cells. **(e)** Subbasal nerve plexus. **(f)** Bowman's membrane. **(g)** Anterior stroma. **(h)** Posterior stroma. **(i)** Endothelium. **(j)** Oblique section through corneal epithelium and anterior stroma – all layers are present. **(k)** Three-dimensional (3D) reconstruction of the whole cornea (Guthoff et al. [3]; used with permission)

aid in differentiating infectious from noninfectious uveitis [15]. It has been used to describe the corneal changes associated with mesodermal dysmorphodystrophy (Weill–Marchesani Syndrome) [16] and dry eyes [17]. *In vivo* corneal confocal microscopy can provide high-quality imaging that can be used to identify the pathological characteristics of traumatic ocular events, such as recurrent corneal erosion [18], and describe age-related corneal changes [19] and the appearance of disorders affecting the cornea such as iridocorneal endothelial syndrome [20] and polymorphous dystrophy [21].

Corneal confocal microscopy is increasingly being used for assessing the subbasal corneal nerve plexus in a variety of different pathological conditions including the effects of long-term contact lens wear, keratoconus [22], dry eye syndrome, neurotrophic keratopathy and infectious keratitis, corneal refractive surgery, corneal transplantation [23, 24], and systemic illnesses, such as diabetes mellitus [25, 26], Fuchs heterochromic cyclitis [27], rheumatoid arthritis [28] and nephropathic cystinosis [29]. Laser-scanning corneal confocal microscopy has also been used *ex vivo* to examine postmortem changes of the central and peripheral human corneal nerves [30].

The transplantation of amniotic membrane to the surface of the eye has been used to promote epithelialization in patients with ocular injuries such as chemical burns and corneal ulcers. Corneal confocal microscopy enables visualization of the corneal epithelium despite the presence of the amniotic membrane [31].

3.3.3 Use in Animal Toxicology and Other Ocular Research

As is the case with most medical instruments, corneal confocal microscopy was primarily developed for and has its most common use in the diagnosis and monitoring of human disease. However, just like the other imaging and analytic techniques discussed in this chapter, corneal confocal microscopy has proven to be useful in animal toxicologic as well as basic research studies. For example, it has been used in several veterinary and toxicologic applications including corneal examination of horses, dogs, cats, and birds [32–35]. A murine model of endotoxin-induced uveitis has been used to study the changes in corneal endothelium to better understand the mechanism of keratic precipitate formation [36]. *In vivo* corneal confocal microscopy was performed after lipopolysaccharide injection in rats. Corneal confocal microscopy images were compared with *ex vivo* corneal endothelium immunostaining and showed numerous round hyperreflective dots on the corneal endothelium, anterior chamber, and anterior stroma. Based on this animal study, *in vivo* corneal confocal may be useful clinically for analyzing keratic precipitates and other corneal changes in patients with uveitis.

The rabbit cornea is well suited to toxicologic, surgical, and device (e.g., contact lens) studies because its size is close to that of the human cornea [37, 38]. Some of the many toxicologic studies using corneal confocal microscopy in rabbit are listed in the reference section [39–45]. Good correlation has been found in rabbit between

in vivo imaging with the corneal confocal microscope and in vitro histologic findings [46]. Wound healing [47, 48] and device [49] studies in rabbit have also made use of the corneal confocal microscope.

Other animal models have also been employed. A study of corneal cosmetic pigmentation in chickens (with potential applications for blind, unsightly human eyes, such as occurs after severe trauma) used corneal confocal microscopy to localize the pigment and assess the surrounding cornea for signs of degeneration and inflammation [50]. In a nonhuman primate study, the safety and efficacy of a topical antibiotic (levofloxacin) following penetrating keratoplasty was monitored with the corneal confocal microscope, and it was determined that the keratocyte structure and stromal organization remained intact [51].

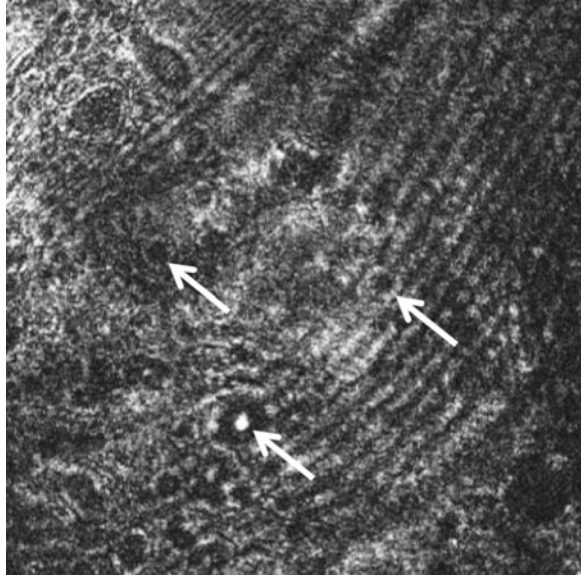
3.3.4 Human Clinical Applications

In the clinic, one of the most important applications for corneal confocal microscopy is to help in the diagnosis of certain infectious processes. Bacteria are too small to be readily identified by *in vivo* microscopy. Fortunately, most bacteria that affect human ocular health can be quickly and inexpensively identified by standard culture methods. More problematic are amoebic and fungal keratitis, both of which are chronic conditions that can masquerade as other pathologies. Furthermore, amoebae and fungi are difficult to culture, often requiring weeks before a definitive diagnosis can be made. Culturing the cornea is an invasive procedure, and the results can vary depending on the skill of the surgeon; however, characteristic morphologic features of amoebae (Fig. 3.4) [52–54] as well as fungal hyphae [55, 56] can be quickly identified with corneal confocal microscopy. The results are immediate, and the sensitivity and specificity profiles are comparable to those of traditional microbiologic culturing [57].

Corneal confocal microscopy was used to determine if patients with dry eye experience changes in corneal nerves and corneal sensation [58]. The epithelium, stroma, and subbasal corneal nerves were evaluated with a corneal confocal microscope. Mechanical, chemical, and thermal sensations were evaluated using a non-contact esthesiometer. A significant decrease in the number and density of subbasal nerves and the density of superficial epithelial cells was observed in patients with dry eyes. The number and density of subbasal nerves was higher in younger patients. A significant decrease was found with respect to mechanical, chemical, and thermal sensitivity which was strongly correlated with the density of subbasal nerves.

Corneal confocal microscopy was also used to investigate the ocular toxicity of an oral antineoplastic drug containing a 5-fluorouracil prodrug by evaluating treated patients using laser-scanning corneal confocal microscopy [59]. Slit-lamp examination revealed epithelial invasion toward the center of the cornea in all examined eyes. *In vivo* corneal confocal microscopy revealed changes the corneal epithelium structure with abnormal epithelial cells and inflammation. Cytologic diagnosis

Fig. 3.4 Corneal confocal microscopic image taken with the HRT Rostock Cornea Module (Heidelberg Engineering) of a human corneal ulcer caused by *Acanthamoeba*. Double-walled trophozoites are apparent (*upper arrows*) as is a highly reflective cyst (*lower arrow*). The cysts can be up to 20 μm in diameter (Courtesy of Sarah M. Nehls, MD, University of Wisconsin School of Medicine and Public Health)



showed moderate dysplasia in one specimen. Hematoxylin and eosin staining revealed that abnormal corneal epithelial sheets lacked the stratified structure of normal epithelium. It was concluded that the oral antineoplastic drug can induce ocular mucositis with dysplasia of the corneal epithelium.

In vivo corneal confocal microscopy has been used to describe the clinical effects of human herpes simplex virus keratitis [60]. Endothelial alterations characteristic of endotheliitis were observed including pseudoguttata, enlarged intercellular gaps, infiltration of inflammatory cells into the endothelial layer, loss of defined cell boundaries, spotlike holes, and endothelial denudation. Although endotheliitis-specific alterations appear to resolve, the corneal endothelium remained irreversibly damaged in some patients.

In patients with nephropathic cystinosis, corneal confocal microscopy has been used to describe the presence of randomly oriented spindle, needle-shaped, and fusiform hyperreflective crystals in all corneal layers except the endothelium with the greatest density observed in the anterior stroma [29]. When used to assess the conjunctival epithelial characteristics in untreated ocular hypertension and in topically treated primary open-angle glaucoma, corneal confocal microscopy revealed the presence of conjunctival microcysts in all hypertensive and glaucomatous eyes [61]. The conjunctiva may therefore be useful for noninvasive assessments of glaucoma pathology.

In one study, *in vivo* corneal confocal microscopy was used to correlate corneal microstructure and recovery of the subbasal nerve plexus following cornea transplantation [62]. Corneas from 42 patients undergoing penetrating keratoplasty were

assessed with laser scanning *in vivo* corneal confocal microscopy and compared with 30 normal controls. After an average of 85 months, significant observations included reductions in epithelial, keratocyte, and endothelial cell densities. There were also significant reductions in sub-basal nerve fiber density and nerve branching. Endothelial cell density decreased with increasing time after surgery, while nerve fiber density increased. Corneal transplantation for keratoconus was associated with higher sub-basal nerve fiber densities than other indications. Neither nerve fiber nor cell density was correlated with improved visual acuity. *In vivo* corneal confocal microscopy revealed substantial reductions in cell density at every level of the transplanted cornea.

3.3.5 *Commercially Available Devices*

Available units:

HRT Rostock Cornea Module (Heidelberg Engineering, Heidelberg, Germany)
(<http://www.heidelbergengineering.com/us/products/hrt-glaucoma-module/cornea-module/>)

Confoscan 4 (Nidek Technologies, Padova, Italy)
(<http://www.nidektechnologies.it/ProductsCS4TechnicalReview.htm>)

3.3.6 *Considerations for Ocular Toxicology Studies*

As a noninvasive way of determining corneal architecture at the cellular level, corneal confocal microscopy is ideally suited to long-term toxicologic studies. Being able to assess corneal health *in vivo* rather than having to rely only on postmortem histopathology can greatly reduce the total number of animals needed since numerous time points can be monitored in each animal.

The Rostock Cornea Module is an add-on to the Heidelberg Retinal Tomograph (HRT). As such, it may be more economical to consider the combination as opposed to separate confocal and scanning laser units.

3.3.7 *Limitations and Caveats*

Even though it is possible to image corneal endothelial cells with the corneal confocal microscope, a dedicated specular microscope with associated image analysis software will image and analyze a wider field with greater numbers of cells [63].

3.4 Specular Photomicroscopy

3.4.1 Basic Principles

Clinical specular microscopes provide a high magnification view of specular reflected light from the corneal endothelium. The specular reflex occurs at the interface of two materials with sufficiently different refractive indices. For example, endothelial cells can be imaged because their refractive index is greater than the adjacent aqueous humor, resulting in reflected light (Fig. 3.5). For a comprehensive review, see McCarey et al. [64].

This imaging technique has been shown to produce highly consistent results [65, 66]. Imaging of the endothelial cells with subsequent analysis of their density and morphology is considered an important endpoint in studies involving therapeutic agents or devices applied to the ocular surface that could impact endothelial function and survival as well as safety assessment of devices implanted into the anterior segment of the eye. Specular imaging is complimentary with the performance of corneal pachymetry (measurement of corneal thickness) that provides an indication of overall corneal endothelial cell health as reflected by their ability to maintain the relatively dehydrated state of the corneal stroma through their pumping action.

3.4.2 Performance Parameters

Specular microscopy is used for *in vivo* imaging and assessing the morphology of the corneal endothelium [67, 68] and central corneal thickness in patients with glaucoma [69] and keratoconus [70] and also following endothelial keratoplasty [71, 72]. Other applications include detecting corneal ectasia following laser *in situ* keratomileusis [73–75], determining central corneal endothelial cell density [76, 77] and endothelial vacuole formation in donor corneas [78].

3.4.3 Use in Animal Toxicology and Other Ocular Research

A sustained increase in intraocular pressure is known to result in the loss of corneal endothelial cells and cause increased corneal thickness. These effects have been documented in monkeys which are commonly used as a model of human glaucoma [79]. One study examined male rhesus monkeys with chronic argon laser-induced ocular hypertension in one eye. Using a noncontact specular microscope, mean central corneal thickness in the hypertensive and normal eyes were similar. A significant loss of endothelial cells was observed in the center of the cornea of laser-treated eyes. Endothelial cell density was inversely related to the duration of intraocular pressure elevation.

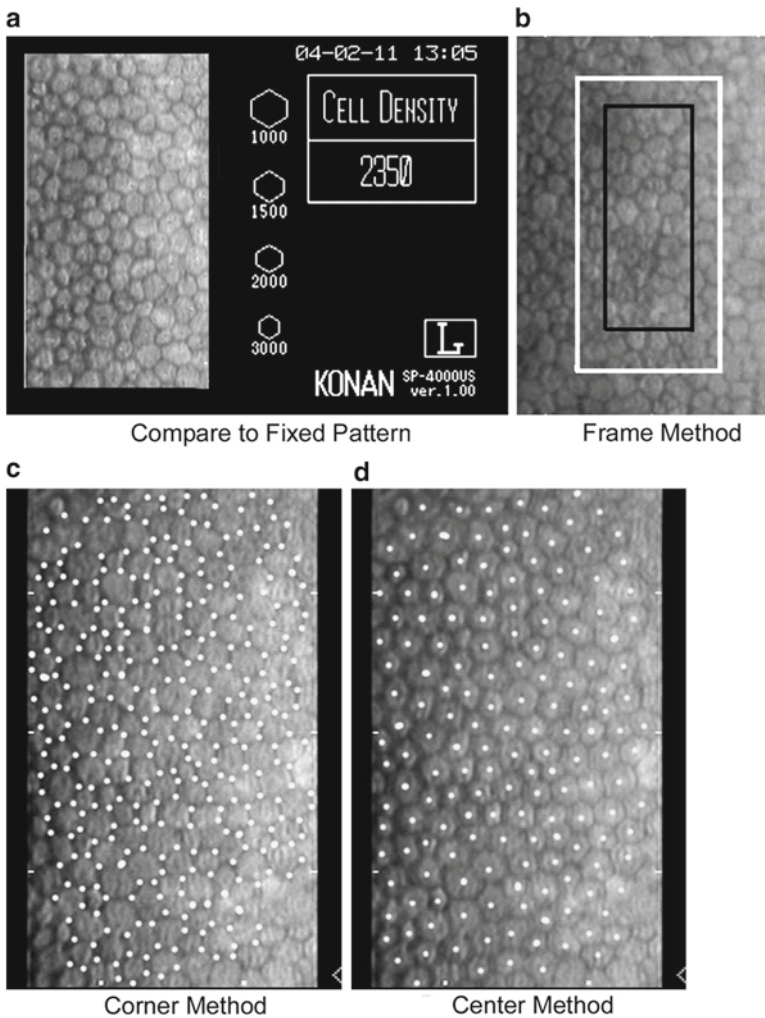


Fig. 3.5 There are four techniques to analyze endothelial cell images: (a) Compare relative cell size to standards, (b) count cells within a predetermined fixed frame with the frame size significantly affecting accuracy, (c) an algorithm using inputted cell corners, and (d) an algorithm using inputted cell centers (McCarey et al. [64]; used with permission)

Other studies using specular microscopy have established the similarity of the normal canine corneal endothelium and that of humans [80, 81]. In one study, spectral microscopy was used to determine the density and morphology of endothelial cells in cynomolgus monkey, dog, and rabbit [82]. All three species in this study had similar endothelial cell morphologies and densities (Figs. 3.6 and 3.7). Furthermore, the endothelial cell densities, as determined by a noncontact spectral microscope, were in statistical agreement with a contact spectral microscope in the rabbit.

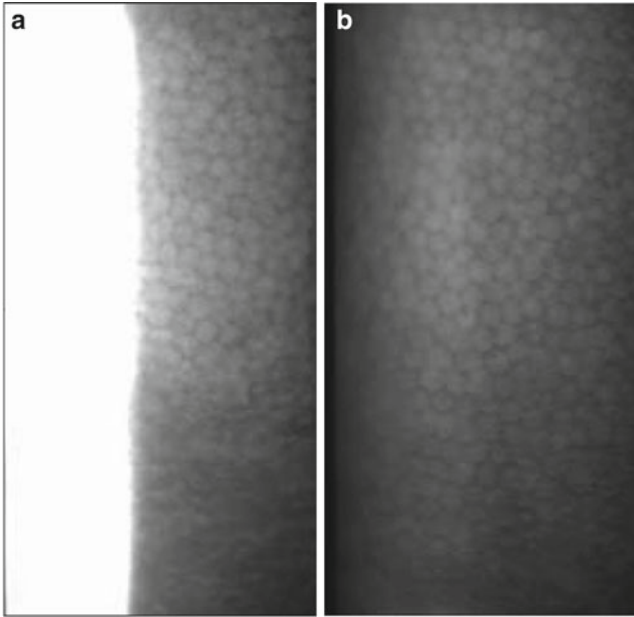


Fig. 3.6 Representative noncontact specular microscopic images of cynomolgus monkey endothelium without (a) and with (b) a plano contact lens on the cornea. Note the use of a plano contact lens on the cynomolgus monkey cornea provides a full-screen image (Miller et al. [82]; used with permission)

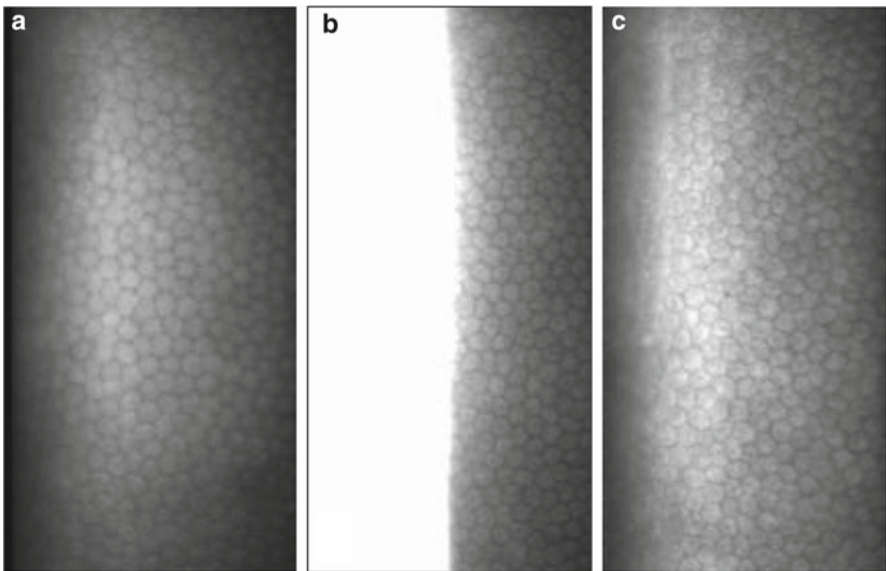


Fig. 3.7 Representative noncontact spectral microscopic images of monkey (with plano contact lens) (a), rabbit (b), and dog (c) endothelium. The morphology and density of the endothelial cells are similar amongst the three species (Miller et al. [82]; used with permission)

The endothelial cell densities in rabbit were also similar to that found by *ex vivo* analysis of the corneas stained with alizarin red.

3.4.4 Human Clinical Applications

Specular microscopy is a noninvasive means for clinically measuring changes in the corneal endothelial cell layer caused by aging, ocular surgical procedures such as LASIK [75, 83] and following the application of pharmacological agents [64].

3.4.5 Commercially Available Devices

3.4.5.1 Contact Specular Microscopes

Available units:

Tomey EM-3000™, Tomey USA, Phoenix, AZ
(http://www.tomeyusa.com/products_EM3000.html)
HAI CL-1000xyz™, HAI Labs, Lexington, AZ
(<http://www.hailabs.com/products/specular/clinical/#cl-1000xyz>)

3.4.5.2 Noncontact Specular Microscopes

Available units:

CellCheck XL™, Konan Medical USA, Inc., Irvine, CA
(<http://www.konan-usa.com>)
HAI CL-1000nc™, HAI Labs, Lexington, AZ
(<http://www.hailabs.com/products/specular/clinical/#cl-1000nc>)

3.4.6 Considerations for Ocular Toxicology Studies

Contact as well as noncontact specular microscopes are available. The contact instruments require topical anesthetic in conscious human patients and are more uncomfortable than noncontact testing. They have the advantage that they flatten the cornea somewhat, which permits a greater field of view that is possible with the noncontact instruments. In the hands of an unskilled operator, corneal abrasion caused by the contact lens is a possibility.

Consistent data can be generated with either contact or noncontact devices; however, there is poor agreement between the two. Thus, the instruments cannot be used interchangeably [84].

Operator experience is critical in obtaining reliable data. Well-defined criteria need to be established for training purposes in acquiring and analyzing images [64].

3.4.7 Limitations and Caveats

Both specular and corneal confocal microscopy are capable of measuring corneal thickness as well as endothelial cell morphology and density; however, each instrument has its own advantages and limitations. The corneal confocal microscope can look at all layers of the cornea and is especially good for certain types of infectious and toxicologic pathologies (see Sect. 3.3); however, specular microscopy has the advantage that it looks at a larger number of endothelial cells. Salvetat et al. [63] found that the confocal microscope (HRT Rostock Cornea Module™, Heidelberg Engineering) significantly underestimated the endothelial cell density in eyes with reduced cell density and overestimated the endothelial cell density in eyes with high cell density compared to the Tomey EM-3000™ (Tomey, USA).

3.5 Scheimpflug Imaging

3.5.1 Basic Principles

Scheimpflug imaging is based on the Scheimpflug principle which describes the orientation of a camera focus plane when the plane of the lens and the plane of the image are not parallel. Using a slit illumination system, a thin layer of the eye is illuminated. This sectional image is photographed from the side view by a rotating Scheimpflug camera. By repeating the process, a series of radially oriented images of the anterior eye chamber can be generated. Analysis of the sectional images can detect tissue boundaries and layers such as anterior and posterior corneal surfaces, iris, and crystalline lens. The stored sectional images can be used to create a 3-dimensional model of the entire anterior eye chamber (Figs. 3.8 and 3.9). For reviews, see Wegener et al. (2009), and Rosales et al. (2009) [85, 86].

3.5.2 Performance Parameters

The Scheimpflug imaging system can be used to measure the shape of the cornea [87] and for objectively assessing lens and cataract changes when used together with lens densitometry [88]. Following cataract surgery, Scheimpflug tomograms are used to measure intraocular lens tilt and decentration [89] and quantify posterior

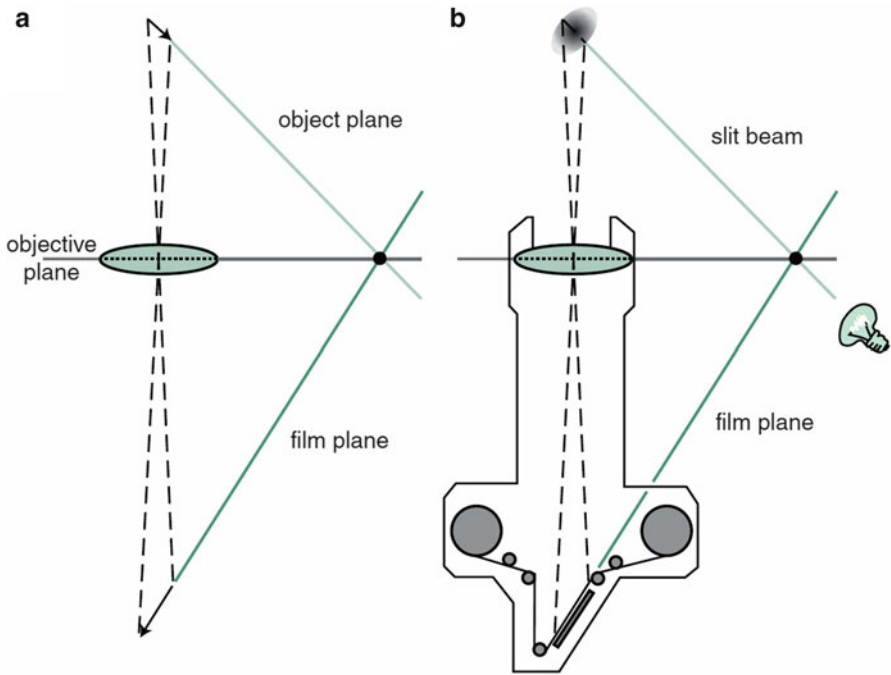


Fig. 3.8 The Scheimpflug principle: (a) geometric conditions of the principle, and (b) optical design of the first Scheimpflug camera (Wegener et al. [86]; used with permission) [85]

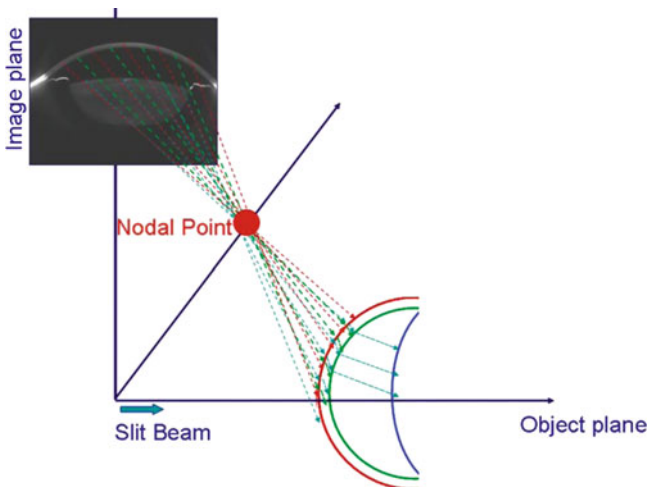
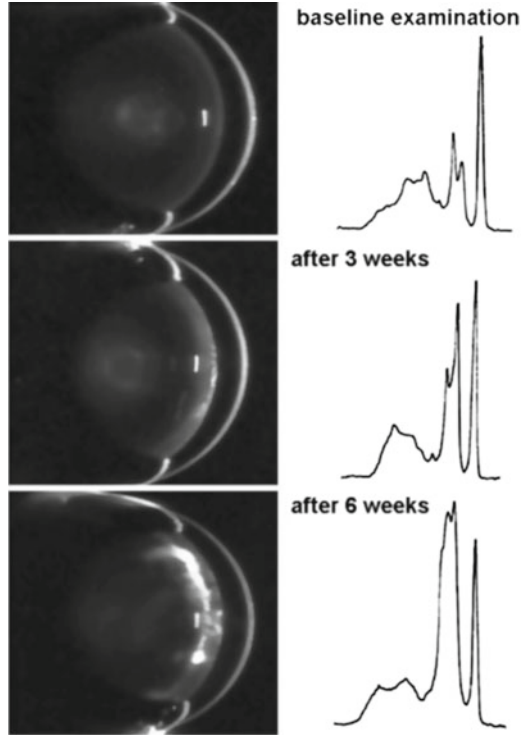


Fig. 3.9 Schematic illustration of the sequential ray tracing through the nodal point of the camera lens performed to correct the optical distortion caused by the ocular components (posterior cornea by the anterior cornea, anterior lens by the anterior and posterior cornea, and posterior lens by anterior and posterior cornea and anterior lens) (Rosales et al. [85]; used with permission) [86]

Fig. 3.10 Series of Scheimpflug images from a rat lens documenting the development of a diabetic cataract. The densitograms on the right show growth of the lens peak (second from the right) over time (Wegener et al. [86]; used with permission)



capsule [90]. Scheimpflug imaging can also measure intraocular lens central optic thickness to determine intraocular lens power [91].

Measuring posterior corneal elevation using the Scheimpflug system is an effective means for distinguishing keratoconus from normal corneas but is less effective for identifying subclinical keratoconus [92]. Scheimpflug imaging has been used to diagnose anterior lenticonus [93], a rare congenital condition which causes part of the crystalline lens capsule and underlying cortex to bulge anteriorly resulting in severe myopia and lenticular irregular astigmatism.

Scheimpflug imaging is also a means for precise localization of retained intraocular foreign bodies [94]. As such, it may prove to be useful in toxicity and efficacy animal studies utilizing intravitreal sustained-release drug implants.

3.5.3 Use in Animal Toxicology and Other Ocular Research

Scheimpflug imaging and the associated quantitative densitometry are valuable adjuncts for assessing the cornea and lens in toxicology studies. For example, in animal toxicity models, lens changes including subclinical ones have been detected and the change in density of light scattering measured (Fig. 3.10) [95–98]. Other

ocular research includes detailed studies of the accommodative mechanisms of the lens and ciliary muscle in rhesus monkeys in order to better understand presbyopia, or loss of near vision with aging in humans (Fig. 3.11) [99–101] (see also Sect. 3.6). As part of the studies on accommodation, Scheimpflug videography has also been developed as a research tool [102].

3.5.4 Human Clinical Applications

Scheimpflug imaging can aid in the diagnosis of subclinical and clinical keratoconus, a degenerative corneal disease characterized by stromal thinning and conical ectasia [103]. Higher levels of vertical coma, primary coma, and coma-like aberrations are present in keratoconic eyes compared to normal eyes [104]. Corneal collagen cross-linking with riboflavin and ultraviolet-A light has been proposed as a treatment for progressive keratoconus. Following treatment, assessment of corneal curvature, elevation, and thickness using Scheimpflug imaging showed visual acuity, and corneal measures remained unchanged, indicating that keratoconus had not progressed [105].

The ocular symptoms of diabetes mellitus include blurred vision, and Scheimpflug imaging has been used to examine changes in ocular refraction and geometry in patients with diabetes [106]. During episodes of hyperglycemia, small hyperopic and myopic shifts of equivalent refractive error were observed; however, there were no significant changes in the shape of the cornea or lens in any patient and no correlations between changes in blood glucose levels and any measured ocular parameters. These results suggest that subjective symptoms of blurred vision during hyperglycemia are not caused by changes in the refractive properties of the diabetic eye.

3.5.5 Commercially Available Devices

Available units:

Pentacam®, Pentacam® HR, Oculus Inc., Lynnwood, WA
(<http://www.pentacam.com>)
Galilei G2, Ziemer Group, Port, Switzerland
(<http://www.ziemergroup.com/products/g2-main.html>)

3.5.6 Considerations for Ocular Toxicology Studies

Excellent pupillary dilation is critical. Some research studies looking at the peripheral anterior structures have used iridectomized animals [99]. Applications for toxicology include the ability to document changes in the geometry of the crystalline

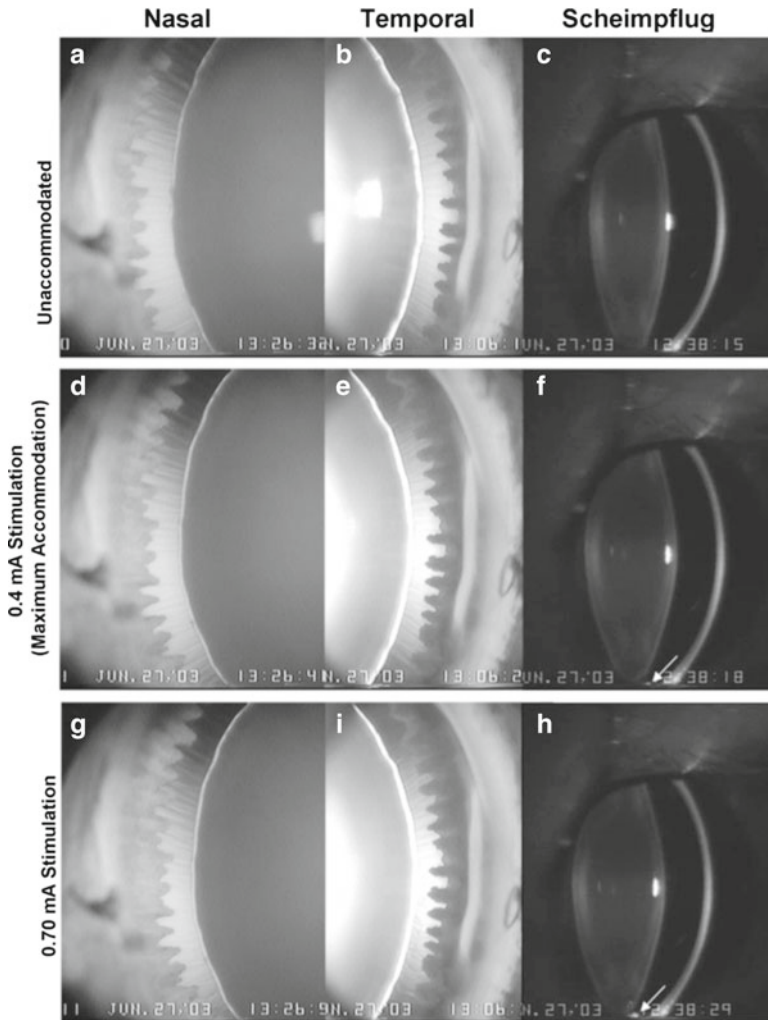


Fig. 3.11 Goniovideography images showing the nasal and temporal quadrants of a 14-year-old rhesus monkey eye in the nonaccommodated state (**a**, **b**) and during maximal (**d**, **e**) and 0.70-mA (**g**, **i**) stimulation. The numbers represent the stimulus current in milliamperes (mA). The zonular fibers appeared taut when the eye was nonaccommodated (**a**, **b**). The lens did not move downward pronouncedly within the eye during accommodation. The circumlental space in both quadrants in the nonaccommodated state was similar superiorly and inferiorly and remained fairly uniform during maximum accommodation. During supramaximal stimulation, the zonular fibers in the accommodated state were more relaxed inferiorly than superiorly but were not oriented predominantly in a downward direction, as in Figure 2 F (Movie 1, <http://www.iovs.org/cgi/content/full/47/3/1087/DC1>). Scheimpflug images show the anterior segment in the nonaccommodated (**c**) state and during maximal (**f**) and 0.70-mA (**h**) stimulation. The inferior ciliary processes (*arrow*) came into view during maximal stimulation (**f**) and touched the inferior lens during the 0.70-mA stimulation (**h**) (Croft et al. [99]; used with permission)

lens and anterior chamber. High-resolution images may be suitable for imaging intracorneal pathologies lens opacities. Scheimpflug imaging may also be useful in monitoring the position of intraocular hardware such as intraocular lenses and pharmaceutical implants.

3.5.7 Limitations and Caveats

Studies with normal volunteers have demonstrated that Scheimpflug imaging results of corneal curvature and anterior chamber measurements [107] and corneal thickness [108] are highly repeatable and the application of geometrical and optical distortion correction algorithms can improve the accuracy of the measurements [89]. When applied to a range of patients, central corneal thickness measures from Scheimpflug, ultrasound and noncontact specular microscopy methods were well-correlated; however, Scheimpflug measures indicate small but significantly greater thicknesses than noncontact specular microscopy or ultrasound [69]. In that study, intraocular pressure was significantly correlated with central corneal thickness measured with noncontact specular microscopy and ultrasound but not the Scheimpflug system.

For measuring central corneal thickness, the results obtained with the Scheimpflug system are similar to those obtained with optical low-coherence reflectometer and ultrasound pachymeters [109] and show better agreement than scanning-slit topography following photorefractive keratectomy [110]; however, central corneal thickness measurements obtained using ultrasound pachymetry were significantly higher than a Scheimpflug camera system and anterior segment optical coherence tomography following laser keratomileusis [111].

The software available with commercial units allows for quantitative assessment of lens opacification in animals and may prove useful for noninvasive quantification of the progression of a cataractous process induced by a test material or implanted device. While testing this in the laboratory, we found it to be more applicable to non-rodent species that have larger anterior segments.

3.6 Ultrasound Biomicroscopy

3.6.1 Basic Principles

Ultrasonography is the workhorse of medical diagnostics in many fields, including ophthalmology. It has the advantage of producing images of internal organs in a noninvasive and nontoxic manner. High-frequency sound waves are generated by a transducer. The reflected waves or echoes are then detected by the same transducer. Timing of the reflected waves generally correlates with distance (an exception is

when internal reflections or “ringing” occurs, as may be caused by a metal foreign body). A computer is used to produce a graph of reflection time vs. intensity (known as an “A scan”). By rapidly sweeping the probe along a plane, the computer can produce a 2-dimensional cross-sectional image showing distances along an *X* and *Y* axis. An additional *Z* axis illustrates the intensity of the reflected waves, the so-called B scan.

Traditionally, the sound frequency in ocular applications has been limited to 10 MHz, which permits detection of structures in the posterior segment of the eye, such as the vitreous, retinal, optic nerve, and orbit. It is particularly useful when media opacities prevent an adequate clinical exam. Beyond simple anatomic identification, the reflected ultrasonic waves give information about tissue density that is often critical in discriminating between tumor types.

More recently, higher ultrasonic frequencies of 12.5–50 MHz [112] and improved computing processing power have been employed to produce image resolutions that rival those of the light microscope. Such imaging is referred to as ultrasound biomicroscopy.

3.6.2 Performance Parameters

Ultrasound biomicroscopy systems are used for imaging the anatomy and pathology of the entire anterior segment including the cornea, iridocorneal angle, anterior chamber, iris, ciliary body, and lens. Consequently, ultrasound biomicroscopy can be used for the diagnosis of glaucoma and diagnostic imaging of ocular cysts and neoplasms [113] and to measure anterior segment parameters including central corneal thickness and anterior chamber depth peripheral iridocorneal angles [114]. It can also be used for evaluating traumatic injury and foreign bodies of the eye and ocular conditions such as siderosis bulbi caused by retained intraocular iron-containing foreign bodies [115].

In addition to diagnosing primary angle-closure glaucoma, ultrasound biomicroscopy can also determine the presence of plateau iris which is a non-pupil blocking cause of glaucoma [116]. In one case report, ultrasound biomicroscopy was used to diagnose pupillary block glaucoma secondary to device remnants remaining in the posterior chamber following phakic intraocular lens implantation [117].

Ultrasound biomicroscopy imaging has several presurgical applications. Prior to phakic intraocular lens implantation, ultrasound biomicroscopy can be used to measure intraocular structures [118] and corneal curvature [119] to improve the accuracy of intraocular lens sizing. Ultrasound biomicroscopy can provide detailed *in vivo*, imaging of primary iris melanoma which may aid in total surgical removal [120] and improved visualization and management of retinoblastoma [121] and determine vertical rectus muscle position prior to surgery [122].

In patients with acute anterior uveitis, ultrasound biomicroscopy can be used to observe severe inflammatory changes including large number of cells in the anterior and posterior chambers, marked edema and exudates in and around the iris and

ciliary body [123]. In patients with unilateral exfoliation syndrome, zonular status in fellow eyes can be assessed prior to cataract extraction may serve as an aid in surgical planning [124].

Ultrasound biomicroscopy has also been used to evaluate the value of cryotherapy for preventing postoperative fibrovascular ingrowth of the anterior retina and sclerotomy sites and recurrent vitreous hemorrhage in patients undergoing pars plana vitrectomy for the treatment of proliferative diabetic retinopathy [125].

3.6.3 Use in Animal Toxicology and Other Ocular Research

Ultrasound biomicroscopy imaging has been used to determine the effect of mydriasis on the anterior segment in healthy dogs following the topical application of 0.5% tropicamide [126]. The result was an increase in the geometric iridocorneal angle and a decrease in the opening of the ciliary cleft, without any effect on the width of the mid-ciliary cleft, on the length of the ciliary cleft, or on the anterior chamber depth. It was concluded that topical tropicamide-induced mydriasis results in changes in the anterior segment which may influence the drainage of aqueous humor.

Ultrasound biomicroscopy imaging was also used to compare two rodent models of glaucoma. One eye of each animal in one strain of rats was treated with episcleral vein cauterization and the other strain with hypertonic saline episcleral vein sclerosis [127]. Eyes treated with episcleral vein cauterization developed higher intraocular pressure than hypertonic saline episcleral vein sclerosis-treated eyes. For all parameters, episcleral vein sclerosis-treated eyes cauterization did not differ significantly from control eyes, while experimental eyes in the hypertonic saline episcleral vein sclerosis group had larger anterior chamber depths and smaller ciliary body areas than control eyes which was found to correlate well with intraocular pressure.

In humans, changes in the angle opening distance following cataract surgery may be clinically useful for evaluating and treating eyes with angle-closure glaucoma or occluded angles. In an animal study, ultrasound biomicroscopy was used to compare the iridocorneal angle and angle opening distance in dogs with and without cataracts [128]. Dogs with cataracts were evaluated for postoperative ocular hypertension with the iridocorneal angle, angle opening distance, and postoperative anterior chamber debris. Dogs with larger presurgical iridocorneal angle and angle opening distance measurements were found to be at greater risk for postoperative ocular hypertension.

Ultrasound biomicroscopy has been employed in rhesus monkeys for studying accommodation, the process by which the eye focuses on near objects. The ciliary muscle is a sphincter muscle inside the eye that suspends the lens via threadlike structures called zonula. During accommodation, the ciliary muscle contracts and moves forward and inward to relax tension via the zonula to the lens. The lens then thickens allowing the eye to focus on nearby objects. With age, the ability to accommodate is lost (presbyopia). Ultrasound biomicroscopy permits detailed and dynamic imaging of the accommodative apparatus in the living eye (Fig. 3.12)

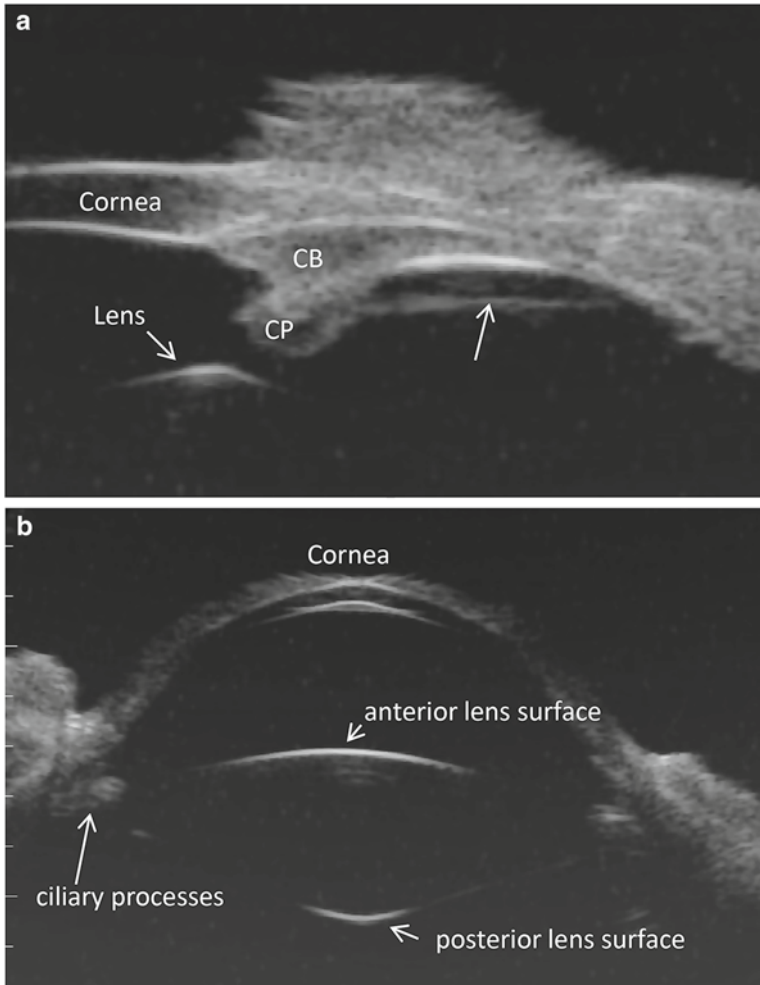


Fig. 3.12 Panel **A**. Ultrasound biomicroscopic overview image in a live rhesus monkey shows a prominent straight line (*arrow*) extending from the pars plicata region of the ciliary body to the ora serrata region separated from the pars plana epithelium by a cleft. *CP* ciliary processes, *CB* ciliary body (Lütjen-Drecoll et al. [129]; used with permission). Panel **B**. Ultrasound biomicroscopic overview image shows the anterior segment in a live young rhesus monkey

[129, 130] as well as other intraocular structures for various scientific studies, such as the study of presbyopia [99, 129, 131]. With new imaging techniques (i.e., high-resolution ultrasound), these events can now be imaged in real time (<http://www.iovs.org/cgi/content/full/51/3/1554/DC1>) [129]. Measurements of the various accommodative structures can be obtained to characterize age-related changes in the eye (Fig. 3.13). In addition, various surgical procedures to disrupt the accommodative apparatus are being employed to further elucidate the mechanisms

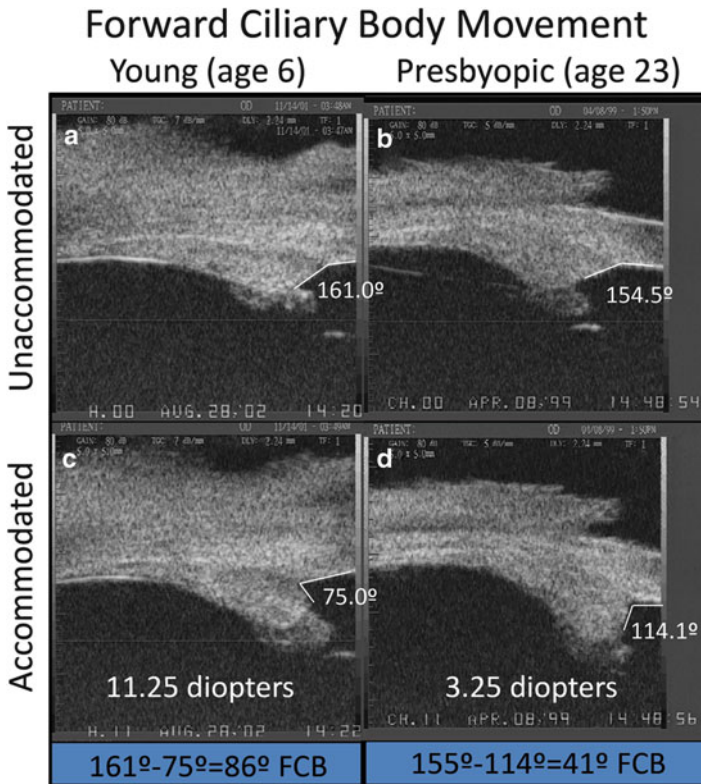


Fig. 3.13 Ultrasound biomicroscopy images of two normal monkey eyes, aged 6 years (A, C) and 23 years (B, D), in the unaccommodated and accommodated states. The change in angle between the anterior aspect of the ciliary body and the inner aspect of the cornea during supramaximal central stimulation was used as a surrogate indicator of forward ciliary body movement (Panels B and D adapted from Croft et al. [99]; used with permission) (Panels A and C adapted from Croft et al. [130]; used with permission)

involved. Ultrasound biomicroscopy plays a key role in this effort (<http://www.iovs.org/cgi/content/full/49/12/5495/DC1>) [131].

3.6.4 Human Clinical Applications

Ultrasound biomicroscopy has been used in clinical trials which compared the effectiveness of different surgical procedures, such as the use of *ab interno* and *ab externo* scleral fixation of posterior chamber intraocular lenses [132].

Changes in anterior segment structures during accommodative stimuli following monofocal intraocular lens implantation were measured using ultrasound

biomicroscopy [133]. Measured parameters included anterior chamber depth, iris/zonule distance, anterior chamber angle, scleral/ciliary process angle, and iris/ciliary process angle. All parameters except the horizontal iris/ciliary process distance and vertical anterior chamber angle and horizontal anterior chamber angle showed significant change during accommodation. An anterior shift of the intraocular lens/capsular bag ciliary processes/sulcus/zonular iris complex was observed. A simultaneous centripetal shift of ciliary bodies and processes was also observed as indicated by a sulcus and capsular bag diameter reduction.

Pigmentary glaucoma is a secondary type of open-angle glaucoma caused by pigment accumulation in the in the trabecular meshwork. Pigment dispersion syndrome is similar but with no evidence of glaucoma. Ultrasound biomicroscopy measured and compared different iridocorneal parameters in eyes affected by pigment dispersion syndrome or pigmentary glaucoma with matched controls [134]. The following parameters were assessed in relaxed and stimulated accommodative state: iris–lens contact, iridocorneal angle, and iris concavity. All ultrasound biomicroscopic parameters showed significant intergroup differences. Iridocorneal angle was the best-performing parameter followed by iris concavity, both in near vision. Receiver operating characteristic (ROC) analysis showed iridocorneal angle and iris–lens contact in near vision to be the most discriminatory parameters. These findings established that iris movement is important in inducing the clinical features of pigment dispersion syndrome and pigmentary glaucoma.

3.6.5 Commercially Available Devices

Available units:

Reflex Ultrasound Bio-Microscope. Reichert Technologies, Depew, NY
(http://www.reichert.com/product_details.cfm?skuId=3006&skuTk=1042101943)
Eye Cubed, Ellex Medical Pty. Ltd., Adelaide, Australia
(<http://www.ellex.com/corp/products/diagnostic-ultrasound/eye-cubed>)

3.6.6 Considerations for Ocular Toxicology Studies

As with any sophisticated measurement instrument, proper operation and consistent data collection require a skilled and experienced operator. Low-frequency devices are available and used routinely in the clinic for relatively straightforward, subjective diagnosis of posterior segment problems such as retinal detachment and ocular tumors; however, the demands of research and ocular toxicologic studies require an understanding of the challenges involved.

Software that is provided by the manufacturer for clinical applications may not be suitable for research. Often greater flexibility is needed to permit off-loading of raw data for recording and image analysis.

3.6.7 Limitations and Caveats

Ultrasonic frequency needs to be chosen to meet the needs of a given study. Higher frequencies result in higher anatomic resolution but also require more time to set up since they must be used with a water bath. Depth of penetration of the sound has an inverse relation to its frequency and thus its resolution. Consequently, detailed ultrasound biomicroscopic images of the retina are not possible in the eyes of large animals or humans.

Preparing an animal for ultrasound biomicroscopy can also be a challenge. A water bath is essential, but the standard eyecup used for humans is inadequate for animals since in most species, the eye is too small and/or the available exposed sclera is limited. The animal needs to be anesthetized and the head position stabilized by an appropriate and often custom-made head holder. The eye is pointed upward and draped with a clear adhesive (Steri-Drape™; 3M Corporation, St. Paul, MN). To create a watertight seal around an animal eye, the fur may need to be trimmed and an additional adhesive such as collodion or benzoin is applied to the skin. A ring stand is a useful means of supporting the Steri-Drape to create a small pool of saline or other appropriate acoustic coupling solution.

A distinct advantage of ultrasound biomicroscopy is the power of the technique not just to see structures but to visualize and quantify their movements in real time for a better understanding of normal physiology, pathophysiology of disease, and device performance.

3.7 Laser Flare-Cell Meter

3.7.1 Basic Principles

The laser flare-cell meter is a noninvasive method for the *in vivo* measurement of aqueous flare (and/or cells) using the principle of laser light scattering detection. The instrument uses a diode laser beam that is projected inside the anterior chamber of the eye. Light scattering occurs as aqueous protein components of inflammation (commonly referred to as “flare”) pass through the focal point of the laser. The intensity of the scattered light is directly proportional to the amount of protein particles present which is detected by a photomultiplier tube, generating an elec-

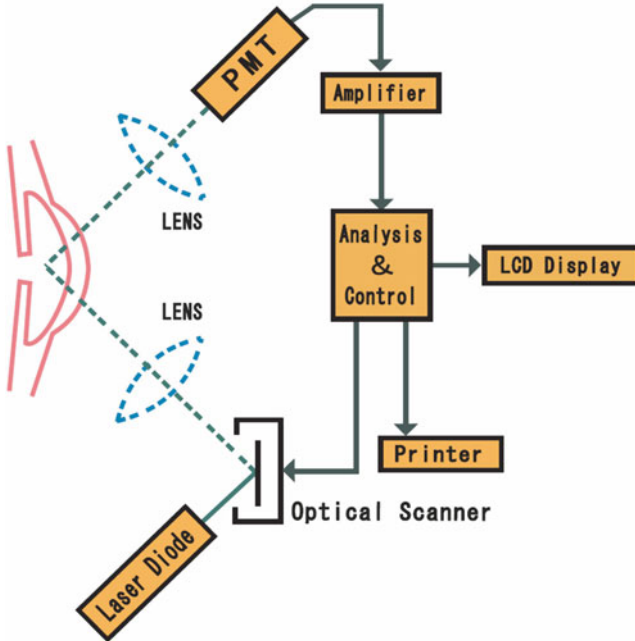


Fig. 3.14 Kowa FM-600 is based on the measurement principle of laser light scattering detection. The instrument uses a diode laser beam to scan a measuring window that is projected inside the anterior chamber of the eye. As an aqueous protein (component of inflammation) passes through the focal point of the laser, light scattering occurs. The intensity of the scattered light (directly proportional to the amount of protein particles, i.e., flare) is detected by a photomultiplier tube (PMT), which generates an electrical signal. These signals are immediately digitized to eliminate outside noise interference and are processed by a computer that displays for user analysis. The unit of measurement employed by the FM-600 is photon counts per millisecond (Kowa FM-600 technical manual; used with permission)

trical signal. The digitized signals are processed by a computer which eliminates outside noise interference and displays the results expressed as photons per millisecond for user analysis (Fig. 3.14). For review and opinion, see Ladas et al. [135], and Herbort et al. [136].

3.7.2 Performance Parameters

Clinical applications of the laser flare meter include assessing uveitis [137], observing the effects of drugs on aqueous humor dynamics, and postoperative inflammation following extracapsular cataract extraction and intraocular lens implantation [138].

3.7.3 Use in Animal Toxicology and Other Ocular Research

The laser flare-cell meter has been shown to objectively quantify inflammation of the anterior chamber of the rabbit eye [137]. Following endotoxin-induced ocular inflammation, a linear relationship between the flare measurements and previously published measures of inflammation; however, false-positive results may occur in cases of severe uveitis. It has also been used to determine the efficacy and time to onset of effect of anti-inflammatory drugs [139–142], topical mydriatics and vasoconstrictors [143], and medicinal herbs [144] on prostaglandin-induced aqueous flare elevation in rabbits. It has also been used to assess the effects of topical carprofen on pilocarpine-induced irritation in dogs [145].

Using a rabbit model, the laser flare-cell meter has been used to evaluate the potential toxicity of intravitreal injections of bevacizumab [146], compare the effects of topical isopropyl unoprostone and latanoprost on prostaglandin-induced aqueous flare [147], and assess the ocular effect of microwaves [148].

3.7.4 Human Clinical Applications

Clinically, the laser flare-cell meter has been used to compare the long-term biocompatibility of intraocular lenses made from different materials in patients with uveitis of various origins [149, 150] and specifically patients with diabetes [151, 152]. Another major application of the laser flare-cell meter includes assessing the safety and efficacy of anti-inflammatory drug therapies before [153] and following cataract extraction [154–157]. It has also been used to assess the effects of postoperative atropine on central and peripheral anterior chamber depth and anterior chamber inflammation following primary trabeculectomy [158].

3.7.5 Commercially Available Device

Available unit:

Kowa FM-600 (Kowa Co. Ltd, Tokyo, Japan)
(http://www.kowa-europe.com/medicals/en/fm_600.php)

3.7.6 Considerations for Ocular Toxicology Studies

Unlike clinical observation, the laser flare meter produces quantitative data that, if collected correctly, is highly repeatable. Furthermore, the sensitivity of the instrument

is superior to that of the human observer such that it can detect subclinical alterations in the anterior chamber protein concentration [159], an important consideration for drug toxicity studies.

3.7.7 Limitations and Caveats

Early models of laser flare meters incorporated the ability to count cells as well as flare; however, subsequent studies indicated that automated cell counting was unreliable except under highly controlled conditions [137]. This problem may result in part from the machine counting cellular debris as cells, an error that is less likely to occur with a human observer. High cellular concentrations are also prone to miscounting since the individual reflected peaks may be too close for the machine to recognize as distinct, resulting in undercounting. With low cellular density, the problem becomes one of obtaining an adequate sample size, whereas a human observer can quickly scan a large portion of the anterior chamber.

In humans, a number of factors may affect the laser flare meter readings, such as aging; medications such as acetazolamide, beta blockers, and pilocarpine; corneal opacity; pupil size; cataract; a shallow anterior chamber; and the presence of an intraocular lens. With the possible exception of pupil size, these would likely not apply to preclinical toxicologic studies. Nevertheless, the laser flare meter results should always be compared to clinical slit-lamp observation [135, 160].

In humans with uveitis, the laser flare meter seems to produce more repeatable results for anterior uveitis than it does for intermediate or posterior uveitis. Therefore, it has been suggested that at least 15 photons in the anterior chamber is the necessary threshold to produce reliable results in intermediate and posterior uveitis [160].

As with any sophisticated measurement device, operator skill and experience are relevant. Inter-operator variability could be an issue for toxicologic studies. Thus, appropriate training procedures and limiting the number of operators could improve consistency.

3.8 Fluorophotometry

3.8.1 Basic Principles

By measuring light emitted by the fluorescent tracer dye fluorescein, fluorophotometry can assess the integrity of various ocular barriers including blood–aqueous and blood–retinal barriers. It is also used for measuring aqueous flow and corneal endothelial permeability. The fluorophotometer projects a vertical slit of blue light into the eye, while a detector which measures fluoresced light is focused on the same point (Fig. 3.15). Only the fluorescence measured at the intersection of the two light paths is recorded. Fluorophotometry was originally designed to measure

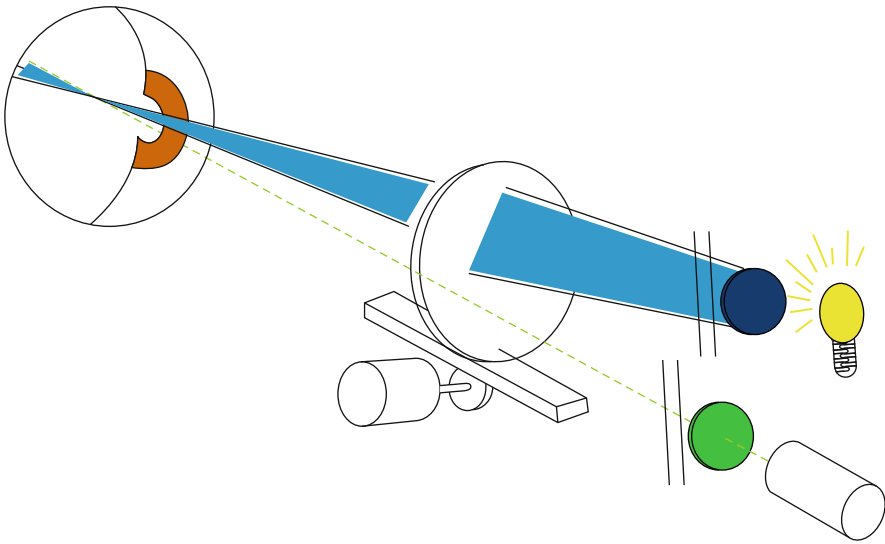


Fig. 3.15 The instrument works by projecting a beam of blue light in the form of a vertical slit into the eye. At the same time, a detector filtered to allow only fluoresced light is focused on the same point in the eye (<http://www.ocumetrics.com>)

the leakage of fluorescein dye from the retina into the vitreous, but it has evolved to meet the needs of various areas of eye research. By accurately measuring fluorescence at discrete points in the eye, researchers can study several aspects ocular physiology (Fig. 3.16).

3.8.2 Performance Parameters

Fluorophotometry can detect increased permeability of the blood–retinal barrier, an early indication of ocular damage in patients with diabetes. Some structures in the eye such as the crystalline lens naturally fluoresce and as people age, glucose reacts with lens proteins to produce new fluorescent compounds. Since patients with diabetes have higher levels of blood glucose, these fluorescent compounds accumulate more quickly and measuring increased lens fluorescence can be used to screen people for diabetes. Similarly, the natural fluorescence of the cornea increases significantly in patients with diabetes and may represent another method for monitoring eye disease in these patients.

Clinically, a fluorophotometer was used to measure corneal fluorescein penetration for diagnosing dry eye disease. Following the topical application of fluorescein, patients with dry eye disease demonstrate increased corneal tissue fluorescence compared with normal subjects [161]. Other uses include measuring the permeability of the blood–retinal and blood–aqueous barriers (Fig. 3.17), vitreous diffusion, lens autofluorescence, aqueous and tear turnover, and cornea endothelial and epithelial permeability.

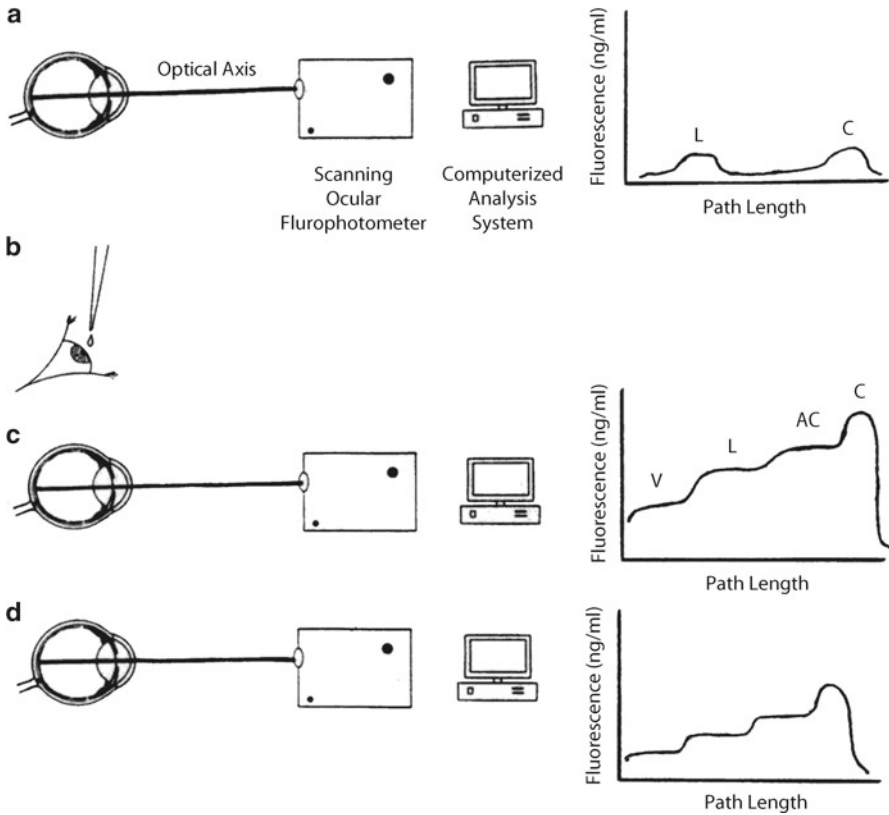


Fig. 3.16 Principles of measurement of aqueous flow by ocular fluorophotometry. **a** Optical axis of eye is scanned for background fluorescence with a scanning ocular fluorophotometer. **b** Topical application of drops of fluorophore (2 % fluorescein) is applied to cornea. **c** After a suitable delay (approximately 15 h), to allow fluorescein to diffuse from the corneal depot to the aqueous humor, the eye is scanned once again. **d** Repeated scans at 30-min to 1-h intervals over a 3–6-h period facilitate monitoring of decline in fluorescence of aqueous humor with time. This can be related mathematically to aqueous flow rate (a calculation often performed by computer) after subtraction of background fluorescence and derivation of anterior chamber volume from keratometry and pachymetry determinations. The graphs to the right of the diagrams indicate typical fluorescence patterns obtained along the optical axis at each stage in the procedure. *C* cornea, *AC* anterior chamber, *L* lens, *V* vitreous (Gabelt et al. [283]; used with permission)

3.8.3 Use in Animal Toxicology and Other Ocular Research

The properties of fluorophotometry make it a valuable research tool for studying a number of illnesses and conditions in animals including diabetes, uveitis, glaucoma, dry eye, and corneal surgery. Fluorophotometry has been used to evaluate the potential pharmacokinetic parameters of drug delivery following various periocular injections [162, 163] and to measure bioavailability of conventional eyedrops [164, 165]. Inflammation caused by bacterial infection or surgery can also increase the permeability

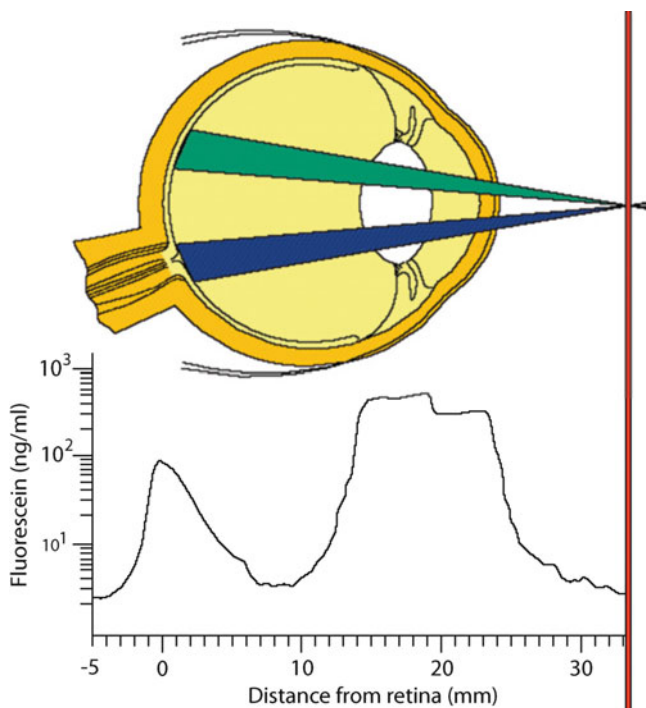


Fig. 3.17 The barrier between the blood system and the anterior segment of the eye is not as tight, so some fluorescein can penetrate it even under normal conditions. However, since the Fluorotron can make a precise measurement of the amount of fluorescein that gets in, it can easily differentiate a normal amount from an abnormally high amount. Inflammation can markedly increase the permeability of the blood–aqueous barrier. Inflammation can be caused by bacterial infection, surgery, and other diseases such as diabetes. A number of drug companies have used Fluorotron to run clinical trials on their anti-inflammatory drugs. These drugs decrease inflammation after surgery and thus also decrease permeability of the blood–aqueous barrier (<http://www.ocumetrics.com>)

of the blood–aqueous barrier, and pharmaceutical companies may use a fluorophotometer to study potential anti-inflammatory drugs.

Measuring the rate of disappearance of fluorescein instilled in the eye is also a useful measure of tear turnover and is of interest to contact lens companies. For example, tear flow estimates under soft lenses are very low compared to rigid lenses. This type of information is useful for studying contact lenses designed for overnight wear. By increasing tear flow under soft lenses, contact lens designers may be able to reduce complications of contact lens wear [166, 167].

Measuring aqueous humor formation *via* fluorophotometry is an important aspect of determining mechanism of action of compounds aimed at lowering intraocular pressure (IOP). Determining what portion of IOP lowering is due to increased outflow *vs.* decreased aqueous humor formation is a critical piece of information in glaucoma therapeutics. Most patients will need several medications of varying and complementary classes to control their IOP in what is a lifelong disease [168–170].

3.8.4 Human Clinical Applications

In humans, the accumulation of fluorescent substances (autofluorescence) is associated with the progression of eye aging and cataract formation. A prospective cohort study using fluorophotometry demonstrated a loss of lens transparency occurs in patients following trabeculectomy for the treatment of in primary open-angle glaucoma [171]. Compared to baseline assessments, this change was significant after 12 months and was not observed in other patients with open-angle glaucoma that did not undergo the procedure.

Fluorophotometry has also been used to assess the efficacy and safety of a stent for the treatment of open-angle glaucoma by measuring changes in aqueous humor dynamics [172]. Using fluorophotometry, aqueous flow and trabecular outflow facility were measured before and after implanting a stent connecting the anterior chamber with Schlemm's canal. Patients treated with stent implants and cataract surgery displayed significantly increased trabecular outflow facility, reduced intraocular pressure, and reduced need for medications compared with patients treated with cataract surgery alone.

Hyaluronic acid has been proposed as a topical agent for the treatment of dry eye disease. To describe the behavior of hyaluronic acid on the ocular surface, hyaluronic acid conjugated with fluorescein was topically applied to the eyes of healthy human volunteers and measured fluorophotometrically [173]. Compared to saline, hyaluronic acid had a longer retention time, possibly by adhering to the surface of the eye.

3.8.5 Commercially Available Devices

Available units:

F-7000 Fluorescence Spectrophotometer

(<http://www.hitachi-hitec.com/global/science/fl/f7000.html>)

F-2500 Fluorescence

(<http://www.sios.net.au/spectrophotometers/hitachi/f-2500-fluorescence>)

Fluorotron™ Master Ocular Fluorophotometers

(<http://www.ocumetrics.com>)

3.8.6 Considerations for Ocular Toxicology Studies

Fluorophotometry can provide objective, quantitative measures of the physiological and pathological state of the retinal vasculature, the pigmented epithelium, the choroid, and the ciliary processes. It is a valuable tool for detecting physiological changes such as inflammation and monitoring treatment progress in preclinical and clinical drug development. A laboratory animal-specific system is commercially available (Fig. 3.18). It has adjustments for the optics of a variety of species, increasing its utility in preclinical work. The performance specifications are the same as for human systems.

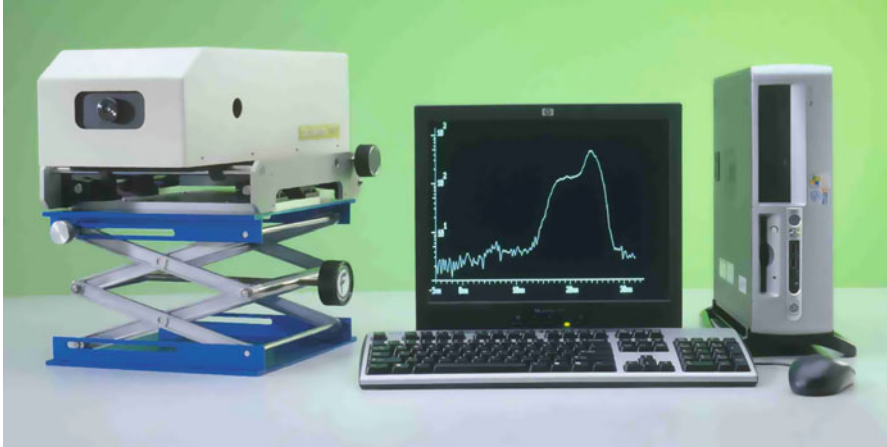


Fig. 3.18 Fluorophotometry is the established method for quantitating the permeability of the blood–retinal barriers and the blood–aqueous barrier. By measuring the concentration profile of the tracer fluorescein within the ocular cavity, the dynamics of intraocular diffusion and elimination can be accurately monitored. The resulting determinations provide indications of the physiological and pathological state of the retinal vasculature, the pigment epithelium, the choroid, and the ciliary processes. The objective and quantitative capabilities of fluorophotometry permit the detection of physiological changes very early in the course of certain diseases and the monitoring of progress in treatment (<http://www.ocumetrics.com>)

3.8.7 *Limitations and Caveats*

Species selection and anesthesia are both important variables in study design. Data are not necessarily comparable across species. Anesthetics can have differential effects depending on the species and level of anesthesia needed to obtain high-quality scans. While the procedure is relatively simple, it takes operator skill to be able to accurately obtain the scans and evaluate the results.

3.9 Scanning Laser Ophthalmoscope (SLO)

3.9.1 *Basic Principles*

Scanning laser ophthalmoscopy is a method of examining the eye using the technique of confocal laser-scanning microscopy. A confocal scanning imager synchronously moves a spot of illumination and a detector over the image. SLO employs mirrors to horizontally and vertically scan a specific region of the retina and create images viewable on a computer monitor. It can provide crisp and complete retinal images without pupil dilation [174] although good dilation may be preferable, especially when obtaining stereoscopic images.

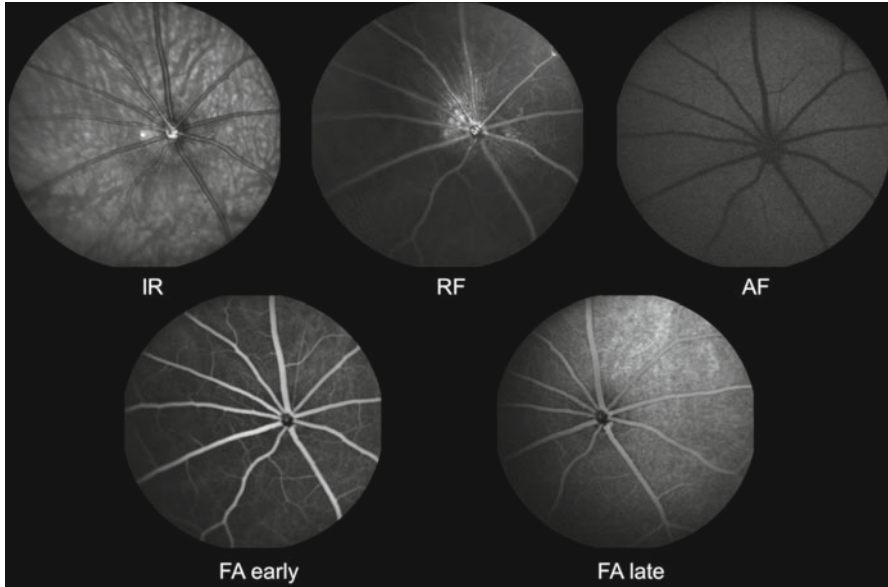


Fig. 3.19 Scanning laser ophthalmoscopic images of rat retinas. *IR* infrared, *RF* red free, *AF* autofluorescence. *FA early*, early phase fluorescein angiogram. *FA late*, late phase fluorescein angiogram (Courtesy Heidelberg Engineering. Images provided to Heidelberg by Sinisa D. Grozdanic, College of Veterinary Medicine, Iowa State University)

3.9.2 Performance Parameters

SLO provides imaging of the retina or cornea of the human eye with a high degree of spatial sensitivity that makes it a very useful aid in the diagnosis management of glaucoma, diabetic retinopathy, macular degeneration, and other retinal disorders. SLO systems have been adapted for use in studying both the anterior and posterior segments of the eye (see Sect. 3.3). For example, Heidelberg Engineering has an anterior segment module (ASM) for their Spectralis™ system that can perform optical coherence tomography on the cornea, iris, and lens.

3.9.3 Use in Animal Toxicology and Other Ocular Research

SLO has been useful in for studying toxicity and for research in animals with large as well as small eyes (Fig. 3.19). Using laboratory small-eyed rodents such as hamsters and gerbils, confocal SLO together with other visualization techniques has been used for the study of human diseases, such as age-related macular degeneration and diabetic macular edema [175]. Confocal SLO has been developed into a technique for assessing corneal surfactant irritation in rabbits and mice [176], the

response of acute anterior chamber inflammation to various treatments [177] and to measure changes in the topography of the optic nerve head following subconjunctival injection of unoprostone (isopropyl unoprostone) in rabbits [178].

Using murine Müller glial cells as potential targets for gene therapy, SLO has been used to detect transgene expression in the mouse retina following intravitreal injection of adeno-associated virus [179]. Confocal SLO has also been used to study cone survival in transgenic mouse models of retinal degeneration [180]. Using a specific strain of engineered knockout mice, SLO together with other histological and biochemical assessments has been used to study the pathogenesis of choroideremia, a progressive X-linked disease characterized by the degeneration of photoreceptors and retinal pigment epithelium [181].

The combination of fluorescence adaptive optics with SLO results in a novel imaging method that enables *in vivo* imaging of nerve fiber layer vasculature in living macaque monkeys [182]. This technique enables researchers to examine the possible role of the nerve fiber layer vasculature in retinal vascular disorders and other eye diseases, such as glaucoma.

3.9.4 Human Clinical Applications

Confocal SLO provides objective and quantitative measurements that are highly reproducible and show very good agreement with clinical estimates of optic nerve head structure and visual function in clinical practice and also in glaucoma trials [183]. For example, confocal SLO studies have shown that baseline Glaucoma Probability Score can be used to predict the development of primary open-angle glaucoma [184]. By comparing normal and glaucomatous eyes using confocal SLO, the retinal nerve fiber layer showed a stronger structure–function association and a higher diagnostic sensitivity for glaucoma detection than the neuroretinal rim [185].

A possible risk factor for glaucoma is central corneal thickness, possibly by affecting the elastic properties of the eye. A study using confocal SLO revealed no significant relationship between these two parameters in healthy eyes [186]. The correlation between the retinal blood flow measured with a retinal functional imager and central macular thickness and volume has also been assessed by a combined spectral scanning laser ophthalmoscopy/optical coherence tomography system [187].

Adaptive optics SLO has also been used to measure disease progression and their response to treatment, such as the use of sustained-release ciliary neurotrophic factor for inherited retinal degeneration [188] and intravitreal bevacizumab for the treatment of radiation retinopathy [189]. The combined use of SLO with spectral-domain optical coherence tomography revealed microstructural changes in eyes with progressive geographic atrophy due to age-related macular degeneration [190]. SLO is an effective means for monitoring the efficacy of treatment of neurodegenerative diseases of the retina in clinical trials [191] and has also been used to assess drug-induced ocular toxicity. For example, SLO has been used to quantify retinal nerve fiber layer and macular thickness loss as markers of retinal damage in patients

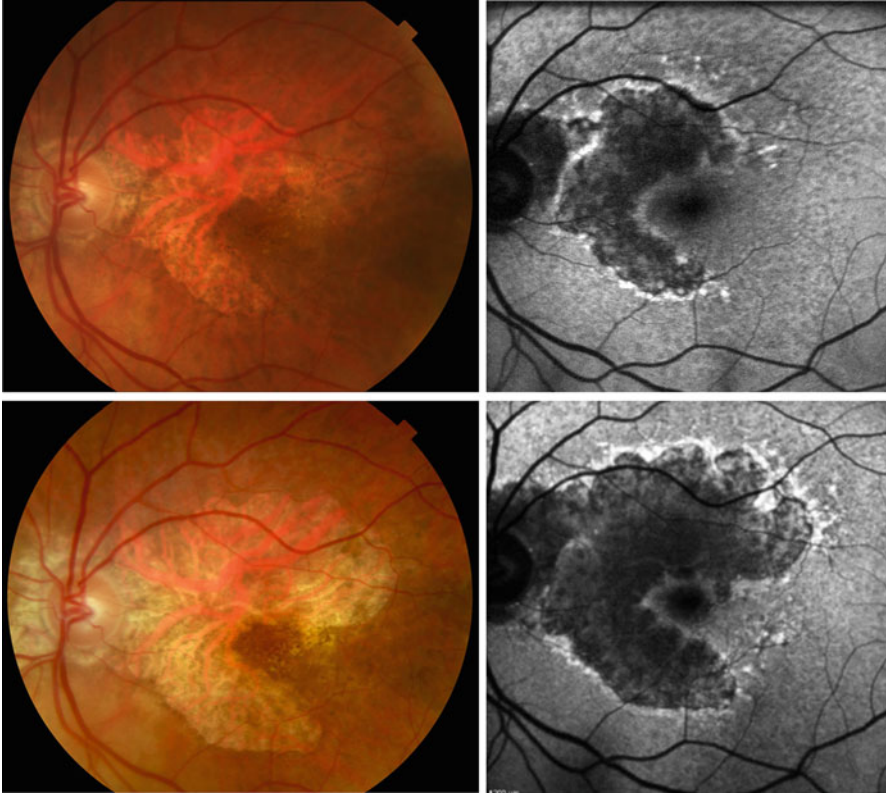


Fig. 3.20 *Left column*, standard white light digital fundus photographs of the retina of an 87-year-old woman with geographic age-related macular degeneration. *Right column*, fundus autofluorescence images taken with a scanning laser ophthalmoscope camera (Heidelberg HRA II). *Top row*, the color and autofluorescence images both taken on the same day. *Bottom row*, the color and autofluorescence images taken on the same day 3 years and 3 months after the *top row* of images. Note the increase in size of the area of atrophy. The autofluorescence images show a decrease in fluorescence compared to normal levels (compare with retina peripheral to the lesion) in the center of the atrophic region; however, the edge of the atrophic region is hyperautofluorescent. Hyperautofluorescence of the retinal pigment epithelium may be an indicator of active degeneration

with vigabatrin-associated vision loss [192]. Examples of SLO fundus imaging for human clinical use are shown in Figs. 3.20, 3.21, and 3.22.

3.9.5 Commercially Available Devices

Available units:

F-10 Scanning Laser Ophthalmoscope, NIDEK, Inc., Fremont, CA
<http://usa.nidek.com/products/scanning-laser-ophthalmoscope>)

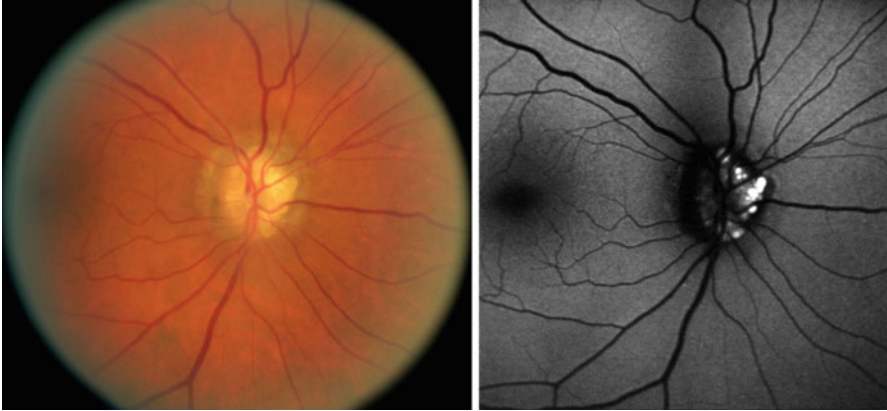


Fig. 3.21 *Left*, color standard digital photograph of an abnormal appearing optic nerve. *Right*, autofluorescence imaged obtained with a scanning laser ophthalmoscope (Heidelberg HRA II). Marked autofluorescence is evident in a nodular pattern consistent with a diagnosis of optic nerve head drusen

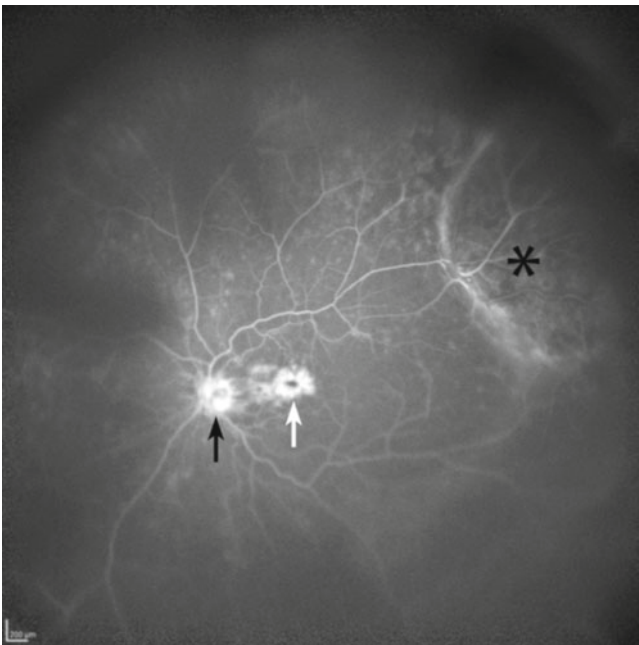


Fig. 3.22 Wide-angle fluorescein angiographic image taken with the Heidelberg HRA II scanning laser ophthalmoscope utilizing the Staurengi contact lens. A mass (choroidal melanoma) is seen in the superotemporal periphery (*asterisk*). The optic nerve (*black arrow*) shows late fluorescein staining, and there is prominent late leakage consistent with cystoid macular edema (*white arrow*) (Courtesy of Diagnostic Services, Flaum Eye Institute, University of Rochester)

This high-definition diagnostic imaging system provides infrared scanning images and is useful for identifying retinal and choroidal pathology.

Heidelberg Retina Tomograph; Heidelberg Engineering, Carlsbad, CA
(<http://www.heidelbergengineering.com/us>)

This confocal scanning laser ophthalmoscope can create a 3-dimensional topographic image of the retina using proprietary software.

3.9.6 Considerations for Ocular Toxicology Studies

In addition to providing high-resolution and repeatable images, other advantages of SLO technology are ease of instrument use, rapid acquisition capability making it suitable for large animal studies, and the advantages of video image capture for angiography that allows the dynamic assessment of dye flow. As with traditional fundus photography, SLO retinal imaging also permits the capture of static stereo image pairs.

3.9.7 Limitations and Caveats

The total acquisition time of SLO scans can be longer than the fraction of a second needed for standard fundus photography. Therefore, eye and head movement can be performance issues. Software has been developed to help compensate for this in conscious humans. Proper attention to anesthesia is required to prevent excessive eye movement in animal studies. Other considerations for animal work include proper positioning of the subject. A head holder can be useful in this regard. Lid speculums can be helpful for animal experiments as are plano corneal contact lenses to prevent drying. As with any sophisticated photographic device used in ocular research, a skilled operator is critical in obtaining reliable and reproducible images.

3.10 Optical Coherence Tomography (OCT)

3.10.1 Basic Principles

Optical coherence tomography (OCT) was developed from a technique called low-coherence interferometry which was used to obtain axial eye length measurements [193]. Low-coherence interferometry requires light to be split and sent to the sample and a reference arm with a mirror. If the length of the path to the reference mirror and tissue match to within the coherence length of the light source, interference occurs when the reflected beams recombine. This can be used to obtain intensity information.

By changing the location of the reference mirror, backscattered tissue intensity levels can be detected from different depths in the tissue sample. Since time-encoded signals are directly obtained, this is referred to as time-domain optical coherence tomography (TD-OCT). Acquisition speed can be improved by detecting backscattering signals in the frequency domain at a given location without moving the reference mirror. There are currently two main ways of doing this. The first to be commonly employed in ophthalmic applications uses frequency information obtained from a broad-bandwidth light source, charge-coupled device camera, and a spectrometer. The signal is then analyzed by a digital signal processor using Fourier analysis. This is referred to either as spectral-domain OCT (SD-OCT) or Fourier-domain OCT (FD-OCT). The latter abbreviation is somewhat unclear as it can be confused with the more general term “frequency-domain OCT,” which encompasses both SD-OCT as well as swept source OCT (SS-OCT). Consequently, SD-OCT is the abbreviation most often used to indicate this type of scanning. A functional extension of SD-OCT known as polarization-sensitive optical coherence tomography has been used for *in vivo* birefringence mapping of the human retina [194]. Figure 3.23 illustrates the difference in resolution between TD-OCT and SD-OCT in scans of cynomolgus monkey maculae.

SS-OCT is accomplished by sweeping a narrow-bandwidth source through a broad range of frequencies and used a photodetector. Using this method, ultrahigh-speed imaging of the retina and optic nerve head provides excellent visualization of the choroid, sclera, and lamina cribrosa [195]. It also has the advantage of less fall-off in signal strength with increasing tissue depth relative to the SD-OCT. Advantages and disadvantages of these systems are summarized in Table 3.1.

Although the axial resolution of both SD- and SS-OCT is somewhat greater than for TD-OCT, the real advantage of frequency domain over time domain is the much higher rates of data acquisition, which permits higher numbers in scan lines and even 3-dimensional imaging [196, 197] without increasing the total testing time.

3.10.2 Performance Parameters

OCT was originally used to obtain optical cross sections of the anterior segment *in vivo* and to evaluate the optic disc and retinal layers such as the retinal nerve fiber layer. It was also used for imaging retinal diseases, such as macular detachment and macular holes, epiretinal membrane, macular edema, and idiopathic central serous chorioretinopathy [193]. Today it is commonly used for the detection, staging, and monitoring of glaucoma [198–203] including highly myopic eyes [204, 205]. OCT may aid in distinguishing glaucoma-related retinal nerve fiber layer thinning from that caused by nonglaucomatous optic neuropathies [206] and can be used to measure angle closure in the different quadrants of the anterior chamber angle [207] and detecting signs of achromatopsia [208]. OCT may reveal ocular injuries such as Descemet’s membrane detachment [209].

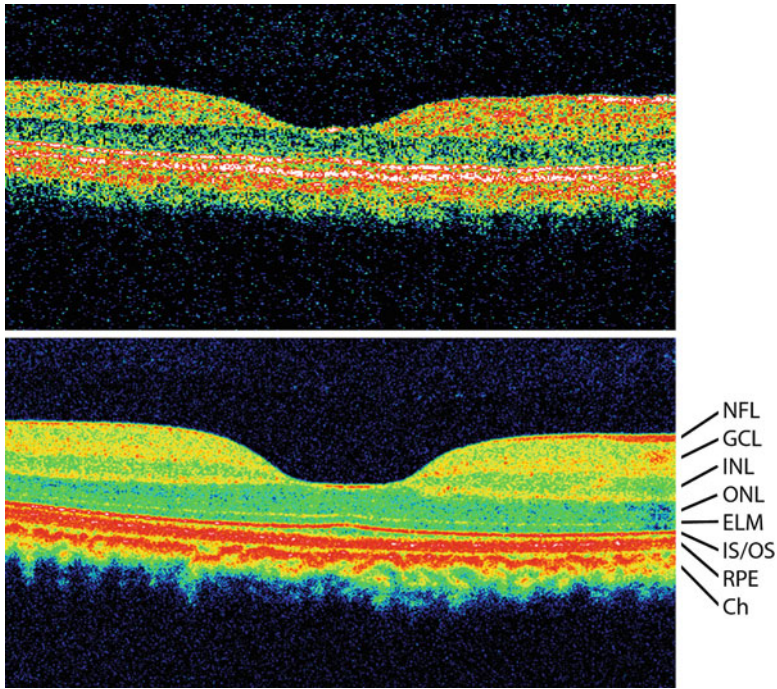


Fig. 3.23 Comparison of time-domain Stratus[®] OCT (*top frame*) with spectral-domain Cirrus[®] OCT (*bottom frame*). Both images are horizontal scans of the central macula of cynomolgus monkeys, originally they were 6 mm scans that have been cropped here to 4 mm for illustration purposes. Several features of retinal anatomy can be visualized better with the higher-resolution SD-OCT. Lines point to the nerve fiber layer (*NFL*), ganglion cell layer (*GCL*), inner nuclear layer (*INL*), outer nuclear layer (*ONL*), external limiting membrane (*ELM*), inner segment/outer segment line (*IS/OS*), retinal pigment epithelium (*RPE*), and choroid (*Ch*)

Table 3.1 Comparison of TD-, SD-, and SS-OCT devices

	Advantages	Disadvantages
TD-OCT	Intensity information acquired in time domain; no complex conjugate image	Moving reference mirror required; limited acquisition rate
SD-OCT	No moving reference mirror; higher sensitivity than TD-OCT; can obtain high scanning speed and axial resolution	Noticeable signal drop-off with depth
SS-OCT	No moving reference mirror; higher sensitivity than TD-OCT; can obtain very high scanning speeds; minimal signal drop-off with depth	Most systems operate at longer wavelengths ($\lambda=1-2 \mu\text{m}$) with lower axial resolution

From: Gabriele et al. [193]

SD-OCT can provide 3-dimensional imaging of structural changes in the optic nerve head lamina cribrosa in patients with optic nerve damage due to glaucoma [210] and measure the inner/outer segment junction to predict visual recovery after macular hole surgery [211]. In one case report, SD-OCT was used to demonstrate a

localized juxta-foveal area of retinal atrophy involving the photoreceptor and retinal pigment epithelium layers following cataract surgery [212].

Using a signal processing algorithm, SD-OCT can provide real-time and artifact-free quantitative imaging of the anterior chamber including the cornea, limbus, iris, anterior lens capsule, trabecular meshwork, and Schlemm's canal [213]. Quantitative surface height maps of the corneal epithelium and endothelium obtained from volumetric data can be used to generate corneal thickness maps.

The use of SD-OCT [214, 215] also enables rapid and sensitive imaging of posterior segments of the human eye *in vivo* such as structural retinal changes in patients with retinitis pigmentosa [216, 217]. OCT can be combined with confocal laser-scanning ophthalmoscopy with integrated simultaneous indocyanine green dye angiography to diagnose of a variety of macular diseases [218].

3.10.3 Use in Animal Toxicology and Other Ocular Research

OCT is suitable for performing various ocular studies in rodents. High-resolution SD-OCT provides high-quality 2- and 3-dimensional *in vivo* imaging of retinal structures in murine models of retinal disease [219, 220]. In albino rats chronically exposed to intense light, OCT and angiographic studies show progressive retinal degeneration and choroidal neovascularization [221] which may represent a model for the study of age-related macular degeneration. SD-OCT has also been used to quantify the effect of experimental optic nerve crush injury in mice by measuring changes in retinal thickness over time [222].

In monkeys, longitudinal SD-OCT imaging has been shown to detect deep optic nerve head changes in experimental glaucoma [223]. These changes were detectable at the onset of Heidelberg Retina Tomograph-defined surface topography depression changes and suggest SD-OCT may aid in the early detection of glaucoma progression in humans. A monkey experimental glaucoma model was also used to investigate correlations between structural and functional measures of early change in glaucoma [224]. Animals were followed over time with SD-OCT, full-field light-adapted flash ERG, 103-hexagon global-flash mfERG (MFOFO), and static perimetry. Significant correlations were found between mfERG root mean square (RMS) amplitude of a glaucoma-sensitive frequency range and peripapillary retinal nerve fiber layer (RNFL) thickness (standard 12° OCT circular scan). Changes in *in vivo* OCT measurements of retinal nerve fiber layer thickness associated with elevated intraocular pressure have also been studied in monkeys [225].

Exposure to high intraocular pressure was found to be associated with the loss of retinal nerve fiber layer over time and OCT measurements corresponded with histomorphometric measurements of the same tissues, highlighting a key feature of animal models – the ability to collect and correlate histologic measures with structural and functional measures. The United States Food and Drug Administration (FDA, Dermatologic and Ophthalmic Drugs Advisory Committee) has expressed a strong interest in objective testing paradigms/strategies such as OCT that have better sensitivity and specificity than subjective visual field testing and are predictive of

functional deficits that affect patient quality of life. In rhesus macaques, SD-OCT has also been used to demonstrate that the RNFL cross-sectional area, not RNFL thickness, provides a more accurate assessment of the retinal ganglion cell axonal content within the eye [226].

3.10.3.1 Segmentation

In addition to its ability to provide high-resolution images of the retina – something approaching *in vivo* histopathology – another potentially huge advantage of OCT is its ability to rapidly quantify various optic nerve and retinal parameters. An example is the determination of RNFL thickness, which is important in monitoring the progression of glaucoma and in identifying optic neuropathies, including toxic neuropathies. Other examples in which the quantitative measurement would be useful are determining the volume of subretinal fluid (such as in serous retinal detachments), measuring the extent of retinal thinning due to drug toxicity or retinitis pigmentosa, or thickening due to edema caused by drug-related vascular leakage, diabetic retinopathy, vascular occlusive disease, or exudative age-related macular degeneration.

Despite the promise of OCT quantification, segmentation (accurate identification of retinal layers) remains challenging. In the case of RNFL thickness, the difficulty arises because the disease toxicity changes are typically on the order of only a few microns. Especially because of their potential application to human glaucoma, new paradigms for RNFL thickness determination are a subject of active research. For example, see Zhu et al. [227]; Vermeer et al. [228]; and Yazdanpanah et al. [229].

The typical macular changes seen clinically with OCT are often much more dramatic than the subtle RNFL thinning of glaucoma, but the problem of quantification for macular analysis is that the retinal layers are often distorted by the disease process [230]. As a result, most of the practical clinical diagnoses are made based on the subjective appearance of the lesions. Nevertheless, efforts are underway to apply quantitative methods to macular OCT scans even with disrupted architecture. For examples, see Malamos et al. [231], and Rathke et al. [232].

Subjective assessment of SD-OCT scans is also valuable in toxicity studies. Similar to human disease, obvious changes such as retinal or vitreous detachment, retinal edema, and RPE scarring (as in macular degeneration) are readily apparent; however, frequency-domain OCT scanning can provide information that goes beyond its nominal resolution. That is because the OCT, in addition to measuring distances, also determines reflectivity of the various layers. This fact has proven useful clinically such as in the assessment of drug toxicity from the chronic use of hydroxychloroquine to treat rheumatologic conditions [233]. In early hydroxychloroquine toxicity, the OCT feature that corresponds to the junction between the inner and outer photoreceptor segments, the so-called IS/OS line is decreased in intensity. Nork et al. showed that the IS/OS line was decreased in intensity three months after

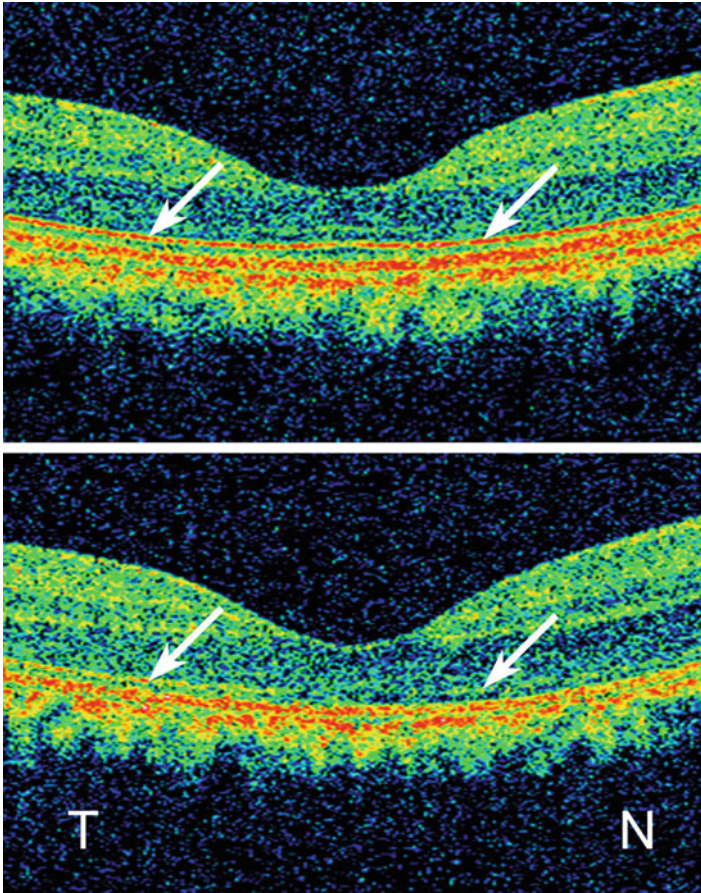


Fig. 3.24 Spectral-domain optical coherence tomograms (SD-OCT) horizontal raster scan of central macula. *Top*, control eye of Cy3 from fovea corresponding to the retinal detachment in the fellow eye. Note the prominent red line (*arrows*) demarcating the photoreceptor inner segment/outer segment (*IS/OS*) junction. *Bottom*, similar section from area of previous retinal detachment after 3 months of reattachment. The IS/OS line is much less reflective. In both frames, the SD-OCT scans are oriented such that the temporal retina (*T*) is on the *left* and nasal retina (*N*) is on the right (Nork et al. [235]; used with permission)

subretinal injection of balanced salt solution in cynomolgus monkeys [234] (Fig. 3.24). Further examination by transmission electron microscopy revealed disruption of the normally tight packing of the outer segment discs (Fig. 3.25). They suggested that a decrease in IS/OS line intensity could be the result of reduced reflectivity at that level. Thus, this particular feature of the SD-OCT is actually providing information about outer segment pathology, a structure formerly accessible only by ultrastructural analysis.

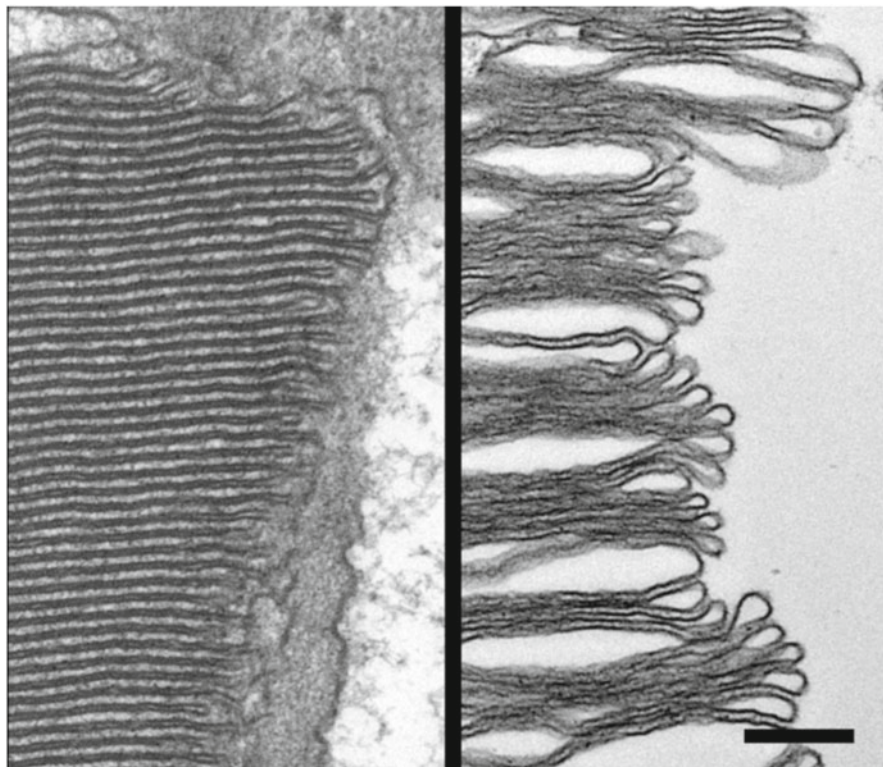


Fig. 3.25 High magnification electron micrograph of rod outer segments. *Left*, control eye of Cy3 from superior retina corresponding to the retinal detachment in the fellow eye. Normal close stacking of discs is evident. *Right*, similar section from area of previous retinal detachment after 3 months of reattachment. Discs are not as tightly packed, having markedly increased intradiscal spaces. Bar = 250 nm (Nork et al. [235]; used with permission)

3.10.4 Human Clinical Applications

High-definition SD-OCT has been used to obtain normative data for macular thickness [236, 237] and retinal nerve fiber layer based on age, ethnicity, gender, optic disc area, and axial length [238]. Other studies have used SD-OCT to measure changes associated with age-related macular degeneration [239, 240]. Ultrahigh-resolution SD-OCT can provide structural intensity images and movies of the human retina *in vivo* [241] and has been used to evaluate changes in retinal anatomy in patients with exudative age-related macular degeneration before and after intravitreal injections of ranibizumab [242]. All treated eyes showed some normalization of macular contour but fibrovascular lesion volume did not change. Using ultrahigh-resolution SD-OCT, this study demonstrated intravitreal treatment with ranibizumab that improves overall retinal architecture although photoreceptor damage may be irreversible.

Table 3.2 Commercially available SD-OCT systems

Device	Manufacturer	Comments
3D-OCT 2000	Topcon, Tokyo, Japan	SD-OCT and high-resolution fundus camera; axial resolution, 5 μm ; axial-scan acquisition rate, 27 kHz
Bioptigen SD-OCT	Bioptigen, Research Triangle Park, NC	Designed for clinical and research use. Includes a handheld probe and microscope setup; axial resolution, 4 μm ; axial-scan acquisition rate, 20 kHz
Cirrus HD-OCT	Carl Zeiss Meditec, Dublin, CA	Includes Guided Progression Analysis software for detecting glaucoma progression; axial resolution, 5 μm ; axial-scan acquisition rate, 27 kHz
RTVue-100	Optovue, Fremont, CA	Multiple scanning protocols for glaucoma detection, including ganglion cell complex analysis; axial resolution, 5 μm ; axial-scan acquisition rate, 26 kHz
SOCT Copernicus	Optopol, Zawiercie, Poland	Includes progression analysis software that incorporates disc damage likelihood scale, asymmetry between the discs, and RNFL thickness; axial resolution, 6 μm ; axial-scan acquisition rate, 27 kHz
Spectral OCT SLO	Opko, Miami, FL	Combines SD-OCT, scanning laser ophthalmoscopy, and microperimetry; axial resolution, 6 μm , axial-scan acquisition rate, 27 kHz
Spectralis OCT	Heidelberg Engineering, Heidelberg, Germany	High-speed SD-OCT device with eye-tracking, fluorescein angiography, ICG angiography, and autofluorescence; axial resolution, 4 μm ; axial-scan acquisition rate, 40 kHz

From: Gabriele et al. [243]

3.10.5 Commercially Available Devices

Available SD-OCT devices are provided in Table 3.2.

3.10.6 Considerations for Ocular Toxicology Studies

The commercially available SD-OCT systems are optimized for human clinical use. As such, they may need to be modified for animal toxicologic studies. For example, the Cirrus™ HD-OCT is designed in such a way that the chin rest is connected directly to an integrated scanner/monitor/computer processor. We have found it necessary to remove the chin rest and modify the electronics accordingly to permit proper configuration for use with anesthetized animals [235]. Because of the smaller ocular size of most research species, modification of contact lenses,

such as the Staurenghi™ 150° contact lens (Heidelberg Engineering), may also be required.

Keeping the cornea moist and thus clear while the animals are anesthetized can be challenging. A hard corneal contact lens with a dry outer surface can maintain optical clarity during prolonged imaging sessions.

As with the hardware, OCT software is also optimized for human clinical applications. Extracting data for detailed statistical analyses can be a challenge with some systems.

Some of the animal models used in toxicology studies are either albinotic or sub-albinotic. Automated segmentation algorithms may have difficulty correctly identifying the retinal layers due to the abnormal reflectivity in these animals.

Finally, OCT is not simply an improved version of photographic ocular imaging. It gives detailed information that is not obtainable *in vivo* by any other means, but it also has some limitations. Similar to histopathology, the OCT images are cross sections. Serial sectioning with either histopathology or OCT can produce a 3-dimensional map but only of limited retinal areas. Color fundus photography can pick of small lesions that could be otherwise missed (see section on Traditional Ocular Fundus Imaging in this chapter).

3.10.7 Limitations and Caveats

Currently, several OCT instrument companies are competing to develop devices with higher scan density and better resolution [244], and several studies comparing OCT devices with other kinds of devices and with each other have been performed.

When the repeatability of retinal nerve fiber layer thickness measurement using OCT was compared with scanning laser polarimetry with variable corneal compensation (GDx-VCC) and optic nerve head topography, the test–retest variability of GDx-VCC and OCT was consistent for all tested stages of disease severity [245]. Except in severe cases, the repeatability of GDx-VCC was better than OCT. The test–retest variability of optic nerve head topography and OCT increased with increasing disease severity for rim area, cup area, and cup-to-disc area ratio, while the vertical cup-to-disc ratio from optic nerve head topography and horizontal cup-to-disc ratio from OCT showed stable test–retest variability through all stages.

One study compared the frequency of scan artifacts, inter-scan reproducibility of macular thickness measurements, and inter-device agreement of three SD-OCT devices (Cirrus HD-OCT, RTVue-100, and Topcon 3D-OCT 1000) devices and one TD-OCT device (Stratus OCT). The TD-OCT scans contained a significantly higher percentage of clinically significant, unacceptable measures of central foveal thickness after manual correction compared with SD-OCT scans [246]. One SD-OCT device (Cirrus HD-OCT) had a significantly lower percentage of clinically significant improper central foveal thickness measures

compared with the other SD-OCT device. All three SD-OCT devices had central foveal subfield thicknesses that were significantly greater than TD-OCT after manual correction. All three SD-OCT devices demonstrated a high degree of reproducibility [244, 247].

Another study also showed SD-OCT data generally showed better reproducibility of retinal nerve fiber layer measurements than TD-OCT [248]. Others have shown that measurements obtained using SD-OCT and TD-OCT should not be compared [249]. For example, when TD-OCT and SD-OCT were used to compare retinal nerve fiber layer in normal subjects and patients with glaucoma, measurements using TD-OCT were generally thicker [250, 251] which may be clinically significant in patients with severe glaucoma. Similarly, anterior chamber angle measurements obtained with different OCT devices show poor agreement [252]. SD-OCT demonstrates significantly better reproducibility of peripapillary RNFL and macular scan thickness measurements over the clinical standard for TD-OCT [253]; however, different OCT systems cannot be used interchangeably for the measurement of macular thickness [254] due in part to differences in segmentation algorithms.

3.11 Scanning Laser Polarimetry (GDx)

3.11.1 Basic Principles

The GDx (an acronym derived from “glaucoma diagnosis”) is a confocal polarimetric scanning laser ophthalmoscope. Scanning laser polarimetry (SLP) uses polarized light to measure the thickness and integrity of the structures of the retinal nerve fiber layer. A scanning unit moves the beam horizontally and vertically on the retina where the beam is split into two components with a relative phase shift proportional to the structural organization of the retinal nerve fiber layer (RNFL) microstructures and RNFL thickness. The GDxPro (Carl Zeiss Meditec, Inc) instrument quantifies the phase shift using the term the term RNFL Integrity™ (RNFL-I™). The RNFL-I is derived from both RNFL thickness and RNFL structural organization. Other retinal imaging devices quantify retinal thickness directly, whereas SLP measures birefringence, a property of tissue that depends on the integrity of retinal ganglion cell axon microtubules and neurofilaments [255].

Structures in the anterior segment (the cornea and lens) are also birefringent. GDx instruments identify anterior segment-based birefringence and compensate for it, so that only the RNFL birefringence is analyzed. There are currently two types of corneal compensation: enhanced corneal compensation (ECC) and variable corneal compensation (VCC). ECC is thought to be superior and is the default setting; VCC is useful for maintaining continuity with historical scans.

Using Guided Progression Analysis software, changes in the polarimetric retinal nerve fiber thickness can be determined and monitored over time [256, 257].

3.11.2 Performance Parameters

The GDx is used for imaging and three-dimensional analysis of the fundus and RNFL in vivo. Its primary role is the detection of glaucoma-induced changes in the RNFL [258, 259]. Scanning laser polarimetry has also recently been used to detect subclinical changes in retinal nerve fiber layer thickness in patients with multiple sclerosis [260, 261].

3.11.3 Use in Animal Toxicology and Other Ocular Research

Scanning laser polarimetry has been used in several animal research studies. In rodents, it has been used to determine the contribution of microtubules in ganglion cell axons to retinal nerve fiber layer birefringence [255]. In monkeys, scanning laser polarimetry has been used to measure retinal nerve fiber layer birefringence. This information can be used for detecting and monitoring retinal nerve fiber layer loss in experimentally induced primate glaucoma [262] and axonal degeneration [263] (Fig. 3.26). Changes in retinal nerve fiber layer birefringence (measured by SLP) precede changes in retinal nerve fiber layer thickness (measured by OCT) following retinal ganglion cell injury [264].

3.11.4 Human Clinical Applications

Numerous human clinical trials have assessed the value of scanning laser polarimetry for the diagnosis of glaucoma [258, 265–268] and shown it to be well-correlated with optical coherence tomography [269–272] and confocal scanning laser ophthalmoscopy [273]. By comparing retinal nerve fiber layer parameters in patients with various degrees of advanced glaucoma, the retinal nerve fiber layer has been shown to be significantly thinner in patients with early glaucoma compared to those in normal subjects [274]. Also, they were significantly thinner in patients with advanced glaucoma compared to patients with early glaucoma. The progressive nature of these changes can be measured over time [256, 275]. Changes in scanning laser polarimetry parameters using variable corneal compensation is a sensitive measure of glaucoma progression [276].

One study compared the ability of optical coherence tomography and scanning laser polarimetry to detect retinal nerve fiber layer abnormalities in multiple sclerosis patients [261]. Although all patients had normal visual acuity and visual fields, the use of optical coherence tomography and scanning laser polarimetry detected retinal nerve fiber layer abnormalities in approximately 50% of evaluated eyes. Subclinical ganglion cell loss can therefore be detected in this patient population despite normal visual function.

Clinical trials for glaucoma therapeutics use endpoints based on functional measurements such as visual field tests. These tests are not highly sensitive and are

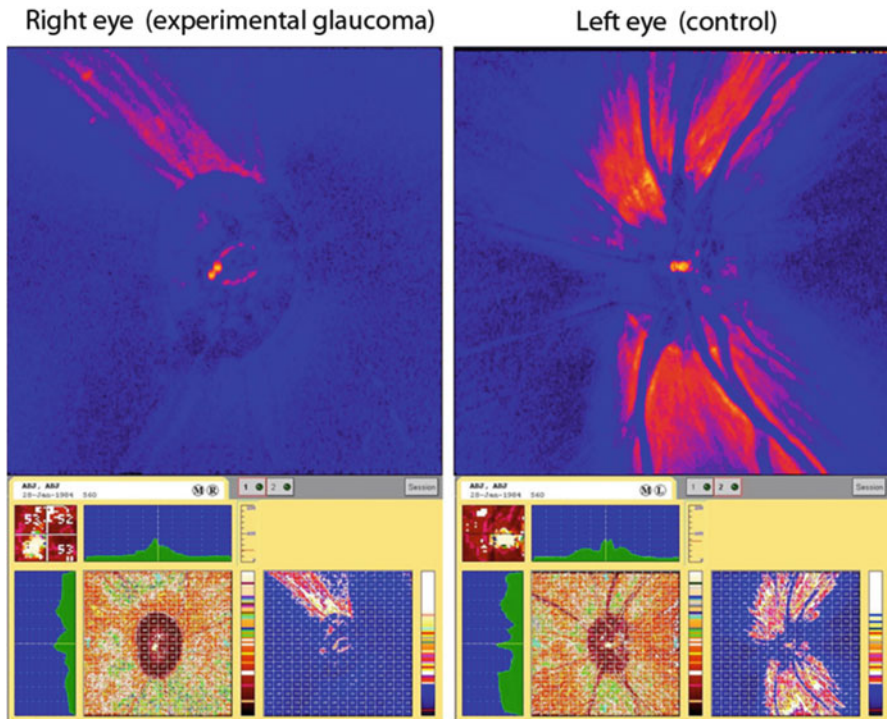


Fig. 3.26 Example of a GDx scan from a monkey with experimental. The GDx scan for this animal shows severe thinning of the nerve fiber layers in the superior and inferior quadrants of the glaucomatous right eye (Gabelt et al. (2011); used with permission)

variable. The United States Food and Drug Administration has agreed that structural measures can be used as endpoints if they can be shown to correlate with functional measures [277]. A recent study showed that glaucomatous eyes with visual field progression had a significantly higher rate of RNFL loss, as measured by the GDxECC, than did non-progressing eyes [257]. In another study comparing structural and functional measures of glaucoma progression, the GDx guided progression analysis (GPA) detected glaucoma progression in a significant number of cases showing progression by conventional methods of automated perimetry, and optic disc photography, suggesting that the GDx GPA is a useful complement in the clinical evaluation and detection of longitudinal change in glaucoma [256].

3.11.5 Commercially Available Devices

Available unit:

The only commercially available scanning laser polarimeter is the GDx (Carl Zeiss Meditec, Inc., Dublin, CA).

(<http://www.meditec.zeiss.com/C1256CAB00599F5D/Contents-Frame/55A2E554EFCFC5B98825726C0001A9A7>)

There have been several iterations of the instrument, using the ECC and VCC mechanisms, as noted above, for calculating the cornea and lens birefringence contributions. The ECC and VCC features were used to compare the structure–function relationship between peripapillary retinal nerve fiber layer retardation and visual field sensitivity measured with standard automated perimetry in patients with glaucoma and normal subjects [278]. The effect of atypical birefringence patterns on this relationship was also assessed. The relationship between retinal nerve fiber layer retardation and standard automated perimetry visual field sensitivity was determined to be stronger in GDx images obtained with ECC. Similar results have been demonstrated in other studies [279].

3.11.6 Considerations for Ocular Toxicology Studies

The older, variable corneal compensation (GDx-VCC) instrument does not provide a “live” view of the area to be scanned and is therefore impractical for animal studies. The GDxPro instrument offers a “live” view as well as the ability to collect multiple images and create mean scans. Several progression analysis options are available (symmetry analysis, TSNIT (an acronym derived from “temporal, superior, nasal, inferior, temporal”), RNFL, and GPA) which are useful in toxicology studies. Since it measures different structural changes than optical coherence tomography, the two instruments should be considered complementary. In practice, however, and reflected by the recent reports available in the literature, the use of GDx is largely being supplanted by the use of advanced OCT units.

3.11.7 Limitations and Caveats

Retinal nerve fiber layer measurements are unaffected by prior photorefractive keratectomy and laser in situ keratomileusis [280]; however, scanning laser polarimetry measurements may be adversely affected when used in patients with peripapillary atrophy [281]. They are also unaffected by optic disc size [282]. Atypical retardation patterns may have a significant effect on the detection of progressive retinal nerve fiber layer loss [201]. Patients with large atypical patterns or pattern fluctuations may show false changes that may appear as glaucomatous progression or mask true changes in the retinal nerve fiber layer. Cataracts and other media opacities can adversely affect image quality parameters.

Acknowledgements The authors thank Michael W. Neider and Hugh D. Wabers for their helpful suggestions.

References

1. National Eye Institute. Advances in optical imaging and biomedical science symposium, Bethesda, MD, 1–2 June 2009. Available: http://www.nei.nih.gov/anniversary/symposia/optical_imaging.asp. Accessed 3 Sept 2012.
2. Erie JC, McLaren JW, Patel SV. Confocal microscopy in ophthalmology. *Am J Ophthalmol*. 2009;148:639–46.
3. Guthoff RF, Zhivov A, Stachs O. In vivo confocal microscopy, an inner vision of the cornea – a major review. *Clin Experiment Ophthalmol*. 2009;37:100–17.
4. Patel DV, McGhee CN. In vivo confocal microscopy of human corneal nerves in health, in ocular and systemic disease, and following corneal surgery: a review. *Br J Ophthalmol*. 2009;9:853–60.
5. Jalbert I, Stapleton F, Papas E, Sweeney DF, Coroneo M. In vivo confocal microscopy of the human cornea. *Br J Ophthalmol*. 2003;87:225–36.
6. Romano AC, Espana EM, Yoo SH, Budak MT, Wolosin JM, Tseng SC. Different cell sizes in human limbal and central corneal basal epithelia measured by confocal microscopy and flow cytometry. *Invest Ophthalmol Vis Sci*. 2003;44:5125–9.
7. Kaufman SC, Musch DC, Belin MW, Cohen EJ, Meisler DM, Reinhart WJ, Udell IJ, Van Meter WS. Confocal microscopy: a report by the American Academy of Ophthalmology. *Ophthalmology*. 2004;111:396–406.
8. Stachs O, Zhivov A, Kraak R, Stave J, Guthoff R. In vivo three-dimensional confocal laser scanning microscopy of the epithelial nerve structure in the human cornea. *Graefes Arch Clin Exp Ophthalmol*. 2007;245:569–75.
9. Zhivov A, Stachs O, Stave J, Guthoff RF. In vivo three-dimensional confocal laser scanning microscopy of corneal surface and epithelium. *Br J Ophthalmol*. 2009;93:667–72.
10. Patel S, McLaren J, Hodge D, Bourne W. Normal human keratocyte density and corneal thickness measurement by using confocal microscopy in vivo. *Invest Ophthalmol Vis Sci*. 2001;42:333–9.
11. McLaren JW, Nau CB, Erie JC, Bourne WM. Corneal thickness measurement by confocal microscopy, ultrasound, and scanning slit methods. *Am J Ophthalmol*. 2004;137:1011–20.
12. Morishige N, Takahashi N, Chikamoto N, Nishida T. Quantitative evaluation of corneal epithelial oedema by confocal microscopy. *Clin Experiment Ophthalmol*. 2009;37:249–53.
13. Pan ZY, Liang J, Zhang QA, Lin JR, Zheng ZZ. In vivo reflectance confocal microscopy of extramammary Paget disease: diagnostic evaluation and surgical management. *J Am Acad Dermatol*. 2012;66(2):e47–53.
14. Mocan MC, Kadayifcilar S, Irkec M. Keratic precipitate morphology in uveitic syndromes including Behçet's disease as evaluated with in vivo confocal microscopy. *Eye (Lond)*. 2009;23:1221–7.
15. Mahendradas P, Shetty R, Narayana KM, Shetty BK. In vivo confocal microscopy of keratic precipitates in infectious versus noninfectious uveitis. *Ophthalmology*. 2010;117:373–80.
16. Roszkowska AM, Aragona P. Corneal microstructural analysis in Weill-Marchesani syndrome by in vivo confocal microscopy. *Open Ophthalmol J*. 2011;5:48–50.
17. Zhang X, Chen Q, Chen W, Cui L, Ma H, Lu F. Tear dynamics and corneal confocal microscopy of subjects with mild self-reported office dry eye. *Ophthalmology*. 2011;118:902–7.
18. Chikama T, Takahashi N, Wakuta M, Morishige N, Nishida T. In vivo biopsy by laser confocal microscopy for evaluation of traumatic recurrent corneal erosion. *Mol Vis*. 2008;14:2333–9.
19. Niederer RL, Perumal D, Sherwin T, McGhee CN. Age-related differences in the normal human cornea: a laser scanning in vivo confocal microscopy study. *Br J Ophthalmol*. 2007;91:1165–9.
20. Le QH, Sun XH, Xu JJ. In vivo confocal microscopy of iridocorneal endothelial syndrome. *Int Ophthalmol*. 2009;29:11–8.
21. Zhang W, Wang J, Wang J, Jing Y. Corneal topography and in vivo confocal microscopy in different types of posterior polymorphous dystrophy. *Life Sci J*. 2011;8:227–38.

22. Efron N, Hollingsworth JG. New perspectives on keratoconus as revealed by corneal confocal microscopy. *Clin Exp Optom*. 2008;91:34–55.
23. Traversi C, Martone G, Malandrini A, Tosi GM, Caporossi A. In vivo confocal microscopy in recurrent granular dystrophy in corneal graft after penetrating keratoplasty. *Clin Experiment Ophthalmol*. 2006;34:808–10.
24. Jonuscheit S, Doughty MJ, Ramaesh K. In vivo confocal microscopy of the corneal endothelium: comparison of three morphometry methods after corneal transplantation. *Eye (Lond)*. 2011;25:1130–7.
25. Malik RA, Kallinikos P, Abbott CA, van Schie CH, Morgan P, Efron N, Boulton AJ. Corneal confocal microscopy: a non-invasive surrogate of nerve fibre damage and repair in diabetic patients. *Diabetologia*. 2003;46:683–8.
26. Cruzat A, Pavan-Langston D, Hamrah P. In vivo confocal microscopy of corneal nerves: analysis and clinical correlation. *Semin Ophthalmol*. 2010;25:171–7.
27. Labbé A, Dupas B, Offret H, Baudouin C, Labetoulle M. Evaluation of keratic precipitates and corneal endothelium in Fuchs' heterochromic cyclitis by in vivo confocal microscopy. *Br J Ophthalmol*. 2009;93:673–7.
28. Villani E, Galimberti D, Viola F, Mapelli C, Del Papa N, Ratiglia R. Corneal involvement in rheumatoid arthritis: an in vivo confocal study. *Invest Ophthalmol Vis Sci*. 2008;49:560–4.
29. Labbé A, Niaudet P, Loirat C, Charbit M, Guest G, Baudouin C. In vivo confocal microscopy and anterior segment optical coherence tomography analysis of the cornea in nephropathic cystinosis. *Ophthalmology*. 2009;116:870–6.
30. Al-Aqaba MA, Alomar T, Miri A, Fares U, Otri AM, Dua HS. Ex vivo confocal microscopy of human corneal nerves. *Br J Ophthalmol*. 2010;94:1251–7.
31. Mimura T, Yamagami S, Usui T, Honda N, Araki F, Amano S. In vivo confocal microscopy of human cornea covered with human amniotic membrane. *Jpn J Ophthalmol*. 2008;52:493–6.
32. Kafarnik C, Fritsche J, Reese S. In vivo confocal microscopy in the normal corneas of cats, dogs and birds. *Vet Ophthalmol*. 2007;10:222–30.
33. Ledbetter EC, Scarlett JM. In vivo confocal microscopy of the normal equine cornea and limbus. *Vet Ophthalmol*. 2009;12:57–64.
34. Ledbetter EC, Kice NC, Matusow RB, Dubovi EJ, Kim SG. The effect of topical ocular corticosteroid administration in dogs with experimentally induced latent canine herpesvirus-1 infection. *Exp Eye Res*. 2010;90:711–7.
35. Ledbetter EC, Irby NL, Kim SG. In vivo confocal microscopy of equine fungal keratitis. *Vet Ophthalmol*. 2011;14:1–9.
36. Trinh L, Brignole-Baudouin F, Labbé A, Raphaël M, Bourges JL, Baudouin C. The corneal endothelium in an endotoxin-induced uveitis model: correlation between in vivo confocal microscopy and immunohistochemistry. *Mol Vis*. 2008;14:1149–56.
37. Li HF, Petroll WM, Moller-Pedersen T, Maurer JK, Cavanagh HD, Jester JV. Epithelial and corneal thickness measurements by in vivo confocal microscopy through focusing (CMTF). *Curr Eye Res*. 1997;16:214–21.
38. Chang JH, Ren HW, Petroll MW, Cavanagh DH, Jester JV. The application of in vivo confocal microscopy and tear LDH measurement in assessing corneal response to contact lens and contact lens solutions. *Curr Eye Res*. 1999;19:171–81.
39. Ichijima H, Petroll WM, Jester JV, Cavanagh HD. Confocal microscopic studies of living rabbit cornea treated with benzalkonium chloride. *Cornea*. 1992;11:221–5.
40. Maurer JK, Li HF, Petroll WM, Parker RD, Cavanagh HD, Jester JV. Confocal microscopic characterization of initial corneal changes of surfactant-induced eye irritation in the rabbit. *Toxicol Appl Pharmacol*. 1997;143:291–300.
41. Liang H, Baudouin C, Pauly A, Brignole-Baudouin F. Conjunctival and corneal reactions in rabbits following short- and repeated exposure to preservative-free tafluprost, commercially available latanoprost and 0.02% benzalkonium chloride. *Br J Ophthalmol*. 2008;92:1275–82.
42. Liang H, Brignole-Baudouin F, Rabinovich-Guilatt L, Mao Z, Riancho L, Faure MO, Warnet JM, Lambert G, Baudouin C. Reduction of quaternary ammonium-induced ocular surface toxicity by emulsions: an in vivo study in rabbits. *Mol Vis*. 2008;14:204–16.

43. Liang H, Baudouin C, Faure MO, Lambert G, Brignole-Baudouin F. Comparison of the ocular tolerability of a latanoprost cationic emulsion versus conventional formulations of prostaglandins: an in vivo toxicity assay. *Mol Vis*. 2009;15:1690–9.
44. Chen W, Li Z, Hu J, Zhang Z, Chen L, Chen Y, Liu Z. Corneal alternations induced by topical application of benzalkonium chloride in rabbit. *PLoS One*. 2011;6:e26103.
45. Liang H, Brignole-Baudouin F, Pauly A, Riancho L, Baudouin C. Polyquad-preserved travoprost/timolol, benzalkonium chloride (BAK)-preserved travoprost/timolol, and latanoprost/timolol in fixed combinations: a rabbit ocular surface study. *Adv Ther*. 2011;28:311–25.
46. Pauloin T, Dutot M, Liang H, Chavinier E, Warnet JM, Rat P. Corneal protection with high-molecular-weight hyaluronan against in vitro and in vivo sodium lauryl sulfate-induced toxic effects. *Cornea*. 2009;28:1032–41.
47. Ivarsen A, Laurberg T, Moller-Pedersen T. Role of keratocyte loss on corneal wound repair after LASIK. *Invest Ophthalmol Vis Sci*. 2004;45:3499–506.
48. Ivarsen A, Moller-Pedersen T. LASIK induces minimal regrowth and no haze development in rabbit corneas. *Curr Eye Res*. 2005;30:363–73.
49. Ichijima H, Petroll WM, Jester JV, Ohashi J, Cavanagh HD. Effects of increasing Dk with rigid contact lens extended wear on rabbit corneal epithelium using confocal microscopy. *Cornea*. 1992;11:282–7.
50. Sirerol B, Walewska-Szafran A, Alio JL, Klonowski P, Rodriguez AE. Tolerance and biocompatibility of micronized black pigment for keratopigmentation simulated pupil reconstruction. *Cornea*. 2011;30:344–50.
51. Gramates PH, McDonald MB, Salib G, Clark L. Safety and efficacy of levofloxacin 1.5% eyedrops in nonhuman primates having penetrating keratoplasty: clinical and laboratory findings. *J Cataract Refract Surg*. 2005;31:1995–8.
52. Winchester K, Mathers WD, Sutphin JE, Daley TE. Diagnosis of *Acanthamoeba* keratitis in vivo with confocal microscopy. *Cornea*. 1995;14:10–7.
53. Mathers WD, Nelson SE, Lane JL, Wilson ME, Allen RC, Folberg R. Confirmation of confocal microscopy diagnosis of *Acanthamoeba* keratitis using polymerase chain reaction analysis. *Arch Ophthalmol*. 2000;118:178–83.
54. Kobayashi A, Ishibashi Y, Oikawa Y, Yokogawa H, Sugiyama K. In vivo and ex vivo laser confocal microscopy findings in patients with early-stage *Acanthamoeba* keratitis. *Cornea*. 2008;27:439–45.
55. Winchester K, Mathers WD, Sutphin JE. Diagnosis of *Aspergillus* keratitis in vivo with confocal microscopy. *Cornea*. 1997;16:27–31.
56. Brasnu E, Bourcier T, Dupas B, et al. In vivo confocal microscopy in fungal keratitis. *Br J Ophthalmol*. 2007;91:588–91.
57. Kanavi MR, Javadi M, Yazdani S, Mirdehghanm S. Sensitivity and specificity of confocal scan in the diagnosis of infectious keratitis. *Cornea*. 2007;26:782–6.
58. Benítez-Del-Castillo JM, Acosta MC, Wassfi MA, Díaz-Valle D, Gegúndez JA, Fernandez C, García-Sánchez J. Relation between corneal innervation with confocal microscopy and corneal sensitivity with noncontact esthesiometry in patients with dry eye. *Invest Ophthalmol Vis Sci*. 2007;48:173–81.
59. Chikama T, Takahashi N, Wakuta M, Nishida T. Noninvasive direct detection of ocular mucositis by in vivo confocal microscopy in patients treated with S-1. *Mol Vis*. 2009;15:2896–904.
60. Hillenaar T, Weenen C, Wubbels RJ, Remeijer L. Endothelial involvement in herpes simplex virus keratitis: an in vivo confocal microscopy study. *Ophthalmology*. 2009;116:2077–86.
61. Ciancaglini M, Carpineto P, Agnifili L, Nubile M, Fasanella V, Mastropasqua L. Conjunctival modifications in ocular hypertension and primary open angle glaucoma: an in vivo confocal microscopy study. *Invest Ophthalmol Vis Sci*. 2008;49:3042–8.
62. Niederer RL, Perumal D, Sherwin T, McGhee CN. Corneal innervation and cellular changes after corneal transplantation: an in vivo confocal microscopy study. *Invest Ophthalmol Vis Sci*. 2007;48:621–6.

63. Salvetat ML, Zeppieri M, Miani F, Parisi L, Felletti M, Brusini P. Comparison between laser scanning in vivo confocal microscopy and noncontact specular microscopy in assessing corneal endothelial cell density and central corneal thickness. *Cornea*. 2011;30:754–9.
64. McCarey BE, Edelhauser HF, Lynn MJ. Review of corneal endothelial specular microscopy for FDA clinical trials of refractive procedures, surgical devices, and new intraocular drugs and solutions. *Cornea*. 2008;27:1–16.
65. Suzuki S, Oshika T, Oki K, Sakabe I, Iwase A, Amano S, Araie M. Corneal thickness measurements: scanning-slit corneal topography and noncontact specular microscopy versus ultrasonic pachymetry. *J Cataract Refract Surg*. 2003;29:1313–8.
66. Ogbuehi KC, Almubrad TM. Repeatability of central corneal thickness measurements measured with the Topcon SP2000P specular microscope. *Graefes Arch Clin Exp Ophthalmol*. 2005;243:798–802.
67. Doughty MJ, Aakre BM. Further analysis of assessments of the coefficient of variation of corneal endothelial cell areas from specular microscopic images. *Clin Exp Optom*. 2008;91:438–46.
68. Bucht C, Söderberg P, Manneberg G. Simulation of specular microscopy images of corneal endothelium, a tool for control of measurement errors. *Acta Ophthalmol*. 2011;89:242–50.
69. Fujioka M, Nakamura M, Tatsumi Y, Kusuhara A, Maeda H, Negi A. Comparison of Pentacam Scheimpflug camera with ultrasound pachymetry and noncontact specular microscopy in measuring central corneal thickness. *Curr Eye Res*. 2007;32:89–94.
70. Uçakhan OO, Ozkan M, Kanpolat A. Corneal thickness measurements in normal and keratoconic eyes: Pentacam comprehensive eye scanner versus noncontact specular microscopy and ultrasound pachymetry. *J Cataract Refract Surg*. 2006;32:970–7.
71. Módis Jr L, Langenbucher A, Seitz B. Corneal endothelial cell density and pachymetry measured by contact and noncontact specular microscopy. *J Cataract Refract Surg*. 2002;28:1763–9.
72. Raecker ME, McLaren JW, Kittleson KM, Patel SV. Endothelial image quality after Descemet stripping with endothelial keratoplasty: a comparison of three microscopy techniques. *Eye Contact Lens*. 2011;37:6–10.
73. Kawana K, Tokunaga T, Miyata K, Okamoto F, Kiuchi T, Oshika T. Comparison of corneal thickness measurements using Orbscan II, non-contact specular microscopy, and ultrasonic pachymetry in eyes after laser in situ keratomileusis. *Br J Ophthalmol*. 2004;88:466–8.
74. Sanchis-Gimeno JA, Lleo-Perez A, Casanova J, Alonso L, Rahhal SM. Inter-observer variability of central corneal thickness measurements using non-contact specular microscopy after laser in situ keratomileusis. *Clin Exp Optom*. 2004;87:15–8.
75. Zhao MH, Zou J, Wang WQ, Li J. Comparison of central corneal thickness as measured by non-contact specular microscopy and ultrasound pachymetry before and post LASIK. *Clin Experiment Ophthalmol*. 2007;35:818–23.
76. Lass JH, Gal RL, Ruedy KJ, Benetz BA, Beck RW, Baratz KH, Holland EJ, Kalajian A, Kollman C, Manning FJ, et al. An evaluation of image quality and accuracy of eye bank measurement of donor cornea endothelial cell density in the Specular Microscopy Ancillary Study. *Ophthalmology*. 2005;112:431–40.
77. Benetz BA, Gal RL, Ruedy KJ, Rice C, Beck RW, Kalajian AD, Lass JH, Cornea Donor Study Group. Specular microscopy ancillary study methods for donor endothelial cell density determination of Cornea Donor Study images. *Curr Eye Res*. 2006;31:319–27.
78. Kanavi MR, Javadi M-A, Chamani T. Specular microscopic features of corneal endothelial vacuolation. *J Ophthalmic Vis Res*. 2011;6:5–7.
79. Ollivier FJ, Brooks DE, Komaromy AM, Kallberg ME, Andrew SE, Sapp HL, Sherwood MB, Dawson WW. Corneal thickness and endothelial cell density measured by non-contact specular microscopy and pachymetry in Rhesus macaques (*Macaca mulatta*) with laser-induced ocular hypertension. *Exp Eye Res*. 2003;76:671–7.
80. Pigatto JAT, Cesar F, Gener Tadeu Pereira GT, et al. Density of corneal endothelial cells in eyes of dogs using specular microscopy. *Braz J Vet Res Anim Sci*. 2006;43:476–80.
81. Pigatto JAT, Cerva C, Freire CD, et al. Morphological analysis of the corneal endothelium in eyes of dogs using specular microscopy. *Pesq Vet Bras*. 2008;28:427–30.

82. Miller JM, Holley GP, Miller PE, Edelhauser HF, Murphy CJ, McCulloh RJ, Christian BJ, Smith PB, Lam TT. Corneal endothelial cell density measurements using noncontact specular microscopy in rabbits, dogs and monkeys. Presented at Association for Research in Vision and Ophthalmology, April 2008, Fort Lauderdale, FL.
83. Al-Ageel S, Al-Muammar AM. Comparison of central corneal thickness measurements by Pentacam, noncontact specular microscope, and ultrasound pachymetry in normal and post-LASIK eyes. *Saudi J Ophthalmol.* 2009;23:181–7.
84. Szalai E, Nemeth G, Berta A, Modis Jr L. Evaluation of the corneal endothelium using non-contact and contact specular microscopy. *Cornea.* 2011;3:567–70.
85. Rosales P, Marcos S. Pentacam Scheimpflug quantitative imaging of the crystalline lens and intraocular lens. *J Refract Surg.* May 2009;25(5):421–428.
86. Wegener A, Laser-Junga H. Photography of the anterior eye segment according to Scheimpflug's principle: options and limitations - a review. *Clin Experiment Ophthalmol.* Jan 2009;37(1):144–154.
87. Chen D, Lam AK. Intra-session and inter-session repeatability of the Pentacam system on posterior corneal assessment in the normal human eye. *J Cataract Refract Surg.* 2007;33:448–54.
88. Kirkwood BJ, Hendicott PL, Read SA, Pesudovs K. Repeatability and validity of lens densitometry measured with Scheimpflug imaging. *J Cataract Refract Surg.* 2009;35:1210–5.
89. de Castro A, Rosales P, Marcos S. Tilt and decentration of intraocular lenses in vivo from Purkinje and Scheimpflug imaging. Validation study. *J Cataract Refract Surg.* 2007;33:418–29.
90. Grewal D, Jain R, Brar GS, Grewal SP. Pentacam tomograms: a novel method for quantification of posterior capsule opacification. *Invest Ophthalmol Vis Sci.* 2008;49:2004–8.
91. Turner SJ, Lee EJ, Hu V, Hollick EJ. Scheimpflug imaging to determine intraocular lens power in vivo. *J Cataract Refract Surg.* 2007;33:1041–4.
92. de Sanctis U, Loiacono C, Richiardi L, Turco D, Mutani B, Grignolo FM. Sensitivity and specificity of posterior corneal elevation measured by Pentacam in discriminating keratoconus/subclinical keratoconus. *Ophthalmology.* 2008;115:1534–9.
93. Xu Y, Hersh PS, Chu DS. Wavefront analysis and Scheimpflug imagery in diagnosis of anterior lenticonus. *J Cataract Refract Surg.* 2010;36:850–3.
94. Arora R, Mehta S, Goyal JL, Pahuja S, Gupta D, Gupta R. Pattern of Scheimpflug imaging in anterior segment foreign bodies. *Eye (Lond).* 2010;24:1304–6.
95. Hockwin O, Wegener A. Syn- and cocataractogenesis. A system for testing subliminal lens toxicity. In: Hockwin O, editor. *Drug-induced ocular side effects and ocular toxicology, concepts toxicol.* Basel: Karger; 1987. p. 241–9.
96. Wegener A, Hockwin O. Animal models as a tool to detect the subliminal cocataractogenic potential of drugs. In: Hockwin O, editor. *Drug-induced ocular side effects and ocular toxicology, concepts toxicol.* Basel: Karger; 1987. p. 250–62.
97. Wegener A, Kaegler M, Stinn W. Age-related light scattering in rat lenses observed in a 2-year inhalation toxicity study. *Ophthalmic Res.* 2002;34:273–80.
98. Böker T, Wegener A, Koch F, Hockwin O. Comparison of Scheimpflug-photography, specular microscopy and scanning electron microscopy to detect corneal changes in toxicity studies in rats. *Lens Eye Toxic Res.* 1990;7:517–29.
99. Croft M, Glasser A, Heatley G, McDonald J, Ebbert T, Kaufman PL. Accommodative ciliary body and lens function in rhesus monkeys. I. Normal lens, zonule and ciliary process configuration in the iridectomized eye. *Invest Ophthalmol Vis Sci.* 2006;47:1076–86.
100. Koretz JF, Neider MW, Kaufman PL, Bertasso AM, DeRousseau CJ, Bito LZ. Slit-lamp studies of the rhesus monkey eye. I. Survey of the anterior segment. *Exp Eye Res.* 1987;44:307–18.
101. Koretz JF, Bertasso AM, Neider MW, True-Gabelt BA, Kaufman PL. Slit-lamp studies of the rhesus monkey eye: II. Changes in crystalline lens shape, thickness and position during accommodation and aging. *Exp Eye Res.* 1987;45:317–26.
102. Subramanian R, Cook C, Croft M, DePaul KL, Neider M, Ferrier NJ, Kaufman PL, Koretz JF. Unilateral real-time Scheimpflug videography to study accommodation dynamics in human eyes. *Invest Ophthalmol Vis Sci.* 2003;44:240.

103. Uçakhan ÖÖ, Cetinkor V, Özkan M, Kanpolat A. Evaluation of Scheimpflug imaging parameters in subclinical keratoconus, keratoconus, and normal eyes. *J Cataract Refract Surg.* 2011;37:1116–24.
104. Piñero DP, Alió JL, Alesón A, Escaf M, Miranda M. Pentacam posterior and anterior corneal aberrations in normal and keratoconic eyes. *Clin Exp Optom.* 2009;92:297–303.
105. Grewal DS, Brar GS, Jain R, Sood V, Singla M, Grewal SP. Corneal collagen crosslinking using riboflavin and ultraviolet-A light for keratoconus: one-year analysis using Scheimpflug imaging. *J Cataract Refract Surg.* 2009;35:425–32.
106. Wiemer NG, Dubbelman M, Ringens PJ, Polak BC. Measuring the refractive properties of the diabetic eye during blurred vision and hyperglycaemia using aberrometry and Scheimpflug imaging. *Acta Ophthalmol.* 2009;87:176–82.
107. Shankar H, Taranath D, Santhirathelagan CT, Pesudovs K. Anterior segment biometry with the Pentacam: comprehensive assessment of repeatability of automated measurements. *J Cataract Refract Surg.* 2008;34:103–13.
108. Miranda MA, Radhakrishnan H, O'Donnell C. Repeatability of corneal thickness measured using an Oculus Pentacam. *Optom Vis Sci.* 2009;86:266–72.
109. Barkana Y, Gerber Y, Elbaz U, Schwartz S, Ken-Dror G, Avni I, Zadok D. Central corneal thickness measurement with the Pentacam Scheimpflug system, optical low-coherence reflectometry pachymeter, and ultrasound pachymetry. *J Cataract Refract Surg.* 2005;31:1729–35.
110. Faramarzi A, Karimian F, Jafarinasab MR, Jabbarpoor Bonyadi MH, Yaseri M. Central corneal thickness measurements after myopic photorefractive keratectomy using Scheimpflug imaging, scanning-slit topography, and ultrasonic pachymetry. *J Cataract Refract Surg.* 2010;36:1543–9.
111. Grewal DS, Brar GS, Grewal SP. Assessment of central corneal thickness in normal, keratoconus, and post-laser in situ keratomileusis eyes using Scheimpflug imaging, spectral domain optical coherence tomography, and ultrasound pachymetry. *J Cataract Refract Surg.* 2010;36:954–64.
112. Konstantopoulos A, Hossain P, Anderson DF. Recent advances in ophthalmic anterior segment imaging: a new era for ophthalmic diagnosis? *Br J Ophthalmol.* 2007;91:551–7.
113. Pavlin CJ, Vásquez LM, Lee R, Simpson ER, Ahmed II. Anterior segment optical coherence tomography and ultrasound biomicroscopy in the imaging of anterior segment tumors. *Am J Ophthalmol.* 2009;147:214–9.
114. Dada T, Sihota R, Gadia R, Aggarwal A, Mandal S, Gupta V. Comparison of anterior segment optical coherence tomography and ultrasound biomicroscopy for assessment of the anterior segment. *J Cataract Refract Surg.* 2007;33:837–40.
115. Sangermani C, Mora P, Mancini C, Vecchi M, Gandolfi SA. Ultrasound biomicroscopy in two cases of ocular siderosis with secondary glaucoma. *Acta Ophthalmol.* 2010;88:1–2.
116. Kumar RS, Baskaran M, Chew PT, Friedman DS, Handa S, Lavanya R, Sakata LM, Wong HT, Aung T. Prevalence of plateau iris in primary angle closure suspects an ultrasound biomicroscopy study. *Ophthalmology.* 2008;115:430–4.
117. Sun CB, Liu Z, Yao K. Ultrasound biomicroscopy in pupillary block glaucoma secondary to ophthalmic viscosurgical device remnants in the posterior chamber after anterior chamber phakic intraocular lens implantation. *J Cataract Refract Surg.* 2010;36:2204–6.
118. Dougherty PJ, Rivera RP, Schneider D, Lane SS, Brown D, Vukich J. Improving accuracy of phakic intraocular lens sizing using high-frequency ultrasound biomicroscopy. *J Cataract Refract Surg.* 2011;37:13–8.
119. Kim KH, Shin HH, Kim HM, Song JS. Correlation between ciliary sulcus diameter measured by 35 MHz ultrasound biomicroscopy and other ocular measurements. *J Cataract Refract Surg.* 2008;34:632–7.
120. Giuliani GP, McGowan HD, Pavlin CJ, Heathcote JG, Simpson ER. Ultrasound biomicroscopic imaging of iris melanoma: a clinicopathologic study. *Am J Ophthalmol.* 2011;151:579–85.

121. Vasquez LM, Giuliari GP, Halliday W, Pavlin CJ, Gallie BL, Héon E. Ultrasound biomicroscopy in the management of retinoblastoma. *Eye (Lond)*. 2011;25:141–7.
122. Solarte CE, Smith DR, Buncic JR, Tehrani NN, Kraft SP. Evaluation of vertical rectus muscles using ultrasound biomicroscopy. *J AAPOS*. 2008;12:128–231.
123. Peizeng Y, Qianli M, Xiangkun H, Hongyan Z, Li W, Kijlstra A. Longitudinal study of anterior segment inflammation by ultrasound biomicroscopy in patients with acute anterior uveitis. *Acta Ophthalmol*. 2009;87:211–5.
124. Sbeity Z, Palmiero PM, Saint-Louis LA, Dorairaj S, Liebmann J, Ritch R. Asymmetric progressive glaucomatous optic neuropathy in a patient with a rare developmental variant of the ophthalmic artery. *J Glaucoma*. 2008;17:699–701.
125. Yeh PT, Yang CM, Yang CH, Huang JS. Cryotherapy of the anterior retina and sclerotomy sites in diabetic vitrectomy to prevent recurrent vitreous hemorrhage: an ultrasound biomicroscopy study. *Ophthalmology*. 2005;112:2095–102.
126. Dulaurent T, Gouille F, Dulaurent A, Mentek M, Peiffer RL, Isard PF. Effect of mydriasis induced by topical instillations of 0.5% tropicamide on the anterior segment in normotensive dogs using ultrasound biomicroscopy. *Vet Ophthalmol*. 2012 Mar;15, Suppl 1:8–13. Epub 2011 Apr 19.
127. Nissirios N, Chanis R, Johnson E, Morrison J, Cepurna WO, Jia L, Mittag T, Danias J. Comparison of anterior segment structures in two rat glaucoma models: an ultrasound biomicroscopic study. *Invest Ophthalmol Vis Sci*. 2008;49:2478–82.
128. Rose MD, Mattoon JS, Gemensky-Metzler AJ, Wilkie DA, Rajala-Schultz PJ. Ultrasound biomicroscopy of the iridocorneal angle of the eye before and after phacoemulsification and intraocular lens implantation in dogs. *Am J Vet Res*. 2008;69:279–88.
129. Lütjen-Drecoll E, Kaufman PL, Wasielewski R, Ting-Li L, Croft MA. Morphology and accommodative function of the vitreous zonule in human and monkey eyes. *Invest Ophthalmol Vis Sci*. 2010;51:1554–64.
130. Croft M, McDonald JP, Nadkarni NV, Lin TL, Kaufman PL. Age-related changes in centripetal ciliary body movement relative to centripetal lens movement in monkeys. *Exp Eye Res*. 2009;89:824–32.
131. Wasielewski R, McDonald JP, Heatley G, Lütjen-Drecoll E, Kaufman PL, Croft MA. Surgical intervention and accommodative responses, II: Forward ciliary body accommodative movement is facilitated by zonular attachments to the lens capsule. *Invest Ophthalmol Vis Sci*. 2008;49:5495–502.
132. Kamal AM, Hanafy M, Ehsan A, Tomerak RH. Ultrasound biomicroscopy comparison of ab interno and ab externo scleral fixation of posterior chamber intraocular lenses. *J Cataract Refract Surg*. 2009;35:881–4.
133. Marchini G, Pedrotti E, Modesti M, Visentin S, Tosi R. Anterior segment changes during accommodation in eyes with a monofocal intraocular lens: high-frequency ultrasound study. *J Cataract Refract Surg*. 2008;34:949–56.
134. Mora P, Sangermani C, Ghirardini S, Carta A, Ungaro N, Gandolfi S. Ultrasound biomicroscopy and iris pigment dispersion: a case-control study. *Br J Ophthalmol*. 2010;94:428–32.
135. Ladas JG, Wheeler NC, Morhun PJ, Rimmer SO, Holland GN. Laser flare-cell photometry: methodology and clinical applications. *Surv Ophthalmol*. 2005;50:27–47.
136. Herbort CP, Tugal-Tutkun I. Editorial: laser flare (cell) photometry: 20 years already. *Int Ophthalmol*. 2010;30:445–7.
137. Ni M, Bloom JN, Lele S, Sotelo-Avila C. A laboratory evaluation of the Kowa laser flare-cell meter for the study of uveitis. *Graefes Arch Clin Exp Ophthalmol*. 1992;230:547–51.
138. Sawa M. Clinical application of laser flare-cell meter. *Jpn J Ophthalmol*. 1990;34:346–63.
139. Abe T, Hayasaka Y, Zhang XY, Hayasaka S. Effects of intravenous administration of FR122047 (a selective cyclooxygenase 1 inhibitor) and FR188582 (a selective cyclooxygenase 2 inhibitor) on prostaglandin-E2-induced aqueous flare elevation in pigmented rabbits. *Ophthalmic Res*. 2004;36:321–6.
140. Shoji N, Oshika T, Amano S, Masuda K. Effects of endothelin receptor antagonists on anterior chamber inflammation induced by intravitreal injection of endothelin-1. *Exp Eye Res*. 1999;69:437–44.

141. Hayasaka Y, Hayasaka S, Zhang XY, Nagaki Y. Effects of topical anti-inflammatory and antiallergic eyedrops on prostaglandin E2-induced aqueous flare elevation in pigmented rabbits. *Arch Ophthalmol*. 2002;120:950–3.
142. Arvind H, Klistorner A, Graham S, Grigg J, Goldberg I, Klistorner A, Billson FA. Dichoptic stimulation improves detection of glaucoma with multifocal visual evoked potentials. *Invest Ophthalmol Vis Sci*. 2007;48:4590–6.
143. Hayasaka Y, Hayasaka S, Zhang XY, Nagaki Y. Effects of topical mydriatics and vasoconstrictors on prostaglandin-E2-induced aqueous flare elevation in pigmented rabbits. *Ophthalmic Res*. 2003;35:256–60.
144. Nagaki Y, Hayasaka S, Abe T, Zhang XY, Hayasaka Y, Terasawa K. Effects of oral administration of Gardeniae fructus extract and intravenous injection of crocetin on lipopolysaccharide- and prostaglandin E2-induced elevation of aqueous flare in pigmented rabbits. *Am J Chin Med*. 2003;31:729–38.
145. Krohne SG, Blair MJ, Bingaman D, Gionfriddo JR. Carprofen inhibition of flare in the dog measured by laser flare photometry. *Vet Ophthalmol*. 1998;1:81–4.
146. Xu W, Wang H, Wang F, Jiang Y, Zhang X, Wang W, Qian J, Xu X, Sun X. Testing toxicity of multiple intravitreal injections of bevacizumab in rabbit eyes. *Can J Ophthalmol*. 2010;45:386–92.
147. Zhang XY, Hayasaka S, Hayasaka Y, Yanagisawa S, Nagaki Y. Effects of isopropyl unoprostone, latanoprost, and prostaglandin E(2) on acute rise of aqueous flare in pigmented rabbits. *Ophthalmic Res*. 2002;34:90–3.
148. Kojima M, Hata I, Wake K, Watanabe S, Yamanaka Y, Kamimura Y, Taki M, Sasaki K. Influence of anesthesia on ocular effects and temperature in rabbit eyes exposed to microwaves. *Bioelectromagnetics*. 2004;25:228–33.
149. Abela-Formanek C, Amon M, Schild G, Schauersberger J, Heinze G, Kruger A. Uveal and capsular biocompatibility of hydrophilic acrylic, hydrophobic acrylic, and silicone intraocular lenses. *J Cataract Refract Surg*. 2002;28:50–61.
150. Abela-Formanek C, Amon M, Kahraman G, Schauersberger J, Dunavoelgyi R. Biocompatibility of hydrophilic acrylic, hydrophobic acrylic, and silicone intraocular lenses in eyes with uveitis having cataract surgery: long-term follow-up. *J Cataract Refract Surg*. 2011;37:104–12.
151. Gatinel D, Lebrun T, Le Toumelin P, Chaine G. Aqueous flare induced by heparin-surface-modified poly(methyl methacrylate) and acrylic lenses implanted through the same-size incision in patients with diabetes. *J Cataract Refract Surg*. 2001;27:855–60.
152. Krepler K, Ries E, Derbolav A, Nepp J, Wedrich A. Inflammation after phacoemulsification in diabetic retinopathy. Foldable acrylic versus heparin-surface-modified poly(methyl methacrylate) intraocular lenses. *J Cataract Refract Surg*. 2001;27:233–8.
153. Meacock WR, Spalton DJ, Bender L, Antcliff R, Heatley C, Stanford MR, Graham EM. Steroid prophylaxis in eyes with uveitis undergoing phacoemulsification. *Br J Ophthalmol*. 2004;88:1122–4.
154. Kruger AJ, Amon M, Abela-Formanek C, Schild G, Kolodjaschna J, Schauersberger J. Postoperative inflammation after lens epithelial cell removal: 2 year results. *J Cataract Refract Surg*. 2001;27:1380–5.
155. Kruger A, Amon M, Abela-Formanek C, Schild G, Kolodjaschna J, Schauersberger J. Effect of heparin in the irrigation solution on postoperative inflammation and cellular reaction on the intraocular lens surface. *J Cataract Refract Surg*. 2002;28:87–92.
156. Papa V, Milazzo G, Santocono M, Servolle V, Sourdille P, Santiago PY, Darondeau J, Cassoux N, LeHoang P. Naproxen ophthalmic solution to manage inflammation after phacoemulsification. *J Cataract Refract Surg*. 2002;28:321–7.
157. Wadood AC, Armbrrecht AM, Aspinnall PA, Dhillon B. Safety and efficacy of a dexamethasone anterior segment drug delivery system in patients after phacoemulsification. *J Cataract Refract Surg*. 2004;30:761–8.
158. Orenge-Nania S, El-Harazi SM, Oram O, Feldman RM, Chuang AZ, Gross RL. Effects of atropine on anterior chamber depth and anterior chamber inflammation after primary trabeculectomy. *J Glaucoma*. 2000;9:303–10.

159. Tugal-Tutkun I, Herbort CP. Laser flare photometry: a noninvasive, objective, and quantitative method to measure intraocular inflammation. *Int Ophthalmol*. 2010;30:453–64.
160. Wakefield D, Herbort CP, Tugal-Tutkun I, Zierhut M. Controversies in ocular inflammation and immunology laser flare photometry. *Ocul Immunol Inflamm*. 2010;18:334–40.
161. Fahim MM, Haji S, Koonapareddy CV, Fan VC, Asbell PA. Fluorophotometry as a diagnostic tool for the evaluation of dry eye disease. *BMC Ophthalmol*. 2006;6:20.
162. Ghate D, Brooks W, McCarey BE, Edelhauser HF. Pharmacokinetics of intraocular drug delivery by periocular injections using ocular fluorophotometry. *Invest Ophthalmol Vis Sci*. 2007;48:2230–7.
163. Lee SJ, Kim ES, Geroski DH, McCarey BE, Edelhauser HF. Pharmacokinetics of intraocular drug delivery of Oregon green 488-labeled triamcinolone by subtenon injection using ocular fluorophotometry in rabbit eyes. *Invest Ophthalmol Vis Sci*. 2008;49:4506–14.
164. Steinfeld A, Lux A, Maier S, Suverkrup R, Diestelhorst M. Bioavailability of fluorescein from a new drug delivery system in human eyes. *British J Ophthalmol*. 2004;88:48–53.
165. Lux A, Maier S, Dinslage S, Suverkrup R, Diestelhorst M. Comparative bioavailability study of three conventional eye drops versus a single lyophilisate. *British J Ophthalmol*. 2003;87:436–40.
166. Virtanen T, Huotari K, Harkonen M, Tervo T. Lacrimal plugs as a therapy for contact lens intolerance. *Eye (Lond)*. 1996;10(Pt 6):727–31.
167. Glasson MJ, Stapleton F, Keay L, Willcox MD. The effect of short term contact lens wear on the tear film and ocular surface characteristics of tolerant and intolerant wearers. *Cont Lens Anterior Eye*. 2006;29:41–7; quiz 49.
168. Toris CB, Zhan GL, Yablonski ME, Camras CB. Effects on aqueous flow of dorzolamide combined with either timolol or acetazolamide. *J Glaucoma*. 2004;13:210–5.
169. Tsukamoto H, Larsson LI. Aqueous humor flow in normal human eyes treated with brimonidine and dorzolamide, alone and in combination. *Arch Ophthalmol*. 2004;122:190–3.
170. Avila MY, Mitchell CH, Stone RA, Civan MM. Noninvasive assessment of aqueous humor turnover in the mouse eye. *Invest Ophthalmol Vis Sci*. 2003;44:722–7.
171. Lazaro C, Benitez-del-Castillo JM, Castillo A, Garcia-Feijoo J, Macias JM, Garcia-Sanchez J. Lens fluorophotometry after trabeculectomy in primary open-angle glaucoma. *Ophthalmology*. 2002;109:76–9.
172. Fernández-Barrientos Y, García-Feijoó J, Martínez-de-la-Casa JM, Pablo LE, Fernández-Pérez C, García SJ. Fluorophotometric study of the effect of the glaukos trabecular microbypass stent on aqueous humor dynamics. *Invest Ophthalmol Vis Sci*. 2010;51:3327–32.
173. Mochizuki H, Yamada M, Hato S, Nishida T. Fluorophotometric measurement of the precorneal residence time of topically applied hyaluronic acid. *Br J Ophthalmol*. 2008;92:108–11.
174. Webb RH, Hughes GW, Delori FC. Confocal scanning laser ophthalmoscope. *Appl Opt*. 1987;26:1492–9.
175. Huber G, Heynen S, Imsand C, von Hagen F, Muehlfriedel R, Tanimoto N, Feng Y, Hammes HP, Grimm C, Peichl L, et al. Novel rodent models for macular research. *PLoS One*. 2010;5:e13403.
176. Furrer P, Plazonnet B, Mayer JM, Gurny R. Application of in vivo confocal microscopy to the objective evaluation of ocular irritation induced by surfactants. *Int J Pharm*. 2000;207:89–98.
177. Xie F, Sun D, Schering A, Nakao S, Zandi S, Liu P, Hafezi-Moghadam A. Novel molecular imaging approach for subclinical detection of iritis and evaluation of therapeutic success. *Am J Pathol*. 2010;177:39–48.
178. Sugiyama T, Mashima Y, Yoshioka Y, Oku H, Ikeda T. Effect of unoprostone on topographic and blood flow changes in the ischemic optic nerve head of rabbits. *Arch Ophthalmol*. 2009;127:454–9.
179. Aartsen WM, van Cleef KW, Pellissier LP, Hoek RM, Vos RM, Blits B, Ehlert EM, Balaggan KS, Ali RR, Verhaagen J, et al. GFAP-driven GFP expression in activated mouse Müller glial cells aligning retinal blood vessels following intravitreal injection of AAV2/6 vectors. *PLoS One*. 2010;5:e12387.

180. Beck SC, Schaeferhoff K, Michalakakis S, Fischer MD, Huber G, Rieger N, Riess O, Wissinger B, Biel M, Bonin M, et al. In vivo analysis of cone survival in mice. *Invest Ophthalmol Vis Sci.* 2010;51:49493–7.
181. Tolmachova T, Wavre-Shapton ST, Barnard AR, MacLaren RE, Futter CE, Seabra MC. Retinal pigment epithelium defects accelerate photoreceptor degeneration in cell type-specific knockout mouse models of choroideremia. *Invest Ophthalmol Vis Sci.* 2010;51:4913–20.
182. Scoles D, Gray DC, Hunter JJ, Wolfe R, Gee BP, Geng Y, Masella BD, Libby RT, Russell S, Williams DR, et al. In vivo imaging of retinal nerve fiber layer vasculature: imaging histology comparison. *BMC Ophthalmol.* 2009;9:9.
183. Greenfield DS, Weinreb RN. Role of optic nerve imaging in glaucoma clinical practice and clinical trials. *Am J Ophthalmol.* 2008;145:598–603.
184. Weinreb RN, Zangwill LM, Jain S, Becerra LM, Dirkes K, Piltz-Seymour JR, Cioffi GA, Trick GL, Coleman AL, Brandt JD, et al. Predicting the onset of glaucoma: the confocal scanning laser ophthalmoscopy ancillary study to the Ocular Hypertension Treatment Study. *Ophthalmology.* 2010;117:1674–83.
185. Leung CK, Medeiros FA, Zangwill LM, Sample PA, Bowd C, Ng D, Cheung CY, Lam DS, Weinreb RN. American Chinese glaucoma imaging study: a comparison of the optic disc and retinal nerve fiber layer in detecting glaucomatous damage. *Invest Ophthalmol Vis Sci.* 2007;48:2644–52.
186. Mumcuoglu T, Townsend KA, Wollstein G, Ishikawa H, Bilonick RA, Sung KR, Kagemann L, Schuman JS. Advanced Imaging in Glaucoma Study Group. Assessing the relationship between central corneal thickness and retinal nerve fiber layer thickness in healthy subjects. *Am J Ophthalmol.* 2008;146:561–6.
187. Landa G, Garcia PM, Rosen RB. Correlation between retina blood flow velocity assessed by retinal function imager and retina thickness estimated by scanning laser ophthalmoscopy/optical coherence tomography. *Ophthalmologica.* 2009;223:155–61.
188. Talcott KE, Ratnam K, Sundquist SM, Lucero AS, Lujan BJ, Tao W, Porco TC, Roorda A, Duncan JL. Longitudinal study of cone photoreceptors during retinal degeneration and in response to ciliary neurotrophic factor treatment. *Invest Ophthalmol Vis Sci.* 2011;52:2219–26.
189. Finger PT, Chin K. Anti-vascular endothelial growth factor bevacizumab (Avastin) for radiation retinopathy. *Arch Ophthalmol.* 2007;125:751–6.
190. Fleckenstein M, Schmitz-Valckenberg S, Adrion C, Krämer I, Eter N, Helb HM, Brinkmann CK, Charbel Issa P, Mansmann U, Holz FG. Tracking progression with spectral-domain optical coherence tomography in geographic atrophy caused by age-related macular degeneration. *Invest Ophthalmol Vis Sci.* 2010;51:3846–52.
191. Charbel Issa P, Troeger E, Finger R, Holz FG, Wilke R, Scholl HP. Structure-function correlation of the human central retina. *PLoS One.* 2010;5:e12864.
192. Wild JM, Robson CR, Jones AL, Cunliffe IA, Smith PE. Detecting vigabatrin toxicity by imaging of the retinal nerve fiber layer. *Invest Ophthalmol Vis Sci.* 2006;47:917–24.
193. Gabriele ML, Wollstein G, Ishikawa H, Kagemann L, Xu J, Folio LS, Schuman JS. Optical coherence tomography: history, current status, and laboratory work. *Invest Ophthalmol Vis Sci.* 2011;52:2425–36.
194. Mujat M, Park BH, Cense B, Chen TC, de Boer JF. Autocalibration of spectral-domain optical coherence tomography spectrometers for in vivo quantitative retinal nerve fiber layer birefringence determination. *J Biomed Opt.* 2007;12:041205.
195. Srinivasan VJ, Adler DC, Chen Y, Gorczynska I, Huber R, Duker JS, Schuman JS, Fujimoto JG. Ultrahigh-speed optical coherence tomography for three-dimensional and en face imaging of the retina and optic nerve head. *Invest Ophthalmol Vis Sci.* 2008;49:5103–10.
196. Nassif N, Cense B, Pierce M, Yun S, Bouma B, Tearney G, Chen T, de Boer J. In vivo high-resolution video-rate spectral-domain optical coherence tomography of the human retina and optic nerve. *Opt Express.* 2004;12:367–76.
197. Makita S, Fabritius T, Yasuno Y. Full-range, high-speed, high-resolution 1 microm spectral-domain optical coherence tomography using BM-scan for volumetric imaging of the human posterior eye. *Opt Express.* 2008;16:8406–20.

198. Kanadani FN, Hood DC, Grippo TM, Wangsupadilok B, Harizman N, Greenstein VC, Liebmann JM, Ritch R. Structural and functional assessment of the macular region in patients with glaucoma. *Br J Ophthalmol*. 2006;90:1393–7.
199. Bowd C. Optical coherence tomography for clinical detection and monitoring of glaucoma? *Br J Ophthalmol*. 2007;91:853–4.
200. Kagemann L, Mumcuoglu T, Wollstein G, Bilonick R, Ishikawa H, Townsend KA, Gabriele M, Fujimoto JG, Schuman JS. Sources of longitudinal variability in optical coherence tomography nerve-fibre layer measurements. *Br J Ophthalmol*. 2008;92:806–9.
201. Medeiros FA, Zangwill LM, Alencar LM, Bowd C, Sample PA, Susanna Jr R, Weinreb RN. Detection of glaucoma progression with stratus OCT retinal nerve fiber layer, optic nerve head, and macular thickness measurements. *Invest Ophthalmol Vis Sci*. 2009;50:5741–8.
202. Townsend KA, Wollstein G, Schuman JS. Imaging of the retinal nerve fibre layer for glaucoma. *Br J Ophthalmol*. 2009;93:139–43.
203. Lee EJ, Kim TW, Weinreb RN, Park KH, Kim SH, Kim DM. Trend-based analysis of retinal nerve fiber layer thickness measured by optical coherence tomography in eyes with localized nerve fiber layer defects. *Invest Ophthalmol Vis Sci*. 2011;52:1138–44.
204. Shoji T, Sato H, Ishida M, Takeuchi M, Chihara E. Assessment of glaucomatous changes in subjects with high myopia using spectral domain optical coherence tomography. *Invest Ophthalmol Vis Sci*. 2011;52:1098–102.
205. Xin D, Greenstein VC, Ritch R, Liebmann JM, De Moraes CG, Hood DC. A comparison of functional and structural measures for identifying progression of glaucoma. *Invest Ophthalmol Vis Sci*. 2011;52:519–26.
206. Pasol J. Neuro-ophthalmic disease and optical coherence tomography: glaucoma look-alikes. *Curr Opin Ophthalmol*. 2011;22:124–32.
207. Sakata LM, Lavanya R, Friedman DS, Aung HT, Gao H, Kumar RS, Foster PJ, Aung T. Comparison of gonioscopy and anterior segment ocular coherence tomography in detecting angle closure in different quadrants of the anterior chamber angle. *Ophthalmology*. 2008;115:769–74.
208. Thomas MG, Kumar A, Kohl S, Proudlock FA, Gottlob I. High-resolution in vivo imaging in achromatopsia. *Ophthalmology*. 2011;118:882–7.
209. Wylegala E, Dobrowolski D, Nowińska A, Tarnawska D. Anterior segment optical coherence tomography in eye injuries. *Graefes Arch Clin Exp Ophthalmol*. 2009;247:451–5.
210. Inoue R, Hangai M, Kotera Y, Nakanishi H, Mori S, Morishita S, Yoshimura N. Three-dimensional high-speed optical coherence tomography imaging of lamina cribrosa in glaucoma. *Ophthalmology*. 2009;116:214–22.
211. Inoue M, Watanabe Y, Arakawa A, Sato S, Kobayashi S, Kadonosono K. Spectral-domain optical coherence tomography images of inner/outer segment junctions and macular hole surgery outcomes. *Graefes Arch Clin Exp Ophthalmol*. 2009;247:325–30.
212. Mansour AM, Yunis MH, Medawar WA. Ocular coherence tomography of symptomatic phototoxic retinopathy after cataract surgery: a case report. *J Med Case Reports*. 2011;5:133.
213. Sarunic MV, Asrani S, Izatt JA. Imaging the ocular anterior segment with real-time, full-range Fourier-domain optical coherence tomography. *Arch Ophthalmol*. 2008;126:537–42.
214. Lee EC, de Boer JF, Mujat M, Lim H, Yun SH. In vivo optical frequency domain imaging of human retina and choroid. *Opt Express*. 2006;14:4403–11.
215. Wakabayashi T, Sawa M, Gomi F, Tsujikawa M. Correlation of fundus autofluorescence with photoreceptor morphology and functional changes in eyes with retinitis pigmentosa. *Acta Ophthalmol*. 2010;88:e177–83.
216. Oishi A, Nakamura H, Tatsumi I, Sasahara M, Kojima H, Kurimoto M, Otani A, Yoshimura N. Optical coherence tomographic pattern and focal electroretinogram in patients with retinitis pigmentosa. *Eye (Lond)*. 2009;23:299–303.
217. Hood DC, Lazow MA, Locke KG, Greenstein VC, Birch DG. The transition zone between healthy and diseased retina in patients with retinitis pigmentosa. *Invest Ophthalmol Vis Sci*. 2011;52:101–8.

218. Rosen RB, Hathaway M, Rogers J, Pedro J, Garcia P, Dobre GM, Podoleanu AG. Simultaneous OCT/SLO/ICG imaging. *Invest Ophthalmol Vis Sci.* 2009;50:851–60.
219. Ruggeri M, Wehbe H, Jiao S, Wang J, Jockovich ME, Rosenfeld PJ, Major JC, McKeown C, Puliafito CA. Ultra high-resolution optical coherence tomography for non-contact ocular imaging of small animals. Presented at Biomedical Optics, Optical Society of America; March 2008, St. Petersburg, FL.
220. Ruggeri M, Wehbe H, Jiao S, Gregori G, Jockovich ME, Hackam A, Duan Y, Puliafito CA. In vivo three-dimensional high-resolution imaging of rodent retina with spectral-domain optical coherence tomography. *Invest Ophthalmol Vis Sci.* 2007;48:1808–14.
221. Albert DM, Neekhra A, Wang S, Darjatmoko SR, Sorenson CM, Dubielzig RR, Sheibani N. Development of choroidal neovascularization in rats with advanced intense cyclic light-induced retinal degeneration. *Arch Ophthalmol.* 2010;128:212–22.
222. Gabriele ML, Ishikawa H, Schuman JS, Bilonick RA, Kim J, Kagemann L, Wollstein G. Reproducibility of spectral-domain optical coherence tomography total retinal thickness measurements in mice. *Invest Ophthalmol Vis Sci.* 2010;51:6519–23.
223. Strouthidis NG, Fortune B, Yang H, Sigal IA, Burgoyne CF. Longitudinal change detected by spectral domain optical coherence tomography in the optic nerve head and peripapillary retina in experimental glaucoma. *Invest Ophthalmol Vis Sci.* 2011;52:1206–19.
224. Luo X, Patel NB, Harwerth RS, Frishman LJ. Loss of the low-frequency component of the global-flash multifocal electroretinogram in primate eyes with experimental glaucoma. *Invest Ophthalmol Vis Sci.* 2011;52:3792–804.
225. Schuman JS, Pedut-Kloizman T, Pakter H, Wang N, Guedes V, Huang L, Pieroth L, Scott W, Hee MR, Fujimoto JG, et al. Optical coherence tomography and histologic measurements of nerve fiber layer thickness in normal and glaucomatous monkey eyes. *Invest Ophthalmol Vis Sci.* 2007;48:3645–54.
226. Patel NB, Luo X, Wheat JL, Harwerth RS. Retinal nerve fiber layer assessment: area versus thickness measurements from elliptical scans centered on the optic nerve. *Invest Ophthalmol Vis Sci.* 2011;52:2477–89.
227. Zhu H, Crabb DP, Schlottmann PG, Ho T, Garway-Heath DF. Floating canvas: quantification of 3D retinal structures from spectral-domain optical coherence tomography. *Opt Express.* 2010;18:24595–610.
228. Vermeer KA, van der Schoot J, Lemij HG, de Boer JF. Automated segmentation by pixel classification of retinal layers in ophthalmic OCT images. *Biomed Opt Express.* 2011;2:1743–56.
229. Yazdanpanah A, Hamarneh G, Smith BR, Sarunic MV. Segmentation of intra-retinal layers from optical coherence tomography images using an active contour approach. *IEEE Trans Med Imaging.* 2011;30:484–96.
230. McIntyre KB, Rasmussen CA, Goulding AK, Bantsev V, Ver Hoeve JN, Kaufman PL, Christian BJ, Nork TM. Spectral domain OCT segmentation accuracy in monkeys. Presented at Association for Research in Vision and Ophthalmology, May 2010, Fort Lauderdale, FL.
231. Malamos P, Ahlers C, Mylonas G, Schutze C, Deak G, Ritter M, Sacu S, Schmidt-Erfurth U. Evaluation of segmentation procedures using spectral domain optical coherence tomography in exudative age-related macular degeneration. *Retina.* 2011;31:453–63.
232. Rathke F, Schmidt S, Schnorr C. Order preserving and shape prior constrained intra-retinal layer segmentation in optical coherence tomography. *Med Image Comput Comput Assist Interv.* 2011;14:370–7.
233. Marmor MF. Comparison of screening procedures in hydroxychloroquine toxicity. *Arch Ophthalmol.* 2012 Apr;130(4):461–9. Epub 2011 Dec 12.
234. Nork TM, Murphy CJ, Kim CB, Ver Hoeve JN, Rasmussen CA, Miller PE, Wabers HD, Neider MW, Dubielzig RR, McCulloh RJ, et al. Functional and anatomic consequences of subretinal dosing in the cynomolgus macaque. *Arch Ophthalmol.* 2012;130:65–75.
235. Nork TM, Murphy CJ, Kim CB, Ver Hoeve JN, Rasmussen CA, Miller PE, Wabers HD, Neider MW, Dubielzig RR, McCulloh RJ, et al. Functional and anatomic consequences of

- subretinal dosing in the cynomolgus macaque. *Arch Ophthalmol*, 14 Aug 2011 [Epub ahead of print].
236. Xu L, Cao WF, Wang YX, Chen CX, Jonas JB. Anterior chamber depth and chamber angle and their associations with ocular and general parameters: the Beijing Eye Study. *Am J Ophthalmol*. 2008;145:929–36.
 237. Grover S, Murthy RK, Brar VS, Chalam KV. Normative data for macular thickness by high-definition spectral-domain optical coherence tomography (spectralis). *Am J Ophthalmol*. 2009;148:266–71.
 238. Budenz DL, Anderson DR, Varma R, Schuman J, Cantor L, Savell J, Greenfield DS, Patella VM, Quigley HA, Tielsch J. Determinants of normal retinal nerve fiber layer thickness measured by Stratus OCT. *Ophthalmology*. 2007;114:1046–52.
 239. Fleckenstein M, Charbel Issa P, Helb HM, Schmitz-Valckenberg S, Finger RP, Scholl HP, Loeffler KU, Holz FG. High-resolution spectral domain-OCT imaging in geographic atrophy associated with age-related macular degeneration. *Invest Ophthalmol Vis Sci*. 2008;49:4137–44.
 240. Khanifar AA, Koreishi AF, Izatt JA, Toth CA. Drusen ultrastructure imaging with spectral domain optical coherence tomography in age-related macular degeneration. *Ophthalmology*. 2008;115:1883–90.
 241. Cense B, Nassif N, Chen T, Pierce M, Yun SH, Park B, Bouma B, Tearney G, de Boer J. Ultrahigh-resolution high-speed retinal imaging using spectral-domain optical coherence tomography. *Opt Express*. 2004;12:2435–47.
 242. Witkin AJ, Vuong LN, Srinivasan VJ, Gorczynska I, Reichel E, Bauman CR, Rogers AH, Schuman JS, Fujimoto JG, Duker JS. High-speed ultrahigh resolution optical coherence tomography before and after ranibizumab for age-related macular degeneration. *Ophthalmology*. 2009;116:956–63.
 243. Gabriele ML, Ishikawa H, Schuman JS, Ling Y, Bilonick RA, Kim JS, Kagemann L, Wollstein G. Optic nerve crush mice followed longitudinally with spectral domain optical coherence tomography. *Invest Ophthalmol Vis Sci*. 2011;52:2250–4.
 244. Považay B, Hofer B, Torti C, Hermann B, Tumlinson AR, Esmaelpour M, Egan CA, Bird AC, Drexler W. Impact of enhanced resolution, speed and penetration on three-dimensional retinal optical coherence tomography. *Opt Express*. 2009;17:4134–50.
 245. DeLeón Ortega JE, Sakata LM, Kakati B, McGwin Jr G, Monheit BE, Arthur SN, Girkin CA. Effect of glaucomatous damage on repeatability of confocal scanning laser ophthalmoscope, scanning laser polarimetry, and optical coherence tomography. *Invest Ophthalmol Vis Sci*. 2007;48:1156–63.
 246. Ho J, Sull AC, Vuong LN, Chen Y, Liu J, Fujimoto JG, Schuman JS, Duker JS. Assessment of artifacts and reproducibility across spectral- and time-domain optical coherence tomography devices. *Ophthalmology*. 2009;116:1960–70.
 247. Sull AC, Vuong LN, Price LL, Srinivasan VJ, Gorczynska I, Fujimoto JG, Schuman JS, Duker JS. Comparison of spectral/Fourier domain optical coherence tomography instruments for assessment of normal macular thickness. *Retina*. 2010;30:235–45.
 248. Kim JS, Ishikawa H, Sung KR, Xu J, Wollstein G, Bilonick RA, Gabriele ML, Kagemann L, Duker JS, Fujimoto JG, et al. Retinal nerve fibre layer thickness measurement reproducibility improved with spectral domain optical coherence tomography. *Br J Ophthalmol*. 2009;93:1057–63.
 249. Leung CK, Cheung CY, Weinreb RN, Qiu Q, Liu S, Li H, Xu G, Fan N, Huang L, Pang CP, et al. Retinal nerve fiber layer imaging with spectral-domain optical coherence tomography: a variability and diagnostic performance study. *Ophthalmology*. 2009;116:1257–63.
 250. Knight OJ, Chang RT, Feuer WJ, Budenz DL. Comparison of retinal nerve fiber layer measurements using time domain and spectral domain optical coherent tomography. *Ophthalmology*. 2009;116:1271–7.
 251. Vizzeri G, Weinreb RN, Gonzalez-Garcia AO, Bowd C, Medeiros FA, Sample PA, Zangwill LM. Agreement between spectral-domain and time-domain OCT for measuring RNFL thickness. *Br J Ophthalmol*. 2009;93:775–81.

252. Leung CK, Li H, Weinreb RN, Liu J, Cheung CY, Lai RY, Pang CP, Lam DS. Anterior chamber angle measurement with anterior segment optical coherence tomography: a comparison between slit lamp OCT and Visante OCT. *Invest Ophthalmol Vis Sci.* 2008;49:3469–74.
253. Schuman JS. Spectral domain optical coherence tomography for glaucoma (an AOS thesis). *Trans Am Ophthalmol Soc.* 2008;106:426–58.
254. Wolf-Schnurrbusch UE, Ceklic L, Brinkmann CK, Iliev ME, Frey M, Rothenbuehler SP, Enzmann V, Wolf S. Macular thickness measurements in healthy eyes using six different optical coherence tomography instruments. *Invest Ophthalmol Vis Sci.* 2009;50:3432–7.
255. Huang XR, Knighton RW. Microtubules contribute to the birefringence of the retinal nerve fiber layer. *Invest Ophthalmol Vis Sci.* 2005;46:4588–93.
256. Alencar LM, Zangwill LM, Weinreb RN, Bowd C, Vizzeri G, Sample PA, Susanna Jr R, Medeiros FA. Agreement for detecting glaucoma progression with the GDx guided progression analysis, automated perimetry, and optic disc photography. *Ophthalmology.* 2010;117:462–70.
257. Grewal DS, Sehi M, Greenfield DS. Detecting glaucomatous progression using GDx with variable and enhanced corneal compensation using Guided Progression Analysis. *Br J Ophthalmol.* 2011;95:502–8.
258. Poinosawmy D, Tan JC, Bunce C, Hitchings RA. The ability of the GDx nerve fibre analyser neural network to diagnose glaucoma. *Graefes Arch Clin Exp Ophthalmol.* 2001;239:122–7.
259. Brusini P, Salvetat ML, Zeppieri M, Tosoni C, Parisi L, Felletti M. Comparison between GDx VCC scanning laser polarimetry and Stratus OCT optical coherence tomography in the diagnosis of chronic glaucoma. *Acta Ophthalmol Scand.* 2006;84:650–5.
260. Frohman EM, Dwyer MG, Frohman T, Cox JL, Salter A, Greenberg BM, Hussein S, Conger A, Calabresi P, Balcer LJ, et al. Relationship of optic nerve and brain conventional and non-conventional MRI measures and retinal nerve fiber layer thickness, as assessed by OCT and GDx: a pilot study. *J Neurol Sci.* 2009;282:96–105.
261. Pueyo V, Ara JR, Almarcegui C, Martin J, Güerri N, García E, Pablo LE, Honrubia FM, Fernandez FJ. Sub-clinical atrophy of the retinal nerve fibre layer in multiple sclerosis. *Acta Ophthalmol.* 2010;88:748–52.
262. Weinreb RN, Bowd C, Greenfield DS, Zangwill LM. Measurement of the magnitude and axis of corneal polarization with scanning laser polarimetry. *Arch Ophthalmol.* 2002;120:901–6.
263. Fortune B, Wang L, Cull G, Cioffi GA. Intravitreal colchicine causes decreased RNFL birefringence without altering RNFL thickness. *Invest Ophthalmol Vis Sci.* 2008;49:255–61.
264. Fortune B, Cull GA, Burgoyne CF. Relative course of retinal nerve fiber layer birefringence and thickness and retinal function changes after optic nerve transection. *Invest Ophthalmol Vis Sci.* 2008;49:4444–52.
265. Reus NJ, Lemij HG. Diagnostic accuracy of the GDx VCC for glaucoma. *Ophthalmology.* 2004;111:1860–5.
266. Shaikh A, Salmon JF. The role of scanning laser polarimetry using the GDx variable corneal compensator in the management of glaucoma suspects. *Br J Ophthalmol.* 2006;90:1454–7.
267. Baraibar B, Sánchez-Cano A, Pablo LE, Honrubia FM. Preperimetric glaucoma assessment with scanning laser polarimetry (GDx VCC): analysis of retinal nerve fiber layer by sectors. *J Glaucoma.* 2007;16:659–64.
268. Reus NJ, de Graaf M, Lemij HG. Accuracy of GDx VCC, HRT I, and clinical assessment of stereoscopic optic nerve head photographs for diagnosing glaucoma. *Br J Ophthalmol.* 2007;91:313–8.
269. Pablo LE, Ferreras A, Schlottmann PG. Retinal nerve fibre layer evaluation in ocular hypertensive eyes using optical coherence tomography and scanning laser polarimetry in the diagnosis of early glaucomatous defects. *Br J Ophthalmol.* 2011;95:51–5.
270. Leung CK, Chan WM, Chong KK, Yung WH, Tang KT, Woo J, Chan WM, Tse KK. Comparative study of retinal nerve fiber layer measurement by Stratus OCT and GDx VCC, I: correlation analysis in glaucoma. *Invest Ophthalmol Vis Sci.* 2005;46:3214–20.

271. Zarei R, Soleimani M, Moghimi S, et al. Relationship between the GDx VCC and Stratus OCT in primary open angle glaucoma. *Iran J Ophthalmol*. 2009;21:55–62.
272. Zareii R, Soleimani M, Moghimi S, Eslami Y, Fakhraie G, Amini H. Relationship between GDx VCC and Stratus OCT in juvenile glaucoma. *Eye (Lond)*. 2009;23:2182–6.
273. Ma KT, Lee SH, Hong S, Park KS, Kim CY, Seong GJ, Hong YJ. Relationship between the retinal thickness analyzer and the GDx VCC scanning laser polarimeter, Stratus OCT optical coherence tomograph, and Heidelberg retina tomograph II confocal scanning laser ophthalmoscopy. *Korean J Ophthalmol*. 2008;22:10–7.
274. Zheng W, Baohua C, Qun C, Zhi Q, Hong D. Retinal nerve fiber layer images captured by GDx-VCC in early diagnosis of glaucoma. *Ophthalmologica*. 2008;222:17–20.
275. Medeiros FA, Alencar LM, Zangwill LM, Sample PA, Susanna Jr R, Weinreb RN. Impact of atypical retardation patterns on detection of glaucoma progression using the GDx with variable corneal compensation. *Am J Ophthalmol*. 2009;148:155–63.
276. Tóth M, Holló G. Increased Long-term measurement variability with scanning laser polarimetry employing enhanced corneal compensation: an early sign of glaucoma progression. *J Glaucoma*. 2008;17:571–7.
277. Weinreb RN, Kaufman PL. Glaucoma research community and FDA look to the future, II: NEI/FDA Glaucoma Clinical Trial Design and Endpoints Symposium: measures of structural change and visual function. *Invest Ophthalmol Vis Sci*. 2011;4:7842–51.
278. Mai TA, Reus NJ, Lemij HG. Structure-function relationship is stronger with enhanced corneal compensation than with variable corneal compensation in scanning laser polarimetry. *Invest Ophthalmol Vis Sci*. 2007;48:1651–8.
279. Reus NJ, Zhou Q, Lemij HG. Enhanced imaging algorithm for scanning laser polarimetry with variable corneal compensation. *Invest Ophthalmol Vis Sci*. 2006;47:3870–7.
280. Aristeidou AP, Labiris G, Paschalis EI, Foudoulakis NC, Koukoura SC, Kozobolis VP. Evaluation of the retinal nerve fiber layer measurements, after photorefractive keratectomy and laser *in situ* keratomileusis, using scanning laser polarimetry (GDx VCC). *Graefes Arch Clin Exp Ophthalmol*. 2010;248:731–6.
281. Kunitatsu S, Tomidokoro A, Saito H, Aihara M, Tomita G, Araie M. Performance of GDx VCC in eyes with peripapillary atrophy: comparison of three circle sizes. *Eye (Lond)*. 2008;22:173–8.
282. Resch H, Deak G, Vass C. Influence of optic-disc size on parameters of retinal nerve fibre analysis as measured using GDx VCC and ECC in healthy subjects. *Br J Ophthalmol*. 2010;94:424–7.
283. Gabelt BT, Kiland JA, Tian B, Kaufman PL. Aqueous humor: Secretion and dynamics. In: Tasman W, Jaeger EA, editors. *Duane's foundations of clinical ophthalmology*, vol. 2. Philadelphia: Lippincott Williams & Wilkins; 2006.

Chapter 4

Emerging Electrophysiological Technologies for Assessing Ocular Toxicity in Laboratory Animals

James N. Ver Hoeve, Robert J. Munger,
Christopher J. Murphy, and T. Michael Nork

Abstract The previous chapter on emerging imaging technologies emphasized new or improved devices that, for the most part, provide anatomic information about the living eye. In this chapter, we will review electrophysiological measures of ocular function. Functional assessment can often confirm and strengthen the anatomical findings. For example, in establishing early hydroxychloroquine (Plaquenil®) toxicity in humans, spectral domain optical coherence tomography (sdOCT) and multifocal electroretinography (mfERG) are frequently used together. Sometimes imaging can provide the most sensitive toxicologic test, such as may be the case for vitreous fluorophotometry and fluorescein angiography in detecting subtle breakdown of the blood-retinal barrier. At other times, functional measures may be the most sensitive. An example from clinical medicine is retinitis pigmentosa, which, early on, may produce only vague subjective symptoms in patients with normal appearing fundi but show a markedly reduced full-field ERG (ffERG). Since the animals used in preclinical toxicologic testing cannot communicate their visual symptoms, a combination of anatomic and functional measures is needed to definitively rule out injury to the visual system.

J.N. Ver Hoeve, M.S., Ph.D.(✉) • T.M. Nork, M.D., M.S., DABO, FARVO (✉)
Ocular Services On Demand, LLC (OSOD)

Department of Ophthalmology and Visual Sciences, University of Wisconsin
School of Medicine and Public Health, Madison, WI, USA
e-mail: verhoeve@wisc.edu; jverhoeve@ocularservices.com; tmnork@wisc.edu;
tmnork@ocularservices.com

R.J. Munger, D.V.M., DACVO
Animal Ophthalmology Clinic Inc., Dallas, TX, USA
e-mail: eyedvm@aol.com

C.J. Murphy, D.V.M., Ph.D., DACVO
Ocular Services On Demand, LLC (OSOD)

Department of Ophthalmology and Vision Science, School of Medicine
and Department of Surgical and Radiological Sciences, School of Veterinary Medicine,
University of California, Davis
e-mail: cjmurphy@ucdavis.edu; cjmurphy@ocularservices.com

4.1 Introduction

As is also the case for imaging, the technological roots of electrophysiology date back to the nineteenth century (for a historical review of the ERG, see De Rouck [1] and for the visual evoked response (VEP), see Harding [2]). Improvements in electronics in the twentieth century and the computer revolution of the late twentieth and early twenty-first centuries have turned electrophysiological testing into a practical and cost-effective way to assess toxicological effects in preclinical studies. The entire neurological visual system can now be tested efficiently, from the photoreceptors to the visual cortex.

The specific type of electrophysiological testing chosen for a given toxicological study will depend on which aspect of the visual system that is most likely to be affected. The ffERG is a relatively straightforward test to administer and provides highly sensitive information about the retina as a whole—especially the photoreceptors and bipolar cells. Where the ffERG falls short is in identifying localized retinal lesions. The mfERG is good for such localized effects but requires some technical skill in properly aligning the stimulus and analyzing the large amount of data it generates. For macular retinal ganglion cell assessment, the pattern reversal electroretinogram (PERG) is useful but requires technical skill for both stimulus alignment and proper refraction of the animal. While the ERG and PERG are limited to retinal function, the visual evoked response (VEP) measures the entire visual system as far as the visual cortex. In combination with the ERG and PERG, the VEP can be useful in identifying the site of functional injury. A recent refinement of the VEP, the multifocal VEP, is showing promise as a means of localizing defects much as, for example, can be done in human subjects with subjective visual field testing.

Needed developments, such as eye-tracking and better software to extract and analyze data of interest, are in the offing and will make functional testing an ever more practical and expected aspect of toxicologic and regulatory testing.

4.2 Full-Field Electroretinography (ERG)

Electroretinography is the measurement of electrical potentials generated by the retina in response to light. The electroretinogram (ERG) is a measure of retinal function, as distinguished from measures of anatomical integrity assessed by imaging or histology. The full-field ERG (FERG) is used in clinical human and veterinary medicine to diagnose a wide variety of hereditary and acquired retinal diseases. Of relevance to the application of ERG in preclinical safety studies is the observation that the ERG may be abnormal or even extinguished (flat) in conditions such as retinitis pigmentosa prior to any anatomical changes observable by ophthalmoscopic examination. Thus, the FERG can provide evidence that a drug is affecting retinal function in the absence of, or prior to, changes in retinal appearance. The FERG may also be useful to determine whether any observations of changes in retinal appearance during a study are in fact altering retinal function. Like other noninvasive methods, the ERG permits repeated assessment during a study without the cost of additional animals that would be required for terminal histology at additional time points.

FERG has been used in research and in the clinic for many years. However, the contribution of the various retinal layers to the FERG waveform continues to be an area of active investigation. This research shows that accurate interpretation of the FERG depends on a strict adherence to standardized or other well-documented stimulation and recording protocols. To supplement information from the FERG, additional ERG tests have been developed to assess retinal ganglion cell function (pattern ERG) and to assess localized retinal areas (multifocal ERG) and will be discussed in separate sections.

4.2.1 Basic Principles

The FERG is the most widely used type of electroretinogram in ocular toxicology studies. It is a “mass response,” that is, all areas of the retina contribute to the ERG waveform recorded from a corneal electrode. An electrode on the cornea and referenced to a nearby point on the orbit is capable of detecting electric fields generated from the retina, but only those cells that are arranged in radially oriented cell layers. This includes the retinal pigment epithelium (RPE), photoreceptor layer, and inner retinal layers, particularly the bipolar cell layer. Nonradially oriented cells in the retina, including ganglion and amacrine cells, do not contribute directly to the standard FERG. The ERG is a complex response that is the sum of the electric field generated by different cell types in different retinal layers. The relative weight of the field generated by a cell type is affected by the state of light adaptation in the cell (background illumination) and the wavelength and duration of the test flash. Thus, careful protocols are needed for the use of this test in ocular toxicology studies. In the past, studies were sometimes incorrectly oversimplified with a single flash response generated (in some instances without dilating the pupil), and such testing ignores the complexity of the retinal components that contribute to the various aspects of the retinal responses, thus failing to detect evidence of a problem. Standards have been established by the International Society for the Clinical Electrophysiology of Vision (ISCEV) for electroretinography in humans and serve as good resources for developing protocols for use in ocular toxicology [3]. These standards are not intended to preclude the use of other protocols as needed but to ensure that as other protocols are used they do adhere to certain standards and their accuracy and reproducibility are standardized.

4.2.2 Performance Parameters

A detailed discussion of the various techniques employed in electroretinography and their interpretation is beyond the scope of this chapter (see [4–7]), but by controlling dark adaptation, background illumination, flash stimuli, and frequency of stimuli, it is possible to evaluate the most critical cellular components that contribute to retinal function. Five basic stimuli conditions recommended by ISCEV for clinical testing in human patients have been used in many toxicology studies, particularly in nonhuman

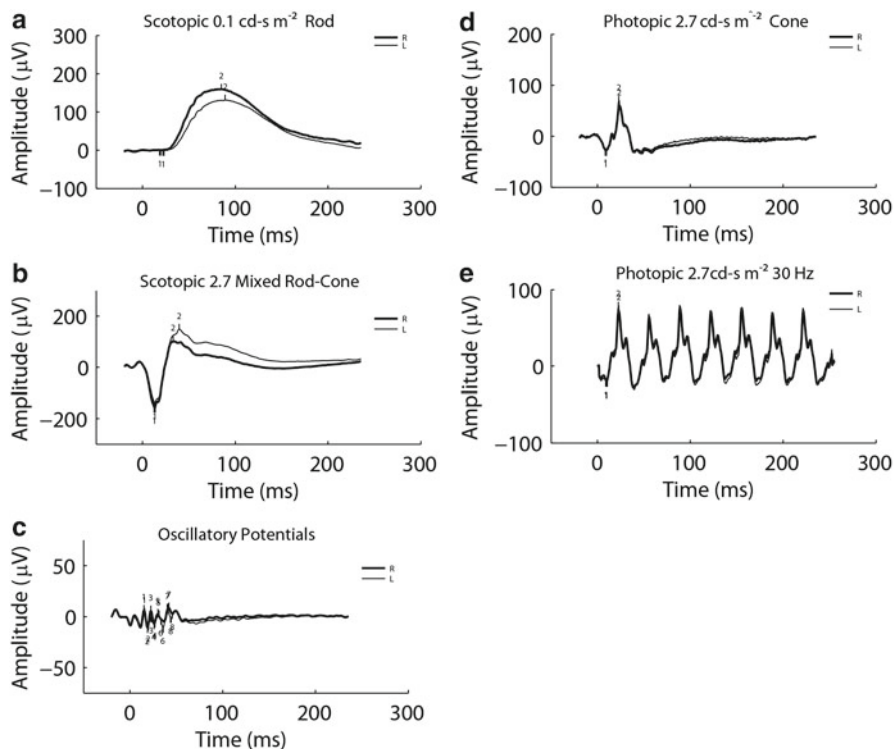


Fig. 4.1 (a) ERG response of the right (top) and left eye (bottom) to a dim flash from the eye of a monkey that has been previously dark-adapted. Cursors have been placed on the waveforms. The voltage difference between cursor 1 and cursor 2 is the amplitude of the *b*-wave. The latency to the peak of the *b*-wave is the implicit time. (b) ERG recorded as in 1A to a bright flash (ISCEV recommends 3 cd-s m⁻²). This stimulus strength elicits a measurable *a*-wave, indicated by cursor 1. This negative voltage waveform is generated by the rod and cone photoreceptors. At moderate flash intensities, there is also a substantial contribution from the on- and off-bipolar cells to the onset and offset of the brief flash stimulus. (c) Oscillatory potentials are derived from the ERG recorded in B by applying a band-pass filter, typically 70–120 Hz to extract the wavelets shown in C. Oscillatory potentials are quantified by summing the amplitude of the individual waves. (d) Light-adapted ERG (photopic) to the same flash stimulus in B. The state of light adaptation completely alters the form of the ERG, underlining the importance of complete dark adaptation and sufficient light adaptation times. (e) Photopic ERG to 30-Hz flicker. Note the quasi-sinusoidal appearance of the ERG at this high repetition rate

primate studies. The ISCEV standard protocols have components for differentiating rod and cone functions, combined photopic responses (so-called maximal response), flicker responses, and oscillatory potentials. A dim stimulus under dark-adapted conditions (a minimum of 20 min in complete dark for nonhuman primates; longer for rod-dominated species such as rodents) will isolate the rod responses and result in a “*b*-wave” generated by bipolar cells with support from Muller cells (Fig. 4.1a). A bright stimulus under the dark-adapted conditions will reveal a combined response



Fig. 4.2 Electroretinograph with full-field photostimulator noted on the right. The animal's head is placed in the photostimulator to achieve uniform flash illumination and maximal efficiency for retinal stimulation

to rods and cones and generate an “*a*-wave” that contains a contribution from the photoreceptors (Fig. 4.1b). Oscillatory potentials on the ascending arm of the *b*-wave originate in the inner plexiform layer of the retina (Fig. 4.1c). By light adapting the retina for at least 10 min with a background (e.g., 30 cd/m²) to bleach rhodopsin in the rods so that they cannot respond, the resulting ERG to a bright white stimulus as the flash is almost exclusively a cone response (Fig. 4.1d). The 30-Hz flicker responses are generated by the cones as rods become refractory at this stimulation rate and are affected if channels in cone photoreceptors cannot repolarize normally (Fig. 4.1e).

The most prominent feature of a typical ERG waveform is the *b*-wave. Practical application of ERG assessment typically involves assessment of *b*-wave amplitude and implicit time or latency, which is the time from stimulus until peak *b*-wave amplitude. For rod, cone, and combined responses, amplitude is measured from the trough of the *a*-wave to the peak of the *b*-wave (or from the base of the *b*-wave when it masks the *a*-wave). Data are often normalized by calculating the percentage relative to prestudy values for individual animal data. It is crucial to collect both prestudy data and data from a control group for comparison. For oscillatory potential and flicker responses, the quality of the waveform is as important as the amplitudes and latencies. Again, a comparison to prestudy values for individual is useful.

The pupils should be maximally dilated, and animals must be sedated to allow proper positioning, usually in a Ganzfeld (Fig. 4.2) device to ensure uniform distribution of light to the retina. Lid specula are used to keep the lids open, and other

positioning measures such as stay sutures may be required to ensure the eyes are in central gaze.

Even with the above standardizations, electroretinographic responses in normal animals are subject to a high degree of variability at different time points and can vary by as much as 25% from one time to the next. Therefore, it is important to compare mean responses of all animals in each group with respect both to the control group as well and the initial baseline means of the responses. An analysis of variance with the prestudy values as the covariate is often performed to assess group differences.

Signal averaging is also a tool that has been used in each individual animal's recordings to eliminate background "noise" (electrical activity from muscle contractions, cardiac activity, and electromagnetic interference from other equipment.), but it is important to space the stimuli adequately to ensure the repeated responses are not so frequent as to bleach rhodopsin and adversely affect components such as the rod responses.

4.2.3 Use in Ocular Toxicology Research

The ERG is increasingly used in preclinical safety studies. It provides a noninvasive assessment of retinal function unavailable through other means. Given the complex nature of the visual cycle, high metabolic rate of the photoreceptors, the visual transduction cascade, and neural processing in the retina required for a normal retinal function, ERG testing may be useful for screening compounds with a wide variety of targets. Target organs may include the eye and any compound that binds melanin in the retinal pigment epithelium, including psychotropic compounds and antimetabolites for neoplastic targets.

4.2.4 Human Clinical Applications

Clinically, the ERG is used primarily to diagnose inherited retinal diseases. For example, a child with nystagmus will have a differential diagnosis list that includes congenital motor nystagmus, neurologic causes, Leber's amaurosis, achromatopsia, and albinism, among others. The scotopic and photopic ERG will both be normal in motor nystagmus and albinism, both will be flat in Leber's congenital amaurosis, and only the photopic ERG will be extinguished in achromatopsia. The ERG is also helpful in assessing the functional effect of foreign intraocular bodies (ocular siderosis) and toxicities.

4.2.5 Commercially Available Devices

Diagnosys LLC, Lowell, MA

<http://www.diagnosysllc.com/home>

LKC Technologies, Inc., Gaithersburg, MD

<http://www.lkc.com>

Electro-Diagnostic Imaging, Inc., Redwood City, CA

<http://www.veris-edi.com>

4.2.6 Considerations for Ocular Toxicology Studies

A complete ERG test using the minimum five conditions will require at least 1 h of dark adaptation, 10 min for electro application, 10 min for scotopic testing, 10 min for light adaptation, and 10 min for photopic testing. While the dark-adapted portion may be overlapped between animals, it is clear that the full ERG test is time-consuming. For species with no macula and a rod-dominated retina, it may be cost-effective to perform only the scotopic tests. It is also time-consuming to individually score the ERG waveforms. An automated processing system may reduce human error and speed the process considerably.

4.2.7 Limitations and Caveats

The FERG has the advantage that it is relatively easy to record (compared with multifocal or pattern ERG), with a relatively large voltage signal (microvolts vs. nanovolts). However, because it is a mass response, the proportional contribution of the retinal that would be removed by a small lesion is often undetectable with the FERG. The FERG is best suited to detecting effects that affect all the cells of a given layer (photoreceptors, bipolar cells) in a similar way. It is important to note that loss of the ganglion cell layer or optic nerve axons is not detectable via the FERG.

4.3 Multifocal Electroretinography (mfERG)

4.3.1 Basic Principles

The full-field ERG gives a mass response recording of retinal activity and is unable to detect small localized regions of impaired activity. For example, a lesion localized to the central fovea of the primate retina would have a normal full-field ERG, but the visual consequences of a lesion in this location would be profound. Fortunately, additional tools have been developed that allow localizing regions of electrical activity within the retina, providing a spatially distributed map of retinal functionality.

Using electrodes placed on the cornea and the skin near the eye, electroretinography measures the electrical response of various types of retinal cells to standardized flashes of light [8, 9]. The resulting signal is displayed as an electroretinogram (ERG) which shows the time course of the signal's voltage amplitude. The ERG is composed of the sum of electrical potentials contributed by different types of retinal

cells including photoreceptors, bipolar cells, and ganglion cells. By altering the stimulus conditions such as flash or pattern stimulus, background lighting, and different colors of stimulus and background, stronger responses from areas of the retina can be elicited. For example, if an ERG is recorded to a dim flash delivered to the dark-adapted eye, the response is from the rod system, while the response from a light-adapted eye is from the cone system. The response evoked from an alternating checkerboard stimulus is due to ganglion cell activity (see Section 4.4 of this chapter on the pattern reversal ERG (PERG)).

In 1992, Sutter and Tran [10] described a means by which regional ERG responses can be determined and mapped in a manner analogous to the way that human visual fields are mapped. This is accomplished by having the subject (either a conscious human or anesthetized animal) gaze at monitor that displays a rapidly changing pattern of white and black hexagons in a pseudorandom pattern (the so-called m-sequence). As is the case with the full-field ERG, only a single active electrode is used (plus a nearby reference electrode and distant indifferent electrode). Computer software then utilizes the complex m-sequence pattern of stimulation to isolate responses from multiple regions of the retina. The regional responses are, individually, similar in appearance to the full-field ERG waveform, that is, a negative going initial wave (N1) followed by a positive wave (P1) plus latter waves (N2 and P2). It also has a high-frequency component that is reminiscent of the full-field ERG oscillatory potentials; however, the cellular origins of the mfERG waveforms may be somewhat different than for the better studied full-field ERG. For example, work by Hood and colleagues [11] suggests that the early waveforms (N1 and P1) may be attributable to responses of the bipolar cells as compared to the full-field ERG in which the first negative going wave (the *a*-wave) is mostly the result of photoreceptor activity. Even so, drug toxicity or disease-related injury to the photoreceptors would have an effect on the mfERG since they are what drive the bipolar and ganglion cells.

Typically 103 or 241 separate stimulus elements are employed that together cover up to $\pm 44^\circ$ of the central visual field. Since the standard full-field ERG testing is the sum of all retinal activity, the multifocal ERG (mfERG) was developed to assess local regions of the retina. The mfERG thus provides spatial information about diseases of the outer retina that could be missed using full-field ERG. For example, a recent study used the mfERG to monitor injury and recovery of retinal function following creation of localized retinal detachments by subretinal injection of balanced salt solution [12].

4.3.2 Performance Parameters

The mfERG can also be used to detect the localized loss of central activity in various maculopathies such as age-related macular degeneration [13], vitelliform maculopathies, macular holes and juvenile retinoschisis, central serous retinopathy [14], vascular disorders, diabetic retinopathy [15], and inflammatory retinal diseases. The mfERG can also be used to detect injury to cone receptors, the inner and outer

plexiform layer, on- and off-bipolar cells, and ganglion cells [8]; however, most of the energy of the mfERG waveform is produced by the outer retina with the ganglion cells contributing only a small component limited to the late wave features. Because of this, the mfERG has not proven practical for monitoring ganglion cell loss, such as seen in human glaucoma [16, 17]. The visual evoked potential VEP and PERG are more useful measures of ganglion cell function. Attempts have been made to improve the sensitivity of the mfERG to inner retinal injury by using slow-flash mfERG [18] or by measuring the so-called optic nerve head component [19, 20]. Even with these refinements, the mfERG is limited in its practical ability to measure ganglion cell function.

4.3.3 Use in Ocular Toxicology Research

A considerable amount of research has been performed using rhesus and cynomolgus monkeys using mfERGs. Initial studies examined retinal changes in experimentally induced glaucoma [21, 22] in the hopes that the mfERG would prove to be an aid in the clinical diagnosis and management of glaucoma. Unfortunately, as noted above, the mfERG waveform has only a weak input from the retinal ganglion cells, the primary cell that is permanently damaged in glaucoma; however, there is mounting evidence that the photoreceptors themselves are injured, but not necessarily lost in glaucoma [23]. To evaluate the relationship between elevated intraocular pressure and the mfERG response, glaucoma was experimentally induced in rhesus and cynomolgus monkeys by using a laser to destroy the trabecular meshwork of one eye [23]. Some animals had undergone prior unilateral optic nerve transection to determine the contribution of ganglion cells to mfERG changes. The results of this study demonstrated species-specific, reversible changes in cone-driven retinal function during periods of elevated intraocular pressure, which can occur in the absence of retinal ganglion cells. The primary effect was an increase in amplitude of the N1 and P1 waveforms (Fig. 4.3). Such increases in the full-field ERG (variously described as supranormal or hyperabnormal) are one of the possible effects of various retinal diseases in humans [24].

4.3.4 Human Clinical Applications

Bevacizumab is a drug used to inhibit angiogenesis. Optical coherence tomography (OCT) and mfERG were used to assess macular function before and after intravitreal administration of bevacizumab in patients with choroidal neovascularization due to age-related macular degeneration [25]. Prior to treatment, OCT showed increased thickening of the fovea and decreased electrical response density in the fovea and parafovea. Three months after treatment, OCT showed resolution of the subretinal fluid, while the mfERG responses in the fovea and parafovea remained unchanged

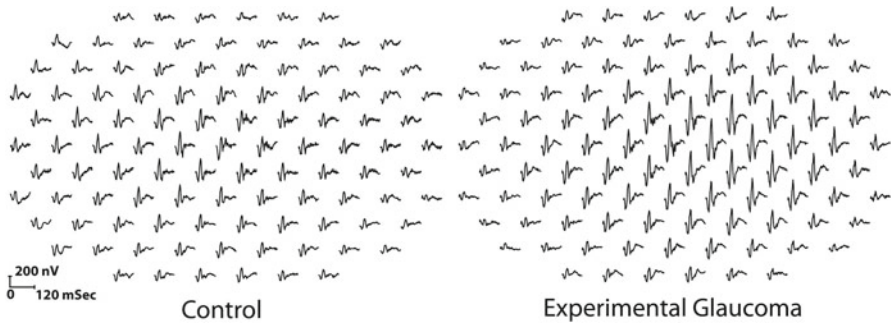


Fig. 4.3 Comparison of unstretched 103 element mfERG traces extending $\pm 44^\circ$ from fixation in a rhesus monkey. The trace array on the *left* is from the control left eye, and the one on the *right* is from the right eye with experimental glaucoma. The traces from the glaucomatous eye are exaggerated or “supranormal” indicating outer retinal (photoreceptor and/or bipolar cell) injury

or slightly improved. The intraocular pressure remained normal, and no inflammation was observed. These results suggest that intravitreal bevacizumab may aid in the treatment of choroidal neovascularization although additional studies are required to establish clinical benefits.

The primary clinical application of the mfERG is to assist in the diagnosis of vision loss by helping to localize the functional defect. An example is monitoring for drug toxicity, such as hydroxychloroquine (Plaquenil®) that initially affects only a small area surrounding the fovea. mfERG testing is often combined with full-field ERG and VEP testing to further characterize the pathology.

4.3.5 Commercially Available Devices

Available Units:

VERIS™ Multifocal System with Integrated Ganzfeld Stimulator and FMS II Stimulator/Refractor/Eye & Fundus Monitoring System

Electro-Diagnostic Imaging, Inc., Redwood City, CA

<http://www.veris-edi.com>

LKC™ Multifocal ERG/VEP with Long Binary m-Sequences

LKC Technologies, Inc., Gaithersburg, MD

<http://www.lkc.com/products/Multi-Focal-ERG/index.html>

4.3.6 Considerations for Ocular Toxicology Studies

There are several aspects of mfERG testing in anesthetized animals that must be taken into account. Unlike conscious humans, the animals will not fixate on the target in the center of the stimulus monitor. Thus, the animals will need to be positioned such that the eye is facing in the proper direction. In our laboratory, we secure the head with

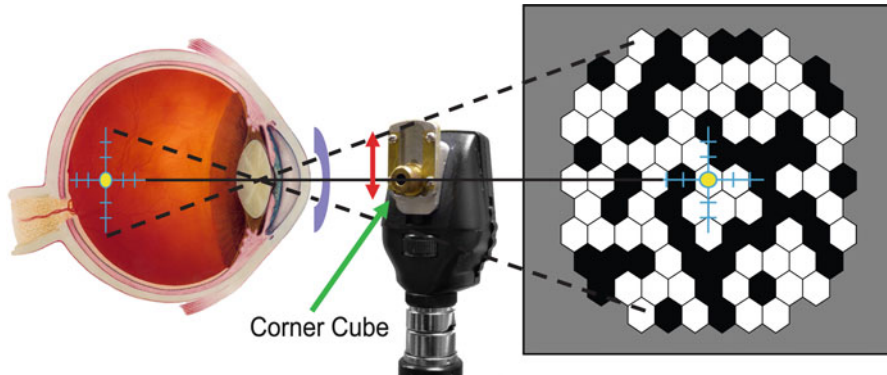


Fig. 4.4 Schematic of alignment method for an anesthetized animal. A direct ophthalmoscope (*center*) is used to project a crosshair onto the desired location, which in primates would typically be the fovea. The ophthalmoscope is then clamped, and a custom-made mirror (corner cube) is raised to back project the crosshairs onto a target screen, which is then moved to line up with the back-projected crosshair. An example of an unstretched stimulus pattern (*right*) used for animal research is shown. An ERG-jet[®] electrode is also illustrated

an oral bit head holder and then align the eye with a reversing ophthalmoscope [26]. A standard direct ophthalmoscope has been modified with a mirror (corner cube). The fovea is identified and placed in the center of the crosshair of the ophthalmoscope, which is then clamped into place. A mirror (corner cube) is slid down to direct the light and crosshair toward the monitor. If necessary, the monitor is then moved to line up with the back-projected crosshair (Fig. 4.4). Newer mfERG systems have camera monitoring systems that permit the operator to project the stimulus directly onto the retina, thus greatly simplifying the alignment process. Even with careful alignment, it is not always possible to exactly center the stimulus. Therefore, it is best with the animals to use an unstretched stimulus (Fig. 4.4) in which slight misalignment is not so critical.

Other considerations for animal toxicity studies are the effects of gender and species [26], electrode placement [27], and anesthesia [28].

4.3.7 Limitations and Caveats

1. mfERG testing in anesthetized animals requires a skilled operator who can troubleshoot technical problems as they arise.
2. There is moderate test-retest variability in the mfERG waveforms that requires averaging over several test periods to extract subtle toxicity effects [23]; however, moderate to marked effects are readily apparent with single recordings.
3. The mfERG generates a tremendous amount of data—essentially normal full-field ERG responses multiplied by 103 or 241. We have found it critical to develop computer software (MATLAB[®], by MathWorks[™], Natick, MA) to assist in data analysis [23].

4.4 Pattern Reversal Electroretinography (PERG)

4.4.1 Basic Principles

The pattern reversal electroretinogram (PERG) is a very small amplitude retinal biopotential generated by a pattern stimulus that is thought to reflect the activation of proximal retinal layers, such as ganglion cells. The PERG thus complements the full-field standard ERG, which is largely driven by distal retinal photoreceptors and bipolar cells. The key feature of the PERG stimulus is that the temporally modulated pattern has no net change in luminance over time. Examples of PERG stimuli include checkerboard patterns in which the black and white squares exchange position every 0.5 s and sinusoidal gratings in which the peaks and troughs alternate phase according to a temporal sine wave. The PERG is most commonly evoked by alternating black and white elements of a checkerboard or by a stripe pattern. The PERG is measured through standard electrodes in contact with the cornea, bulbar conjunctiva, or via periocular skin electrodes. PERG stimuli may be chromatic (red/green, blue/yellow) or achromatic (black/white) with the caveat that the pattern stimulus must be in optimal refraction through the recording electrode. Isolated amplification systems and low-noise recording environments are necessary because the PERG is indeed a very small signal ($\sim 2 \mu\text{V}$) compared with the ERG elicited by full-field stimulation ($>200 \mu\text{V}$). Averaging of a large number of stimulus reversals is commonly needed to achieve an adequate signal-to-noise ratio (SNR). The many stimulus factors affecting the PERG include the spatial frequency of the pattern, temporal rate of phase reversal, luminance, contrast, and chromaticity of the pattern, waveform processing method, type and arrangement of electrodes, background illumination, retina stimulus position, refractive error, and patient age [29].

The PERG was first described by Riggs and colleagues [30–34] who documented its spatial and temporal properties. Maffei then showed that sectioning the optic nerve in cat, monkey, and rat resulted in a gradual decline in the PERG while the standard full-field ERG was unchanged [35–37]. Subsequent research showed that the PERG is markedly affected in human glaucoma [29, 38–45] and inner retinal dysfunction [46–51] as would be expected of a measure of ganglion cell function.

4.4.2 Performance Parameters

Stimuli used for the PERG are similar to those used for the pattern reversal visual evoked potential (PRVEP). The temporal aspects of stimulation determine to a large extent the shape of the PERG waveform. Figure 4.5 shows the PERG elicited by a slow ($<6/\text{s}$) pattern alternation from an example used for illustration in the ISCEV standard. This is the “transient” PERG. The steady-state PERG is elicited by faster temporal rates ($>8/\text{s}$). Figure 4.6 shows the results of the classic Maffei and Fiorentini [52] experiment in which they recorded steady-state PERGs following optic nerve

Fig. 4.5 Idealized pattern ERG from ISCEV standard (From Holder et al. [141])

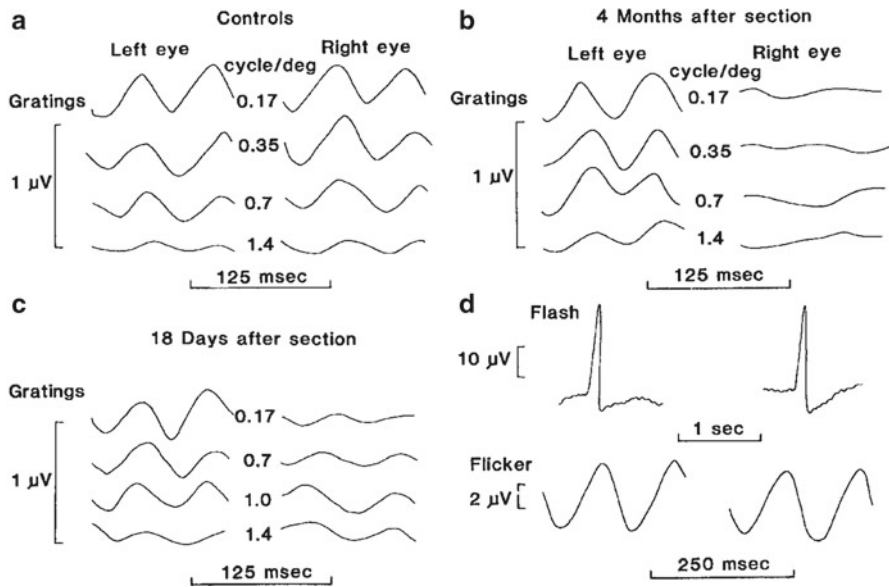
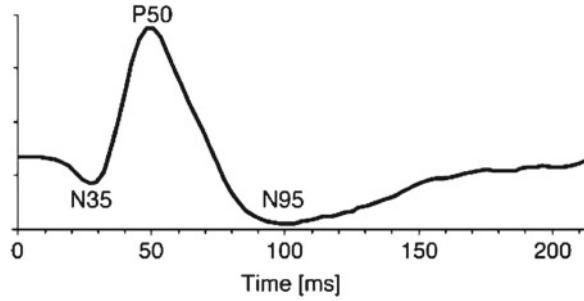


Fig. 4.6 Results of the classic Maffei and Fiorentini [52] experiment in which they recorded steady-state PERGs following optic nerve transection. Note the loss of the steady-state PERG at 4 months while transient flash ERG and steady-state full-field flash ERGs remained unchanged [52]

transaction. Note the loss of the steady-state PERG at 4 months while transient flash ERG and steady-state full-field flash ERGs remained unchanged.

The outcome variables from the transient PERG are the amplitude and peak latencies of the waves labeled in Fig. 4.5, namely, the negative voltage waves with average peak latencies of 35 and 95 ms straddling the prominent P50 positive voltage wave with an average latency of 50 ms. The N95 component is the waveform feature that has been linked with retinal ganglion cell function, whereas the P50 is associated with a distal retinal component. As shown in the idealized transient PERG wave in Fig. 4.5, the amplitude of the PERG is on the order of just a few μvolts, requiring the experimenter to ensure very low levels of noise during the recording. The steady-state

PERG (Fig. 4.6) assumes a quasi-sinusoidal appearance, and typically the amplitude and phase of the second harmonic of the signal are used for analysis.

When properly used, the PERG provides a highly sensitive biomarker for retinal ganglion cell function [29, 53–55]. Clinical studies have examined the utility of the PERG in the diagnosis and assessment of glaucoma and ocular hypertension [45, 53, 56, 57]. These studies have shown that the PERG is markedly reduced in human glaucoma and that some PERG stimuli (high temporal frequency, multiple check sizes) may be optimal for identifying patients with incipient glaucomatous damage [44, 53]. Despite a large body of research showing the value of the technique, routine clinical application of the PERG in glaucoma management has remained elusive.

4.4.3 Use in Animal Toxicology and Other Ocular Research

As expected, the PERG is markedly altered in animal models of glaucoma and ocular hypertension. PERG is also reduced in murine models of spontaneous glaucoma [51, 58, 59]. Porciatti has shown that the PERG declines markedly with age in the DBA/2J mouse, which develops a pigmentary glaucoma postnatally (Fig. 4.7). PERGs are also sensitive to experimental glaucoma in monkeys [60–63].

Although the PERG is a technically demanding potential to record, in animals it can provide similar information to the cortical VEP and may be much easier to obtain than the VEP. For example, PERGs have been used to measure psychophysical responses in pigeons [64, 65]; however, of note is the finding that in pigeons, transection of the optic nerve does not abolish the PERG [48, 66, 67], which suggests that in the pigeon, retinal ganglion cells are not the generators of the PERG and that other cell types in the inner retina (e.g., amacrine) may play an important role. Nevertheless, with the caveat that species differences may be critically important, the PERG may provide an estimate of spatial acuity in smaller animals more readily than the VEP in some experimental situations. Work from Frishman and colleagues has delineated the specific pathways in the C57BL/6 mouse that give rise to the PERG [68].

4.4.4 Use in Human Clinical Research

In addition to studies of glaucoma, there is a substantial body of research using the PERG to document pathologic changes in the retina in patients with idiopathic Parkinson's disease [71–75]. These studies suggest that in addition to higher cortical functions, there is evidence of retinal function in these patients. Visual symptoms including a decline in the PERG may be an important indicator of cognitive decline in patients with Parkinson's disease [76]. In children with optic nerve hypoplasia (ONH), the N95 component of the PERG is diminished, but ONH may also involve more distal layers of the retina [77]. The N95 component of PERG, together with full-field ERGs and the flash VEP, has been found to be predictive of visual

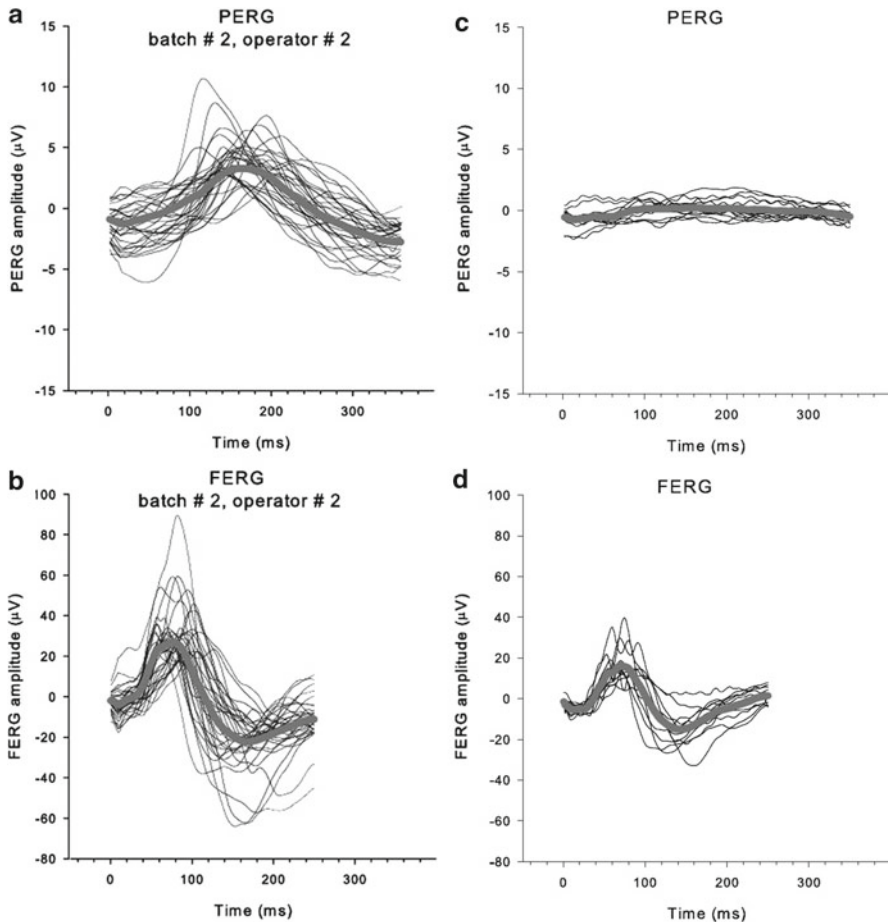


Fig. 4.7 (a) PERG and (b) full-field ERG (FERG) recorded from 22 3–4-month-old DBA/2J mice. *Thin lines*: individual waves; *thick lines*: averages. (c) PERG recorded from six older DBA/2J mice (12–14 months old). (d) FERG from same animals as in (c). Note the selective reduction of the PERG and preservation of the FERG, reflecting selective loss of ganglion cells (From Porciatti et al. [65])

outcomes in children with ONH [78]. The PERG has also been used to monitor macular function following laser treatment in patients with macular degeneration [79, 80]. These studies have demonstrated that, in addition to the N95 ganglion cell component, the PERG is also useful marker of macular function.

The PERG has not been used extensively as a biomarker for toxic exposures. However, in one case report, transient PERG and transient pattern VEP were used to assess ocular status in Amazon gold miners who chronically inhaled mercury vapor [81].

4.4.5 *Commercially Available Devices*

Available Units:

Diagnosys LLC, Lowell, MA

<http://www.diagnosysllc.com/home>

LKC Technologies, Inc., Gaithersburg, MD

<http://www.lkc.com>

Electro-Diagnostic Imaging, Inc., Redwood City, CA

<http://www.veris-edi.com>

Cadwell Laboratories, Inc., Kennewick, WA

<http://www.cadwell.com>

Electrical Geodesics, Inc., Eugene, OR

<http://www.egi.com>

4.4.6 *Considerations for Ocular Toxicology Studies*

The PERG is a technically demanding recording. Refraction and optical clarity are essential to obtain meaningful results. For many PERG recordings, a fiber electrode [82, 83] is useful to avoid optical distortions created from standard contact lens ERG electrodes. For animals, it is necessary to be able to refract the animals using streak retinoscopy or other means. In addition, the stimulus must be aligned optically with the fovea or other retinal landmark using a reversing ophthalmoscope or other suitable optical technique. Because of the low signal amplitude, there may be ambiguity with placement of the cursors used to measure amplitude and peak latency or implicit time, particularly in animals with experimentally reduced PERGs. New methods have been introduced for improving the reliability of cursor placement in high-noise recordings [84].

4.4.7 *Limitations and Caveats*

The PERG is a small amplitude signal that is typically generated from a pattern displayed on a computer monitor. Older CRT monitors may create a large electromagnetic field that could be synchronized with the stimulus. Thus, it is critical to measure the PERG in the apparatus used with zero contrasts (no visible pattern) in order to ensure recordings are free from artifact. Of great importance is the fact that LED displays have backlit features that may introduce a luminance artifact that could masquerade as a PERG. As indicated from work with pigeons reviewed above, there may be large species differences in the relative contribution to the PERG from retinal ganglion cells versus other cells of the inner retina, making it necessary to validate the PERG in each species.

4.5 Visual Evoked Potential (VEP)

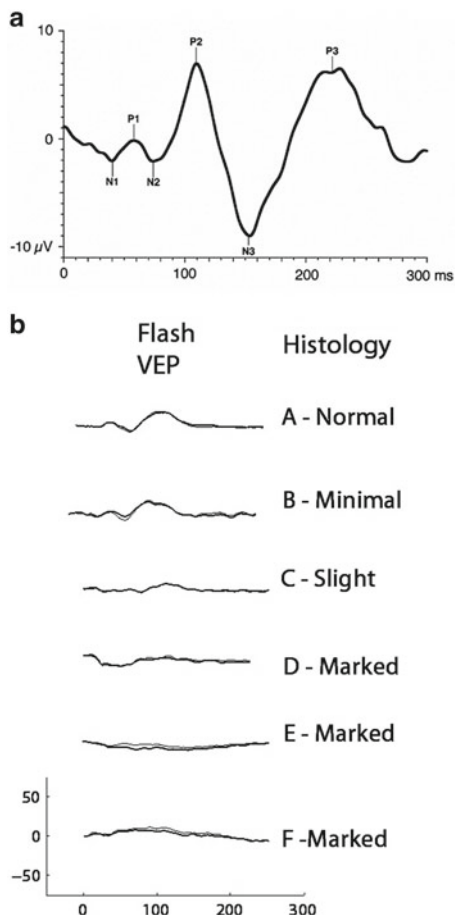
4.5.1 Basic Principles

Visual evoked potentials (VEPs) are changes in electric fields generated in the cerebral cortex when activated by visual stimulation. See Nunez and Srinivasa [85] and Regan [86] for reviews. VEPs are typically recorded noninvasively via scalp electrodes positioned over the occipital lobe, although for research purposes, VEPs may be recorded from electrodes placed directly on the surface of the cortex. In order to achieve sufficient amplitude to be recorded from scalp electrodes, the visual stimulus must elicit a time-locked activation of cortical neurons. An action potential traveling down an axon releases a neurotransmitter into the synapse which binds with a receptor on the membrane of the target cell which alters current flowing into the cell. This current flow generates an electromagnetic field. If there is sufficient depolarization of the target cell, an action potential is generated that transmits the signal via the target cell's axon to the next cell; however, only volume-conducted magnetic and electric fields generated by the current flow into the cell bodies are detectable extracellularly from surface electrodes. Action potentials per se are not recordable via scalp electrodes. Detection of magnetic field dipoles requires highly specialized low-temperature detectors which have been rarely used outside of research. Electric fields are measured as the potential difference between the active electrode and a reference electrode over a nonactive site. Only the synchronous activation of very large numbers of neurons (compound activity) can result in a summed potential (an electric field created by changes in intracellular ionic concentrations) that is large enough to be recorded from the scalp. Note also that the orientation of the dipole within the cortical tissue must be radial with respect to the recording electrodes in order to be detected; orthogonally oriented dipoles are not detected. It is for this reason that VEPs are often recorded using several electrode montages. Unlike single-unit recordings, the VEP represents a mode of response that must be common throughout the cortex. Another advantage of the VEP as an imaging technique includes the fact that it is a relatively fast measure, typically resolved within 250 ms, compared with fMRI, which takes orders of magnitude longer to resolve.

4.5.1.1 Averaging

The classic technique for obtaining a VEP uses “averaging” to extract the small field potential from the much larger background EEG. In the classic averaging method, a visual stimulus is presented, such as a strobe flash, checkerboard pattern reversal, or grating onset at a fairly slow rate (2 s^{-1}), and the occipital EEG (electrode placement at O1 and O2 plus a midline Oz channel is common) is digitized in time-ordered bins for a given period, typically 300 ms following the stimulus [87]. The voltage in each time bin is summed across the number of stimulations, typically 64 or greater. The signal-to-noise ratio (SNR) increases with the square root of the number of

Fig. 4.8 (a) Ideal flash visual evoked potentials (FVEPs) recorded from human showing the major waveforms using ISCEV VEP standard. From Odom et al. [87]. (b) FVEPs recorded from six monkeys under anesthesia. On the right is the histologist's rating of the degree of optic nerve atrophy. FVEPs are depressed or abolished in animals with evidence of atrophy judged "marked" (From Dubielzig et al. [103])



stimulations; thus, there is a large gain in SNR with the initial stimulations, and benefits diminish at very high numbers of stimulations. Poststimulus epochs where the occipital EEG voltage is consistently above zero will sum to a positive VEP "wave," whereas EEG that is negatively correlated with stimulus onset will sum to a negative voltage wave, and activity that is unrelated to the stimulus will, in the long run, sum to zero. Figure 4.8a shows an idealized VEP evoked by flash stimulation, and Fig. 4.9a shows a VEP evoked by pattern reversal (PRVEP) stimulation, both following the ISCEV standard example [87]. It is also possible to record VEPs from a "steady-state" stimulus (ssVEPs)—a flash or pattern reversal that is presented at a temporal rate that is sufficiently rapid to drive the cortex in a quasi-sinusoidal output. The amplitude and phase of the harmonics of the ssVEPs can be extracted with a Fourier transform or other frequency-domain techniques, avoiding traditional averaging. In certain applications, ssVEPs are more efficient than time-averaged VEPs but at the expense of losing detail about the waveform. VEPs are also classified by the spatial aspects of the stimulus. Common spatial patterns include strobe flash, checkerboards, dartboards, sinusoidal gratings, and vernier offsets.

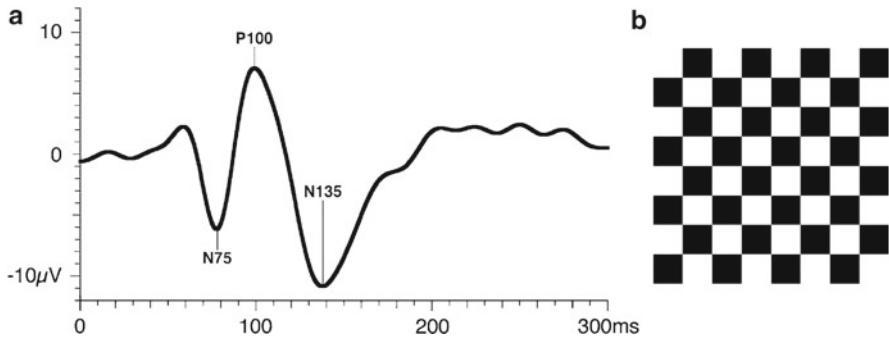


Fig. 4.9 (a) Ideal pattern reversal VEP recorded from human showing the major waveforms using ISCEV VEP standard. From Odom et al. [101]. (b) Checkerboard pattern used in PRVEP. The transient PRVEP shown is the average cortical response elicited by the exchange of black and white checks at a rate of 2 s^{-1}

4.5.1.2 Frequency Labeling

The Fourier transform of a steady-state VEP contains energy peaks at the fundamental and the harmonics of the temporal frequency of the stimulus. In frequency labeling techniques, the stimulus is modulated in time while another stimulus attribute, for example, spatial frequency, is swept through a range [86]. A narrow-band digital filter that passes only the energy at the stimulus frequency is applied to the occipital EEG, and the resulting amplitude and phase are plotted as a function of the swept stimulus attribute. This situation is analogous to an amplitude-modulated (AM) radio: the flickering of the stimulus is the “carrier frequency,” and the amplitude of the demodulated signal from the EEG is similar to the loudness of the radio signal. Frequency labeling methods are the basis of the “sweep VEP” acuity in which the spatial frequency (inverse of bar width) of a grating is increased while the light and dark bars are exchanging position at a constant rate. In humans, the intersection of the slope of the sweep VEP with $0 \mu\text{V}$ (or background EEG noise) correlates well with subjective acuity as determined by an eye chart. Frequency labeling has been applied to VEP measurement of vernier acuity [88], motion [89, 90], and binocular interactions [91, 92].

4.5.1.3 Cross-Correlation Methods

Recently, the multifocal or m-sequence methodology has been applied to VEPs. Sutter [93–95] introduced a pseudorandom stimulation method based on the m-sequence that has found widespread clinical application in the form of multifocal ERGs and multifocal VEPs [16, 96–99]. In a simple cross-correlation, the stimulus sequence is correlated with a channel of recorded EEG. The offset between the stimulus sequence and recorded physiology is then shifted one sample at a time, and the correlation is repeated. If this procedure is repeated for the desired number of post-stimulus msec, the shape of the evoked potential is recovered. The m-sequence is a pseudorandom series of stimulus sequences for multiple stimulus inputs with the

unique property that the correlation between all possible pairs of sequences is exactly zero. This means that the cross-correlation between one pseudorandom m-sequence and the recorded physiology is independent from all other inputs. The mfVEP can be thought of as creating a “spatial dissection” of the VEP waveform across the visual field. In humans, mfVEPs often show polarity inversion around the calcarine sulcus corresponding to the upper and lower visual fields. The standard PRVEP averages across these individual waves, probably contributing to interindividual variability.

A multifocal VEP typically uses 60 small checkerboard patterns that alternate black and white according to an m-sequence (Fig. 4.10). The m-sequence allows extraction of VEPs from each of 60 locations across the visual field; however, the technique is not limited to the standard checkerboard pattern. In addition, the multifocal VEP requires recording from at least two orthogonal occipital EEG channels [11, 100].

4.5.1.4 Visual Physiology

A vast body of research in visual physiology has shown that separate, often “parallel” central visual pathways are activated by distinct classes of stimulus features. See Regan (1989) for a review [86]. Cortical areas that are activated by a uniform flash of light differ substantially from those activated by the onset of a pure spatial frequency luminance grating, an isoluminant color patch, edges, or coherent motion. In addition, application of these methods to animal testing must take into consideration the differences between species in spatial resolution, contrast, and color sensitivity. Thus, it is of utmost importance to select the appropriate VEP stimulus paradigm based on what is known about the functional anatomy of the visual system and how that system may be affected by a given experimental manipulation.

VEPs are affected by any degradation of the visual signal between eye and cortex. Image clarity, retinal dysfunction, and lesions within the central visual pathways all may affect the VEP. For this reason, in order to interpret the VEP as an indicator of optic nerve or cortical function, a retinal basis for the dysfunction must be ruled out. For animal work, this typically involves combining the VEP with ERG and/or retinal imaging.

The International Society for Clinical Electrophysiology of Vision has established a standard for a subset of VEP stimulus and recording conditions that represent basic clinical assessment and which can be obtained by most clinical electrophysiology laboratories [87, 101]. The three most common VEP stimulus conditions are:

1. Flash VEP elicited by a brief luminance increment (flash) which subtends a visual field of at least 20°
2. Pattern reversal VEPs (PRVEP) elicited by checkerboard stimuli with large 1° (60 min) and small 0.25° (15 min) checks
3. Pattern onset/offset VEPs elicited by checkerboard stimuli with large 1° (60 min) and small 0.25° (15 min) checks

These ISCEV VEP standards are meant to apply only to human recordings. Spatial acuity varies greatly across species; thus, the size of the stimulus elements needs to be adjusted accordingly. An ISCEV standard has not yet been published for multifocal VEP.

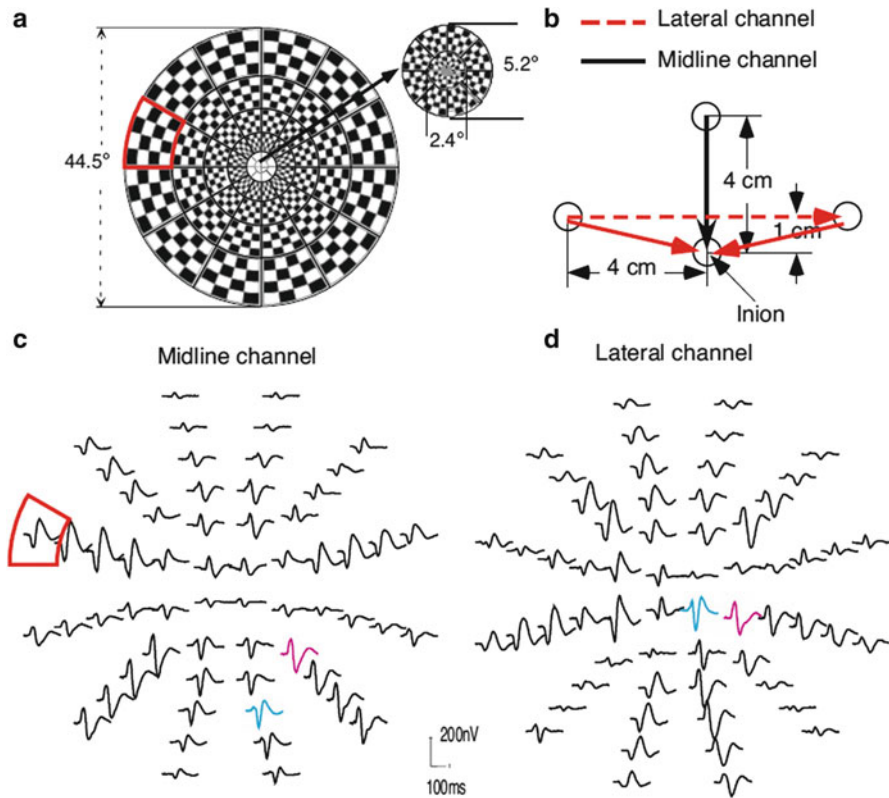


Fig. 4.10 Multifocal VEP stimulus and electrode montage. From Zhang et al. [100]. (a) 60 \times 4 dartboard pattern. Each pattern reverses according to the pseudorandom m-sequence. Insert shows dimensions of the innermost portions of the mfVEP stimulus. (b) Recording montage shown in a vertically oriented midline channel and a horizontally oriented lateral channel. (c,d) mVEP outputs from midline and lateral channels. Note that areas that appear reduced (e.g., row of VEPs in midline channel just below horizontal midline) are large in the lateral channel and vice versa, a likely indication that the dipole generating the electric field changes orientation relative to the two recording channels at these locations

4.5.2 Performance Parameters

The most common outcome measures from the standard “transient” PRVEP recorded to flash or pattern stimulation are the amplitudes and peak latencies of the prominent negative and positive voltage waves [87]. In human clinical studies, the PRVEP “P100” wave, a positive voltage wave with a peak latency of 100 ms that is elicited by a reversing checkerboard pattern, is the most common outcome measure. The P100 has a more uniform appearance across subjects (i.e., lower intersubject variability) compared with the flash VEP, which may have multiple wavelets. The flash VEP typically has a large negative/positive wave with the positive or “P2” wave showing latencies between 90 and 115 ms, depending on the laboratory so that identification

of these major waves is usually unambiguous. The advantage of the flash VEP is that it does not require accurate fixation or refraction, which is the case with the pattern VEP. Flash VEPs are technically much less difficult to record than PRVEP. Refraction and alignment of the stimulus are not required, although the FVEP may be less sensitive than the PRVEP in some human diseases. We have found the FVEP is depressed in monkeys with idiopathic bilateral optic atrophy (Fig. 4.8b), and this is an important ophthalmologic finding when screening animals for participation in ocular studies [102, 103]. In animals with a retina that contains a high-resolution macula, PRVEPs are generated primarily by the central $\sim 9^\circ$ [86]. Thus, the standard PRVEP is sensitive to macular and optic nerve insults but far less sensitive to damage to the visual structures supporting peripheral vision.

Steady-state VEP outcome measures typically are amplitude and phase in the VEP at the stimulation frequency (including harmonics) derived by spectral analysis. The output from a frequency-labeled VEP is the stimulus parameter that elicits a criterion response (e.g., the minimum stripe width, contrast, or vernier offset). Multifocal VEPs are less widely used than flash or PRVEP but are gaining use clinically when visual field defects are suspected or confirm field delays in diagnosis of optic neuropathies.

4.5.3 Use in Animal Toxicology and Other Ocular Research

Research with humans has shown that PRVEPs are sensitive to the spatial frequency of the checkerboard grating pattern and therefore can be used to estimate acuity. We have used PRVEP to estimate acuity in dogs [104] and albino and pigmented rats (Fig. 4.11) [105]. Like the pattern electroretinogram (PERG), the PRVEP requires precise refraction for the distance of the stimulator to the animal's eye.

The sweep VEP “frequency labeling” technique can markedly decrease the time needed to establish the relationship between VEP amplitude and spatial frequency or bar width with good reliability. We found, in a group of difficult-to-test children with albinism and nystagmus, that sweep VEP acuity in infancy was predictive of visual acuity later in childhood when the child was capable of reading the eye chart. We have applied this method to acuity testing in the anesthetized rhesus macaque and have found sweep VEP acuity to be highly sensitive to refractive error (Fig. 4.12) [106].

The multifocal VEP technique has been applied only recently in nonclinical studies. We have conducted mfVEPs in anesthetized nonhuman primates using luminance stimulation from seven large central hexagons to assess field-specific VEPs (Fig. 4.13) [107] and found it sensitive for detecting glaucoma. Recently, we reported that the mfVEP in the anesthetized monkey is sensitive to experimental glaucoma and may reflect neuroprotective properties of memantine [108]. Recording VEPs from mice has many obvious advantages in studies of neuroprotection; however, relatively few studies using the VEP technique in mice have been reported. Peachey [109] showed that it is feasible to perform serial recordings with the flash VEP from wild-type mice and the FVEP is delayed in Akt-DD mice that have enhanced

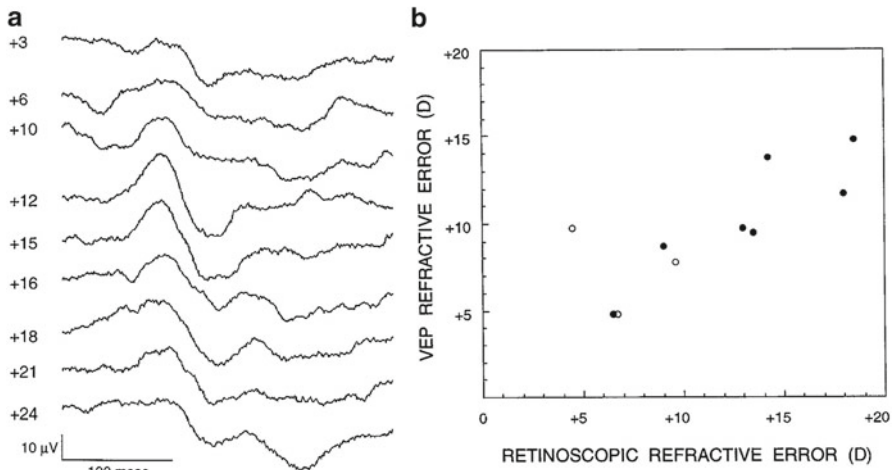


Fig. 4.11 PRVEP refraction in the rat. (a) PRVEP waveforms recorded from anesthetized, dilated, and cycloplegic pigmented rat showing higher amplitude PRVEP was elicited when a +12.00 diopter trial lens was placed in front of the eye. (b) Estimated VEP refraction as a function of retinoscopy in pigmented (*dark circles*) and albino (*open circles*) rats (From Mutti et al. [105])

optic nerve myelination or abnormalities in the density of the nodes of Ranvier (Fig. 4.14). Flash VEPs in mice have been used to assess ganglion cell death in naturally occurring murine models of glaucoma (Fig. 4.15) [110], optic atrophy [111], and (recording from the surface of the cortex) in the osteopetrotic knockout [112].

VEP has been used to correlate dose-effect relationships in rats between exposures to industrial chemicals such as perchloroethylene [113], and together with other imaging techniques, VEP has been used to assess the ocular safety of drugs. In rabbits, for example, it has been used to study the possible toxicity of intravitreal injections of bevacizumab [114] and ketorolac tromethamine [115].

4.5.4 Human Clinical Applications

VEPs have been used for many years in neurology and neuro-ophthalmology in diagnosing demyelinating diseases of the optic nerve and visual system (Fig. 4.16). Optic neuritis typically manifests as a unilateral inflammation of the optic nerve that often precedes a diagnosis of multiple sclerosis. Whereas latency to the positive peak in the VEP elicited by a checkerboard is normally 100 ms with an upper limit of 115 ms, depending on the age of the patient and the specific equipment and technique used in a given laboratory, a patient with optic neuritis may have peak latencies of the “P100” delayed as long as 130–150 ms.

VEPs are altered by occupational exposure to a variety of industrial chemicals, for example, acrylamide and N-methylolacrylamide [116, 117] and dietary

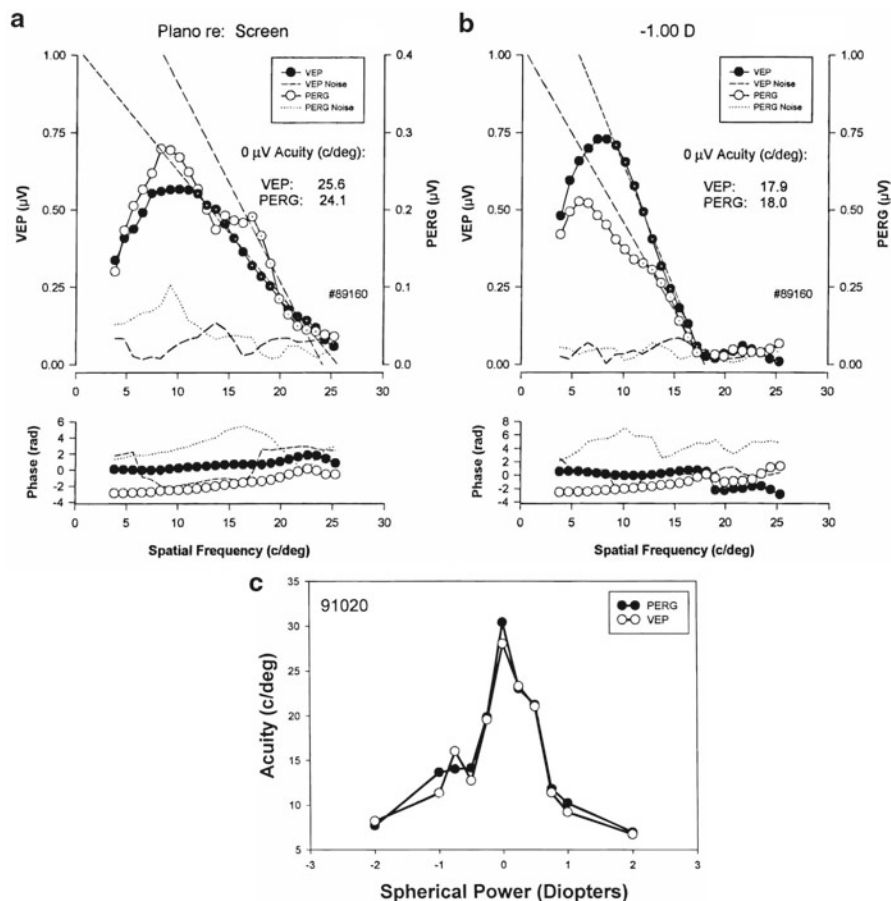


Fig. 4.12 “Sweep VEP” acuity estimation in an anesthetized monkey. **(a)** The amplitude and phase of the VEP (and simultaneously recorded PERG) in response to a steady-state (15 Hz) grating are plotted as a function of the spatial frequency of the grating. Regression lines through the descending portion of the sweep VEP interpolate to acuity of 25.6 c/deg. **(b)** A -1.00 diopter lens reduces acuity to 17.9 cycles/deg. **(c)** A plot of sweep VEP acuity versus lens power demonstrated the sensitivity of the VEP to blur (From Ver Hoeve et al. [106])

methylmercury and polychlorinated biphenyls in children [117]. Clinically, VEPs have been used to detect adverse drug-related ocular effects, such as hydroxychloroquine toxicity in patients undergoing treatment for rheumatoid arthritis and systemic lupus erythematosus [118], although the multifocal ERG is a more direct and widely used adjunctive test for the ring scotomas that typify this toxicity [119, 120]. Ethambutol is a first-line treatment for tuberculosis with a potential side effect of the development of significant optic atrophy. PRVEP P100 latencies have been shown to detect subclinical toxicity in a group of 52 patients [121]. Flash VEP has been

Fig. 4.13 Luminance multifocal VEP elicited by seven large hexagons recorded simultaneously with the multifocal ERG to this stimulus in a monkey with a unilateral experimental optic nerve transection. The VEP from transected right eye is completely extinguished while the ERG remains robust and slightly enhanced relative to the normal fellow eye (OS) (From Maertz et al. [107])

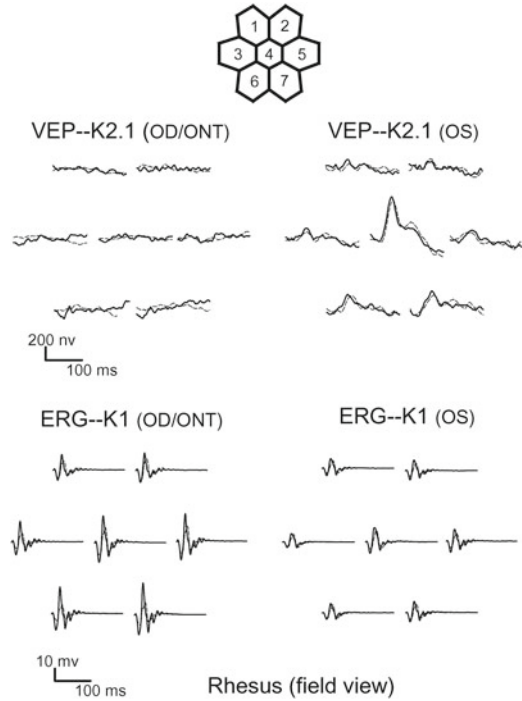
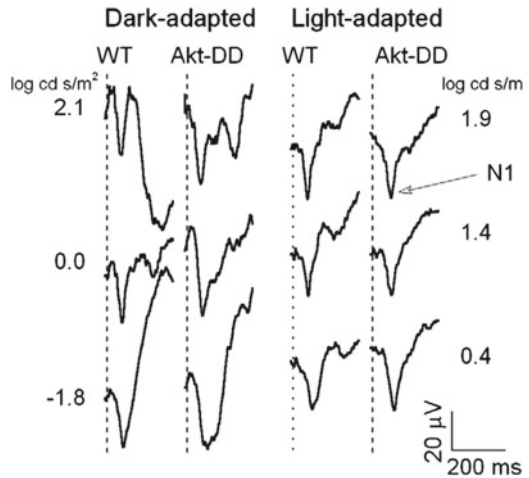


Fig. 4.14 Flash VEPs recorded from wild-type (*WT*) and *Akt-DD* mice with a phenotype of overmyelinated optic nerves (From Yu et al. [109])



included in evaluation for predicting clinical visual loss following traumatic optic neuropathy [122]. Other examples of clinical applications of VEP include studying the effects of diet on the development of visual acuity in premature infants [123] and the effect of drug treatment on visual changes in patients with Parkinson’s disease [124, 125].

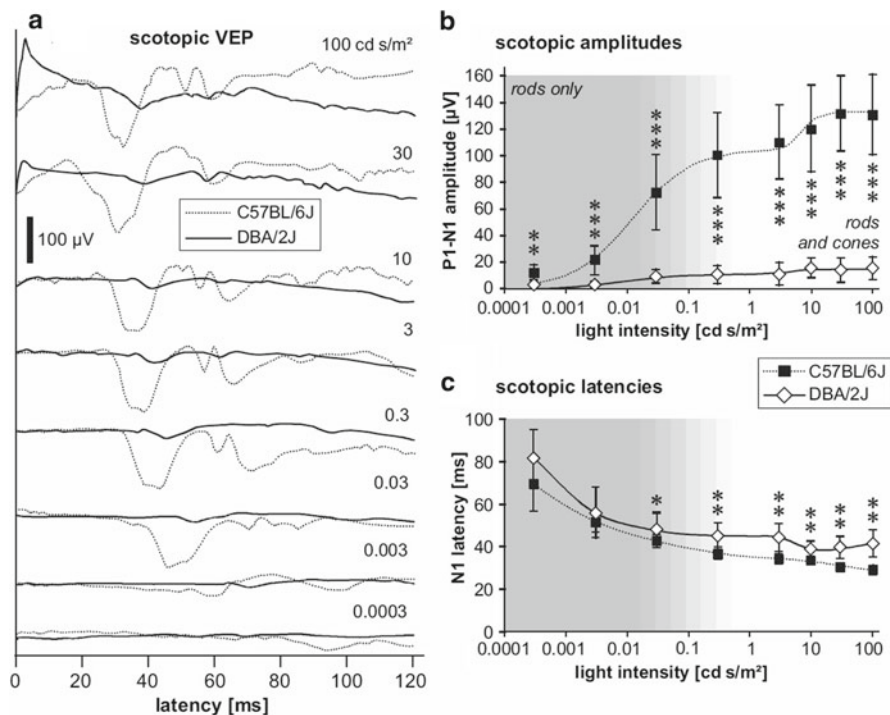


Fig. 4.15 VEPs recorded under scotopic and photopic conditions in a normal strain (C57BL/6J) and a mouse with congenital anterior pigmentary angle closure glaucoma (DBA/2J). Note marked reduction in VEP amplitude in mice with congenital glaucoma, exceeding ERG decreases (not shown) (From Heiduschka et al. [110])

Glaucoma is a neurodegenerative disorder of the optic nerve and brain with insidious onset and loss of peripheral vision. Because of the dependence of the traditional checkerboard VEP on the papillomacular nerve bundle, it has not been considered an appropriate test, although there are some indications that the FVEP [126] and pattern VEP, particularly with a blue-yellow pattern, [127] may be sensitive to early glaucomatous damage. Combining PRVEP with PERG has been shown to improve sensitivity and specificity for discrimination of open-angle glaucoma from ocular hypertension [128]. With sufficient post-processing and extensive control data, multifocal visual evoked potentials (mfVEP) have been shown to be sensitive for detection of glaucoma and for measuring the progression of glaucomatous field defects [9, 129–132]. Interocular and dichoptic multifocal visual evoked potentials (mfVEP) may improve detectability of visual field loss and other defects caused by glaucoma [133, 134]. Other recent applications have shown the mfVEP to be sensitive to recovery following optic neuritis [135–137]. It has also been used to demonstrate clinical improvements in visual acuity and macular edema secondary to vein occlusion following intravitreal injection of bevacizumab [138]. Changes in VEP were correlated with industrial lead exposure [139] and n-hexane [140].

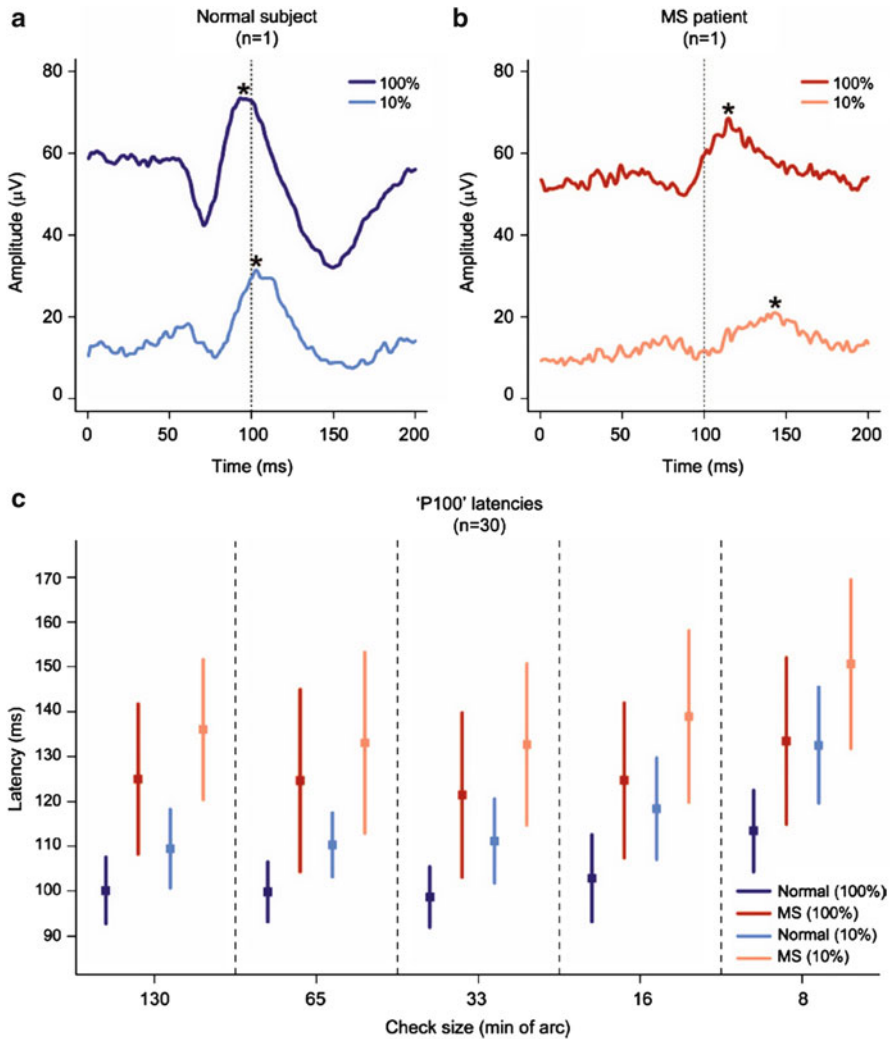


Fig. 4.16 (a) PRVEP recorded from a normal subject at high and low contrast. (b) PRVEPs from a patient with multiple sclerosis. (c) PRVEP latency increases as check size decreases for low and high contrast check patterns (From Thurtell et al. [142])

4.5.5 Commercially Available Devices

Available Units:

Diagnosys LLC, Lowell, MA

<http://www.diagnosysllc.com/home>

LKC Technologies, Inc., Gaithersburg, MD

<http://www.lkc.com>

Electro-Diagnostic Imaging, Inc., Redwood City, CA

<http://www.veris-edi.com>

Cadwell Laboratories, Inc., Kennewick, WA

<http://www.cadwell.com>

Electrical Geodesics, Inc., Eugene, OR

<http://www.egi.com>

4.5.6 Considerations for Ocular Toxicology Studies

The VEP is particularly useful when it is important to know whether visual signals are reaching and being processed by the cortical areas. At many stages of drug development, it may be sufficient to use only ERG to evaluate toxicity; however, because the ERG is not sensitive to loss of retinal ganglion cell function and VEPs depend on an intact retinal ganglion cell layer, VEPs can be a valuable adjunct to an ocular safety evaluation program. It is also important to consider the fact that pattern VEP is generated primarily from the macular regions (in species with a macula). Thus, for the primate, the cat, and, to a lesser extent, the dog, the VEP may be used to assess central retinal function. For example, in macular degeneration, the full-field ERG is often normal due to the relatively small portion of the entire retina that is affected, whereas the PRVEP is greatly depressed. Additional applications include the necessity to assess central neural function in ocular and CNS drug development studies. Frequently, compounds are developed with sites of action that could potentially affect brain function independently of retinal function. In these instances, the VEP may be a useful add-on to ERG studies while the animal is anesthetized.

4.5.7 Limitations and Caveats

In general, recording VEPs requires monitoring attention and fixation in humans and monitoring level of anesthesia and alignment of the stimulus with the retina in animals. Flash VEP stimulation is far less dependent on fixation and optic clarity than pattern VEPs; however, the flash VEP is less sensitive to manipulations that might affect, for example, acuity. There are several major types of pattern VEPs, with specific caveats and limitations. The principal caveat is that the subject must be accurately refracted for testing distance. Inaccurate refraction can result in marked decreases in VEP. Alignment of the pattern stimulus with the retina is also essential. Eye position should be continuously monitored during PRVEP testing. Drift in eye position during testing can seriously degrade the VEP. The situation is even more critical in the multifocal pattern VEP where alignment of the center of the dartboard pattern with the fovea throughout testing is critical.

Interpretation of the VEP is largely dependent on the stimulus paradigm that was used for testing: flash VEP testing shows that luminance (light/dark) signals are

reaching the cortex, PRVEP shows that local changes in contrast and contour are responded to by cortex, and the mfVEP shows that cortical responses are full throughout the central visual field.

References

1. De Rouck AF. History of the electroretinogram. In: Heckenlively JR, Arden GB, editors. Principles and practice of clinical electrophysiology of vision. Cambridge, MA: The MIT Press; 2006. p. 3–10.
2. Harding GFA. History of visual evoked cortical testing. In: Heckenlively JR, Arden GB, editors. Principles and practice of clinical electrophysiology of vision. Cambridge, MA: The MIT Press; 2006. p. 15–9.
3. Marmor MF, Fulton AB, Holder GE, Miyake Y, Brigell M, Bach M. ISCEV Standard for full-field clinical electroretinography (2008 update). *Doc Ophthalmol.* 2009;118:69–77.
4. Narfstrom K, Ekesten B, Rosolen SG, Spiess BM, Percicot CL, Ofri R. Guidelines for clinical electroretinography in the dog. *Doc Ophthalmol.* 2002;105:83–92.
5. Narfstrom K. Electroretinography in veterinary medicine—easy or accurate? *Vet Ophthalmol.* 2002;5:249–51.
6. Robson JG, Frishman LJ. Dissecting the dark-adapted electroretinogram. *Doc Ophthalmol.* 1998;95:187–215.
7. Robson JG, Saszik SM, Ahmed J, Frishman LJ. Rod and cone contributions to the a-wave of the electroretinogram of the macaque. *J Physiol.* 2003;547:509–30.
8. Hood DC. Assessing retinal function with the multifocal technique. *Prog Retin Eye Res.* 2000;19:607–46.
9. Hood DC, Odel JG, Chen CS, Winn BJ. The multifocal electroretinogram. *J Neuroophthalmol.* 2003;23:225–35.
10. Sutter EE, Tran D. The field topography of ERG components in man—I. The photopic luminance response. *Vision Res.* 1992;32:433–46.
11. Hood DC, Frishman LJ, Saszik S, Viswanathan S. Retinal origins of the primate multifocal ERG: implications for the human response. *Invest Ophthalmol Vis Sci.* 2002;43:1673–85.
12. Nork TM, Murphy CJ, Kim CB, Ver Hoeve JN, Rasmussen CA, Miller PE, Wabers HD, Neider MW, Dubielzig RR, McCulloh RJ, et al. Functional and anatomic consequences of subretinal dosing in the cynomolgus macaque. *Arch Ophthalmol.* 2012;130:65–75.
13. Li J, Tso MO, Lam TT. Reduced amplitude and delayed latency in foveal response of multifocal electroretinogram in early age related macular degeneration. *Br J Ophthalmol.* 2001;85:287–90.
14. Kretschmann U, Bock M, Gockeln R, Zrenner E. Clinical applications of multifocal electroretinography. *Doc Ophthalmol.* 2000;100:99–113.
15. Shimada Y, Li Y, Bearnse Jr MA, Sutter EE, Fung W. Assessment of early retinal changes in diabetes using a new multifocal ERG protocol. *Br J Ophthalmol.* 2001;85:414–19.
16. Hood DC, Greenstein VC, Holopigian K, Bauer R, Firoz B, Liebmann JM, Odel JG, Ritch R. An attempt to detect glaucomatous damage to the inner retina with the multifocal ERG. *Invest Ophthalmol Vis Sci.* 2000;41:1570–9.
17. Holopigian K, Greenstein VC, Seiple W, Hood DC, Ritch R. Electrophysiologic assessment of photoreceptor function in patients with primary open-angle glaucoma. *J Glaucoma.* 2000;9:163–8.
18. Bearnse Jr MA, Han Y, Schneck ME, Adams AJ. Retinal function in normal and diabetic eyes mapped with the slow flash multifocal electroretinogram. *Invest Ophthalmol Vis Sci.* 2004;45:296–304.
19. Sutter EE, Bearnse Jr MA. The optic nerve head component of the human ERG. *Vision Res.* 1999;39:419–36.

20. Hood DC, Bearse Jr MA, Sutter EE, Viswanathan S, Frishman LJ. The optic nerve head component of the monkey's (*Macaca mulatta*) multifocal electroretinogram (mERG). *Vision Res.* 2001;41:2029–41.
21. Frishman LJ, Saszik S, Harwerth RS, Viswanathan S, Li Y, Smith 3rd EL, Robson JG, Barnes G. Effects of experimental glaucoma in macaques on the multifocal ERG. Multifocal ERG in laser-induced glaucoma. *Doc Ophthalmol.* 2000;100:231–351.
22. Hare WA, Ton H, Ruiz G, Feldmann B, Wijono M, WoldeMussie E. Characterization of retinal injury using ERG measures obtained with both conventional and multifocal methods in chronic ocular hypertensive primates. *Invest Ophthalmol Vis Sci.* 2001;42:127–36.
23. Nork TM, Kim CB, Heatley GA, Kaufman PL, Lucarelli MJ, Levin LA, Ver Hoeve JN. Serial multifocal electroretinograms during long-term elevation and reduction of intraocular pressure in non-human primates. *Doc Ophthalmol.* 2010;120:273–89.
24. Heckenlively JR, Tanji T, Logani S. Retrospective study of hyperabnormal (supranormal) electroretinographic responses in 104 patients. *Trans Am Ophthalmol Soc.* 1994;92:217–31.
25. Moschos MM, Brouzas D, Apostolopoulos M, Koutsandrea C, Loukianou E, Moschos M. Intravitreal use of bevacizumab (Avastin) for choroidal neovascularization due to ARMD: a preliminary multifocal-ERG and OCT study. Multifocal-ERG after use of bevacizumab in ARMD. *Doc Ophthalmol.* 2007;114:37–44.
26. Kim CB, Ver Hoeve JN, Kaufman PL, Nork TM. Interspecies and gender differences in multifocal electroretinograms of cynomolgus and rhesus macaques. *Doc Ophthalmol.* 2004;109:73–86.
27. Kim CB, Ver Hoeve JN, Kaufman PL, Nork TM. Effects of reference electrode location on monopolar-derived multifocal electroretinograms in cynomolgus monkeys. *Doc Ophthalmol.* 2005;111:113–25.
28. Kim CBY, Ver Hoeve JN, Nork TM. The effect of pentobarbital sodium and propofol anesthesia on multifocal electroretinograms in rhesus macaques. *Doc Ophthalmol* 2011 (Dec. 28 [Epub]).
29. Rimmer S, Katz B. The pattern electroretinogram: technical aspects and clinical significance. *J Clin Neurophysiol.* 1989;6:85–99.
30. Riggs LA. The human electroretinogram. *AMA Arch Ophthalmol.* 1958;60:739–49; discussion 749–54.
31. Riggs LA. Progress in the recording of human retinal and occipital potentials. *J Opt Soc Am.* 1969;59:1558–66.
32. Dodt E. The electrical response of the human eye to patterned stimuli: clinical observations. *Doc Ophthalmol.* 1987;65:271–86.
33. Riggs LA, Johnson EP, Schick AM. Electrical responses of the human eye to moving stimulus patterns. *Science.* 1964;144:567.
34. Lawwill T. The bar-pattern electroretinogram for clinical evaluation of the central retina. *Am J Ophthalmol.* 1974;78:121–6.
35. Maffei L, Fiorentini A. Electroretinographic responses to alternating gratings in the cat. *Exp Brain Res.* 1982;48:327–34.
36. Maffei L, Fiorentini A, Bisti S, Hollander H. Pattern ERG in the monkey after section of the optic nerve. *Exp Brain Res.* 1985;59:423–5.
37. Berardi N, Domenici L, Gravina A, Maffei L. Pattern ERG in rats following section of the optic nerve. *Exp Brain Res.* 1990;79:539–46.
38. Ringens PJ, Vijfinkel-Bruinenga S, van Lith GH. The pattern-elicited electroretinogram. I. A tool in the early detection of glaucoma? *Ophthalmologica.* 1986;192:171–5.
39. Porciatti V, Falsini B, Brunori S, Colotto A, Moretti G. Pattern electroretinogram as a function of spatial frequency in ocular hypertension and early glaucoma. *Doc Ophthalmol.* 1987;65:349–55.
40. Wanger P, Persson HE. Pattern-reversal electroretinograms from normotensive, hypertensive and glaucomatous eyes. *Ophthalmologica.* 1987;195:205–8.
41. Weinstein GW, Arden GB, Hitchings RA, Ryan S, Calthorpe CM, Odom JV. The pattern electroretinogram (PERG) in ocular hypertension and glaucoma. *Arch Ophthalmol.* 1988;106:923–8.
42. Korth M, Horn F, Storck B, Jonas J. The pattern-evoked electroretinogram (PERG): age-related alterations and changes in glaucoma. *Graefes Arch Clin Exp Ophthalmol.* 1989;27:123–30.

43. Pfeiffer N, Bach M. The pattern-electroretinogram in glaucoma and ocular hypertension. A cross-sectional and longitudinal study. *Ger J Ophthalmol.* 1992;1:35–40.
44. Ventura LM, Porciatti V, Ishida K, Feuer WJ, Parrish 2nd RK. Pattern electroretinogram abnormality and glaucoma. *Ophthalmology.* 2005;112:10–9.
45. Porciatti V, Ventura LM. Physiologic significance of steady-state pattern electroretinogram losses in glaucoma: clues from simulation of abnormalities in normal subjects. *J Glaucoma.* 2009;18:535–42.
46. Atilla H, Tekeli O, Ornek K, Batioglu F, Elhan AH, Eryilmaz T. Pattern electroretinography and visual evoked potentials in optic nerve diseases. *J Clin Neurosci.* 2006;13:55–9.
47. Kirkham TH, Coupland SG. Abnormal pattern electroretinograms with macular cherry-red spots: evidence for selective ganglion cell damage. *Curr Eye Res.* 1981;1:367–72.
48. Porciatti V, Francesconi W, Bagnoli P. The pigeon pattern electroretinogram is not affected by massive loss of cell bodies in the ganglion layer induced by chronic section of the optic nerve. *Doc Ophthalmol.* 1985;61:41–7.
49. Armington JC, Adolph AR. Local pattern electroretinograms and ganglion cell activity in the turtle eye. *Int J Neurosci.* 1990;50:1–11.
50. Vaegan Graham SL, Goldberg I, Millar TJ. Selective reduction of oscillatory potentials and pattern electroretinograms after retinal ganglion cell damage by disease in humans or by kainic acid toxicity in cats. *Doc Ophthalmol.* 1991;77:237–53.
51. Porciatti V, Saleh M, Nagaraju M. The pattern electroretinogram as a tool to monitor progressive retinal ganglion cell dysfunction in the DBA/2J mouse model of glaucoma. *Invest Ophthalmol Vis Sci.* 2007;48:745–51.
52. Maffei L, Fiorentini A. Electroretinographic responses to alternating gratings before and after section of the optic nerve. *Science.* 1981;211:953–5.
53. Bach M, Hoffmann MB. Update on the pattern electroretinogram in glaucoma. *Optom Vis Sci.* 2008;85:386–95.
54. Holder GE. Pattern electroretinography (PERG) and an integrated approach to visual pathway diagnosis. *Prog Retin Eye Res.* 2001;20:531–61.
55. Holder GE. Electrophysiological assessment of optic nerve disease. *Eye.* 2004;18:1133–43.
56. Ventura LM, Porciatti V. Pattern electroretinogram in glaucoma. *Curr Opin Ophthalmol.* 2006;17:196–202.
57. Fredette MJ, Anderson DR, Porciatti V, Feuer W. Reproducibility of pattern electroretinogram in glaucoma patients with a range of severity of disease with the new glaucoma paradigm. *Ophthalmology.* 2008;115:957–63.
58. Nagaraju M, Saleh M, Porciatti V. IOP-dependent retinal ganglion cell dysfunction in glaucomatous DBA/2J mice. *Invest Ophthalmol Vis Sci.* 2007;48:4573–9.
59. Saleh M, Nagaraju M, Porciatti V. Longitudinal evaluation of retinal ganglion cell function and IOP in the DBA/2J mouse model of glaucoma. *Invest Ophthalmol Vis Sci.* 2007;48:4564–72.
60. Johnson MA, Drum BA, Quigley HA, Sanchez RM, Dunkelberger GR. Pattern-evoked potentials and optic nerve fiber loss in monocular laser-induced glaucoma. *Invest Ophthalmol Vis Sci.* 1989;30:897–907.
61. Marx MS, Podos SM, Bodis-Wollner I, Howard-Williams JR, Siegel MJ, Teitelbaum CS, Maclin EL, Severin C. Flash and pattern electroretinograms in normal and laser-induced glaucomatous primate eyes. *Invest Ophthalmol Vis Sci.* 1986;27:378–86.
62. Marx MS, Podos SM, Bodis-Wollner I, Lee PY, Wang RF, Severin C. Signs of early damage in glaucomatous monkey eyes: low spatial frequency losses in the pattern ERG and VEP. *Exp Eye Res.* 1988;46:173–84.
63. Viswanathan S, Frishman LJ, Robson JG. The uniform field and pattern ERG in macaques with experimental glaucoma: removal of spiking activity. *Invest Ophthalmol Vis Sci.* 2000;41:2797–810.
64. Hodos W, Ghim MM, Potocki A, Fields JN, Storm T. Contrast sensitivity in pigeons: a comparison of behavioral and pattern ERG methods. *Doc Ophthalmol.* 2002;104:107–18.
65. Porciatti V, Hodos W, Signorini G, Bramanti F. Electroretinographic changes in aged pigeons. *Vision Res.* 1991;31:661–8.

66. Bagnoli P, Porciatti V, Francesconi W, Barsellotti R. Pigeon pattern electroretinogram: a response unaffected by chronic section of the optic nerve. *Exp Brain Res.* 1984;55:253–62.
67. Blondeau P, Lamarche J, Lafond G, Brunette JR. Pattern electroretinogram and optic nerve section in pigeons. *Curr Eye Res.* 1987;6:747–56.
68. Miura G, Wang MH, Ivers KM, Frishman LJ. Retinal pathway origins of the pattern ERG of the mouse. *Exp Eye Res.* 2009;89:49–62.
69. Bodis-Wollner I. Visual electrophysiology in Parkinson's disease: PERG, VEP and visual P300. *Clin Electroencephalogr.* 1997;28:143–7.
70. Calzetti S, Franchi A, Taratufolo G, Groppi E. Simultaneous VEP and PERG investigations in early Parkinson's disease. *J Neurol Neurosurg Psychiatry.* 1990;53:114–17.
71. Nightingale S, Mitchell KW, Howe JW. Visual evoked cortical potentials and pattern electroretinograms in Parkinson's disease and control subjects. *J Neurol Neurosurg Psychiatry.* 1986;49:1280–7.
72. Peppe A, Stanzione P, Pierelli F, De Angelis D, Pierantozzi M, Bernardi G. Visual alterations in de novo Parkinson's disease: pattern electroretinogram latencies are more delayed and more reversible by levodopa than are visual evoked potentials. *Neurology.* 1995;45:1144–8.
73. Sartucci F, Orlandi G, Lucetti C, Bonuccelli U, Murri L, Orsini C, Porciatti V. Changes in pattern electroretinograms to equiluminant red-green and blue-yellow gratings in patients with early Parkinson's disease. *J Clin Neurophysiol.* 2003;20:375–81.
74. Tagliati M, Bodis-Wollner I, Yahr MD. The pattern electroretinogram in Parkinson's disease reveals lack of retinal spatial tuning. *Electroencephalogr Clin Neurophysiol.* 1996;100:1–11.
75. Tartaglione A, Oneto A, Bandini F, Favale E. Visual evoked potentials and pattern electroretinograms in Parkinson's disease and control subjects. *J Neurol Neurosurg Psychiatry.* 1987;50:1243–4.
76. Archibald NK, Clarke MP, Mosimann UP, Burn DJ. The retina in Parkinson's disease. *Brain.* 2009;132:1128–45.
77. McCulloch DL, Garcia-Filion P, van Boemel GB, Borchert MS. Retinal function in infants with optic nerve hypoplasia: electroretinograms to large patterns and photopic flash. *Eye (Lond).* 2007;21:712–20.
78. McCulloch DL, Garcia-Filion P, Fink C, Chaplin CA, Borchert MS. Clinical electrophysiology and visual outcome in optic nerve hypoplasia. *Br J Ophthalmol.* 2010;94(8):1017–23. Epub 2009 Dec 2. PMID: 19955198 [PubMed - indexed for MEDLINE].
79. Birch DG, Anderson JL, Fish GE, Jost BF. Pattern-reversal electroretinographic follow-up of laser photocoagulation for subfoveal neovascular lesions in age-related macular degeneration. *Am J Ophthalmol.* 1993;116:148–55.
80. Birch DG, Anderson JL, Fish GE, Jost BF. Pattern-reversal electroretinographic acuity in untreated eyes with subfoveal neovascular membranes. *Invest Ophthalmol Vis Sci.* 1992;33:2097–104.
81. da Costa GM, dos Anjos LM, Souza GS, Gomes BD, Saito CA, Pinheiro Mda C, Ventura DF, da Silva Filho M, Silveira LC. Mercury toxicity in Amazon gold miners: visual dysfunction assessed by retinal and cortical electrophysiology. *Environ Res.* 2008;107:98–107.
82. Odom JV, Maida TM, Dawson WW, Hobson R. Pattern electroretinogram: effects of reference electrode position. *Doc Ophthalmol.* 1987;65:297–306.
83. Dawson WW, Trick GL, Litzkow CA. Improved electrode for electroretinography. *Invest Ophthalmol Vis Sci.* 1979;18:988–91.
84. Fisher AC, Hagan RP, Brown MC. Automatic positioning of cursors in the transient pattern electroretinogram (PERG) with very poor SNR using an Expert System. *Doc Ophthalmol.* 2007;115:61–8.
85. Nunez P, Srinivasa R. Electric fields of the brain. The neurophysics of EEG. New York: Oxford University Press; 2006.
86. Regan D. Human brain electrophysiology: evoked potentials and evoked magnetic fields in science and medicine. London: Elsevier; 1989.
87. Odom JV, Bach M, Brigell M, Holder GE, McCulloch DL, Tormene AP, Vaegan. ISCEV standard for clinical visual evoked potentials (2009 update). *Doc Ophthalmol.* 2009;120:111–19.
88. Hou C, Good WV, Norcia AM. Validation study of VEP vernier acuity in normal-vision and amblyopic adults. *Invest Ophthalmol Vis Sci.* 2007;48:4070–8.

89. Mirabella G, Norcia AM. Neural correlates of transformational apparent motion. *Perception*. 2008;37:1368–79.
90. Norcia AM, Wesemann W, Manny RE. Electrophysiological correlates of vernier and relative motion mechanisms in human visual cortex. *Vis Neurosci*. 1999;16:1123–31.
91. Norcia AM, Hale J, Pettet MW, McKee SP, Harrad RA. Disparity tuning of binocular facilitation and suppression after normal versus abnormal visual development. *Invest Ophthalmol Vis Sci*. 2009;50:1168–75.
92. Struck MC, Ver Hoeve JN, France TD. Binocular cortical interactions in the monofixation syndrome. *J Pediatr Ophthalmol Strabismus*. 1996;33:291–7.
93. Bearse Jr MA, Sutter EE. Imaging localized retinal dysfunction with the multifocal electroretinogram. *J Opt Soc Am A Opt Image Sci Vis*. 1996;13:634–40.
94. Sutter E. The interpretation of multifocal binary kernels. *Doc Ophthalmol*. 2000;100:49–75.
95. Sutter EE. Imaging visual function with the multifocal m-sequence technique. *Vision Res*. 2001;41:1241–55.
96. Fortune B, Demirel S, Zhang X, Hood DC, Johnson CA. Repeatability of normal multifocal VEP: implications for detecting progression. *J Glaucoma*. 2006;15:131–41.
97. Hood DC, Zhang X, Greenstein VC, Kangovi S, Odel JG, Liebmann JM, Ritch R. An interocular comparison of the multifocal VEP: a possible technique for detecting local damage to the optic nerve. *Invest Ophthalmol Vis Sci*. 2000;41:1580–7.
98. Klistorner AI, Graham SL. Multifocal pattern VEP perimetry: analysis of sectoral waveforms. *Doc Ophthalmol*. 1999;98:183–96.
99. Yang EB, Hood DC, Rodarte C, Zhang X, Odel JG, Behrens MM. Improvement in conduction velocity after optic neuritis measured with the multifocal VEP. *Invest Ophthalmol Vis Sci*. 2007;48:692–8.
100. Zhang X, Hood DC. A principal component analysis of multifocal pattern reversal VEP. *J Vis*. 2004;4:32–43.
101. Odom JV, Bach M, Brigell M, Holder GE, McCulloch DL, Tormene AP, Vaegan. ISCEV standard for clinical visual evoked potentials (2009 update). *Doc Ophthalmol*. 2010;120:111–19.
102. Fortune B, Wang L, Bui BV, Burgoyne CF, Cioffi GA. Idiopathic bilateral optic atrophy in the rhesus macaque. *Invest Ophthalmol Vis Sci*. 2005;46:3943–56.
103. Dubielzig RR, Leedle R, Nork TM, Ver Hoeve JN, Christian BJ. Bilateral optic atrophy: A background finding in cynomolgus macaques used in toxicologic research. Presented at Association for Research in Vision and Ophthalmology, May 2009, Fort Lauderdale, FL.
104. Murphy CJ, Mutti DO, Zadnik K, Ver HJ. Effect of optical defocus on visual acuity in dogs. *Am J Vet Res*. 1997;58:414–18.
105. Mutti DO, Ver Hoeve JN, Zadnik K, Murphy CJ. The artifact of retinoscopy revisited: comparison of refractive error measured by retinoscopy and visual evoked potential in the rat. *Optom Vis Sci*. 1997;74:483–8.
106. Ver Hoeve JN, Danilov YP, Kim CB, Spear PD. VEP and PERG acuity in anesthetized young adult rhesus monkeys. *Vis Neurosci*. 1999;16:607–17.
107. Maertz NA, Kim CB, Nork TM, Levin LA, Lucarelli MJ, Kaufman PL, Ver Hoeve JN. Multifocal visual evoked potentials in the anesthetized non-human primate. *Curr Eye Res*. 2006;31:885–93.
108. Gabelt BT, Rasmussen CA, Tektas OY, Kim CB, Peterson JC, Nork TM, Ver Hoeve JN, Lütjendrecoll E, Kaufman PL. Structure/function studies and the effects of memantine in monkeys with experimental glaucoma. *Invest Ophthalmol Vis Sci*. 2012 Apr 30;53(4):2368–76.
109. Yu M, Narayanan SP, Wang F, Morse E, Macklin WB, Peachey NS. Visual abnormalities associated with enhanced optic nerve myelination. *Brain Res*. 2011;1374:36–42.
110. Heiduschka P, Julien S, Schuetttauf F, Schnichels S. Loss of retinal function in aged DBA/2J mice - New insights into retinal neurodegeneration. *Exp Eye Res*. 2009;91:779–83.
111. Heiduschka P, Schnichels S, Fuhrmann N, Hofmeister S, Schraermeyer U, Wissinger B, Alavi MV. Electrophysiological and histologic assessment of retinal ganglion cell fate in a mouse model for OPA1-associated autosomal dominant optic atrophy. *Invest Ophthalmol Vis Sci*. 2010;51:1424–31.

112. Michaelson MD, Bieri PL, Mehler MF, Xu H, Arezzo JC, Pollard J, Kessler JA. CSF-1 deficiency in mice results in abnormal brain development. *Development*. 1996;122:2661–72.
113. Boyes WK, Bercegeay M, Oshiro WM, Krantz QT, Kenyon EM, Bushnell PJ, Benignus VA. Acute perchloroethylene exposure alters rat visual-evoked potentials in relation to brain concentrations. *Toxicol Sci*. 2009;108:159–72.
114. Xu W, Wang H, Wang F, Jiang Y, Zhang X, Wang W, Qian J, Xu X, Sun X. Testing toxicity of multiple intravitreal injections of bevacizumab in rabbit eyes. *Can J Ophthalmol*. 2010;45:386–92.
115. Komarowska I, Heilweil G, Rosenfeld PJ, Perlman I, Loewenstein A. Retinal toxicity of commercially available intravitreal ketorolac in albino rabbits. *Retina*. 2009;29:98–105.
116. Goffeng LO, Heier MS, Kjuus H, Sjöholm H, Sørensen KA, Skaug V. Nerve conduction, visual evoked responses and electroretinography in tunnel workers previously exposed to acrylamide and N-methylolacrylamide containing grouting agents. *Neurotoxicol Teratol*. 2008;30:186–94.
117. Saint-Amour D, Roy MS, Bastien C, Ayotte P, Dewailly E, Després C, Gingras S, Muckle G. Alterations of visual evoked potentials in preschool Inuit children exposed to methylmercury and polychlorinated biphenyls from a marine diet. *Neurotoxicology*. 2006;27:567–78.
118. Heravian J, Saghafi M, Shoeibi N, Hassanzadeh S, Shakeri MT, Sharepoor M. A comparative study of the usefulness of color vision, photostress recovery time, and visual evoked potential tests in early detection of ocular toxicity from hydroxychloroquine. *Int Ophthalmol*. 2011;31:283–9.
119. Marmor MF, Holder GE, Seeliger MW, Yamamoto S. Standard for clinical electroretinography (2004 update). *Doc Ophthalmol*. 2004;108:107–14.
120. Marmor MF. New American Academy of Ophthalmology recommendations on screening for hydroxychloroquine retinopathy. *Arthritis Rheum*. 2003;48:1764.
121. Menon V, Jain D, Saxena R, Sood R. Prospective evaluation of visual function for early detection of ethambutol toxicity. *Br J Ophthalmol*. 2009;93:1251–4.
122. Tabatabaei SA, Soleimani M, Alizadeh M, Movasat M, Mansoori MR, Alami Z, Foroutan A, Joshaghani M, Safari S, Goldiz A. Predictive value of visual evoked potentials, relative afferent pupillary defect, and orbital fractures in patients with traumatic optic neuropathy. *Clin Ophthalmol*. 2011;5:1021–6.
123. Harding CO, Gillingham MB, van Calcar SC, Wolff JA, Verhoeve JN, Mills MD. Docosahexaenoic acid and retinal function in children with long-chain 3-hydroxyacyl-CoA dehydrogenase deficiency. *J Inher Metab Dis*. 1999;22:276–80.
124. Sartucci F, Orlandi G, Bonuccelli U, Borghetti D, Murri L, Orsini C, Domenici L, Porciatti V. Chromatic pattern-reversal electroretinograms (ChPERGs) are spared in multiple system atrophy compared with Parkinson's disease. *Neurol Sci*. 2006;26:395–401.
125. Sener HO, Akbostanci MC, Yucesan C, Dora B, Selcuki D. Visual evoked potentials in Parkinson's disease—correlation with clinical involvement. *Clin Neurol Neurosurg*. 2001;103:147–50.
126. Watts MT, Good PA, O'Neill EC. The flash stimulated VEP in the diagnosis of glaucoma. *Eye (Lond)*. 1989;3:732–7.
127. Korth M, Nguyen NX, Junemann A, Martus P, Jonas JB. VEP test of the blue-sensitive pathway in glaucoma. *Invest Ophthalmol Vis Sci*. 1994;35:2599–610.
128. Parisi V, Miglior S, Manni G, Centofanti M, Bucci MG. Clinical ability of pattern electroretinograms and visual evoked potentials in detecting visual dysfunction in ocular hypertension and glaucoma. *Ophthalmology*. 2006;113:216–28.
129. Fortune B, Demirel S, Zhang X, Hood DC, Patterson E, Jamil A, Mansberger SL, Cioffi GA, Johnson CA. Comparing multifocal VEP and standard automated perimetry in high-risk ocular hypertension and early glaucoma. *Invest Ophthalmol Vis Sci*. 2007;48:1173–80.
130. Hood DC, Thienprasiddhi P, Greenstein VC, Winn BJ, Ohri N, Liebmann JM, Ritch R. Detecting early to mild glaucomatous damage: a comparison of the multifocal VEP and automated perimetry. *Invest Ophthalmol Vis Sci*. 2004;45:492–8.
131. Thienprasiddhi P, Greenstein VC, Chu DH, Xu L, Liebmann JM, Ritch R, Hood DC. Detecting early functional damage in glaucoma suspect and ocular hypertensive patients with the multifocal VEP technique. *J Glaucoma*. 2006;15:321–7.

132. Wangsupadilok B, Greenstein VC, Kanadani FN, Grippo TM, Liebmann JM, Ritch R, Hood DC. A method to detect progression of glaucoma using the multifocal visual evoked potential technique. *Doc Ophthalmol*. 2009;118:139–50.
133. Arvind H, Klistorner A, Graham S, Grigg J, Goldberg I, Klistorner A, Billson FA. Dichoptic stimulation improves detection of glaucoma with multifocal visual evoked potentials. *Invest Ophthalmol Vis Sci*. 2007;48:4590–6.
134. Arvind H, Graham S, Leaney J, Grigg J, Goldberg I, Billson F, Klistorner A. Identifying preperimetric functional loss in glaucoma: a blue-on-yellow multifocal visual evoked potentials study. *Ophthalmology*. 2009 Jun;116(6):1134–41. Epub 2009 Apr 23. PMID: 19395037.
135. Klistorner A, Arvind H, Nguyen T, Garrick R, Paine M, Graham S, O'Day J, Yiannikas C. Multifocal VEP and OCT in optic neuritis: a topographical study of the structure-function relationship. *Doc Ophthalmol*. 2009;118:129–37.
136. Klistorner A, Graham S, Fraser C, Garrick R, Nguyen T, Paine M, O'Day J, Grigg J, Arvind H, Billson FA. Electrophysiological evidence for heterogeneity of lesions in optic neuritis. *Invest Ophthalmol Vis Sci*. 2007;48:4549–56.
137. Klistorner A, Fraser C, Garrick R, Graham S, Arvind H. Correlation between full-field and multifocal VEPs in optic neuritis. *Doc Ophthalmol*. 2008;116:19–27.
138. Pai SA, Shetty R, Vijayan PB, Venkatasubramaniam G, Yadav NK, Shetty BK, Babu RB, Narayana KM. Clinical, anatomic, and electrophysiologic evaluation following intravitreal bevacizumab for macular edema in retinal vein occlusion. *Am J Ophthalmol*. 2007;143:601–6.
139. Hirata M, Kosaka H. Effects of lead exposure on neurophysiological parameters. *Environ Res*. 1993;63:60–9.
140. Kutlu G, Gomceli YB, Sonmez T, Inan LE. Peripheral neuropathy and visual evoked potential changes in workers exposed to n-hexane. *J Clin Neurosci*. 2009;16:1296–9.
141. Holder GE, Brigell MG, Hawlina M, Meigen T, Vaegan BM, International Society for Clinical Electrophysiology of Vision. ISCEV standard for clinical pattern electroretinography-2007 update. *Doc Ophthalmol*. 2007;114:111–16.
142. Thurtell MJ, Bala E, Yaniglos SS, Rucker JC, Peachey NS, Leigh RJ. Evaluation of optic neuropathy in multiple sclerosis using low-contrast visual evoked potentials. *Neurology*. 2009;73:1849.

Chapter 5

Toxicologic Pathology of the Eye: Histologic Preparation and Alterations of the Anterior Segment

Kenneth A. Schafer and James A. Render

Abstract The identification of microscopic toxicologic changes in eyes is influenced by many factors. Important factors include *in vivo* procedures, such as route of administration to the eye, and procedures involved in preparation of the microscopic ocular sections. A wide variety of toxins may affect all parts of the eye and ocular adnexa and must be differentiated from iatrogenic and spontaneous changes. Both toxic and spontaneous changes may occur in certain species of animals, certain strains of animals, or at certain ages; therefore, a good understanding of potential changes, as well as knowledge of the normal ocular anatomy, physiology, and function, is essential. This chapter focuses on the histologic preparation of ocular tissues and findings involving the anterior segment, uvea, and ocular adnexa and is followed by a chapter focusing on the lens and posterior segment of the eye.

5.1 Introduction

The detection and identification of microscopic toxicologic changes is influenced by many factors. For example, one needs to have an understanding of comparative ocular anatomy in order to differentiate variations in normal anatomical structures of different species from treatment-related changes in these structures. Smith et al. [1] and Prince [2] provide a review of the ocular anatomy of the mouse and rabbit, respectively, and others provide broader discussions of comparative ocular anatomy [3–5].

K.A. Schafer, D.V.M., DACVP, FIATP (✉)
Vet Path Services, Inc., Mason, OH, USA
e-mail: kschafer@vetpathservicesinc.com

J.A. Render, D.V.M., Ph.D., DACVP
NAMSA, Northwood, OH, USA

The detection of microscopic findings requires an awareness of clinical ocular findings observed via direct ophthalmoscopy, indirect ophthalmoscopy, and often slit lamp biomicroscopy [6–8]. These methods, along with additional techniques used in ophthalmology, can detect the exact location of findings and thus challenge the pathologist to provide a microscopic correlate. Detection of microscopic changes requires preparation of good quality histologic sections that have proper orientation and minimal tissue artifacts. Ocular findings need to be accurately classified as spontaneous, iatrogenic, or treatment-related and labeled with the proper diagnostic term.

Toxicologic pathologic evaluation begins with a review of the protocol. In addition to typical features of a study protocol, procedures used in the collection, fixation, trimming, processing, embedding, and ocular section preparation should be reviewed [9]. With oral administration, the globe will most likely be evaluated in a standard manner. However, direct dosing to the eye may result in ocular changes in specific locations that will require customized sampling of ocular tissue. Examples include localized superficial findings in the cornea following topical administration of a drug and findings in the vitreous or retina following intravitreal injections. Pathology laboratory personnel should be familiar with all ocular procedures used in studies and if not, should conduct a methods development study prior to the toxicity study to ensure that good quality sections will be prepared.

Development of the eye and ocular teratogenesis have been discussed in the literature including several comprehensive reviews [10–16]. Although ocular development is similar for humans and animals, the timing of events varies among humans and animals [12, 17]. Ocular findings occurring in neonatal or young animals are often characterized as developmental and are often identified during prestudy examinations. When using mice, especially genetically engineered mice, it is advantageous to know the anticipated effects on the eye of the induced genetic mutation [1].

5.2 Preparation for Microscopic Ocular Examination

Toxicologic ophthalmic pathology involves the detection and accurate characterization of macroscopic and microscopic toxicologic ocular findings. Macroscopic findings are often detected by use of the clinical ophthalmic examination; therefore, clinical ocular findings should be available at the time of necropsy, trimming, and microscopic examination. Microscopic correlates to ophthalmic findings should be determined, when possible.

The detection of ocular findings is not possible unless the histologic ocular sections are of good quality with the proper orientation and minimal tissue artifacts [9, 18, 19]. Obtaining ocular sections of good quality requires good communication between the pathologist and those involved in the clinical examination, postmortem procedures, and preparation of sections. Pathology laboratory personnel handling ocular tissue need to be familiar with all procedures (i.e., enucleation, fixation, trimming, processing, embedding, sectioning, and staining) required for good section quality.

In general, if fewer individuals are involved in the process (enucleation through section preparation), there are fewer artifacts.

Enucleation begins with a review of the ophthalmic findings which may be in the form of descriptions, diagrams, or images [20]. All globes should be enucleated as soon as possible after death (i.e., the beginning of the postmortem examination) to minimize postmortem autolysis, especially of the retina [18, 21]. Globes and the optic nerve should always be handled as gently as possible with minimal tension to avoid artifacts, such as retinal detachment, myelin in the subretinal space, and artifacts (i.e., spherical to irregularly shaped hyaline bodies) in the optic nerve [22–24]. At least 0.5 cm of the retrobulbar optic nerve should remain attached to the globe so that a cross section of the optic nerve can be prepared. For most studies, the extraocular muscles, orbital glands, and other orbital tissues should be carefully removed from around the globe prior to fixation for the following reasons: (1) allows for a gross examination of the globe, (2) exposes natural landmarks used for trimming (e.g., long posterior ciliary artery), and (3) facilitates fixation of intraocular structures (e.g., retina). For rodents, removal of the Harderian gland will allow visualization and collection of the retrobulbar optic nerve for cross sectioning. If needed, extraocular tissues may be fixed separately and processed. If globes are being collected for an ocular irritation study, then bulbar conjunctiva should be retained with the globe. For sub-Tenon's depot injections, extraocular tissue may need to be left intact to evaluate the injection site.

Prior to fixation, globes (especially those of albino rodents) may need to be marked with tattoo ink, an indelible dye, or a suture as a landmark for trimming. By convention, the mark is usually placed at the 12 o'clock position [1]. In addition, both globes should be identified as right (oculus dexter [OD]) or left (oculus sinister [OS]) at the time of enucleation, and the identification should be maintained throughout the process of section preparation.

The purpose of fixation is to preserve ocular tissues with minimal artifacts. There are many different fixatives used for fixation of the eye, but none are ideal. All fixatives have advantages and disadvantages which are important to understand in order to choose the most appropriate one for a given situation. Since there is variability in results among histotechnology laboratories using the same fixative, a pilot study is necessary to develop the method for each fixative in each laboratory to ensure that good quality ocular sections are obtained. The appearance of the ocular tissue is partially determined by the ingredients in the fixative used [25–27]. Depending on the fixative, immersion fixation (i.e., fixatives containing glacial acetic acid) should be sufficient for obtaining good sections of globes. In addition to immersion, optimal fixation with glutaraldehyde-based fixatives requires an intraocular injection of the fixative or the creation of a small window through which the fixative can diffuse. Systemic perfusion of the head is not necessary unless ocular tissues are going to be processed for plastic embedding and examination of sections at a thickness of 1 μm or examined by transmission electron microscopy. Systemic perfusion may cause inconsistent results or artifacts, especially if the perfusion pressure is too high (e.g., spaces beneath the retinal pigment epithelium) or if the fixative is too cold.

Fixatives containing glutaraldehyde (1–6%, buffered with monobasic and dibasic sodium phosphate) have proven to be an acceptable fixative for rodent globes (24-h immersion) and nonrodent globes (injection or window techniques followed by 48-h immersion). After initial fixation, globes are then stored in 10% neutral buffered formalin (NBF) [28, 29]. Glutaraldehyde is often combined with 10% NBF for light microscopy and is combined with paraformaldehyde for transmission electron microscopy [30, 31]. Generally, advantages of glutaraldehyde fixation of globes include (1) no vacuolation of the corneal epithelium and endothelium, (2) visible outlines of lenticular fibers, and (3) visible outlines of photoreceptor outer segments [28]. Possible artifacts of glutaraldehyde fixation include (1) a few spaces in the corneal stroma, (2) lenticular cracks, (3) distorted shape of cornea and lens of rodents due to altered tissue osmolarity, (4) cellular vacuolation in the inner nuclear layer, and (5) vacuolation in the inner and outer segments [28].

Other fixatives that are commonly used (i.e., Davidson's, modified Davidson's, Bouin's, and Zenker's solutions) contain glacial acetic acid and appear to penetrate relatively quickly for good fixation, especially the retina [1, 25, 32]. Glacial acetic acid provides good preservation of nuclei and helps prevent hardening of tissues (especially the lens) but causes cells to swell which may result in artifacts. Davidson's or a modified Davidson's solution contains a combination of buffered formalin, ethanol, glacial acetic acid, and distilled water. These fixatives are frequently used for fixation of rodent globes [33, 34]. Fixation times vary depending on the size of the globe and include 6–24 h for rodent globes and 24–48 h for rabbit, monkey, or dog. Prolonged exposure to glacial acetic acid should be avoided because of artifacts. After initial fixation, the globes should be rinsed and placed in 10% NBF for at least 24 h before trimming. The main advantage of these fixatives is the general good fixation of rodent globes and retinas of all species. In addition, tissues fixed in Davidson's fixative may also be used for immunohistochemistry. The main disadvantages of Davidson's solution include an opaque gross appearance of the globe and the occurrence of artifacts after prolonged fixation which include (1) corneal epithelial vacuolation, (2) clefts in the corneal stroma, (3) corneal endothelial cell vacuolation, (4) shattering of the lens, (5) liquefaction and globule formation in the lens of monkeys resembling cataract, (6) lens swelling which may result in rupture of the lens capsule in rodents, and (7) indistinct appearance of rods and cones. Tissues fixed with Davidson's are not suitable for electron microscopy.

Bouin's solution and Zenker's solution are fixatives that have been widely used in the past for fixation of the retina but have been largely replaced by other fixatives because of disposal issues [25–27]. Bouin's solution contains picric acid and is also potentially explosive in the dried state. Zenker's solution, as well as some other fixatives, contains mercuric chloride [22, 25, 26, 28, 35].

Regardless of the type of fixative used, the ratio of the volume of the globe to the fixative should be at least one part globe to at least ten parts fixative. Gauze may be placed on top of the globe to ensure it stays submerged, and wide-mouth containers should be used. The container should be at least a couple of centimeters wider than the globe to allow for complete exposure of the globe to the fixative.

As mentioned, immersion fixation of nonrodent globes with glutaraldehyde needs to be enhanced by increasing the exposure of internal ocular structures,

especially the retina. This may be accomplished by injecting fixative into the vitreous chamber or creating a small window in the globe after some initial fixation. Intravitreal injection of a fixative is accomplished by the insertion of a small (25–27 ga) needle into the vitreous chamber through the sclera at a point just posterior to equator (thickest part of globe and parallel to the limbus). The needle should be directed posteriorly to avoid contacting the lens, and the injection should not be in the desired plane of section for microscopic examination. For most species, the needle should be inserted (with syringe attached) along the nasal or temporal aspect of the plane of the long posterior ciliary artery. For nonhuman primates, the point of insertion of the needle is 90° superior or inferior to the long posterior ciliary artery. The fixative should be slowly injected into the vitreous body until the globe feels turgid (volumes of 0.15–0.3 ml are common). If done correctly, compression artifacts are usually not observed. After injecting the fixative, the globe should be submerged in the same fixative.

A globe should not be incised prior to fixation because it causes the globe to be distorted, but a small (~5 mm) window may be created in a globe that has undergone immersion fixation for 5–30 min without distortion. As with the injection technique, the window should not be located in the desired plane of section. To make a window, the globe should be positioned with the cornea down, and the position of the long posterior ciliary artery should be noted. A cut with a sharp tissue slicer blade through the sclera is made to create a small (~5 mm diameter) window along a peripheral parasagittal plane. This window will usually be at the nasal or temporal position for nonprimates and a superior or inferior position for primates.

After initial fixation, the globe may be transferred into 10% NBF to ensure that it will be firm for trimming. At the time of trimming, the globe may be examined for any abnormalities or for the location of medical devices [36]. Findings observed should be recorded along with any other comments pertaining to the preparation of the ocular tissue. The grossing process may be enhanced by transillumination.

Trimming begins by being aware of clinical ocular findings. Generally, standard sections of the globe will be adequate for evaluation, but trimming may need to be modified depending on ophthalmic findings or ocular conditions (e.g., injection site or globe with an implanted medical device). The proper standard plane of section should be one that is uniform for all globes of a certain species, unless otherwise specified [18]. For nonprimates, the uniform section should be a vertical midsagittal plane that is through the pupil and includes the optic disc [20]. This will result in a superior portion and an inferior portion. For canine globes, the tapetum lucidum will be in the superior portion, and for globes of rabbits, the inferior aspect of the globe is larger (optic nerve to limbus) than the superior aspect. For primates, the standard ocular section for systemic studies should include the macula. This area contains a central depression, the fovea, but it is generally not necessary for this structure to be present in the histologic section. By trimming along this plane of section, the temporal aspect (optic nerve to limbus) of the primate globe is longer than the nasal aspect. Primate globes may be trimmed vertically in intravitreal studies, but it would be necessary to obtain multiple sections in order to evaluate the macula and the optic disc. For all species, a cross section of retrobulbar optic nerve should be obtained for examination.

Generally, globes are trimmed in a posterior-anterior direction to ensure that the optic nerve will be in the section. When trimming, the globe should be placed on a block of paraffin or other trimming board. The long posterior ciliary artery extending from the optic nerve along a horizontal plane toward the temporal limbus and medial limbus should be located. The blade (i.e., long tissue slicer blade or other very sharp blade, such as a disposable microtome blade) is positioned perpendicular to the posterior ciliary artery for vertical planes of section and parallel for horizontal planes of section. The end of the blade initiates the cut which is smooth, downward, and forward cutting into the globe. A sawing motion should be avoided to avoid artifacts (e.g., lens luxation and retinal detachment). The blade will meet some resistance at the lens, so put hands on each side of the blade and push down through the lens and cornea. The vitreous body should stay as a gel and helps to keep the lens and retina in place. Some histotechnologists advocate the removal of the vitreous to avoid retinal detachment, especially for primate eyes, but this is not necessary and will make the vitreous unavailable for examination. The trimmed globe should be put into a megacassette because standard cassettes are too thin except for rodent globes. Trimming globes thinly in order to fit into a standard cassette results in retinal detachment and other artifacts. A window should be created in the upper domed portion of the globe in the cassette to prevent the formation of bubbles during embedding. The window should not be any larger than necessary to avoid hitting the lens, if possible, but large enough so the trimmed globe will not project above the edges of the megacassette. For trimming a globe that has a window created at the time of fixation, the window can be covered with a finger to “seal” it. Since a window already exists in the globe, additional trimming may not be needed.

An alternative method for trimming globes of animals is one that is similar to a method used for human globes [21, 37]. This method avoids hitting the lens but requires a lot more facing of the paraffin block and is generally not used for safety studies.

Globes of rodents need minor or no trimming. For globes of rats, a parasagittal cut is made through the globe removing a small (1–2 mm thick) calotte. This will leave the optic nerve, lens, and most of the cornea in the larger section. The globes of mice are small enough that they do not need to be trimmed and can be embedded whole.

The globes of albino rodents are small and diffusely white which may make it difficult to get uniform sections, especially when fixed in certain fixatives (i.e., Davidson’s fixative). Applying a dot of pasty tattoo ink or tissue dye to the superior aspect of the globe at the time of enucleation may be helpful. This mark should be along a superior-inferior midline plane. With a uniform plane of section, measurements of certain ocular structures, such as the outer nuclear layer of the sensory retina (i.e., nuclei of the rods and cones) may be obtained, thus creating a “spider graph” [38].

Generally, globes of animals in toxicity studies are processed along with nonocular tissues, but separate processors with separate processing procedures may be used [18, 21, 32, 37, 39]. To aid in sectioning the lens, cedarwood oil may be used in the processor prior to xylene, and low-melting-point paraffins with plastic polymers may be used for processing and embedding.

Embedding is an important phase in the process that can contribute to artifacts [18]. The window created at fixation or trimming is useful in removing air bubbles and for making sure that the lens is in complete contact with the bottom of the embedding mold. Not having a complete section of lens may be a problem especially for larger globes with relatively large lenses (e.g., dog).

Sectioning of the blocks may be troublesome for the histotechnologist [18, 32, 37]. Techniques may vary depending upon the species of animal, but the main problems consist of not getting good sections of the lens [39]. Removing the lens and embedding it separately should be avoided. Chilling the paraffin blocks gradually from room temperature to freezer temperature helps to avoid cracking and crumbling, especially of the lens. Softening of the lens by turning the block face down on gauze located on ice and applying 10% ammonium hydroxide, glycerin, or soap to the block may help improve section quality [39–41]. Another troublesome issue is getting sections of optic disc or optic nerve of albino rodents. For these animals, a dye or tattoo ink may be applied to the optic nerve at the time of enucleation, and candling the block to observe the location of the optic nerve may be another option.

After the sections are obtained from the block, ribbons are placed on a water bath. The water bath should be cleaned of tissue debris between ribbons to avoid extraneous tissue from getting into ocular sections. Generally, low-temperature paraffin is used, so the temperature of the water bath does not need to be excessively hot. Heat causes the globe to expand, but overexpansion causes the tissue not to adhere to the glass slides (e.g., glaucomatous globes) and causes artifacts (e.g., spaces within ocular tissues). The temperature of the water bath is generally 2° above the melting point of the paraffin. To help in the adherence of the ocular tissue to the glass slide, poly-L-lysine, extra gelatin, or other material may be placed in the water bath [37]. Some histotechnologists use two water baths. One is at room temperature for initial contact of the ribbon with the water to remove wrinkles and the second at a higher temperature to allow for expansion. After the sections are adhered to the glass slides, they are slowly dried in a horizontal position in a warm (60°) oven overnight. Generally, for most toxicity studies, the ocular sections are stained with hematoxylin and eosin, but specific ocular structures may be enhanced with special stains or immunohistochemistry [18, 20]. For example, periodic acid-Schiff stain is used to stain basement membranes (e.g., Descemet's membrane, lenticular capsule, basal lamina of ciliary epithelium) and the mucin in conjunctival goblet cells.

5.3 Descriptive Terminology

Good quality ocular sections should help in the identification of ocular changes. Terms used to describe gross and microscopic ocular changes should be specific as to the location within the eye and specific as to the type of ocular change. By knowing the plane of section, terms, such as anterior, posterior, superior, inferior, temporal, nasal, inner, outer, central, and peripheral, may be used along with the specific structure of the eye that has a finding. The type of ocular finding should also be as

specific as possible. For example, a gross loss of transparency of the lens should be referred to as a lenticular opacity, since the finding may be reversible (i.e., cold cataract) or irreversible (i.e., cataract) [42–44]. Microscopically, features, such as liquefaction and globule formation in the lenticular cortex, are considered to represent lenticular cortical degeneration, and the combination of clinical and microscopic findings indicates that the lenticular change is a permanent change (i.e., cataract). In addition, since the retina is composed of many different types of cells, the use of retinal degeneration may be too vague. For one study, retinal degeneration might represent loss of ganglion cells, and in another study, retinal degeneration might represent changes associated with photoreceptors. Use of precise diagnostic terms for ocular findings helps to eliminate confusion.

5.4 Extraocular Tissues (Ocular Adnexa)

The extraocular tissues include the eyelids and the contents of the orbit. The orbit is a bony fossa that contains the globe, optic nerve, extraocular muscles, orbital fascia, adipose tissue, various types of glands, and the third eyelid, in some species [2–4, 7, 32, 45].

5.4.1 Eyelids

Each eyelid is composed of an outer cutaneous surface and an inner surface lined by palpebral conjunctiva. Mucin from goblet cells in the conjunctiva forms the inner layer of the tear film. At the palpebral margin are the sebaceous meibomian glands. Secretions of the meibomian glands form the outer layer of the tear film.

Eyelid alterations may be spontaneous or due to toxicity. Spontaneous alterations may be congenital, inflammatory, hyperplastic, or neoplastic. For example, entropion (i.e., inward folding of the eyelids) can occur as congenital defects in rabbits and as a sequel to inflammation in any animal. Entropion can damage the conjunctiva and cornea with affected rabbits exhibiting blepharospasm, conjunctivitis, epiphora, and corneal ulceration. Another example of a spontaneous finding is the incomplete formation of the palpebral fissure described in 4–5-week-old Swiss mice Crl:CD1(ICR)BR [46].

Inflammation of the eyelid may involve several structures (e.g., blepharitis in Göttingen minipig) or just specific structures, such as the meibomian gland (i.e., meibomian adenitis) [47]. Inflammation of the meibomian glands includes the presence of lymphocytes, neutrophils, and macrophages and may result in glandular dysfunction (i.e., decreased secretion). Meibomian gland dysfunction can lead to a decreased tear film and keratoconjunctivitis sicca (KCS) (i.e., dry eye) [48]. Similar effects may be expected in humans. Inflammation of the eyelids also includes spontaneous, nonspecific dermal mononuclear cell infiltrates (Fig. 5.1).

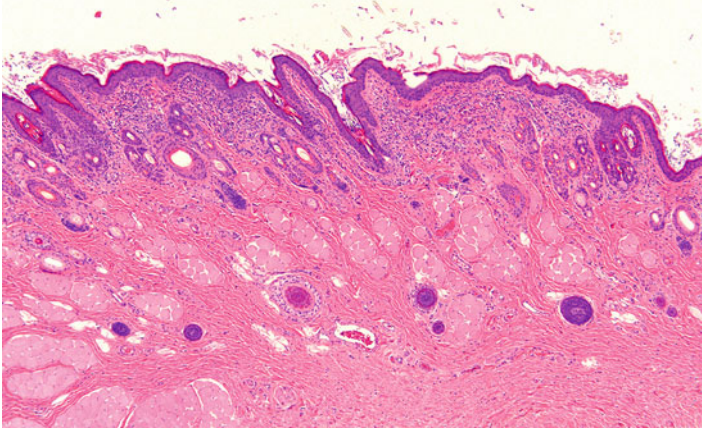


Fig. 5.1 The upper eyelid from a control rabbit has diffuse infiltrates of lymphocytes and plasma cells in the dermis as a spontaneous change. H&E. 5× objective

Neoplasms may arise from any of the structures in the eyelid, including the skin. Neoplasms reported in rats include squamous papilloma, squamous cell carcinoma, schwannoma, melanoma, granular cell tumor, basal cell tumor, sebaceous adenoma, malignant fibrous histiocytoma, and sarcoma [49].

Several drugs and chemicals can cause alterations involving the eyelids [50]. Edema of the eyelid can occur from systemic administration of iminodipropionitrile to monkeys.

Polychlorinated biphenyl (PCB) poisoning produces a chloracne condition in humans and affects sebaceous glands including the meibomian gland [51]. In monkeys, PCBs and similar compounds cause swelling of eyelids with meibomian gland hypersecretion and abnormal pigmentation of the conjunctiva. Microscopically, meibomian glands often contain keratin cysts with atrophy of the glands, increased numbers of layers of epithelial cells in the ducts, dilated ducts, and increased mitotic figures in basal cells [52–56].

Chronic application of topical epinephrine [57] to rabbit eyes results in a syndrome that has been called meibomian gland dysfunction. Features include plugging of the orifice of glands, microcysts, and opacification and enlargement of the gland. Ducts have increased stratification and keratinization, while the lumen is dilated with retention of desquamated epithelium.

Retinoids have been recognized to have effects on the meibomian gland. Isotretinoin (13-cis-retinoic acid), a therapy for acne vulgaris and keratinizing dermatoses, has been associated with side effects of blepharoconjunctivitis in 20–45% of human patients [58]. Systemic treatment of adult New Zealand white rabbits produces mild conjunctival erythema and crusting of the eyelid margins [58, 59]. These correlate microscopically with thickened meibomian gland ducts and ductal epithelium. The amount of acinar tissue is decreased due to degeneration and necrosis of acinar cells and accompanied by periacinar fibrosis. Additional changes

include accentuation of the basal cells and decreases in basaloid cells lining acini with a lack of inflammation [58, 59].

Toxaphene administered orally to cynomolgus monkeys has been reported to produce local effects in the meibomian gland. Affected monkeys had inflammation, enlargement, or both, of the meibomian gland due to impacted diverticula in both the upper and lower lids causing accumulations of glandular secretions [60].

Systemic administration of small molecule inhibitors of epidermal growth factor receptor (EGFR) may produce granulomatous inflammation of the meibomian gland. This is suspected to be a pharmacologic effect due to a failure to secrete glandular content and continued production leading to subsequent glandular rupture. Release of glandular lipids into the surrounding tissue causes a granulomatous response.

Prostaglandin analogs (latanoprost, travoprost, and bimatoprost) are topically applied drugs that decrease intraocular pressure. In addition, there is lengthening of eyelashes (hypertrichosis) [61–64].

5.4.2 *Extraocular Muscles*

The extraocular muscles consist of six muscles (four rectus muscles and two oblique muscles) and, in species such as the dog and rabbit, the retractor bulbi [4, 7, 65]. The dorsal, ventral, and medial rectus muscles and the ventral oblique muscle are innervated by the oculomotor (III) nerve. The lateral rectus and retractor bulbi muscles are innervated by the abducens (VI) nerve. The dorsal oblique muscle is innervated by the trochlear (IV) nerve.

Extraocular muscles may be affected by light exposure and retrobulbar injections [66]. After 24 h of light exposure, extraocular muscles of rats were infiltrated with numerous neutrophils and mononuclear cells with myofiber degeneration. With time, neutrophilic infiltrates decreased and mononuclear cells persisted. Myoblasts formed to replace fragmented myofibers. Extraocular muscles may develop areas of inflammation (e.g., granulomas) associated with periorbital or retrobulbar injections and should be examined following these injections (Fig. 5.2).

5.4.3 *Orbital Glands*

Except for the rodent's Harderian gland, most of the glands of the lacrimal system are not examined in routine toxicology studies but will often be examined in ocular toxicology studies. Since lacrimal glands and lacrimal structures may vary among different species, such as some species having the gland of the third eyelid and dogs having orbital glands that are not lacrimal glands (i.e., zygomatic salivary gland in the dog), it is important to be aware of these differences so that personnel involved in the collection of lacrimal structures can locate the intended structures [2–4, 7, 67–71].

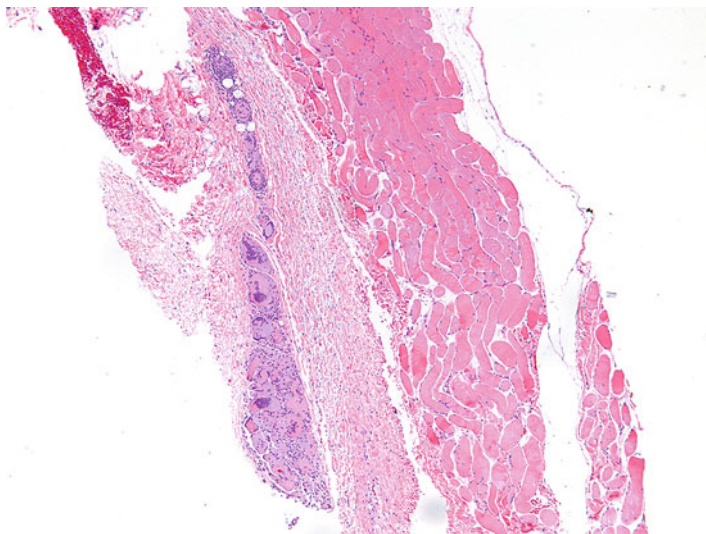


Fig. 5.2 Granuloma adjacent to an extraocular muscle in a rabbit given an injection into the periorbital soft tissues. Granuloma consists of numerous large, foamy, and eosinophilic macrophages, some of which are multinucleate. H&E. 5× objective

Rodents have intraorbital and extraorbital lacrimal glands and a harderian gland [7, 68]. Cytomegaly and karyomegaly, along with nuclear pseudoinclusions, are features identified in the glands with males having a greater degree of these features than females. These differences may be explained by differences in gene expression in males versus females that may be associated with sex steroids [72].

Harderian glands are tubuloalveolar, merocrine glands without an intraglandular duct system [69, 70]. Harderian glands are usually larger in females than males and lymphoid cells may be present. The lipid-containing secretion contains porphyrins, mainly protoporphyrin IX, which may be a potential photosensitizer when activated by ultraviolet and blue components of daylight. The lumina may contain brown accretions which accumulate with age and may be associated with atrophy, granulomatous inflammation, and sclerosis. The amount of porphyrin in the gland is affected by castration, administration of androgens or estrogens, and nutritional deficiencies of riboflavin or vitamin A [69, 73, 74].

In the rabbit, the Harder's gland may be referred to as a harderian gland but is different in gross and microscopic appearance than the harderian gland of rodents and does not produce porphyrins. The Harder's gland is grossly composed of a white lobe and a pink lobe. The white lobe has smaller lumina and the cytoplasm contains larger lipid droplets. The pink lobe has larger lumina and stains more intensely with hematoxylin and eosin stain (Fig. 5.3). Small foci of lymphocytes are found sporadically in the lacrimal and Harder's glands in rabbits [68].

The main effect resulting from alterations in lacrimal glands is increased secretion (i.e., dacryorrhea) or decreased secretion leading to KCS. The morphologic

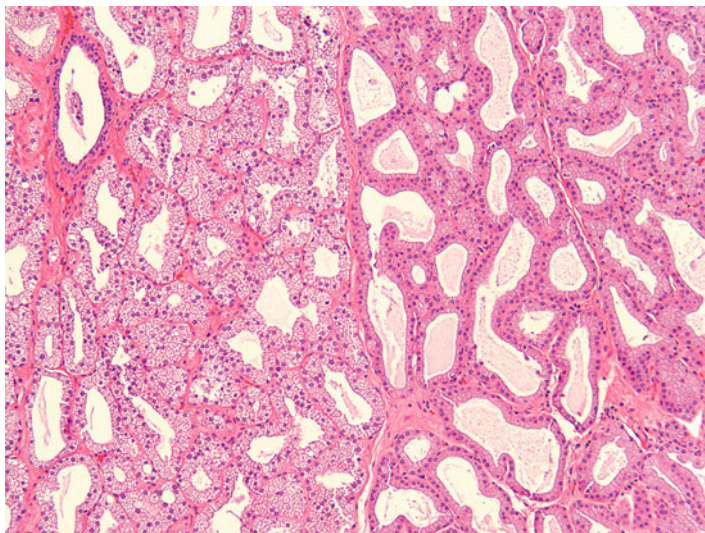


Fig. 5.3 Normal rabbit Harder's gland. The adjacent pink (left) and white (right) lobes are readily distinguishable based on morphology. H&E. 10× objective

changes that may be observed in lacrimal glands following injury are relatively limited. These include degeneration, necrosis (either oncotic or apoptotic), hypertrophy, atrophy, inflammation, and pigment accumulations. Focal lacrimal glandular hyperplasia, diffuse hyperplasia, or squamous metaplasia of ductal epithelium in rats may occur as a regenerative response to glandular damage [75]. Squamous metaplasia may be observed infrequently in the nictitating gland in dogs (Fig. 5.4).

Harderian gland alteration (i.e., metaplasia), or harderianization, of the lacrimal gland is characterized as normal-appearing harderian acini in an otherwise normal lacrimal gland. Harderianization occurs as early as 3 weeks and increases with age and in the glands of both sexes, but males tend to have a greater incidence and extent of the change than females. The relative occurrence has been shown to be decreased with castration [76, 77]. Lacrimal gland alteration also occurs in rabbits and is characterized as normal lacrimal gland acini in the Harder's gland (Fig. 5.5).

Alterations of the lacrimal gland include minimal lymphoplasmacytic cell infiltration, especially in the rabbit, and focal glandular hyperplasia and squamous hyperplasia of ductal epithelium in rats [75, 76]. Hyperplasia generally occurs as a regenerative response to degeneration or inflammation [75]. Experimentally, diffuse acinar hyperplasia occurs in rats infused with recombinant human growth factor and is characterized by an increased number of cells per acinus, cell hypertrophy, anisokaryosis, accumulation of cell debris, and brown pigmentation [78].

Hyperplasia of the lacrimal gland may occur in aged rodents and appears to be more common in mice than aged rats or hamsters [49, 75, 79–81]. Hyperplasia of the lacrimal glands may be associated with degeneration and inflammation with squamous metaplasia of ducts [75].

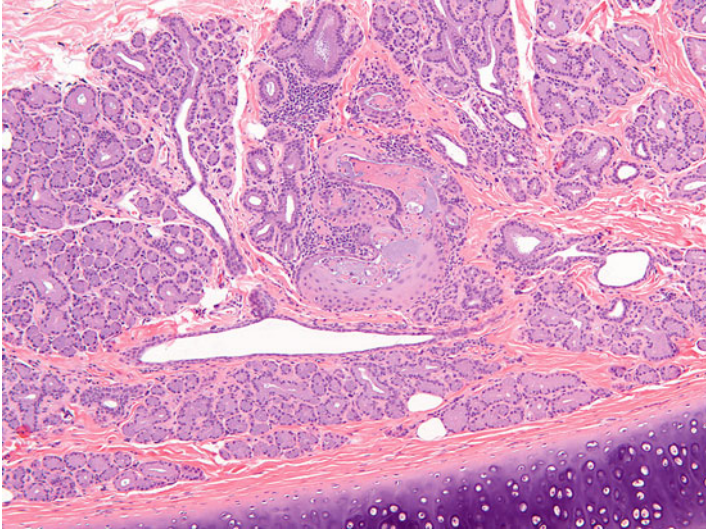


Fig. 5.4 Gland of the third eyelid from a control dog. The gland has focal squamous metaplasia. H&E. 10x objective

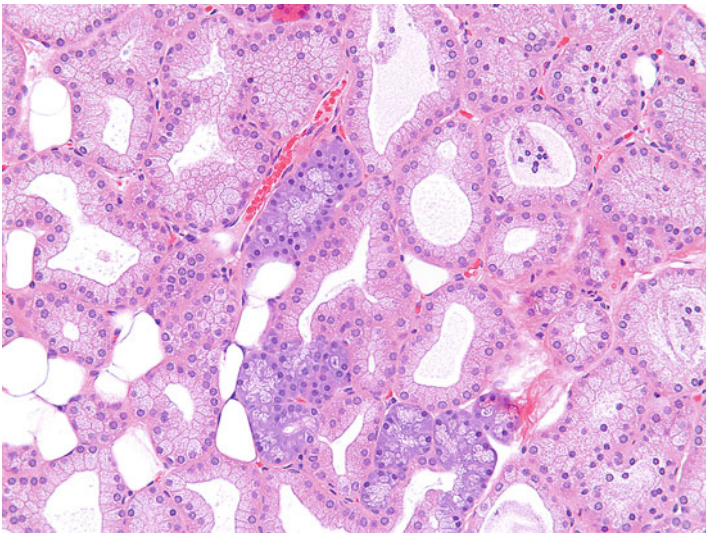


Fig. 5.5 Harder's gland from a rabbit. Lacrimal gland alteration consisting of a cluster of basophilic acini morphologically similar to lacrimal gland acini located within the pink lobe of the Harder's gland. H&E. 20x objective

In contrast to other periorbital tissues, lacrimal glands are sensitive to radiation injury. Radiation injury of ocular adnexa initially manifests acutely within 48 h of irradiation of the lacrimal glands. Degeneration and apoptosis or necrosis of the acinar cells occurs as a dose-dependent phenomenon. Ionizing radiation that exceeds

35Gy fractionated at 1.8–2.0 Gy (180–200 rad) per fraction increases the risk of lacrimal damage [82]. The ductular epithelium is also susceptible, but to a lesser degree than the acinar epithelium. Degenerating cells may have enlarged nuclei. Necrosis leads to a neutrophilic inflammatory response, and with time, there are decreased numbers of serous acini and atrophy of remaining serous acini. Periocular tissues will likely be edematous and diffusely infiltrated with neutrophils. However, this periocular tissue reaction may be due to vascular endothelial injury and not to glandular injury per se, as blood vessels are dilated and have hypertrophic endothelium [83, 84].

Drugs may affect lacrimal glands by decreasing lacrimal secretion resulting in KCS, but species susceptibility may vary [85]. For example, practolol, a β -adrenergic receptor blocker, induces adverse ocular effects in humans, but not in animal models [86].

Lacrimal glands of dogs are affected by treatment with sulfonamide and 5-aminosalicylic acid [85, 87]. Sulfonamides have been reported to produce decreased tear production and subsequent KCS in dogs. The glands have chronic inflammation with atrophy and replacement by fibrous connective tissue, plasma cells, and lymphocytes. Atrophy of the lacrimal glands may occur in dogs following administration of 5-aminosalicylic acid for 1 year [88]. Atrophy and lymphoid cell infiltration occurs in the lacrimal glands, the glands of the nictitating membrane, and the parotid salivary glands. These dogs develop KCS with flattening and desquamation of superficial corneal epithelial cells, stunting and loss of cell surface microvilli, decreased density of cell cytoplasm, and disruption of anterior cell membranes. Corneal changes include inflammation, vascularization, and proliferation of fibroblasts. However, KCS does not appear to have been reported in human patients chronically treated with 5-aminosalicylic acid.

Inflammatory reactions in lacrimal glands can also be stimulated by various cytokines. These experiments have largely been for the purpose of developing models of autoimmune dacryoadenitis. Interleukin-1 injected into the lacrimal gland inhibits neural- and agonist-induced protein secretion with decreased tear output [89]. Associated with this is a severe inflammatory response that is reversible within 7–13 days after injection. The inflammation leads to destruction of lacrimal gland acinar epithelium. During resolution, there is increased proliferation of acinar and ductal epithelium with ultimate recovery to normal tear production. Interleukin-12 and interleukin-18 will also result in injury to the lacrimal gland, but without infiltrates of inflammatory cells [90]. Injection of these cytokines together via the intraperitoneal route results in apoptosis of serous acinar cells. Administration of either cytokine alone had no effects on these glands.

Another change in lacrimal glands is discoloration due to an accumulation of pigments. 7-Acetyl-1,1,3,4,4,6-hexamethyl-1,2,3,4-tetrahydronaphthalene (AHTN) is a fragrance material in consumer products that resulted in a green discoloration of lacrimal gland in female rats, but not male rats [91]. Discoloration was also noted in the liver and lymph nodes with reversal of the discoloration occurring in the liver, but not lacrimal gland. No microscopic correlate to the green discoloration of the lacrimal gland was observed.

Practolol administration to dogs results in a macroscopic dark brown to black discoloration of the lacrimal glands [92]. Microscopically, fine, dark brown pigment granules are present in the apical or supranuclear cytoplasm of the serous acinar lacrimal epithelial cells. Ultrastructurally, these correspond to membrane-bound dense bodies. In another study, practolol administration to dogs resulted in decreased tear flow and lymphocytic infiltrates into the lacrimal gland, but changes did not occur when a related compound (carteolol) was administered [85]. Phenazopyridine accumulates selectively in the lacrimal glands, nictitating glands, and glands of Moll, resulting in pigmentation [93]. Clinical effects include blepharospasm, photophobia, purulent conjunctivitis, and corneal ulceration, presumably from decreased tear production. Grossly, within 48 h of oral administration, phenazopyridine causes dark brown to black pigmentation of the lacrimal gland and gland of the third eyelid. Microscopically, brown to black pigment is visible in glandular acini within 48 h and accumulated with time. Neutrophilic infiltrates occur within 3–6 days of administration, and ultrastructurally, immature secretory granules containing phenazopyridine occur within 24 h as an osmiophilic material interspersed with normal granule constituents. With time, granules in acinar cells become pleomorphic or fuse.

Botulinum toxin B, a treatment for hypersecretion of lacrimal glands, blocks muscarinic receptors and when injected directly into the lacrimal gland suppresses lacrimation for 4–5 months in human patients. In mice, a similar physiologic effect can be produced, resulting in KCS, but without histologic changes in lacrimal glands [94, 95]. Similarly, administration of a muscarinic receptor agonist in rats results in corneal opacity with neovascularization [96]. Both lacrimal glands and harderian glands undergo hypertrophy which is suspected to be an adaptive response to the blockade. Diminution of lacrimal secretions is also observed with administration of other antispasmodic agents [97].

Common spontaneous microscopic findings of the Harder's gland in rabbits include variability in the size of the lumina with scattered aggregates of dilated acini, minimal lymphoplasmacytic cell infiltrates, and focal areas of atrophy. Spontaneous findings involving the rodent harderian gland are common and include degeneration, especially in older animals, which may be characterized by atrophy of glandular acini, mineralization, fibrosis, and cyst formation. Additional spontaneous findings in harderian glands include inflammatory cell (neutrophils, lymphocytes, plasma cells) infiltrates, inflammation (dacryoadenitis), and excessive secretion of porphyrin (chromodacryorrhea).

Chromodacryorrhea may be caused by stress, necrosis or inflammation of the harderian gland, or administration of cholinergic drugs [98, 99]. Inflammation and necrosis may be caused by a viral disease (i.e., sialodacryoadenitis virus [SDV]) that occurs in young rats and mice [100]. The infection involves salivary glands, lacrimal glands, and harderian glands. The necrosis and edema of the harderian gland results in orbital swelling and proptosis of the globe which leads to corneal ulceration and keratitis. Other causes of necrosis, edema, and inflammation of the harderian gland include retro-orbital trauma from venipuncture, exposure to certain drugs (e.g., 4-chloronitrobenzene in rats), and exposure of albino rats to high-intensity light for 12–24 h (Fig. 5.6) [101–104]. Exposure of albino mice to constant light

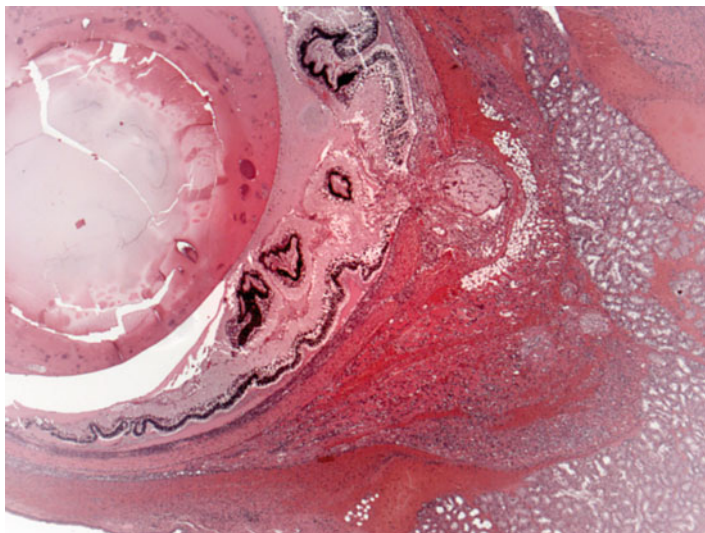


Fig. 5.6 Globe and adjacent tissues from a rat with iatrogenic trauma from retro-orbital blood collection. Multiple changes include necrosis, hemorrhage, and inflammation of periorbital tissues and intraocular exudation with serous retinal detachment. H&E. 2.5× objective

for as little as 24 h results in exophthalmos. Microscopically, the harderian gland has swollen secretory cells with an obliteration of glandular lumina. With time, glandular lumina contain lipid and cellular debris, and lining cells vary in appearance from columnar to squamous. Mitotic figures, leukocytes, and macrophages are present, along with necrosis of glandular cells and edema [102]. With cessation of the exposure, harderian gland changes regress within about a week.

Inflammation of the harderian gland may also occur following exposure to exogenous chemicals.

Several agents, such as albuterol, have been shown to produce enlargement of the harderian gland [105]. Chronic aflatoxin administration to the Syrian hamster will result in hyperplasia and epithelial atypia of the harderian gland [106]. With time, some of these changes progress to papillary cystadenomas and solid adenomas. Recombinant human epidermal growth factor administered systemically has resulted in changes in the harderian gland of rats that include an increased numbers of epithelial cells per acinus, increased cell size, accumulation of cell debris in acinar lumina, and occasional areas of degenerating cells with pyknotic nuclei [78].

Atropine sulfate, a mydriatic often used in nonrodent species during ophthalmic examinations, causes a suppression of expulsion of secretory material [107]. Changes include dilation of acinar lumina and accumulations of brownish pigment. The increased brown pigment correlated with increased levels of porphyrin pigments in these glands. Glandular epithelial degeneration occurred in some animals which may have been associated with the prolonged accumulation of the porphyrin. The degeneration was characterized by thinning of the epithelium with formation of larger cytoplasmic vacuoles.

Many different agents and conditions cause effects in the harderian gland. Administration of the neuroleptic timipirone causes increases in the number of accretions of porphyrin in mice [108]. In rats, accumulation of porphyrin occurs with dietary pantothenic acid deficiency and results in hypertrophy of the harderian gland [109]. Atrophy of the harderian gland occurs following exposure to xenobiotics, and administration of retinoids causes a decrease in the weights of harderian glands due to a decrease in acini and small nuclei, indicating inactivity [110].

Since the harderian gland develops to a significant degree after birth, prenatal exposure to an agent (e.g., the herbicide 2,4-dichlorophenyl-p-nitrophenyl ether) may result in degeneration after birth [111].

Spontaneous hyperplasia of the harderian gland may occur in aged rodents and appears to be more common in mice than aged rats or hamsters [49, 75, 79–81]. At times, hyperplasia of the harderian gland of the rat (i.e., Fischer 344) may be associated with degeneration, inflammation, and ductular squamous metaplasia [75].

5.4.4 Nictitating Membrane

The third eyelid (i.e., nictitating membrane, membrane nictitans) is a fold of conjunctiva that contains a cartilaginous plate surrounded ventromedially by a lacrimal gland (i.e., gland of the third eyelid, nictitans gland) which contributes to the production of tears [4, 112]. The inner conjunctival covering (i.e., bulbar conjunctiva) of the third eyelid contains numerous lymphoid nodules which can undergo lymphoid hyperplasia. The third eyelid is present in many laboratory animals (e.g., rabbits, dogs, minipigs) but is absent in rodents and primates. Retraction of the globe into the orbit by the retractor bulbi muscle or sinking of the globe into the orbit because of bulbar pain or a small size (e.g., microphthalmia or phthisis bulbi) allows the third eyelid to passively cover the cornea. Large red masses protruding from the third eyelid at the medial canthus may be the result of swelling and protrusion of the nictitating membrane [113, 114].

5.4.5 Lacrimal and Lymphoid Drainage

The products of the lacrimal glands flow over the cornea and are drained away via puncta in the eyelid margins that open into canaliculi and lacrimal sacs. The canaliculi travel a short distance vertically in the lid margin, then horizontally before connecting with the lacrimal sac. The canaliculi are lined by nonkeratinizing, stratified squamous epithelium. The lacrimal sac is located in the lacrimal fossa, a depression in the medial wall of the orbit. The lacrimal sac is lined by stratified columnar epithelium containing goblet cells. From the lacrimal sac, the nasolacrimal duct forms as a downward extension and can be histologically evaluated in appropriate nasal sections. The lymphatic drainage for the lacrimal glands and harderian glands is via periauricular and submandibular nodes in humans. Sampling

of similar nodes in laboratory animal species should be considered when dosing via a topical route.

Treatment-related findings occur in the nasolacrimal duct. Hyperplasia of the lining epithelium of the nasolacrimal duct of rats has been noted following systemic treatment with recombinant human epidermal growth factor (EGF) [78]. Findings include a duct with an increased mucosal thickness, loss of cilia, and occasional pyknotic nuclei. EGF is secreted and cleared by the harderian gland and is eventually drained into the nasolacrimal duct. Interestingly, there was no corneal change, but corneal healing has been noted to be enhanced in cats and rabbits treated with EGF [115, 116].

Inflammation of the nasolacrimal duct is associated with chronic administration of antihistamines to rats and has been associated with the presence of stents [117, 118]. Hydrophilic coatings of the stents appear to decrease foreign body reactions and increase patency. Blockage of the nasolacrimal duct from inflammation or implanting a stent may result in epiphora (i.e., excessive tearing). Administration of docetaxel has been associated with this finding [119]. Cyalume, a chemiluminescent material, has been used to clinically evaluate the nasolacrimal system in human patients and does not injure the nasolacrimal duct but has resulted in findings in other locations [120].

5.4.6 Orbital Fascia and Other Orbital Contents

Orbital fascia consists of periorbita, Tenon's capsule (i.e., fascia bulbi), and fascial sheaths of extraocular muscles [4, 7, 45]. Other structures include the retro-orbital sinus in mice and retro-orbital plexus in rats which are used for venipuncture.

An increase in the size of intraorbital contents results in an anterior protrusion of the globe (i.e., proptosis or exophthalmos). The cause is often the result of inflammation but could potentially be due to orbital neoplasia or the result of toxicity. In animals, orbital edema may be due to systemic administration of p-phenylenediamine and exophthalmos may be due to systemic administration of acetonitrile, aminocaproic acid, organic cyanides, or vitamin A [50].

5.4.7 Neoplasia of Lacrimal and Harderian Glands

Neoplasia of the harderian gland and lacrimal gland may occur in aged rodents and appears to be more common in mice than rats or hamsters [49, 75, 79–81]. Most tumors in rats are adenomas, with papillary, or cystic acinar differentiation, but orbital schwannoma has been reported [76]. The incidence depends on strain (e.g., Fischer 344, Osborne-Mendel and Wistar rats) but may be as much as 0.5–15% [81]. Harderian gland adenomas are frequently well-demarcated masses that compress the adjacent parenchyma, but usually do not have a well-defined capsule. They are

papillary, cystic, or a combination and are composed of pseudoglandular structures and form arborizing and folded fingerlike fronds. Fronds are composed of a delicate fibrovascular core lined by cells that are usually tall columnar with foamy amphiphilic cytoplasm. The cells usually form a single layer, but areas are frequently present that give the appearance of having a basal layer of normal-appearing cells “capped” by smaller cells adjacent to the lumen. Harderian gland adenocarcinomas are usually well differentiated, differing from adenomas by greater atypia, invasion, and metastasis. Undifferentiated adenocarcinomas often contain a single large cytoplasmic vacuole, and mitotic figures are uncommon [121–123]. Harderian gland adenocarcinomas can metastasize to the eye and spread systemically [49, 76, 123]. Harderian gland tumors in mice may be induced by various agents, including ionizing radiation and genotoxic carcinogens [50, 81]. Harderian adenocarcinoma has been induced experimentally in rats by repeated injections with 10% urethane or when fed a low-fat diet containing 0.03% 2-acetylaminofluorene [49].

5.5 Cornea

The cornea is composed of several transparent layers that include (1) the precorneal tear film; (2) an outer, nonpigmented, nonkeratinized, and stratified squamous epithelial layer; (3) the anterior limiting membrane (i.e., Bowman’s layer) in primates; (4) an avascular stromal layer; (5) Descemet’s membrane; and (6) the corneal endothelium [4, 7, 124]. The function of the cornea is to transmit and refract light.

The results of iatrogenic intervention may result in various degrees of corneal opacity and should be distinguished from alterations due to toxicity. Some procedures such as surgery or an injection of a test article may affect all layers of the cornea. It is important to be aware of iatrogenic causes of corneal lesions that may be observed in the course of a toxicology study. Although most pathologists microscopically examine the eye in toxicology studies of systemically administered compounds, there are times when the test article is administered locally to the eye. In these studies, the pathologist needs to be aware of the route of administration and the alterations that may be present due to that route of administration. These effects are most notable when there is a surgical procedure or injection of the test article. Complications, or the lack thereof, should be documented. Corneal alterations that may be observed include an incision site and suture material as well as needle tracks from an injection. If the cornea is incised, complications may include inflammatory reactions to infected incision sites, down growth of corneal epithelium into the incision site, islands of corneal epithelium within the cornea that may become epithelial inclusion cysts (Fig. 5.7), corneal epithelial growth on the endothelial surface of the cornea, loss of corneal endothelium, deposition of foreign material into the eye or incision site or needle track (Fig. 5.8), and entrapment of the iris in the incision site (Fig. 5.9) [20]. For both incisions and needle tracks captured in histologic sections, the corneal stroma may be focally disorganized, which may or may not be sufficient to be observed as corneal opacity on ophthalmic or gross examination.

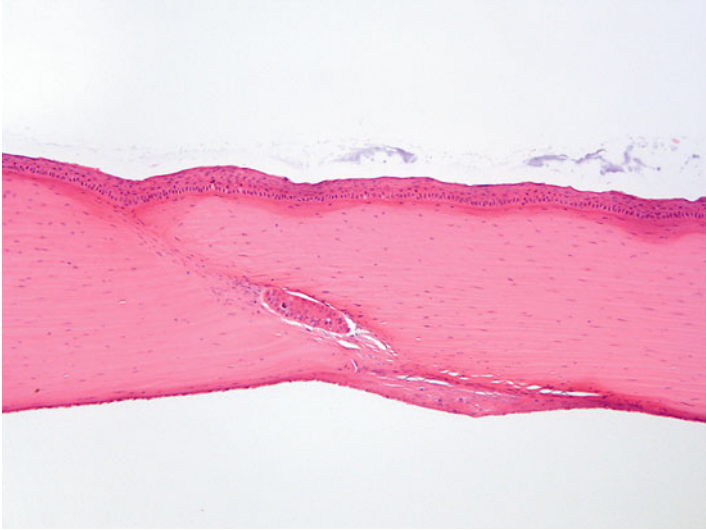


Fig. 5.7 Cornea from a rabbit two weeks following a surgical procedure. The incision site has a nest of corneal epithelium entrapped in the stroma, which, given sufficient time, may develop into a cyst. The endothelial surface has a focal area of retrocorneal membrane development. H&E. 10× objective

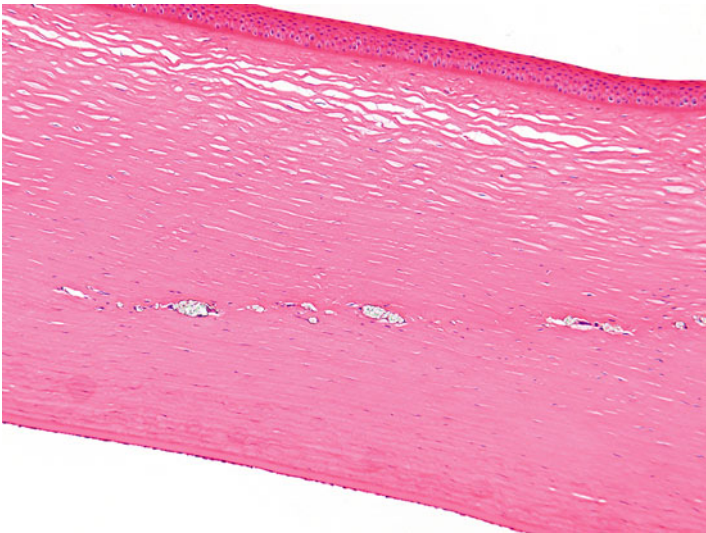


Fig. 5.8 Injection site in the cornea from a dog. There is a linear area of deposition of crystalline material from the injection remaining in the corneal stroma. H&E. 10× objective

In addition to iatrogenic findings, there are various alterations that occur spontaneously or in response to toxicity. Some changes may be localized to specific layers of the cornea, but more often than not, multiple layers of the cornea are affected. Toxic effects of the cornea have a tendency to affect either the outer cornea or the



Fig. 5.9 Iridal entrapment in a rabbit. The iris is entrapped in a healing corneal incision. Note the suture cross sections near the corneal surface. H&E. 5× objective

inner cornea. Toxic effects may be the result of a topical application or may be associated with systemic effects. Systemically administered drugs can also affect the cornea by secretion into the tear film (and therefore irritate the cornea directly), by injury of the lacrimal gland which removes the protective tear film which results in damage, or by inhibiting the protective corneal reflexes through depression of the central nervous system.

5.5.1 Macroscopic Corneal Opacities

Corneal opacities are noted on ophthalmic or macroscopic examination and refer to loss of transparency of the cornea. These are often due to mineralization, especially in rodents. Corneal opacities in rats may be diffuse or punctate and reversible or permanent. Diffuse corneal opacities occur in rats, especially males, and increase in incidence with age [125]. They may be punctate, focal lesions that give the cornea the dimpled gross appearance of an orange peel. Diffuse or focal opacities may be associated with or accompanied by conjunctivitis, keratitis, and corneal ulceration [126]. As such, corneal opacity is a nonspecific term that may correlate with multiple microscopic alterations.

In rats, corneal opacity as a spontaneous change may be unilateral or bilateral and tends to occur in males greater than or equal to 18 weeks of age. They correspond with multiple deposits of fine, white granules on the corneal surface grossly or deposits of basophilic fine granules or basophilic laminated plaques in the corneal basement membrane microscopically [127]. Corneal degeneration with superficial

punctate opacities has been reported in Sprague-Dawley and Wistar rats of various ages and of both sexes [128]. Corneal opacities generally occur with an increased incidence with increased age in Sprague-Dawley rats [126, 127]. Others have reported reflective opacities in rats to be corneal crystalline deposits, with a higher incidence in males, that are usually bilateral, multifocal, and punctate, and usually in nasal locations oriented horizontally along the palpebral fissure [129].

Corneal abnormalities as spontaneous occurrences in mice on ophthalmic or gross examination have been reported in various strains [122, 126, 128, 130, 131]. Diffuse corneal opacities are infrequent in mice but increase in incidence with age and are due to mineralization of the anterior stroma [126]. Hubert reported corneal abnormalities in 4–5-week-old Swiss mice Crl:CD1(ICR)BR [46]. MRL mice with features of hyperparathyroidism have been described with corneal changes [132, 133]. Opacities in mice may be due to infrequent cage cleaning or cage environment, where urease-positive bacteria may increase ambient cage ammonia levels [130]. It has been suggested that some strains of mice may have a genetic predisposition. Therapeutic agents such as azathioprine and meticorten have been described as causing corneal opacities as well. In spontaneous diabetic KK mice, calcium is present as extracellular deposits of fine basophilic granules or as dense strips at the junction between the epithelium and the stroma, with older lesions tending to have neovascularization and minimal cellular infiltrates of neutrophils and mononuclear cells [132, 134].

5.5.2 Superficial Corneal Alterations

Changes in the corneal epithelium to superficial injury or toxicity include edema, erosions or abrasions, and ulcers from necrosis [135]. Grant characterizes the corneal changes from chemical burns from contact with liquids and solids; contact with gases, vapors, and dusts; or changes from systemic substances [50]. Chemical burns may cause immediate caustic injuries. Examples include alkalis and acids which not only affect the epithelium but also the stroma with edema and loss of mucopolysaccharides leading to opacification. The opacification is often accompanied by vascularization. Gases, vapors, and dusts may include a stinging sensation and result in tearing. Most substances that induce lacrimation can injure the cornea if the concentration is high enough. Findings include epithelial edema, vacuolation, delayed healing, or inflammation. Corneal epithelial edema is initially intracellular and appears as perinuclear pallor. With progression, there is pericellular fluid accumulation with the potential for bulla formation. An erosion (i.e., abrasion) is the partial desquamation of corneal epithelium and is usually due to focal mechanical trauma of a foreign body, such as dust particles. Since the defect does not extend past the corneal epithelial basement membrane, it may not be discernible on ophthalmic examination. With extension through the epithelial basement membrane (i.e., ulcer), the stroma will retain fluorescein. Ulceration may occur as a result of an initial abrasion with a bacterial infection. Abrasions are occasionally observed

in the corneal epithelium in large animals [136]. Although in histologic section abrasions appear like small “craters” in the epithelium, they are likely instead linear. Microscopically, abrasions containing crowded cells in the basal layer are indicative of healing. Generally, the corneal epithelium heals quickly [137].

Hypertyrosinemia has been demonstrated to produce corneal opacities in laboratory animals [138–140]. Excessive tyrosine fed in the diet to rats produces initially an edema of the corneal epithelium with subsequent infiltrate of neutrophils into the superficial epithelial layers [139]. This progresses to neutrophilic infiltrates throughout the epithelium and eventually to infiltrates and edema of the corneal stroma. In rabbits, similar changes have been described with hypertyrosinemia with ophthalmic observations of pinpoint opacities and “glittering pre-endothelial structures” on slit lamp [138]. Microscopically, the corneal epithelium had focal proliferations with vacuolation of basal epithelial layers. Scattered epithelial cells underwent necrosis. Hypertyrosinemia induced by 2-(2-nitro-4-trifluoromethylbenzoyl)-cyclohexane-1,3-dione (NTBC), which is a potent inhibitor of 4-hydroxyphenylpyruvate dehydrogenase, produced corneal opacities in dogs, but not rats or rhesus monkeys [140]. All three species had elevations of serum tyrosine and aqueous tyrosine, indicating that there are some species-specific differences that lead to the corneal opacity with hypertyrosinemia.

Keratitis in various animal species is occasionally observed. These have been suspected to be due to environmental irritants such as ammonia and dusts from the bedding and feed, reduced lacrimal secretion, trauma, or exophthalmos [68, 130, 141]. Several strains of mice have had corneal opacities with histologic correlates of chronic inflammation of the corneal epithelium and anterior corneal stroma that included such features as ulcers and erosions, acute keratitis, neovascularization, and mineralization of the basement membrane [130]. These may be considered iatrogenic in the sense that they are an artifact of the test system, although animal colony management should reduce or eliminate these as a common occurrence.

5.5.3 Corneal Irritation or Local Toxicity

Adverse effects of drugs or ocular medical devices (i.e., contact lenses) on the outer cornea can be determined by use of the Draize ocular irritation scoring method and its various modifications [17, 142–146]. Currently, some of the features of a clinical adverse reaction are being predicted by use of *in vitro* or *ex vivo* assays such as the bovine corneal opacity and permeability assay (BCOP) [147, 148]. The BCOP will largely mirror *in vivo* responses, except for the absence of an inflammatory response or neovascularization in these *in vitro* and *ex vivo* assays.

The various responses to irritating substances such as alkalis, acids, and surfactants from direct contact to the cornea have been studied to better understand the pathology as well as to serve as benchmarks in the development of *in vitro* and *ex vivo* substitutes to *in vivo* testing [135, 149–154]. Alkali burns are caused by saponification of cell membranes, allowing greater penetration of the injurious chemical, making

alkali burns usually the most severe injury. Acid burns are caused by coagulation and precipitation of cellular proteins, and the natural buffering of tissues tends to limit the injury of acids as compared to alkalis [151]. Surfactants generally produce a milder injury than acids or alkalis. Surfactants are broadly classified as cationic, anionic, or nonanionic based on their chemical structure, but cationic surfactants tend to produce the greatest injury due to the precipitation of cellular proteins [17]. Anionic surfactants are intermediate and tend to cause cell lysis, while nonionic surfactants do not produce protein precipitation or cell lysis [150]. Regardless of the nature of the chemical, they all can produce erosion, denudation, and necrosis of the corneal epithelium [135]. Greater irritant capacity generally corresponds with greater extent and depth of injury. Mild irritants are therefore confined to the epithelium, while moderate irritants will injure the corneal stroma, and severe irritants will affect the deep stroma and possibly the corneal endothelium. Affected corneal stroma will be edematous and have necrosis and lysis of keratocytes. The corneal endothelium may be lost. With time, the cornea will respond with keratocyte regeneration, neovascularization, conjunctivalization, or epidermalization of the corneal epithelium. The degree of response will reflect the initial depth and area of injury. It should be noted that although the corneal epithelium is first and often most greatly affected, this may not always be the case. For bleaching agents, it was noted that the corneal stromal injury was greater than the corneal epithelial injury [153]. Severe or perforating keratitis may lead to inflammation of the iris (i.e., iritis), anterior uvea (i.e., anterior uveitis), inner aspect of the globe (i.e., endophthalmitis), or the whole globe (i.e., panophthalmitis). With chronic inflammation affecting most or all of the globe, then shrinkage and distortion of the globe (i.e., phthisis bulbi) can occur.

The outer cornea may be injured due to desiccation from an acute or chronic loss of tear film. The tear film may be compromised by a lack of production or a lack of covering of the corneal surface. A lack of production may be due to inflammation of the lacrimal gland or administration of certain pharmacological compounds, including local anesthetics, anticholinergic compounds, or anticholinesterases, which decrease lacrimal secretions. Compounds that affect the lacrimal gland or meibomian glands may result in a minimal, reversible changes in the cornea (e.g., keratinization) or, if more severe, a chronic condition involving the cornea, KCS. Changes in the cornea associated with KCS include keratinization, epidermalization, pigmentation, fibrosis, and neovascularization of the superficial stroma and possibly mononuclear or mixed inflammatory cell infiltration.

Acute corneal desiccation may occur following general anesthesia as an iatrogenic cause of corneal changes [155, 156]. Desiccation in the interpalpebral area leading to keratoconjunctivitis sicca and associated secondary uveitis is reported in rats following general anesthesia with a combination of xylazine and ketamine [157]. Animals undergoing general anesthesia will often have incomplete closure of the eyes (lagophthalmos). Even if the anesthesia is not prolonged, desiccation of the areas of cornea not covered by the eyelids will occur by evaporation following breakup of the precorneal tear film, which can happen in seconds to minutes. In humans, the time required for injury is longer than in rodents, with no changes

reported in human eyes up to approximately 100 min. In addition to lagophthalmos, general anesthesia may also reduce the production and the stability of tears [155]. Microscopically, corneal desiccation may result in changes of degeneration or erosion and thinning and ulceration of the corneal epithelium. Changes generally will be acute to subacute, and the changes of chronic KCS would not be anticipated as iatrogenic changes in laboratory animals. Several authors have described drug-induced corneal opacities related to narcotic analgesics or prolonged anesthesia [157–159]. For example, a single administration of the long-acting narcotic analgesic 1-alpha-acetylmethadol to male Sprague-Dawley rats resulted in localized corneal opacities mainly in central, nasal, or inferior-nasal regions after 3–5 days [159]. Microscopically, these animals had thickened corneal epithelium, loss of cellular polarity, hyalinization of the basement membrane, stromal vascularization, spindle cell proliferation, inflammation, and frank perforation. It was considered likely that this was due to adverse effects on corneal sensory innervation, blinking, or tear formation, instead of direct chemical effect on the corneal epithelium.

Although not due to lagophthalmos and drying, other anesthetic agents have been associated with corneal epithelial changes. These include administration of agents such as cocaine, tetracaine, and proparacaine. Chronic use of these anesthetics may alter the plasma membrane integrity of corneal epithelial cells, cause release of enzymes such as lactate dehydrogenase, and cause decreases in mitochondrial dehydrogenase activity [160]. Corneal opacities have been reported in rats following administration of morphine and narcotic analgesics [159]. Microscopically, there may be thinning of the corneal epithelium, and generally, these are acute or subacute and do not progress to the changes of chronic keratoconjunctivitis sicca.

Chronic desiccation of the cornea leading to KCS may also be the result of anterior displacement of the cornea. This may occur as the result of an enlarged globe (e.g., glaucoma) or from anterior displacement of the entire globe (exophthalmos, proptosis) secondary to orbital swelling. Inflammation of the Harderian gland with chromodacryorrhea from repeated orbital bleeding or from a viral infection (e.g., sialodacryoadenitis) may also be causes [100]. Anterior displacement of the cornea appears to affect males more than females. Treatment with clonidine induces exophthalmos and a reduction in tear flow in mice and rats resulting in flattening and desquamation of corneal epithelium and vacuolation of basal cells. These changes may progress to keratoconjunctivitis and anterior uveitis [141].

In addition to irritants and loss of tear film, corneal epithelial lesions may be produced by drugs that inhibit mitosis and reduce the proliferative capacity of the corneal basal epithelium. A variety of antineoplastic agents are known to affect the cornea, and these often present clinically in patients as punctate keratitis [161]. For example, the antineoplastic drug, capecitabine, is converted to 5-fluorouracil *in vivo* and is concentrated in tears. Clinical signs in dogs include multiple erosions of the cornea with superficial corneal epithelial pigmentation and neovascularization [162]. Microscopically, the corneal epithelial basal cells were disorganized and had an abnormal morphology resulting in a thinned corneal epithelium. Thinning

(i.e., atrophy) of the corneal epithelium with progression to ulceration and inflammation also occurred in dogs given inhibitors of oxidosqualene cyclase [163]. Atrophy has also been described in human patients treated with triparanol, a late stage blocker of cholesterol synthesis [164, 165]. Decreases or alterations in tear production may occur with oxidosqualene inhibitors related to reductions in the lipid-rich glands such as the meibomian glands [166].

Hyperplasia of the corneal epithelium may occur as a nonspecific response to injury such as to topical chemical injury as described above. Conjunctivalization is a metaplastic response where the corneal epithelium transforms into the appearance of conjunctiva, with goblet cell differentiation and irregular thickness. A chronic change observed in the corneal epithelium of mice is goblet cell metaplasia [167]. Hyperplasia has also been observed with systemically administered compounds, a notable example being EGF [168]. High doses of systemically administered recombinant EGF produced diffuse, uniform thickening of the corneal epithelium due to an increased number of layers of corneal epithelial cells overlying basal cells that were hypertrophic and hyperplastic.

Although uncommon, localized corneal proliferation may occur, especially in chronic studies. Corneal hyperplasia may be observed as a focal, diffuse, or nodular thickening of the corneal epithelial layer and is not considered to be preneoplastic [167]. Hyperplasia may be accompanied by keratinization. Corneal proliferation may include squamous cell hyperplasia, epithelial hyperplasia, squamous cell papilloma, and squamous cell carcinoma as chronic changes in rats. Squamous cell carcinoma is not known as a spontaneous finding in mice [169]. The corneal surface epithelium may be focally thickened due to congenital findings such as corneal dermoids. A corneal dermoid is the localized presence of tissue appearing as skin within the cornea. The finding may be unilateral or bilateral and will be discovered on prestudy ophthalmic examinations. These have been described in the rat, hairless and haired guinea pig, rabbit, and dog [170–174].

Squamous cell hyperplasia and acute keratitis have been induced in female HRA/Skh mice treated with 8-methoxypsoralen combined with UV radiation [175].

5.5.4 Superficial Corneal Stromal Alterations

Alterations in Bowman's layer in primates include edema, spheroidal degeneration, or interruptions and may or may not be noted as corneal opacities. Edema of Bowman's layer is usually associated with edema in the overlying epithelium or the underlying stroma and is manifested by decreased eosinophilia of this layer microscopically. Spheroidal degeneration of Bowman's layer is considered collagen deposition and appears as extracellular spherical deposits. This change occurs as a sequela of chronic actinic exposure in humans. Interruptions in Bowman's layer are often traumatic or related to surgery. Since Bowman's layer does not regenerate, these interruptions will be filled in either with overlying corneal epithelium or with fibrous connective tissue from the underlying stroma.

5.5.4.1 Subepithelial Corneal Mineralization

Corneal mineralization can be due to multiple causes. Corneal dystrophy is a term commonly used in veterinary ophthalmic pathology to encompass many of these changes. However, corneal dystrophies are defined as spontaneously occurring, noninflammatory changes bilaterally affecting the central cornea with no associated systemic disease, when narrowly defined by the definitions used in human ophthalmology. Thus, narrowly defined, true corneal dystrophies as a primary disease appear to be rare in animals, while the more nonspecific calcific band keratopathies are relatively common. Calcific band keratopathy occurs in human patients in association with a variety of ocular and systemic diseases including chemical and physical injury, chronic glaucoma, and phthisis bulbi. It may also accompany hyperparathyroidism or vitamin D poisoning [176]. Hypercalcemia produces bilateral findings and may extend to include calcification of the bulbar conjunctiva [177]. In humans, it also usually involves Bowman's layer.

Calcific band keratopathies, which as previously mentioned are also commonly referred to as corneal dystrophies in laboratory animals, are mineralized or calcified deposits presenting microscopically as basophilic granularity along the corneal epithelial basement membrane [178]. The extent and severity of secondary changes varies with animal strain, age, and experimental conditions [125]. The macroscopic lesion is often characterized by a central, bilateral, and elliptical band in the area underlying the palpebral fissure [179]. More advanced findings may consist of epithelial necrosis, foreign body reaction, and scarring. Often, experimental corneal calcification is the result of trauma, which causes edema and proliferation of fibroblasts. These cells synthesize and release glycosaminoglycans into damaged regions, where the calcification develops; the free anionic groups of glycosaminoglycans tend to bind calcium [180].

Drying of the cornea is an important mechanism of mineralization because evaporation of the tear film from the cornea results in supersaturation and precipitation of calcium in the superficial corneal stroma. Band keratopathy may develop due to inability to cover the underlying cornea with the lids, as well as high ammonia levels from urease-positive bacteria in the bedding [130]. In mice, it may be due to harderian gland adenoma leading to proptosis and keratitis.

A true corneal dystrophy has been described in the American Dutch belted rabbit and the New Zealand white rabbit. The American Dutch belted rabbit develops opacities involving the corneal epithelium, basement membrane, and superficial stroma that are noted clinically with the use of a slit lamp. Microscopically, the basement membrane is thickened, and the overlying epithelium is thinned and disorganized. The underlying corneal stroma is also often disorganized [181]. The corneal dystrophy reported in the New Zealand white rabbits is characterized by a normal basement membrane, but the overlying epithelium is irregular with both thickened and thinned areas [182]. Calcification or mineralization of the cornea independent of these corneal dystrophies has been reported in rabbits due to local trauma, hypervitaminosis D, and administration of dihydrotachysterol [158, 183–185]. Corneal injury potentiates the corneal calcification produced by the

hypercalcemia of dihydrotachysterol in rabbits. Calcification also occurs in the rabbit cornea in response to immunogenic uveitis combined with hypercalcemia [186].

Experimental corneal calcification in the rabbit has been produced by mild irritation with carbon dioxide laser [183]. Ultrastructurally, numerous spherules of fine crystals were within the basement membrane of the corneal epithelium. Some calcific spherules were also present in membrane-bound vesicles within the cytoplasm of keratocytes. These deposits stained black with von Kossa silver stain and red with alizarin red S stain, indicating the presence of calcium. Additionally in rabbits, — morphine appears to cause drying of the cornea [158] with development of exophthalmos in treated rabbits.

In rats, corneal mineralization, often referred to as corneal dystrophy, is a condition where calcium and phosphorus is deposited in the superficial cornea in a diffuse or punctate distribution along the palpebral fissure [179]. It is postulated that changes in the corneal microenvironment (e.g., pH or ion concentration) can cause calcium to precipitate [128, 177]. Strains of rats involved include Wistar, Sprague-Dawley, and Fischer 344 [122, 126, 128, 130, 178]. In Sprague-Dawley, Fischer 344, and Wistar rats, mineralization occurs more in males than females [129]. A syndrome called spontaneous corneal dystrophy has been described in Fischer 344 rats that have extracellular electron-dense deposits of calcium and phosphorus in basement membranes of corneal epithelial cells and other tissues (e.g., renal tubular basement) such that the condition is not strictly limited to the cornea and therefore does not fit the strict definition of corneal dystrophy used in human ophthalmology [178, 187]. Band keratopathy can occur in rats due to the increased dietary content of vitamin D₃, local ocular disease, or systemic abnormalities in calcium-phosphate metabolism [131]. Excess vitamin D causes similar findings in the corneas of albino and pigmented guinea pigs. However, the guinea pig cornea appears to be much less susceptible to experimental corneal calcification than the rat or the rabbit.

In the rat, de-epithelialization of the central or entire cornea is effective in inducing corneal calcification. Other treatments in the rat, including isoproterenol, alloxan [188, 189], increased dietary vitamin D₃ [185], subcutaneous administration of morphine sulfate, and suturing the eyelids open, all can be associated with corneal calcification.

Meador et al. described corneal mineralization associated with epicardial mineralization in SCID mice with deposition of mineralized material in the corneal basement membrane or in thin clefts at the epithelial/stromal junction [192]. In more severe instances, deposits were surrounded by macrophages. The corneal epithelium was variably thinned and dystrophic.

5.5.4.2 Corneal Pigmentation

There are many different causes of corneal pigmentation. Brown, hemosiderin-laden macrophages may be present in the anterior chamber and adherent to the endothelium or in the corneal stroma following hemorrhage; yellow particles in the

anterior layers of the cornea have been reported in the human cornea following administration of compounds containing gold [191]; and pigmentation occurs following administration of minocycline, amiodarone, phenothiazines, antimalarials, and salts containing silver [192–194]. Pigmentation may also be a consequence of migration of melanocytes from the conjunctiva associated with neovascularization and reparative responses from previous ulceration.

5.5.4.3 Corneal Stromal Edema

Nonspecific alterations in the stroma include edema and inflammation. Stromal edema is characterized by increased thickness of the stroma due to increased interstitial fluid. Inflammatory cells may infiltrate as part of the edema process. Expansion of the stroma by edema disrupts the regular arrangement of the collagen bundles of the stroma, producing opacity. Proper histologic processing is important to appreciate corneal edema, as artifacts can lead to notable differences in corneal thickness as observed on histologic slides.

5.5.4.4 Corneal Inflammation

Corneal inflammation is almost always accompanied by edema. Inflammation first presents grossly as perilimbal hyperemia. With time, cells migrate into the corneal epithelium and stroma. When inflammation is severe, cells will migrate from the iris into the anterior chamber (hypopyon) and then into the cornea. Nonulcerative inflammation, such as superficial keratopathy, if minor, can heal without any residual opacity. Stromal keratopathy involves the stromal layer and will likely be vascularized. Ulcerative corneal inflammation usually has a bacterial component that follows the initial injury. Sequelae to keratopathy include scars, which microscopically appear as fibrosis and will be clinically opaque. Keratectasia (i.e., ectatic cicatrix), descemetocoele, and adherent leukoma may form. Pterygium is conjunctival growth onto the cornea and should be distinguished from pseudopterygium which is the extension of a conjunctival flap over the cornea. Keratectasia (ectatic cicatrix), descemetocoele, adherent leukoma, and corneal staphyloma are the more serious consequences of ulceration.

Keratitis and sequelae are often related to injury and increase with age, with the rat having a greater incidence of keratitis than the mouse [125, 126]. Keratitis has been associated with SDV and coagulase-positive *Staphylococci* [100, 125, 129]. Corneal scars, with superficial vascularization, may be attributed to prior trauma [129]. Large animals such as the dog and monkey tend to have only infrequent keratitis, and the incidence in the dog has been report to be as low as 0.5%. In dogs, this has been attributed to dust and bedding and may be exacerbated when ocular defense mechanisms are depressed following administration of pharmacological agents.

Keratitis may be a manifestation of photosensitization after exposure to phenothiazine, methoxsalen, or other photosensitizing compounds [17, 50]. Ultraviolet

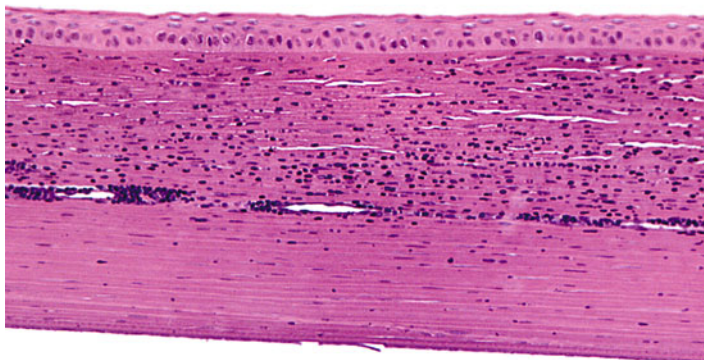


Fig. 5.10 Cornea from a rabbit. The cornea is infiltrate by numerous inflammatory cells, and a relatively large vessel extends laterally through the corneal stroma. H&E. 20× objective

radiation exposure and phototoxicity have been demonstrated to occur in humans and a variety of animal species with the cornea being one site of injury [161]. UV radiation has been associated with marked loss of keratocytes in mice [195]. Phototoxicity following exposure to *Penicillium viridicatum* culture material includes epithelial changes in the cornea, such as ballooning degeneration, proliferation and thickening of the corneal epithelium, and thinning of the corneal stroma [196]. Changes in the corneal stroma include corneal vascularization, fibrosis, and inflammation that may lead to keratoconus and rupture of the globe. The observed thinning of the cornea with UV light and the thickening demonstrated with some photosensitizers suggest that there may be effects related to differences in the physical energy injury.

5.5.4.5 Corneal Neovascularization

Neovascularization is the vascularization of a normally avascular corneal stroma (Fig. 5.10). It is a common response to corneal injury and is often associated with inflammatory mediators [197, 198]. Corneal neovascularization may be observed in nude or hairless mice [167, 199]. Blood vessels interfere with transparency by their physical presence and participate in inflammation. Vascularization of the cornea is a beneficial repair response to inflammation, although, as a sequela, it may produce opacities due to the persistence of nonperfused ghost vessels visible on ophthalmic examination as linear opacities. Vascularization will be confined only to the injured cornea and does not generally involve healthy cornea. Findings often associated

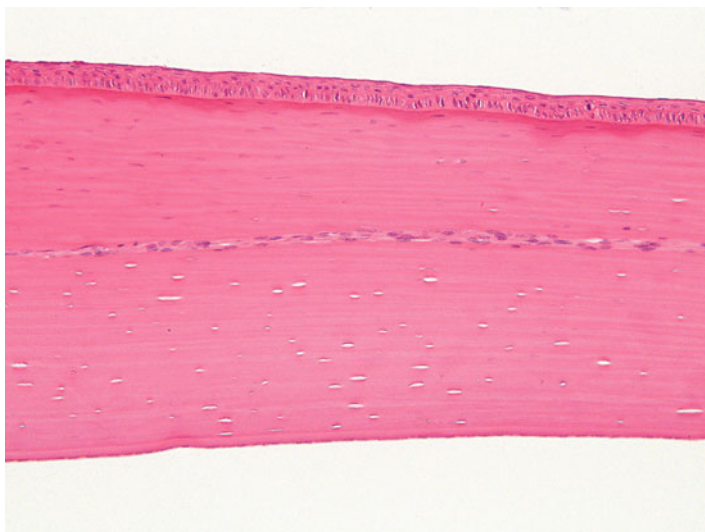


Fig. 5.11 Cornea from a rabbit. A nerve traverses laterally through the corneal stroma and is occasionally observed as a normal structure. H&E. 20× objective

with corneal neovascularization include conjunctival congestion, corneal stromal edema, and inflammation.

Neovascularization has also been associated with deficiencies of tryptophan, riboflavin, vitamin A, and zinc [200, 201]. Some compounds can induce neovascularization, such as EP4-prostaglandin E2 agonists. When this compound was administered topically, corneal neovascularization was induced as if either through a pharmacologic or inflammatory mechanism [202]. The induction of neovascularization may be inhibited by administration of compounds such as anti-vascular endothelial growth factor (VEGF) antibodies [203].

Not all corneal stromal vascularization is neovascularization. Limbal vessels can occasionally extend a short distance into the peripheral cornea. This finding is observed in the corneas of rabbits with no other corneal or limbal changes and is considered to represent normal finding. Careful examination of multiple sections of the eye from control animals can help differentiate normal variability from abnormality. In addition, corneal nerves may occasionally be observed within sections and should not be confused with neovascularization (Fig. 5.11).

5.5.4.6 Lipid Keratopathy and Corneal Phospholipidosis

Corneal lipidosis can be observed on occasion as either a spontaneous or induced change. Lipid deposition in the cornea of rabbits and dogs has been observed in animal colonies. Rabbits with altered lipid metabolism, notably the Watanabe WHHL

rabbit or rabbits on high-fat diets, are susceptible to corneal lipidosis [204–207]. The eyes have grossly visible corneal opacities, initially as clouding of the medial ventral cornea, which will progress to pearly corneal opacities extending to the central and lateral cornea. Microscopically, the anterior corneal stroma has infiltrates of cells with necrosis and cellular infiltrates. Infiltrates consisted of large, pale, and foamy macrophages. Foci of necrosis contained Sudan black-positive materials. Corneal lipidosis may also be drug induced, with birefringent crystals in outer stroma that are visible with polarized light and stain with Sudan black. The guinea pig also may present with lipid deposition as part of a disease process including conjunctivitis, keratitis, and keratoconjunctivitis sicca [208].

In dogs, corneal lipidosis is a rare spontaneous change but when it occurs may present as marginal, zonal, or epithelial forms [209]. In beagle dogs on life span toxicology studies of radionuclides, similar corneal opacities have been observed with microscopic changes of amorphous to crystalline lipid deposits in the anterior cornea [209]. These appeared to be a spontaneous change in aged dogs, as no evidence of a systemic hypercholesterolemia was detected. However, deposits were determined to be neutral fats, phospholipids, and cholesterol [210].

Cationic amphiphilic drugs are recognized to produce phospholipidosis of the cornea. Chloroquine, tamoxifen, and other drugs in humans produce corneal deposits characterized by lipid in lysosomes of the corneal epithelium and keratocytes [161, 211–213]. In humans, the phospholipidosis is reversible and associated with little or no visual impairment [191]. Corneal phospholipidosis is also described in rats and dogs [214–216] and could occur in any species dosed with cationic amphiphilic compounds. Histologically, phospholipidosis in the cornea appears as clear lipidosis-like alterations in the corneal epithelial cells and keratocytes with bluish granules with hematoxylin and eosin staining. Semithin sections demonstrate densely staining toluidine blue positive, irregular cytoplasmic inclusions [215]. Transmission electron microscopy shows the typical lamellar and crystalline-like inclusions. Tilorone, an immunostimulatory agent that causes increased production of interferon, has been shown to produce both phospholipidosis and mucopolysaccharidosis in rats. The phospholipidosis is typical and reversible, while the mucopolysaccharidosis occurs as deposits of glycosaminoglycans in lysosomes of the corneal epithelium and keratocytes which persist for long periods [217, 218].

5.5.5 *Deep Corneal Alterations*

Descemet's membrane undergoes changes secondary to changes in the overlying corneal stroma or underlying corneal endothelium. With expansion of the corneal stroma, such as with edema, Descemet's membrane may develop tears (i.e., stria), and the edges of large tears in Descemet's membrane often coil when examined microscopically (Fig. 5.12). Deep ulceration of the corneal stroma may result in anterior displacement of Descemet's membrane into the stromal defect forming a descemetocoele. Since Descemet's membrane is continuously produced by corneal

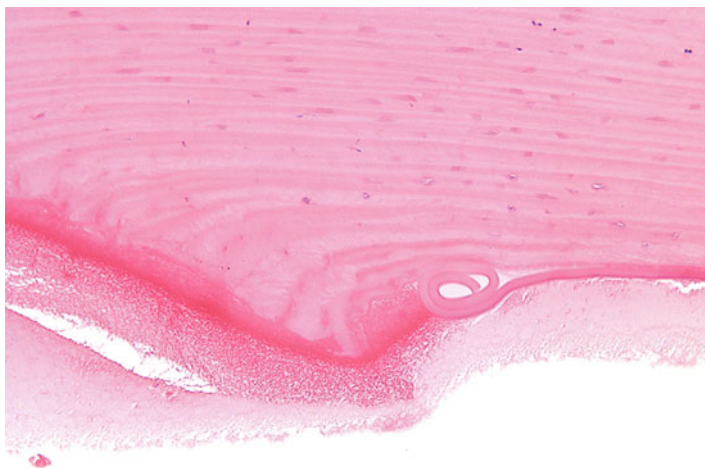


Fig. 5.12 Cornea from a rabbit 1 day following a surgical procedure. The incision site (left) has coiling of Descemet's membrane (right). H&E. 20× objective

endothelium, it will become thickened with age or can undergo duplication [219]. Degenerative changes in Descemet's membrane will manifest as irregular or diffuse thickening and are generally due to disease of the subjacent corneal endothelium. Descemet's membrane may extend onto structures of the filtration angle (i.e., descemetization), and cellular material may be embedded within it as a result of transcorneal injections.

Degeneration or loss of the corneal endothelium, with sufficient time, will result in irregular thickening of Descemet's membrane. Since Descemet's membrane is continuously laid down during the life of an animal, where the endothelium is healthy and active, Descemet's membrane will continue to be expanded. In those areas where the endothelium is not actively laying down Descemet's membrane, it gives the impression of local thinning, which is only a relative change.

The corneal endothelium is important in maintaining fluid balance within the corneal stroma, so a morphologic or functional loss of corneal endothelial cells results in diffuse corneal edema and opacification. When the inhibition is the result of a compound, the resulting opacity is often diffuse in comparison to localized injury. Intracameral implantation of medical devices can lead to a physical loss of the endothelium and may demonstrate this localized opacity. Compounds that are known to injure the corneal endothelium include 5-fluorouracil, local anesthetics, methylene blue, and tobramycin. Compounds such as methylhydrazine, 1,2-dichloroethane, 1,2-dibromoethane, and 1,2-dichloroethylene have been reported to cause corneal endothelial cell injury in animal studies, but not in humans [50]. With sufficient time, loss of the corneal endothelial cells causes irregular thinning of Descemet's membrane from a lack of continuous deposition and normal thickening.

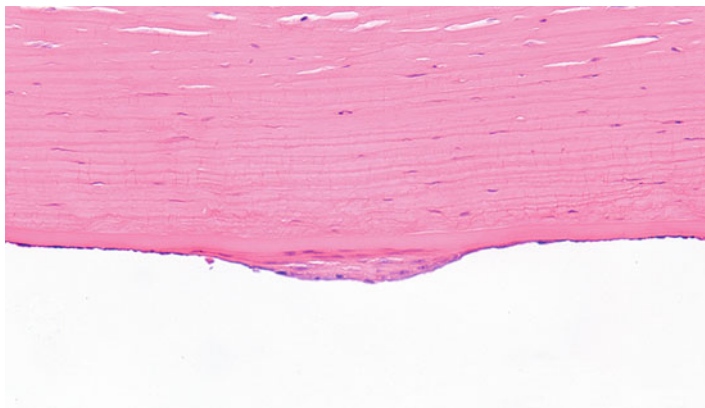


Fig. 5.13 Cornea from a dog that had a device implanted in the anterior chamber. The posterior surface of the cornea has a focal area of endothelial hyperplasia. H&E. 20× objective

The corneal endothelium has limited regenerative capacity which does vary some by species. For example, endothelial cells of nonhuman primates, dogs, and cats enlarge and migrate instead of proliferating, but in the rabbit, endothelial cells proliferate but may not provide a functional barrier [220–222]. In humans, the endothelium is thought not to proliferate at all or, if it does, not at a rate sufficient to replace lost cells since there is decreased corneal endothelial density with age. Therefore, injury to the corneal endothelium in a toxicology study is generally not an acceptable result. Human corneal endothelium has been shown *in vitro* to have proliferative capacity, even from aged patients, but that capacity requires a strong mitogenic signal [223]. Similar observations have been made with corneas of other species, in that there is proliferative capacity when cultured *in vitro*, but there is still a tendency for decreased corneal endothelial density with age for rhesus macaques, rats, mice, and rabbits. At times, some limited endothelial proliferation can be observed in laboratory animals (Fig. 5.13).

With the limited regenerative capacity of the corneal endothelium, the loss of corneal endothelium is repaired by spreading and decreased density of the existing endothelium (Fig. 5.14). This can manifest as attenuation microscopically, where corneal endothelial nuclei are fewer and spaced farther apart. Detection of such a change requires detailed comparison with concurrent controls and consistent orientation of the eye, since there are differences in endothelial density dorsally as compared to ventrally. However, this is probably better assessed with specular microscopy, described elsewhere in this book. With a greater degree of endothelial loss, where the remaining endothelium cannot migrate and spread over the defect, a fibrous membrane (i.e., retrocorneal membrane) may form [224] (Fig. 5.15). The origin of the retrocorneal membrane is thought to be from keratocytes or from corneal endothelial cells that have undergone a metaplastic change to fibrocytes [225]. A retrocorneal membrane would be expected to result in permanent corneal

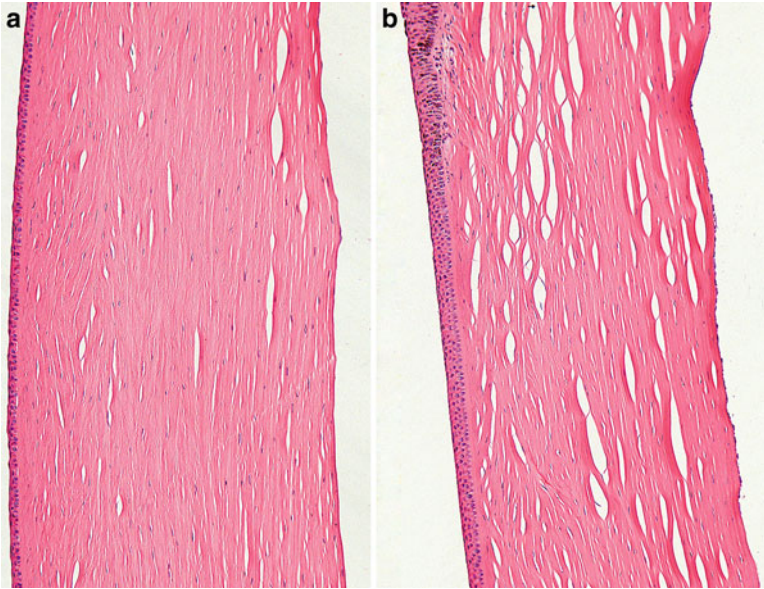


Fig. 5.14 Cornea from a monkey that had a device implanted in the anterior chamber. The inferior cornea (**a**) has a paucity of endothelial cells as compared to the superior cornea (**b**). The corneal endothelium is attenuated and widely spaced. H&E. 20× objective

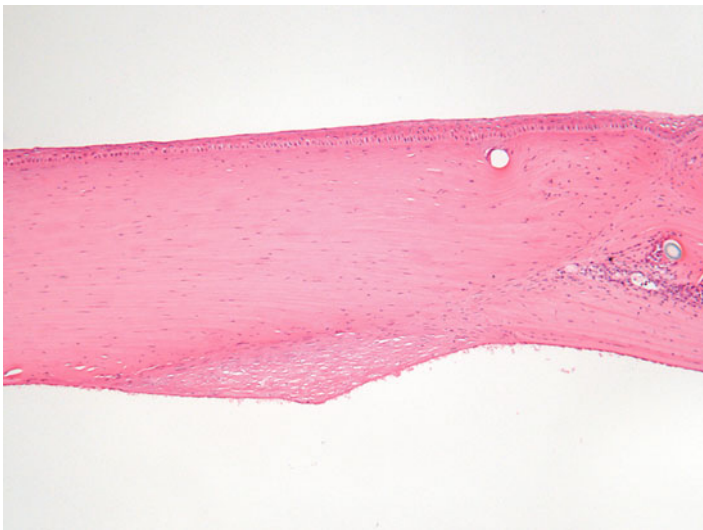


Fig. 5.15 Cornea from a rabbit 2 weeks after a surgical procedure. A retrocorneal membrane has formed at the incision site on the posterior surface of the cornea where the endothelium was lost. Note the disorganization of the stroma at the incision site and the cross sections of suture material. H&E. 10× objective

opacity in affected areas. Loss of endothelium may also result in adherence of the iris to the posterior corneal surface which is anterior synechia.

Injury to endothelial cells can be recognized ultrastructurally as loss of surface microvilli, alterations in surface apical processes, rounding of cells, separation of cells, death, and loss of cells from the basement membrane. In response to cellular stress, endothelial cells produce excess basement membrane that accumulates between the basal surface of the endothelial cells and Descemet's membrane. This may progress to the above-mentioned fibrous metaplasia and the formation of a retrocorneal membrane [17]. Protective mechanisms associated with glutathione are important in maintaining cell viability. Endothelial cells may be damaged directly by instillation of material into the anterior chamber during surgical procedures [17].

Chemical features in the local environment including ionic concentration, bicarbonate levels, pH, and tonicity affect the corneal endothelium. Damage to endothelial cells can generally be categorized into two major mechanisms: alterations in passive permeability or alterations in function. For example, benzalkonium chloride, a surfactant, will cause endothelial cell separation and therefore will increase permeability. Dimethyl sulfoxide has been associated with corneal opacification, and this may also reasonably be related to increased permeability of the endothelial layer. Hydrogen peroxide and other drugs or substances that inhibit catalase or glutathione activity will affect endothelial membranes and ion pumps due to the increases in free radicals. Drugs that affect the endothelium can reach the anterior chamber by direct diffusion if given topically or through filtration during the formation of aqueous fluid if given systemically. Damage to the endothelium can also be a secondary event to the administration of phototoxic chemicals such as rose bengal or chlorpromazine, which produce free radicals when exposed to ultraviolet or visible spectrum light [226–228]. Anything that may affect corneal endothelial metabolism and the function of sodium-potassium ATPase pumps may result in corneal swelling.

Fischer 344 rats have been described with endothelial dystrophy. Dense opacities are observed unilaterally or bilaterally in the deep cornea as spots of 1–2 mm in size. These may be caused by antidepressants in young F344 rats [229].

5.6 Sclera and Episclera

The sclera is composed of collagenous connective tissue and serves as a supportive frame for the globe [4, 7]. The vascularized layer between the bulbar conjunctiva and the sclera is the episclera.

5.6.1 Scleral and Episcleral Alterations

The sclera is generally not primarily involved in ocular toxicity but may be secondarily involved such as being diffusely stretched when the globe enlarges (i.e., buphthalmos) due to glaucoma or due to focal stretching (i.e., ectasia) secondary to posterior

coloboma. Osseous or cartilaginous metaplasia of the sclera occurs as an aging change in rats (Fischer 344) [76]. Posteriorly, drugs may be deposited in the suprachoroidal space [230] or sub-Tenon's space near the macula in primates.

The episclera may contain mononuclear or mixed inflammatory cells secondary to irritation or inflammation of the cornea. With the increasing development of intraocular therapies, the sclera is frequently a barrier that must be breached, such that incision sites and sutures or injection tracks may be apparent in section. Healing of the sclera is mostly by cells from the episclera. With small, uncomplicated wounds, there is ingrowth of fibroblasts and occasionally of blood vessels either from the episclera or the uvea. With larger wounds, there may be incarceration or prolapse of other ocular tissues.

The only known drug class that specifically affects the sclera is the bisphosphonates [231]. In humans, bisphosphonates, specifically pamidronate, have been shown to cause scleritis within 6–48 h post intravenous injection. Bisphosphonates in general can cause ophthalmitis, but the scleritis appears to be specific for this drug class.

5.7 Conjunctiva

The corneal epithelium abruptly becomes bulbar conjunctiva at the limbus. The bulbar conjunctiva covers the episclera and extends as palpebral conjunctiva onto the inner surface of the eyelids and over the third eyelid [4, 7, 112]. Conjunctiva is composed of a single row of epithelial cells that appear as squamous epithelium near the palpebral margins and goblet cells in areas less exposed. The density of goblet cells is not homogeneous in the palpebral conjunctiva.

The conjunctival epithelium is supported by an underlying connective tissue stroma that contains lymphoid aggregates in nonrodents referred to as conjunctiva-associated lymphoid tissue (CALT) and is generally considered to be part of the mucosa-associated lymphoid tissue (MALT) system [232–235]. Some authors have in the past identified this as chronic inflammation and if exuberant, it very well may be. Rats and mice do not normally have lymphoid follicles in the conjunctiva, such that their formation in that location should be considered an abnormality [232]. As determined by evaluating rabbits, newborns have no lymphoid follicles in the conjunctiva, while adolescents have rapidly increasing amounts of lymphoid tissue that stabilizes during young adulthood and steadily declines with advancing age [236]. The lymphoid tissue in the conjunctiva is greater in the palpebral conjunctiva than in the bulbar conjunctiva and greater in the conjunctiva of the upper lid than the lower lid [235]. The conjunctival lymphoid tissue is largely located such that it overlies the cornea when the lids are closed, which is thought to be an important part of ocular immune surveillance [234]. The lymphoid tissue exists as individual lymphocytes and plasma cells scattered in the stroma as well as well-defined follicles, some of which will have germinal centers. It is important to note the relative amounts of lymphoid tissues when examining the conjunctiva of the eye, as increases or decreases may be related to test article administration, especially when that administration is ocular. Decreases in number and size of lymphoid follicles can be

observed with the topical administration of anti-inflammatory agents. The nictitating membrane is also a site where lymphoid tissue is frequently present and should be considered part of the CALT.

The limbus, which is the border between the conjunctiva and the cornea, will often have small aggregates of lymphocytes in the stroma subjacent to the epithelium. These are common findings in monkeys, dogs, and rabbits but, like CALT, do not occur in normal rats and mice.

The palpebral conjunctiva of rabbits often contains a few heterophils which may increase in number as a response to irritation or infection.

5.7.1 *Conjunctival Alterations*

Inflammation of the conjunctiva (i.e., conjunctivitis) is often associated with corneal inflammation or inflammation of the anterior segment. This is because the cornea is continuous with the conjunctiva and because the conjunctiva is the source of vessel for corneal vascularization and a route for ingress of inflammatory cells into the cornea and anterior chamber. On gross examination, the inflammation will be manifested as hyperemia or congestion and edema (i.e., chemosis) of the mucous membranes. If there was previous hemorrhage, gross discoloration of the conjunctiva may be visible, or hemosiderin pigment deposition may be present in histologic section. Conjunctivitis and keratoconjunctivitis are reported infrequently as spontaneous changes in laboratory animals with the majority of papers describing it in nonhuman primates more so than other species [126, 136, 237, 238]. However, the incidence reported in nonhuman primates is approximately 1% [238].

Acute conjunctivitis may present with grossly identifiable exudates, consisting of mucus, sloughed epithelial cells, exudation of serous fluid and fibrin, and inflammatory cells. If the injury is great enough, this exudate can form a pseudomembrane adhered to the conjunctiva and cornea, or if there is loss of epithelium, it can form a tightly adherent true membrane. Grossly, there will likely also be chemosis and hyperemia of conjunctival vessels. Conjunctivitis frequently occurs in rabbits and is often due to bacteria which may have gained access to the conjunctival sac via the nasolacrimal duct. Eyelids may be swollen or closed with serous, mucous, or purulent discharge [239]. If chronic, the discharge can cause a loss of hair on the face below the medial canthus. Inflammation may be associated with respiratory disease, and *Pasteurella multocida* is frequently cultured. However, this organism can be present in grossly normal eyes.

With chronic conjunctivitis, a spectrum of changes may occur, depending on the duration, severity, and cause of the injury. Goblet cells are often increased in number, and the epithelium is hyperplastic with crypt-like infoldings. Lymphoid follicles may be increased in number and prominence, enough so that they are readily apparent on a careful gross examination. Vessels may also have perivascular infiltrates of inflammatory cells.

Sequela of conjunctivitis may include the continued increased density of goblet cells and epithelial folds. However, if there is epidermalization, there may actually be decreases in or an absence of goblet cells, due to the transition to a stratified squamous

epithelium. In some instances, this stratified squamous epithelium may be keratinizing. With stromal scarring, the eye may become dry (i.e., xerophthalmia) due to constriction and obstruction of lacrimal glands and decreases in goblet cells.

Various agents can cause conjunctivitis, and many of those mentioned causing keratitis will also produce conjunctivitis. Ricin topically applied to the eyes is an exception, where the conjunctiva and sclera will develop a necrotizing inflammatory reaction; the cornea will have only a sparse neutrophilic infiltrate limited to the most peripheral areas [240].

Miscellaneous conjunctival alterations include amyloidosis, squamous cell metaplasia, squamous papilloma, squamous cell carcinoma, mucoepidermoid carcinoma, microgranuloma, and pseudopterygium [49]. Conjunctival microgranuloma may appear in the bulbar conjunctiva of older rats. The finding consists of small accumulations of macrophages with calcific deposits beneath the conjunctival epithelium and may occur with corneal mineralization [127, 131, 187]. Pseudopterygium is characterized by a sheet-like overgrowth of bulbar conjunctiva that extends over the cornea in the rabbit. Pseudopterygium is a spontaneous change infrequently observed [20]. The flap is not associated with irritation or inflammation. Microscopically, the flap consists of a loose connective tissue stroma covered by epithelium on both sides. There are usually no adhesions between the flap and either the eyelid or the cornea, and the flap of tissue will often grow back after removal.

The conjunctiva is one site of local application of test articles. When subconjunctival injections are part of the study design, the conjunctiva should be evaluated microscopically, especially in the area of the injection. With depot injections, granulomas and other reactions may be observed (Fig. 5.16).

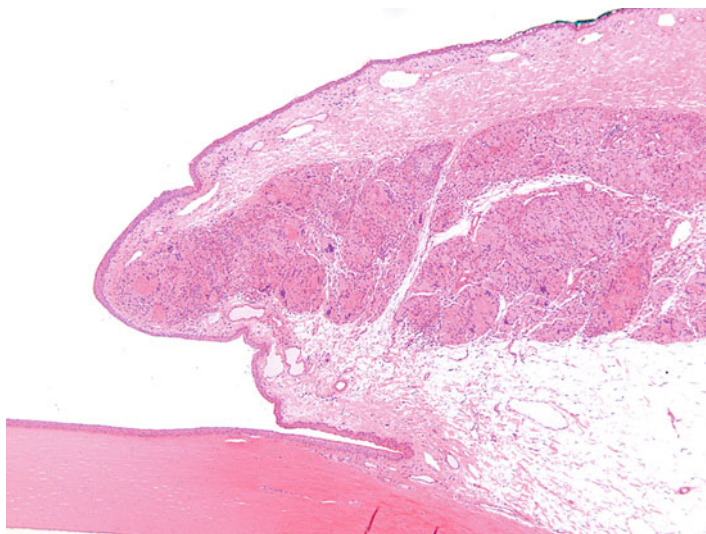


Fig. 5.16 Conjunctiva from a rabbit given a subconjunctival depot injection. The loose connective tissue is expanded by an aggregate of foamy macrophages and multinucleate giant cells. H&E, 5 \times objective

5.8 Uvea

The uvea or the vascular tunic of the globe includes the iris, ciliary body, and choroid [4, 7, 32, 241]. The choroid includes the tapetum lucidum in some species.

Since the uvea is the vascular tunic of the eye, it is often involved in intraocular inflammation. Intraocular inflammation needs to be prevented or minimized quickly in order to prevent permanent damage to the specialized structures of the eye. Ocular immunity is reviewed by Biros [242] but includes features such as a blood-eye barrier, an absence of lymphatic vessels, a semiconfined microenvironment, tissue-specific antigen presenting cells, and innate immune cells [242].

5.8.1 Uveal Alterations

Drug-induced morphological changes involving the uvea of laboratory animals consist of edema, inflammation, degeneration, abnormal pigmentation, cytoplasmic vacuolation, cellular necrosis, or changes in the intraocular pressure (IOP). Colchicine, naphthol, and urethane cause edema, inflammation, or degeneration of the ciliary body [50]. Naphthalene causes degeneration of the ciliary body and the choroid, and pyriithione causes edema and degeneration of the choroid [50]. Drug-induced changes must be differentiated from spontaneous findings which may be congenital, traumatic, inflammatory, degenerative, metaplastic, and proliferative processes [46, 126, 243, 244].

5.8.1.1 Pigmentary Changes

Increased or decreased pigmentation may occur following administration of compounds [245]. Drug-induced darkening of the iris occurs in cynomolgus monkeys and humans with topical administration of the prostaglandin F_{2a} analogs latanoprost, travoprost, and bimatoprost [246–248]. The increased pigmentation is due to an increase in melanin synthesis [249]. The sympathetic nervous system is important in the development of iris pigmentation [250].

Proliferation of melanin-containing cells in the iris may be induced in hooded rats treated neonatally with urethane [251], but was not observed when Wistar rats were used.

Depigmentation of the uvea may occur as a result of inflammation or edema.

5.8.1.2 Cytoplasmic Vacuolation

Cytoplasmic vacuolation may occur in the epithelium of the iris, ciliary body, or both and may be due to a variety of causes. A fairly common cause of vacuolation is due to phospholipids. This may be caused by many compounds and will vary by species.

For example, disobutamide, a piperidine antiarrhythmic drug, causes vacuolation of the epithelial cells of the iris and other cells in dogs, but not rats [252]. Phospholipidosis may involve the pigmented iridal epithelial cells of monkeys and can cause alterations in the appearance of the tapetum lucidum in dogs. Other causes of vacuolation include dilation of the endoplasmic reticulum and cell swelling. Diffuse cytoplasmic vacuolation of the iridal and ciliary epithelium occurred in albino and pigmented rabbits treated with 6-aminonicotinamide [253]. Extensive cytoplasmic vacuolation of both pigmented and nonpigmented ciliary epithelial cells occurred in cynomolgus monkeys following administration of a novel anticancer agent [254]. The ciliary body appeared swollen and had a decreased amount of pigment.

5.8.1.3 Uveal Inflammation and Trauma

Inflammation of the uvea may be caused by an immunological or a toxicological mechanism [137, 255]. Drug-related inflammation of the anterior uvea occurs in humans and is associated with the antiviral cidovir, antituberculous drug rifabutin, palmidronic acid, sulfonamides, streptokinase, and topical metipranolol [256]. Acute inflammation occurs in the anterior uvea after injection of a compound such as an antiviral agent [257]. Inflammation of the uvea may be a manifestation of toxicity in animals, such as inflammation of the ciliary body (i.e., cyclitis) that occurs after administration of cyclophosphamide to rats [258].

Inflammation as a manifestation of toxicity must be differentiated from spontaneous inflammation occurring as a background change. Rats and aged mice may develop spontaneous inflammation of the anterior uvea (i.e., iridocyclitis) [126]. The NIH Hartley strain of guinea pig is susceptible to experimental autoimmune uveitis [259]. Mononuclear cell infiltration into the ciliary body (rabbits and monkeys), choroid (monkeys), iris (rabbit), and filtration angle (rabbit) is a nonspecific change that occurs relatively frequently [68, 260] (Fig. 5.17). In the rabbit, spontaneous anterior uveal inflammation is more common than choroidal inflammation, but unilateral uveal inflammation of undetermined cause may occur [261]. In dogs, inflammation of the choroid may cause the tapetum lucidum to have a red discoloration [261]. If intraocular inflammation persists, then secondary changes occur, such as adhesions or fibrosis [20].

Trauma to the globe, irritation from an intracameral (i.e., within the anterior chamber) injection, or implantation of a medical device may cause inflammation with or without secondary changes. Secondary ocular changes include adhesion of the iris to the lens (i.e., posterior synechia), adherence of the iris to the cornea (i.e., anterior synechia), ciliary edema, proteinaceous fluid in the anterior chamber (i.e., aqueous flare), neutrophils in the anterior chamber (i.e., hypopyon), or hemorrhage in the anterior chamber (i.e., hyphema). Injection of material into the vitreous cavity through the pars plana will leave an injection track. Ocular findings associated with the needle track include prolapse of the ciliary epithelium or the vitreous upon removal of the needle, or intravitreal inflammation. The iris may respond to surgical trauma or irritation by a fibroproliferative response in rabbits; a similar response may be observed in humans.

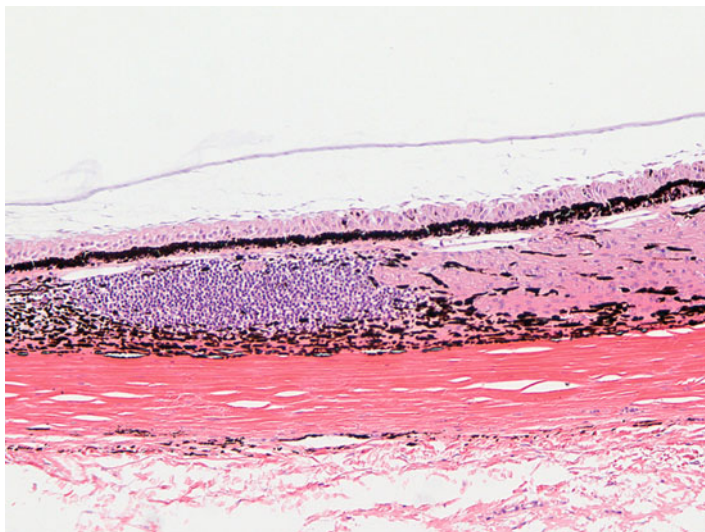


Fig. 5.17 Pars plana of the ciliary body of a monkey with infiltrates of lymphocytes. These are commonly observed as spontaneous changes in monkeys. H&E. 10× objective

5.8.1.4 Miscellaneous Uveal Findings

Miscellaneous uveal findings may be associated with administration of a compound or may be spontaneous background changes. Iris atrophy is generally not observed in laboratory animals but may be found in (C57L X A/He) F1 mouse [167]. Initially, small holes appear that may coalesce with microscopic disorganization of the normal iridal appearance. The ciliary epithelial basement membranes of dogs may become thickened following administration of an anticholinesterase pesticide [262]. Systemic administration of silver lactate to rats results in silver grain deposition in the iris and ciliary body [263]. The deposits are located on the basement membranes and within the pigmented epithelial cells. Background findings include mineralization in the iris of rodents [264] or the presence of foci of heterotopic bone (i.e., osseous choristoma or osseous metaplasia) within the ciliary body of guinea pigs [208, 265, 266]. Fischer 344 rats, but not Sprague-Dawley rats, develop choroidal adiposity as a response to systemic PPAR-gamma agonist administration [267]. The choroidal adiposity is characterized by increased adipocytes between the choroid and the sclera.

5.8.1.5 Intraocular Pressure and Glaucoma

The IOP can be increased or decreased. Intraocular pressure may be increased by subconjunctival injections of compounds, intraocular injection of compounds, and by topical application of compounds, but other possibilities should also be considered.

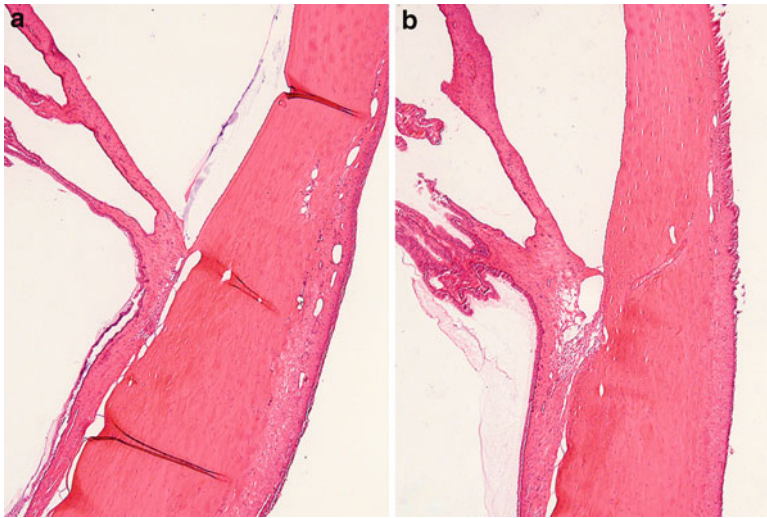


Fig. 5.18 Trabecular meshwork from rabbits. (a) Congenital goniodysgenesis. Note the narrowing of the filtration angle and absences of trabecular meshwork for aqueous fluid filtration. The animal had buphthalmos and increased intraocular pressure. (b) Normal trabecular meshwork. H&E. 5 \times objective

Drugs that dilate the pupil or limit the constriction of the pupil cause the anterior chamber to be shallow and the filtration angle to be narrow [268]. This may possibly lead to an increase in the IOP, and a prolonged increase in IOP results in structural changes (i.e., glaucoma). Obviously, glaucoma is a significant problem in human ophthalmology, and a variety of therapeutics and surgical techniques are aimed at decreasing IOP.

Features of glaucoma include increased size of the globe (i.e., buphthalmos or buphthalmia), breaks in Descemet's membrane (i.e., stria), diffuse corneal edema, thinning of the tunics (i.e., retina, uvea, sclera), luxation of the lens, and cupping of the optic disc. Thinning of the retina begins with loss of the ganglion cells (i.e., inner retinal degeneration) followed by loss of neurons with cell bodies in the inner nuclear layer. As the globe becomes stretched, the sensory retina may become separated (i.e., retinal detachment) from the retinal pigment epithelium (RPE) leading to degeneration of photoreceptors (i.e., outer retinal degeneration).

Buphthalmos occurs as a unilateral or bilateral, autosomal recessive inherited defect in New Zealand white rabbits [269] (Fig. 5.18), and beagles may develop open-angle glaucoma as an inherited autosomal recessive disorder [270]. Glaucoma largely develops as a result of impaired drainage of aqueous humor from the anterior chamber from maldevelopment (i.e., goniodysgenesis) or secondary to other ocular findings. Abnormal development of structures of the filtration angle often involves faulty development of the pectinate ligament. When the pectinate ligament is poorly developed, the root of the iris is located adjacent to the peripheral margin of Descemet's membrane. There may be splitting and extension of Descemet's

membrane onto structures around the pectinate ligament (i.e., descemetization). Increased production of aqueous has been suggested to be a cause of increased IOP, but demonstration of this cause is rare.

The increased IOP causes a thin-walled globe, diffuse bluish corneal opacity, and cupping of the optic disc, especially because of the poorly developed lamina cribrosa in rabbits [271]. In general, enlargement of the globe may interfere with adequate hydration of the cornea resulting in drying of the cornea with possible inflammation (i.e., keratoconjunctivitis) and possibly corneal trauma [261, 272]. With time, secondary lens luxation and ciliary atrophy may occur. In addition to the development of glaucoma from maldevelopment (primary glaucoma), glaucoma may develop as a secondary effect.

Secondary glaucoma occurs when normal aqueous filtration becomes obstructed. Glaucoma may be secondary to inflammation, neoplasia, neovascular growth, or lens luxation [20]. For example, rodents develop glaucoma after inflammation in the anterior segment, particularly if adhesions occur [273–276]. Mechanical causes of secondary glaucoma include adhesion of the iris to the peripheral cornea (i.e., anterior synechia) or infiltration of the filtration meshwork by inflammatory or neoplastic cells, to mention a few causes. Older DBA/2J (D2) mice develop glaucoma due to dispersion of ocular pigment [277]. Affected mice develop elevated IOP pigment dispersion, pigment epithelial atrophy, anterior synechia, ganglion cell loss, optic disc cupping, and optic nerve atrophy. IOP may increase following administration of intraocular materials in laboratory animals. Some substances that obstruct aqueous outflow include particulates such as calcium carbonate, cotton, talc, sanguinarine, and India ink. Viscous solutions such as methyl cellulose can also slow aqueous outflow [50]. Other substances, such as alloxan, cresol, and phenol, destroy endothelial cells, including those lining the trabecular meshwork, causing an inflammatory reaction.

IOP may be decreased in some instances. Inflammation is an important cause of decreased IOP. Cardiac glycosides, including digitoxin, digoxin, lanatoside C, and ouabain reduce the IOP by interfering with the formation of aqueous through inhibition of Na/K-ATPase in the ciliary body. Iodoacetate and quinine reduce IOP by damage to the iris and ciliary body and reduction of aqueous production [50]. Topical application of prostaglandin F2c reduces IOP and increases the uveoscleral outflow resulting in edema and dilatation of intramuscular spaces of the ciliary body of cynomolgus monkeys [278].

5.8.1.6 Tapetal Alterations

Since dogs are commonly used in toxicity studies, alterations involving the tapetum lucidum are often observed in laboratory beagles [245]. Since the tapetum lucidum is not present in humans, treatment-related findings may not be relevant to human safety assessment [279]. To help determine if treatment-related tapetal findings have relevance to humans, beagles which do not have an observable tapetum lucidum are sometimes used [280]. These dogs have tapetal cells, but they are lacking

intracytoplasmic rodlets [281]. For example, administration of imidazoquinoline to normal beagles results in tapetal and retinal changes, but the use of atapetal beagles results in no retinal changes [282].

The principal toxicity-related finding involving the tapetum lucidum is a loss of tapetal cells. Since young beagles are generally used for toxicity studies, age-related loss of tapetal cells can be eliminated as a possible cause for the loss [283, 284]. Degeneration or necrosis of tapetal cells may be accompanied by inflammation which may cause the tapetum lucidum to appear red or be absent [261]. Additional findings that may accompany tapetal cell degeneration include inflammation of the retina (i.e., chorioretinitis), edema, hemorrhage, or retinal detachment.

Toxicity involving the tapetum lucidum of beagles may be subdivided into zinc chelators and nonchelators. Since tapetal cells contain a high concentration of zinc, administration of zinc chelators, such as hydroxypyridinethione or pyrithione, to dogs causes tapetal and choroidal necrosis and edema with a secondary retinopathy [254, 261, 285, 286]. Administration of the zinc chelator ethambutol causes fluffy-white discoloration of the tapetum [261]. This change is reversible and is probably due to altered refraction because of disorganization of tapetal cell rodlets. Administration of hydroxypyridinethione results in retinal edema and detachment in addition to tapetal cell necrosis [261]. Administration of the chelating agent pyrithione also causes tapetal and choroidal necrosis and edema [254, 288].

Toxicity involving the tapetum lucidum of beagles is observed with non-chelators such as enrofloxacin, CGS14796C (a potential aromatase inhibitor), 1192U90 (an antipsychotic agent), dithizone, edentate, and ethylenediamine derivatives [50, 289, 290]. Compounds that do not cause chelation may also cause tapetal edema, degeneration, retinal edema, and retinal detachment in dogs and tapetal atrophy in cats [291]. These changes were specific for the tapetum since no retinal changes were observed in primates, rats, rabbits, or atapetal beagles [50].

5.8.1.7 Developmental Uveal Findings

Findings associated with toxicity of the uvea of laboratory animals must be differentiated from spontaneous uveal findings. Many of the spontaneous findings are congenital and easily differentiated from a finding associated with toxicity by being observed during the prestudy ocular examination. Developmental anomalies involving the uvea may be unilateral or bilateral, occur in a variety of laboratory animals (rat, mice, hamster, rabbit, beagle dog), and include ectopic pupil (beagle dog), persistent pupillary membrane or strands (beagle dog, Sprague-Dawley rat, Crj:CD (SD) rat, Göttingen minipig, Yucatan micropig, mice, Syrian hamster), iridal coloboma (rat), posterior coloboma (beagle dog, rat), and alterations in iridal color [47, 100, 125, 126, 129, 261, 292–294].

5.8.1.8 Uveal Neoplasia

In general, spontaneous uveal neoplasia rarely occurs in the common laboratory animals. In mice, they are generally malignant, with the exception of iridal adenoma of the nonpigmented iridal epithelium [167]. Some neoplasms metastasize to the globe (e.g., harderian gland carcinoma) or may be induced, such as fibrosarcoma induced by intraocular implantation of a suture containing 20-methylcholanthrene [169].

Rats develop spindle cell neoplasms which include uveal malignant melanoma [295], uveal leiomyoma [296], and malignant and benign intraocular Schwannoma [297]. In guinea pigs, malignant lymphoma, including T cell lymphoma and reticulosarcoma, has been reported to involve the choroid [298, 299], and uveal malignant melanoma has been reported in rabbits [300]. In the mouse, secondary tumors, such as malignant lymphoma and harderian gland carcinoma, can spread to the globe [167, 301, 302].

Spontaneously occurring uveal melanomas have been reported in albino rat strains including Sprague-Dawley, Wistar, and F344 [49]. Uveal melanomas in the rat consist of bundles and whorls of spindle-shaped cells with a perivascular orientation, possibly containing epithelioid cells and areas of necrosis. Mitotic figures may be numerous. The neoplasm generally involves the anterior uvea but may involve the choroid and extend into adjacent ocular structures. Neoplastic cells are positive for S-100 protein and vimentin intermediate filament.

Uveal malignant melanoma is generally not a neoplasm that occurs in albino mice and is rare in pigmented mice, such as B6C3F1 mice [81, 302]. In B6C3F1/Cr1BR mice, intraocular melanomas are noninvasive, well-pigmented, epithelioid neoplasms originating in the choroid with no metastasis [302]. In these mice, malignant melanoma usually originates in a lymphoid organ and metastasizes to the choroid resulting in retinal detachment [167]. Uveal malignant melanoma in the mouse may metastasize to the lymph node, spleen, and thymus.

Uveal melanoma has been induced by intravitreal instillation of nickel subsulfide or N-methyl-N-nitrosourea and by oral administration of ethionine combined with 2-acetylaminofluorene [303, 304]. Uveal melanoma has been induced in pigmented August hooded rats by subcutaneous injection of urethane or N-hydroxyurethane during the neonatal period [49]. Metastasis to the lung has been reported.

Uveal leiomyoma in the rat consists of whorls of spindle cells, occasionally around blood vessels, that are reported to be positive for desmin [296]. The cells contain myofibrils that can be demonstrated with phosphotungstic acid hematoxylin (PTAH) stains and by transmission electron microscopy.

Intraocular schwannoma arises from the iris or ciliary body but involves adjacent ocular structures [75]. The neoplasm is composed of plump spindle-shaped cells with abundant eosinophilic cytoplasm arranged in parallel rows and palisades around blood vessels. Neoplastic cells may have positive immunoreactivity for S-100, and desmosomes may be detected, ultrastructurally. Mitotic figures may be numerous and areas of necrosis may be present.

References

1. Smith RS, Nishina PM, Ikeda S, Jewett P, Zabaleta A, John SWM. Interpretation of ocular pathology in genetically engineered and spontaneous mutant mice. In: Ward JM, Mahler JF, Maronpot RR, editors. Pathology of genetically engineered mice. Ames: Iowa State University Press; 2000. p. 217–31.
2. Prince JH. The rabbit in eye research. Springfield: Charles C Thomas Pub.; 1964.
3. Prince JH. Comparative anatomy of the eye. Springfield: Charles C Thomas Pub.; 1956.
4. Samuelson DA. Ophthalmic anatomy. In: Gelatt KN, editor. Veterinary ophthalmology. 4th ed. Ames: Blackwell; 2007. p. 37–148.
5. Kuiper B, Boeve MH, Jansen T, Roelofs-van Emden ME, Thuring JW, Wijnands MV. Ophthalmologic examination in systemic toxicity studies: an overview. *Lab Anim*. 1997;31(2):177–83.
6. Munger RJ. Veterinary ophthalmology in laboratory animal studies. *Vet Ophthalmol*. 2002;5(3):167–75.
7. Rubin LF. Comparative anatomy of the eye. In: Hockwin O, Green K, Rubin LF, editors. Manual of oculotoxicity testing of drugs. Stuttgart: Gustav Fischer Verlag; 1992. p. 12–44.
8. Schiavo DM. Special topics about the use of laboratory animals in toxicology – an ophthalmoscopic assessment. In: Hockwin O, Green K, Rubin LF, editors. Manual of oculotoxicity testing of drugs. Stuttgart: Gustav Fischer Verlag; 1992. p. 9–20.
9. Short BG. Safety evaluation of ocular drug delivery formulations: techniques and practical considerations. *Toxicol Pathol*. 2008;36(1):49–62.
10. Aguirre GD, Rubin LF, Bistner SI. Development of the canine eye. *Am J Vet Res*. 1972;33(12):2399–414.
11. Cook C, Sulik K, Wright K. Embryology. In: Wright KW, editor. Pediatric ophthalmology and strabismus. St. Louis: Mosby-Year Book; 1995. p. 3–59.
12. Cook CS. Ocular embryology and congenital malformations. In: Gelatt KN, editor. Veterinary ophthalmology. 4th ed. Ames: Blackwell Publishing; 2007. p. 3–36.
13. O’Rahilly R. The timing and sequence of events in the development of the human eye and ear during the embryonic period proper. *Anat Embryol (Berl)*. 1983;168(1):87–99.
14. Stromland K, Miller M, Cook C. Ocular teratology. *Surv Ophthalmol*. 1991;35(6):429–46.
15. Smith RS, Koa WW-Y, John SWM. Ocular development. In: Smith RS, editor. Systematic evaluation of the mouse eye: anatomy, pathology, and biomethods. Boca Raton: CRC Press; 2002. p. 45–63.
16. Hoar RM. Embryology of the eye. *Environ Health Perspect*. 1982;44:31–4.
17. Whiteley HE, Peiffer RL. The eye. In: Haschek WM, Rousseaux CG, editors. Haschek and Rousseaux’s handbook of toxicologic pathology. Salt Lake City: Academic; 2002. p. 539–84.
18. Ramos M, Reilly CM, Bolon B. Toxicological pathology of the retina and optic nerve. In: Bolon B, Butt MT, editors. Fundamental neuropathology for pathologists and toxicologists: principles and techniques. Hoboken: Wiley; 2011. p. 385–412.
19. Somps CJ, Greene N, Render JA, Aleo MD, Fortner JH, Dykens JA, et al. A current practice for predicting ocular toxicity of systemically delivered drugs. *Cutan Ocul Toxicol*. 2009;28(1):1–18.
20. Dubielzig R, Ketring KL, McLellan GJ, Albert DM. Veterinary ocular pathology: a comparative review. Edinburgh: Saunders Elsevier; 2010.
21. Saunders LZ, Rubin LF. Ophthalmic pathology of animals. New York: S. Karger; 1975.
22. Thompson SW, Luna LG. An atlas of artifacts encountered in the preparation of microscopic tissue sections. Springfield: Charles C Thomas Pub.; 1978.
23. Fix AS, Garman RH. Practical aspects of neuropathology: a technical guide for working with the nervous system. *Toxicol Pathol*. 2000;28(1):122–31.
24. Smith RS, Hawes NL, Miller J, Sundberg JP, John SWM. Photography and necropsy. In: Smith RS, editor. Systematic evaluation of the mouse eye: anatomy, pathology, and biomethods. Boca Raton: CRC Press; 2002. p. 251–64.

25. Luna LG. Manual of histology staining methods of the Armed Forces Institute of Pathology. 3rd ed. New York: McGraw-Hill Book Co.; 1968.
26. Preece A. A manual for histotechnologists. 3rd ed. Boston: Little, Brown and Co.; 1972.
27. Sheehan DC, Hrapchak BB. Theory and practice of histotechnology. 2nd ed. Columbus: Battelle; 1980.
28. Saby JA, Sigler RE, Klaus S. Comparison of fixatives for histologic evaluation of the canine eye. *J Histotechnol.* 1991;14:251–5.
29. Yanoff M, Fine BS. Glutaraldehyde fixation of routine surgical eye tissue. *Am J Ophthalmol.* 1967;63(1):137–40.
30. Feeney-Burns L, Burns RP, Anderson RS. Ultrastructure and acid phosphatase activity in hereditary cataracts of deer mice. *Invest Ophthalmol Vis Sci.* 1980;19(7):777–88.
31. Anderson R, Shearer TR. Glycol methacrylate sections of the crystalline lens. *Stain Technol.* 1986;61(6):381–2.
32. Weisse I. Microscopic examination of the eye. In: Hockwin O, Green K, Rubin LF, editors. Manual of ophthalmology testing of drugs. Stuttgart: Gustav Fischer Verlag; 1992. p. 137–63.
33. Latendresse JR, Warbritton AR, Jonassen H, Creasy DM. Fixation of testes and eyes using a modified Davidson's fluid: comparison with Bouin's fluid and conventional Davidson's fluid. *Toxicol Pathol.* 2002;30(4):524–33.
34. Humason GL. Histochemistry and special procedures. Animal tissue techniques. San Francisco: Freeman; 1979.
35. Levy MC, Covatta TJ, Morris C, Aschner HH. Technique for preparing histologic sections of dogs' and rabbits' eyes in paraffin. *Arch Ophthalmol.* 1965;73:122–3.
36. Georger M. Concepts in the routine preparation of eye specimens. *Histo-Logic.* 2002;2:34–6.
37. Prophet EB. Technique for processing eye specimens. *Histo-Logic.* 1976;1:75–6.
38. Lee ES, Flannery JG. Transport of truncated rhodopsin and its effects on rod function and degeneration. *Invest Ophthalmol Vis Sci.* 2007;48(6):2868–76.
39. Smith RS, Zabeleta A, John SWM, Bechtold LS, Ikeda S, Relyea MJ, et al. General and special histopathology. In: Smith RS, editor. Systematic evaluation of the mouse eye: anatomy, pathology, and biomethods. Boca Raton: CRC Press; 2002. p. 265–97.
40. Duncan S. Microtomy and staining of cataract lens. *Histo-Logic.* 1981;11:160–1.
41. Lewis PA. Ocular Histology. 27th Annual Symposium/Convention, National Society for Histotechnology; Sept 22–27; Charlotte, NC2001.
42. Bermudez MA, Vicente AF, Romero MC, Arcos MD, Abalo JM, Gonzalez F. Time course of cold cataract development in anesthetized mice. *Curr Eye Res.* 2011;36(3):278–84.
43. Delaye M, Clark JI, Benedek GB. Identification of the scattering elements responsible for lens opacification in cold cataracts. *Biophys J.* 1982;37(3):647–56.
44. Lo WK. Visualization of crystallin droplets associated with cold cataract formation in young intact rat lens. *Proc Natl Acad Sci U S A.* 1989;86(24):9926–30.
45. Eglitis I. The orbital fascia. In: Prince JH, editor. The rabbit in eye research. Springfield: Charles C. Thomas Pub.; 1964. p. 28–37.
46. Hubert MF, Gerin G, Durand-Cavagna G. Spontaneous ophthalmic lesions in young Swiss mice. *Lab Anim Sci.* 1999;49(3):232–40.
47. Loget O. Spontaneous ocular findings and esthesiometry/tonometry measurement in the Göttingen minipig (Conventionally and microbiologically defined). In: Weisse I, Tripathi RC, Hockwin O, editors. Ocular toxicology. New York: Springer; 1995. p. 351–62.
48. LeDoux MS, Zhou Q, Murphy RB, Greene ML, Ryan P. Parasympathetic innervation of the meibomian glands in rats. *Invest Ophthalmol Vis Sci.* 2001;42(11):2434–41.
49. Ackerman LJ, Yoshitomo K, Fix AS, Render JA. Proliferative lesions of the eye in rats. *OSS. Guides for Toxicologic Pathology.* Washington, D.C.: STP/ARP/AFIP; 1998.
50. Grant WM. Toxicology of the eye. 3rd ed. Springfield: Charles C. Thomas Pub.; 1986.
51. Fischbein A, Rizzo JN, Solomon SJ, Wolff MS. Oculodermatological findings in workers with occupational exposure to polychlorinated biphenyls (PCBs). *Br J Ind Med.* 1985; 42(6):426–30.

52. Ohnishi Y, Kohno T. Polychlorinated biphenyls poisoning in monkey eye. *Invest Ophthalmol Vis Sci.* 1979;18(9):981–4.
53. Brewster DW, Elwell MR, Birnbaum LS. Toxicity and disposition of 2,3,4,7,8-pentachlorodibenzofuran (4PeCDF) in the rhesus monkey (*Macaca mulatta*). *Toxicol Appl Pharmacol.* 1988;93(2):231–46.
54. Arnold DL, Bryce F, Stapley R, McGuire PF, Burns D, Tanner JR, et al. Toxicological consequences of Aroclor 1254 ingestion by female rhesus (*Macaca mulatta*) monkeys. Part 1A. Prebreeding phase: clinical health findings. *Food Chem Toxicol.* 1993;31(11):799–810.
55. Tryphonas L, Truelove J, Zawidzka Z, Wong J, Mes J, Charbonneau S, et al. Polychlorinated biphenyl (PCB) toxicity in adult cynomolgus monkeys (*M. fascicularis*): a pilot study. *Toxicol Pathol.* 1984;12(1):10–25.
56. Tryphonas L, Arnold DL, Zawidzka Z, Mes J, Charbonneau S, Wong J. A pilot study in adult rhesus monkeys (*M. mulatta*) treated with Aroclor 1254 for two years. *Toxicol Pathol.* 1986;14(1):1–10.
57. Jester JV, Nicolaidis N, Kiss-Palvolgyi I, Smith RE. Meibomian gland dysfunction. II. The role of keratinization in a rabbit model of MGD. *Invest Ophthalmol Vis Sci.* 1989;30(5):936–45.
58. Kremer I, Gatton DD, David M, Gatton E, Shapiro A. Toxic effects of systemic retinoids on meibomian glands. *Ophthalmic Res.* 1994;26(2):124–8.
59. Lambert RW, Smith RE. Pathogenesis of blepharoconjunctivitis complicating 13-cis-retinoic acid (isotretinoin) therapy in a laboratory model. *Invest Ophthalmol Vis Sci.* 1988;29(10):1559–64.
60. Bryce F, Iverson F, Andrews P, Barker M, Cherry W, Mueller R, et al. Effects elicited by toxaphene in the cynomolgus monkey (*Macaca fascicularis*): a pilot study. *Food Chem Toxicol.* 2001;39(12):1243–51.
61. Hejkal TW, Camras CB. Prostaglandin analogs in the treatment of glaucoma. *Semin Ophthalmol.* 1999;14(3):114–23.
62. Johnstone MA, Albert DM. Prostaglandin-induced hair growth. *Surv Ophthalmol.* 2002;47 Suppl 1:S185–202.
63. Al-Jazzaf AM, DeSantis L, Netland PA. Travoprost: a potent ocular hypotensive agent. *Drugs Today (Barc).* 2003;39(1):61–74.
64. Law SK. Bimatoprost in the treatment of eyelash hypotrichosis. *Clin Ophthalmol.* 2010;4:349–58.
65. Prince JH, Eglitis I. Extraocular muscles. The rabbit in eye research. Springfield: Charles C Thomas Pub.; 1964. p. 57–71.
66. O’Steen WK, Kraeer SL, Shear CR. Extraocular muscle and Harderian gland degeneration and regeneration after exposure of rats to continuous fluorescent illumination. *Invest Ophthalmol Vis Sci.* 1978;17(9):847–56.
67. Katsuta O, Yamaguchi-Onozawa M, Okazaki K, Itoh T, Okazaki Y, Tsuchitani M. Gross and microscopic anatomy of the extraorbital lacrimal gland of the common marmoset (*Callithrix jacchus*). *Comp Med.* 2000;50(6):609–12.
68. Greaves P. *Histopathology of preclinical toxicity studies.* 3rd ed. New York: Academic; 2007.
69. Sakai T. The mammalian harderian gland: morphology, biochemistry, function and phylogeny. *Arch Histol Jpn.* 1981;44(4):299–333.
70. Nagai M, Nagai T, Yamamoto M, Goto K, Bishop TR, Hayashi N, et al. Novel regulation of delta-aminolevulinic synthase in the rat harderian gland. *Biochem Pharmacol.* 1997;53(5):643–50.
71. Eglitis I. The glands. In: Prince JH, editor. *The rabbit in eye research.* Springfield: Charles C. Thomas Pub.; 1964. p. 38–56.
72. Sullivan DA, Jensen RV, Suzuki T, Richards SM. Do sex steroids exert sex-specific and/or opposite effects on gene expression in lacrimal and meibomian glands? *Mol Vis.* 2009;15:1553–72.

73. Krinke AL, Schaetti PH, Krinke GJ. Changes in the major ocular glands. In: Mohr U, Dungworth DL, Capen CC, editors. Pathobiology of the aging rat. Washington, DC: ILSI Press; 1994.
74. Spike RC, Johnston HS, McGadey J, Moore MR, Thompson GG, Payne AP. Quantitative studies on the effects of hormones on structure and porphyrin biosynthesis in the harderian gland of the female golden hamster: I. The effects of ovariectomy and nitrogen administration. *J Anat.* 1985;142:59–72.
75. Mohr U. Fascicle No. 7: Central Nervous System, Heart, Eye, Mesothelium. In: Mohr U, editor. International Classification of Rodent Tumours: Part 1: The Rat, IARC Publications, No 122. Lyon: World Health Organization, International Agency for Research on Cancer; 1994. p. 34-51.
76. Yoshitomo K, Boorman GA. Eye and associated glands. Pathology of the Fischer rat: reference and atlas. San Diego: Academic Press; 1990. p. 239–59.
77. Sashima M, Hatakeyama S, Satoh M, Suzuki A. Harderianization is another sexual dimorphism of rat exorbital lacrimal gland. *Acta Anat (Basel).* 1989;135(4):303–6.
78. Breider MA, Bleavins MR, Reindel JF, Gough AW, de la Iglesia FA. Cellular hyperplasia in rats following continuous intravenous infusion of recombinant human epidermal growth factor. *Vet Pathol.* 1996;33(2):184–94.
79. Haseman JK, Hailey JR, Morris RW. Spontaneous neoplasm incidences in Fischer 344 rats and B6C3F1 mice in two-year carcinogenicity studies: a national toxicology program update. *Toxicol Pathol.* 1998;26(3):428–41.
80. Goodman DG, Ward JM, Squire RA, Chu KC, Linhart MS. Neoplastic and nonneoplastic lesions in aging F344 rats. *Toxicol Appl Pharmacol.* 1979;48(2):237–48.
81. Krinke GJ, Fix AS, Jacobs M, Render JA, Weisse I. Eye and harderian gland. In: Mohr U, editor. International classification of rodent tumors the mouse. Heidelberg: Springer; 2001. p. 347–59.
82. Parsons JT. Radiation toxicity to the visual system. *J Neuroophthalmol.* 2004;24(3):193–4.
83. Stephens LC, Schultheiss TE, Peters LJ, Ang KK, Gray KN. Acute radiation injury of ocular adnexa. *Arch Ophthalmol.* 1988;106(3):389–91.
84. Gazda MJ, Schultheiss TE, Stephens LC, Ang KK, Peters LJ. The relationship between apoptosis and atrophy in the irradiated lacrimal gland. *Int J Radiat Oncol Biol Phys.* 1992; 24(4):693–7.
85. Kaswan RL, Martin CL, Chapman Jr WL. Keratoconjunctivitis sicca: histopathologic study of nictitating membrane and lacrimal glands from 28 dogs. *Am J Vet Res.* 1984; 45(1):112–8.
86. Tanaka N, Ohkawa T, Hiyama T, Nakajima A. Evaluation of ocular toxicity of two beta blocking drugs, carteolol and practolol, in beagle dogs. *J Pharmacol Exp Ther.* 1983;224(2):424–30.
87. Trepanier LA. Idiosyncratic toxicity associated with potentiated sulfonamides in the dog. *J Vet Pharmacol Ther.* 2004;27(3):129–38.
88. Barnett KC, Joseph EC. Keratoconjunctivitis sicca in the dog following 5-aminosalicylic acid administration. *Hum Toxicol.* 1987;6(5):377–83.
89. Zoukhri D, Macari E, Kublin CL. A single injection of interleukin-1 induces reversible aqueous-tear deficiency, lacrimal gland inflammation, and acinar and ductal cell proliferation. *Exp Eye Res.* 2007;84(5):894–904.
90. Kimura-Shimmyo A, Kashiwamura S, Ueda H, Ikeda T, Kanno S, Akira S, et al. Cytokine-induced injury of the lacrimal and salivary glands. *J Immunother.* 2002;25 Suppl 1:S42–51.
91. Api AM, Smith RL, Pipino S, Marczylo T, De Matteis F. Evaluation of the oral subchronic toxicity of AHTN (7-Acetyl-1,1,3,4,4,6-hexamethyl-1,2,3,4-tetrahydronaphthalene) in the rat. *Food Chem Toxicol.* 2004;42(5):791–801.
92. Tsuchitani M, Narama I, Kohda S. Accumulation of pigment granules in lacrymal gland epithelium in practolol-treated beagle dogs. *J Comp Pathol.* 1989;100(3):237–43.
93. Slatter DH, Davis WC. Toxicity of phenazopyridine. Electron microscopical studies of canine lacrimal and nictitans glands. *Arch Ophthalmol.* 1974;91(6):484–6.

94. Keegan DJ, Geerling G, Lee JP, Blake G, Collin JR, Plant GT. Botulinum toxin treatment for hyperlacrimation secondary to aberrant regenerated seventh nerve palsy or salivary gland transplantation. *Br J Ophthalmol.* 2002;86(1):43–6.
95. Suwan-apichon O, Rizen M, Rangsin R, Herretes S, Reyes JM, Lekhanont K, et al. Botulinum toxin B-induced mouse model of keratoconjunctivitis sicca. *Invest Ophthalmol Vis Sci.* 2006;47(1):133–9.
96. Dethloff LA, Wilga P, Seefeld M, Ulloa H, Hawkins K, Petrere J. Effects of sustained low-level muscarinic agonism in rats. *Food Chem Toxicol.* 1994;32(8):753–62.
97. Majeed SK, Gopinath C, Heywood R. A report on drug-induced kerato-conjunctivitis sicca in dogs. *J Comp Pathol.* 1987;97(4):385–91.
98. Mason G, Wilson D, Hampton C, Wurbel H. Non-invasively assessing disturbance and stress in laboratory rats scoring chromodacryorrhea. *Alt Lab Anim.* 2004;32(Supple 1):153–9.
99. Harkness JE, Ridgway MD. Chromodacryorrhea in laboratory rats (*Rattus norvegicus*): etiologic considerations. *Lab Anim Sci.* 1980;30(5):841–4.
100. Heywood R. Some clinical observations on the eyes of Sprague-Dawley rats. *Lab Anim.* 1973;7(1):19–27.
101. McGee MA, Maronpot RR. Harderian gland dacryoadenitis in rats resulting from orbital bleeding. *Lab Anim Sci.* 1979;29(5):639–41.
102. Kurisu K, Sawamoto O, Watanabe H, Ito A. Sequential changes in the harderian gland of rats exposed to high intensity light. *Lab Anim Sci.* 1996;46(1):71–6.
103. Strum JM, Shear CR. Constant light exposure induces damage and squamous metaplasia in harderian glands of albino mice. *Tissue Cell.* 1982;14(1):149–61.
104. Travlos GS, Mahler J, Ragan HA, Chou BJ, Bucher JR. Thirteen-week inhalation toxicity of 2- and 4-chloronitrobenzene in F344/N rats and B6C3F1 mice. *Fundam Appl Toxicol.* 1996;30(1):75–92.
105. Libretto SE. A review of the toxicology of salbutamol (albuterol). *Arch Toxicol.* 1994; 68(4):213–6.
106. Herrold KM. Aflatoxin induced lesions in Syrian hamsters. *Br J Cancer.* 1969;23(3): 655–60.
107. Iwai H, Tagawa Y, Hayasaka I, Yanai T, Masegi T. Effects of atropine sulfate on rat harderian glands: correlation between morphological changes and porphyrin levels. *J Toxicol Sci.* 2000;25(3):151–9.
108. Kajimura T, Satoh H, Nomura M. Effect of hyperprolactinemia induced by neuroleptic agent, timiperone, on porphyrin content of mouse harderian gland. *J Toxicol Sci.* 1997; 22(3):219–29.
109. Eida K, Kubota N, Nishigaki T, Kikutani M. Harderian gland. V. Effect of dietary pantothenic acid deficiency on porphyrin biosynthesis in harderian gland of rats. *Chem Pharm Bull(Tokyo).* 1975;23(1):1–4.
110. da Costa JR, Lucif S, Lopes RA. Effect of hypervitaminosis A on the harderian gland in rats. A morphologic and morphometric study. *Int J Vitam Nutr Res.* 1978;48(2):113–22.
111. Gray Jr LE, Kavlock RJ, Chernoff N, Ferrell J, McLamb J, Ostby J. Prenatal exposure to the herbicide 2,4-dichlorophenyl-p-nitrophenyl ether destroys the rodent harderian gland. *Science.* 1982;215(4530):293–4.
112. Eglitis I. The eyelids. In: Prince JH, editor. *The rabbit in eye research.* Springfield: Charles C Thomas Pub.; 1964. p. 72–85.
113. Richardson VCG. *Diseases of domestic guinea pigs.* 2nd ed. London: Blackwell Science; 2000.
114. Percy D, Barthold S. *Pathology of laboratory rodents and rabbits.* Ames: Iowa State University Press; 2001.
115. Brazzell RK, Stern ME, Aquavella JV, Beuerman RW, Baird L. Human recombinant epidermal growth factor in experimental corneal wound healing. *Invest Ophthalmol Vis Sci.* 1991;32(2):336–40.
116. Rich LF, Hatfield JM, Louiselle I. The influence of epidermal growth factor on cat corneal endothelial wound healing. *Curr Eye Res.* 1991;10(9):823–30.

117. Greenman DL, Cronin GM, Dahlgren R, Allen R, Allaben W. Chronic feeding study of pyrilmamine in Fischer 344 rats. *Fundam Appl Toxicol.* 1995;25(1):1–8.
118. Wilhelm KE, Grabolle B, Urbach H, Tolba R, Schild H, Paulsen F. Evaluation of polyurethane nasolacrimal duct stents: in vivo studies in New Zealand rabbits. *Cardiovasc Intervent Radiol.* 2006;29(5):846–53.
119. Kintzel PE, Michaud LB, Lange MK. Docetaxel-associated epiphora. *Pharmacotherapy.* 2006;26(6):853–67.
120. Vettese T, Hurwitz JJ. Toxicity of the chemiluminescent material Cyalume in anatomic assessment of the nasolacrimal system. *Can J Ophthalmol.* 1983;18(3):131–5.
121. Carlton WW, Render JA. Adenoma and adenocarcinoma, harderian gland, mouse, rat and hamster. In: Jones TC, Mohr U, Hunt RD, editors. *Monographs on pathology of laboratory animals: eye and ear.* Berlin: Springer; 1991. p. 133–7.
122. Tucker MJ. Special sense organs and associated tissues. In: Tucker MJ, editor. *Diseases of the Wistar Rat.* London: Taylor and Francis; 1997. p. 237–45.
123. Sheldon WG, Curtis M, Kodell RL, Weed L. Primary harderian gland neoplasms in mice. *J Natl Cancer Inst.* 1983;71(1):61–8.
124. Prince JH. Cornea, trabecular region, and sclera. In: Prince JH, editor. *The rabbit in eye research.* Springfield: Charles C Thomas Pub.; 1964. p. 86–139.
125. Taradach C, Regnier B, Perraud J. Eye lesions in Sprague-Dawley rats: type and incidence in relation to age. *Lab Anim.* 1981;15(3):285–7.
126. Taradach C, Greaves P. Spontaneous eye lesions in laboratory animals: incidence in relation to age. *Crit Rev Toxicol.* 1984;12(2):121–47.
127. Shibuya K, Satou K, Sugimoto K, Saitoh T, Ihara M, Itabashi M, et al. Background data on spontaneous ophthalmic lesions in Crj:CD(SD)IGS rats. In: Matsuzawa T, Inoue H, editors. *Biological reference data on CD(SD) IGS rats – 1999.* Yokohama: Best Printing Co. Ltd.; 1999. p. 60–2.
128. Bellhorn RW, Korte GE, Abrutyn D. Spontaneous corneal degeneration in the rat. *Lab Anim Sci.* 1988;38(1):46–50.
129. Kuno H, Usui T, Eydeloth RS, Wolf ED. Spontaneous ophthalmic lesions in young Sprague-Dawley rats. *J Vet Med Sci.* 1991;53(4):607–14.
130. Van Winkle TJ, Balk MW. Spontaneous corneal opacities in laboratory mice. *Lab Anim Sci.* 1986;36(3):248–55.
131. Carlton WW, Render JA. Calcification of the cornea. In: Jones TC, Mohr U, Hunt RD, editors. *Monographs on pathology of laboratory animals: eye and ear.* Berlin: Springer; 1991. p. 16–20.
132. Mittl R, Galin MA, Opperman W, Camerini-Davalos RA, Spiro D. Corneal calcification in spontaneously diabetic mice. *Invest Ophthalmol.* 1970;9(2):137–45.
133. Hoffman RW, Yang HK, Waggle KS, Durham JB, Burge JR, Walker SE. Band keratopathy in MRL/l and MRL/n mice. *Arthritis Rheum.* 1983;26(5):645–52.
134. Huang LH, Sery TW. Corneal degeneration in a congenitally diabetic inbred strain of mouse. *Br J Ophthalmol.* 1971;55(4):266–71.
135. Jester JV, Maurer JK, Petroll WM, Wilkie DA, Parker RD, Cavanagh HD. Application of in vivo confocal microscopy to the understanding of surfactant-induced ocular irritation. *Toxicol Pathol.* 1996;24(4):412–28.
136. Schmidt RE. Ophthalmic lesions in non-human primates. *Vet Pathol.* 1971;8(1):28–36.
137. Riley MV, Green K. Comparative physiology and biochemistry of the eye. In: Hockwin O, Green K, Rubin LF, editors. *Manual of oculotoxicity testing of drugs.* Stuttgart: Gustav Fischer Verlag; 1992. p. 45–80.
138. Weber U, Sons HU, Lenz W, Bernsmeier H. Experimental tyrosine keratopathy in rabbits. *Klin Monbl Augenheilkd.* 1986;188(6):587–9.
139. Beard ME, Burns RP, Rich LF, Squires E. Histopathology of keratopathy in the tyrosine-fed rat. *Invest Ophthalmol.* 1974;13(12):1037–41.
140. Lock EA, Gaskin P, Ellis M, Provan WM, Smith LL. Tyrosinemia produced by 2-(2-nitro-4-trifluoromethylbenzoyl)-cyclohexane-1,3-dione (NTBC) in experimental animals and its relationship to corneal injury. *Toxicol Appl Pharmacol.* 2006;215(1):9–16.

141. Kast A. Keratoconjunctivitis sicca and sequelae, mouse and rat. In: Jones TC, Mohr U, Hunt RD, editors. Monographs on pathology of laboratory animals: eye and ear. Berlin: Springer; 1991. p. 29–37.
142. Draize JH, Woodward G, Calvery HO. Method for the study of irritation and toxicity of substances applied topically to the skin and mucous membranes. *J Pharmacol Exp Ther.* 1944;82:377–90.
143. Gershbein LL, McDonald JE. Evaluation of the corneal irritancy of test shampoos and detergents in various animal species. *Food Cosmet Toxicol.* 1977;15(2):131–4.
144. Wilhelmus KR. The Draize eye test. *Surv Ophthalmol.* 2001;45(6):493–515.
145. Roggeband R, York M, Pericoi M, Braun W. Eye irritation responses in rabbit and man after single applications of equal volumes of undiluted model liquid detergent products. *Food Chem Toxicol.* 2000;38(8):727–34.
146. DeRosa AJ. Toxic keratopathy. *Int Ophthalmol Clin.* 1998;38(4):15–22.
147. Curren DR, Evans MG, Raabe H, Ruppalt RR, Harbell J. Correlation of histopathology, opacity, and permeability of bovine corneas exposed *in vitro* to known ocular irritants. *Vet Pathol.* 2000;37:557.
148. Sina JF, Galer DM, Sussman RG, Gautheron PD, Sargent EV, Leong B, et al. A collaborative evaluation of seven alternatives to the Draize eye irritation test using pharmaceutical intermediates. *Fundam Appl Toxicol.* 1995;26(1):20–31.
149. Maurer JK, Parker RD. Light microscopic comparison of surfactant-induced eye irritation in rabbits and rats at three hours and recovery/day 35. *Toxicol Pathol.* 1996;24(4):403–11.
150. Maurer JK, Parker RD, Carr GJ. Ocular irritation: microscopic changes occurring over time in the rat with surfactants of known irritancy. *Toxicol Pathol.* 1998;26(2):217–25.
151. Maurer JK, Parker RD. Microscopic changes with acetic acid and sodium hydroxide in the rabbit low-volume eye test. *Toxicol Pathol.* 2000;28(5):679–87.
152. Jester JV, Molai A, Petroll WM, Parker RD, Carr GJ, Cavanagh HD, et al. Quantitative characterization of acid- and alkali-induced corneal injury in the low-volume eye test. *Toxicol Pathol.* 2000;28(5):668–78.
153. Maurer JK, Molai A, Parker RD, Li L, Carr GJ, Petroll WM, et al. Pathology of ocular irritation with bleaching agents in the rabbit low-volume eye test. *Toxicol Pathol.* 2001;29(3):308–19.
154. Maurer JK, Molai A, Parker RD, Li LI, Carr GJ, Petroll WM, et al. Pathology of ocular irritation with acetone, cyclohexanol, parafluoroaniline, and formaldehyde in the rabbit low-volume eye test. *Toxicol Pathol.* 2001;29(2):187–99.
155. White E, Crosse MM. The aetiology and prevention of peri-operative corneal abrasions. *Anaesthesia.* 1998;53(2):157–61.
156. Guillet R, Wyatt J, Baggs RB, Kellogg CK. Anesthetic-induced corneal lesions in developmentally sensitive rats. *Invest Ophthalmol Vis Sci.* 1988;29(6):949–54.
157. Williams DL. Ocular disease in rats: a review. *Vet Ophthalmol.* 2002;5(3):183–91.
158. Fabian RJ, Bond JM, Drobeck HP. Induced corneal opacities in the rat. *Br J Ophthalmol.* 1967;51(2):124–9.
159. Roerig DL, Hasegawa AT, Harris GJ, Lynch KL, Wang RI. Occurrence of corneal opacities in rats after acute administration of l-alpha-acetylmethadol. *Toxicol Appl Pharmacol.* 1980;56(2):155–63.
160. Grant RL, Acosta D. Comparative toxicity of tetracaine, proparacaine and cocaine evaluated with primary cultures of rabbit corneal epithelial cells. *Exp Eye Res.* 1994;58(4):469–78.
161. Fraunfelder FT, Fraunfelder FW, Chambers WA. *Clinical ocular toxicology.* Philadelphia: Saunders Elsevier; 2008.
162. Zarfoss M, Bentley E, Milovancev M, Schmiedt C, Dubielzig R, McAnulty J. Histopathologic evidence of capecitabine corneal toxicity in dogs. *Vet Pathol.* 2007;44(5):700–2.
163. Pyrah IT, Kalinowski A, Jackson D, Davies W, Davis S, Aldridge A, et al. Toxicologic lesions associated with two related inhibitors of oxidosqualene cyclase in the dog and mouse. *Toxicol Pathol.* 2001;29(2):174–9.

164. Kirby TJ. Cataracts produced by triparanol. (MER-29). *Trans Am Ophthalmol Soc.* 1967;65:494-543.
165. Kirby Jr TJ, Achor RW, Perry HO, Winkelmann RK. Cataract formation after triparanol therapy. *Arch Ophthalmol.* 1962;68:486-9.
166. Funk J, Landes C. Histopathologic findings after treatment with different oxidosqualene cyclase (OSC) inhibitors in hamsters and dogs. *Exp Toxicol Pathol.* 2005;57(1):29-38.
167. Geiss V, Yoshitomo K. Eyes. In: Maronpot RR, Boorman GA, Gaul BW, editors. *Pathology of the mouse.* St. Louis: Cache River Press; 1999. p. 471-90.
168. Reindel JF, Gough AW, Pilcher GD, Bobrowski WF, Sobocinski GP, de la Iglesia FA. Systemic proliferative changes and clinical signs in cynomolgus monkeys administered a recombinant derivative of human epidermal growth factor. *Toxicol Pathol.* 2001; 29(2):159-73.
169. Patz A, Wulff LB, Rogers SW. Experimental production of ocular tumors. *Am J Ophthalmol.* 1959;48(1, Part 2):98-117.
170. Gupta BN. Scleral dermoid in a guinea pig. *Lab Anim Sci.* 1972;22(6):919-21.
171. Nichols CW, Yanoff M. Dermoid of a rat cornea. *Pathol Vet.* 1969;6(3):214-6.
172. Horikiri K, Ozaki K, Maeda H, Narama I. Corneal dermoid in two laboratory beagle dogs. *Jikken Dobutsu.* 1994;43(3):417-20.
173. Otto G, Lipman NS, Murphy JC. Corneal dermoid in a hairless guinea pig. *Lab Anim Sci.* 1991;41(2):171-2.
174. Styer CM, Ferrier WT, Labelle P, Griffey SM, Kendall LV. Limbic dermoid in a New Zealand white rabbit (*Oryctolagus cuniculus*). *Contemp Top Lab Anim Sci.* 2005;44(6):46-8.
175. Dunnick JK, Forbes PD, Eustis SL, Hardisty JF, Goodman DG. Tumors of the skin in the HRA/Skh mouse after treatment with 8-methoxypsoralen and UVA radiation. *Fundam Appl Toxicol.* 1991;16(1):92-102.
176. Porter R, Crombie AL. Corneal calcification as a presenting and diagnostic sign in hyperparathyroidism. *Br J Ophthalmol.* 1973;57(9):665-8.
177. O'Connor GR. Calcific band keratopathy. *Trans Am Ophthalmol Soc.* 1972;70:58-81.
178. Losco PE, Troup CM. Corneal dystrophy in Fischer 344 rats. *Lab Anim Sci.* 1988; 38(6):702-10.
179. Shibuya K, Sugimoto K, Satou K. Spontaneous ocular lesions in aged Crj:CD(SD)IGS rats. *Anim Eye Res (Jpn).* 2001;20(15-19):95-9.
180. Ocumpaugh DE, Obenberger J. Experimental corneal calcification: a radioautographic and histochemical study. *Clin Orthop Relat Res.* 1970;69:162-71.
181. Moore CP, Dubielzig R, Glaza SM. Anterior corneal dystrophy of American Dutch belted rabbits: biomicroscopic and histopathologic findings. *Vet Pathol.* 1987;24(1):28-33.
182. Port CD, Dodd DC. Two cases of corneal epithelial dystrophy in rabbits. *Lab Anim Sci.* 1983;33(6):587-8.
183. Fine BS, Berkow JW, Fine S. Corneal calcification. *Science.* 1968;162(3849):129-30.
184. Muirhead JR, Tomazzoli-Gerosa L. Animal models of band keratopathy. In: Tabbara K, Cello R, editors. *Animals models of band keratopathy.* Springfield: Charles C. Thomas Pub.; 1984. p. 221-32.
185. Obenberger J, Ocumpaugh DE, Cubberly MG. Experimental corneal calcification in animals treated with dihydrotachysterol. *Invest Ophthalmol.* 1969;8(5):467-74.
186. Economon JW, Silverstein AM, Zimmerman LE. Band keratopathy in a rabbit colony. *Invest Ophthalmol.* 1963;2:361-8.
187. Bruner RH, Keller WF, Stitzel KA, Sauers LJ, Reer PJ, Long PH, et al. Spontaneous corneal dystrophy and generalized basement membrane changes in Fischer-344 rats. *Toxicol Pathol.* 1992;20(3 Pt 1):357-66.
188. Friend J, Ishii Y, Thoft RA. Corneal epithelial changes in diabetic rats. *Ophthalmic Res.* 1982;14(4):269-78.
189. Obenberger J. Calcification in corneas with alloxan-induced vascularization. *Am J Ophthalmol.* 1969;68(1):113-9.
190. Meador VP, Tyler RD, Plunkett ML. Epicardial and corneal mineralization in clinically normal severe combined immunodeficiency (SCID) mice. *Vet Pathol.* 1992;29(3):247-9.

191. Davidson SI, Rennie IG. Ocular toxicity from systemic drug therapy. An overview of clinically important adverse reactions. *Med Toxicol.* 1986;1(3):217–24.
192. Johnston AM, Memon AA. Mystery of the blue pigmentation. *N Engl J Med.* 1999;340(20):1597–8.
193. Morrow GL, Abbott RL. Minocycline-induced scleral, dental, and dermal pigmentation. *Am J Ophthalmol.* 1998;125(3):396–7.
194. Sanchez AR, Rogers 3rd RS, Sheridan PJ. Tetracycline and other tetracycline-derivative staining of the teeth and oral cavity. *Int J Dermatol.* 2004;43(10):709–15.
195. Newkirk KM, Chandler HL, Parent AE, Young DC, Colitz CM, Wilkie DA, et al. Ultraviolet radiation-induced corneal degeneration in 129 mice. *Toxicol Pathol.* 2007;35(6):819–26.
196. Budiarto IT, Carlton WW, Tuite JF. Phototoxic syndrome induced in mice by rice cultures of *Penicillium viridicatum* and exposure to sunlight. *Pathol Vet.* 1970;7(6):531–46.
197. Klintworth GK, Burger PC. Neovascularization of the cornea: current concepts of its pathogenesis. *Int Ophthalmol Clin.* 1983;23(1):27–39.
198. Huang AJ, Li DQ, Li CH, Shang TY, Hernandez E. Modulation of corneal vascularization. *Ocul Surf.* 2005;3(4 Suppl):S190–3.
199. Niederkorn JY, Ubelaker JE, Martin JM. Vascularization of corneas of hairless mutant mice. *Invest Ophthalmol Vis Sci.* 1990;31(5):948–53.
200. Carter-Dawson L, Tanaka M, Kuwabara T, Bieri JG. Early corneal changes in vitamin A deficient rats. *Exp Eye Res.* 1980;30(3):261–9.
201. Leure-dupree AE. Vascularization of the rat cornea after prolonged zinc deficiency. *Anat Rec.* 1986;216(1):27–32.
202. Aguirre SA, Huang W, Prasanna G, Jessen B. Corneal neovascularization and ocular irritancy responses in dogs following topical ocular administration of an EP4-prostaglandin E2 agonist. *Toxicol Pathol.* 2009;37(7):911–20.
203. Kim TI, Chung JL, Hong JP, Min K, Seo KY, Kim EK. Bevacizumab application delays epithelial healing in rabbit cornea. *Invest Ophthalmol Vis Sci.* 2009;50(10):4653–9.
204. Garibaldi BA, Goad ME. Lipid keratopathy in the Watanabe (WHHL) rabbit. *Vet Pathol.* 1988;25(2):173–4.
205. Sebesteny A, Sheraidah GA, Trevan DJ, Alexander RA, Ahmed AI. Lipid keratopathy and atheromatosis in an SPF laboratory rabbit colony attributable to diet. *Lab Anim.* 1985;19(3):180–8.
206. Stock EL, Mendelsohn AD, Lo GG, Ghosh S, O'Grady RB. Lipid keratopathy in rabbits. An animal model system. *Arch Ophthalmol.* 1985;103(5):726–30.
207. Janes RG. Changes in the rabbit's eye caused by cholesterol feeding. *Am J Ophthalmol.* 1964;58:819–28.
208. Williams D, Sullivan A. Ocular disease in the guinea pig (*Cavia porcellus*): a survey of 1000 animals. *Vet Ophthalmol.* 2010;13(Suppl):54–62.
209. Spangler WL, Waring GO, Morrin LA. Oval lipid corneal opacities in beagles. *Vet Pathol.* 1982;19(2):150–9.
210. Roth AM, Ekins MB, Waring 3rd GO, Gupta LM, Rosenblatt LS. Oval corneal opacities in beagles. III. Histochemical demonstration of stromal lipids without hyperlipidemia. *Invest Ophthalmol Vis Sci.* 1981;21(1 Pt 1):95–106.
211. D'Amico DJ, Kenyon KR, Ruskin JN. Amiodarone keratopathy: drug-induced lipid storage disease. *Arch Ophthalmol.* 1981;99(2):257–61.
212. Turdumambetova G, Bredehorn T, Duncker GI. Ocular side-effects associated with amiodarone therapy. *Klin Monbl Augenheilkd.* 2005;222(6):485–92.
213. Mantyjärvi M, Tuppurainen K, Ikaheimo K. Ocular side effects of amiodarone. *Surv Ophthalmol.* 1998;42(4):360–6.
214. Lullmann H, Lullmann-Rauch R. Tamoxifen-induced generalized lipidosis in rats subchronically treated with high doses. *Toxicol Appl Pharmacol.* 1981;61(1):138–46.
215. Drenckhahn D, Jacobi B, Lullmann-Rauch R. Corneal lipidosis in rats treated with amphiphilic cationic drugs. *Arzneimittelforschung.* 1983;33(6):827–31.
216. Bicer S, Fuller GA, Wilkie DA, Yamaguchi M, Hamlin RL. Amiodarone-induced keratopathy in healthy dogs. *Vet Ophthalmol.* 2002;5(1):35–8.

217. Lullmann-Rauch R. Mucopolysaccharidosis (MPS) in ocular tissues as induced by amphiphilic di-cationic drugs. *Lens Eye Toxic Res.* 1990;7(3-4):263-79.
218. Hein L, Lullmann-Rauch R. Mucopolysaccharidosis and lipidosis in rats treated with tilorone analogues. *Toxicology.* 1989;58(2):145-54.
219. Kafarnik C, Murphy CJ, Dubielzig RR. Canine duplication of Descemet's membrane. *Vet Pathol.* 2009;46(3):464-73.
220. Gwin RM, Warren JK, Samuelson DA, Gum GG. Effects of phacoemulsification and extracapsular lens removal on corneal thickness and endothelial cell density in the dog. *Invest Ophthalmol Vis Sci.* 1983;24(2):227-36.
221. Yee RW, Geroski DH, Matsuda M, Champeau EJ, Meyer LA, Edelhauser HF. Correlation of corneal endothelial pump site density, barrier function, and morphology in wound repair. *Invest Ophthalmol Vis Sci.* 1985;26(9):1191-201.
222. Van Horn DL, Sendele DD, Seideman S, Bucu PJ. Regenerative capacity of the corneal endothelium in rabbit and cat. *Invest Ophthalmol Vis Sci.* 1977;16(7):597-613.
223. Joyce NC. Proliferative capacity of the corneal endothelium. *Prog Retin Eye Res.* 2003;22(3):359-89.
224. Sherrard ES, Rycroft PV. Retrocorneal membranes. I. Their origin and structure. *Br J Ophthalmol.* 1967;51(6):379-86.
225. Silbert AM, Baum JL. Origin of the retrocorneal membrane in the rabbit. *Arch Ophthalmol.* 1979;97(6):1141-3.
226. Hull DS, Green K, Laughter L. Cornea endothelial rose bengal photosensitization. Effect on permeability, sodium flux, and ultrastructure. *Invest Ophthalmol Vis Sci.* 1984;25(4):455-60.
227. Bartlett JD. Ophthalmic toxicity by systemic drugs. In: Chiou GCY, editor. *Ophthalmic toxicology.* New York: Raven Press, Ltd.; 1992. p. 175-81.
228. Hull DS, Csukas S, Green K. Chlorpromazine-induced corneal endothelial phototoxicity. *Invest Ophthalmol Vis Sci.* 1982;22(4):502-8.
229. Vonvoigtlander PF, Kolaja GJ, Block EM. Corneal lesions induced by antidepressants: a selective effect upon young Fischer 344 rats. *J Pharmacol Exp Ther.* 1982;222(1):282-6.
230. Olsen TW, Feng X, Wabner K, Conston SR, Sierra DH, Folden DV, et al. Cannulation of the suprachoroidal space: a novel drug delivery methodology to the posterior segment. *Am J Ophthalmol.* 2006;142(5):777-87.
231. French DD, Margo CE. Postmarketing surveillance rates of uveitis and scleritis with bisphosphonates among a national veteran cohort. *Retina.* 2008;28(6):889-93.
232. Chodosh J, Nordquist RE, Kennedy RC. Comparative anatomy of mammalian conjunctival lymphoid tissue: a putative mucosal immune site. *Dev Comp Immunol.* 1998;22(5-6):621-30.
233. Ruskell GL. Organization and cytology of lymphoid tissue in the cynomolgus monkey conjunctiva. *Anat Rec.* 1995;243(2):153-64.
234. Knop E, Knop N. The role of eye-associated lymphoid tissue in corneal immune protection. *J Anat.* 2005;206(3):271-85.
235. Knop N, Knop E. Conjunctiva-associated lymphoid tissue in the human eye. *Invest Ophthalmol Vis Sci.* 2000;41(6):1270-9.
236. Cain C, Phillips TE. Developmental changes in conjunctiva-associated lymphoid tissue of the rabbit. *Invest Ophthalmol Vis Sci.* 2008;49(2):644-9.
237. Fujihira S, Matsumoto M, Yoshizawa K, Oishi Y, Iwanami K, Fujii T. Naturally occurring ophthalmic lesions in cynomolgus monkeys used in toxicity and pharmacological studies. *Anim Eye Res Jpn.* 1994;13(3-4):147-54.
238. Shimoi A, Kakinuma C, Kuwayama C, Watanabe M. Comparison of spontaneous minor lesions in wild-caught and laboratory-bred monkeys. *J Toxicol Pathol.* 1998;11:85-94.
239. Flatt RE. Bacterial diseases. In: Weisbroth S, Flatt RE, Kraus AL, editors. *The biology of the laboratory rabbit.* New York: Academic Press; 1974. p. 194-236.
240. Strocchi P, Dozza B, Pecorella I, Fresina M, Campos E, Stirpe F. Lesions caused by ricin applied to rabbit eyes. *Invest Ophthalmol Vis Sci.* 2005;46(4):1113-6.

241. Prince JH, Eglitis I. The uvea. In: Prince JH, editor. The rabbit in eye research. Springfield: Charles C Thomas Pub.; 1964. p. 140–71.
242. Biros DJ. Ocular immunity. In: Gelatt KN, editor. Veterinary ophthalmology. 4th ed. Ames: Blackwell Publishing; 2007. p. 223–35.
243. Park SA, Jeong SM, Yi NY, Kim MS, Jeong MB, Suh JG, et al. Study on the ophthalmic diseases in ICR mice and BALB/c mice. *Exp Anim*. 2006;55(2):83–90.
244. Jeong MB, Kim NR, Yi NY, Park SA, Kim MS, Park JH, et al. Spontaneous ophthalmic diseases in 586 New Zealand white rabbits. *Exp Anim*. 2005;54(5):395–403.
245. Rubin LF, Weisse I. Species differences relevant for ocular toxicity studies. In: Hockwin O, Green K, Rubin LF, editors. Manual of oculotoxicity testing of drugs. Stuttgart: Gustav Fischer Verlag; 1992.
246. Brown SM. Increased iris pigment in a child due to latanoprost. *Arch Ophthalmol*. 1998;116(12):1683–4.
247. Eisenberg DL, Camras CB. A preliminary risk-benefit assessment of latanoprost and unoprostone in open-angle glaucoma and ocular hypertension. *Drug Saf*. 1999;20(6):505–14.
248. Stjerschantz JW, Albert DM, Hu DN, Drago F, Wistrand PJ. Mechanism and clinical significance of prostaglandin-induced iris pigmentation. *Surv Ophthalmol*. 2002;47 Suppl 1:S162–75.
249. Lindquist NG, Larsson BS, Stjerschantz J. Increased pigmentation of iridial melanocytes in primates induced by a prostaglandin analogue. *Exp Eye Res*. 1999;69(4):431–6.
250. Gesundheit B, Greenberg M. Medical mystery: brown eye and blue eye—the answer. *N Engl J Med*. 2005;353(22):2409–10.
251. Roe FJ, Millican D, Mallett JM. Induction of melanotic lesions of the iris in rats by urethane given during the neonatal period. *Nature*. 1963;199:1201–2.
252. Koizumi H, Watanabe M, Numata H, Sakai T, Morishita H. Species differences in vacuolation of the choroid plexus induced by the piperidine-ring drug disubutamide in the rat, dog, and monkey. *Toxicol Appl Pharmacol*. 1986;84(1):125–48.
253. Render JA, Carlton WW. Toxic effects of 6-aminonicotinamide, uvea, rabbit. In: Jones TC, Mohr U, Hunt RD, editors. Monographs on pathology of laboratory animals: eye and ear. Berlin: Springer; 1991. p. 50–4.
254. Gopinath C, Prentice DE, Lewis DJ. The eye and ear. In: Gopinath C, Prentice DE, Lewis DJ, editors. Atlas of experimental toxicological pathology. Lancaster: MTP Press; 1987. p. 145–55.
255. Potts AM, Gonasun LM. Toxic responses of the ocular and visual system. In: Duoll J, Klaassen CD, Amdur MO, editors. Toxicology: the basic science of poisons. New York: MacMillan; 1980. p. 275–310.
256. Fraunfelder FW, Rosenbaum JT. Drug-induced uveitis. Incidence, prevention and treatment. *Drug Saf*. 1997;17(3):197–207.
257. Heywood R. Clinical and laboratory assessment of visual dysfunction. In: Hayes AC, editor. Toxicology of the eye, ear and other special sense organs. New York: Raven Press, Ltd; 1985. p. 61–77.
258. Levine S. Cyclitis induced by cyclophosphamide, rat. In: Jones TC, Mohr U, Hunt RD, editors. Monographs on pathology of laboratory animals: eye and ear. Berlin: Springer; 1991. p. 38–9.
259. McMaster PR, Wong VG, Owens JD. The propensity of different strains of guinea pigs to develop experimental autoimmune uveitis. *Mod Probl Ophthalmol*. 1976;16:62–71.
260. Sinha DP, Cartwright ME, Johnson RC. Incidental mononuclear cell infiltrate in the uvea of cynomolgus monkeys. *Toxicol Pathol*. 2006;34(2):148–51.
261. Rubin LF. Atlas of veterinary ophthalmoscopy. Philadelphia: Lea and Febiger; 1974.
262. Pleština R, Piuković-Pleština M, Roberts DV. Effect of anticholinesterase pesticides on the eye and on vision. *Crit Rev Toxicol*. 1978;6(1):1–23.
263. Rungby J. Experimental argyrosis: ultrastructural localization of silver in rat eye. *Exp Mol Pathol*. 1986;45(1):22–30.
264. Faccini JM. Mouse histopathology. Philadelphia: Elsevier Science; 1990.

265. Griffith JW, Sassani JW, Bowman TA, Lang CM. Osseous choristoma of the ciliary body in guinea pigs. *Vet Pathol.* 1988;25(1):100–2.
266. Brooks DE, McCracken MD, Collins BR. Heterotopic bone formation in the ciliary body of an aged guinea pig. *Lab Anim Sci.* 1990;40(1):88–90.
267. Donnelly KB, Berridge B, Long GG, Schafer KA, Reynolds VL, Sullivan JM, et al. Peroxisome proliferator activated receptor gamma (PPAR γ) agonist-mediated ocular choroid adiposity: Strain sensitivity differences between Fischer 344 and Sprague-Dawley rats. *Toxicol Pathol.* 2007;35(1):189.
268. Hadjikitoutis S, Morgan JE, Wild JM, Smith PE. Ocular complications of neurological therapy. *Eur J Neurol.* 2005;12(7):499–507.
269. Peckman JC. The rabbit: pathology. In: Gad SC, editor. *Animal models in toxicology.* Boca Raton: CRC/Taylor and Francis; 2007. p. 449–74.
270. Gelatt KN, Gum GG, Gwin RM, Bromberg NM, Merideth RE, Samuelson DA. Primary open angle glaucoma: inherited primary open angle glaucoma in the beagle. *Am J Pathol.* 1981;102(2):292–5.
271. Lindsey JR, Fox RR. Inherited diseases and variations. In: Manning PJ, Ringler DH, Newcomer CE, editors. *The biology of the laboratory rabbit.* New York: Academic Press; 1994. p. 239–319.
272. Suckow MA, Douglas FA. *The laboratory rabbit.* Boca Raton: CRC Press; 1997.
273. McMenamin PG. Dendritic cells and macrophages in the uveal tract of the normal mouse eye. *Br J Ophthalmol.* 1999;83(5):598–604.
274. McMenamin PG. The distribution of immune cells in the uveal tract of the normal eye. *Eye (Lond).* 1997;11(Pt 2):183–93.
275. Butler TL, McMenamin PG. Resident and infiltrating immune cells in the uveal tract in the early and late stages of experimental autoimmune uveoretinitis. *Invest Ophthalmol Vis Sci.* 1996;37(11):2195–210.
276. Pras E, Neumann R, Zandman-Goddard G, Levy Y, Assia EI, Shoenfeld Y, et al. Intraocular inflammation in autoimmune diseases. *Semin Arthritis Rheum.* 2004;34(3):602–9.
277. John SW, Smith RS, Savinova OV, Hawes NL, Chang B, Turnbull D, et al. Essential iris atrophy, pigment dispersion, and glaucoma in DBA/2 J mice. *Invest Ophthalmol Vis Sci.* 1998;39(6):951–62.
278. Lutjen-Drecoll E, Tamm E. Morphological study of the anterior segment of cynomolgus monkey eyes following treatment with prostaglandin F $_2$ alpha. *Exp Eye Res.* 1988;47(5):761–9.
279. Heywood R. Drug-induced retinopathies in the Beagle dog. *Br Vet J.* 1974;130(6):564–9.
280. Heywood R. An anomaly of the ocular fundus of the Beagle dog. *J Small Anim Pract.* 1972;13(4):213–5.
281. Bellhorn RW, Bellhorn MB, Swarm RL, Impellizzeri CW. Hereditary tapetal abnormality in the beagle. *Ophthalmic Res.* 1975;7:250–60.
282. Schiavo DM. Retinopathy from administration of an imidazoquinazoline to beagles. *Toxicol Appl Pharmacol.* 1972;23(4):782–3.
283. Haggerty GC, Peckman JC, Thomassen RW, Gad SC. The dog. In: Gad SC, editor. *Animal models in toxicology.* 3rd ed. Boca Raton: CRC Press; 2007. p. 563–662.
284. Heywood R, Hepworth PL, Van Abbe NJ. Age changes in the eyes of the Beagle dog. *J Small Anim Pract.* 1976;17(3):171–7.
285. Delahunt CS, Stebbins RB, Anderson J, Bailey J. The cause of blindness in dogs given hydroxypyridinethione. *Toxicol Appl Pharmacol.* 1962;4:286–91.
286. Moe RA, Kirpan J, Linegar CR. Toxicology of hydroxypyridinethione. *Toxicol Appl Pharmacol.* 1960;2:156–70.
287. Budinger JM. Diphenylthiocarbazone blindness in dogs. *Arch Ophthalmol.* 1961;71:304–10.
288. Snyder FH, Buehler EV, Winek CL. Safety evaluation of zinc 2-pyridinethiol 1-oxide in a shampoo formulation. *Toxicol Appl Pharmacol.* 1965;7:425–37.

289. Schiavo DM, Green JD, Traina VM, Spaet R, Zaidi I. Tapetal changes in beagle dogs following oral administration of CGS 14796 C, a potential aromatase inhibitor. *Fundam Appl Toxicol.* 1988;10(2):329–34.
290. Dillberger JE, Peiffer RL, Dykstra MJ, O'Mara M, Patel DK. The experimental antipsychotic agent 1192U90 targets tapetum lucidum in canine eyes. *Toxicol Pathol.* 1996;24(5):595–601.
291. Cloyd GG, Wyman M, Shaddock JA, Winrow MJ, Johnson GR. Ocular toxicity studies with zinc pyridinethione. *Toxicol Appl Pharmacol.* 1978;45(3):771–82.
292. Saint-Macary G, Berthoux C. Ophthalmologic observations in the young Yucatan micropig. *Lab Anim Sci.* 1994;44(4):334–7.
293. Hubert MF, Gillet JP, Durand-Cavagna G. Spontaneous retinal changes in Sprague Dawley rats. *Lab Anim Sci.* 1994;44(6):561–7.
294. Bellhorn RW. Survey of ocular findings in 16- to 24-week-old beagles. *J Am Vet Med Assoc.* 1973;162(2):139–41.
295. Everitt JI, Shaddock JA. Melanoma of the uvea, rat. In: Jones TC, editor. *Monographs on pathology of laboratory animals: eye and ear.* Berlin: Springer; 1991. p. 40–3.
296. Owen RA, Duprat P. Leiomyoma of the iris, Sprague-Dawley rat. In: Jones TC, Mohr U, Hunt RD, editors. *Monographs on pathology of laboratory animals: eye and ear.* Berlin: Springer; 1991. p. 47–9.
297. Yoshitomi K, Boorman GA. Intraocular and orbital malignant Schwannomas in F344 rats. *Vet Pathol.* 1991;28(6):457–66.
298. Congdon CC, Lorenz E. Leukemia in guinea-pigs. *Am J Pathol.* 1954;30(2):337–59.
299. Steinberg H. Disseminated T-cell lymphoma in a guinea pig with bilateral ocular involvement. *J Vet Diagn Invest.* 2000;12(5):459–62.
300. Peiffer RL, Pohm-Thorsen L, Corcoran K. Models in ophthalmology and vision research. In: Manning PJ, Ringler DH, Newcomer CE, editors. *The biology of the laboratory rabbit.* 2nd ed. New York: Academic Press; 1994. p. 410–33.
301. Squire RA, Goodman DG, Valerio MG, Fredrickson TN, Strandberg JD, Levitt MH, et al. Tumors. In: Benirschke K, Gamer FM, Jones TC, editors. *Pathology of laboratory animals.* New York: Springer; 1978. p. 1051–252.
302. Ernst H, Rittinghausen S, Mohr U. Melanoma of the eye, mouse. In: Jones TC, Mohr U, Hunt RD, editors. *Monographs on pathology of laboratory animals: eye and ear.* Berlin: Springer; 1991. p. 44–7.
303. Albert DM, Gonder JR, Papale J, Craft JL, Dohlman HG, Reid MC, et al. Induction of ocular neoplasms in Fischer rats by intraocular injection of nickel subsulfide. *Invest Ophthalmol Vis Sci.* 1982;22(6):768–82.
305. Albert DM, Puliafito CA, Haluska FG, Kimball GP, Robinson NL. Induction of ocular neoplasms in Wistar rat by N-methyl-N-nitrosourea. *Exp Eye Res.* 1986;42(1):83–6.

Chapter 6

Toxicologic Pathology of the Eye: Alterations of the Lens and Posterior Segment

Kenneth A. Schafer and James A. Render

Abstract The identification of microscopic toxicologic changes in the lens and posterior segment is influenced by many factors. Important factors include *in vivo* procedures, such as route of administration, and procedures involved in preparation of the eye for microscopic examination which have been discussed in the previous chapter. A wide variety of toxins may affect the lens and posterior segment, but toxic changes must be differentiated from iatrogenic and spontaneous changes. Both the toxic and spontaneous changes may be influenced by the type of species, strain of animal, or an animal's age. Understanding these differences, as well as knowledge of the normal anatomy, physiology, and function of ocular structures, will help in detecting toxicologic changes. This chapter is a continuation of the previous chapter with a focus on findings of the lens and posterior segment of the eye.

6.1 Introduction

As indicated in the previous chapter, the detection and identification of microscopic toxicologic changes are influenced by many factors. This is especially true for changes in the lens and structures of the posterior chamber. The detection of microscopic findings of the lens requires an awareness of clinical ocular findings observed via ophthalmoscopy and slit lamp biomicroscopy. For detection of findings in the posterior segment of the eye, it is important to have knowledge of the clinical findings observed via direct and indirect ophthalmoscopy [1–4]. These methods, along with additional techniques used in ophthalmology, can detect the exact

K.A. Schafer, D.V.M., DACVP, FIATP (✉)
Vet Path Services, Inc., Mason, OH, USA
e-mail: kschafer@vetpathservicesinc.com

J.A. Render, D.V.M., Ph.D., DACVP
NAMSA, Northwood, OH, USA

location of findings and thus challenge the pathologist to provide a microscopic correlate. As discussed in the previous chapter, detection of microscopic changes requires good communication among the clinical examiner, the pathology technical staff, and the pathologist. The preparation of good quality histologic sections is necessary for detailed histologic evaluation. Specialized structures, such as the retinal macula of primates, need to be examined, and examination of a cross section of the optic nerve will help in assessing the health of retinal ganglion cells.

6.2 Lens

There are many references covering the embryology, anatomy, physiology, and biochemistry of the lens [3, 5–13]. The lens epithelium proliferates to form lens fibers throughout the life of the animal. This results in compression of the lens nucleus and eventually hardening (i.e., nuclear sclerosis). Throughout life, the anterior lens epithelium continues to deposit basement membrane causing thickening. Focal proliferation of lens epithelium may occur, especially in rats.

Terms used to describe changes in the lens should be descriptive and accurate. For example, a gross loss of transparency of the lens should be referred to as a lenticular opacity, since the finding may be reversible (i.e., cold cataract) or irreversible (i.e., cataract) [14–16]. Microscopically, features such as liquefaction and globule formation in the lenticular cortex are considered to represent lenticular cortical degeneration, and the combination of clinical and microscopic findings indicate that the lenticular change is a permanent change (i.e., cataract). Use of precise diagnostic terms for ocular findings helps to eliminate confusion.

6.2.1 *Reversible Lenticular Opacification*

Reversible opacification of the lens may be induced by various stimuli including cold temperature, anoxia, asphyxia, dehydration, stress, and drugs [17]. Microscopically, reversible changes include prominent suture lines from the swelling of adjacent lens fibers, minimal swelling of individual lens fibers in the outer cortex without any degenerative or other microscopic changes. A cold cataract is a reversible change in the lens especially in rodents. The lenses appear opaque, but microscopically, there are no changes, and the opacity is reversible.

There are several compounds that cause acute reversible white clouding of the anterior rodent lens within 1 or 2 hours, including opiates, opioids, and phenothiazine [18]. The loss of transparency of the anterior lens may be due to temporary decreases in hydration from an arrest in blinking resulting in excessive exposure and evaporation from the front of the eye. Swelling of individual lens fibers without degenerative changes may be observed microscopically. In addition, triparanol-induced opacities are sometimes reversible [19].

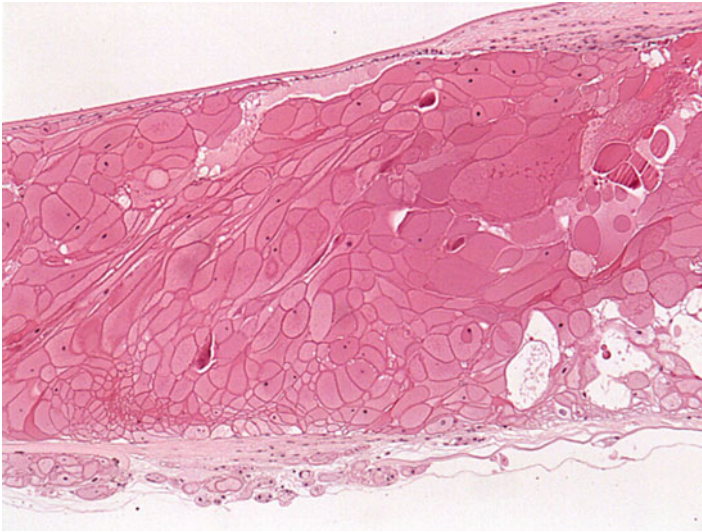


Fig. 6.1 Lens from a monkey with spontaneously occurring cataracts. Histologic changes in the lens include swelling of lens fibers (bladder cells), vacuolation, and proliferation of lens epithelium (upper right). H&E. 10× objective

6.2.2 Microscopic Lenticular Findings

Any lenticular finding, including cataract, should be characterized as unilateral or bilateral, focal or diffuse, and whether it involves the capsule; subcapsular epithelium; posterior subcapsular cortex; anterior, equatorial, or posterior cortex; or nucleus. Irreversible microscopic changes that likely correlate with opacity include bladder cells, clefts, vacuoles, liquefaction, lens fiber fragmentation, Morgagnian globules, collapse of the lens capsule, and dystrophic mineralization. Changes characteristic of a cataract generally include degeneration and necrosis of lenticular fibers but may involve the lenticular epithelium (Fig. 6.1). Lenticular epithelial cells can migrate along the posterior capsule and undergo proliferation with or without fibrous metaplasia (Fig. 6.2). The degree of involvement varies from minimal to marked [20].

6.2.3 Spontaneous Lenticular Opacities

It is common for lenticular opacities to occur in rodents [21]. Mice appear to develop more lenticular opacities than rats, and minor opacities are common in young mice [22]. Diffuse opacification and vacuoles around suture lines occur with increasing age of mice, and lenticular opacities may be strain specific (e.g., Crl:CD1[®](ICR)BR mice) [22].



Fig. 6.2 Lens from a rabbit 2 weeks after a lensectomy procedure. Portions of the transparent implanted intraocular lens are visible (arrowhead). The anterior lenticular epithelium is hyperplastic and undergoing fibrous metaplasia. Lens fibers that were not removed during the procedure are swollen. H&E. 10× objective

Various types of optical changes are considered to be background changes in the lens of rats, and some may be inherited [23]. Spontaneous changes in the lens may involve the cortex with loss of transparency or be associated with lens capsule rupture [21, 24]. Changes associated with anterior suture lines are common in older rats [20, 25, 26], and opacities involving the anterior suture lines appear to be common in spontaneously hypertensive rats [27]. Lesions of the posterior cortex may occur in the rat, especially young rats that have focal opacities associated with remnants of hyaloid vessels [20, 21]. Posterior capsular cataract appears as one or more small granular plaques and is common in older animals [21]. Swollen lens fibers are observed in a peripheral arcuate pattern in Sherman rats and as striations in the anterior cortex in Sprague-Dawley rats [20, 26, 28].

Other laboratory animals may develop spontaneous lenticular opacities. Hamsters have few spontaneous opacities, but spontaneous opacities of anterior cortex and nucleus occur in young hamsters, and striations within the cortex and posterior cortical cataract occurs with advancing age in hamsters [21]. Congenital cataracts are reported in the guinea pig [29]. Posterior cortical pinpoint lens opacities have been described in the Götting minipig and Yucatan micropig [30].

In Beagles, anterior and posterior suture opacities have been described in animals at approximately 15 weeks to 3 years [31–36]. Bilateral vacuoles or punctate opacities near suture lines at the periphery of the posterior cortex occur in young laboratory beagles, and age-related lenticular changes are well characterized in laboratory beagle dogs [21]. Posterior sutures may be pronounced in very young

dogs [31, 32] and in older dogs [21, 33]. Cataracts that occur in young beagles often involve the posterior aspect of the lens and may be pinpoint [21, 34]. Findings include posterior polar subcapsular streaks or small plaques [35]. Posterior capsular and cortical opacities increase with age in the beagle dog [21, 33, 36].

With the continuous production of lens fibers, there is constant compression of the lenticular nucleus, and the optical density of the nucleus increases slowly with age (i.e., nuclear sclerosis) [20, 26]. Nuclear sclerosis must be differentiated from nuclear cataract. Nuclear cataract can occur, especially in rodents, and is more common in mice than rats. Spontaneous nuclear cataracts are rare in rats but do occur in Sprague-Dawley rats. Unilateral nuclear cataract has been reported as age-related in Sprague-Dawley rats. Inherited nuclear cataracts also occur in Sprague-Dawley rats [21, 27, 37]. Nuclear opacities occur in spontaneous hypertensive rats of the Okomoto strain, and nuclear cataract has been observed in hamsters [21]. A nonprogressive focal opacity of the fetal nucleus has been reported in beagles, but focal opacities and spontaneous nuclear cataracts are rare [25]. Focal nuclear opacities occur in Göttingen minipig [38], dog, Sprague-Dawley rat, and Yucatan micropig. Increases in nuclear densities after 1 year have been reported in the rat [25].

Granulomatous inflammation focused on the lens occurs in rabbits, especially dwarf rabbits, and occurs with rupture of the lens capsule (i.e., phacoclastic uveitis) [39]. Although not always detected in the affected globe, *Encephalitozoon cuniculi* is thought to be the cause. Although the pathogenesis is not completely understood, vertical transmission occurring during lens development is a possible source of the infection.

Aging associated with cataract formation has been reviewed [40] and is thought to be the net result of oxidative stress [24]. Oxidative stress decreases superoxide dismutase and GSH activities, increases free radical formation, and increases protein aggregation [40–42]. The Emory mouse is a model for age-related cataract in humans.

6.2.4 Lenticular Toxicity

Only a few substances have been shown to cause cataract in humans, but many compounds have been shown to cause cataract in animals [18, 43–45]. This may be due to the large number of compounds tested in animals. Cataract may be caused by many different mechanisms and may be induced in laboratory animals by various factors [18, 46, 47]. Factors influencing cataract formation include aging, disrupted metabolism, nutritional deficiency, and exposure to oxygen radicals, X-ray radiation, microwave radiation, gamma radiation, and UVA or UVB light [18, 46, 48, 49].

“Sugar” cataract is produced by high concentrations of galactose, xylose, or glucose and has been demonstrated in rats [18, 48]. These sugars are converted to sugar alcohols which become trapped in the lens and osmotically attract water into the lens. This results in excessive hydration, swelling of cells and fibers, and fluid between fibers. High lens glucose is metabolized by aldose reductase pathway to sorbitol, and increased amounts of sorbitol causes hyperosmotic stress on lens fibers with the potential for cataract. The high blood glucose conditions of diabetes mellitus

or induced by administration of alloxan or streptozotocin cause persistent hyperglycemia and eventually a “sugar” cataract in rats and rhesus monkeys [48, 50]. Polyol (sugar alcohols such as sorbitol and xylitol) accumulation and protein glycation in diabetic mice have been described as well [41]. In addition to increased sugars, tryptophan deficiency can cause cataract in the rat [51].

Several compounds cause cataract. Acetaminophen causes cataract by decreasing GSH levels [18]. Naphthalene causes cataract through a P450-glutathione-dependent mechanism [52] and is cataractogenic and retinotoxic (retinal edema) in the rabbit [53]. Diquat induces the production of free radicals and structural changes in lens fibers in the rat and dog [50]. Repeated subcutaneous injections of buthionine sulfoximine causes osmotic swelling along suture boundaries in the anterior cortex but eventually spreads to the rest of the lens [24]. Administration of phenylalanine or chlorophenylalanine results in a protein disturbance and cataract [50]. Disruption of lipid metabolism may result in cataract. Triparanol inhibits cholesterol synthesis and thus cell membrane production [48]. Administration of aminopyridine inhibits oxidosqualene cyclase and blocks cholesterol synthesis at hydroxymethylglutaryl-coenzyme A (HMGCoA). The result is necrosis and swelling of fibers at equator [50]. U18666A, an inhibitor of enzymatic reduction of desmosterol to cholesterol, produces permanent nuclear cataract. Agents that cause hypolipemia, such as styryl-hexahydroindolinol and AY-9944, have been associated with cataracts [54].

Cataract formation may have multiple causes. Selenite causes nuclear cataract in young rats [55]. Inhibition of enzymes or disruption in protein metabolism causes cataract and may be due to compounds such as chlorophenylalanine, phenylhydrazopropionitrile, mimosine, and naphthalene [18]. Administration of naphthoquinone inhibits Na/K-ATPase leading to an electrolyte disturbance and osmotic swelling of lens fibers [50]. Radiomimetic cataracts are similar to those produced by radiation [18]. Compounds that produce this effect include busulfan, dibromomannitol, dimethylaminostyrylquinoline, iodoacetate, nitrogen mustard, tretamine, and triaziquone. Posterior subcapsular cataract is produced by a variety of glucocorticoids in humans, but these are difficult to replicate in animals [18]. Uncoupling of oxidative phosphorylation caused by 2,4-dinitrophenol produces cataract in humans, but not in the dog and rat [50].

6.2.5 Lenticular Epithelial Alterations

Changes in uniformity, such as swelling of lens fibers and variation in shapes of lens cells, may be noted in the germative zone before opacity occurs. Lenticular epithelial cells may undergo focal hyperplasia in older rats. Administration of 4-diethylaminoethoxy- α -ethyl-benzhydrol to rats caused inflammation of the cornea and anterior uvea with secondary lenticular epithelial proliferation followed by pyknosis and fiber degeneration. Perturbation of cell division may occur following ionizing radiation or the administration of 4-*p*-dimethylaminostyryl and busulfan [50]. UV light is a possible factor in age-related cataracts because UVB radiation causes epithelium to undergo apoptosis and hyperplasia, as well as anterior suture

disintegration. Vacuolation of lens epithelium occurs following administration of SK&F 86466, an alpha2 adrenoreceptor antagonist. Antineoplastic antimetabolic agents affect mitotically active cells in the germative zone of lens epithelium with changes noted at the equator [18]. Lenticular epithelial cells may undergo focal proliferation in the aged rat or following surgery or trauma (Fig. 6.2).

Neoplasms of the lens do not appear to occur spontaneously in laboratory animals.

6.2.6 Lens Capsule Alterations

The lens capsule is continuously produced by the anterior lens epithelium, such that the anterior capsule will increase in thickness with age and may be notably thicker than the posterior capsule. With intraocular surgical techniques in preclinical studies, there is the potential for nicks in the lens capsule, which may result in adjacent opacities and lens fiber changes. Infrequently, intravitreal injections of some soluble therapeutics may diffuse into the lens capsule and produce abnormal staining, although producing no ophthalmologic changes. One example is basophilic staining of the lens capsule and optic disc following intravitreal injection of oligonucleotides (Figs. 6.3 and 6.4).

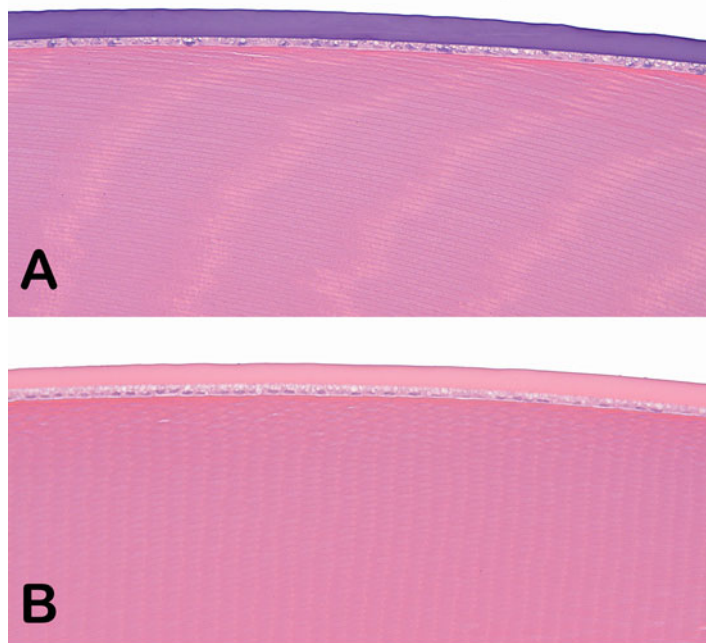


Fig. 6.3 Lenses from rabbits on an intravitreal injection study. (a) The soluble test article tended to accumulate in the lens capsule and caused basophilic staining. (b) Lens capsule of a vehicle-treated rabbit was unremarkable. No abnormal ophthalmic examination findings were observed. H&E. 20× objective

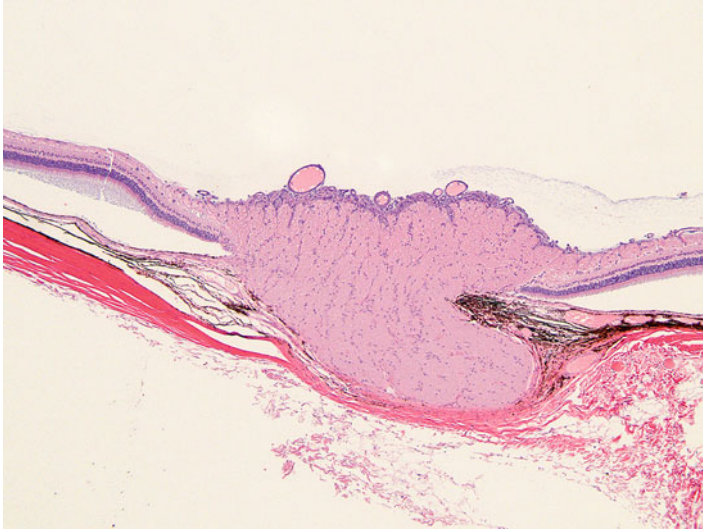


Fig. 6.4 The optic disc from the same rabbit in Fig. 6.3a. The inner limiting membrane was basophilic. No fundusoscopic examination correlates were observed. H&E. 5× objective

6.3 Vitreous Body

The vitreous humor is a transparent, jellylike material that fills the vitreous chamber [3, 5, 13, 56]. Alterations of the vitreous may be congenital, spontaneous, or iatrogenic associated with drug administration.

6.3.1 *Spontaneous Vitreal Alterations*

Many of the spontaneous background findings involving the vitreous body are various types of remnants of embryological structures, especially the hyaloid vessels. The embryologic vessels surrounding the developing lens (the tunica vasculosa lentis), hyaloid vessels, or both may persist. If there is a proliferation of connective tissue in addition to the blood vessels, the finding is classified as persistent hyperplastic primary vitreous (PHPV). This finding has been reported in the Sprague-Dawley rat [57]. Persistent hyaloid vessels have been reported in rats [20, 25, 57–60], Swiss mice [22], Göttingen minipigs [38], and Yucatan micropigs [61] but is a common congenital finding in many species. Persistent hyaloid vessels are rare in laboratory primates [53]. In the rat, there are patent hyaloid arteries that persist up to 6 days of age and close between 1 and 3 weeks [20]. Remnants of the hyaloid vessels are still present at 6 weeks in a majority (60%) of rats with a few (2%) containing blood. By the age of 26 weeks, a few (5–6%) of the rats have hyaloid remnants and an occasional rat (1%) will have a hyaloid remnant at 1 year of age.

Intravitreal hemorrhage is rare in dogs but common in rats [53]. Vascularization of the vitreous may cause intravitreal bleeding which may lead to vitreal traction bands on the retina. When hyaloid vessels are patent, blood extends into the vitreous. This is the main cause of vitreous hemorrhage reported in the mouse [Cri:CD1(ICR)BR] [22] and rat [20, 57, 58]. Erythrocytes are engulfed by phagocytic cells resulting in brown-pigmented cells in the vitreous [57]. Persistent hyperplastic vitreous causes defects in the posterior lens capsule which may result in a posterior polar cataract [53]. Preretinal arteriolar loops which extend into the vitreous are uncommon findings in beagles and can be detected during the pretest study period. They are caused by a defect in the inner limiting membrane of the retina [53].

In humans, rheological (the gel-liquid state of the vitreous) changes may occur in the central vitreous. A liquefaction process may occur in dogs and may cause separation of the posterior cortex from the retinal inner limiting membrane, predisposing to retinal tears and rhegmatogenous retinal detachment [5]. Hyaluronic acid provides viscoelasticity but also acts as a barrier to the diffusion of macromolecules into the vitreous, unless that barrier is disrupted by trauma. The vitreous is a storage site for retinal metabolites and protects the lens and retina from toxic compounds. Pathologic processes leading to decreased hyaluronic acid concentration and vitreal liquefaction will affect the nutrient supply, waste removal, and drug delivery in the posterior segment. In most species, holes and liquefaction (i.e., syneresis) occur in older individuals, especially in the central or intermediate zones [5].

Asteroid bodies or asteroid hyalosis are small, opaque bodies consisting of calcium-lipid complexes within the vitreous. These have been described in beagles 3–8 years of age [21, 33, 62]. Fibrosis and calcification of the vitreous are occasionally seen in the rat, mouse, and hamster [21].

6.3.2 Iatrogenic Vitreal Findings

Most of the changes in the vitreous in ophthalmic studies are iatrogenic and due to the administration of a compound or device to treat the retina [63]. These findings include inflammation, plasmoid vitreous, hemorrhage, liquefaction, and displacement (possibly causing retinal detachment). Inflammatory infiltrates often consist of macrophages, which will phagocytose and attempt to clear poorly soluble materials via migration out the optic nerve. Inflammatory infiltrates and hemorrhage may lead to progressive neovascularization [21]. The vitreous may prolapse through intravitreal injection tracks.

6.3.3 Toxicologic Vitreal Findings

In addition to the physical changes associated with the intravitreal administration of a compound, there may be a toxic effect involving the vitreous and the adjacent structures (i.e., the lens and retina). Intravitreal injection of commercially available ketorolac tromethamine in rabbits resulted in retinal toxicity [64].

6.4 Retina

There are many references covering the embryology, anatomy, physiology, and biochemistry of the retina, and retinal anatomy is also covered elsewhere in this book [3, 5, 13, 65]. In general, the retinal structure is similar among species, but there are a few differences in ocular anatomy among laboratory animal species, for example, the macula in primates [5, 66]. The retina consists of the inner transparent sensory (neurosensory) retina and the outer retinal pigmented epithelium (RPE) separated by a potential space, the subretinal space. Axons of retinal ganglion cells converge to form the optic nerve. The peripheral sensory retina abruptly becomes the inner ciliary epithelium and the RPE abruptly becomes the pigmented ciliary epithelium at the ora ciliaris (ora serrata in humans and nonhuman primates).

The layers of the retina, from external to internal, are the RPE, the photoreceptor layer (i.e., layer of rods and cones), the outer limiting membrane (OLM), the outer nuclear layer (ONL), the outer plexiform layer (OPL), the inner nuclear layer (INL), the inner plexiform layer (IPL), the ganglion cell layer (GCL), the nerve fiber layer (NFL), and the inner limiting membrane (ILM).

Generally, morphologic changes in the retina are permanent, so early detection of toxicity is important [67]. The primary methods of clinically evaluating the retina for toxicity are indirect ophthalmoscopy (fundoscopy) and flash electroretinogram (ERG), although clinical evaluation may also involve fluorescein angiography, confocal scanning laser tomography, ultrasonography, and optical coherence tomography [2, 53, 66, 68, 69].

Terms used to describe changes in the retina should be descriptive and accurate. For example, the outer displacement of a photoreceptor nucleus into the layer of inner and outer segments should be referred to as photoreceptor displaced nuclei which may be normal or may be one of several changes that may cumulatively be referred to as retinal degeneration. Since the retina is composed of many different types of cells, the use of retinal degeneration may be a vague term. For one study, retinal degeneration might represent loss of ganglion cells, and in another study, retinal degeneration might represent changes associated with photoreceptors. Use of precise diagnostic terms for retinal findings helps to eliminate confusion.

6.4.1 *Spontaneous Retinal Alterations*

Retinal findings generally involve retinal vessels, photoreceptors, or ganglion cells. Spontaneous findings need to be differentiated from treatment-related toxicities. Vascular findings are often a reflection of a systemic condition such as spontaneous preretinal arteriolar loops in dogs or possibly alterations associated with atherosclerosis such as calcification or changes associated with hypertension leading to hemorrhage or edema. Occasionally, spontaneous retinal changes are observed without a clear pathogenesis (Fig. 6.5).

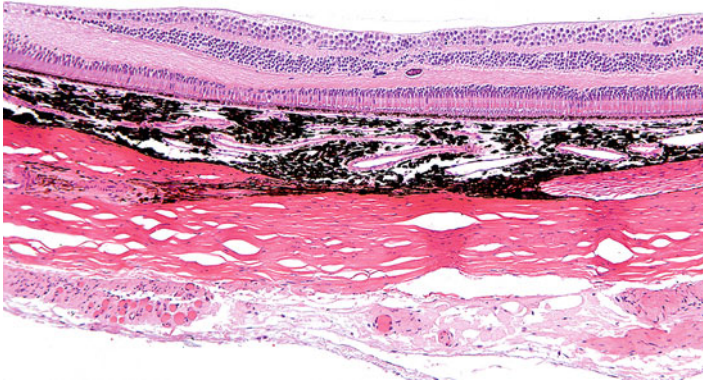


Fig. 6.5 Retina from a monkey. Fovea is to the *left*. On prestudy ophthalmic examination, a retinal “scar” was identified adjacent to the fovea. The retina has loss of cells in the outer nuclear layer and inner nuclear layer. The photoreceptor, inner plexiform, and outer plexiform layers are focally thinned. The outer plexiform layer has a focus of mineralization. H&E. 10× objective

Alterations involving photoreceptors include dysplasia, dystrophy, and degeneration. The term retinal dysplasia is used to describe focal or multifocal disorganization of the sensory retina due to faulty development and is usually characterized by retinal rosettes, abnormal alignment of photoreceptor cells, and possibly cellular degeneration [70]. Retinal folds are occasionally diagnosed as retinal dysplasia clinically and microscopically, but should be given a separate diagnosis. Since the retina of the rat at birth is considered to be equivalent in development to the human retina at 4–5 months gestation, it is possible to create experimental developmental findings in the eyes of rat pups [70]. For example, retinal dysplasia has been produced by administration of cytosine arabinose, cycasin, N-methyl-N-nitrosourea (NMU), and trimethyltin [37, 70–72]. Spontaneous retinal dysplasia occurs in many laboratory animals, especially rats and rabbits, but does occur rarely in laboratory beagles [53]. In the rat, retinal dysplasia generally consists of unilateral linear elevations of the retina of varied lengths [37]. Sprague-Dawley rats have different types of retinal dysplasia. Retinal dysplasia may be unilateral or bilateral and characterized by focal or occasionally diffuse absence of outer layers of the sensory retina. This form occurs more frequently in males and increases in incidence with age [73]. Another form of retinal dysplasia occurs in Sprague-Dawley rats at 7–10 weeks of age and is referred to as linear retinopathy, retinochoroidal degeneration or atrophy, retinal dysplasia or dystrophy, or choroid defect [21, 25, 37, 57, 73, 74]. The finding is generally unilateral and consists of thinning from focal loss of the outer layers of the sensory retina with direct abutment of the INL to the choroid or even sclera.

Inherited retinal degeneration is a condition that generally affects photoreceptors, the RPE, or both and varies in the time of onset with a tendency to progress in severity. The hereditary condition occurs in several strains of mice, including several mutant and transgenic mouse strains, rats, and monkeys, but is rarely observed in hamsters and laboratory beagles [21, 22, 53, 75–80, 81–85]. One example is retinal dystrophy in the Royal College of Surgeons (RCS) rat that has a spontaneous mutation for a gene that encodes a receptor critical for phagocytosis of shed outer segments [80, 84, 85]. The RCS rat lacks the ability to phagocytose shed discs, resulting in photoreceptor loss, reduced numbers of nuclei in the ONL, and debris between the RPE and photoreceptors [77]. Other examples of retinal dystrophy include Wag/Rij and Osborne-Mendel stains of rats [53, 78, 84].

Treatment-related degeneration of photoreceptors needs to be differentiated from spontaneous (including inherited) retinal degeneration, especially senile retinal degeneration, a condition characterized by the gradual decrease in the number of photoreceptors, especially rods, and thinning of the ONL with age for all of the laboratory animal species, especially rodents [66]. Since rodents have a relatively short lifespan in comparison to other laboratory animals, it is easier to observe senile retinal degeneration in these species. Senile retinal degeneration can affect enough of the retina such that retinal atrophy is the preferred term. Changes can advance to a degree that the retina consists of just a fibrous layer with glial cells and occasional neurons [21, 24, 74, 86–92]. Age-related effects have been reported in various laboratory animals including aged CD-1 and B6C3F1 mice, and in albino rats including Chbb/THOM strain, Fischer 344, Sprague-Dawley, and Wistar-Furth rats [21, 74, 86–92]. For example, the ONL in F344 rats decreases in cellular thickness from 12 cells thick at 3 months to less than 8 cells thick at 18 months [90]. In Wistar rats, the incidence of senile retinal atrophy can reach 10% in both males and females at 2 years [88].

Since the peripheral retina is thinner than the central retina, degeneration associated with aging is more noticeable in this region and may begin with microcystoid changes in the RPE. Changes typical of senile peripheral retinal degeneration include retinal thinning with a loss of nuclei in the ONL and INL, fusion of the nuclear layers, displacement of photoreceptor nuclei into the inner and outer segment layers, hypertrophy of the RPE, and possibly migration of RPE cells or macrophages into the sensory retina [21, 53, 79, 87, 90, 93]. Infiltration of heavily pigmented cells into the subretinal space may be detached RPE cells or possibly macrophages.

Some strains of mice, especially those background strains used for knockin/knockout transgenic studies such as FVB mice, carry a photoreceptor gene mutation (*rd/rd*) that leads to progressive retinal atrophy with age [75, 82] (Fig. 6.6). Selection of an appropriate strain is important if the eye is to be a focus of interest in these engineered animal models [94].

The normal, gradual loss of photoreceptors with age may be detected by the displacement of photoreceptor nuclei into the inner and outer segment layers in normal retinas of humans and laboratory animals including monkeys, pigs, cats, dogs, rabbits, guinea pigs, rats, mice, and hamsters [93, 95]. Displaced photoreceptor

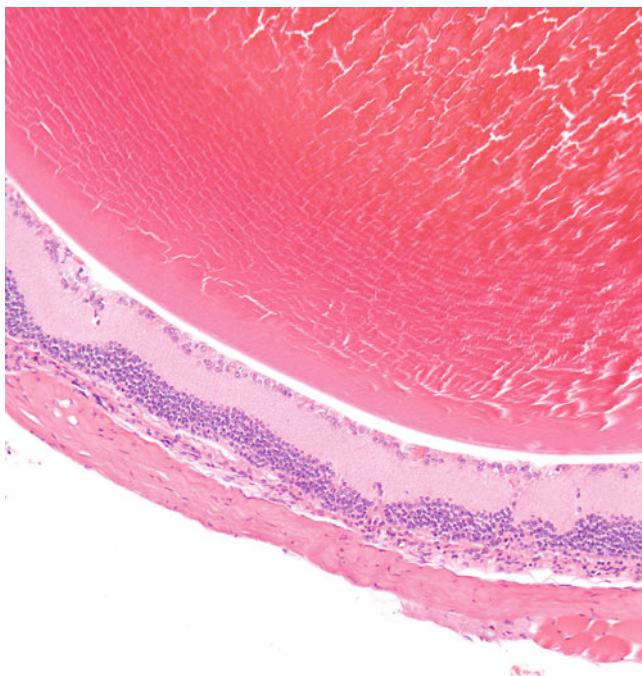


Fig. 6.6 Eye from an FVB mouse. The retina has loss of the photoreceptor and outer nuclear layers due to a mutation in a photoreceptor gene. H&E. 10× objective

nuclei (PDN) are generally low in number and contain a normal density of chromatin, but the number may vary. Occasionally, nuclei are small with condensed chromatin and referred to as pyknotic nuclei (especially in nonhuman primates). These PDN are distributed over the entire retina but more frequently in the periphery. They have a tendency to be more frequent in the retina of very young rats, rats exposed to high ambient light intensities, aged rats, or in globes with ocular disease (e.g., senile macular degeneration or cataract), or in the retina of individuals with systemic disorders (e.g., diabetes mellitus and septicemia). The nuclei eventually undergo degeneration and are removed by the RPE. Since PDN may or may not be occurring with other findings in the retina, PDN may be a separate diagnosis.

A condition to consider when evaluating the retina of albino animals for toxicity, especially from long-term studies, is phototoxic or light-induced retinopathy. The exact mechanism of light-induced retinal degeneration is unknown but may involve phototransduction or oxidative mechanisms with free radical liberation in the photoreceptor outer segments [96]. The primary ocular mechanism for controlling light exposure is constriction of the pupil by the pigmented iris [66, 97, 98]. Light-induced retinal degeneration has been reported in pigmented rats when pupils are dilated and in pigs exposed to constant illumination for at least 1 month when their pupil size remained relatively large with constant illumination [97, 99].

Uveal pigmentation of nonalbino animals, especially of the iris, absorbs light and protects the retina from light-induced damage [100–104]. This condition has been described in rats, mice, monkeys, rabbits, and miniature pigs [22, 46, 57, 99, 100, 104–108]. In rats, females have a tendency to be more affected than males. Exposure to light contributes to the natural aging process, but short-exposure to high light intensity or long exposure to low levels of artificial lighting may cause photoreceptor degeneration [87]. For example, photoreceptor degeneration is more pronounced in rats housed under light intensity of 32 foot-candles than rats housed under light intensity of 1 foot-candle, but even though the overall room light intensity may be within the acceptable limits, the light exposure of animals on the top of a cage rack has greater light exposure than animals on the bottom of the cage rack [87, 88, 90, 100, 103, 109, 110]. In long-term toxicology studies, age-related and light-associated retinal lesions are common. Therefore, it is critical that a light intensity (12 h light/12 h dark) of 60–200 lux not be exceeded [66, 87, 90, 111, 112]. In addition to light intensity, other factors that influence the development of phototoxic retinopathy include wavelength, duration of exposure, length of time for dark-adaptation, age of initial exposure, maturity of the retina, body temperature, albinism, decreased prior daily light exposure, changes in light/dark cycle length, and diet including a deficiency or excess of vitamin A or deficiency of vitamin E or taurine [21, 46, 53, 66, 91, 100, 101, 113, 114]. In general, light-induced retinal degeneration is more prominent in the central retina, and rods are more sensitive than cones. Alterations include a decrease in the thickness of the ONL; disorganization and thinning of the layers of outer segments and inner segments; the presence of normal appearing or darkly stained, pyknotic photoreceptor nuclei in the layers of the outer and inner segments and in the subretinal space; and possibly astrocyte proliferation and Müller cell activation [100, 112, 115]. Normally, the ONL is thicker than the INL, but with light-induced retinopathy, the thickness of the ONL may appear similar to the thickness of the INL, and the layer of inner and outer segments will appear thinner and disorganized. The ONL gradually thins and eventually disappears.

A common change occurring especially in dogs, monkeys, and humans is peripheral cystoid retinal degeneration (Fig. 6.7) [39, 53]. It is described as a normal change in virtually all human patients by 8 years of age and consists of single to multiple vacuoles in the peripheral retina in the INL, IPL, and OPL [116]. This finding is noted in the superior nasal quadrant of dogs as early as 8 weeks and in the peripheral temporal retina of monkeys with age. This background change should be distinguished from retinoschisis, which is splitting of the retinal layers [39, 53].

Ganglion cells are lost as a spontaneous condition in rhesus and cynomolgus monkeys as part of idiopathic optic neuropathy. Loss of ganglion cells in the macular region correlates with loss of axons in the temporal aspect of the optic nerve [117, 118].

The sensory retina may focally bulge inward with the photoreceptors possibly separating from the underlying RPE forming a retinal fold [37]. Spontaneous retinal folds have been reported in many species of laboratory animals including mice, rats, (Sprague-Dawley, Wistar), rabbits, and dogs, especially young animals [22, 53, 57]. In young animals, when present histologically, these may be Lange's folds, which



Fig. 6.7 Peripheral retina from a dog with peripheral cystoid retinal degeneration. Multiple cyst-like spaces expand the retina with loss of layers and organization. H&E. 10× objective

are artifactual folds related to fixation [119, 120]. Some retinal folds may be recognized during the prestudy examination and appear as short gray to brown lines in the nontapetal area of the canine fundus or short gray or white lines [53, 66]. This finding is common in young beagles and may decrease with age. Folds usually affect outer layers of the retina and, in rabbits, they occur in the region of the medullary rays [53]. They may be associated with preretinal traction membranes or subretinal hemorrhage and develop into focal retinal detachment [33, 53]. Retinal folds may be congenital in Sheffield-Wistar rats and associated with microphthalmia or other intraocular anomalies. Depending on the plane of histologic section, retinal folds may resemble a rosette [121].

Spontaneous retinal detachment is uncommon in laboratory animals but may occur rarely in B6C3F1 mice, rats (Sprague-Dawley), dogs, and laboratory monkeys [24, 53, 57]. Funduscopically, retinal detachment appears as a gray membrane and may be associated with preretinal traction membranes, rhegmatogenous change associated with retinal holes or tears, or the presence of fluid or hemorrhage within the subretinal space [53]. Traction membranes may develop secondarily to disruptions of the vitreous body and be due to contraction bands of organized tissue within the vitreous or be due to neovascular disease or intraocular surgery. Serous or exudative retinal detachment consists of fluid in the subretinal space and may develop secondarily to hypertension. Other causes include retinal detachment secondary to buphthalmos, caused by glaucoma, trauma, and the administration of compounds. Dithizone causes retinal edema and exudation, leading to secondary retinal detachment, and administration of diphenyl thiocarbazonone causes retinal detachment in the dog, but not in cat, rat, rabbit, or monkey [18, 53].

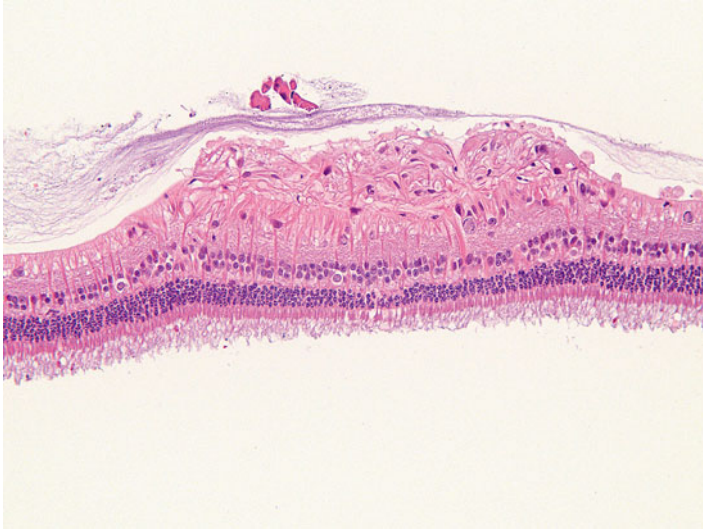


Fig. 6.8 Rabbit retina with focal gliosis expanding the nerve fiber layer. Retinal gliosis is infrequent and of unknown origin. H&E. 20× objective

True retinal detachment needs to be differentiated from artifactual retinal detachment. In addition to obvious causes, such as traction membranes and the presence of fluid or hemorrhage in the subretinal space, the RPE cells are hypertrophied and individualized, giving them a “tombstone” appearance when the retinal detachment is not artifactual. With time, retinal detachment will result in photoreceptor degeneration.

6.4.2 Retinal Inflammation, Trauma, and Gliosis

Retinal inflammation may occur spontaneously or may be induced experimentally. Spontaneous inflammation of the retina is rare in laboratory animals but may occur as a unilateral finding secondary to trauma [53, 122]. Retinal inflammation usually occurs secondarily to inflammation of the choroid and results in retinal degeneration. For example, multifocal serous chorioretinitis has been reported in the beagle dog with focal retinal detachment and focal loss of photoreceptors. Experimentally in mice, there are virally induced retinitis models and autoimmune disease models induced by immunization with retinal S-antigen or interphotoreceptor retinoid-binding protein [24]. The latter model involves an infiltration of neutrophils and mononuclear inflammatory cells in the retina.

Retinal gliosis has been observed as a focal finding localized around the optic disc and is confined entirely to the retina in rats (Fig. 6.8) [123]. The finding consists

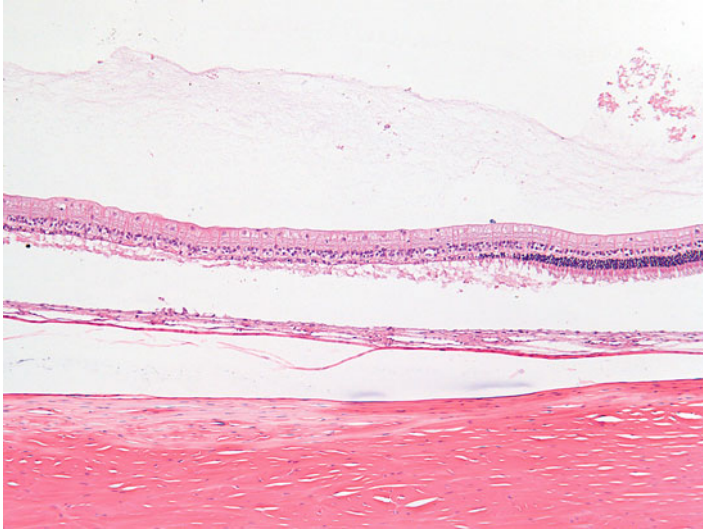


Fig. 6.9 Retinal degeneration in a rabbit 2 weeks after phacoemulsification lensectomy using hydrodissection. There is loss of photoreceptors which is thought to be associated in the surgical procedure. H&E. 10× objective

of an expanded NFL containing cells with elongated nuclei, fibrillar eosinophilic cytoplasm, and indistinct membranes. These cells are positive for anti-glial fibrillary acidic protein (GFAP) indicating their origin as glial cells [123].

Focal retinal degeneration can occur as a consequence of surgical trauma from procedures such as phacoemulsification lensectomy (Fig. 6.9).

6.4.3 Retinal Pigment Epithelium Alterations

Changes in the RPE have been reviewed [124, 125]. Because of the functional relationship between the RPE and photoreceptor cells, photoreceptor changes are frequently secondary to RPE changes. Toxicity-related alterations involving the RPE must be differentiated from artifacts. For example, the presence of crystalloid bodies between RPE and tapetum lucidum is an artifact observed in control beagles considered to be associated with glutaraldehyde fixation.

There are several morphologic changes that can be observed in the RPE. One common change is hypertrophy. Hypertrophy may be diffuse and uniform, possibly due to an increase in smooth endoplasmic reticulum from increased metabolic activity of the cells or focal with or without an apparent cause. Focal hypertrophy of RPE cells is often associated with retinal detachment (Fig. 6.10), retinal folds, or trauma. The affected RPE cells appear individualized with a domed apical portion (“tombstone” appearance). Additional changes in the RPE

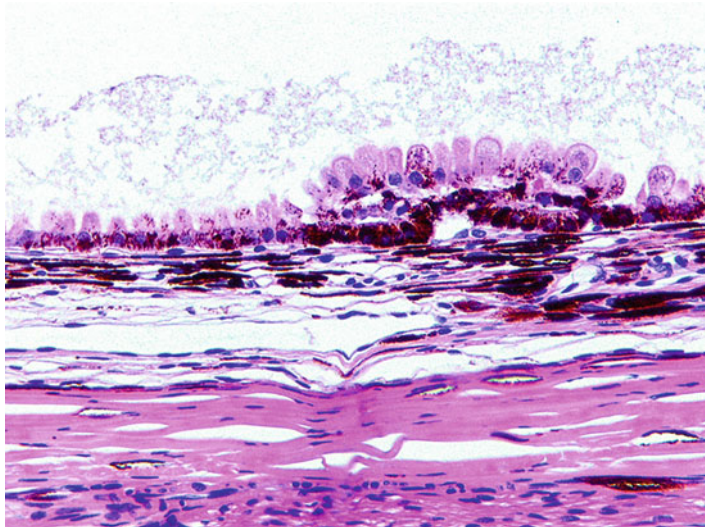


Fig. 6.10 Retinal pigment epithelium from a control dog on a 3-month oral toxicity study. The retina was noted to have tears early in the study and had completely detached by the end of the study. Cause of tears and detachment were undetermined. The underlying RPE has undergone hypertrophy and hyperplasia, demonstrating the classic “tombstoning” appearance. H&E. 20x objective

include retraction of apical pigment granules, loss of polarity, hyperplasia, migration into the subretinal space or sensory retina, accumulation of deposits or cellular components, degeneration, fibroblastic or osteoblastic metaplasia, and the formation of subretinal membranes.

Since the RPE engulfs and degrades photoreceptor outer segments, lipofuscin may accumulate with age [125]. As this occurs, the number of melanin granules decreases. This change is especially noticed as a spontaneous finding in the RPE of rabbits, especially Dutch belted rabbits (Fig. 6.11). The brown deposits which accumulate within the cytoplasm of rabbits have the ultrastructural appearance of lipofuscin. Affected cells often occur around the optic disc or under the most peripheral retina, but may be present in other locations. Eventually, the cells extend into the subretinal space and become disassociated with outer segments. There is often concurrent focal retinal detachment with degeneration.

Loss of cellular polarity, loss of apical villi, and depigmentation occur when the RPE cells are responding to injury or may be observed as a spontaneous change in the retinas of rabbits. Injured RPE cells retract melanosomes from the apical processes and become rounded, giving the appearance of hypertrophy. Rounded RPE may migrate into the subretinal space. RPE cells have a distinct morphology with apical microvilli and basal infoldings. Loss of apical microvilli may be indicative of impaired phagocytosis of photoreceptor discs, and there may be a reduced number of phagolysosomes. Depigmentation is usually from a fusion of melanosomes, and a loss of basal infoldings may be indicative of impaired transport processes.

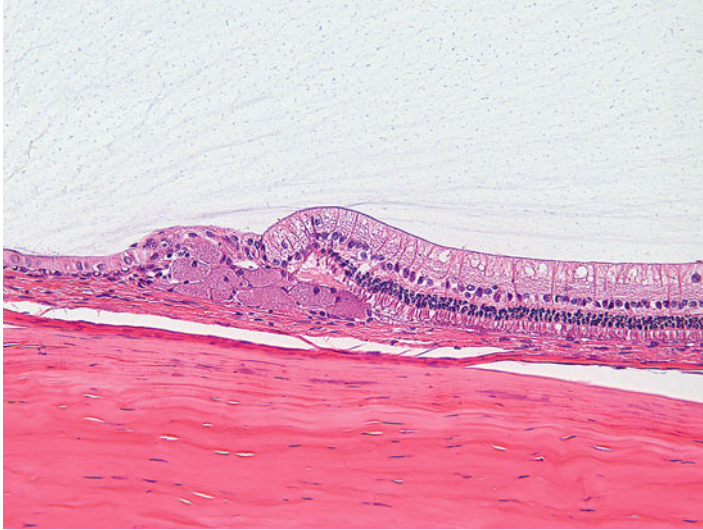


Fig. 6.11 Peripheral retina from a rabbit. There are multiple hypertrophied retinal pigment epithelial cells with granular cytoplasm due to lipofuscin, occurring as a spontaneous change. H&E. 20× objective

RPE cells may undergo hyperplasia with or without metaplasia in response to stimuli that include injuries, chronic inflammation, and long-standing retinal detachment with traction. Hyperplastic RPE cells appear immature with limited differentiation and may form multiple layers between the choroid and the photoreceptor layer. RPE cells also have the potential to differentiate into fibroblasts and secrete a collagenous extracellular matrix forming a membrane between the RPE and Bruch's membrane, which may consist of multiple cell layers interspersed between collagen-rich extracellular matrix. The membranes may be vascularized or nonvascularized.

Deposits of extracellular matrix components may accumulate between the RPE and Bruch's membrane in monkeys [125] and other species (Fig. 6.12). These deposits are similar to drusen which occur as a degenerative change in the human eye. Drusen-like bodies consisting of subretinal concretions on Bruch's membrane can occur in the macula of nonhuman primates as an aging change and may be associated with focal retinal detachment [66, 126, 127] (Fig. 6.13).

6.4.4 Retinal Toxicity: General

Retinal and RPE changes associated with various drug and chemical toxicities have previously been reviewed [1, 18, 44, 86, 128, 129]. Alterations involving the sensory retina consist of vascular changes, degeneration of ganglion cells, degeneration of photoreceptors, degeneration of other neurons, and reactive glial cells. Müller cells

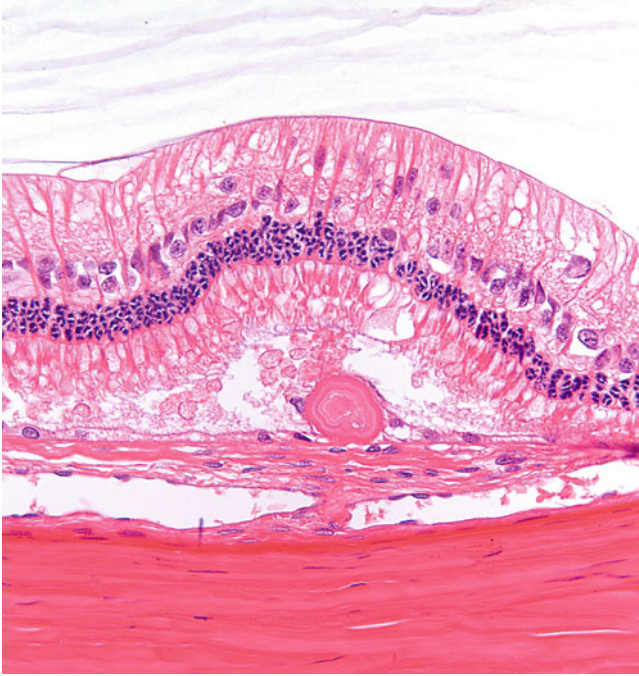


Fig. 6.12 Rabbit peripheral retina with a drusen-like deposit located below the photoreceptor layer and associated with the RPE. H&E. 40× objective

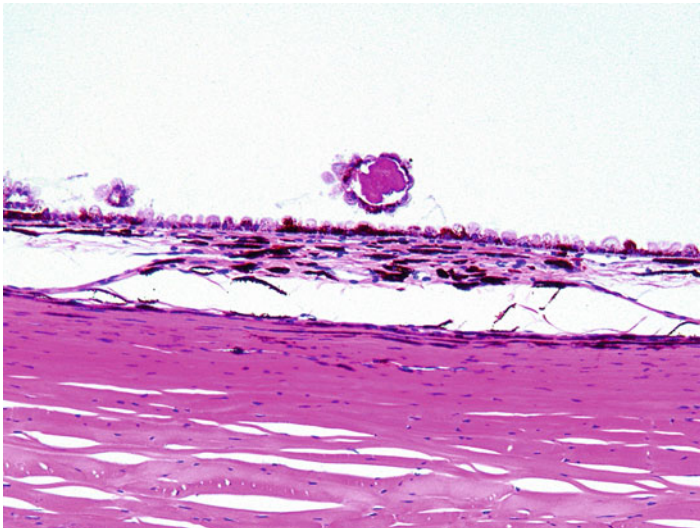


Fig. 6.13 Drusen-like deposits from the same dog as in Fig. 6.10. The drusen-like deposit is in an area of focal retinal detachment. Note that the drusen-like deposit in this animal appears to be surrounded by RPE cells. H&E. 10× objective

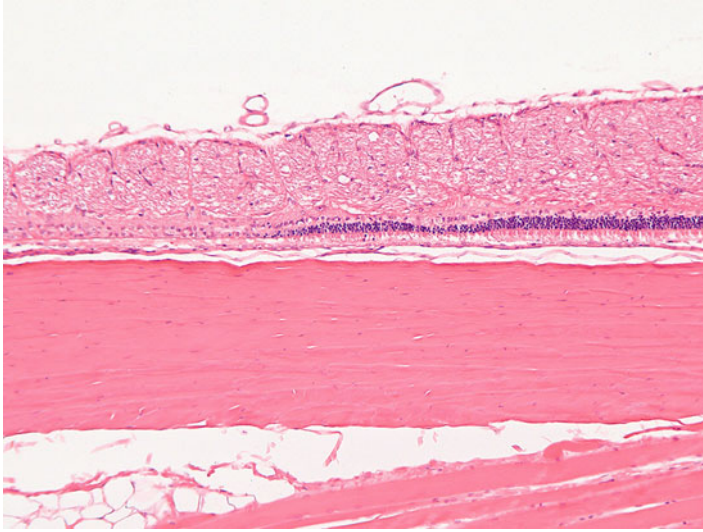


Fig. 6.14 Segmental retinal degeneration in a rabbit following an intravitreal injection. H&E. 10 \times objective

may be a target of toxicity, such as in D, L α -amino adipic acid toxicity, with changes consisting of cytoplasmic vacuolation and necrosis [130]. Some compounds, such as trimethyltin, fenthion, and D,L-2-amino-3-phosphonopropionate, may produce alterations in more than one type of retinal cell [18, 44] (Fig. 6.14). Trimethyltin most frequently and most severely affects the inner segments of photoreceptors resulting in intracytoplasmic, membrane-bound vacuoles and dense bodies, but changes are also present in ganglion cells and neurons of the INL [131]. D,L-2-amino-3-phosphonopropionate is structurally related to aspartate, an excitatory amino acid neurotransmitter, and causes severe degeneration of all retinal layers of the neonatal rat.

The predicative value of retinal findings in laboratory animals with respect to the determination of ocular toxicity may vary between rodent and nonrodent species and between animals and humans [132]. For example, enrofloxacin is an antimicrobial agent that has interspecies differences in sensitivity to retinal toxicity [133, 134]. Changes include acute blindness, ophthalmoscopic evidence of increased tapetal reflectivity, attenuation and loss of retinal blood vessels, and changes in tapetal coloration [133, 134].

Retinal lesions in animals may be difficult to correlate to retinal lesions in humans. Some drugs (e.g., ethambutol) that cause retinal lesions in laboratory animals do not appear to cause visual disturbances or retinal changes in humans [135]. The toxicity may be related to melanin binding. Drugs that bind to melanosomes can alter ion composition, especially calcium. Melanin may also have biochemical differences among species. Melanin in the RPE of hamsters is ultrastructurally different than the melanin in mice and this difference may account for interspecies differences in retinal toxicity [136].

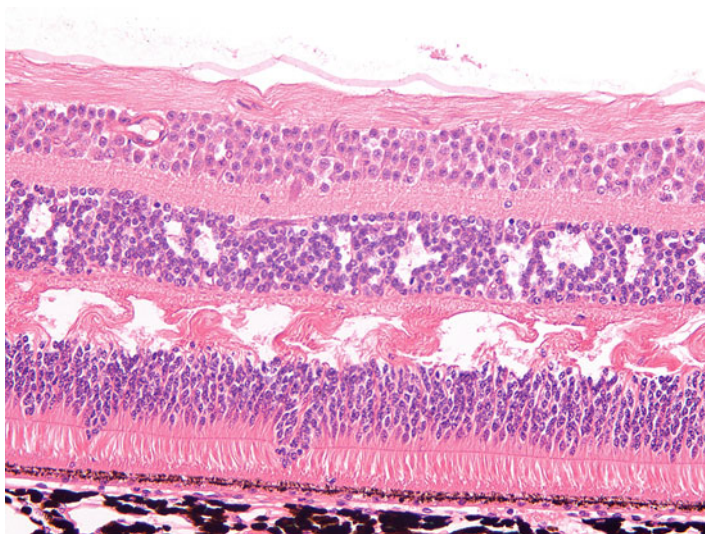


Fig. 6.15 Retinal changes in a monkey given an intravitreal injection. Degenerative changes include disruption of the external limiting membrane with extension of the outer nuclear layer nuclei into the photoreceptor layer. In addition, there is vacuolation of the outer plexiform layer, and vacuolation of the inner nuclear layer. H&E. 40× objective

Vigabatrin (gamma-vinyl GABA), an enzyme-activated, irreversible inhibitor of GABA transferase, is associated with visual disturbance in human patients. Patients treated with vigabatrin had peripheral field visual defects, but the macula was spared [137]. The precise pathology was unclear [138]. In a preclinical 90-day rat study, there was mild disorganization of the ONL and displacement of photoreceptor nuclei. These changes were more prominent in the periphery of the retina and occurred as dose-related findings in albino Sprague-Dawley rats, but not in the retina of pigmented Lister-Hooded rats [50, 137]. It is thought that vigabatrin is detoxified by melanin [139, 140].

The most common finding in the retina associated with toxicity is, which may consist of apoptosis, necrosis, and atrophy and may be associated with vacuolation and inflammation (Fig. 6.15). Retinal degeneration is a term generally used to describe a loss of retinal tissue, but needs further definition in a toxicity study as to the actual change, the portion of the retina involved, and the extent of involvement. In general, toxicities have an effect on the inner retina, principally the ganglion cells, or on the outer retina, principally the photoreceptors or RPE, and toxicities can be observed in a variety of laboratory animals [141]. Initial degenerative changes may result in a shortening of the outer segments. This change can be a reversible change as long as the photoreceptor is still viable. Generally, this acute phase of outer retinal degeneration is not detected clinically and may not be noted microscopically. Retinal degeneration is more easily detected after there is more advanced shortening and disorganization of the inner and outer segments of photoreceptors, especially with thinning of the ONL due to loss of photoreceptor

nuclei. Microscopic findings of degeneration are similar to those mentioned for spontaneous photoreceptor degeneration and may include mitochondrial swelling, disorientation of outer segment membrane discs, and disruption of the photoreceptor cells with vacuolation. Retinal degeneration may occur as a spontaneous (hereditary, aging, exposure to light nutritive deficiency, or following inflammation or trauma) or iatrogenic (e.g., laser) finding and must be differentiated from toxicity. Cellular and humoral autoimmune mechanisms may also contribute to retinal degeneration [142].

6.4.5 Retinal Toxicity: Vascular Alterations

Changes in the retinal vasculature associated with toxicity include necrosis, vascular proliferation, microaneurysm, vessel thickening, or calcification and may lead to retinal hemorrhage or edema. Retinal hemorrhage associated with toxicity must be differentiated from other causes such as coagulopathies, retinal hypertension, vascular disease, ocular trauma, or chest compression during handling of rodents [37]. Retinal vascular changes may be evaluated clinically by vascular angiography and microscopically by trypsin digestion of whole mounts of the retina [143]. Examples of vascular toxicity include vascular proliferation within the subretinal space due to urethane anesthesia and retinal edema due to administration of naphthalene to rabbits [53].

6.4.6 Retinal Toxicity: Ganglion Cells

Ganglion cell degeneration leading to loss of ganglion cells may be directly due to toxicity, but may be a spontaneous condition or secondary to glaucoma. Examples of toxicity include carbon disulfide or doxorubicin [144, 145]. Doxorubicin toxicity causes an inhibition of slow transport resulting in neurofilamentous axonal swelling and necrosis [145].

Toxicity mainly involving the ganglion cells occurs with monosodium glutamate (humans) and ethambutol (rats and humans) [135]. Glutamate causes neuronal depolarization resulting in an influx of sodium, calcium, and chloride, resulting in cell swelling and necrosis with loss of cells in the GCL and the INL and vacuolation in plexiform layers in the rat and mouse [146–148]. Intravitreal injection of excitatory amino acids such as monosodium glutamate into the eyes of rats produced ultrastructural alterations including swelling of the nucleus, cytoplasmic matrix, mitochondria, and dendritic processes of ganglion cells. Later there was loss of cytoplasmic components, nuclear pyknosis and cell shrinkage, and phagocytosis of degenerated dendritic processes by Müller cells [147]. The severity of alterations produced in the retina of mice by parenteral administration of glutamate increased with age up to the tenth postnatal day, but beyond 10 days of age, lesions were difficult to produce even with lethal doses.

Overstimulation of the N-methyl-D-aspartate (NMDA) type of glutamate receptor results in a loss of ganglion cells and their axons and eventually a reduction in the IPL. This loss in ganglion cells is mediated through an influx of extracellular calcium through voltage-gated calcium channels. NMDA and glutamate receptors have also been implicated in toxicity associated with retinal ischemia and the release of nitric oxide by endothelial cells. Ethambutol toxicity is characterized by bilateral, focal axonal swellings within the optic nerves of rats and visual disturbances in human patients. It is mediated through an excitotoxic pathway [135, 138].

With loss of ganglion cells there is degeneration of the optic nerve best appreciated by microscopic examination of a cross section.

Additional retinal cells may be involved in toxicity such as cells in the INL due to sodium L-glutamate or domoic acid, amacrine cells due to kainic acid, and multiple cell types due to AY9944 or L-cystine [146, 149, 150]. Not all species have ganglion cell involvement. For example, methanol toxicity produces ganglion cell injury in humans and nonhuman primates, but not in the rabbit or dog [53].

Chloroquine inhibits lysosomal enzyme activity or protein synthesis in ganglion cells, photoreceptors, and RPE in humans and animals [53, 138, 151–153]. Melanin binding facilitates the concentration and accumulation of chloroquine within the RPE. However, binding of drug to melanin may also serve as a protective mechanism [138, 151–153]. The effects of chloroquine may be irreversible after cessation [154]. Chloroquine adversely affects the retina of humans, rats, cats, dogs, rabbits, pigs, and monkeys and results in intracellular accumulations of membranous phospholipid inclusions (myeloid bodies) within ganglion cells and to lesser degree photoreceptors and RPE cells. Quinine in the dog leads to ganglion cell destruction and retinal atrophy, while the rabbit is less sensitive [53, 138, 151–153, 154].

Vacuolation of ganglion cells is associated with drug-induced lipidosis. Degenerative changes can occur in ganglion cells, neurons with nuclei in the INL, Muller cells, and RPE cells and associated drugs include anorectics, antidepressants, antimalarials, antihistamines, hypocholesterolemic agents, and immunostimulants. Involved animals include rabbits, mice, cats, dogs, monkeys, and guinea pigs.

6.4.7 Retinal Toxicity: Photoreceptors

Retinal degeneration associated with various drug and chemical toxicities has been reviewed [18, 129]. Compounds primarily affecting the photoreceptor cells include aminophenoxyalkane, chloroquine, fluoride, iodate, iodoacetate, piperidylchlorophenothiazine, and vitamin A. Methyl 2-(ureidoxy) propionate (MUP) produces fragmentation and disorganization of the outer segments with outward migration of photoreceptor cell nuclei and phagocytosis of photoreceptor debris by RPE [156]. Urethane produced changes in the photoreceptors that resembled hereditary retinal degeneration [31] including fragmentation and vacuolation of outer segments of photoreceptor cells and accumulation of debris and macrophages. With time there was depletion of melanosomes in the RPE and extension of vascularized tufts or

proliferating RPE into the sensory retina. Ethylenimine and 4,4'-diaminosiphenylmethane caused selective atrophy of rods and cones in the retina of the cat but not in several other laboratory animal species. Single administration of NMU in adult mice or rabbits causes photoreceptor degeneration by apoptosis [157]. Intrauterine exposure to NMU in mice results in retinal rosette formation [83].

The mechanism of chemically induced retinal degeneration varies with compound and species. For example, D,L-(*p*-trifluoromethylenyl) isopropylamine hydrochloride causes anoxia in the choroid of dogs resulting in degenerative changes in the photoreceptors and the RPE [158]. Rose Bengal injures the endothelium of the choroid and choriocapillaris causing occlusion and eventual ischemic damage to the RPE.

The site and severity of injury within the retina may also vary due to the high degree of subspecialization among neurons of the different retinal layers [131]. It may be difficult to determine the primary cell type affected by a compound based on morphology alone.

Because spontaneous lesions also occur in the retina of laboratory animals and may be similar to those produced by toxicity, it is sometimes difficult to separate chemically induced retinal changes from senile or genetic disorders or light-induced retinopathy. For some compounds, the only manifestation of toxicity may be an increase in the incidence or an earlier age of onset of spontaneous lesions [21].

6.4.8 Toxicity: Retinal Pigment Epithelium

Alterations in the RPE due to toxicity are similar to the previously discussed spontaneous findings in the RPE [124, 125]. These include intracellular accumulations, loss of polarity with dedifferentiation, depigmentation, degeneration, necrosis, atrophy, hyperplasia, migration into the subretinal space, formation of subretinal membranes, and metaplasia. Effects on the RPE may be primary with secondary effects on photoreceptors or secondary to primary effects involving the photoreceptors. Real alterations involving the RPE must be differentiated from artifacts.

Chlorpromazine causes pigmentary changes in the RPE as well as the cornea and lens and may be the result of drug interactions with ultraviolet light [151, 152]. Phenothiazine derivatives cause pigmentary changes throughout the eye, including the RPE, cornea, lens, retina, conjunctiva, sclera, eyelids, pupils, and lacrimal system. Phenothiazine binding to melanin, especially in the choroid, is retinotoxic. Accumulation of phenothiazine or its derivatives (piperidylchlorophenothiazine, thioridazine, chlorpromazine) in the RPE [159] causes clinical retinopathy in man and retinal toxicity in cats, but not rabbits, rats, guinea pigs, or dogs. The primary retinal target is photoreceptors, especially rods with excessive shedding of photoreceptor outer segments. The RPE accumulates lipofuscin and melanolysosomes and eventually atrophies.

In addition to species considerations, ocular pigmentation may influence retinotoxicity of some compounds in rodents. For example, in chronic lead retinopathy in

rats, pathologic changes in the retina were less severe in pigmented rats than a non-pigmented strain [160]. Albino animals have an absence of melanin and this absence may make them more or less susceptible than pigmented animals [66]. Compounds are routinely evaluated for their tendency to bind to melanin, and those that do are examined for their potential to cause retinal toxicity based on the presence of melanin in the human eye. However, mere binding to melanin by a drug does not mean that it will cause toxicity, and in fact it may provide protection. Nonetheless, pigmented animals are often used in ocular research in order to assess as best as possible potential melanin-associated toxicity in humans.

There are various compounds that affect the RPE, including antiproliferative drugs, calcium channel blockers, carbonic anhydrase inhibitors, metabolic inhibitors that affect functions such as ion transport, interphotoreceptor cell matrix production, carbohydrate synthesis, protein synthesis, and lysosomal enzyme activity [18, 44, 129]. Copper and iron can accumulate within the RPE. Ferrous ions promote the formation of peroxidation damage. Changes in RPE cells following treatment with high dose of desferrioxamine in rats and rabbits include loss of villi from the apical surface, patchy depigmentation, vacuolation of the cytoplasm, swelling and calcification of mitochondria, and disorganization of the plasma membrane [161]. Bruch's membrane adjacent to the degenerating RPE cells was thickened.

Other compounds that affect the RPE by disrupting the normal interactions between the photoreceptor outer segments include aminophenoxyalkane, fluoride, iodate, naphthalene, and aspartate [18, 159, 162]. Examples of toxicities in which both the RPE and photoreceptors have changes include zinc chelators, vitamin A, 4,4"-methylenedianiline, naphthol, nitroaniline, and aluminum chloride [126, 163–165]. Zinc chelators in rats produce non-membrane-bound, electron opaque, scalloped inclusions in basal cytoplasm of RPE [165]. Vitamin A produces increased lipid droplets and mitochondrial degeneration in rats. Compounds that interfere with phagocytosis of photoreceptor outer segment disc include colchicine, adenylate cyclase drugs, or nonsteroidal anti-inflammatory drugs that modulate prostaglandin-mediated immune responses.

Quinolines or drugs containing a quinoline ring affect the retina, RPE, cornea, and lens. The effects are due to inhibition of lysosomal enzyme activity or protein synthesis [139, 151, 152, 166] and are progressive after cessation [154]. The RPE has a specific toxicity associated with melanin binding that facilitates concentration in the RPE of drug to melanin. This may also serve as a protective mechanism. Functionally quinolines compromise the RPE and lead to breakdown of the outer blood-retinal barrier [53].

RPE deposits can consist of lipids. Oxalate crystals from hyperoxaluria due to renal failure or subcutaneous dibutyl oxalate can occur in the RPE [125]. Zinc chelators produce non-membrane-bound electron opaque cytoplasmic inclusions in the RPE [163]. 2-Aminoxy propionic acid causes disruption of the photoreceptor outer segments and secondary increases in lysosomal bodies and phagosomes in the RPE in rats [156].

Degeneration of the RPE is characterized by swelling and vacuolation of mitochondria and the endoplasmic reticulum. This progresses to disintegration and loss

of the cells resulting in atrophy due to the missing RPE cells. RPE cells may undergo degeneration with aging but also may undergo degeneration and necrosis due to trauma, sensory retinal detachment, and toxicity followed by hyperplasia [167]. Thinning of the RPE with loss of photoreceptor outer segments occurs with intraperitoneal administration of aluminum chloride in rats [165]. Necrosis of RPE cells occurs following systemic administration of aminophenoxyalkanes [162, 168]. Intravenous administration of sodium fluoride and sodium or potassium iodate causes primary degeneration to the RPE with secondary changes in the photoreceptors. Systemic lead toxicity is characterized by swelling and lipofuscin accumulation in RPE of rabbits with eventual photoreceptor degeneration and alterations in the blood-retinal barrier [125].

6.4.9 Retinal Vacuolation

Vacuolation is a degenerative change that can occur in various cells in the retina or in various retinal layers. For example, hexachlorophene causes vacuolation and degeneration of the photoreceptor outer segments [53, 129, 169]. Cationic amphiphilic drugs result in an accumulation of phospholipids in the RPE (retinal lipidosis) and appear as lamellated or crystalloid cytoplasmic inclusions. These drugs include amiodarone, chloroamitriptyline, chlorphentermine, clomipramine, imipramine, iprindole, aminoglycosides, and other compounds that interfere with enzymatic degradation of phospholipids and are partially reversible upon discontinuation of treatment [126, 170–173]. There may be cell type specificity of cationic amphiphilic drug toxicity. For example, chloroquine and 4,4'-diethy-aminoethoxyhexestrol mainly affect neurons and Muller cells, while triparanol affects the RPE and Muller cells, and chlorcyclizine affects both RPE and sensory retinal cells. This variability may be due to the varying affinity for particular polar lipids. The RPE is particularly at risk because of its role in phagocytosis and processing of large amounts of membranous material from tips of rod outer segments [172]. The role of phospholipidosis of the RPE in causing visual impairment in humans is unclear.

6.4.10 Retinal Neoplasia

Primary neoplasia of the retina (retinoblastoma) has not been reported to occur spontaneously in laboratory animals but has been induced experimentally in the rat following intraocular injection of nickel sulfide [174, 176] and in transgenic mice [175]. Neoplasms induced by nickel sulfide contain mitotic figures and pseudorosettes (Homer Wright type). The retinoblastoma in transgenic mice had rosettes and pseudorosettes of small cells consistent with photoreceptor cells. In addition to primary neoplasia, the retina may be infiltrated by neoplastic cells from neoplasms of other tissues.

6.5 Optic Nerve

The optic nerve is composed of axons of retinal ganglion cells, glial cells, and septa from the pia mater. Ganglion cell axons converge to form the optic disc (optic papilla, optic nerve head) and then traverses the lamina cribrosa (bulbar or intraocular optic nerve), pass through the orbit (retrobulbar or intraorbital optic nerve), and pass through the optic foramen (intracanalicular optic nerve) to become the intracranial optic nerve. Fibers from the left and right optic nerves come together at the optic chiasm. Axons continue as the optic tracts and eventually synapse with neurons in locations such as the lateral geniculate body and rostral colliculus [5].

The optic disc has a slight and variable peripheral elevation and a variable central depression (physiologic cup). The physiologic cup is present in dogs but prominent in rabbits. Based on this anatomical structure, a microscopic examination includes a section through the optic disc and a cross section of retrobulbar optic nerve.

6.5.1 *Developmental Abnormalities of the Optic Nerve*

Spontaneous changes are often congenital anomalies but may develop after birth. Congenital changes can be detected on a prestudy examination and may include conditions such as a decreased size from congenital aplasia, hypoplasia, or dysplasia; cavitation from congenital coloboma; and depression of the optic disc from congenital glaucoma. Aplasia or hypoplasia of the optic nerve has been reported in beagles, rats, and mice [53]. Congenital aplasia or hypoplasia usually occurs as a unilateral finding in rats. Microscopically, optic nerve hypoplasia is characterized by the absence of the inner layers of the retina, especially the GCL. Optic nerve dysplasia has been reported in Sprague-Dawley rats [177]. Cavitation of the optic disc, with or without involvement of adjacent structures, is indicative of congenital posterior coloboma. Posterior coloboma occurs in young Sprague-Dawley rats [57], but in the rat, coloboma may also involve the iris and may be associated with microphthalmia as an inherited trait [53]. Coloboma must be distinguished from a central depression of the optic disc that occurs as a result of degeneration from glaucoma, and the anterior segment should be examined to determine if this change is primary or secondary.

6.5.2 *Degeneration, Inflammation, and Edema of the Optic Nerve*

Changes that may occur during a study include degeneration, inflammation, and optic disc edema (papilledema). The main spontaneous background finding of the optic nerve is degeneration. In Wistar rats, degeneration may be unilateral and consists of loss of axons and gliosis of the optic nerve and the optic tracts [178].



Fig. 6.16 Longitudinal section of an optic nerve from a monkey with asymmetric optic nerve atrophy. The temporal portion of the nerve (*right*) has a relatively increased cellularity due to a loss of axons. H&E. 2.5× objective

Various types of optic nerve abnormalities are observed in rhesus monkeys [53], but most cases of optic atrophy occur in young rhesus monkeys and are unilateral, not progressive, and found during routine exam of fundus [53]. In monkeys, optic nerve degeneration is manifested in rhesus and cynomolgus monkeys as idiopathic optic neuropathy [117, 118] (Figs. 6.16 and 6.17). This condition is characterized by reduction of nuclei within the macular region of the temporal retinal ganglion cell layer, thinning of the temporal retinal nerve fiber layer due to axonal loss, temporal pallor of optic disc, loss of axons and gliosis of the temporal optic nerve, and spaces within the INL of the temporal retina. This condition is similar to the condition described by Rubin in primates, “leukoencephalomyelosis” [53]. This condition was characterized by papillomacular degeneration and pallor of the optic disc with or without other neurologic or systemic disease. It was bilateral and almost symmetrical [53].

Degeneration of the optic nerve is generally the result of a loss of ganglion cells in the retina and causes include glaucoma, aging, and toxicities. Optic nerve alterations associated with glaucoma includes necrosis with malacia, gliosis, and the formation of a cup within the optic disc [39]. Optic nerve fibers decrease with age in animals and humans [179]. For example, there is a decrease in the number of nerve fibers, increased number of astrocytes, and an increase in meningeal membranes in the optic nerve of Sprague-Dawley rats as they age [180]. With loss of ganglion cells, there is degeneration of the optic nerve that is best appreciated by examination of a cross section microscopically.

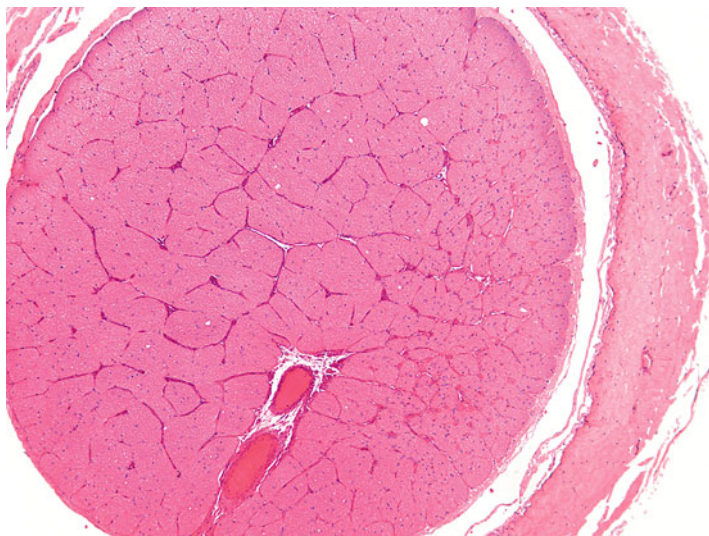


Fig. 6.17 Cross section of an optic nerve from a monkey with asymmetric optic nerve atrophy involving temporal portion of the nerve H&E. 2.5× objective

Toxic optic neuropathy has been reported with numerous compounds in humans and many compounds in laboratory animals [18, 181]. Changes observed during a study may include degeneration, edema, and inflammation. Administration of ethambutol resulted in bilateral focal axonal swelling without demyelination in the optic chiasm and optic tracts of albino rats [136, 182] with changes also occurring in monkeys [183]. Other compounds causing optic nerve degeneration include clioquinol and organophosphate pesticides in dogs [183–185]. Other degenerative changes include a loss of axons in the optic nerve and optic chiasm with reactive gliosis and vascular endothelial proliferation. These changes may occur following ionizing radiation [186].

Terms for inflammation of the optic nerve and papilla are optic neuritis and optic papillitis, respectively. During an ophthalmic examination, optic neuritis might be a term used when the optic disc is indistinct. Microscopically, there are usually no inflammatory cells present, and possibly no changes present; therefore, the term should be avoided.

Although not specifically inflammation, macrophages bearing test article may be observed within the optic nerve in intravitreal ocular toxicology studies (Fig. 6.18). Poorly soluble materials in the vitreous will be phagocytosed by macrophages and carried out of the eye via the optic nerve to the vessels of the optic nerve. Because of this route of clearance, ophthalmitis rarely occurs without concurrent optic neuritis [187].

Papilledema is edema of the optic disc or optic papilla and is characterized by a projection of the optic disc into the vitreous chamber. Papilledema may or may not

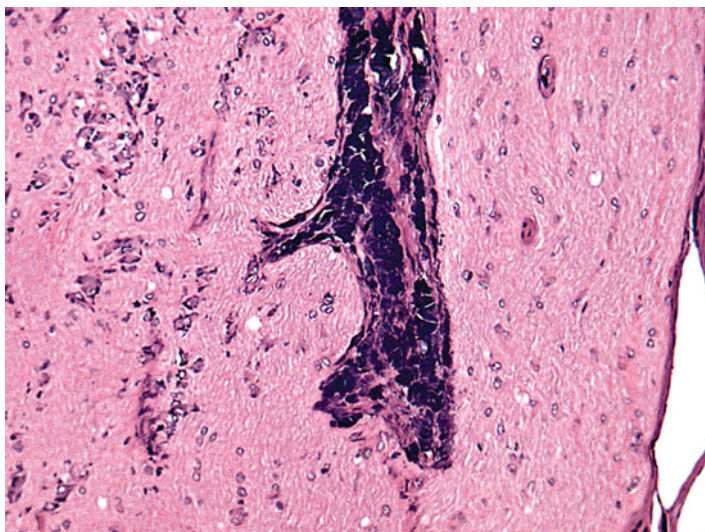


Fig. 6.18 Optic nerve from a rabbit given an intravitreal injection of a poorly soluble excipient. The vessel in the optic nerve is surrounded by macrophages containing the excipient as an apparent clearance mechanism. H&E. 20× objective

have accompanying destruction of axons and myelin. The term, optic disc swelling, may be a better descriptive term to use initially because in addition to edema, optic disc swelling can be due to accumulation of neurofilaments. This change occurs with the administration of β,β' -iminodipropionitrile to guinea pigs, dogs, and primates [188]. The finding can be secondary to increased intracranial pressure due to an intracranial mass or the result of constriction of the optic foramen from a vitamin A deficiency, or an orbital mass. Vitamin A deficiency causes constriction of the optic foramen and papilledema with pallor of the optic disc [53]. Papilledema and optic neuritis have been induced by intradermal injection of spinal cord emulsified with Freund's adjuvant [189]. Examples of papilledema from toxicity include salicylanilide, rafoxanide in the dog, and male fern (*Dryopteris filix-mas*) in cattle [53, 190]. Papilledema can be induced in humans and primates with administration of methanol, but not in lower mammals due to differences in metabolism.

6.5.3 Optic Nerve Neoplasia

Neoplasia of the optic nerve is rare in laboratory animals but reported in rats [191]. Spontaneous neoplasms include glioma, ganglioneuroma, and meningioma. Benign and malignant orbital schwannomas have been reported to be associated with the optic nerve. Astrocytoma has been induced by administration of a nickel compound.

References

1. Kuiper B, Boeve MH, Jansen T, Roelofs-van Emden ME, Thuring JW, Wijnands MV. Ophthalmologic examination in systemic toxicity studies: an overview. *Lab Anim.* 1997;31(2):177–83.
2. Munger RJ. Veterinary ophthalmology in laboratory animal studies. *Vet Ophthalmol.* 2002;5(3):167–75.
3. Rubin LF. Comparative anatomy of the eye. In: Hockwin O, Green K, Rubin LF, editors. *Manual of oculotoxicity testing of drugs.* Stuttgart: Gustav Fischer Verlag; 1992. p. 12–44.
4. Schiavo DM. Special topics about the use of laboratory animals in toxicology – an ophthalmoscopic assessment. In: Hockwin O, Green K, Rubin LF, editors. *Manual of oculotoxicity testing of drugs.* Stuttgart: Gustav Fischer Verlag; 1992. p. 9–20.
5. Samuelson DA. Ophthalmic anatomy. In: Gelatt KN, editor. *Veterinary ophthalmology.* 4th ed. Ames: Blackwell; 2007. p. 37–148.
6. Prince JH. *Comparative anatomy of the eye.* Springfield: Charles C Thomas Publications; 1956.
7. Aguirre GD, Rubin LF, Bistner SI. Development of the canine eye. *Am J Vet Res.* 1972;33(12):2399–414.
8. Cook C, Sulik K, Wright K. Embryology. In: Wright KW, editor. *Pediatric ophthalmology and strabismus.* St. Louis: Mosby-Year Book; 1995. p. 3–59.
9. Cook CS. Ocular embryology and congenital malformations. In: Gelatt KN, editor. *Veterinary ophthalmology.* 4th ed. Ames: Blackwell Publishing; 2007. p. 3–36.
10. Stromland K, Miller M, Cook C. Ocular teratology. *Surv Ophthalmol.* 1991;35(6):429–46.
11. Smith RS, Koa WW-Y, John SWM. Ocular development. In: Smith RS, editor. *Systematic evaluation of the mouse eye: anatomy, pathology, and biomethods.* Boca Raton: CRC Press; 2002. p. 45–63.
12. Prince JH. *The rabbit in eye research.* Springfield: Charles C Thomas Publications; 1964.
13. Riley MV, Green K. Comparative physiology and biochemistry of the eye. In: Hockwin O, Green K, Rubin LF, editors. *Manual of oculotoxicity testing of drugs.* Stuttgart: Gustav Fischer Verlag; 1992. p. 45–80.
14. Bermudez MA, Vicente AF, Romero MC, Arcos MD, Abalo JM, Gonzalez F. Time course of cold cataract development in anesthetized mice. *Curr Eye Res.* 2011;36(3):278–84.
15. Delaye M, Clark JI, Benedek GB. Identification of the scattering elements responsible for lens opacification in cold cataracts. *Biophys J.* 1982;37(3):647–56.
16. Lo WK. Visualization of crystallin droplets associated with cold cataract formation in young intact rat lens. *Proc Natl Acad Sci U S A.* 1989;86(24):9926–30.
17. Fraunfelder FT, Burns RP. Acute reversible lens opacity: caused by drugs, cold, anoxia, asphyxia, stress, death and dehydration. *Exp Eye Res.* 1970;10(1):19–30.
18. Grant WM. *Toxicology of the eye.* 3rd ed. Springfield: Charles C. Thomas; 1986.
19. Rathbun WB, Harris JE, Vagstad G, Gruber L. The reversal of triparanol-induced cataract in the rat. IV. Reduced sulfhydryl groups in soluble protein and glutathione. *Invest Ophthalmol.* 1973;12(5):388–90.
20. Heywood R. Some clinical observations on the eyes of Sprague-Dawley rats. *Lab Anim.* 1973;7(1):19–27.
21. Taradach C, Greaves P. Spontaneous eye lesions in laboratory animals: incidence in relation to age. *Crit Rev Toxicol.* 1984;12(2):121–47.
22. Hubert MF, Gerin G, Durand-Cavagna G. Spontaneous ophthalmic lesions in young Swiss mice. *Lab Anim Sci.* 1999;49(3):232–40.
23. Peiffer RP. Inherited cataracts, mouse. In: Jones TC, Mohr U, Hunt RD, editors. *Monographs on pathology of laboratory animals: eye and ear.* Berlin: Springer; 1991. p. 55–60.
24. Geiss V, Yoshitomo K. Eyes. In: Maronpot RR, Boorman GA, Gaul BW, editors. *Pathology of the mouse.* St. Louis: Cache River Press; 1999. p. 471–90.
25. Taradach C, Regnier B, Perraud J. Eye lesions in Sprague-Dawley rats: type and incidence in relation to age. *Lab Anim.* 1981;15(3):285–7.

26. Balazs T, Ohtake S, Noble JF. Spontaneous lenticular changes in the rat. *Lab Anim Care*. 1970;20(2):215–19.
27. Koch H-R, Fischer A, Kaufmann H. Occurrence of cataracts in spontaneously hypertensive rats. *Ophthalmic Res*. 1977;9(3):189–93.
28. Balazs T, Rubin L. A note on the lens in aging Sprague-Dawley rats. *Lab Anim Sci*. 1971;21(2):267–8.
29. Williams D, Sullivan A. Ocular disease in the guinea pig (*Cavia porcellus*): a survey of 1000 animals. *Vet Ophthalmol*. 2010;13(Suppl):54–62.
30. Loget O, Saint-Macary G. Comparative study of ophthalmological observations in the Yucatan micropig and in the Gottingen minipig. *Scand J Lab Anim Sci*. 1998;25 Suppl 1:173–9.
31. Bellhorn RW. Survey of ocular findings in 16- to 24-week-old beagles. *J Am Vet Med Assoc*. 1973;162(2):139–41.
32. Bellhorn RW. A survey of ocular findings in eight- to ten-month-old beagles. *J Am Vet Med Assoc*. 1974;164(11):1114–16.
33. Heywood R, Hepworth PL, Van Abbe NJ. Age changes in the eyes of the beagle dog. *J Small Anim Pract*. 1976;17(3):171–7.
34. Heywood R. Developmental changes in the lens of the young beagle dog. *Vet Rec*. 1971;88(16):411–14.
35. Heywood R. Juvenile cataracts in the beagle dog. *J Small Anim Pract*. 1971;12(3):171–7.
36. Schiavo DM, Field WE. The incidence of ocular defects in a closed colony of beagle dogs. *Lab Anim Sci*. 1974;24:51–6.
37. Hubert MF, Gillet JP, Durand-Cavagna G. Spontaneous retinal changes in Sprague Dawley rats. *Lab Anim Sci*. 1994;44(6):561–7.
38. Loget O. Spontaneous ocular findings and esthesiometry/tonometry measurement in the Göttingen minipig (Conventionally and microbiologically defined). In: Weisse I, Tripathi RC, Hockwin O, editors. *Ocular toxicology*. New York: Springer; 1995. p. 351–62.
39. Dubielzig R, Ketring KL, McLellan GJ, Albert DM. *Veterinary ocular pathology: a comparative review*. Edinburgh: Saunders Elsevier; 2010.
40. Wegener A. Aging of the lens, and models to study this phenomenon. In: Mohr U, Dungworth DL, Capen CC, editors. *Pathobiology of the aging rat*. Washington, DC: ILSI Press; 1994. p. 91–107.
41. Lee AYW, Chung SSM. Contributions of polyol pathway to oxidative stress in diabetic cataract. *FASEB J*. 1999;13(1):23–30.
42. Obara Y. The oxidative stress in the cataract formation. *Nihon Ganka Gakkai Zasshi*. 1995;99(12):1303–41.
43. Render JA, Carlton WW. Induced cataracts, lens, rat. In: Jones TC, Mohr U, Hunt RD, editors. *Monographs on pathology of laboratory animals: eye and ear*. Berlin: Springer; 1991. p. 63–73.
44. Whiteley HE, Peiffer RL. The eye. In: Haschek WM, Rousseaux CG, editors. *Haschek and Rousseaux's handbook of toxicologic pathology*. Salt Lake City: Academic; 2002. p. 539–84.
45. Fraunfelder FT, Fraunfelder FW, Chambers WA. *Clinical ocular toxicology*. Philadelphia: Saunders Elsevier; 2008.
46. Peiffer RL, Porter DP. Light-induced retinal degeneration, rat. In: Jones TC, Mohr U, Hunt RD, editors. *Monographs on pathology of laboratory animals: eye and ear*. Berlin: Springer; 1991. p. 82–7.
47. Peiffer RP. Radiation-induced cataracts, mouse and rat. In: Jones TC, Mohr U, Hunt RD, editors. *Monographs on pathology of laboratory animals: eye and ear*. Berlin: Springer; 1991. p. 73–81.
48. Gehrig PJ. The cataractogenic activity of chemical agents. *CRC Crit Rev Toxicol*. 1971;1(1):93–118.
49. Wegener AR. In vivo studies on the effect of UV-radiation on the eye lens in animals. *Doc Ophthalmol*. 1994;88(3–4):221–32.
50. Robinson M. Organs of special sense I: the eye. In: Turton J, Hooson J, editors. *Target organ pathology a basic text*. Bristol: Taylor and Francis; 1998. p. 405–19.

51. Render JA, Carlton WW. Cataract due to tryptophan deficiency, rat. In: Jones TC, Mohr U, Hunt RD, editors. *Monographs on pathology of laboratory animals: eye and ear*. Berlin: Springer; 1991. p. 61–3.
52. Rathbun WB, Holleschau AM, Cohen JF, Nagasawa HT. Prevention of acetaminophen- and naphthalene-induced cataract and glutathione loss by CySSME. *Invest Ophthalmol Vis Sci*. 1996;37(5):923–9.
53. Rubin LF. *Atlas of veterinary ophthalmoscopy*. Philadelphia: Lea and Febiger; 1974.
54. Bagdon RE, Engstrom RG, Kelly LA, Hartman HA, Robison RL, Viesscher GE. Hypolipidemic activity and toxicity studies of a styryl-hexahydroindolinol, 34–250. *Toxicol Appl Pharmacol*. 1983;69(1):12–28.
55. Shearer TR, Ma H, Fukiage C, Azuma M. Selenite nuclear cataract: review of the model. *Mol. Vis*. 1997;3:8.
56. Prince JH. The vitreous. In: Prince JH, editor. *The rabbit in eye research*. Springfield: Charles C Thomas Publications; 1964. p. 372–84.
57. Kuno H, Usui T, Eydelloth RS, Wolf ED. Spontaneous ophthalmic lesions in young Sprague-Dawley rats. *J Vet Med Sci*. 1991;53(4):607–14.
58. Shibuya K, Satou K, Sugimoto K, Saitoh T, Ihara M, Itabashi M, et al. Background data on spontaneous ophthalmic lesions in Crj:CD(SD)IGS rats. In: Matsuzawa T, Inoue H, editors. *Biological reference data on CD(SD) IGS rats – 1999*. Yokohama: Best Printing Co. Ltd.; 1999. p. 60–2.
59. Hebel R, Stromberg MW. *Anatomy and embryology of the laboratory rat*. Worthsee: BioMed Verlag; 1986.
60. Shibuya K, Satou K, Fujii T, Nunoya T, Tajima M. Spontaneous ophthalmic lesions in Sprague-Dawley, Wistar, and Fischer 344 rats. *Anim Eye Res (Jpn)*. 1997;16:1–10.
61. Saint-Macary G, Berthoux C. Ophthalmologic observations in the young Yucatan micropig. *Lab Anim Sci*. 1994;44(4):334–7.
62. Haggerty GC, Peckman JC, Thomassen RW, Gad SC. The dog. In: Gad SC, editor. *Animal models in toxicology*. 3rd ed. Boca Raton: CRC Press; 2007. p. 563–662.
63. Short BG. Safety evaluation of ocular drug delivery formulations: techniques and practical considerations. *Toxicol Pathol*. 2008;36(1):49–62.
64. Komarowska I, Heilweil G, Rosenfeld PJ, Perlman I, Loewenstein A. Retinal toxicity of commercially available intravitreal ketorolac in albino rabbits. *Retina*. 2009;29(1):98–105.
65. Prince JH, McConnell DG. Retina and optic nerve. In: Prince JH, editor. *The rabbit in eye research*. Springfield: Charles C Thomas Publications; 1964. p. 385–448.
66. Hockwin O, Green K, Rubin LF. *Manual of oculotoxicity testing of drugs*. Stuttgart: Gustav Fischer Verlag; 1992.
67. Crews SJ. Macular changes following retinal detachment procedures. *Bibl Ophthalmol*. 1968;75:337–47.
68. Dietrich UM. Ophthalmic examination and diagnostics. Part 3: diagnostic ultrasonography. In: Gelatt KN, editor. *Veterinary ophthalmology*. 4th ed. Philadelphia: Blackwell Publishing Professional; 2007. p. 507–35.
69. Källberg ME. Ophthalmic examination and diagnostics. Part 2: ocular imaging. In: Gelatt KN, editor. *Veterinary ophthalmology*. Ames: Blackwell Publishing; 2007. p. 484–506.
70. Percy DH, Danylchuk KD. Experimental retinal dysplasia due to cytosine arabinoside. *Invest Ophthalmol Vis Sci*. 1977;16(4):353–64.
71. Hirono I. Carcinogenicity and neurotoxicity of cycasin with special reference to species differences. *Fed Proc*. 1972;31(5):1493–9.
72. Herrold KM. Pigmentary degeneration of the retina induced by N-methyl-N-nitrosourea. An experimental study in syrian hamsters. *Arch Ophthalmol*. 1967;78(5):650–3.
73. Schardein JL, Lucas JA, Fitzgerald JE. Retinal dystrophy in Sprague-Dawley rats. *Lab Anim Sci*. 1975;25(3):323–6.
74. Lin WL, Essner E. An electron microscopic study of retinal degeneration in Sprague-Dawley rats. *Lab Anim Sci*. 1987;37(2):180–6.

75. Pittler SJ, Baehr W. Identification of a nonsense mutation in the rod photoreceptor cGMP phosphodiesterase beta-subunit gene of the rd mouse. *Proc Natl Acad Sci U S A*. 1991;88(19):8322–6.
76. Drager UC, Hubel DH. Studies of visual function and its decay in mice with hereditary retinal degeneration. *J Comp Neurol*. 1978;180(1):85–114.
77. Von Sallmann L, Grimes P. Spontaneous retinal degeneration in mature Osborne-Mendel rats. *Arch Ophthalmol*. 1972;88(4):404–11.
78. Lai YL, Jacoby RO, Jones AM, Papermaster DS. A new form of hereditary retinal degeneration in Wag/Rij rats. *Invest Ophthalmol*. 1975;14(1):62–7.
79. Aguirre GD, Ray J, Stramm LE. Diseases of the retinal pigment epithelium-photoreceptor complex in nonrodent animals models. In: Marmor MF, Wolfensberger TJ, editors. *The retinal pigment epithelium*. Oxford: Oxford University Press; 1998.
80. Matuk Y. Inherited retinal degeneration, RCS rat. In: Jones TC, Mohr U, Hunt RD, editors. *Monographs on pathology of laboratory animals: eye and ear*. Berlin: Springer; 1991. p. 92–100.
81. Gregory CY, Bird AC. Cell loss in retinal dystrophies by apoptosis—death by informed consent! *Br J Ophthalmol*. 1995;79(2):186–90.
82. Sidman RL, Green MC. Retinal degeneration in the mouse: location of the RD locus in linkage Group XVII. *J Hered*. 1965;56:23–9.
83. Smith SB, Yielding KL. Retinal degeneration in the mouse. A model induced transplacentally by methylnitrosourea. *Exp Eye Res*. 1986;43(5):791–801.
84. Dowling JE, Sidman RL. Inherited retinal dystrophy in the rat. *J Cell Biol*. 1962;14:73–109.
85. Li LX, Turner JE. Inherited retinal dystrophy in the RCS rat: prevention of photoreceptor degeneration by pigment epithelial cell transplantation. *Exp Eye Res*. 1988;47(6):911–17.
86. Heywood R. Drug-induced retinopathies in the beagle dog. *Br Vet J*. 1974;130(6):564–9.
87. Weisse I, Stotzer H, Seitz R. Age- and light-dependent changes in the rat eye. *Virchows Arch A Pathol Anat Histol*. 1974;362(2):145–56.
88. Tucker MJ. Special sense organs and associated tissues. In: Tucker MJ, editor. *Diseases of the Wistar rat*. London: Taylor and Francis; 1997. p. 237–45.
89. Lin WL, Essner E. Retinal dystrophy in Wistar-Furth rats. *Exp Eye Res*. 1988;46(1):1–12.
90. Lai YL, Jacoby RO, Jonas AM. Age-related and light-associated retinal changes in Fischer rats. *Invest Ophthalmol Vis Sci*. 1978;17(7):634–8.
91. Lai YL, Jacoby RO, Yao PC. Animal model: peripheral retinal degeneration in rats. *Am J Pathol*. 1979;97(2):449–52.
92. Kudow S, Itabashi M, Takehara K, Tajima M. Ophthalmoscopic and pathologic studies of retinal degeneration in the rats. *Anim Eye Res (Jpn)*. 1984;3:17–21.
93. Lai YL, Masuda K, Mangum MD, Lug R, Macrae DW, Fletcher G, et al. Subretinal displacement of photoreceptor nuclei in human retina. *Exp Eye Res*. 1982;34(2):219–28.
94. Smith RS, Sundberg JP. Strain background disease characteristics. In: Smith RS, editor. *Systematic evaluation of the mouse eye: anatomy, pathology, and biomethods*. Boca Raton: CRC Press; 2002. p. 67–75.
95. Lai YL. Outward movement of photoreceptor cells in normal rat retina. *Invest Ophthalmol Vis Sci*. 1980;19(8):849–56.
96. Organisciak DT, Winkler BS. Retinal light damage: practical and theoretical considerations. In: Chader G, Osborne N, editors. *Progress in retinal research*. New York: Pergamon Press; 1994. p. 1–29.
97. Rapp LM, Williams TP. The role of ocular pigmentation in protecting against retinal light damage. *Vision Res*. 1980;20(12):1127–31.
98. LaVail MM, Gorrin GM, Repaci MA. Strain differences in sensitivity to light-induced photoreceptor degeneration in albino mice. *Curr Eye Res*. 1987;6(6):825–34.
99. Dureau P, Jeanny JC, Clerc B, Dufier JL, Courtois Y. Long term light-induced retinal degeneration in the miniature pig. *Mol Vis*. 1996;2:7.
100. Noell WK, Walker VS, Kang BS, Berman S. Retinal damage by light in rats. *Invest Ophthalmol*. 1966;5(5):450–73.

101. Bellhorn RW. Lighting in the animal environment. *Lab Anim Sci.* 1980;30(2 Pt 2):440–50.
102. Williams DL. Laboratory animal ophthalmology. In: Gelatt KN, editor. *Veterinary ophthalmology*. 4th ed. Ames: Blackwell Publishing; 2007. p. 1336–69.
103. Noell WK, Albrecht R. Irreversible effects on visible light on the retina: role of vitamin A. *Science.* 1971;172(3978):76–9.
104. LaVail MM, Gorrin GM. Protection from light damage by ocular pigmentation: analysis using experimental chimeras and translocation mice. *Exp Eye Res.* 1987;44(6):877–89.
105. Tso MOM. Photic maculopathy in rhesus monkeys: a light and electron microscopy study. *Invest Ophthalmol Vis Sci.* 1973;12:17–34.
106. Tso MO, Woodford BJ. Effect of photic injury on the retinal tissues. *Ophthalmology.* 1983;90(8):952–63.
107. Lawill T. Effects of prolonged exposure of rabbit retina to low-intensity light. *Invest Ophthalmol Vis Sci.* 1973;12:45–51.
108. Harkness JE, Wagner JE. *The biology and medicine of rabbits and rodents*. 3rd ed. Philadelphia: Lea and Febiger; 1989.
109. Greenman DL, Bryant P, Kodell RL, Sheldon W. Influence of cage shelf level on retinal atrophy in mice. *Lab Anim Sci.* 1982;32(4):353–6.
110. Perez J, Perentes E. Light-induced retinopathy in the albino rat in long-term studies. An immunohistochemical and quantitative approach. *Exp Toxicol Pathol.* 1994;46(3):229–35.
111. Stotzer H, Weisse I. Etiology of retinal degeneration in rats during toxicity experiments. *Naunyn Schmiedebergs Arch Pharmakol.* 1970;266(4):460–1.
112. O’Steen WK, Shear CR, Anderson KV. Retinal damage after prolonged exposure to visible light. A light and electron microscopic study. *Am J Anat.* 1972;134(1):5–21.
113. Kuwabara T, Funahashi M. Light damage in the developing rat retina. *Arch Ophthalmol.* 1976;94(8):1369–74.
114. O’Steen WK, Anderson KV, Shear CR. Photoreceptor degeneration in albino rats: dependency on age. *Invest Ophthalmol.* 1974;13(5):334–9.
115. Kuwabara T, Gorn RA. Retinal damage by visible light. An electron microscopic study. *Arch Ophthalmol.* 1968;79(1):69–78.
116. Yanoff M, Fine BS. *Ocular pathology*. 5th ed. Philadelphia: Mosby; 2002.
117. Fortune B, Wang L, Bui BV, Burgoyne CF, Cioffi GA. Idiopathic bilateral optic atrophy in the rhesus macaque. *Invest Ophthalmol Vis Sci.* 2005;46(11):3943–56.
118. Reedle R, Dubielzig R, Christian B. Bilateral optic atrophy in cynomolgus monkey. *Vet Pathol.* 2008;45(5):781.
119. Gartner S, Henkind P. Lange’s folds: a meaningful ocular artifact. *Ophthalmology.* 1981;88(12):1307–10.
120. French J, Halliday J, Scott M, Adkins D, Liess C, Waterton JC, et al. Retinal folding in the term rabbit fetus—developmental abnormality or fixation artifact? *Reprod Toxicol.* 2008;26(3–4):262–6.
121. Poulson R, Hayes B. Congenital retinal folds in Sheffield-Wistar rats. *Graefes Arch Clin Exp Ophthalmol.* 1988;226(1):31–3.
122. Greaves P. *Histopathology of preclinical toxicity studies*. 3rd ed. New York: Academic; 2007.
123. Adams ET, Auerbach S, Blackshear PE, Bradley A, Gruebbel MM, Little PB, et al. Proceedings of the 2010 National Toxicology Program Satellite Symposium. *Toxicol Pathol.* 2011;39(1):240–66.
124. Marmor MF, Wolfensberger TJ. *The retinal pigment epithelium: function and disease*. Oxford: Oxford University Press; 1998.
125. Mecklenburg L, Schraermeyer U. An overview on the toxic morphological changes in the retinal pigment epithelium after systemic compound administration. *Toxicol Pathol.* 2007;35(2):252–67.
126. Dawson WW, Ulshafer RJ, Engel HM, Hope GM, Kessler MJ. Macular disease in related rhesus monkeys. *Doc Ophthalmol.* 1989;71(3):253–63.

127. Ishibashi T, Sorgente N, Patterson R, Ryan SJ. Pathogenesis of drusen in the primate. *Invest Ophthalmol Vis Sci.* 1986;27(2):184–93.
128. Ramos M, Reilly CM, Bolon B. Toxicological pathology of the retina and optic nerve. In: Bolon B, Butt MT, editors. *Fundamental neuropathology for pathologists and toxicologists: principles and techniques.* Hoboken: Wiley; 2011. p. 385–412.
129. Frame SR, Carlton WW. Toxic retinopathy, rat, mouse, and hamster. In: Jones TC, Mohr U, Hunt RD, editors. *Monographs on pathology of laboratory animals: eye and ear.* Berlin: Springer; 1991. p. 116–24.
130. Pedersen OO, Karlson RL. Destruction of Muller cells in the adult rat by intravitreal injection of D,L-alpha-aminoadipic acid. An electron microscopic study. *Exp Eye Res.* 1979;28(5):569–75.
131. Bouldin TW, Goines ND, Krigman MR. Trimethyltin retinopathy. Relationship of subcellular response to neuronal subspecialization. *J Neuropathol Exp Neurol.* 1984;43(2):162–74.
132. Heywood R. Histopathological and laboratory assessment of visual dysfunction. *Environ Health Perspect.* 1982;44:35–45.
133. Wiebe V, Hamilton P. Fluoroquinolone-induced retinal degeneration in cats. *J Am Vet Med Assoc.* 2002;221(11):1568–71.
134. Gelatt KN, van der Woerd A, Ketring KL, Andrew SE, Brooks DE, Biros DJ, et al. Enrofloxacin-associated retinal degeneration in cats. *Vet Ophthalmol.* 2001;4(2):99–106.
135. Heng JE, Vorwerk CK, Lessell E, Zurakowski D, Levin LA, Dreyer EB. Ethambutol is toxic to retinal ganglion cells via an excitotoxic pathway. *Invest Ophthalmol Vis Sci.* 1999;40(1):190–6.
136. Buyukmihci N, Goehring-Harmon F. Histology and fine structure of the hamster retinal pigment epithelium. *Acta Anat (Basel).* 1982;112(1):36–46.
137. Butler WH, Ford GP, Newberne JW. A study of the effects of vigabatrin on the central nervous system and retina of Sprague Dawley and Lister-Hooded rats. *Toxicol Pathol.* 1987;15(2):143–8.
138. Hadjikoutis S, Morgan JE, Wild JM, Smith PE. Ocular complications of neurological therapy. *Eur J Neurol.* 2005;12(7):499–507.
139. Eves P, Smith-Thomas L, Hedley S, Wagner M, Balafa C, Mac Neil S. A comparative study of the effect of pigment on drug toxicity in human choroidal melanocytes and retinal pigment epithelial cells. *Pigment Cell Res.* 1999;12(1):22–35.
140. Dayhaw-Barker P. Retinal pigment epithelium melanin and ocular toxicity. *Int J Toxicol.* 2002;21(6):451–4.
141. Barnett KC. Retinal atrophy. *Vet Rec.* 1965;77(51):1543–60.
142. Chant SM, Meyers-Elliott RH. Autoimmunity: a possible factor in the development of retinal degeneration in the RCS rat. *Clin Immunol Immunopathol.* 1982;22(3):419–27.
143. Fischer MW, Slatter DH. Preparation and orientation of canine retinal vasculature. A modified trypsin digestion technique. *Austr J Ophthalmol.* 1978;6:46–50.
144. Ide T. Histopathological studies on retina, optic nerve, and arachnoidal membrane of mouse exposed to carbon disulfide poisoning. *Nihon Ganka Gakkai Zasshi.* 1958;62A:85–108.
145. Parhad IM, Griffin JW, Clark AW, Koves JF. Doxorubicin intoxication: neurofilamentous axonal changes with subacute neuronal death. *J Neuropathol Exp Neurol.* 1984;43(2):188–200.
146. Lucas DR, Newhouse JP. The toxic effect of sodium L-glutamate on the inner layers of the retina. *AMA Arch Ophthalmol.* 1957;58(2):193–201.
147. Sisk DR, Kuwabara T. Histologic changes in the inner retina of albino rats following intravitreal injection of monosodium L-glutamate. *Graefes Arch Clin Exp Ophthalmol.* 1985;223(5):250–8.
148. Rothman SM, Olney JW. Glutamate and the pathophysiology of hypoxic-ischemic brain damage. *Ann Neurol.* 1986;19(2):105–11.
149. Lessell S, Craft JL, Albert DM. Kainic acid induces mitoses in mature retinal neurones in rats. *Exp Eye Res.* 1980;30(6):731–8.

150. Pedersen OO, Karlsen RL. The toxic effect of L-cysteine on the rat retina. A morphological and biochemical study. *Invest Ophthalmol Vis Sci.* 1980;19(8):886–92.
151. Griffin JD, Garnick MB. Eye toxicity of cancer chemotherapy: a review of the literature. *Cancer.* 1981;48(7):1539–49.
152. Harrison RJ. Ocular adverse reactions to systemic drug therapy. *Adv Drug React Bull.* 1996;180:683–6.
153. Porter JB. A risk-benefit assessment of iron-chelation therapy. *Drug Saf.* 1997;17:407–21.
154. Davidson SI, Rennie IG. Ocular toxicity from systemic drug therapy. An overview of clinically important adverse reactions. *Med Toxicol.* 1986;1(3):217–24.
155. Tsai RK, Lee YH. Reversibility of ethambutol optic neuropathy. *J Ocul Pharmacol Ther.* 1997;13(5):473–7.
156. Lee KP, Gibson JR, Sherman H. Retinopathic effects of 2-aminoxy propionic acid derivatives in the rat. *Toxicol Appl Pharmacol.* 1979;51(2):219–32.
157. Yuge K, Nambu H, Senzaki H, Nakao I, Miki H, Uyama M, et al. N-methyl-N-nitrosourea-induced photoreceptor apoptosis in the mouse retina. *In Vivo.* 1996;10(5):483–8.
158. Delahunt CS, O'Connor RA, Yeary RA, Kuwabara T. Toxic retinopathy following prolonged treatment with dl-(p-trifluoromethylphenyl) isopropylamine (P-1727) in experimental animals. *Toxicol Appl Pharmacol.* 1963;5(3):298–305.
159. Potts AM. Retinotoxic and choroidotoxic substances. *Invest Ophthalmol.* 1962;1:290–303.
160. Santos-Anderson RM, Tso MO, Valdes JJ, Annau Z. Chronic lead administration in neonatal rats: electron microscopy of the retina. *J Neuropathol Exp Neurol.* 1984;43(2):175–87.
161. Rahi AH, Hungerford JL, Ahmed AI. Ocular toxicity of desferrioxamine: light microscopic histochemical and ultrastructural findings. *Br J Ophthalmol.* 1986;70(5):373–81.
162. Collins RF, Cox VA, Davis M, Edge ND, Hill J, Rivett KF, et al. The antischistosomal and retinotoxic effects of some nuclear substituted aminophenoxyalkanes. *Br J Pharmacol Chemother.* 1967;29(2):248–58.
163. Leure-duPree AE. Electron-opaque inclusions in the rat retinal pigment epithelium after treatment with chelators of zinc. *Invest Ophthalmol Vis Sci.* 1981;21(1 Pt 1):1–9.
164. Amemiya T. Cytochemical and electron microscopic examination of the retina of rats with hypervitaminosis A. *Acta Soc Ophthalmol Jpn.* 1967;71:2236–51.
165. Lu ZY, Gong H, Amemiya T. Aluminum chloride induces retinal changes in the rat. *Toxicol Sci.* 2002;66(2):253–60.
166. Wilhelmus KR, Keener MJ, Jones DB, Font RL. Corneal lipidosis in patients with the acquired immunodeficiency syndrome. *Am J Ophthalmol.* 1995;119(1):14–9.
167. Gao H, Hollyfield JG. Aging of the human retina. Differential loss of neurons and retinal pigment epithelial cells. *Invest Ophthalmol Vis Sci.* 1992;33(1):1–17.
168. Lee KP, Valentine R. Pathogenesis and reversibility of retinopathy induced by 1,4-bis(4-aminophenoxy)-2-phenylbenzene (2-phenyl-APB-144) in pigmented rats. *Arch Toxicol.* 1991;65(4):292–303.
169. Towfighi J, Gonatas NK, McCree L. Hexachlorophene retinopathy in rats. *Lab Invest.* 1975;32(3):330–8.
170. Lullmann-Rauch R. Lipidosis of the retina due to cationic amphiphilic drugs, rat. In: Jones TC, Mohr U, Hunt RD, editors. *Monographs on pathology of laboratory animals: eye and ear.* Berlin: Springer; 1991. p. 87–92.
171. Lullmann H, Lullmann-Rauch R. Tamoxifen-induced generalized lipidosis in rats subchronically treated with high doses. *Toxicol Appl Pharmacol.* 1981;61(1):138–46.
172. Lullmann H, Mosinger EU. Increased lysosomal enzyme activities in tissues of rats suffering from chlorphentermine induced lipidosis. *Biochem Pharmacol.* 1979;28(7):1015–16.
173. Drenckhahn D, Lullmann-Rauch R. Drug-induced retinal lipidosis: differential susceptibilities of pigment epithelium and neuroretina toward several amphiphilic cationic drugs. *Exp Mol Pathol.* 1978;28(3):360–71.
174. Albert DM, Gonder JR, Papale J, Craft JL, Dohlman HG, Reid MC, et al. Induction of ocular neoplasms in Fischer rats by intraocular injection of nickel subsulfide. *Invest Ophthalmol Vis Sci.* 1982;22(6):768–82.

175. O'Brien JM, Marcus DM, Niffenegger AS, Bernards R, Carpenter JL, Windle JJ, et al. Trilateral retinoblastoma in transgenic mice. *Trans Am Ophthalmol Soc.* 1989;87:301–22; discussion 22–6.
176. Shaddock JA, Everitt JJ. Retinoblastoma, experimental, rat and hamster. In: Jones TC, Mohr U, Hunt RD, editors. *Monographs on pathology of laboratory animals: eye and ear.* Berlin: Springer; 1991. p. 114–16.
177. Shibuya K, Tajima N, Nunoya T. Optic nerve dysplasia associated with meningeal defect in Sprague-Dawley rats. *Vet Pathol.* 1998;35(5):323–329.
178. Shibuya K, Tajima M, Yamate J. Unilateral atrophy of the optic nerve associated with retrograde and anterograde degenerations in the visual pathways in Slc: Wistar rats. *J Vet Med Sci.* 1993;55(6):905–12.
179. Balazsi AG, Rootman J, Drance SM, Schulzer M, Douglas GR. The effect of age on the nerve fiber population of the human optic nerve. *Am J Ophthalmol.* 1984;97(6):760–6.
180. Cavallotti D, Cavallotti C, Pescosolido N, Iannetti GD, Pacella E. A morphometric study of age changes in the rat optic nerve. *Ophthalmologica.* 2001;215(5):366–71.
181. McCaa CS. Anatomy, physiology and toxicology of the eye. In: Hayes AC, editor. *Toxicology of the eye, ear and other special sense organs.* New York: Raven Press, Ltd.; 1985. p. 1–15.
182. Lessell S. Histopathology of experimental ethambutol intoxication. *Invest Ophthalmol Vis Sci.* 1976;15(9):765–9.
183. Heywood R. Clinical and laboratory assessment of visual dysfunction. In: Hayes AC, editor. *Toxicology of the eye, ear and other special sense organs.* New York: Raven; 1985. p. 61–77.
184. Suzuki H, Ishikawa S. Ultrastructure of the ciliary muscle treated by organophosphate pesticide in beagle dogs. *Br J Ophthalmol.* 1974;58(11):931–40.
185. Uga S, Ishikawa S, Mukuno K. Histopathological study of canine optic nerve retina treated by organophosphate pesticide. *Invest Ophthalmol Vis Sci.* 1977;16(9):877–81.
186. Crompton MR, Layton DD. Delayed radionecrosis of the brain following therapeutic x-radiation of the pituitary. *Brain: J Neurol.* 1961;84:85–101.
187. Saunders LZ, Rubin LF. *Ophthalmic pathology of animals.* New York: S. Karger; 1975.
188. Parhad IM, Griffin JW, Miller NR. Optic disc swelling. *Comp Pathol Bull AFIP.* 1986;19:2–3.
189. Rao NA, Tang RA, Irving GWI. Demyelinating optic neuritis: model no. 166. In: Jones TC, Hackel DB, Migaki G, editors. *Handbook: animals models of human disease.* Washington, DC: Registry of Comparative Pathology, Armed Forces Institute of Pathology; 1979. p. 1–2.
190. Brown WR, Rubin L, Hite M, Zwickey RE. Experimental papilledema in the dog induced by a salicylanilide. *Toxicol Appl Pharmacol.* 1972;21(4):532–41.
191. Ackerman LJ, Yoshitomo K, Fix AS, Render JA. Proliferative lesions of the eye in rats. *OSS. Guides for toxicologic pathology.* Washington, DC: STP/ARP/AFIP; 1998.

Chapter 7

Nonclinical Regulatory Aspects for Ophthalmic Drugs

Andrea B. Weir and Susan D. Wilson

Abstract Development of ocular products and novel delivery systems for the treatment of retinal and other ocular conditions is an active area of drug development. In the United States of America (USA), regulatory expectations for the nonclinical studies needed to support clinical development of ocular products are not yet defined in a guidance document. Similar to other drugs, however, therapeutics directly administered to the eye undergo safety evaluation in nonclinical studies to support clinical trials and, ultimately, drug approval. The nonclinical testing strategy for an ocular drug (i.e., drugs applied directly onto or into the eye) will be impacted by a number of indication-specific factors including route of administration; extent of systemic exposure, which may be relatively limited especially for some sustained-release delivery systems; and whether the drug is a new molecular entity (NME) or an already approved drug. The nonclinical programs to support development and approval of ocular drugs, therefore, will variably differ from nonclinical programs for drugs administered orally or via other systemic routes. A regulatory perspective on the types of nonclinical safety and toxicity studies appropriate for ocular therapeutics is outlined in this chapter.

A.B. Weir, Ph.D., DABT (✉)
Charles River Laboratories, Preclinical Services, Reno, NV, USA
e-mail: andrea.weir@crl.com

S.D. Wilson, D.V.M., Ph.D. (✉)
Aclairo Pharmaceutical Development Group, Inc., Vienna, VA, USA
e-mail: swilson@aclairo.com

7.1 Introduction

Development of ocular products (i.e., products administered directly on or into the eye), which include both drugs and novel delivery systems for the treatment of retinal and other ocular conditions, is an active area of drug development. Over 30 drugs have been approved by the US Food and Drug Administration (FDA) from 2004 to 2011 and are delineated in Table 7.1. The approved products include NMEs, new formulations, new indications, new manufacturers, and new combinations, with the designation identified under New Drug Application (NDA) chemical type in Table 7.1. As shown in Fig. 7.1, most of the recent FDA approvals, almost 50%, were for reformulations of previously approved drugs as opposed to NMEs.

A number of clinical trials for therapeutics to treat ocular conditions are ongoing. In April 2011, ClinicalTrials.gov, a website offering up-to-date information on federally and privately supported clinical trials, listed clinical trials for approximately 150 ocular diseases. A partial list of clinical trials that were open in April 2011 is shown in Table 7.2. The clinical trials include those that are recruiting participants, will be doing so in the future, or are evaluating drugs available for individuals with a serious disease who cannot participate in clinical trials (e.g., a patient who might not live sufficiently close to a clinical trial site). The clinical trials include new entities that have not yet been approved as well as approved drugs.

In the USA, regulatory expectations for the nonclinical studies needed to support the safety of ocular products are not yet defined in a dedicated guidance document. Similar to other drugs, however, therapeutics administered directly on or into the eye undergo safety evaluation in nonclinical studies to support clinical trials and drug approval. Reports from the nonclinical studies are submitted to the US FDA, initially as part of Investigational New Drug (IND) applications to allow the conduct of clinical trials, then ultimately as part of NDAs or Biologics License Applications (BLA) to gain approval for marketing. Also similar to drugs for other indications, drugs for ophthalmic application include new molecular/new biologic entities as well as reformulations of drugs that have already been approved for both ocular and other routes of administration. The nonclinical testing strategy for an ocular drug, however, will be impacted by a number of indication or drug-specific factors, including route of administration (e.g., topical, intravitreal) and extent of systemic exposure. The route- and indication-specific factors result in nonclinical programs for ocular drugs that variably differ from the programs for compounds administered orally or via other systemic routes. Additionally, the ocular product class itself can influence the type of nonclinical program considered appropriate to support safety. Specifically, a more robust nonclinical program might be appropriate for a class of compounds with a novel mechanism of action vs. compounds for which the mechanism of action has been well characterized.

This chapter provides a regulatory perspective on the types of nonclinical safety and toxicity studies needed to support development of ocular therapeutics. This chapter focuses on FDA/Center for Drug Evaluation and Research's (CDER) regulatory expectations for the nonclinical development of ophthalmic drugs that are administered via an ocular route, such as topical application or intravitreal injection.

Table 7.1 Ophthalmic drugs approved by the FDA from March 2004 through April 2011^a

Approval date	Drug name	NDA chemical type ^b	Indication ^c	Route of administration
Mar 2004	Iquix (levofloxacin)	3	Treatment of bacterial corneal ulcers	Topical
Jun 2004	Istalol (timolol maleate)	3	Treatment of ↑ IOP due to ocular hypertension or open-angle glaucoma	Topical
Dec 2004	Zylet (loteprednol etabonate+ tobramycin)	4	Steroid-responsive inflammation associated with presence or risk of bacterial ocular infection	Topical
Dec 2004	Visionblue (trypan blue)	1	Staining of lens anterior capsule as an aid in ophthalmic surgery	Injection into anterior chamber
Dec 2004	Macugen (pegaptanib sodium)	1	Neovascular (wet) age-related macular degeneration	Intravitreal
Dec 2004	Pataday (olopatadine hydrochloride)	3	Treatment of itching associated with allergic conjunctivitis	Topical
Mar 2005	Bromday (bromfenac sodium)	3	Treatment of postoperative inflammation and pain after cataract extraction	Topical
Apr 2005	Retisert (fluocinolone acetonide)	3	Treatment of chronic noninfectious uveitis of the posterior segment	Intravitreal implant
Aug 2005	Alphagan P (brimonidine tartrate)	3	Treatment of ↑ IOP due to open-angle glaucoma or ocular hypertension	Topical
Aug 2005	Nevanac (nepafenac)	1	Treatment of pain and inflammation associated with cataract surgery	Topical
Jun 2006	Lucentis (ranibizumab)	1 (New biological entity)	Neovascular (wet) age-related macular degeneration	Intravitreal
Sep 2006	Travatan Z (travoprost)	5	Macular edema following retinal vein occlusion	Topical
Dec 2006	Alaway (ketotifen fumarate)	5	Treatment of ↑ IOP due to open-angle glaucoma or ocular hypertension	Topical
Apr 2007	Azasite (azithromycin)	3	Temporary relief of itching due to allergic/irritant conjunctivitis	Topical
Oct 2007	Combigan (brimonidine tartrate + timolol maleate)	4	Bacterial conjunctivitis	Topical
			Adjunctive or replacement treatment of ↑ IOP due to glaucoma or ocular hypertension	Topical

(continued)

Table 7.1 (continued)

Approval date	Drug name	NDA chemical type ^b	Indication ^c	Route of administration
Nov 2007	Triescence (triamcinolone acetonide)	3, 6	Treatment of sympathetic ophthalmia, temporal arteritis, uveitis, ocular inflammation unresponsive to topical corticosteroids, and visualization during vitrectomy	Intravitreal
Jun 2008	Trivaris (triamcinolone acetonide)	3	Sympathetic ophthalmia, temporal arteritis, uveitis, and ocular inflammation unresponsive to topical corticosteroids	Intravitreal
Jun 2008	Durezol (difluprednate)	1	Treatment of inflammation and pain associated with ocular surgery	Topical
Jul 2008	Navstel (hypromellose, dextrose, glutathione, CaCl ₂ , MgCl ₂ , KCl, NaHCO ₃ , NaCl, Na ₃ PO ₄)	3	Intraocular irrigating solution for use during surgical procedures	Intraocular
Oct 2008	Akten (lidocaine hydrochloride)	5	Ocular surface anesthesia	Topical
Feb 2009	Tobradex ST (tobramycin + dexamethasone)	3	Steroid-responsive inflammation associated with presence or risk of bacterial ocular infection	Topical
Feb 2009	Membraneblue (trypan blue)	5	Ocular staining to aid in ophthalmic posterior surgery and facilitating removal of epiretinal tissue	Injection – epiretinal tissues or intravitreal
May 2009	Besivance (besifloxacin hydrochloride)	1	Treatment of bacterial conjunctivitis	Topical
Jun 2009	Ozurdex (dexamethasone)	3	Treatment of macular edema following retinal venous occlusion	Intravitreal injection
Jul 2009	Acuvail (ketorolac tromethamine)	5	Treatment of noninfectious uveitis of the posterior segment	
Sep 2009	Bepreve (bepotastine besilate)	1	Treatment of pain and inflammation after cataract surgery	Topical
			Treatment of itching associated with allergic conjunctivitis	Topical

Sep 2009	Zirgan (ganciclovir)	3	Treatment of acute herpetic keratitis (dendritic ulcers)	Topical
May 2010	Zymaxid (gatifloxacin)	5	Treatment of bacterial conjunctivitis	Topical
Jun 2010	Isopto Carpine (pilocarpine hydrochloride)	3	Treatment of ↑ IOP due to open-angle glaucoma and ocular hypertension Management of acute angle-closure glaucoma Prevention of postoperative ↑ IOP associated with laser surgery	Topical
Jul 2010	Lastacraft (alcaftadine)	1	Induction of mitosis Prevention of itching associated with allergic conjunctivitis	Topical
Aug 2010	Lumigan (bimatoprost)	5	Treatment of ↑ IOP due to open-angle glaucoma and ocular hypertension	Topical
Nov 2010	Moxeza (moxifloxacin)	3	Treatment of bacterial conjunctivitis	Topical
Apr 2011	Lotemax (loteprednol etabonate)	3	Treatment of ocular postoperative inflammation and pain	Topical

^a Information obtained from (<http://www.accessdata.fda.gov/scripts/cder/drugsatfda/index.cfm?fuseaction=Reports.Menu>)

^b Designation of chemical type based on FDA classification: 1 new molecular entity, 2 new ester, new salt, or other noncovalent derivative, 3 new formulation, 4 new combination, 5 new manufacturer, 6 new indication

^c Indication generally derived from approved package insert
IOP intraocular pressure

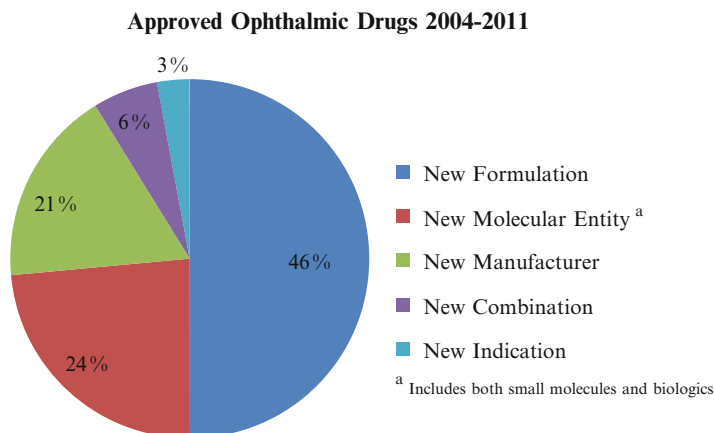


Fig. 7.1 Approved ophthalmic drugs from 2004 to 2011. A total of 33 drugs were reviewed and categorized according to NDA chemical type

Table 7.2 Open clinical trials for drugs intended to treat ocular conditions (small molecules and biologics)

Indication	Number of clinical trials
Conjunctival diseases	72
Diabetic retinopathy	70
Dry eye syndrome	36
Macular degeneration	147
Ocular hypertension	121

7.2 Overview of the Drug Development Process

In the USA as well as in other countries, it is illegal to test new drugs in or to market new drugs to humans without prior approval from the US FDA or the appropriate regulatory body. In order to support the development and approval of drugs, including drugs to treat ocular disease, companies need to present data to the FDA to demonstrate the safety and efficacy of the products being investigated. Generating and reviewing the data required to develop a drug is a multidisciplinary process from both the company and FDA perspective. Drug development involves input from experts in clinical trial design and data evaluation, chemistry and manufacturing, biostatistics, microbiology, and pharmacology/toxicology.

Multiple drug candidates are screened using various assays in the discovery phase of drug development, from which the lead candidate is selected for further development. Nonclinical pharmacology and toxicology studies are needed to support the initiation of clinical trials with the identified drug candidate, and additional nonclinical studies are conducted throughout the drug development process to support the various clinical development phases. Clinical trials are divided into three basic phases as defined in regulations [1], specifically Phases 1, 2, and 3 (Table 7.3).

Table 7.3 Phases of clinical trials

Phase 1	Phase 2	Phase 3
Closely monitored Conducted in patients or normal volunteers	Closely monitored Evaluate the effectiveness of a drug for a given indication(s) in patients with the disease	Intended to gather information relating to efficacy and safety to allow characterization of risk vs. benefit
Determine pharmaco- kinetics, metabolism and/or pharmacology, and potential side effects of escalating doses and, if possible, obtain early evidence of efficacy	Establish short-term side effects and risks	Several hundred to several thousand subjects
Generally 20–80 subjects	Usually no more than several hundred subjects	

In order to initiate a Phase 1 clinical trial, sponsors (i.e., the companies developing drugs) submit an IND to the FDA. The INDs contain data from the appropriate nonclinical studies, a protocol for the proposed clinical trial, information defining the manufacture of the drug, as well as other pertinent information. If the FDA agrees that the data outlined in the IND support the safety of the proposed clinical trial, sponsors can initiate their clinical program. If the FDA does not agree that the IND adequately supports safety, the company's program is placed on clinical hold (i.e., clinical trials cannot proceed in the USA) until the safety concern is resolved to the satisfaction of the FDA. As clinical trials progress, sponsors continue to submit nonclinical studies and other information to FDA for review and comment. Once the sponsor has completed all of the appropriate studies to support approval of their drug for marketing, they submit an NDA or BLA for small molecules and biologics, respectively (small molecules vs. biologics are addressed in Sect. 7.6). The properties of approved drugs, including indication, dosing regimen, and potential adverse effects, are described in the approved package insert, which is also referred to as labeling. Nonclinical data, primarily those obtained from genotoxicity, reproductive toxicology, and carcinogenicity studies, are included in the labeling.

The different types of nonclinical studies and their timing within the drug development process are defined in Sect. 7.7. As noted, sponsors need to present nonclinical and clinical data as well as chemistry and manufacturing data to the FDA to support the safety and efficacy of the products being investigated. A team of reviewers at FDA/CDER evaluates the data contained in the INDs and NDAs/BLAs. The team members include the following: medical officers (i.e., clinicians with appropriate expertise in the given indication), nonclinical pharmacology/toxicology reviewers, chemists, clinical pharmacologists, microbiologists, and biostatisticians. The nonclinical pharmacology/toxicology reviewers generally hold PhDs in pharmacology, toxicology, or another life science.

It is possible for sponsors to meet with the FDA throughout the drug development process [2]. The types of FDA meetings, which are identified as Types A, B,

Table 7.4 Meetings with FDA

Type A	Dispute resolution meetings Meetings to discuss clinical holds Special protocol assessment meetings Should be scheduled within 30 days of FDA's receipt for request
Type B	Pre-IND meeting Certain end-of-phase 1 meetings End-of-phase 2 meetings Pre-NDA/BLA meeting Should be scheduled within 60 days of FDA's receipt of a request
Type C	Any meeting other than type A or B Should be scheduled to occur within 75 days of FDA's receipt of a request

and C, are described in Table 7.4. Sponsors submit formal requests for each of the meetings. If the meeting is granted by the FDA, sponsors will provide the FDA with a meeting package outlining the intent of the meeting, the questions that the sponsor is requesting the FDA to address, and the appropriate background information and relevant data. During the pre-IND meeting, sponsors can present their IND-enabling plan (i.e., nonclinical studies conducted to support the safety of clinical trial[s] proposed in the initial submission) with FDA. During the end-of-Phase 2 meeting, sponsors can review completed nonclinical studies and present their plan to support Phase 3 clinical trials and marketing. At the pre-NDA/BLA meeting, the sponsor should confirm with FDA that there are no gaps in their nonclinical program.

7.3 Regulation of Ophthalmic Products

In the USA, the FDA is responsible for the regulation of all classes of ophthalmic drugs. Additionally, FDA is responsible for the regulation of devices that are being used to deliver ophthalmic drugs. The centers, offices, and divisions within FDA that are responsible for the regulation of ophthalmic products are depicted in Fig. 7.2.

The FDA/CDER is responsible for the regulation of the majority of the ophthalmic drug products. The scope of the drugs that FDA/CDER regulates encompasses small molecules, biologics, synthetic peptides, and oligonucleotides. The biologics are comprised primarily of monoclonal antibodies and their fragments, as well as recombinant human proteins such as cytokines and fusion proteins. Like many other organizations, FDA/CDER undergoes periodic reorganizations. Due to workload and other considerations, the ophthalmic drug products have been combined into a division with other drug classes (based on indication) as opposed to being in their own division. Since approximately 1990, the ophthalmic drugs have been paired with five different groups. Although the clinical ophthalmic review staff generally remains the same with the reorganizations, there are often changes in the nonclinical

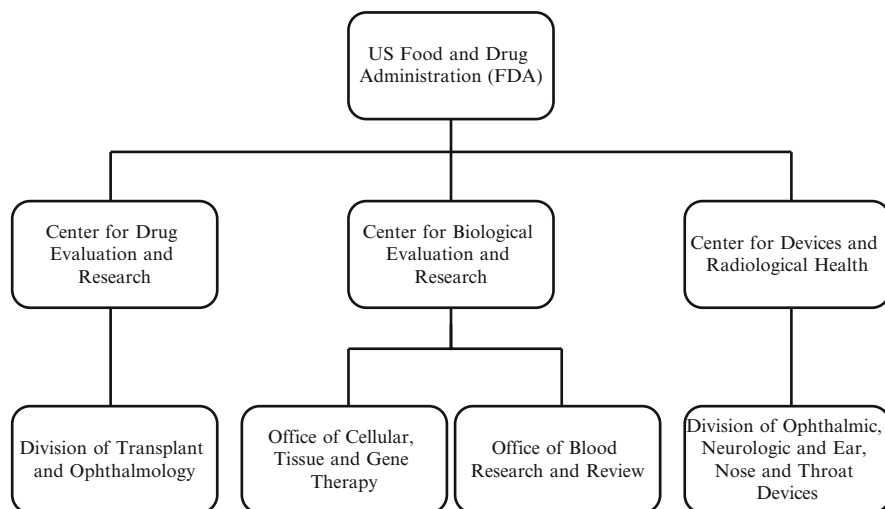


Fig. 7.2 The centers, offices, and divisions within FDA responsible for the regulation of ophthalmic products

reviewers. Consequently, there may be a loss of consistency with regard to nonclinical expectations and review practices for the ophthalmic drug products.

Pharmaceutical and biopharmaceutical companies are actively pursuing drug candidates from the various drug classifications (e.g., small molecules, biologics, devices) for the treatment of ocular diseases ranging from conjunctival and corneal disorders to retinal diseases. In order to facilitate delivery of ophthalmic drug products, especially to the posterior chamber of the eye, companies are developing devices and other novel delivery systems or are forming partnerships with companies capable of developing delivery systems. As noted, devices are regulated by the FDA Center for Devices and Radiological Health (CDRH). If the therapeutic product consists of a drug that utilizes a device for delivery, the product may be designated as a drug-device combination. The regulatory review of drug-device combinations often involves interaction between CDER and CDRH [3]. If the principle therapeutic moiety is the drug component, however, CDER will typically be the lead center evaluating the product. Combination products are discussed in greater detail in Sect. 7.8.2.

7.4 Nonclinical Guidance Documents and Good Laboratory Practice Regulation

The FDA/CDER's expectations for each of the review disciplines referenced in Sect. 7.2 are defined in guidance documents. Guidance documents can be grouped into two basic categories, those generated within FDA/CDER and those generated

Table 7.5 Selected FDA guidance documents pertaining to nonclinical testing to support clinical drug development

Selected FDA nonclinical guidance documents
Estimating the maximum safe starting dose in initial clinical trials for therapeutics in adult healthy subjects (2005)
Genotoxic and carcinogenic impurities in drug substances and products: recommended approaches (Draft, 2008)
Immunotoxicology evaluation of investigational new drugs (2002)
Nonclinical safety evaluation of drug or biologic combinations (2006)
Nonclinical safety evaluation of reformulated drug products and products intended for administration by an alternate route (Draft, 2008)

Table 7.6 ICH guidance pertaining to nonclinical testing to support clinical drug development

ICH guidance documents
ICH S1A; The need for long-term rodent carcinogenicity studies of pharmaceuticals (1996)
ICH S1B; Testing for carcinogenicity of pharmaceuticals (1998)
ICH S1C(R2); Dose selection for carcinogenicity studies of pharmaceuticals (2008)
ICH S2(R1); Genotoxicity testing and data interpretation for pharmaceuticals intended for human use (2011)
ICH S3A; Toxicokinetics: the assessment of systemic exposure in toxicity studies (1995)
ICH S3B; Pharmacokinetics: guidance for repeated dose tissue distribution studies (1995)
ICH S4A; Duration of chronic toxicity testing in animals (1999)
ICH S5A; Detection of toxicity to reproduction for medicinal products (1994) ^a
ICH S5B; Detection of toxicity to reproduction for medicinal products: addendum on toxicity to male fertility (1996) ^a
ICH S6(R1); Addendum: preclinical safety evaluation of biotechnology-derived pharmaceuticals (2011)
ICH S7A; Safety pharmacology studies for human pharmaceuticals (2001)
ICH S7B; Nonclinical evaluation of the potential for delayed ventricular repolarization (QT interval prolongation) by human pharmaceuticals (2005)
ICH S8; Immunotoxicity studies for human pharmaceuticals (2006)
ICH S9; Nonclinical evaluation for anticancer pharmaceuticals (2010)
ICH M3(R2); Nonclinical safety studies for the conduct of human clinical trials and marketing authorization for pharmaceuticals (2010)

^aOn the ICH website, the ICH S5A and S5B guidances are combined into a single document. The content of S5A and S5B, however, were not changed upon combination

under the International Conference on Harmonisation (ICH) process. Both the FDA/CDER and ICH guidances can be found on the FDA website at <http://www.fda.gov/Drugs/GuidanceComplianceRegulatoryInformation/Guidances/default.htm>. The FDA/CDER nonclinical guidance documents generally are prepared by a working group consisting of the nonclinical pharmacology and toxicology reviewers within CDER. A partial list of FDA guidance documents is provided in Table 7.5.

The ICH process involves an international cooperative effort to globally harmonize regulatory expectations for drug development. A list of ICH guidances pertaining to nonclinical development is listed in Table 7.6.

Nonclinical studies intended to support the safety of clinical trials, such as general toxicology and safety pharmacology studies, need to be conducted in compliance with good laboratory practice (GLP). Primary pharmacology and pharmacokinetic (PK) studies, including absorption, distribution, metabolism, and excretion (ADME) studies, are not required to be conducted according to GLP. It is not uncommon, however, for PK and ADME studies to be conducted in accordance with GLP regulations. Requirements for meeting GLP compliance are defined in the Code of Federal Regulations, 21 CFR 58 [4]. The GLP requirement pertains to all aspects of a nonclinical toxicology study. For example, it requires the following:

1. That there is a study director who has overall responsibility for the conduct of the study
2. That there is a quality assurance unit at the testing facility to monitor each study
3. That there is an analytical method for determining the concentration of test article in the dosing solution(s) used to treat the animals

Contract research organizations (CROs) that conduct nonclinical studies to support drug development and pharmaceutical and biopharmaceutical companies conducting such studies themselves should be capable of conducting studies in compliance with GLP. Because a detailed discussion of GLP compliance is beyond the scope of this chapter, readers are encouraged to refer to the cited CFR for additional information.

7.5 Types of Drug Products

Drug products that are either under development or approved can be divided into the following different categories: NMEs, combination drug products, and reformulations. Before considering the various categories in more detail, it is important to define the difference between drug substance and drug product. The former term refers to the unformulated active ingredient, while the latter refers to the complete dosage form. In addition to the drug substance, the drug product contains excipients that are typically inert substances used to create a suitable clinical formulation for the drug. Excipients include fillers, extenders, diluents, solvents, emulsifiers, preservatives, flavors, absorption enhancers, sustained-release matrices, and coloring agents [5].

An NME is defined as an active ingredient that has never been marketed in the USA in any form. If the NME is a chemically synthesized small molecule, it is referred to as a new chemical entity (NCE). On the other hand, if the NME is a biotechnology-derived protein, such as a monoclonal antibody, it is referred to as a new biological entity (NBE).

As drugs are undergoing development or after they are approved, sponsors might choose to further develop the drug as a combination product. Combination products can be subdivided into three categories: fixed-dose combination (FDC), co-packaged,

Table 7.7 Definition of combination product designation

Fixed-dose combination	Two or more separate active ingredients combined in a single-dosage form
Co-packaged	Two or more separate drug products packaged together in their final dosage form
Adjunctive therapy	A patient is maintained on a second drug product that is used in conjunction with the primary treatment. Relative doses are not fixed, and the different drugs or biologics may or may not be given at the same time. They may be co-packaged

and adjunctive therapies [6]. The combination product designations are defined in Table 7.7. Nonclinical considerations for combination ocular products are provided in Sect. 7.8.2.

In addition to developing combination products, sponsors might choose to reformulate a drug product. Reformulation may or may not be associated with a change in route of administration. Generally, additional nonclinical studies are needed to address a change in formulation, especially if it is associated with a change in route of administration. Nonclinical considerations for reformulated ocular drug products are addressed in FDA Guidance for Industry and Review Staff, Nonclinical Safety Evaluation of Reformulated Drug Products and Products Intended for Administration by an Alternate Route [7] and discussed in Sect. 7.8.1.

Both drug substances and drug products can contain impurities. Impurities are defined as any component that is not the drug substance or an excipient in the drug product. They can include by-products, starting materials, degradants, reagents, ligands, and catalysts. The FDA/CDER nonclinical reviewers work closely with the chemistry reviewers in the center to ensure that the safety of impurities is adequately evaluated. Impurities in the drug substance and drug product, including residual solvents, are addressed in ICH guidance documents [8–10]. In addition, the draft FDA guidance, Genotoxic and Carcinogenic Impurities in Drug Substances and Products: Recommended Approaches, addresses a specific concern with respect to impurities [11].

7.6 Biologics vs. Small Molecules and Species Selection

Before considering the types of nonclinical studies needed to support the development of the ophthalmic drugs, it is important to consider differences between chemically synthesized small molecules and biologics. Biologics have properties that distinguish them from small molecules and influence their nonclinical testing strategy. A detailed discussion of the nonclinical development of biologics is beyond the scope of this chapter but is provided in the ICH S6(R1), Preclinical Safety Evaluation of Biotechnology-derived Pharmaceuticals [12]. Additionally, a detailed discussion relating to multiple aspects of biologics development can be

Table 7.8 Comparison of small molecules vs. biologics

Small molecules	Biologics
Chemically synthesized organic molecule	Proteins obtained from living cells
Greater potential for off-target effects due to the potential for chemical impurities, active/reactive metabolites, extensive distribution in the body, and activity at multiple receptors or enzymes	Highly targeted, due to lack of chemical impurities and active/reactive metabolites and decreased potential for extensive distribution as a result of large molecular weight
Generally active and, therefore, potentially toxic in many species	Activity and toxicity generally limited to animals possessing the intended receptor or epitope (i.e., pharmacologically relevant animal model/species)
Pharmacokinetic and pharmacologic considerations when selecting species for nonclinical studies	Primarily pharmacologic considerations when selecting relevant species for nonclinical studies
Generally no or negligible potential for immunogenicity	Animals can frequently mount an immune response (immunogenicity) to biologics

found in the text entitled *Preclinical Safety Evaluation of Biopharmaceuticals* [13]. A summary of the key differences between biologics and small molecules is provided in Table 7.8.

Nonclinical studies for both small molecules and biologics should be conducted in species that are relevant for extrapolation to humans. Relevance can be established based on pharmacology, metabolism, and anatomical considerations. Pharmacological relevance, which refers to a drug's ability to bind to the intended receptor or other target and elicit the intended pharmacological effect, tends to be more of an issue with biologics but may apply to small molecules as well. The ICH guidance for biologics, ICH S6(R1), clearly states that toxicology studies in nonrelevant species can be misleading and are discouraged [12]. In the case of chemically synthesized small molecules, relevance can be defined, at least in part, by metabolism. A cross-species metabolic stability test that includes metabolic profiling should be conducted using an appropriate *in vitro* system, such as isolated hepatocytes from humans and laboratory animals, prior to selecting species for toxicology studies of a small molecule.

Ocular anatomical considerations of the various species used in toxicology studies, which may factor into species selection, are addressed in detail in Chap. 1 of this text. With few exceptions, ocular toxicology studies are conducted in nonrodents (e.g., rabbits, dogs, monkeys, and pigs) due to eye size and other anatomical considerations. Although the eyes of rabbits and dogs differ from those of humans, they are routinely used for ocular toxicology studies. Monkey eyes most closely resemble the human eye, and monkeys are often considered the most appropriate species for intravitreal and other treatments administered to the posterior segment of the eye. They are, however, used less frequently than rabbits or dogs due, at least in part, to cost and ethical issues.

Systemic bioavailability refers to the amount of drug absorbed into the systemic circulation following oral or parenteral administration relative to that achieved

following intravenous (iv) administration. While bioavailability does not truly define relevance per se, it can be used to select the most appropriate species especially for orally administered compounds. It is generally only a minor consideration for ophthalmic drugs.

7.7 Types of Nonclinical Studies Needed for New Molecular Entities Intended for Ophthalmic Indications

Pharmacology and toxicology studies, which are conducted in laboratory animals and/or in vitro systems, are frequently referred to as nonclinical or preclinical to distinguish them from the clinical trials conducted in humans. Even though selected sections of some of the available guidance documents apply to ophthalmic drugs, there are no published guidance documents dedicated to ophthalmic drugs per se. In 1998, FDA/CDER's Division of Anti-inflammatory, Analgesic, and Ophthalmic Drug Products presented a poster at the Society of Toxicology meeting on nonclinical development of ophthalmic drug products, which focused on drugs applied topically to the eye. The poster presentation was followed in 1999 by one that addressed intravitreal drug products. Although the abstracts and handouts from these sessions are dated, sponsors still use the documents to some extent as references for the nonclinical development of ophthalmic drug products. Since 1999, FDA/CDER's pharmacologists/toxicologists have presented their expectations at various scientific meetings, such as Society of Toxicology and other venues, but they have not yet published a guidance document on the topic.

The ICH M3(R2) guidance document defines the types of nonclinical studies needed to support drug development in general and when the studies should be conducted in the development process [14]. The need for the various studies as part of the nonclinical development strategy for ophthalmic drug products vs. a systemically administered drug is summarized in Table 7.9.

A discussion of the different types of studies delineated in Table 7.9 is provided in Sects. 7.7.1, 7.7.2, 7.7.3, 7.7.4, 7.7.5, 7.7.6, 7.7.7, 7.7.8 and 7.7.9. Information from the FDA/CDER nonclinical pharmacology/toxicology reviews for Macugen, Nevanac, Durezol, Besivance, Bepreve, and Lastacaft, six NCEs approved from 2004 through 2010, as well as Lucentis, an NBE, was included in the discussion to provide examples. Bepreve and Nevanac were approved in Japan as orally administered drugs prior to their approval in the USA. Similarly, Durezol was approved in Japan and Europe as a topical formulation for dermatological indications prior to US approval. Information from the nonclinical reviews can be useful and informative in defining nonclinical programs for other NMEs. There are, however, limitations that should be kept in mind when reviewing the information. For example, it is not always apparent whether a sponsor conducted studies on their own initiative or based on FDA request nor is it always apparent whether the drug was previously in development for another route of administration or indication that might have influenced the available nonclinical data and/or nonclinical strategy.

Table 7.9 Comparison of nonclinical studies designed to support an ophthalmic drug vs. a drug administered orally or parenterally

Study type	Needed for ophthalmic drug	Needed for systemically administered drug
Pharmacology	Yes	Yes
In vitro metabolic stability and plasma protein binding for humans and animals	Yes	Yes
Pharmacokinetics	Yes	Yes
Safety pharmacology	Often no	Yes
Genotoxicity	Yes (generally limited to small molecules)	Yes (generally limited to small molecules)
General toxicology	Yes (generally using an ocular and systemic route of administration)	Yes (generally limited to the clinical route of administration)
Reproductive toxicology		
Fertility	Potential for waiver	Yes
Embryo-fetal development	Generally yes	Yes
Pre-, postnatal development	Potential for a waiver	Yes
Photosafety	Yes	Yes
Carcinogenicity	Potential for a waiver	Yes (if needed)
Tissue cross-reactivity	Yes (generally limited to monoclonal antibodies)	Yes (generally limited to monoclonal antibodies)

7.7.1 Pharmacology

Pharmacology studies can be divided into three categories: primary pharmacodynamics, secondary pharmacodynamics, and safety pharmacology. Primary and secondary pharmacodynamics studies are conducted for ocular as well as systemically administered drugs. In contrast, the need for stand-alone safety pharmacology studies is generally limited to systemically administered drugs. The need to conduct studies to evaluate potential drug-drug pharmacodynamic interactions for ophthalmic drug products is generally limited, and a determination as to whether the studies are indicated should be on a case-by-case basis.

Primary pharmacodynamics studies explore the pharmacology of a drug in relation to its intended therapeutic effect and can include both *in vitro* and *in vivo* studies. The studies are designed to define the mechanism of action of a compound as well as efficacy in animal models of disease, when available. Secondary pharmacodynamics studies, on the other hand, explore the pharmacology of a drug outside of its intended therapeutic effect. Safety pharmacology studies investigate the potential for undesirable effects of a drug on physiological functions, such as cardiovascular (CV), respiratory, and central nervous system (CNS) function [15].

The regulatory expectations for primary and secondary pharmacodynamics studies are not well defined, but the studies are intended to provide a basis for predicting

clinical efficacy. Primary and secondary pharmacodynamics studies do not generally need to be conducted in compliance with GLP. Most companies conduct at least a limited battery of *in vitro* and *in vivo* primary pharmacodynamic studies designed to define a compound's mechanism(s) of action, characterize intended target specificity and selectivity, and demonstrate activity in relevant animal models of disease when available. The types of studies conducted are dependent upon the proposed target of the compound and the clinical indication being pursued. For example, the sponsoring company for Lastacaft (alcaftadine), an antihistamine indicated for prevention of itching associated with allergic conjunctivitis, conducted *in vitro* experiments demonstrating the binding of the drug to H₁ and H₂ receptors and mast cell stabilization following IgE binding. Additionally, they demonstrated evidence of efficacy in animal models of allergy [16].

As noted, the potential for secondary pharmacodynamic effects is generally more of an issue for a small molecule compared to a biologic due to the potential for off-target effects as a result of chemical impurities, active or reactive metabolites, frequently extensive distribution in the body, and greater promiscuity with respect to selectivity. It is not unusual for companies to conduct an *in vitro* screen of potential activity at a number of receptors and enzymes.

Safety pharmacology studies investigate the potential adverse effects of a compound on physiological systems, primarily the CV and respiratory systems and the CNS (i.e., systems acutely essential to support life). Indeed, an assessment of these three functions constitutes the core battery of safety pharmacology studies that should generally be conducted prior to human exposure [15]. Typically, CV safety pharmacology studies are conducted in conscious, unrestrained nonrodents outfitted with implanted telemetry devices. The respiratory studies are usually conducted in rats using plethysmography. The CNS studies are typically conducted in rats as well. Other systems, such as renal and gastrointestinal, may be evaluated as well, but these are considered supplemental studies that should be conducted on a case-by-case basis after considering nonclinical and clinical data.

Safety pharmacology studies are conducted in compliance with GLP. The ICH S7A guidance entitled Safety Pharmacology Studies for Human Pharmaceuticals addresses the scope and conduct of the studies and identifies situations in which safety pharmacology studies might not be needed [15]. The guidance states that the studies might not be needed for locally applied compounds, such as ophthalmic drugs, for which the pharmacology is well characterized and systemic exposure or distribution to other tissues is low.

Consistent with this guidance, the core battery of safety pharmacology studies was not conducted using the typical methods for any of the six NCEs approved from 2004 through 2010, with the exception of Macugen. It was not apparent from the nonclinical review for Macugen whether the sponsor conducted the studies on their own initiative or if FDA requested them [17]. The review for Nevanac [18] indicated that although stand-alone studies were conducted to assess CNS, CV, and respiratory function, the methods used were not always standard. For other drugs, assessment of safety pharmacology parameters was limited to endpoints routinely included

in repeat-dose toxicology studies (e.g., electrocardiograms [ECG] in nonrodent species) or stand-alone studies of only selected physiological functions. For example, an assessment of CNS/behavioral and CV function, but not respiratory function, was conducted for Lastacaft [16], and a non-GLP CV study in anesthetized dogs was performed for Bepreve [19].

The position stated in ICH S7A that safety pharmacology studies may not be warranted for topically administered compounds, including ophthalmics, is further supported by the nonclinical review for Besivance (besifloxacin). In that document [20], the nonclinical reviewer stated that safety pharmacology data were not relevant for besifloxacin because systemic exposure following clinical ocular dosing is very low. In addition, the review for Bepreve [19] indicated that the available safety pharmacology data (e.g., standard toxicology endpoints, non-GLP CV study) were adequate because the systemic exposure following ocular administration is low.

The timing recommendation for the conduct of safety pharmacology studies is prior to initiation of clinical trials. If the intended ophthalmic drug is an NME and first in class, the potential liability with respect to safety pharmacology following systemic exposure is not known. In addition, no clinical data are available to determine if the level of exposure observed in the animal ocular toxicity studies extrapolates to humans. For a first-in-class NME ophthalmic drug, therefore, safety pharmacology assessment may be warranted even if systemic exposure is anticipated to be very low and even if not specifically requested by the FDA. The assessment may be conducted, however, in a well-designed nonclinical toxicology study and not as a stand-alone study, an approach that is consistent with ICH M3(R2) [14].

There are scenarios for which clinical data are not necessarily needed to determine whether or not nonclinical safety pharmacology studies are warranted. A decision regarding the need for safety pharmacology studies can be made based on nonclinical PK or toxicology data. Specifically, a sponsor might consider conducting safety pharmacology if systemic exposure following ocular administration is higher than anticipated in animals or if systemic effects are observed in ocular toxicology studies.

7.7.2 In Vitro Metabolic Stability and Plasma Protein Binding for Humans and Animals

The ICH M3(R2) guidance recommends that in vitro metabolic and plasma protein binding data be evaluated prior to initiating clinical trials [14]. The in vitro metabolic studies can be conducted with hepatocytes, microsomal preparations, or, infrequently, liver slices and the protein binding studies with plasma. The species evaluated should include humans as well as the animal species utilized in nonclinical toxicology studies. The studies are often conducted using radiolabeled drug. Considering the relatively low systemic exposure that results from ocular routes of

administration, the relevance of the above studies to ophthalmic drugs may not always be entirely clear. However, considering that systemic effects can occur when drugs are administered via the ocular route (e.g., Timoptic) [21] and the studies are recommended prior to having exposure data in humans, it is generally considered appropriate to conduct the studies.

7.7.3 *Pharmacokinetics/Toxicokinetics*

In the case of compounds dosed via ocular routes of administration, PK evaluation should encompass assessment of systemic exposure (i.e., blood, plasma, or serum levels) as well as distribution and levels in ocular tissues (e.g., cornea, conjunctiva, sclera, iris, ciliary body, lens, vitreous, retina, optic nerve, and aqueous humor) for a given drug. Assessment of systemic exposure should be included as part of the nonclinical toxicology studies regardless of the route of administration. The exposure data generated in toxicology studies are referred to as toxicokinetics (TK). Blood should be obtained at selected time points during the course of the nonclinical toxicology study, typically following the first and last dose administration of the compound to the animals. The time points at which the samples are obtained as well as the number of time points selected should be adequate to characterize the kinetics of the drug, to determine the maximum drug concentration (C_{\max}), and to calculate the half-life. Selection of time points can be particularly challenging for ophthalmic drugs that have a sustained release from depot formulations or following administration of a drug-device combination. It is important to continue sampling for an adequate duration following administration of the sustained-release product to demonstrate when the drug is apparently cleared from the systemic circulation and eye.

Apparent clearance from the systemic circulation does not necessarily reflect clearance of test article from the eye, especially for depot drugs administered by intravitreal injection. Consequently, characterization of ocular distribution is needed to define the kinetics and clearance of the drug from the eye. For logistical reasons, it is most appropriate to assess ocular distribution in a study specifically designed for that purpose. Using radiolabeled compounds for the studies conducted with small molecular weight drugs results in increased sensitivity; however, the use of radioactive compounds is not needed from a regulatory perspective. Although more sensitive, radiolabeled studies potentially have limitations if only the radioactivity levels are quantitated but the radiolabeled moieties are not characterized. It is also important to emphasize that although distribution studies can be applicable to biologics, data generated using radiolabeled proteins might be difficult to interpret because radiolabeled amino acids can be incorporated into endogenous proteins and peptides. If systemic distribution has been shown to be negligible, systemic distribution studies are not warranted.

According to ICH M3(R2), systemic exposure data in the species used in general toxicology studies generally should be evaluated prior to the initiation of clinical trials, but further PK studies (e.g., absorption, distribution, metabolism, and excretion) are generally not needed until prior to Phase 3 clinical trials [14]. Notably, FDA generally expects that ocular distribution studies be conducted prior to initiating clinical trials.

Table 7.10 Genotoxicity testing strategies – ICH S2(R1) recommendations

Option	Testing battery
1.	<p>Bacterial test for gene mutations in bacteria</p> <p>An in vitro cytogenetic test for chromosomal damage or an in vitro mouse lymphoma Tk gene mutation assay</p> <p>In vivo test for genotoxicity, generally a test for chromosomal damage using rodent hematopoietic cells, either for micronuclei or for chromosomal aberrations in metaphase cells</p>
2.	<p>Bacterial test for gene mutation in bacteria</p> <p>An in vivo test for genotoxicity with 2 different tissues, usually an assay for micronuclei using rodent hematopoietic cells and a second in vivo assay (typically, this would be a DNA strand breakage assay in liver, unless otherwise justified); assays may be incorporated into repeat-dose toxicity study if dose/exposure is adequate</p>

It is generally considered that the melanin-binding capability of a drug should be assessed. If a drug binds to melanin, then PK and toxicology studies should include a species with pigmented eyes. Evaluation of the nonclinical reviews for the six ophthalmic NCEs demonstrated that in addition to conducting standard melanin-binding assays, class effects and/or results of tissue distribution studies can be used to investigate the potential for melanin binding [16, 18–20].

7.7.4 Genotoxicity

The need for genotoxicity studies is generally limited to small molecules and applies to both ocular and systemically administered drugs. Testing may not be limited, however, to the active ingredient. It can be extended to excipients and impurities, which are discussed later in this chapter. The recently released ICH guidance document for genotoxicity testing, ICH S2(R1), Guidance on Genotoxicity Testing and Data Interpretation for Pharmaceuticals Intended for Human Use, outlines two options for the standard genotoxicity battery as well as details relating to various aspects of the genotoxicity assays [22]. The two options are shown in Table 7.10.

In general, the companies developing the six NCEs conducted the genotoxicity studies defined in Option 1 of Table 7.10. To ensure adequate exposure in the in vivo studies, animals were dosed parenterally and not by the intended ophthalmic route of administration. In some cases, however, additional studies were conducted. For example, unscheduled DNA synthesis (UDS) was assessed for Besivance [20]. The rationale for the study being conducted was not clear but may have been related to a genotoxicity profile that the FDA reviewer classified as typical for fluoroquinolones. Specifically, Besivance was positive for mutagenicity in some bacterial strains, was clastogenic in Chinese hamster ovary cells, and was positive in the in vivo mouse micronucleus assay. As noted by the FDA reviewer, however, the UDS assay is particularly insensitive. Genotoxicity assays with major metabolites and a Syrian hamster embryo (SHE) cell assay were conducted with Macugen and the metabolites even though the standard

Table 7.11 Length of nonclinical toxicology to support clinical trials of various durations^a

Maximum duration of clinical trial	Recommended minimum duration of repeat-dose toxicity studies to support clinical trials	
	Rodents	Nonrodents
Up to 2 weeks	2 weeks ^b	2 weeks ^b
Between 2 weeks and 6 months	Same as clinical trial	Same as clinical trial
>6 months	6 months	9 months ^c

^aTable as presented in ICH M3(R2)

^bIn the USA, extended single-dose studies can be used to support single-dose clinical trials. In an extended single-dose study, animals receive a single dose. One group of animals is sacrificed within 24–72 h following dosing and a second group following a 14-day recovery period. Additionally, clinical studies of less than 14 days can be supported using toxicology studies of the same duration as the proposed clinical study

^cAccording to ICH M3(R2), studies of 6-month duration in nonrodents are considered acceptable in Europe. Conditions under which 6-month studies would be appropriate in the USA or Japan are addressed in ICH M3(R2). It should be noted that according to ICH S6(R1), 6 months is considered a sufficient maximum duration for biologics

battery of genotoxicity assays was negative for Macugen. The studies were conducted to support a request for waiver of carcinogenicity, which was granted by the FDA [17].

Because biologics are proteins, it is not expected that they will interact with DNA or other chromosomal material. That position is presented in the ICH S6(R1) guidance [12]. Consistent with the guidance, genotoxicity studies were not conducted to support the approval of Lucentis [23], a recombinant humanized monoclonal antibody fragment.

7.7.5 General Toxicology Studies

General toxicology studies are needed for ocular as well as systemically administered drugs. In order to support the development of ophthalmic drug products, general toxicology studies need to be conducted using two routes of administration, the intended ocular route and a systemic route (e.g., oral, iv). In the case of systemically administered drugs, the route of administration used in toxicology studies is generally limited to the intended clinical route. The purpose of the ocular toxicology study is to assess ocular and systemic toxicity following treatment via the clinically relevant ocular route of administration. Systemic exposure following administration of the drug by the ocular route is generally very low or negligible, precluding adequate characterization of the systemic toxicity profile. Thus, in order to define the systemic toxicity of an ophthalmic drug, studies are conducted using an oral or parenteral route.

Toxicology studies are needed throughout the drug development process to support the various phases of clinical trials. As defined in the ICH M3(R2) guidance document [14] and as outlined in Table 7.11, the duration of the toxicology study

Table 7.12 Duration of the nonclinical toxicology studies to support marketing approval^a

Duration of indicated treatment	Rodent	Nonrodent
Up to 2 weeks	1 month	1 month
>2 weeks to 1 month	3 months	3 months
>1–3 months	6 months	6 months
>3 months	6 months	9 months ^b

^aTable as presented in ICH M3(R2)

^bAccording to ICH M3(R2), studies of 6-month duration in nonrodents are considered acceptable in Europe. Conditions under which 6-month studies would be appropriate in the USA or Japan are addressed in ICH M3(R2). It should be noted that according to ICH S6(R1), the guidance for biologics, 6 months is considered a sufficient maximum duration for biologics

needed to support clinical development increases with the duration of the clinical trial. As indicated in Table 7.11, there are regional differences in the recommended duration of nonclinical toxicology studies.

In general for the USA, the duration of the nonclinical toxicology study needs to be at least of comparable duration to the clinical trial it is designed to support for either ocular toxicity studies or studies to assess systemic toxicity of an ophthalmic drug (i.e., drug administered by the oral or parenteral route). In addition, FDA will typically expect to see a 9-month chronic toxicity study in a nonrodent for small molecules, with the acceptability of a 6-month study the exception rather than the rule.

The maximum duration of the nonclinical toxicology studies required to support marketing of a drug regardless of administration route is dependent on the duration of treatment and is outlined in Table 7.12. The three regions, USA, Europe, and Japan, are in general agreement with the appropriate duration of the toxicology studies except for the recommended duration of the chronic nonrodent study.

The FDA/CDER does not have a guidance document addressing the nonclinical toxicology study design. However, there are documents, such as the FDA's Center for Food Safety and Applied Nutrition's Redbook [24], the OECD (Organisation for Economic Co-operation and Development) guidelines [25–27], as well as other publications [28, 29], that address the topic. Briefly, such studies should be conducted in compliance with GLP. Nonclinical toxicology studies generally consist of four groups: a control or vehicle group and three treatment groups receiving a low, mid, and high dose of the test article. The dosing frequency and duration (Tables 7.11 and 7.12) should be appropriate for the intended clinical usage. Toxicity is assessed based on clinical observation, body weight, food consumption, ECG (nonrodents only), ophthalmic examination, clinical pathology (hematology, clinical chemistry, coagulation, and urinalysis), gross necropsy, organ weight, and histopathology data. To confirm exposure and define the TK profile, blood samples are obtained at appropriate time points after dosing and analyzed for serum or plasma levels of drug. In addition, dosing formulations are analyzed at various time points throughout the study to demonstrate that the formulations are properly prepared and that the animals are being dosed at the intended dose levels.

7.7.5.1 Systemic Toxicology Studies for Ocular Drug Products

As noted, the toxicity profile of the compound cannot generally be fully characterized in ocular toxicology studies because systemic exposure following ocular administration of compounds is typically low. The nonclinical development program for ophthalmic drugs that are NCEs/NBEs, therefore, includes toxicity studies conducted using a systemic route of administration, such as oral or iv. In general, the oral route of administration may be more appropriate for compounds applied topically to the eyes because such compounds are frequently swallowed and ultimately end up in the gastrointestinal tract. On the other hand, the iv route is generally considered more appropriate for compounds injected into the posterior chamber of the eye because such compounds have relatively direct access to the bloodstream. The repeat-dose systemic toxicology studies for Lastacaft, Besivance, Bepreve, and Nevanac, all of which are applied topically to the eyes, were conducted using the oral route of administration [16, 18–20]. In the case of Macugen, which is administered via intravitreal injection, the systemic studies were conducted via the iv route [17].

The number of species that has been requested by the FDA for evaluation of general toxicology has changed over the years. At one time, a single species, typically a rodent, was considered adequate to address the systemic toxicity following the oral or parenteral administration of an ophthalmic drug. More recently, however, general toxicology studies in a rodent and nonrodent species have been required to support the development of an ophthalmic drug. The FDA may accept limiting systemic toxicity studies to a single species, possibly rodent, if (1) the compound being evaluated belongs to a class with an established safety profile, (2) toxicity in a single species following adequate systemic exposure is of low order, and/or (3) systemic exposure following ocular administration is shown to be low. In the case of Lastacaft, Besivance, and Bepreve, the rat and dog were used for systemic toxicology studies [16, 19, 20]. In contrast, only rats were used for repeat-dose systemic toxicology for Macugen and Nevanac [17, 18]. No systemic toxicity studies were conducted for Lucentis, which is administered intravitreally [23]. As discussed in Sect. 7.10, scientific justification for a nonclinical testing strategy utilizing a single species for an NCE/NBE should be presented to the FDA early in the development program (e.g., at a pre-IND meeting) to obtain concurrence with the approach.

The frequency of administration should be appropriate for the frequency of dosing in the clinic and should factor in the duration of exposure following dosing in the clinic vs. nonclinical setting. For example, if monthly injections into the eye could potentially result in sustained release of the compound, then the frequency of administration in the systemic toxicology study should be increased accordingly to either mimic or, preferably, to exaggerate the potential duration of exposure. In the case of Macugen, which is injected into patients' eyes every six weeks, rats received daily iv injections for 13 weeks [17].

The formulation used in systemic toxicology studies should be appropriate for the route of administration. It is not necessary, and is frequently not feasible, to test the ophthalmic formulation via a systemic route of administration. If the ophthalmic

formulation contains novel excipients (i.e., excipients that are not in approved ophthalmic products), however, it may be necessary to conduct toxicity studies with the excipient (discussed in Sect. 7.8.3).

7.7.5.2 Ocular Toxicology Studies

Ocular toxicology studies are conducted to define the ocular and systemic effects of a compound following ocular administration. A number of factors, including species selection, method of compound administration, and endpoints for assessing toxicity, need to be considered when planning ocular toxicology studies.

As for systemic toxicology, the number of species that has been requested by the FDA for ocular toxicology studies has changed over the years. Previously, a single species, typically a nonrodent, was considered adequate to address potential ocular toxicity. Currently, ocular toxicology studies for an NME are generally conducted in two nonrodent species, but there can be exceptions. Factors to consider when choosing the number of species include the nature of the compound, mechanism of action, and indication. Using two species would likely be required by the FDA for compounds having one or more of the following properties: (1) first in a chemical class to be tested, (2) an NME (but not first in class), and/or (3) a novel mechanism of action. In contrast, one species might be more appropriate for compounds belonging to a class known to have a favorable safety profile or in the case of an NBE for which there is only a single pharmacologically relevant species.

A number of factors should be considered when selecting a species for ocular toxicology studies, including melanin binding, anatomical considerations, and, in the case of biologics, species specificity. If a compound binds to melanin, then ocular toxicology studies should be conducted in species with pigmented eyes. For compounds to be injected or implanted into the eye, as in the case of device-based delivery platforms, one of the primary considerations is the size of the eye. Specifically, the eye of the selected species needs to be large enough to accommodate the mode of administration being used. In the case of biologics, species specificity should be considered. Based on ICH S6(R1), toxicology studies with biologics should be limited to relevant animal models, defined as animals in which the biologic is active due to the presence of a receptor or, in the case of a monoclonal antibody or antibody fragment, the epitope [12]. Techniques for identifying a relevant animal model for a biologic include flow cytometry, immunohistochemistry, and/or functional assays. The approach(es) used should be customized to the biologic.

Generally, ocular toxicology studies are conducted in one or two nonrodent species, such as rabbit, monkey, dog, or pig. Although dogs have a tapetum (refer to Chap. 1 of this text for additional information), an anatomical feature that distinguishes them from humans, rabbits, monkeys, and pigs, it does not preclude use of the dog in ocular toxicology studies conducted for regulatory purposes. Indeed, dogs were used in combination with rabbits for the ocular toxicology

studies conducted to support the development and approval of Besivance, Bepreve, and Durezol [19, 20, 30] and in combination with rabbits and monkeys to support the same for Macugen [17]. Dogs were not used for the ocular toxicology studies conducted for Lastacaft, Nevanac, or Lucentis [16, 18, 23]. While rodents might be appropriate for ocular toxicology studies being conducted early in the drug development process (i.e., screening studies), they are not appropriate models for ocular studies intended to support the safety of clinical trials due, in part, to the small size of their eyes. Although the nonhuman primate may be considered to be the most appropriate animal model for ocular toxicology studies because of similarities to the human eye, their use was very limited for the six NCEs approved from 2004 to 2010. Nonhuman primates were used to assess ocular toxicity in only two NCEs, Macugen and Nevanac. The maximum duration of the ocular toxicity studies in the nonhuman primates was three months with studies of longer duration for Macugen conducted in the rabbit and/or dog [17, 18]. Nonhuman primates were not used in the other four of the six drugs [16, 19, 20, 30]. Generally ocular toxicity studies were conducted in two species [18–20, 30]. The exceptions were Macugen, for which ocular toxicity studies were conducted in three species [17], the rabbit, dog, and monkey, and Lastacaft, which utilized a single species, the rabbit [16]. The ocular toxicology studies for Lucentis, an NBE, were limited to monkeys [23].

Route and frequency of administration, duration of treatment, and the formulation to be tested should be considered when planning and conducting ocular toxicology studies. The route of administration should be the same as that being used in the clinic. The frequency of administration should at least be equal to that intended for the clinical usage. The appropriate duration for these studies is comparable to that outlined in the ICH M3(R2) guidance document [14] for general toxicology studies (Tables 7.11 and 7.12).

The clinical formulation should be used in the ocular toxicology studies as well as a formulation in which the concentration of active compound exceeds that in the clinical formulation (i.e., enriched formulations), if possible. The goal of utilizing enriched formulations is to exaggerate the exposure that will occur in the clinic. If it is not technically feasible to enrich a formulation, the frequency of administration used in the ocular toxicology studies should be increased to exaggerate the clinical treatment regimen. For example, in the 4- and 13-week ocular toxicology studies conducted with Bepreve in the rabbit and dog, respectively, and in the 26-week study conducted in dogs, the active ingredient was administered as a 1.5% solution, which is the same as the clinical formulation. However, the dosing frequency was up to eight times daily as compared to twice daily in the clinic [19]. In the case of device-based delivery systems, the amount of compound delivered should be increased to the extent feasible. Possible approaches for achieving this goal include not only increasing the drug concentration in the device but increasing the number of devices implanted relative to the clinical regimen.

It is not unusual for the clinical formulation to evolve over the course of development. Depending on the nature of the change (e.g., excipient that potentially alters

Table 7.13 Standard endpoints evaluated in nonclinical ocular toxicity studies

Ocular endpoints	Systemic endpoints
Gross observations	Observations
Slit lamp biomicroscopy	Body weight
Funduscopy	Food consumption
Tonometry	Clinical pathology
Electroretinography	Necropsy
Histopathology	Organ weights
	Histopathology
	Toxicokinetics
	Immunogenicity (biologics)

the PK of the drug), additional studies to assess the ocular toxicity of the formulation may be required. The nonclinical studies, which may include short-term ocular toxicity studies that evaluate toxicity and/or PK following ocular administration, are designed to bridge (i.e., termed bridging studies) to the existing nonclinical toxicity data.

Ocular toxicology studies include endpoints for assessing both ocular and systemic toxicity. The endpoints typically evaluated as a minimum are shown in Table 7.13. Depending on the duration of the study, the ocular endpoints, with the exception of histopathology, are generally evaluated at multiple time points. The methodologies for specifically characterizing the ocular toxicity of a drug in the nonclinical studies are discussed in detail in Chaps. 2, 3, 4, 5, and 6.

7.7.6 Reproductive Toxicology Studies

Reproductive toxicology studies address the effects of compounds on all phases of reproduction, ranging from fertility through postnatal development. The studies, which are described in detail in the ICH S5 documents [31, 32], can be divided into three phases: (1) fertility and early embryonic development (Segment I), (2) embryo-fetal development (Segment II), and (3) pre- and postnatal development (Segment III). In general, all stages of reproduction need to be assessed for systemically administered drugs. There is, however, the potential for flexibility with ocular drugs due to the potential for limited systemic exposure. For biologics administered via the ocular route of administration, pharmacological relevance can impact the manner in which reproductive toxicology is assessed. Reproductive toxicology testing for biologics is addressed in ICH S6(R1) [12].

Reproductive toxicology studies conducted to support the safety of ophthalmic drugs should use a systemic route of administration. Embryo-fetal development studies generally are needed for all NCEs, regardless of the level of systemic

exposure following ocular administration. It might be possible under certain circumstances, however, to obtain concurrence from the FDA that fertility and early embryonic development and/or pre- and postnatal development studies are not warranted. Factors that should be considered when determining whether the Segment I and III studies are needed include, but are not limited to:

1. Nature of the compound – for example, first in class vs. a member of an established class, cause for concern
2. Mechanism of action – for example, novel and/or not well defined vs. well understood
3. Systemic exposure following ocular administration, specifically clinical exposure relative to exposure levels causing toxicity in systemic nonclinical toxicology studies
4. Toxicity profile relative to systemic exposure
5. Clinical indication, with the studies less likely to be needed when the compound is intended to treat a serious condition with limited treatment options or in a geriatric patient population

In order to obtain concurrence that the studies are not needed, a request for a waiver should be submitted to FDA/CDER's Division of Transplant and Ophthalmology Drug Products.

Although there is the potential to obtain a waiver for all reproductive studies except the embryo-fetal development studies, the full battery of reproductive toxicity studies were conducted for all of the NCEs [16, 18–20, 30] except for Macugen. In the case of Macugen, reproductive toxicology testing, specifically embryo-fetal development, was limited to a GLP study conducted in mice using iv administration and a non-GLP study in rabbits using intravitreal administration [17]. It was not evident from the pharmacology/toxicology reviews whether the decision to conduct Segment I, II, and III studies was driven by specific FDA requests/recommendations or whether it was an internal decision by the sponsor. No reproductive toxicology studies were conducted for the US approval of Lucentis [23].

7.7.7 Photosafety

Photosafety, while an area of varying concern for regulatory authorities and the pharmaceutical industry for over 30 years, has garnered more attention from both groups in the last several years. The interest is reflected in the issuance of the FDA photosafety guidance document [33], the inclusion of photosafety evaluation in ICH M3(R2) [14], and, most recently, the planned development of the ICH S10 photosafety guidance document [34]. Whether ocular photosafety evaluations will be addressed in ICH S10 and the potential impact of any such inclusion on ophthalmic drug development is not known. Most nonclinical evaluations of ocular phototoxicity have been performed for drugs that are intended to be administered via the oral or iv route, and there has historically been little interest in photosafety evaluation of

drugs administered by topical instillation or intravitreal administration. The standard thinking for topical instillation was that the residence time on the eye of a drug administered by topical installation is very brief and evaluation for photosafety could potentially be performed using a standard dosing regimen and study design. Consequently, there has generally been minimal to no concern for the potential phototoxicity of topically instilled ophthalmic drugs. Interest in photosafety evaluation with topical instillation, however, has recently increased, and the concern can be successfully evaluated in a nonclinical rat model. In addition, the development of methods for photosafety evaluation of drugs administered by the intravitreal route is under way, in response to requests from industry to evaluate drugs administered following drug administration by this route (Learn, Personal Communication, April 2012).

7.7.8 Carcinogenicity Studies

The conditions under which carcinogenicity studies are needed are addressed in the ICH S1A guidance document [35]. Carcinogenicity studies generally are required for compounds when the expected clinical use is continuous for at least six months or for drugs used in a chronic intermittent manner. With regard to pharmaceuticals administered via the ocular route, ICH S1A states that unless there is a cause for concern and/or notable systemic exposure occurs following ocular administration, carcinogenicity studies are not warranted. Cause for concern can result from demonstration of carcinogenic potential relevant to humans in the product class, a structural alert suggestive of carcinogenic risk, evidence of preneoplastic lesions in repeat-dose toxicity studies, and/or long-term tissue retention of parent compound and/or metabolite resulting in pathophysiological responses. As for the reproductive toxicology studies, a request for a waiver of the carcinogenicity studies for a chronically administered ophthalmic drug should be submitted to FDA/CDER's Division of Transplant and Ophthalmology Products. The factors that should be considered when preparing the scientific justification for a waiver are the same as defined for reproductive toxicology studies with the exception of drugs to be used in the elderly. The FDA/CDER generally expects carcinogenicity studies to be conducted for drugs to be used in the elderly.

No carcinogenicity studies were conducted for three of the six identified NCEs that did not meet the criteria outlined in ICH S1A for conducting the studies [35], specifically Besivance, Durezol, and Nevanac [18, 20, 30]. Of the three NCEs intended for chronic use, Lastacaft, Bepreve, and Macugen, carcinogenicity studies were conducted for Bepreve only [19]. According to the nonclinical reviews for Macugen and Lastacaft, carcinogenicity studies were waived. The rationale for granting the waiver for Lastacaft was based on negative results in an extensive panel of genetic toxicology studies, an expectation of intermittent clinical dosing, low carcinogenicity potential for the antihistamine class, lack of carcinogenicity concern for the drug and its major metabolite based on structural alert analysis, an absence

of preneoplastic lesions in the oral repeated dose toxicology studies, no indication of long-term retention in tissues, and low systemic exposure following topical ocular administration [16]. In the review for Macugen, the pharmacology/toxicology reviewer indicated that the waiver was based on the “drug’s property,” negative results in a SHE cell assay, and results of the other nonclinical studies that were conducted [17].

Standard 2-year carcinogenicity assays in rodents can be of limited value for biologics because rodents are frequently not a relevant model or may develop antidrug antibodies that preclude long-term testing. In addition, assessment of carcinogenic potential in rodents using a homologous protein is considered of limited value. If an assessment of the carcinogenic potential is needed for a biologic based on duration of treatment and patient population, ICH S6(R1) recommends that the strategy could be based on a weight of evidence approach using data from a variety of sources [12]. Data to be considered can include published data, information on class effects, detailed information on target biology and mechanism of action, in vitro data, data from chronic toxicity studies, and clinical data. As for a small molecule, the magnitude of systemic exposure in patients will be a factor in determining the need for carcinogenicity assessment. Carcinogenicity was not assessed for Lucentis. However, a rationale was not provided in the FDA/CDER pharmacology/toxicology review of the BLA for Lucentis [23].

7.7.9 Tissue Cross-Reactivity

Tissue cross-reactivity (TCR) studies utilize immunohistochemistry to define the binding of monoclonal antibodies to their targets. The TCR studies can be conducted using frozen sections of human and animal tissues to define potential target organs and to identify a relevant species for nonclinical testing. Guidance relating to TCR studies can be found in ICH S6(R1) [12]. A tissue cross-reactivity study was conducted with human tissues to support the clinical development and approval of Lucentis [23].

7.8 Nonclinical Approaches for Reformulated Drugs, Combination Drug Products, Excipients, and Impurities

7.8.1 Reformulated Products

As demonstrated in Table 7.1 and Fig. 7.1, a significant proportion of approved ophthalmic drugs, almost 50%, are reformulations of previously approved drug substances. In March 2008, FDA/CDER published a draft guidance defining the nonclinical expectations for reformulated drug products and products intended for

use by an alternate route of administration [7]. The following recommendation is provided regarding ocular drug products:

If the active ingredient has not been used by the ocular route, then toxicity studies in two species with complete eye and systemic evaluation of the appropriate duration should be carried out with the new formulation. In certain cases, studies in one most appropriate species may be adequate. Optimal design of these studies would include the evaluation of ocular and systemic PK. Ocular toxicity can be assessed using slit lamp biomicroscopy (with fluorescein staining), tonometry and histopathology. Nonclinical ocular toxicology studies generally should be conducted with vehicle control and complete formulation groups.

The guidance, however, does not define cases in which one species might be appropriate nor does it address the expectations for drugs that have already been approved for use via the ocular route.

The pharmacology/toxicology reviews for reformulated ocular drugs provide insight into the different strategies that have been successfully used to gain approval for reformulated ocular drugs. Reformulated ophthalmic drugs can be grouped into two basic categories. The first category includes drugs that are already approved for an ophthalmic indication but are being reformulated to alter the properties of an already-approved product (e.g., enhance ocular bioavailability, change to a more appropriate preservative). The second category includes drugs already approved for use via an oral, subcutaneous (sc), iv, or other nonocular route. Regardless of the category, bridging studies will likely be needed and often include ocular PK and toxicology studies in at least one species.

An example of a drug that would fall into the first category is Trivaris, triamcinolone acetonide injectable suspension (80 mg/mL), which was approved by the FDA in 2008. According to the FDA summary review, an injectable triamcinolone-containing formulation using benzyl alcohol as a preservative, Kenalog-40, has been used to treat ocular inflammatory conditions that are not responsive to topical steroids [36]. While the Kenalog-40 formulation had an acceptable safety profile, a rare association between the benzyl alcohol preservative and noninfectious endophthalmitis has been noted. Trivaris is a preservative-free formulation of triamcinolone acetonide developed for intravitreal use. To support development and approval of the reformulated product, the sponsor that developed Trivaris conducted an ocular PK study and a 3-month ocular toxicology study in New Zealand white (NZW) rabbits with triamcinolone acetonide [37].

An example of a drug that would fall into the second category is AzaSite, 1% azithromycin solution, approved by the FDA in 2007 for the treatment of bacterial conjunctivitis caused by susceptible bacterial strains. Previously, systemic formulations of azithromycin have been approved [38]. In order to support the development and approval of AzaSite, the sponsor conducted ocular PK studies in NZW rabbits, ocular toxicology studies with AzaSite 1% for up to one month in Dutch-belted rabbits, and an ocular toxicology with vehicle excipients for up to 52 weeks in NZW rabbits [39].

It should be remembered that each reformulated product is unique and has its own potential concerns. The approaches used in the two examples cited, therefore,

might not be appropriate for all reformulated products. While, as noted, the non-clinical reviews for reformulated products provide insight into possible approaches, it is recommended that FDA be consulted for each individual product.

7.8.2 Combination Products

Nonclinical approaches for evaluation of combination drugs are addressed in FDA/CDER's guidance document entitled Nonclinical Safety Evaluation of Drug or Biologic Combinations and in ICH M3(R2) [6, 14]. Although neither document specifically addresses ophthalmic drug products, the concepts in both are applicable. Both documents provide information for sponsors to consider in determining whether a combination toxicology study is needed. For example, according to ICH M3(R2):

Nonclinical combination toxicology studies generally are not recommended to support small clinical trials of relatively short duration (e.g., phase 2 clinical trials up to 3 months in duration) for two late stage products for which there are no significant toxicological concerns based on available data even if there is not adequate clinical experience with co-administration. However, nonclinical combination toxicology studies, generally limited to a single relevant species, are recommended before larger-scale or long-term combination studies and for marketing.

Combination drug products may be comprised of either one or more approved drugs, one or more NCEs/NBEs, or an approved product(s) plus one or more NCEs/NBEs. The FDA guidance suggests that in addition to the available nonclinical package for the various components of the combination drug product, there are a number of factors that will impact whether or not additional nonclinical studies are warranted. The other factors include previous human experience with the combination; the potential for a pharmacodynamic, PK, toxic, or chemical interaction; the seriousness, reversibility, and/or monitorability of any potential interaction; and the margin of safety for each drug in the combination. The design of any additional nonclinical studies will be dependent on the intended clinical usage, with a single species acceptable based on similarity of toxicity profile across species and relevance to or concordance with humans. The sponsor will need to provide a scientific justification to the FDA and obtain concurrence for the proposed nonclinical strategy [6].

Two combination products for ophthalmic use approved since 2004 were identified. The products include Zylet, a combination of loteprednol etabonate and tobramycin for treatment of steroid-responsive ocular inflammatory conditions, and Combigan, a combination of brimonidine tartrate and timolol maleate for the reduction of increased intraocular pressure associated with glaucoma or ocular hypertension. In the case of Zylet, the sponsor conducted a 14-day and 6-month ocular toxicology study in Dutch-belted rabbits in addition to a pharmacology study and ocular distribution studies in NZW and Dutch-belted rabbits, respectively [40].

Similarly, the sponsor for Combigan conducted a 6-month ocular toxicity study in NZW rabbits as well as several absorption and distribution studies. A 1- and 3-month toxicology study was conducted primarily to qualify, or characterize the toxicity profile of, the levels of a new impurity at the proposed specification limits. The studies, however, included both stressed (i.e., stored under accelerated conditions of 40°C and 20% relative humidity for 7 months) and non-stressed combination test article. Evaluation of impurities is discussed in more detail in Sect. 7.8.4. The FDA reviewer concluded that no pharmacology studies were warranted for Combigan because there was extensive clinical use of the two drugs being prescribed together to reduce intraocular pressure [41]. It is unclear from the reviews as to whether the ocular toxicology studies conducted for Zylet and Combigan were required by the FDA but may be warranted, in part, due to the inherent sensitivity of the eye as a target organ for both nonspecific and specific toxicity effects.

7.8.3 Excipients

Guidance relating to the need to assess in nonclinical studies the toxicity of excipients, also referred to as inactives to distinguish them from the drug substance, can be found in FDA's Nonclinical Studies for the Safety Evaluation of Excipients [5]. Information on inactive ingredients present in FDA-approved drug products can be found in a listing of inactive ingredients on the FDA website (<http://www.accessdata.fda.gov/scripts/cder/iig/index.cfm>). According to information provided on the website, once an inactive ingredient appears in an approved product for a particular route of administration, the inactive is no longer considered novel. When using the information from the inactive ingredients website, it is important to consider the concentration of the inactive being used in the drug being developed compared to the concentration in the approved product(s) administered by the relevant route.

As part of the review process of any submission, the FDA/CDER nonclinical reviewer ensures that the sponsor has adequately addressed the safety of excipients. For example, in the nonclinical review for Durezol, the reviewer noted that the inactive ingredients in the formulation, castor oil and polysorbate 80, had a history of ocular use or were tested in rabbit eyes. The reviewer concluded that the inactives were acceptable for use at the proposed concentrations. It is unclear whether the test article used in the 4-week ocular toxicity in NZW rabbits was the intended clinical formulation, but the sponsor conducted a 7-day ocular irritation study with polysorbate 80 in NZW rabbits at a concentration comparable to that present in the clinical formulation [30].

If an excipient is novel, the toxicity profile will need to be fully characterized. In general, as outlined in FDA Guidance Nonclinical Safety Studies for the Safety Evaluation of Pharmaceutical Excipients [5], the evaluation of a novel excipient is similar to that for an NME, although the risk-benefit considerations are notably different for an inactive ingredient vs. a therapeutic agent.

7.8.4 *Impurities*

As with other routes of administration, there are impurity thresholds for drugs administered by the ocular route. The ICH Q3 guidance documents address impurities in a general sense and propose a nonclinical approach for qualifying impurities [8, 9]. The proposed levels requiring qualification, while applicable to drugs administered orally or by iv, intramuscular, or sc injection, for example, may not be applicable to ophthalmic drugs. If the level of the impurity in the clinical or to-be-marketed ophthalmic formulation exceeds what was assessed in the nonclinical ocular toxicity studies, additional qualification in nonclinical studies may be required. Advice from the FDA is recommended to determine the acceptability of impurity levels and the need for additional studies to qualify any impurity.

The FDA has developed a draft guidance that defines approaches for assessing the genotoxic and carcinogenic potential of impurities and steps to be taken if such an impurity is identified [11]. Additionally, ICH is in the process of developing a guidance document for genotoxic impurities, which is scheduled to be completed in 2013 [42].

As noted, the impurity profile of the drug product (e.g., chemical characteristics and levels present) used in the nonclinical toxicology studies should ideally be the same or higher as that proposed for clinical trials. During the course of drug development, however, changes in manufacturing and other events can occur that can result in the need to conduct additional studies to qualify impurities. For example, the sponsoring company for Combigan conducted a 1- and 3-month ocular toxicology study in NZW rabbits, a bacterial mutation assay, and a chromosomal aberration assay to address the safety of an impurity [41]. Toxicology studies conducted to qualify impurities can be limited to the impurity. More commonly, however, and especially for general toxicology studies, the test article is comprised of the drug substance containing exaggerated levels of the impurity. The test article used to qualify the impurity of concern for Combigan was the drug substance with exaggerated levels of the impurity.

7.9 **Extrapolation of Nonclinical Data to Clinical Trials and Use in Labeling**

Data generated in nonclinical toxicology studies are used to support the safety of clinical trials and marketing approval. Specifically, the studies define the toxicity profile of a compound, which includes identifying target organs, dose-response relationships for adverse effects, and reversibility or delayed onset of effects. The toxicity profile obtained in nonclinical studies aids in the design of the clinical trials with respect to appropriate monitoring, exclusion of vulnerable patients from the clinical trial, and/or limiting dose escalation and/or dosing duration. The goal is to avoid toxic doses and ensure that the trial can adequately identify possible adverse events.

Different approaches, identified in the reviews of the six NCEs approved between 2004 and 2010 and discussed in Sect. 7.7, were used to define the ocular safety factor for extrapolating nonclinical data to humans [16, 19, 20, 30]. The approaches include a direct comparison of the nonclinical and clinical dosing regimens without calculating a safety factor per se as well as a comparison of the nonclinical ocular no observed effect level (NOEL) to the clinical dose after normalizing doses to vitreal volume or conjunctival surface area. Of the two approaches, dose normalization for the relevant ocular compartment provides a more scientifically reasonable approach for extrapolating data across species with regard to ocular effects. The no observed adverse effect level (NOAEL), however, is considered a more appropriate dose for comparison than the NOEL since not all drug effects are necessarily adverse. The rationale for the approach used to calculate safety margins was not always clear, and other approaches likely could have been justified. In some cases, multiple approaches might be appropriate. Regardless of the approach, the route of administration and ocular distribution of the compound should be considered when selecting the best approach for extrapolating nonclinical data to humans.

In contrast to the ocular safety, calculating a systemic safety factor is more straightforward. Two basic approaches can be used, comparing the NOAEL dose from nonclinical studies to the clinical dose based on either a body weight or surface area dose equivalency or by comparing systemic drug exposure achieved in animals at the NOAEL to that achieved in patients. In general, the preferred method is a comparison of systemic drug exposure (generally area under the curve) when the data are available. The default method for small molecules in the absence of exposure data is a surface area dose equivalency unless body weight comparisons can be justified. For biologics, however, the appropriate method depends upon a number of factors, including the molecular weight of the protein.

7.10 Scientific and Regulatory Advice

Companies developing ophthalmic drug products face a number of challenges in the nonclinical arena. First, FDA/CDER has not released a guidance document for the nonclinical development of ophthalmic drugs. As noted, however, certain FDA and ICH guidance documents address selected issues relevant to ophthalmic drugs. Second, there are a number of issues unique to the ocular route of delivery that need to be addressed during the drug development process. For example, the number of species considered appropriate for ocular and systemic general toxicology studies can vary depending upon the nature of the compound being developed. Additionally, the scope of the studies required to support the development of ophthalmic drugs (e.g., whether reproductive toxicology or carcinogenicity studies are needed) is dependent on a number of factors such as extent of systemic exposure or whether the product is a first-in-class NME or is in a class for which the pharmacology and toxicology are generally well understood. Third, scientific knowledge and understanding with respect to drug development is continually evolving, and regulatory

decisions may be based on proprietary data to which only the FDA has access. Finally, the various available guidance documents may appear to be somewhat vague or ambiguous, in part, because it is not possible to address all scenarios that arise during drug development but also in an effort to accommodate scientific advances as they relate to drug development.

Companies need to balance their development timeline with the time needed to obtain regulatory guidance and concurrence on the nonclinical testing strategy throughout the development process. Development timelines, however, are often aggressive. Companies, therefore, may also need to balance their development timeline with the regulatory risk of not obtaining FDA concurrence for a proposed nonclinical strategy, especially if the strategy is not standard or if the drug being evaluated presents nonstandard concerns or issues. Ideally, timelines should allow for the preparation of requests for FDA recommendations/advice or waivers and for FDA/CDER's evaluation and responses to requests for guidance or waivers. Importantly, companies should also factor in the time required to conduct additional study(ies) if concurrence for a nonclinical approach is not obtained or a waiver is not granted. In order to successfully meet drug development challenges, companies should consider the following approaches: (1) be familiar with the available guidance documents that contain information relevant to ophthalmic drugs, (2) take advantage of meetings with FDA/CDER (e.g., pre-IND and end-of-phase 2 meetings), (3) provide complete justification and rationale for nonclinical development plans in regulatory submissions, (4) include someone with expertise in nonclinical development in interactions with FDA/CDER, and (5) be prepared to negotiate with FDA/CDER.

References

1. Code of Federal Regulations Title 21: Part 312, Section 312.21; <http://www.accessdata.fda.gov/scripts/cdrh/cfdocs/cfcfr/CFRSearch.cfm?fr=312.21>
2. FDA Guidance for Industry, Formal meetings between the FDA and sponsors or applicants, 2009; <http://www.fda.gov/downloads/Drugs/GuidanceComplianceRegulatoryInformation/Guidances/ucm153222.pdf>
3. Code of Federal Regulations Title 21: Part 3, Sec 3.2[e]; http://edocket.access.gpo.gov/cfr_2008/aprqttr/21cfr3.2.htm
4. Code of Federal Regulations Title 21: Part 58 <http://www.accessdata.fda.gov/scripts/cdrh/cfdocs/cfcfr/cfrsearch.cfm?cfrpart=58>
5. FDA Guidance for Industry, Nonclinical Studies for the Safety Evaluation of Pharmaceutical Excipients, 2005; <http://www.fda.gov/downloads/Drugs/GuidanceComplianceRegulatoryInformation/Guidances/UCM079250.pdf>
6. FDA Guidance for Industry, Nonclinical Safety Evaluation of Drug or Biologic Combinations, 2006; <http://www.fda.gov/downloads/Drugs/GuidanceComplianceRegulatoryInformation/Guidances/UCM079243.pdf>
7. FDA Guidance for Industry and Review Staff, Nonclinical Safety Evaluation of Reformulated Drug Products and Products Intended for Administration by an Alternate Route, 2008; <http://www.fda.gov/downloads/Drugs/GuidanceComplianceRegulatoryInformation/Guidances/UCM079245.pdf>

8. ICH Q3A(R2), Impurities in New Drug Substances, 2008; <http://www.fda.gov/downloads/Drugs/GuidanceComplianceRegulatoryInformation/Guidances/UCM073385.pdf>
9. ICH Q3B(R2), Impurities in New Drug Products, 2006; <http://www.fda.gov/downloads/Drugs/GuidanceComplianceRegulatoryInformation/Guidances/UCM073389.pdf>
10. ICH Q3C(R5), Impurities: Guidelines for Residual Solvents, 1997; <http://www.fda.gov/downloads/Drugs/GuidanceComplianceRegulatoryInformation/Guidances/UCM073394.pdf>
11. FDA Guidance, Genotoxic and Carcinogenic Impurities in Drug Substances and Products: Recommended Approaches, 2008; <http://www.fda.gov/downloads/Drugs/GuidanceComplianceRegulatoryInformation/Guidances/UCM079235.pdf>
12. ICH S6(R1), Pre-clinical Safety Evaluation of Biotechnology-derived Pharmaceuticals, 2011; http://www.ich.org/fileadmin/Public_Web_Site/ICH_Products/Guidelines/Safety/S6_R1/Step4/S6_R1_Guideline.pdf
13. Cavagnaro J, editor. Preclinical safety evaluation of biopharmaceuticals: a science-based approach to facilitating clinical trials. Hoboken: Wiley; 2008.
14. ICH M3(R2), Nonclinical Safety Studies for the Conduct of Human Clinical Trials, 2010; <http://www.fda.gov/downloads/Drugs/GuidanceComplianceRegulatoryInformation/Guidances/UCM073246.pdf>
15. ICH S7A, Safety Pharmacology Studies for Human Pharmaceuticals, 2001; <http://www.fda.gov/downloads/Drugs/GuidanceComplianceRegulatoryInformation/Guidances/UCM074959.pdf>
16. Lastacast: Pharmacology Review – NDA 022134, http://www.accessdata.fda.gov/drugsatfda_docs/nda/2010/022134s000PharmR.pdf
17. Macugen: Pharmacology Review – NDA 021756; 2004; http://www.accessdata.fda.gov/drugsatfda_docs/nda/2004/21-756_Macugen_pharmr.pdf
18. Nevanac: Pharmacology Review – NDA 021862, http://www.accessdata.fda.gov/drugsatfda_docs/nda/2005/021862s000_Nevanac_pharmr.pdf
19. Bepreve: Pharmacology Review – NDA 022288, http://www.accessdata.fda.gov/drugsatfda_docs/nda/2009/022288s000_PharmR.pdf
20. Besivance: Pharmacology Review – NDA 022308; http://www.accessdata.fda.gov/drugsatfda_docs/nda/2009/022308s000_PharmR.pdf
21. Timoptic (Label). Aton Pharma; Lawrenceville, NJ. 2009; http://www.accessdata.fda.gov/drugsatfda_docs/label/2011/018086s0751b1.pdf
22. ICH S2(R1), Guidance on Genotoxicity Testing and Data Interpretation for Pharmaceuticals Intended for Human Use, 2008; http://www.ich.org/fileadmin/Public_Web_Site/ICH_Products/Guidelines/Safety/S2_R1/Step4/S2R1_Step4.pdf
23. Lucentis: Pharmacology Review – BLA 125156, http://www.accessdata.fda.gov/drugsatfda_docs/nda/2006/125156s0000_Lucentis_PharmR.pdf
24. FDA Guidance for Industry and Other Stakeholders: Toxicological Principles for the Safety Assessment of Food Ingredients, Redbook 2000, Chapter IV; <http://www.fda.gov/downloads/Food/GuidanceComplianceRegulatoryInformation/GuidanceDocuments/FoodIngredientsandPackaging/Redbook/UCM222779.pdf>
25. OECD, Draft OECD Guideline for the Testing of Chemicals, Test Guideline 452: Chronic Toxicity Studies, November 2008; <http://www.oecd.org/dataoecd/30/44/41753317.pdf>
26. OECD Guideline for the Testing of Chemicals, Test Guideline 408: Repeated Dose 90-day Oral Toxicity Study in Rodents, September 1998; <http://www.oecdilibrary.org/docserver/download/fulltext/9740801e.pdf?expires=1335528071&id=id&accname=freeContent&checksum=338E6174AA3EDF887E12F72F6453FD3F>
27. OECD Guideline for the Testing of Chemicals, Test Guideline 409: Repeated Dose 90-day Oral Toxicity Study in Non-Rodents, September 1998; <http://browse.oecdbookshop.org/oecd/pdfs/free/9740901e.pdf>
28. Woolley A. A guide to practical toxicology: evaluation, prediction, and risk. 2nd ed. New York: Informa Healthcare; 2008. p. 134–42.
29. Wilson NH, Hardisty JF, Hayes JR. Short-term, subchronic, and chronic toxicology studies. In: Hayes AW, editor. Principles and methods of toxicology. 4th ed. Philadelphia: Taylor & Francis; 2001. p. 917–58.

30. Durezol: Pharmacology Review – NDA 022212; 2008; http://www.accessdata.fda.gov/drug-satfda_docs/nda/2008/022212s000_PharmR.pdf
31. ICH S5A, Detection of Toxicity to Reproduction for Medicinal Products, 1994; <http://www.fda.gov/downloads/Drugs/GuidanceComplianceRegulatoryInformation/Guidances/UCM074950.pdf>
32. ICH S5B, Detection of Toxicity to Reproduction for Medicinal Products: Addendum on Toxicity to Male Fertility, 1996; <http://www.fda.gov/downloads/Drugs/GuidanceComplianceRegulatoryInformation/Guidances/UCM074954.pdf>
33. FDA Guidance for Industry, Photosafety Testing, 2003; <http://www.fda.gov/downloads/Drugs/GuidanceComplianceRegulatoryInformation/Guidances/UCM079252.pdf>
34. ICH S10, Photosafety Evaluation of Pharmaceuticals: Final concept paper, 2010; http://www.ich.org/fileadmin/Public_Web_Site/ICH_Products/Guidelines/Safety/S10/Concept_Paper/S10_Final_Concept_Paper_June_2010x.pdf
35. ICH S1A, The Need for Long-term Rodent Carcinogenicity Studies of Pharmaceuticals, 1996; <http://www.fda.gov/downloads/Drugs/GuidanceComplianceRegulatoryInformation/Guidances/UCM074911.pdf>
36. Trivaris: Summary Review – NDA 022220, 2008; http://www.accessdata.fda.gov/drugsatfda_docs/summary_review/2008/022220s000_SUMR.pdf
37. Trivaris: Pharmacology Review – NDA 022220, 2008; http://www.accessdata.fda.gov/drug-satfda_docs/nda/2008/022220s000_PharmR.pdf
38. Azasite: Clinical Review – NDA 050810, 2007; http://www.accessdata.fda.gov/drugsatfda_docs/nda/2007/050810s000_MedR.pdf
39. Azasite: Pharmacology Review – NDA 050810, 2007; http://www.accessdata.fda.gov/drug-satfda_docs/nda/2007/050810s000_PharmR.pdf
40. Zylet: Pharmacology Review – NDA 050804, 2003; http://www.accessdata.fda.gov/drug-satfda_docs/nda/2004/50804_Zylet%20Ophthalmic%20Suspension_pharmr.PDF
41. Combigan: Pharmacology Review – NDA 021398, 2002; http://www.accessdata.fda.gov/drugsatfda_docs/nda/2007/021398s000_PharmR.pdf
42. ICH M7: Assessment and Control of DNA Reactive (mutagenic) Impurities in Pharmaceuticals to Limit Potential Carcinogenic Risk: Final concept paper, 2010. http://www.ich.org/fileadmin/Public_Web_Site/ICH_Products/Guidelines/Multidisciplinary/M7/M7_Final_Concept_Paper_June_2010.pdf

Chapter 8

Ocular Toxicity Regulatory Considerations for Nondrug Food and Drug Administration (FDA) Products and the Environmental Protection Agency (EPA)

Christopher Bartlett

Abstract The regulatory requirements for ocular toxicity of nondrug FDA products and the EPA are designed to identify the hazard of the material and ensure that labels have the proper use instructions and warnings. This is different from the Food, Drug, and Cosmetic Act (FDCA) process for drug development which is designed to determine the risk based on the exposure of the investigational drug. The regulatory guidance for cosmetics falls under the FDCA and is focused on ensuring that manufacturers produce safe products with proper use instructions and eye warnings. Other consumer products are regulated by the Consumer Product Safety Commission (CPSC) under the Federal Hazardous Substances Act (FHSA). The Federal Insecticide, Fungicide, and Rodenticide Act (FIFRA) is responsible for registering pesticides and ensuring safe and proper use. Development of new industrial chemicals is regulated by the Toxic Substances Control Act (TSCA). The regulatory guidelines associated with these acts provide recommendations to use the Draize eye test for evaluation of ocular toxicity. However, each regulatory guidance for different substance categories has slightly different guidance for the Draize eye test methodology, the interpretation of the results, and conclusions based on the results. While the standard test to evaluate ocular toxicity has been the Draize eye test since the 1940s, significant efforts are currently under way to develop and validate alternative assays to identify ocular toxicity hazard, replace the Draize eye test, and modify the regulatory landscape.

C. Bartlett, Ph.D. (✉)
SciMetrika LLC, Durham, NC, USA
e-mail: cbartlett@scimetrika.com

8.1 Introduction

In the previous chapter, regulatory considerations for drug products that are regulated by the FDA's Center for Drug Evaluation and Research (CDER) were presented. With the exception of drug products, the FDA permits the majority of consumer products (e.g., cosmetics) to be marketed without premarket authorization but has set forth guidance under the FDCA that requires products to be safe and "prohibits the marketing of adulterated or misbranded cosmetics in interstate commerce" [1]. This requires the manufacturer to comply with monographs and guidance published by the FDA Center for Food Safety and Applied Nutrition (CFSAN) and substantiate the safety of the product prior to marketing. Supporting the safety of a product often requires ocular toxicity testing to define the ocular hazard of the product and ensure proper labeling to protect consumers and workers from potential ocular hazards. For example, a cosmetic manufacturer developing a new eyeliner is responsible for testing the product to demonstrate that it is safe for the intended use and providing a label with the product that has an ingredient list, use instructions, and appropriate warnings.

Household products are regulated by the Consumer Product Safety Commission (CPSC) under the authority of the Consumer Product Safety Act (CPSA) [2]. The CPSC is committed to protecting consumers and families from products that pose a fire, electrical, chemical, or mechanical hazard or can injure children.

Similar to the FDA drug process, the EPA requires premarket approval for pesticides/antimicrobial products under Federal Insecticide, Fungicide, and Rodenticide Act (FIFRA) [3]. The focus of this premarket approval process by the EPA is to characterize the hazards associated with the use of the substances. Part of defining the hazard of a substance is to define the ocular hazard. Based on test results characterizing the ocular hazard of a substance, the EPA has established language for the use instructions and warnings permitted on the labels.

Industrial chemicals regulated under the Toxic Substances Control Act (TSCA) require a premanufacture notification be submitted to EPA, which provides the agency the opportunity to review and manage the potential risk of the material [4]. These premanufacture notifications require submission of all of the product chemistry and test data generated from the chemical. While no specific requirements are set forth, ocular toxicity testing is often analyzed for these chemicals.

Ocular toxicity tests are one of the four most commonly conducted product safety tests [5]. The Draize eye test [6] is the only acceptable ocular toxicity test for regulatory purposes and is the standard that all regulatory agencies use for evaluation of ocular toxicity hazard. However, each agency uses the results of the test slightly differently and classifies the potential for hazard using different schemes. It is important to know which regulations govern a specific product in order to follow the appropriate Draize eye testing scheme, based on the material's chemical properties, to ensure a product has been properly categorized and labeled.

8.2 Regulatory Overview

In 1938, the US congress issued the Federal Food, Drug, and Cosmetic Act (FDCA) which extended regulatory control to cosmetics in response to the public display of blinding that occurred as a result of administration of an aniline-based eyelash dye. The regulation required manufacturers to assess product safety prior to marketing of products. The Draize eye test was developed by the Dermal and Ocular Toxicity branch in the FDA's Division of Pharmacology in 1940 for the toxicological appraisal of a given compound or preparation intended for therapeutic, cosmetic, or other topical use. It has been the standard recommended by the FDA to assess cosmetic products since its development. These testing procedures were adopted by the Consumer Product Safety Commission (CPSC) in 1972 [7].

As described in Table 8.1 below, agencies such as the FDA and EPA, have been created in the USA in part to promote the general welfare of US citizens by protecting them from harmful exposures to consumer and other products [7]. In the twentieth century, several additional acts (FIFRA, TSCA, Federal Hazardous Substances Act (FHSA) have given regulatory authority to the agencies beyond the FDA and EPA to ensure the safety of chemicals and consumer products. While these regulations do not mandate any testing, they do require assurance of a product's safety. Product safety is substantiated by conducting toxicology tests. Animals have long been used to evaluate and predict potential adverse effects from human exposure, and the Draize rabbit eye test was developed to support ocular toxicity testing and hazard identification. All of the agencies with consumer product regulatory responsibilities use the Draize eye test as the standard assay with some variance in the guidance on how to conduct the assay [1–4].

8.2.1 Testing Guidelines

Several agencies, EPA, FDA, CPSC, and OSHA, have designated specific test guidelines for assessing ocular toxicity (Table 8.2). All of the testing guidelines provide standards for conducting the Draize eye test, but, due to variations in the

Table 8.1 US laws that govern ocular toxicity of nondrug FDA products and the EPA [7]

Legislation	Agency	Substance/product
FDCA (1938)	Department of Health and Human Services (FDA)	Pharmaceuticals and cosmetics
FIFRA (1947)	EPA	Pesticides
FHSA (1964) and TSCA (1977)	Department of Agriculture and EPA	Agriculture and industrial products
CPSC (1972)	Consumer Product Safety Commission	Household products
OSHA (1970)	Department of Labor (OSHA)	Occupational materials

Table 8.2 Current regulations that require ocular safety testing [9]

Agency	Authority created	Regulation	Test guideline
EPA	FIFRA (1947), TSCA (1977)	40 CFR 156	OPPTS 870.2400
CPSC	FHSA (1964)	16 CFR 1500	16 CFR 1500.42
FDA	FDCA (1938)	21 CFR 501–523	16 CFR 1500.42
OSHA	OHSA (1970)	29 CFR 1910	16 CFR 1500.42

Table 8.3 Comparison summary of testing guidelines [9]

Test method component	EPA (TG OPPTS 870.2400)	FHSA (16 CFR 1500.42)	OECD (TG 405)
Number of animals used to make decision	1 to screen for corrosive, then $n \geq 2$	1 Animal based on Maximum score in any animal on any day	1 Animal based on Maximum score in any animal on any day
Quantity in test eye	0.1 ml or 0.1 g	0.1 ml or 0.1 g	0.1 ml or 0.1 g
Observation times	1, 24, 48, 72 h, and daily thereafter until lesions clear or 21 days	24, 48, and 72 h	1, 24, 48, 72 h, and daily thereafter until lesions clear or 21 days
Post-dosing irrigation	24 h unless substance is shown to be irritating	24 h	Liquids: 24 h Solids: 1 h

nature of concern over the different regulated products, the guidelines for conducting the assay vary among the agencies. The Organization for Economic Cooperation and Development (OECD) has standardized methods for a number of toxicology tests, including the Draize eye test [8]. In general, 0.1 mL (liquid) or 0.1 g (solid) is placed on the conjunctival sac of one eye of the rabbit, and the other eye serves as an untreated control. Observations are made, and irritation is scored 1, 24, 48, and 72 h postexposure and daily thereafter until the lesion clears or for 21 days. Irritation is measured by observing corneal opacity, iritis, and conjunctival redness and swelling. Optional assessments can also be conducted using light microscopy or fluorescein, but in practice these assessments are rarely conducted [9].

While all three testing guidelines that accompany current regulations are based on the Draize rabbit eye test [6], differences exist in the assay methodologies. OPPTS 870.2400 follows the OECD Test Guideline, TG 405 for Draize eye testing, more closely than 16 CFR 1500.42. EPA guidance requires studies to be carried out for 21 days to evaluate for reversible/irreversible effects, while FHSA only requires 3 days of observation. Other differences in the assay guidance are described in Table 8.3.

8.2.2 Hazard Classification Schemes and Labeling Requirements

The desired outcome of ocular toxicity testing based on the testing guidelines defined by regulatory agencies is to classify the ocular hazard of the substance. This allows for the material to be assigned to a group within the agencies' hazard

Table 8.4 Ocular toxicity assays and regulatory conclusions

Assay	Test type	Assay endpoint	Prediction utility
Bovine corneal opacity and permeability	Isolated eye assay	Barrier function – fluorescein permeability	Conjunctival endpoints
EpiOcular	3D epithelial cell models	Cytotoxicity	Cytotoxicity/irritation
HET-CAM/CAMVA	Chicken egg membrane	Vascular effects	Corneal lesions and iritis

classification scheme and ensures proper labeling of a material and to provide instructions and warnings. As described above, the Draize eye test is still the test standard recommended by the different regulatory guidelines/guidances, but the interpretation of the results and the subsequent classification schemes vary among the agencies. The Draize eye test is necessary for materials like pesticides that require premarket authorization and hazard and labeling classification, while some industries like personal care products that do not require premarket approval or standardized classification and labeling have greater flexibility in substantiating ocular safety. While a push for alternative assays is ongoing and will be discussed in a later section, no alternative assays are used for hazard classification and labeling.

8.2.2.1 Cosmetics

Cosmetics marketed in the United States are regulated by the FDCA and the Fair Packaging and Labeling Act (FPLA) [1]. Cosmetic products and ingredients are not subject to premarket approval with the exception of colorants, which must meet approved standards in CFR, and certain banned materials. Therefore, cosmetic firms are responsible for substantiating the safety of their products and ingredients prior to marketing. Failure by the cosmetic firm to substantiate safety prior to marketing puts them in violation of the FDCA and potentially subjects them to penalties or recalls. In addition to substantiating safety, the FPLA requires the cosmetic not be misbranded. The label must contain a complete ingredient list, proper warnings, and use instructions and must not contain false claims. Since substantiating the safety of cosmetic products prior to marketing is the responsibility of the cosmetic manufacturer and the specific methodology/approach is not mandated, manufacturers have the flexibility to use varying approaches. For example, many cosmetic firms have moved away from the standard Draize eye test to support ocular safety and have begun to use in vitro alternative assays like the EpiOcular assay to substantiate the safety of their products. Table 8.4 lists many of the common in vitro alternative assays currently in use.

8.2.2.2 Pesticides

As mentioned before, pesticides undergo registration prior to marketing. To ensure the safe use of pesticides, human health, environmental health, and efficacy data are required for submission to EPA. Part of the submission is an ocular toxicity

Table 8.5 EPA classification scheme for ocular toxicity [9]

EPA category	In vivo effect observed
I	Corrosive; irreversible corneal involvement or irritation persisting more than 21 days
II	Corneal involvement or irritation clearing in 8–21 days
III	Corneal involvement or irritation clearing in ≤ 7 days
IV	Minimal effects clearing within 24 h

Table 8.6 Eye warning labels for EPA classification scheme [9]

EPA category	Signal word	Statements	Protective equipment/actions
I	Danger	Corrosive. Causes irreversible eye damage. Do not get in eyes or on clothing	Wear protective eyewear, goggles, face shield, or safety glasses. Wash thoroughly with soap and water after handling and before eating, drinking, chewing gum, or using tobacco. Remove and wash contaminated clothing prior to reuse
II	Warning	Causes substantial but temporary eye injury. Do not get in eyes or on clothing	Same as category I
III	Caution	Causes moderate eye irritation. Avoid contact with eyes or clothing	Wear protective eyewear, goggles, face shield, or safety glasses. Wash thoroughly with soap and water after handling and before eating, drinking, chewing gum, or using tobacco
IV	Caution (optional)	None required	None required, but may choose category III

test to determine the ocular hazard of the substance. Animals are tested according to the EPA test guidance OPPTS 870.2400. The conclusions drawn from the test result in classification of the substance and provide recommendations for the product label. In the EPA classification scheme, the most severe response seen in an animal is used for classification, which means that in a test with multiple animals, the classification is ultimately based on the most severe response by one animal. The classification scheme in Table 8.5 demonstrates how the results of the ocular toxicity test determine the hazard category of the substance.

The EPA category dictates the language for the warning label of the pesticide. The language described in the pesticide EPA Label Review Manual [10] is above in Table 8.6.

Table 8.7 FHSA classification scheme for ocular toxicity [11]

Positive response for a single rabbit (≥ 1 of the following at 24, 48, or 72 h)	<i>In vivo</i> effect
Corneal ulceration (other than a fine stippling)	<i>First test</i> – If $\geq 4/6$ of animals are positive, the test is positive. If ≤ 1 of animal is positive, the test is negative. If 2/6 or 3/6 of animals are positive, the test is repeated using a different group of six animals.
Corneal opacity ≥ 1	
Iritis ≥ 1	
Conjunctival swelling and/or redness ≥ 2	<i>Second test</i> – If $\geq 3/6$ of animals are positive, the test is positive. If 0/6 is positive, the test is negative. If 1/6 or 2/6 of animals are positive, the test is repeated using a different group of six animals. <i>Third test</i> – Should a third test be needed, the test is positive if $\geq 1/6$ of animals are positive. If 0/6 is positive, the test is negative.
	<i>Note:</i> Classification as an eye irritant hazard can result from as few as 22% of animals showing a positive response (e.g., $2/6 + 1/6 + 1/6 = 4/18$)

8.2.2.3 Industrial Chemicals

TSCA provides the EPA with the authority to require reporting, record-keeping and testing requirements, and restrictions relating to chemical substances and/or mixtures excluding, among others, food, drugs, cosmetics, and pesticides [4].

Section 5 of TSCA mandates the EPA's New Chemicals Program which helps manage the potential human health and environmental risk of new chemicals by serving as a "gatekeeper" that can identify conditions, up to and including a ban on production, to be placed on the use of a new chemical before it is entered into commerce. Anyone who plans to manufacture or import a new chemical substance for a nonexempt (e.g., nonfood, drug, cosmetic, or pesticide) commercial purpose is required by section 5 of TSCA to provide EPA with notice before initiating the activity [4].

Regarding ocular toxicity, industrial chemicals can be classified either by the EPA classification scheme described above or by Occupational Health and Safety Act (OSHA) which uses FHSA classification system and is more sensitive than the EPA (see Table 8.7).

8.2.2.4 Household Products

The CPSC is charged with protecting the public from unreasonable risks and injuries from thousands of consumer products, including household products [2]. CPSC does this by:

- Developing voluntary standards with industry
- Issuing and enforcing mandatory standards or banning consumer products if no feasible standard would adequately protect the public
- Obtaining the recall of products or arranging for their repair
- Conducting research on potential product hazards
- Informing and educating consumers through the media, state and local governments, and private organizations and by responding to consumer inquiries

Table 8.8 Comparison summary of agency classification schemes [11]

Classification scheme	Animals per test	Measurement benchmark	Corrosive determination	Other
EPA	At least 3	Maximum score in any animal on any day	Can be determined by one animal screen	Most severe response used for classification
FHSA	6	Maximum score in any animal on any day	≥1 animal with irreversible alterations	Tiered testing possible
GHS	At least 3	Calculate average severity over all 3 time points	Dependent on injury ≥1 or 2 animals (see Table 8.9 – effects for category 1)	Requires 2/3 animals demonstrating positive response

Table 8.9 GHS classification scheme for ocular toxicity [11]

GHS category	In vivo effect
I	≥1 animal with CO ≥4 at any time or ≥2 animals with mean CO ≥3 or IR ≥1.5 or ≥1 animal with CO or IR ≥1 or CC or CR ≥2 which is not expected to reverse or does not fully reverse within 21 days
2A	≥2 animals with mean CO or IR ≥1 or CC or CR ≥2 which fully reverses within 21 days
2B	≥2 animals with mean CO or IR ≥1 or CC or CR ≥2 which fully reverses within 7 days

CC conjunctival chemosis, *CO* corneal opacity, *CR* conjunctival redness, *IR* iritis

Therefore, household product safety must be substantiated to avoid CPSC enforcement action. The CPSC uses the same test guidance as the FDA (16 CFR 1500.42) and monitors products and institutes enforcement in a similar post market surveillance manner.

8.2.2.5 Comparison of Classification Schemes

Recent analysis by ICCVAM revealed that 36% of the chemicals currently classified and labeled as eye irritation hazards by US hazard classification regulations (FHSA, OSHA, EPA, CPSC) would not be classified and labeled as eye hazards using United Nations (UN) Globally Harmonized System of Classification and Labeling of Chemicals (GHS) eye irritation criteria [12]. OSHA has recently proposed to adopt the GHS criteria to replace the current OSHA Hazard Communication Standard, and other US agencies are also considering a switch to the less conservative classification. The reduced eye hazard labeling from using the GHS classification criteria is attributable to two differences: the number of positive animal responses required for classification and a significant difference in the criteria that must be met for eye injuries to be considered positive responses. These differences described in Table 8.8 lead to reduced classification of eye hazard under the GHS classification system compared to US regulations.

Table 8.9 describes the specifics of the GHS classification scheme.

8.3 Current Regulatory Initiatives

While the Draize eye test is the standard, it is not without limitations. It has high interlaboratory variability, subjective scoring of injury, and imperfect predictive value for human irritants (correctly predict toxic materials 85% of the time, overestimates toxicity 10% of the time, and underestimates 5% of the time). However, the most significant criticism of the Draize eye test has been for causing undue pain and distress for test animals. In an attempt to meet the goals of the three Rs – refinement, reduction, and replacement – all of the testing guidelines have also been modified over time as more information has been collected that can allow for comparisons to be made between chemical properties and ocular toxicity in order to reduce or refine the number of animals used. For example, in an attempt to refine the process to lessen distress and discomfort of the animals, chemicals that are strongly acidic ($\text{pH} < 2$) or alkaline ($\text{pH} > 11.5$) are generally excluded from testing as these compounds would likely cause adverse effects to any mucous membrane. Also, the test has been modified to limit the test volume to refine the assay [8].

Due to the concerns around animal testing, investigation of alternative assays is under way to replace the Draize eye test. Currently, agencies are collaborating to validate alternative approaches. This effort is being led by the Interagency Coordinating Committee on the Validation of Alternative Methods (ICCVAM) Authorization Act of 2000 (42 U.S.C. 285l-3) which created ICCVAM as a permanent interagency committee of National Institute of Environmental Health Sciences (NIEHS) under the National Toxicology Program (NTP) Interagency Center for the Evaluation of Alternative Toxicological Methods (NICEATM) in order to [5]

establish, wherever feasible, guidelines, recommendations, and regulations that promote the regulatory acceptance of new or revised scientifically valid toxicological tests that protect human and animal health and the environment while reducing, refining, or replacing animal tests and ensuring human safety and product effectiveness.

NICEATM-ICCVAM has created a committee representing 15 agencies of the US government to establish criteria for validating alternative assays to replace whole animal testing of ocular corrosiveness or irritancy. The 15 agencies are:

Agency for Toxic Substances and Disease Registry (ATSDR)
Consumer Product Safety Commission (CPSC)
Department of Defense (DOD)
Department of Energy (DOE)
Department of the Interior (DOI)
Department of Transportation (DOT)
Environmental Protection Agency (EPA)
Food and Drug Administration (FDA)

- Office of the Commissioner
- Center for Drug Evaluation and Research (CDER)
- Center for Devices and Radiological Health (CDRH)
- Center for Food Safety and Applied Nutrition (CFSAN)
- National Center for Toxicological Research (NCTR)

- Center for Biologics Evaluation and Research (CBER)
- Center for Veterinary Medicine (CVM)

National Cancer Institute (NCI)

National Institute of Environmental Health Sciences (NIEHS)

National Institutes of Health (NIH)

National Institute for Occupational Safety and Health (NIOSH)

National Library of Medicine (NLM)

Occupational Safety and Health Administration (OSHA)

US Department of Agriculture (USDA)

The types of assays under review can be grouped into tissue tests, cell tests, or nonliving systems (see Table 8.4). While no single *in vitro* test is accepted as an alternative to Draize testing, these alternative assays can be used in a tiered testing system to reduce the number of animals in the testing paradigm [13, 14]. The major criterion in evaluating an alternative assay is its predictive ability as compared to existing results of the Draize assay. None of the alternatives reviewed to date have been determined to have the ability to produce or predict an inflammatory response. They also do not indicate the course of the injury development or the course of injury recovery. While the alternative tests are reasonably consistent at identifying irritant or corrosive substances, they have difficulty with some chemical classes (surfactants, alcohols, organic solvents, or solids) [13, 14] that have more complex interactions that are not accurately predicted in an *in vitro* model.

8.4 Product Development Process and Regulatory Considerations

While the standard for ocular toxicity testing remains the Draize eye test, animal testing has come under considerable scrutiny, and the search for acceptable alternative assays has become a priority for many industries. Cosmetic and personal care product companies have led the initiative to reduce or eliminate animal testing as their practices become a source of public criticism. In the late 1970s, it was estimated that eye irritation testing accounted for up to one-fourth of all animals used in toxicity testing [7]. With the advance of science in the early 1980s, cosmetic companies began to investigate alternatives as the public exerted pressure on their corporate conscience. Investigation of *in vitro* alternative methods led by industry organizations Cosmetics Europe – The Personal Care Association (previously COLIPA) and the Personal Care Products Council (previously CTFA) has led to many viable alternatives (see Table 8.4). In fact, a number of consumer product companies are able to support the safety of products based on historical data and *in vitro* methods.

The most general approach for assessing ocular toxicity in the current regulatory environment for products that do not require premarket approval is:

1. Review current literature
2. Conduct Quantitative Structure Activity Relationship (QSAR) investigation

3. In vitro testing
4. Draize testing (if required)

Given the language within the actual regulations, no testing is mandated for products that do not require premarket registration (e.g., cosmetics) as long as the manufacturer determines they have the necessary information to support the safety of the product. Therefore, if the manufacturer feels they have sufficient information to support the product, they can stop at any of the steps above. In fact, many cosmetic companies use in vitro testing to substantiate the ocular safety of eye products. This is different than substances (e.g., pesticides) that require premarket registration in which they must submit mandated test data for review by the agency and, therefore, Draize eye testing is necessary.

While the current regulatory standard is the Draize eye test, work led by agencies such as ICCVAM are attempting to identify alternative ocular toxicity testing assays and strategies that allow for ensuring the safety of new chemicals and consumer products while limiting the use of animal testing.

References

1. FDA Authority Over Cosmetics. 2005, March. <http://www.fda.gov/Cosmetics/GuidanceComplianceRegulatoryInformation/ucm074162.htm>
2. Consumer Product Safety Commission. <http://www.cpsc.gov/about/about.html>. Accessed 15 March 2012.
3. Federal, insecticide, fungicide, and Rodenticide Act. <http://www.epa.gov/agriculture/lfra.html>
4. Summary of the Toxic Substances Control Act. <http://www.epa.gov/lawsregs/laws/tsca.html>
5. The NTP Interagency Center for Evaluation of Alternative Methods and the Interagency Coordinating Committee on the Validation of Alternative Methods. <http://iccvam.niehs.nih.gov/>
6. Draize JH, et al. Methods for the study of irritation and toxicity of substances applied topically to the skin and mucous membranes. *J Pharmacol Exp Ther.* 1944;82:377–90.
7. Wilhelmus K. The Draize eye test. *Surv Ophthalmol.* 2001;45(6):493–515.
8. OECD Guideline for the Testing of Chemicals, Test Guideline 405: Acute Eye Irritation/Corrosion. <http://www.oecd.org/dataoecd/7/23/48108995.pdf>
9. Summary of Current Ocular Safety Testing Guidelines and Criteria Used for Hazard Classification and Labeling in the US. <http://iccvam.niehs.nih.gov/meetings/Implement-2011/Ocular-present/4-McCall.pdf>
10. EPA Label Review Manual Chapter 7. 2007. <http://www.epa.gov/oppfead1/labeling/lrm/>
11. Reduced Eye Hazard Labeling Resulting from Using Globally Harmonized System (GHS) Instead of Current U.S. Regulatory Classification Criteria. May 14, 2010. http://ntp.niehs.nih.gov/NTP/About_NTP/SACATM/2010/June/Materials/GHSAnalysis.pdf
12. Globally Harmonized System of Classification and Labelling of Chemicals (GHS). United Nations Economic Commission for Europe. 2007. http://www.unece.org/trans/danger/publi/ghs/ghs_rev02/02files_e.html
13. Brantom PG, et al. Summary report of the COLIPA international validation study of alternatives to the draize rabbit eye irritation test. *Toxicol In Vitro.* 1997;11:141–79.
14. Bradlow JA, Wilcox NL. Workshop on eye irritation testing: practical applications of non-whole animal alternatives. *Food Chem Toxic.* 1997;35:1–11.

About the Editors

Andrea Weir is Senior Scientific Advisor at Charles River Laboratories, Navigators Consulting group. In this position, she provides scientific and regulatory advice to clients to ensure that their nonclinical development strategies are consistent with the expectations of regulatory agencies. She has advised clients on the nonclinical development of ophthalmic drug products and provided presentations on the same topic at various meetings. From 1993 to 2005, she was employed by the Food and Drug Administration (FDA), gaining experience in the scientific and regulatory aspects of traditional small molecules and biotechnology-derived products, including ophthalmic drug products. Andrea Weir is a member of the Society of Toxicology and a Diplomate of the American Board of Toxicology.

Margaret Collins is Associate Director of Research and Program Director for Ophthalmology in the Toxicology section of Charles River Laboratories, Inc, Preclinical Services, Nevada. She has served as a councilor, president and founding member of the Ocular Toxicology Specialty Section in the Society of Toxicology. She is also a member of the Association for Research in Vision and Ophthalmology. In addition to contract research, Margaret Collins has previously taught university-level biology courses and conducted basic research in biotransformation and model development.

Index

A

- Acanthamoeba, 64
- Accommodation, 73, 77
- Acetaminophen, 224
- Achromatopsia, 95
- Adaptive optics, 91
- Advances in optical imaging and biomedical sciences, 55
- Age-related macular degeneration, 98
- Aminopyridine, 224
- Amniotic membrane, 62
- Amoebic and fungal keratitis, 63
- Angle-closure glaucoma, 76
- Anterior lens capsule, 97
- Anterior lenticonus, 72
- Aqueous flare, 81
- Aqueous humor, 8–9, 87
- A scan, 76
- Assessing ocular toxicity
 - corneal thickness, 49
 - corneal perfusion, 49
 - corneal wound healing, 49
 - direct and indirect ophthalmoscopy
 - albino rat fundus, 43
 - BOA, 46
 - canine fundus, 43
 - glial (neuroepithelial) choristoma, 45
 - optic nerve and temporal retina, 47
 - peripapillary myelination, 45
 - photographic documentation, 41
 - posterior uveitis, 40
 - primate fundus, 44
 - rabbit fundus, 42
 - vitreous haze, 41, 46
 - electroretinography, 49
 - FA, 50
 - OCT, 50, 52
 - ocular ultrasonography, 50
 - pachymetry and specular endothelial microscopy, 49
 - photography, 41, 42, 45
 - pupil dilation, 25
 - slit-lamp biomicroscopy
 - anterior vitreous, 28, 32
 - aqueous flare, 32
 - aqueous humor, 27
 - cataracts, 30–32
 - corneal degeneration/dystrophy, 28
 - corneal epithelial dystrophy, 29
 - corneal scar, 29
 - dilation, 28
 - Draize scoring system, 38
 - Dutch belted rabbits, 28
 - epithelial dystrophy, 28
 - fibrin formation, 37
 - Hackett-McDonald scoring system, 30
 - hyphema, 38
 - hypopyon, 38
 - nonpigmented cells, 27, 38
 - pigment epithelial cells, 27, 28, 38
 - portable models, 26, 27
 - pupillary light responses, 27, 28
 - red blood cells, 38
 - Sprague-Dawley rat, 28
 - SUN system, 30, 37
 - table-mounted models, 26, 27
 - Tyndall effect, 27, 31, 32
 - uveitis, 32
 - tonometry, 47–48
- Asteroid hyalosis, 59, 60, 227
- Autofluorescence, 88

B

Baseline imaging, 57
 Behcet's disease, 60
 Bevacizumab, 83
 Bilateral optic atrophy (BOA), 46
 Bioavailability, 86
 Biologics License Applications (BLA),
 260, 265
 Biorefringence 103
 Birefringence mapping, 95
 Blood aqueous barrier, 84, 87
 Blood-retinal barrier, 17, 59, 84, 85, 89, 123,
 244, 245
 Bovine corneal opacity and permeability assay
 (BCOP), 181
 Bruch's membrane, 237
 B scan, 76

C

Cataracts, 30–32, 77
 lenticular opacities
 aging, 223
 nuclear cataract, 223
 lenticular toxicity
 causes, 224
 factors affecting, 223
 sugar cataract, 223–224
 ciliary body (*see Uvea*)
 CellCheck XLTM, 69
 Center for Drug Evaluation and Research
 (CDER), 260
 Central nervous system (CNS), 273
 Central serous chorioretinopathy, 95
 Choroid, 13, 17, 95, 243. *See also Uvea*
 Choroidal melanoma, 93
 Chromodacryorrhea, 173
 Ciliary body, 9. *See also Uvea*
 Cirrus HD-OCT, 101
 Comparative ocular anatomy
 aqueous humor, 8–9
 choroid, 13, 17
 conjunctiva, 5–6, 196
 cornea, 6–7
 eyelids, 2–5
 fundus, 12, 13
 human and nonhuman primate eyes, 2, 3
 lens, 9–11
 macular region, 14, 15
 pre-corneal tear film, 6
 retina, 12, 14, 15
 sclera, 7–8
 subretinal space, 18
 suprachoroidal space, 18

 tapetum lucidum, 17
 tenon's capsule/sub-tenon's space, 18
 uvea, 18
 vitreous humor, 10, 12
 Confocal laser-scanning microscopy, 89
 Confoscan 4, 65
 Conjunctiva, 5–6
 alterations
 acute conjunctivitis, 196
 chemosis (edema), 196
 conjunctival microgranuloma, 197
 inflammation, 196
 pseudopterygium, 197
 bulbar conjunctiva, 195
 CALT and MALT system, 195
 limbus, 196
 palpebral conjunctiva, 195
 Consumer Product Safety Act (CPSA), 296
 Consumer Product Safety Commission
 (CPSC), 296
 Contact lenses, 58, 87
 Cornea, 6–7
 anatomy, 7, 177
 irritation, 181–184
 anesthetic agents, 182
 chronic desiccation, 182
 epithelial lesions, 182
 hyperplasia, 184
 irritating substances, 181
 deep corneal alterations
 corneal endothelium degeneration, 191
 descemet's membrane, 190–191
 endothelial cells injury, 191–194
 endothelial density, 192
 iatrogenic findings, 177–179
 opacities, 179–180
 pigmentation, 186–187
 stromal alterations
 pigmentation, 186–187
 edema, 187
 inflammation, 187
 lipid keratopathy and corneal
 phospholipidosis, 189–190
 neovascularization, 188–189
 mineralization, 185–186
 superficial alterations
 hypertyrosinemia, 181
 keratitis, 181
 stromal alterations, 184
 ulceration, 180–181
 thickness, 7
 toxicity, 181–184
 toxic effects, 179
 Corneal compensation, 103

Corneal confocal microscopy, 60
 animal toxicology and ocular research,
 62–63
 commercially available devices, 65
 human clinical applications
 amoebae, 63, 64
 corneal transplantation, 65
 endothelial alterations, 64
 nephropathic cystinosis, 64
 slit-lamp examination, 63
 limitations and caveats, 65
 ocular toxicology studies, 65
 performance parameters, 60, 62
 principles, 60, 61
 Corneal endothelial permeability, 84
 Corneal endothelium, 7, 66, 177, 191–194
 Corneal pachymetry, 66
 Corneal phospholipidosis, 189–190
 Corneal wound healing, 49
 Cystoid macular edema, 93

D

Densitometry, 72
 Descemet's membrane detachment, 95, 177
 3D-OCT 2000101 Bioptigen SD-OCT, 101
 Diabetes, 85
 Diabetic retinopathy, 98
 Differences in segmentation algorithms, 103
 Diquat, 224
 Displaced photoreceptor nuclei (DPN),
 230–231. *See also* Photoreceptor
 displaced nuclei (PDN)
 Draize scoring system, 38
 Drug implants, 72
 Drug toxicity, 98
 Drusen-like bodies, 237
 Dry eyes, 62
 Dysplasia, retinal, 229

E

Electrophysiological technologies
 full-field electroretinography, 124–125
 a-wave, 127
 b-wave, 126
 commercially available devices,
 128–129
 dark-adapted, 126
 Ganzfeld, 127
 30-Hz flicker, 127
 ISCEV, 125
 limitations and caveats, 129
 ocular toxicology research, 128

ocular toxicology studies, 129
 oscillatory potentials, 127
 photopic, 128
 photopic responses, 126
 scotopic, 128
 signal averaging, 128
 multifocal electroretinography
 age-related macular degeneration, 130
 central serous retinopathy, 130
 commercially available devices, 132
 diabetic retinopathy, 130
 experimental glaucoma, 132
 hydroxychloroquine, 132
 inflammatory disease, 130
 juvenile retinoschisis, 130
 limitations and caveats, 133
 macular holes, 130
 m-sequence pattern, 130
 multifocal ERG, 130
 ocular toxicology research, 131, 132
 optic nerve transection, 131
 reversing ophthalmoscope, 133
 supranormal, 132
 vitelliform maculopathies, 130
 pattern reversal electroretinography
 C57BL/6, 136
 commercially available devices, 138
 DBA/2J, 136
 experimental glaucoma, 136
 LED displays, 138
 macular degeneration, 137
 N95, 135
 reversing ophthalmoscope, 138
 P50, 135
 Signal-to-Noise Ratio, 134
 steady-state PERGs, 134–135
 sweep VEP, 141
 transient PERG, 134
 vernier acuity, 141
 visual evoked potential
 acrylamide and N-methylolacrylamide,
 145
 averaging, 139
 binocular interactions, 141
 central visual pathways, 142
 commercially available devices,
 149–150
 cortical generator, 139, 141,
 142, 150
 ethambutol, 146
 experimental glaucoma, 144
 flash VEP, 142
 murine glaucoma, 145
 hydroxychloroquine toxicity, 146

- Electrophysiological technologies (*cont.*)
- idiopathic bilateral optic atrophy, 140, 144
 - lead exposure, 148
 - limitations and caveats, 150–151
 - methylmercury and polychlorinated biphenyls, 146
 - motion, 141
 - multiple sclerosis, 145
 - n-hexane, 148
 - ocular toxicology studies, 150
 - optic atrophy, 145
 - optic nerve transection, 147
 - optic neuritis, 145
 - osteopetrotic knockout, 145
 - pattern onset/offset VEPs, 142
 - pattern reversal VEPs, 142
 - “P100” wave, 143
 - Signal-to-Noise Ratio, 139
 - steady-state stimulus (ssVEPs), 140
 - sweep, 141, 146
 - systemic lupus erythematosus, 146
 - vernier acuity, 141
- Electroretinography, 25, 49
- Endothelial cell density, 65
- Endothelial keratoplasty, 66
- Endotheliitis, 64
- Endotoxin-induced ocular inflammation, 83
- Endotoxin-induced uveitis, 62
- Enhanced corneal compensation (ECC), 103, 106
- Environmental protection agency (EPA)
- alternative toxicity testing, 303–304
 - Draize eye test, 303
 - hazard classification schemes and labeling requirements
 - agency classification schemes, 302
 - cosmetics, 296
 - GHS classification scheme, 302
 - household products, 301, 302
 - industrial chemicals, 301
 - pesticides, 299, 300
 - testing guidelines, 297–298
 - US regulations, 297
- Epiretinal membrane, 95
- Episclera, 194–195
- Episcleral vein cauterization, 77
- Esthesiometer, 63
- Exfoliation syndrome, 77
- Extraocular tissues
- extraocular muscles, 168
 - eyelid, 166–168
 - lacrimal and lymphoid drainage, 175–176
 - nictitating membrane, 175
 - orbital fascia and intraorbital contents, 176
 - orbital glands
 - harderian gland (*see* Harderian glands)
 - lacrimal glands, 168–175
- Eye Cubed, 80
- Eyelids, 2–4
- blinking, 4, 5
 - components, 166
 - drainage system, 3
 - epidermal growth factor receptor, 168
 - eyeball exposure, 4
 - inflammation, 166
 - isotretinoin, 167–168
 - neoplasms, 167
 - nictitating membrane, 5, 6, 175
 - poisoning, 167
 - prostaglandin analogs, 168
 - spontaneous alterations, 166
 - systemic absorption, 4
 - topical epinephrine, 167
 - toxaphene, 168
 - toxicity, 167–168
- F**
- Federal Hazardous Substances Act (FHSA), 297
- FERG. *See* Full-field electroretinography (FERG)
- Fixed-dose combination (FDC), 269, 270
- Fourier-domain Optical coherence tomography, 95
- Fluorescein angiography (FA), 25, 58–60
- capillary transition stage, 50
 - early venous, 50
 - hyperfluorescence, 50
 - hypofluorescence, 50
 - late recirculation phases, 50
 - late venous, 50
 - neovascularization, 50
 - phases, 50
 - prearteriolar, 50
 - retinal arteriolar, 50
 - stages, 51
- F-7000 Fluorescence Spectrophotometer, 88
- F-2500 Fluorescence Spectrophotometer, 88
- Fluorophotometry
- animal toxicology and ocular research, 86–87
 - commercially available devices, 88
 - human clinical applications, 88
 - limitations and caveats, 89
 - ocular toxicology studies, 88–89
 - performance parameters, 85, 87
 - principles, 84–86

- FluorotronTM Master Ocular
Fluorophotometer, 88
- Food and Drug Administration (FDA),
260–266
- Frequency-domain Optical coherence
tomography, 95
- Fuchs heterochromic cyclitis, 62
- Full-field electroretinography (FERG),
124–125
- a-wave, 127
 - b-wave, 126
 - commercially available devices, 128–129
 - dark-adapted, 126
 - 30-Hz flicker, 127
 - ISCEV, 125
 - limitations and caveats, 129
 - ocular toxicology research, 128
 - ocular toxicology studies, 129
 - oscillatory potentials, 127
 - photopic, 128
 - photopic responses, 126
 - scotopic, 128
 - signal averaging, 128
- Fundus autofluorescence, 92
- 5-Fluorouracil, 63
- G**
- Ganglion cell axon microtubules, 103
- Galilei G2, 73
- GDx. *See* Scanning laser polarimetry (GDx)
- Genotoxicity, 265, 273, 277–278
- Geographic age-related macular
degeneration, 92
- Glaucoma, 95, 98, 104, 200–202
- Glaucoma probability score, 91
- Glial (neuroepithelial) choristoma, 45
- Goldmann lens, 57
- Goniovideography, 74
- Good Laboratory Practice (GLP), 24, 269
- H**
- HAI CL-1000ncTM, 69
- HAI-CL-1000xyz, 69
- Hard corneal contact lens 102
- Harderian glands, 6
- albuterol, 174
 - atrophy, 175
 - 2, 4-dichlorophenyl-p-nitrophenyl ether, 175
 - gross and microscopic appearance, 169
 - hyperplasia, 175
 - inflammation and necrosis, 170
 - lipid-containing secretion, 169
 - neoplasia, 176–177
 - neuroleptic timipirone, 175
 - recombinant human epidermal growth
factor, 174
 - spontaneous findings, 175
- Head holder, 94
- Histologic preparation, 160–165
- embedding, 165
 - enucleation, 161
 - fixation, 161–163
 - preparation, 160–161
 - sectioning, 165
 - trimming, 163–164
- HRT Rostock Cornea Module, 65
- Human herpes simplex virus keratitis, 64
- Hydroxychloroquine, 59, 60, 98
- Hypertyrosinemia, 181
- I**
- Imaging technologies, 53, 55
- Indirect ophthalmoscopy, 39
- Infectious keratitis, 62
- Inflammation
- conjunctiva, 196–197
 - cornea, 187–188
 - eyelid, 166–168
 - harderian glands, 169
 - uvea, 199
- Indocyanine green dye angiography, 97
- Inherited retinal degeneration, 230
- International Society for the Clinical
Electrophysiology of Vision
(ISCEV), 125
- ERG, 126
 - pattern ERG, 135
 - VEP standard, 140–142
- Intraocular pressure (IOP), 25, 47,
200–201
- Intravitreal injection of adeno-associated
virus, 91
- Investigational New Drug Application (IND),
260, 265
- Iridocorneal endothelial syndrome, 62
- Iris, 8. *See also* Uvea
- K**
- Keratic precipitates, 60
- Keratitis, 181
- Keratoconus, 62, 65, 72
- Keratomileusis, 66
- Keratoplasty, 64
- KOWA FM-600, 83

L

- Lacrimal drainage, 5, 6, 175–176
- Lacrimal glands, 6, 169–175
 - alterations, 170–175
 - atropine sulfate, 174
 - botulinum toxin B, 173
 - discoloration, 172
 - drugs affecting, 172–175
 - focal squamous metaplasia, 170
 - glandular epithelial degeneration, 170
 - harderianization, 170
 - inflammatory reactions, 172
 - morphologic changes, 170–175
 - neoplasia, 176–177
 - practolol, 173
 - radiation injury, 171–172
- Lamina cribosa, 95
- Laser flare-cell meter
 - animal toxicology and ocular research, 83
 - commercially available device, 83
 - human clinical applications, 83
 - limitations and caveats, 84
 - ocular toxicology studies, 83–84
 - performance parameters, 82
 - principles, 81–82
- LASIK, 69
- Latanoprost, 83
- Lens densitometry, 70
- Lens, 9–11, 220
 - capsule alterations, 225–226
 - Davidson's fixative artifacts, 162
 - epithelial alterations, 224–225
 - epithelium, 220
 - lenticular cortical degeneration, 220
 - lenticular opacity, 220
 - lenticular toxicity, 223–224
 - microscopic lenticular findings
 - cataract, 221–225
 - proliferation, 221
 - reversible opacification, 220
 - spontaneous lenticular opacities
 - aging, 223
 - diffuse opacification and vacuoles, 221
 - granulomatous inflammation, 223
 - nuclear cataract, 223
 - posterior capsular and cortical opacities, 222
- Levofloxacin, 63
- Lid speculums, 94
- Lipid keratopathy, 189–190
- Lipopolysaccharide, 62
- Low-coherence tomography, 94
- Lowering intraocular pressure, 87

M

- Macular detachment, 95
- Macular edema, 95
- Macular thickness, 103
- Macular holes, 95
- Mesodermal dysmorphodystrophy, 62
- mfERG. *See* Multifocal electroretinography (mfERG)
- Microscopic ocular examination
 - conjunctiva (*see* Conjunctiva)
 - cornea (*see* Cornea)
 - extraocular tissues (*see* Extraocular tissues)
 - preparation
 - embedding, 165
 - enucleation, 161
 - fixation and fixatives, 161–163
 - sectioning, 165
 - trimming, 163–164
 - terminology, 165–166
 - uveal alterations
 - choroidal adiposity, 200
 - cytoplasmic vacuolation, 198–199
 - developmental uveal findings, 203
 - drug-induced morphological changes, 198
 - intraocular pressure and glaucoma, 200–202
 - iris atrophy, 200
 - neoplasia, 204
 - pigmentary changes, 198
 - tapetal alterations, 202–203
 - uveal inflammation and trauma, 199
- Multifocal electroretinography (mfERG)
 - age-related macular degeneration, 130
 - central serous retinopathy, 130
 - commercially available devices, 132
 - diabetic retinopathy, 130
 - experimental glaucoma, 132
 - hydroxychloroquine, 132
 - inflammatory disease, 130
 - juvenile retinoschisis, 130
 - limitations and caveats, 133
 - macular holes, 130
 - m-sequence pattern, 130
 - multifocal ERG, 130
 - ocular toxicology research, 131, 132
 - optic nerve transection, 131
 - reversing ophthalmoscope, 133
 - supranormal, 132
 - vitelliform maculopathies, 130
- Multiple sclerosis, 104

N

- Naphthalene, 224
- Neoplasia
 - optic nerve, 249
 - retina, 245
- Nephropathic cystinosis, 64
- Neurofilaments, 103
- Neutrophic keratopathy, 62
- New Drug Application (NDA), 260, 265
- Nictitating membrane, 5, 175
- Nondrug Food and Drug Administration
 - animal testing, 303–304
 - Draize eye test, 303
 - hazard classification schemes and labeling requirements
 - agency classification schemes, 302
 - cosmetics, 300
 - GHS classification scheme, 302
 - household products, 301, 302
 - industrial chemicals, 301
 - pesticides, 299, 300
 - historical data and in vitro methods, 304
 - testing guidelines, 297–298
 - US regulations, 297
- Nonhuman primate (NHP), 2, 15
- No observed adverse effect level (NOAEL), 291
- No observed effect level (NOEL), 291

O

- OCT. *See* Optical coherence tomography (OCT)
- Ocular and systemic general toxicology studies, 277–282
- Ocular ultrasonography, 50
- Open angle glaucoma, 64, 88, 91
- Ophthalmic drugs
 - biologics vs. small molecules, 270–272
 - carcinogenicity, 265, 273, 278, 285–286, 291
 - clinical trials, 264, 265
 - combination products, 267–269, 288–289
 - drug development process
 - clinical trials, 264–267
 - FDA meetings, 265, 266
 - nonclinical pharmacology/toxicology, 265
 - excipients, 269, 277, 281, 289
 - FDA, 260–266
 - FDA/CDER, 260, 266–267

- genotoxicity, 265, 273, 277–278
 - GLP, 269
 - ICH guidance, 268
 - impurities, 270, 290
 - NOAEL, 291
 - ocular and systemic general toxicology, 278–283
 - pharmacokinetics/toxicokinetics, 276–277
 - pharmacology
 - primary pharmacodynamics, 273–274
 - safety pharmacology, 273–275
 - secondary pharmacodynamic effects, 273–274
 - photosafety, 273, 284–285
 - reformulated products, 286–288
 - regulation, 266–267
 - reproductive toxicology studies, 283–284
 - TCR, 286
 - types of, drug products, 269–270
 - in vitro metabolic and plasma protein binding data, 275–276
- Ophthalmoscopy**
- albino rat fundus
 - choroidal vessels, 43
 - optic disc, 43
 - bilateral optic atrophy (BOA), 46
 - binocular indirect ophthalmoscopy, 40
 - BOA, 46
 - canine fundus
 - non-tapetal fundus, 43
 - optic disc, 43
 - tapetal fundus, 43
 - direct, 39–40
 - fundus, 40
 - glial (neuroepithelial) choristoma, 45
 - indirect, 39–40
 - optic nerve and temporal retina, 47
 - peripapillary myelination, 45
 - photographic documentation, 41
 - photography, 41
 - posterior uveitis, 40, 41
 - primate fundus
 - choroid, 44
 - fovea, 44
 - macula, 44
 - optic disc, 44
 - retinal pigment epithelium (RPE), 44
 - rabbit fundus
 - choroidal vessels, 42
 - optic disc, 42
 - retinal vessels, 42
 - vitreous haze, 40, 41, 46

Optical coherence tomography (OCT), 25, 50, 52, 94
 animal toxicology and ocular research
 segmentation, 98–100
 United States Food and Drug Administration, 97–98
 commercially available devices, 101
 human clinical applications, 100
 limitations and caveats, 102–103
 mfERG, 131
 ocular toxicology studies, 101–102
 performance parameters, 95–97
 principles, 94–96

Optic disc, 95

Optic nerve, 12
 atrophy, 247, 248
 degeneration, 246, 247
 developmental abnormalities, 246
 ganglion cell axons, 246
 inflammation, 248
 neoplasia, 249
 optic disc, 246
 papilledema, 246, 248–249
 physiologic cup, 246
 toxic optic neuropathy, 248

Optic nerve crush injury, 97

Optic nerve head drusen, 93

Orbital glands, 168–175
 Harderian gland (*see* Harderian gland)
 Harder's gland, 169
 lacrimal gland (*see* Lacrimal gland)

Orbital contents, 176

Orbital plexus, 176

Orbital sinus, 176

Outer segment pathology, 99, 229–232

P

Pachymetry, 24

Pachymetry and specular endothelial microscopy, 49

Paget's disease, 60

Papilledema, 248–250

Pattern reversal electroretinography (PERG), 134
 C57BL/6, 136
 commercially available devices, 138
 DBA/2J, 136
 experimental glaucoma, 136
 human clinical research, 136–137
 LED displays, 138
 macular degeneration, 137
 N95, 135

reversing ophthalmoscope, 133
 P50, 135
 Signal-to-Noise Ratio, 134
 steady-state PERGs, 134–135
 transient PERG, 134

Pattern reversal visual evoked potential (PRVEP), 142, 144, 145

Pentacam®, 73

Periocular injection, 86

PERG. *See* Pattern reversal electroretinography (PERG)

Pharmacokinetics (PK), 273, 276, 277

Pharmacology
 primary pharmacodynamics, 273–274
 safety pharmacology, 273–275
 secondary pharmacodynamic effects, 273–274

Photomultiplier tube, 81

Photoreceptor displaced nuclei (PDN). *See* Displaced photoreceptor nuclei (DPN)

Pigmentary glaucoma, 80, 202

Pigment dispersion syndrome, 80, 202

PK. *See* Pharmacokinetics (PK)

Plano corneal contact lens, 94

Polymorphous dystrophy, 62

Posterior chamber intraocular lenses, 79

Posterior subcapsular cataract, 224

Prostaglandin-induced aqueous flare, 83

PRVEP. *See* Pattern reversal visual evoked potential (PRVEP)

Pseudoguttata, 64

R

Radiomimetic cataracts, 224

Ranibizumab, 100

Reflex ultrasound biomicroscope, 80

Retina, 12–17
 gliosis, 234
 inflammation, 234
 morphologic changes, 228
 retinal pigment epithelium alterations (*see* Retinal pigment epithelium)

spontaneous alterations
 displaced photoreceptor nuclei, 230–231
 ganglion cells loss, 232
 knockin/knockout transgenic studies, 230
 light-induced retinal degeneration, 232
 microcystoid changes, RPE, 230, 232
 peripheral cystoid retinal degeneration, 232

- photoreceptors, 228–232
- retinal detachment, 233–234
- retinal folds, 232
- uveal pigmentation, 232
- vascular findings, 228
- structure, 228
- surgical trauma, 235
- toxicity
 - D,L-2-amino-3-phosphonopropionate, 239
 - enrofloxacin, 239
 - ethambutol, 239
 - ganglion cell degeneration, 241–242
 - Müller cells, 237–239
 - photoreceptors, 240–241
 - retinal degeneration, 240–241
 - retinal neoplasia, 245
 - retinal pigment epithelium, 243–245
 - retinal vacuolation, 245
 - sensory retinal alterations, 237–243
 - trimethyltin, 239
 - vascular alterations, 241
 - vigabatrin, 240
- Retinal detachment, 99, 233–234
- Retinal nerve fiber layer (RNFL), 95, 97, 98, 103
- Retinal pigment epithelium (RPE), 15, 17, 243–245
 - extracellular matrix components deposition, 237
 - hyperplasia, 237
 - hypertrophy, 235, 236
 - lipofuscin accumulation, 236
 - photoreceptor changes, 228–243
 - Retinitis pigmentosa, 97
- RTVue-100, 101
- S**
- Scanning laser ophthalmoscope (SLO)
 - animal toxicology and ocular research, 90–91
 - commercially available devices, 92, 94
 - human clinical applications, 91–93
 - limitations and caveats, 94
 - ocular toxicology studies, 94
 - performance parameters, 90
 - principles, 89
- Scanning laser polarimetry (GDx), 103
 - animal toxicology and ocular research, 104, 105
 - commercially available devices, 105–106
 - human clinical applications, 104, 105
 - limitations and caveats, 106
 - ocular toxicology studies, 106
 - pathology, 200–202
 - performance parameters, 104
 - principles, 103
- Scheimpflug imaging
 - animal toxicology and ocular research, 72–74
 - commercially available devices, 73
 - human clinical applications, 73
 - limitations and caveats, 75
 - ocular toxicology studies, 73, 75
 - performance parameters, 70, 72
 - principles, 70, 71
- Schlemm's canal, 88, 95
- Sclera, 7, 8, 95, 194
 - alterations, 194–195
- SD-OCT. *See* Spectral-domain optical coherence tomography (SD-OCT)
- Segmentation, 98
- Selenite, 224
- Signal-to-noise ratio (SNR), 139, 140
- Slit-lamp biomicroscopy
 - anterior vitreous, 28
 - aqueous flare, 32
 - aqueous vitreous, 32
 - cataracts, 30–32
 - corneal degeneration/dystrophy, 28
 - corneal epithelial dystrophy, 29
 - corneal scar, 29
 - dilation, 28
 - Draize scoring system, 38
 - Dutch belted rabbits, 28
 - epithelial dystrophy, 28
 - fibrin formation, 37
 - Hackett-McDonald scoring system, 30
 - hyphema, 38
 - hypopyon, 38
 - nonpigmented cells, 27, 38
 - pigment epithelial cells, 27, 28, 38
 - portable models, 26, 27
 - pupillary light responses, 27, 28
 - red blood cells, 38
 - Sprague-Dawley rat, 28
 - SUN system, 30, 37
 - table-mounted models, 26, 27
 - Tyndall effect, 27, 31, 32
 - uveitis, 32
- SLO. *See* Scanning laser ophthalmoscope (SLO)
- SLP. *See* Scanning laser polarimetry (SLP)
- SOCT Copernicus, 101

- Spectral-domain optical coherence tomography (SD-OCT), 95
 advantages and disadvantages, 96
 central macula, 99
 commercially available devices, 101
 development of, 55
 and functional (electrophysiologic) findings, 59
 high-resolution, 97
 and histopathology, 58
 signal processing algorithm, 97
 subjective assessment, 98
 TD-OCT, 103
 ultrahigh-resolution, 100
 use of, 97
- Spectral OCT SLO, 101
- Spectralis OCT, 101
- Specular endothelial microscopy, 24–25
- Specular photomicroscopy
 animal toxicology and ocular research, 66–69
 commercially available devices
 contact, 69
 noncontact, 69
 human clinical applications, 69
 limitations and caveats, 70
 ocular toxicology studies, 69–70
 performance parameters, 66
 principles, 66, 67
- Standardization of Uveitis Nomenclature (SUN) System, 30
- Starengi contact lens, 58, 93, 102
- Steopsis, 57
- Stereopsis, 57
- Sugar cataract, 223–224
- Swept source-domain Optical coherence tomography, 95
- Swept source OCT (SS-OCT), 95, 96
- T**
- Tapetum lucidum, 17. *See also* Uvea alterations, 202–203
- Tear turnover, 87
- Terminology, 165–166
- Time-domain optical coherence tomography (TD-OCT), 95, 96, 102, 103
- Tissue cross-reactivity (TCR), 286
- Tomey EM-3000TM, 69
- Tonometry, 24
 cornea applanation, 47, 48
 induction-impaction, 47
 pneumotonograph, 48
 rebound tonometer, 47
- Toxic Substances Control Act (TSCA), 296
- Trabecular meshwork, 9, 95
- Trabeculectomy, 83, 88
- Traditional ophthalmic fundus imaging, 56
 baseline images, 57
 cross-sectional analysis, 58
 digital images, 57
 dose-response changes, 58
 fluorescein angiography, 59, 60
 high-resolution images, 57
 rapid, subjective interpretation, 58
 recovery, 58
 retrospective analysis, 58
 SD-OCT and functional (electrophysiologic) findings, 59
 stereopsis, 57
- Transgene expression, 91
- Triparanol, 224
- TS NIT, 106
- U**
- Ultrasonography, 25
- Ultrasound biomicroscopy
 animal toxicology and ocular research, 77–79
 commercially available devices, 80
 human clinical applications, 79–80
 limitations and caveats, 81
 ocular toxicology studies, 80–81
 performance parameters, 76–77
 principles, 75–76
- Uvea, 18, 197–198. *See also* Iris, Ciliary body, Choroidal alterations
 choroidal adiposity, 200
 cytoplasmic vacuolation, 198–199
 developmental uveal findings, 203
 drug-induced morphological changes, 198–203
 intraocular pressure and glaucoma, 200–202 (*see also* Glaucoma diagnosis) iris atrophy, 200
 neoplasia, 204
 pigmentary changes, 198
 tapetal alterations, 202–203
 uveal inflammation and trauma, 199
 intraocular inflammation, 199
- Uveitis, 62, 83, 199
- V**
- Variable corneal compensation (VCC), 103, 106
- Vascular occlusive disease, 98

- Vigabatrin, 92, 240
- Visual evoked potentials (VEPs)
- acrylamide and N-methylolacrylamide, 145
 - averaging, 139
 - binocular interactions, 141
 - central visual pathways, 142
 - commercially available devices, 149–150
 - cortical generator, 139, 141, 142, 150
 - ethambutol, 146
 - experimental glaucoma, 144
 - flash VEP, 142
 - glaucoma, 145
 - hydroxychloroquine toxicity, 146
 - idiopathic bilateral optic atrophy, 140, 144
 - lead exposure, 148
 - limitations and caveats, 150–151
 - methylmercury and polychlorinated biphenyls, 146
 - motion, 141
 - multiple sclerosis, 145
 - n-hexane, 148
 - ocular toxicology studies, 150
 - optic atrophy, 145
 - optic nerve transection, 147
 - optic neuritis, 145
 - osteopetrotic knockout, 145
 - pattern onset/offset VEPs, 142
 - pattern reversal VEPs, 142
 - “P100” wave, 143
 - performance parameters, 143–144
 - Signal-to-Noise Ratio, 139
 - steady-state stimulus (ssVEPs), 140
 - sweep, 141, 146
 - systemic lupus erythematosus, 146
 - vernier acuity, 141
- Vitreous body
- iatrogenic vitreal findings, 227
 - spontaneous background findings
 - asteroid hyalosis, 227
 - fibrosis and calcification, 227
 - hyaloid vessels, 226
 - intravitreal hemorrhage, 227
 - rheological changes, 227
 - toxicologic findings, 227
- W**
- Water bath, 81, 165
- Weill-Marchesani syndrome, 62
- Z**
- Zonula adherens, 59
- Zonula, 77